Author:
He, Horatio

Title:
Advances in Living Crystallisation-Driven Self-Assembly

Towards Biological Applications of Uniform 1D and 2D Polymer-Based Micelles with Controlled Dimensions

Advances in Living Crystallisation-Driven Self-Assembly: Towards Biological Applications of Uniform 1D and 2D Polymer-Based Micelles with Controlled Dimensions

Yunxiang He

A thesis submitted to the University of Bristol in conformity with the requirements for the degree of Doctor of Philosophy in the School of Chemistry, Faculty of Science

Jan 2019

Word count: 39,353

Abstract

Nano- to micro-scale (10^{-9}-10^{-6} m) objects abundant in nature such as the enzymes in biological processes and cells in tissues exhibit many distinctive functionalities. Most of these natural species possess hierarchical structures and are created, at least in part, via a bottom-up strategy termed self-assembly. It is a challenge for synthetic chemists to achieve assemblies with complex hierarchy and precise control in each tier by the traditional top-down method in manufacturing. However, applying a bottom-up approach mimicking self-assembly in nature to synthetic chemistry could assist in the fabrication of new materials with novel structures and properties. For example, this is achieved with block copolymer (BCP) self-assembly whereby microphase segregation of chemically immiscible polymer blocks occurs. In solution, amphiphilic BCPs have been shown to exhibit self-organization behaviour via a variety of non-covalent interactions to afford micelles with a diverse range of morphologies on the nanoscale. Only recently, unprecedented control over BCP micelle morphologies and dimensions have been shown with BCPs containing a crystalline-core forming block. By using a seeded-growth method, both one- and two-dimensional (1D and 2D) micelles and complex supermicelles have been fabricated with precisely controlled sizes via a process termed living crystallisation-driven self-assembly (CDSA). The work in this thesis presents an extension of the living CDSA strategies to BCPs with a degradable organic core-forming block and explores the potential applications of well-controlled 1D fibre-like micelles in biomedicine.

Chapter 1 provides a general introduction to the relevant topics surrounding the research presented in this thesis. Nanostructures prepared by self-assembly in nature is first briefly discussed, followed by the principles of BCP self-assembly. Living CDSA will be discussed, focussing on the efficiency in precise control over the structure dimensions in 1D and 2D, as well as the fabrication of functional hierarchical supermicelles. Finally, selected work on 1D fibre-micelle applications in drug delivery systems (DDS) and structures based on poly(*L*-lactide) (PLLA) are presented.

High aspect ratio structures have been reported to be advantageous in DDS, however fibre-like micelles are difficult to attain morphologically pure and with controlled dimensions. In **Chapter 2**, uniform fibre-like micelles based on poly(ferrocenyldimethylsilane) (PFS) and polyfluorene (PF) have been

prepared for cellular uptake investigations. Living CDSA has been extensively studied with PFS-containing BCPs and has led to the formation of a wide range of structures with well-defined dimensions. PF-based nanoparticles have been widely used in bioimaging due to their inherent fluorescent characteristics. Dual-fluorescence and cancer cell targeting PF-based micelles have been prepared and PFS-based fluorescent micelles have been shown to enter HeLa cells in cellular uptake studies.

Biodegradable and biocompatible PLLA are promising materials for applications in DDS. However, the preparation of uniform PLLA-based high aspect ratio structures is challenging. **Chapter 3** presents the living CDSA of BCP containing a PLLA core-forming block. The main work focus on the optimization of the preparation of uniform fibre-like micelles with controlled length of PLLA-containing diblock copolymers by employing additional solvent additives. It is proposed that the balance of PLLA chain solvation and intermolecular H-bonding has significant effects on the epitaxial growth of the micelles. Solvent additives have been shown to also optimise the seeded-growth other PLLA-containing diblock copolymers whereby complex block co-micelles can be fabricated.

Chapter 4 expands the micelle morphology and dimension control from 1D to 2D via a charge-terminated PLLA homopolymer and a blend of PLLA homopolymer and diblock copolymer. Complex spatial segmented block co-platelet micelles have been prepared. Functional platelet micelles have been shown to template inorganic nanoparticles. Square scarf-like micelles based on a hybrid of 1D fibre-like micelles and 2D diamond-shaped micelles are obtained by sequentially using PLLA homopolymer and diblock copolymer.

Finally, **Chapter 5** summarises the progresses achieved in this thesis which contributes to the understanding of living CDSA of organic crystallizable polymers. The future research directions have been discussed which are geared towards functional nanostructures manufacturing, potential applications in catalysis and biomedicine.

Acknowledgements

I would not have been able to complete my PhD studies without the great funding support of my parents and the help and guidance from my friends, colleagues and supervisors.

In particular, I would like to thank Professor Ian Manners for providing the opportunity for me to join the group and the important academic guidance he has provided me throughout my project. I would also like to thank Professor Charl Faul for useful suggestions and supportive encouragement in the struggling times.

I also greatly appreciate the help and support from George Whittell and Deborah O'Hanlon Manners. Without their help on projects, lab issues and social activities, I could not have enjoyed my PhD life in Bristol.

I would also like to give special thanks to Dr. Ali Nazemi, Dr. Holly Baum, Dr. Xuhui Jin, Diego Garcia Hernandez, Dr. Xiaoming He, Prof. Robert Richardson, Dr. Jean-Charles Eloi, Jonathan Jones, Dr. Robert Harniman, Dr. George Whittell, Prof. Rachel O'Reilly and Prof. Andrew Dove for their contributions to this thesis.

I really appreciate the fun time and experience with the intelligent and lovely people in Bristol. Without their kind and useful help, cares, suggestions and discussions in both lab works and life events, I would not finish the Ph.D. It is not possible to name them all here, but special thanks must go to Becca, Alastair, Alex O, Becs, Ben M, Carl Hu, C. Boott, C. Ellis, Christian, Dicker, Diego B, Djen, Emily K, Eric, Erin, Esther, Feng, Henry, Hongjing, Huda A, Huda Shaikh, Huibin, Jay, Jess G, Jia, John F, Josh, Kazu, Laura, Liam, Lipeng, Luke, Maha, Macros, Marius, Matt R, Nan, Naomi, Nikki, Nouf, Oli, P. Choi, Pan, Qiwei, Renhua, Sammy P, Saurabh, Steve S, Theresa, Titel, Tomoya, Uli, Veronica, Vince, Wei Lyu, Xiaohua, Xiaoyu, Yang and Yifan. I must also thank the BCS CDT for providing my Ph.D funding and my lovely 2014 cohort people: Ali, Bin, David, Jess, Kate, Krishna, Harper, Paul and Siying.

Last but not least, I would like to thank my great and lovely family members: my parents, my grandmas, my uncles and aunties and my cousins. Without their loves and cares, I would not have come this far.

Declaration

I declare that the work in this dissertation was carried out in accordance with the requirements of the University's Regulations and Code of Practice for Research Degree Programmes and that it has not been submitted for any other academic award. Except where indicated by specific reference in the text, the work is the candidate's own work. Work done in collaboration with, or with the assistance of, others, is indicated as such. Any views expressed in the dissertation are those of the author.

Yunxiang He

University of Bristol

Jan 2019

Contents

List of Figures

List of Supplementary Figures

List of Tables

List of Schemes

Abbreviations

-b-	-block-
-m-	-micelle block-
-r-	-random-
-g-	-graft-
[cat]	Catalyst
0D	Zero-dimensional
1D	One-dimensional
2D	Two-dimensional
3D	Three-dimensional
Å	Ångström
AFM	Atomic force microscopy
AIBN	2,2′-Azobis(2-methylpropionitrile)
A_n	Number-average area
A_w	Weight-average area
BCP	Block copolymer
BODIPY	Boron-dipyrromethene
χ	Flory-Huggins interaction parameter
C	Celsius
CDSA	Crystallisation-driven self-assembly
$CDCl_3$	Deuterated chloroform
$CHCl_3$	Chloroform
CLSM	Confocal laser scanning microscopy
cm	Centimetre
CMC	Critical micelle concentration
CTA	Chain transfer agent
d	Doublet
D	Diameter
D	Diffusion constant
$Đ_M$	Molar mass dispersity
Da	Dalton
DAPI	4′,6-Diamidino-2-phenylindole
DBU	1,8-Diazabicyclo[5.4.0]undec-7-ene
DCM	Dichloromethane
Dioxane	1,4-Dioxane
DLS	Dynamic light scattering
DMEM	Dulbecco's modified eagle's media
DMF	Dimethylformamide
DMPA	2,2-Dimethoxy-2-phenylacetophenone

DMSO	Dimethyl sulfoxide
DOSY	Diffusion ordered spectroscopy
DP_n	Number-average degree of polymerisation
DSC	Differential scanning calorimetry
EDX	Energy-dispersive X-ray spectroscopy
eq	Equivalent
EtOH	Ethanol
f	Volume fraction
FA	Folic acid
FT-IR	Fourier-transform infrared spectroscopy
GPC	Gel permeation chromatography
H_2O	water
h	Hour
H-bond	Hydrogen-bond
Hz	Hertz
I	Intensity
i-PrOH	2-Propanol
K	Kelvin
kV	Kilovolt
kW	Kilowatt
L_D	Exciton diffusion lengths
L_n	Number-average length
L_w	Weight-average length
M	Molar
m	Multiplet
MALDI-TOF	Matrix assisted laser desorption/ionisation time of flight
MeOH	Methanol
meV	Mili-electronvolt
mg	Miligram
MHz	Megahertz
min	Minute
mL	Mililitre
mM	Milimolar
μm	Micrometer
mmol	Milimole
M_n	Number-average molecular weight
mol	Mole
m_{unimer}/m_{seed}	Unimer-to-seed mass ratio
M_w	Weight-average molecular weight

N	Degree of polymerisation
n	Number
$N_{agg,A}$	Two-dimensional aggregation number
$N_{\mathrm{agg,L}}$	Linear aggregation number
NHS	N-hydroxysuccinimide
nm	Nanometre
NMR	Nuclear magnetic resonance
NP	nanoparticle
$^{\mathrm{o}}$	Degree
OPV	Oligo(*p*-phenylenevinylene)
p	Packing parameter
P2VP	Poly(2-vinylpyridine)
P3HT	Poly(3-hexylthiophene)
PAA	Poly(acrylic acid)
PAGE	Poly(allyl glycidyl ether)
PCL	Poly(caprolactone)
PDTF	Poly(di-*n*-hexylfluorene)
PDMA	Poly(*N*,*N*-dimethylacrylamide)
PDMAEMA	Poly(dimethylaminoethyl methacrylate)
PDMS	Polydimethylsiloxane
PDTC	Poly(2,2-dimethyltrimethylene carbonate)
PE	Polyethylene
PEE	Polyethylethylene
PEG	Poly(ethylene glycol) or poly(ethylene oxide)
PF	Polyfluorene
PFS	Poly(ferrocenyldimethylsilane)
PFTMC	Poly(spiro[fluorene-9,5'-[1,3]dioxin]-2'-one)
PI	Polyisoprene
PISA	Polymerisation induced self-assembly
PL	Photoluminescence
PLLA	Poly(*L*-lactide)
PDLA	Poly(D-lactide)
PMMA	Poly(methyl methacrylate)
PMVS	Poly(methylvinylsiloxane)
PNIPAm	Poly(N-isopropylacrylamide)
ppm	Parts per million
PPV	Poly(p-phenylene vinylene)
PS	Polystyrene
Q	Magnitude of scattering vector
QPT	Quaternised polythiophene
R	Rate of addtion

r	Reactivity ratio
ρ	Density
RAFT	Reversible addition-fragmentation chain-transfer
RNA	Ribonucleic acid
ROP	Ring-opening polymerisation
rpm	Revolutions per minute
s	Seconds
s	Singlet
σ	Standard deviation
SAED	Selected-area electron diffraction
SAXS	Small-angle X-ray scattering
SLD	Scattering-length density
SLS	Static light scattering
STEM	Scanning transmission electron microscopy
t	Triplet
TMDS	1,1,3,3-tetramethyldisiloxane
TEG	Triethylene glycol
TFA	Trifluoroacetic acid
TFE	Trifluoroethanol
Tg	Glass transition temperature
TGA	Thermogravimetric
THF	Tetrahydrofuran
T_m	Melting point transition
TMEDA	Tetramethylethylenediamine
TMV	Tobacco mosaic virus
UV	Ultraviolet radiation
v	volume
V_3	1,3,5-Trimethyl-1,3,5-trivinylcyclotrisiloxane
WAXS	Wide-angle X-ray scattering
W_n	Number-average width
wt%	Weight percent
W_w	Weight-average width
δ	Chemical shift
λ	Wavelength

Chapter 1 **Introduction**

1.1. Nanoscale Synthesis

1.1.1. 'Top-down', 'Bottom-up' and Self-assembly

Materials on the nano-to-micro length scales (10^{-9} - 10^{-6} m) are desirable in many applications, especially in nanomedicine.[1-3] There are two main approaches in nanoscale fabrication: 'top-down' and 'bottom-up'. Top-down methods involve scaling down a bulk material by selectively removing materials, until a nanomaterial is obtained.[4] The traditional fabrication of most everyday objects is limited by a scale visible to the naked eye (ca. $>10^{-4}$ m), and only a limited number of production methods can make complex microscale objects.[5-7] It is a challenge to prepare well-defined structures on the nano- to micro-scale using top-down methods due to the requirements concerning the high precision and resolution of the equipment in fabrication.

In contrast, bottom-up approaches involve assembling small building blocks together to create a larger length scale material.[3, 4] Chemical synthesis is a bottom-up method, forming bonds between atoms to afford molecules on the order of 10^{-10} m. However, to fabricate macromolecules on the length scale of 10^{-6} m with uniform size requires joining thousands of atoms with well-defined connections, which would be extremely inefficient and challenging.[8]

Self-assembly is an alternative bottom-up approach which can efficiently afford structures on a variety of length scales.[3, 9, 10] In this thesis, self-assembly is described as an automatic process of assembling building blocks into organised well-ordered structures via non-covalent interactions without external stimuli.[11-13]

1.1.2. Nanoscale Self-Assembly in Nature

Nature is superior to synthetic chemists in terms of the ability to produce complex structures with various sizes, especially for those which have dimensions on the nano- to macro-scales.[14-16] For example,

most biological materials found in nature are built into hierarchical structures by assembly of small sub-units.[17] The hierarchical structure plays an important role in determining the properties and functions of the assembled bulk materials which may not be shown by each sub-unit individually.[18] Self-assembly is used by nature to prepare these materials via a process that is driven by a multitude of non-covalent interactions.[14, 17, 19-21] A summary of commonly used non-covalent interactions are shown in Table 1.1.[22-25] Hydrogen-bonding (H-bonding) is one of the most common non-covalent interactions in biological materials.[26-28]

Table 1.1. Summary of typical non-covalent interactions.[22-25]

Non-covalent interactions	Strength (kJ/mol)	Distance
Ionic	250	1 nm – 1 μm
Dipole-dipole	5-50	0.1 nm – 1 nm
Hydrogen bonding	10-65	0.1 nm – 1 nm
π-π	0-50	0.1 nm – 1 nm
Van der Waals	<10	1 nm – 10 nm
Hydrophobic effects	Difficult to access	1 nm – 100 nm

Proteins are well-defined functional biological materials that are fabricated by self-assembly.[29] The hierarchical structure of proteins can be resolved into four levels and the order in each level is significant to the properties and functions. The primary structure is the sequence of covalently linked amino acids. The secondary structure involves amino acid assemblies such as α-helices or β-sheets, which are held together by H-bonding interactions. The tertiary structures are the aggregates or bundles of these helices or sheets formed via hydrophobic interactions. The quaternary structures are usually formed by the assembly of the tertiary structures as building blocks.[14, 21, 29]

As a result of the subject matter of this thesis, namely the preparation of uniform one dimensional (1D) fibre-like nanoparticles, two examples of fibre-like biological structures produced by nature will be briefly described. Collagen (Figure 1.1), which consists of almost one quarter of the total protein content

in most animals, is a good example of a well-studied protein with a hierarchical structrue.[30-32] The remarkable functions of collagen are derived from its unique tertiary structure, the formation of which is driven by H-bonding interactions.[33] The primary structure of collagen is a chain with a triplet repeat sequence of glycine-proline-hydroxyproline (Gly-Pro-Hyp) with generally more than 1,000 residues. Each chain folds into an α-helix by intramolecular H-bonding among the amino acid sequences to afford the α-helix secondary structure. The tertiary structure is a triple helix consisting of three α-helix chains held together by both strong (N-H···O) and weak (C-H···O) intermolecular H-bonding interactions, which is considered as a fundamental unit of collagen. The quaternary structure achieves functions by organising triple helices in different ways: tensile strength in tendon is generated by bundling; the hard rigidity in bone and teeth arises by calcification of the interspace; and flexibility in skin and cartilage is generated by cross-linking and intricate rearrangement.[32]

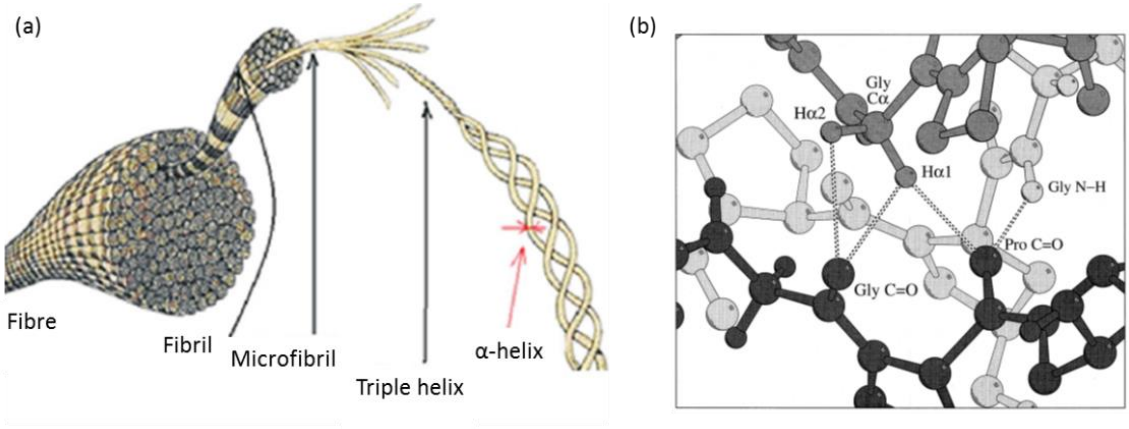

Figure 1.1. (a) Schematic representation of hierarchical structures of collagen fibre, and (b) schematic representation of H-bonding networks in collagen triple helix structures. Reproduced with permission from reference 33 and 34.

Tobacco mosaic virus (TMV) (Figure 1.2) is another example of a natural well-defined hierarchical structure formed by self-assembly, but on a much larger length scale (ca. 300 nm) compared with collagen triple helix (ca. 1.6 nm).[34-36] TMV contains a ribonucleic acid (RNA) strand protected by a protein capsid. The strand of RNA in TMV is ca. 6,400 nucleotides in length and is surrounded by a helical arrangement of 2,130 protein sub-units each containing 158 amino acid residues. When forming the virus, 34 protein sub-units first assemble around one end of the RNA strand into a hollow disc shape

with a screw dislocation, which is considered as the nucleation step. This allows further protein sub-units to helically bind to obtain a final hollow cylindrical capsid with a length ca. 300 nm and a diameter ca. 18 nm. H-bonding interactions among the residues in the protein sub-units contribute to the stability of the cylindrical capsid.[35, 37]

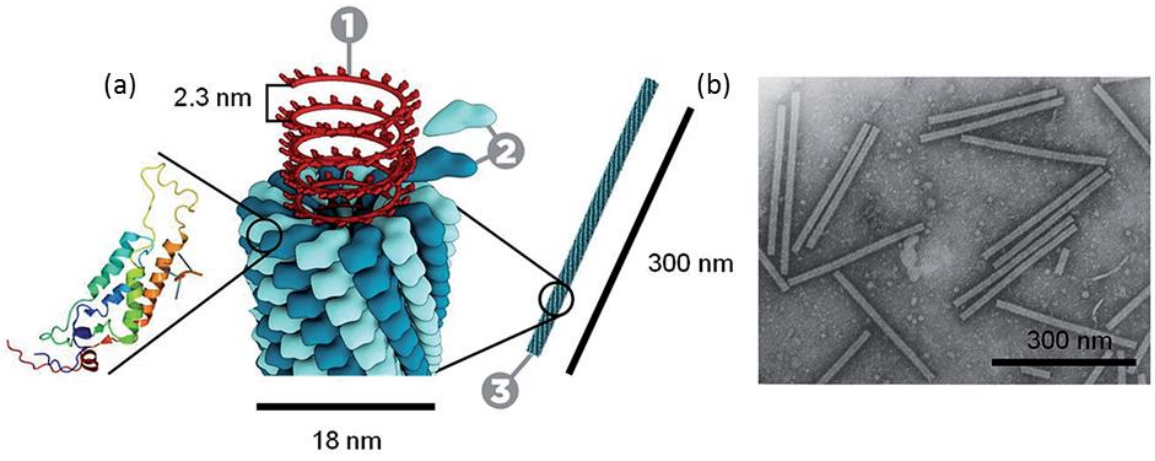

Figure 1.2. (a) Schematic representation and (b) Transmission election microscopy (TEM) image of the tobacco mosaic virus. One molecule of single strand RNA (1) surrounded by 2130 coat proteins (2) that make up the virus capsid (3). Reproduced with permission from reference 38.

1.2. Block Copolymer Self-Assembly

Block copolymer (BCP) self-assembly has been employed by materials scientists to fabricate well-defined objects on the nanoscale, this is a bottom-up strategy mimicking self-assembly found in nature.[38, 39] BCPs are covalently linked homopolymer blocks with different chemical and physical properties.[40] Due to special molecular composition, BCPs have a unique microphase separation property, which will result in considerable complex nanostructures.[41] With the recent advances in controlled polymerization techniques,[42-44] such as living ring-opening polymerizations, controlled radical polymerizations (CRP) and post-polymerization modification reactions, complex BCP architectures with controlled molecular weights and narrow molecular weight distributions have been achieved.[41] Such BCPs provide opportunities for the controlled preparation of nanostructures by microphase separation in bulk or the formation of core-shell nanoparticles (micelles) in solution.[45, 46]

1.2.1. Solid State Self-Assembly of BCP

Microphase separation of A-B linear diblock copolymers in the solid state has been studied extensively by both experiment[47, 48] and simulations.[39, 49-52] The process is driven by the unfavourable mixing enthalpy of the immiscible blocks which outweighs the entropic loss from localizing junctions at the interface and chain stretching.[47] The microphase separation of a well-defined A-B BCP can result in different morphologies (Figure 1.3), including spheres (S), cylinders (C), gyroids (G) and lamellae (L). the morphology is governed by three factors: the relative volume fractions of A and B blocks (f_A and f_B), the total degree of polymerization (DP_n: N) and the Flory-Huggins interaction parameters of A and B (χ).[40, 47, 53] In the self-assembly process, the system minimizes the number of A-B contacts to achieve a thermodynamically preferred state with the lowest A-B interfacial energy and least chain stretching.[38] A theoretical phase diagram of A-B BCP behaviour in bulk is shown in **Figure 1.3**.

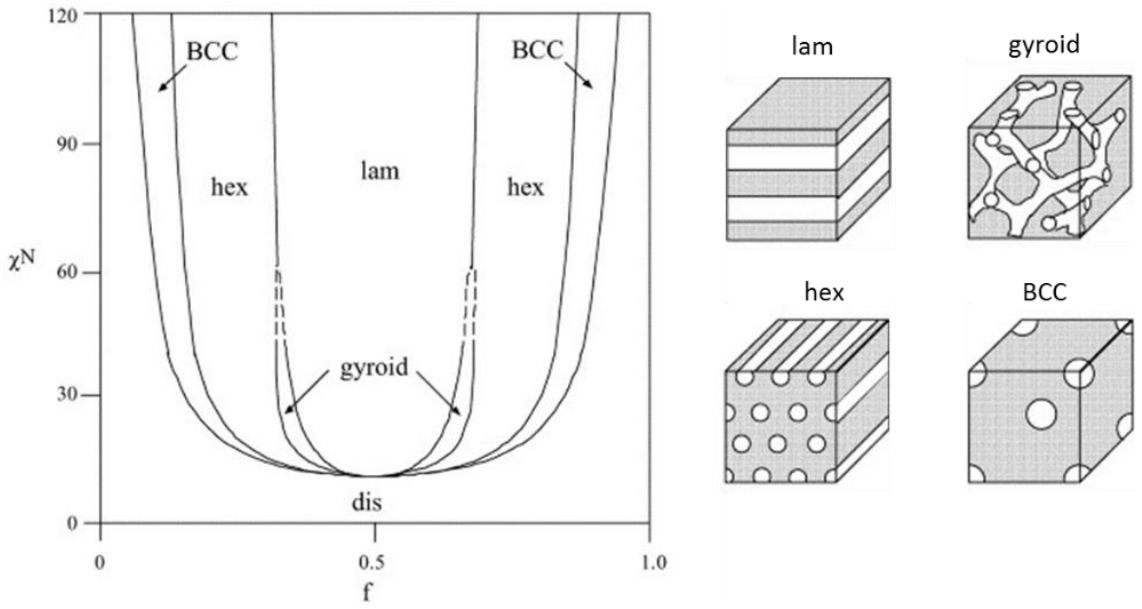

Figure 1.3. Theoretical phase diagram for a A-B diblock copolymer, regions of stability of disordered (dis), lamellar (lam), gyroid (gyroid), hexagonal (hex) and body-centred cubic (BCC) phases are indicated. Reproduced with permission from reference [54].

More complex and novel morphologies can be achieved by the self-assembly of triblock copolymer. This increases the complexity of the BCP systems by increasing the number of interaction parameters.[48,

[55-57] The self-assembly of BCPs is also affected by external factors such as electrical fields,[58] mechanical forces[59] and the interaction between the BCP and substrate (thin film self-assembly).[60, 61]

1.2.2. Solution State Self-Assembly of BCP with an Amorphous Core-Forming Block

Solution self-assembly of BCPs has been well-studied since 1990[38, 46, 62] and most studies focus on diblock copolymers with an amorphous core-forming block.[62-68] In this section, the principles of solution self-assembly will be briefly discussed with A-B diblock copolymers containing an amorphous core-forming block. Solution self-assembly of BCPs is generally conducted by dispersing the BCP into a selective solvent (or solvent mixture) for one block, while the other block collapses by solvophobic effects to afford core-shell micelle structures with varied morphologies.[38, 69] Although nanoparticles formed in solution seek the minimum free energy state similar with that in bulk self-assembly, the complexity is dramatically greater due to the presence of solvent.[38, 70-72] Three competing contributions are important to the overall free energy and therefore the observed morphology: intercoronal interactions, core-coronal interfacial energy and core-chain packing. The solvation of the corona in solvents results in an increase in the volume of the corona. This leads to corona chain stretching and an entropic penalty. Due to the preference for the least contact between the solvophobic core and solvent molecules, the interfacial energy plays a key role. Due to solvophobicity, the aggregation of core chains results in a decrease in the entropy of the system.

BCP self-assembly in solution can be regarded as a comparable process to the self-assembly of surfactants, in which the core-forming block mimics the hydrophobic tail and the corona-forming block mimics the polar head group of a surfactant molecule. The packing parameter (p) can also be used to describe and predict the thermodynamically favoured morphology formed in solution, which possesses a similar definition with that defined in surfactant self-assembly,

$$p = \frac{v}{a_o l_c} \qquad \text{(Equation.1)}$$

Where v is the hydrophobic core-forming block volume, a_o is the core-corona interface area and l_c is the core-forming block length.[71, 73-75] When $p \leq 1/3$, spherical micelles are observed; when $1/3 \leq p \leq ½$, rod- or -worm like micelles are observed; when $½ \leq p \leq 1$, bilayer structures are formed (Figure 1.4).

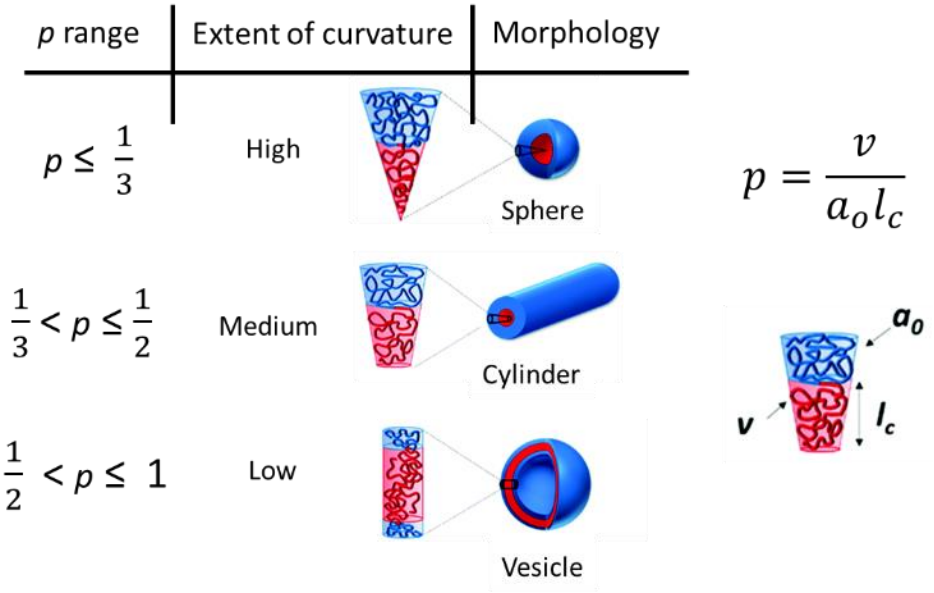

Figure 1.4. Schematic representation of effects of packing parameters on morphology formation in BCP solution state self-assembly. Reproduced with permission from reference [76].

However, the packing parameter can only predict the morphology formed in the equilibrium state. Unlike surfactant molecules, BCPs possess very low critical micelle concentrations (CMC) and extremely slow chain exchange rate.[38] This leads to BCPs often forming kinetically trapped morphologies in solution in most cases, which are far from equilibrium state.[77, 78] In addition, due to the difficulties in examining the dissolution of the polymer in different solvents, the parameter a_o is difficult to calculate, which further affects the calculation of p. This makes the prediction of the morphology in the equilibrium state a challenge in practice. Therefore, using a phase diagram to predict the BCP morphologies in solution is very limited to the specific BCP composition and solvent conditions. On the other hand, most out-of-equilibrium morphologies are stable under ambient conditions.[67, 69, 71, 79] This allows the preparation and applications of well-defined novel kinetically-trapped structures by optimization of the self-assembly conditions.[67, 77, 80-83]

Instead of using the value of *p*, the relative volume fractions of hydrophobic and hydrophilic blocks are commonly used to predict morphology formation.[76, 79] A good example would be early studies on polystyrene-*block*-poly(acrylic acid) (PS-*b*-PAA).[62] By altering the block length ratios, selective solvent/common solvent contents and additives, a series of morphologies have been achieved (Figure 1.5).[38, 62] The morphology evolution affected by core block volume fractions has also been observed in a process termed polymerization-induced self-assembly (PISA), where the BCP micelles are formed *in situ* during the polymerization.[84-87] With the increase of the core block length, the observed morphology transformed from spheres to cylinders to vesicles, which possess a lower degrees of core-corona interfacial curvature.

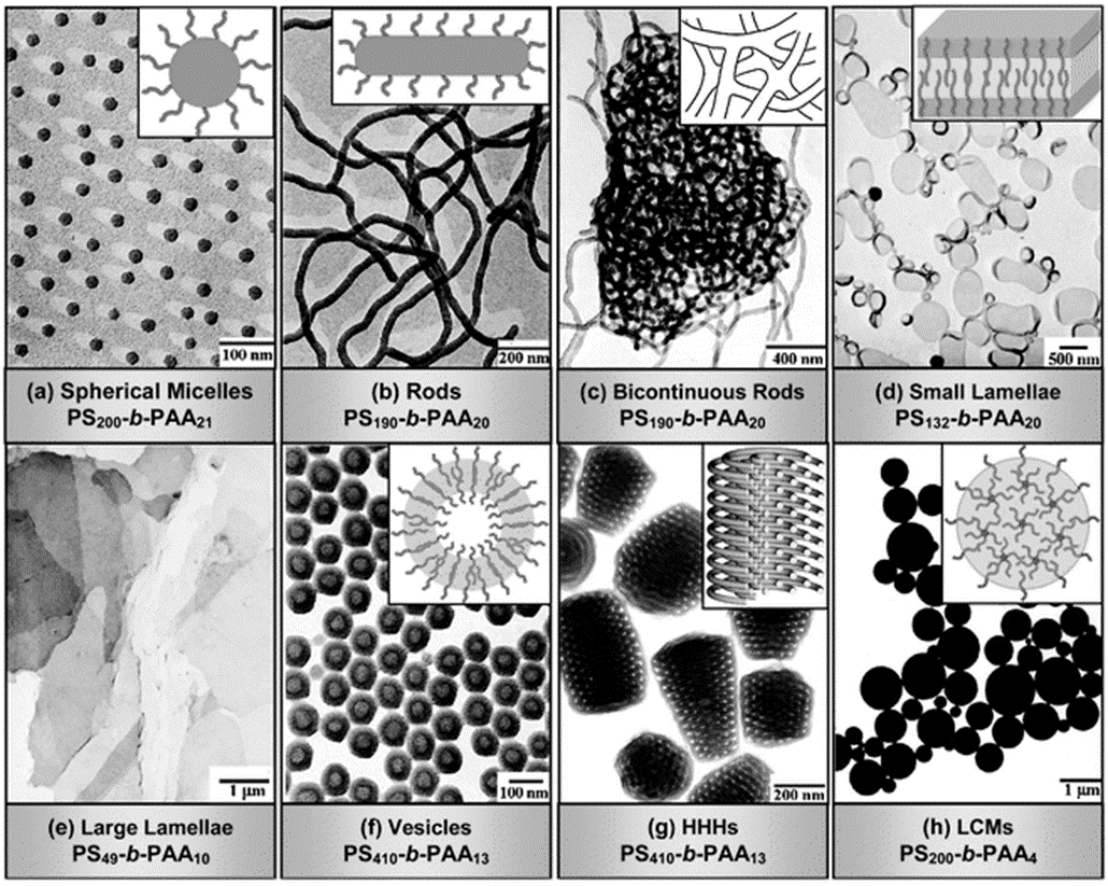

Figure 1.5. TEM images of various morphologies formed by PS-*b*-PAA with different polymer compositions. HHHs: hexagonally packed hollow hoopes, LCMs: large compound micelles. Reproduced with permission from reference [38].

More complex morphologies can be achieved by solution self-assembly by increasing the BCP architecture complexity and fine-tuning the kinetic and thermodynamic constraints. These include patchy or multi-compartment structures, helices, toroids and networks.[68, 88-91]

1.3. Crystallisation-Driven Self-Assembly (CDSA)

As discussed above, spherical micelles and vesicles are the major morphologies being obtained from solution self-assembly of BCPs with amorphous core-forming blocks. By using a crystallisable polymer as the core-forming block in BCPs, the self-assembly behaviour is altered dramatically, as such cylinders and platelets are now the major morphologies formed in solutions. This process is termed crystallisation-driven self-assembly (CDSA).[92, 93] The main difference comes from the additional contribution to the system, the enthalpy of crystallisation of the core-forming block (Table 1.2). In the past two decades, CDSA has been shown as an effective method to develop complex nanostructures[70, 94] with a vast range of crystallisable polymers as core-forming blocks, such as poly(ferrocenyldimethylsilane) (PFS)[95-99], polyethylene (PE)[100-104], poly(ε-caprolactone) (PCL)[105-109], poly(*L*-lactide) (PLLA)[110-114], polycarbonate[115, 116], poly(3-heylthiophene) (P3HT)[117-119] and oligo(p-phenylenevinylene) (OPV)[120, 121].

Table 1.2. A comparison between self-assembly of BCPs with an amorphous and crystalline core.

	Amorphous core	**Crystalline Core**
Driving Force	$G_{core} + G_{interface} + G_{corona}$	$G_{core} + G_{interface} + G_{corona} + G_{crystallization}$
Morphology	Difficult to predict	Low interfacial curvature
Factors	Dependent on chain stretching, interfacial energy, and corona chain stretching	Dependent on the crystallinity of the core

1.3.1. Crystallisation Mechanism

To achieve desired morphologies or alter the geometries of self-assembled nanoparticles, it is essential to understand the crystallisation behaviour of BCPs in solutions. A brief introduction on micelle formation of crystalline-amorphous diblock copolymers will be described in this section.

Two mechanisms are generally considered in the micelle formation process.[122, 123] The first one involves self-assembly followed by crystallisation. In the self-assembly process, the solvophobic core-forming block, which prefers minimum contact with the solvent, gives rise to spherical micelles with an amorphous core at first. This process can be considered as a spontaneously triggered microphase separation of the amphiphilic diblock copolymers. Afterwards the amorphous core starts to crystallise to form the nucleus for micelle formation. The core chain can either crystallise in the constrained spherical morphology (formed during microphase separation) or reorganise to crystallise (break-out) to develop into other morphologies by controlling the self-assembly conditions.[94, 124, 125] The second mechanism involves the homogeneous nucleation followed by elongation. This process is triggered by the initial nuclei formation via thermal fluctuations in the system, followed by the continuation of crystallisation on the growth surface by inducing more polymer chains.[126] Generally, the morphology formation in CDSA of BCPs relies on the competition between microphase separation and crystallisation, which are two self-organisation motions.

1.3.2. Factors Affecting Morphologies in CDSA

According to mechanistic studies on BCP crystallisation, changing the factors affecting the microphase separation behaviour and the core crystallisation would affect the final morphology obtained in solution.[94] These factors include the molecular characteristics of BCPs, the relative volume ratio between core and corona block, micelle concentration, solvent selectivity and temperature. By fine-tuning these parameters, the accessible morphologies are not limited to the common geometries (fibre-like micelles and platelet micelles) and other complex and hierarchical structures can be achieved, such as petal-like micelles, branched micelles and dendrites.[96, 101, 127-132]

Theoretical studies. In an important theoretical study, a model for BCP micelles with a crystalline core was proposed and the self-assembly process was studied (Figure 1.6).[93] In the model, the solvophobic crystallisable core chain folds adjacently and is aligned parallel to the short axis of the core, and a sharp boundary divides the core from the solvent-swollen corona. The junctions of the core and corona are constrained on the surface. The coronal blocks are grafted to the junctions on the surface. Additionally, core chain crystallisation and coronal chain stretching were suggested as two aspects in determining the formation of equilibrium morphologies during self-assembly. The core chains fold to crystallise and the chain folding determines the packing modes of the core-forming block, which also determines the grafted chain density and core geometry. The crystallisation of the core favours the growth of the micelles, because the increased size of the micelles would reduce the overall surface area of the core, which also minimizes the contract between the core and solvent. In contrast, due to the constrained core-corona junctions on the surface, the flexible corona chains are highly stretched along the normal to the surface,[93, 94] which causes a substantial loss in entropy. As a result, the micelles halt further growth to compensate for the entropic penalty. From this model, platelets were found to be the most common morphology. By increasing the corona block length, cylindrical and star-like micelles could be achieved. However, the crew-cut micelles (micelles from rod-coil BCP, no core chain folding)[133, 134] were unstable. The study also suggested that such micelles with a crystalline core could be used as seeds to induce homopolymer-like crystallisation to control the crystal fold size.

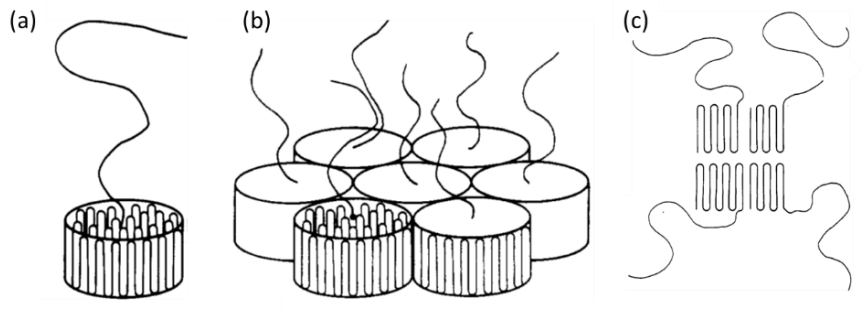

Figure 1.6. Schematic representations of crystalline-core micelles based on the model presented by Vilgis and Halperin. (a) A coil-crystalline diblock copolymer molecule in solution with the core chain undergoing fold crystallisation, (b) core chain packing in a lamella and (c) a star-like micelle with folded crystalline core. Reproduced with permission from reference [135].

Experimental studies. Experimental studies have been carried out on factors which impact the morphology of BCP micelles obtained from CDSA in solution. By varying self-assembly conditions, such as the relative ratio of the core and corona block, temperature and solvent conditions, different morphologies (thermodynamically stable or kinetically trapped) have been obtained.

By using poly(ε-caprolactone)-*block*-poly(ethylene glycol) (PCL-*b*-PEG) with different PCL (core-forming block) block lengths, a micellar morphology transition was observed from spherical to fibre-like to platelet micelles.[105, 127] With an increase of PCL block length, the number of chain folds increased and the density of grafted corona chain decreased, which resulted in the favoured formation of low curvature morphologies. In the studies with poly(ferrocenyldimethylsilane) (PFS)-based diblock copolymers, BCPs with a core-corona block ratio larger than 1:3 favoured the platelet micelle formation, while a small core-corona block ratio between 1:20 and 1:3 favoured the cylindrical micelles.[97, 136] In other studies on poly(*N*,*N'*-dimethylacrylamide)-*b*-poly(*L*-lactide)-*b*-poly(*N*,*N'*-dimethylacrylamide) (PDMA-*b*-PLLA-*b*-PDMA), both kinetically trapped (fibre-like micelles) and thermodynamically favoured morphologies (platelet micelles) were achieved by varying the volume factions of corona forming block.[137] With BCP containing a short PDMA corona-forming block, 1D fibre-like micelles were kinetically trapped due to fast crystallisation. In the case of long PDMA chains, 2D platelet micelles were obtained as the thermodynamically favoured morphology due to the slow crystallisation caused by the increased overall solubility of the BCP.

Kinetically trapped morphologies could be obtained by altering the conditions which would change the core crystallisation. Polyethylene-*b*-poly(*N*,*N*-dimethylacrylamide) (PE-*b*-PDMA) formed micelles with a PE molten core by direct dissolution in H_2O at 25 °C. After heating above the T_m of PE and cooling to 25 °C, micelles with a crystalline core were obtained.[100, 101, 129]

Similarly, kinetic trapping of PFS-*b*-poly(2-vinylpyridine) (PFS-*b*-P2VP) micelles (spherical and cylindrical micelles) was observed in a selective solvent for the P2VP block.[138] When common solvents were added into the system to improve the solvent quality for the PFS block, thermodynamically favoured platelet micelles were obtained.

1.4. Living Crystallisation Driven Self-Assembly

CDSA of BCPs can be carried out in a living manner to control the dimensions of the morphologies in solution. This process is termed 'living CDSA'.[92, 139, 140] This section will give a brief introduction on living CDSA of 1D PFS-containing micelles, followed by controlling micelles in different dimensions. Micelles prepared by the living CDSA of other crystallisable polymers will be discussed.

1.4.1. Living CDSA of BCPs with a PFS Core-Forming Block

CDSA of PFS-containing BCPs in selective solvents direct from a solid or unimer (solvated polymer in common solvent) state always affords micelles with uncontrolled dimensions (i.e. polydisperse in length for 1D micelles, Figure 1.7b). This is due to the different nucleation time of polymer chains in solution during self-assembly under homogeneous nucleation conditions. For 1D fibre-like micelles, the length was characterized by L_n (number average micelle length) and length dispersity L_w/L_n (L_w is weight average micelle length). Near monodisperse (L_w/L_n <1.10) short fragments of the 1D fibre-like micelles, which are known as 'seeds'(Figure 1.7c), can be achieved upon vigorous sonication.[141] The termini of the seeds have exposed faces which are active nucleation sites for further polymer chains to epitaxially grow from. When extra unimer was added to the seeds, elongated fibre-like micelles with uniform length could be obtained in solution (Figure 1.7d) due to the higher rate of epitaxial crystallisation from the seeds (pre-existing nucleus) compared with self-nucleation. By varying the amount of the added unimer, the micelle growth showed a linear relationship between the micelle length and the unimer-to-seed mass ratios. This process is analogous to living covalent polymerization, where the seeds behave as the initiator and the added unimers behave as the unconsumed monomer. Due to the micelle elongation involving adding unimer to seeds, this method is termed 'seeded-growth' (Figure 1.7a bottom). The prepared micelles can be stable in solution for a prolonged amount of time with no change in micelle length or dispersity.[139, 140] This suggests that the micelles are kinetically trapped and no unimer exchange occurs among the micelles.

'Self-seeding'(Figure 1.7a bottom), as another living CDSA method, has been reported to provide 1D PFS micelles with uniform length and narrow length distribution.[142-144] Similar to seeded-growth, seed micelles are fragmented by sonication and heated to an elevated temperature, where less crystalline regions of the micelle dissociate to release unimers whilst the higher crystallinity regions survive and can act as seeds. The less crystalline region is formed by the kinetical trapping of the BCP chains during self-assembly.[122, 144, 145] Upon cooling, the dissociated unimers grow from the seed termini to afford elongated micelles with uniform lengths. To achieve uniform length fibres by self-seeding, strict temperature conditions need to be set and optimised, as an exponential relationship between micelle length and temperature is typically observed in the micelle growth process. In addition, each set of self-seeding conditions is very specific to one batch of seed micelles, as the micellar crystallinity is related to the thermal history. Therefore, the reproducibility of self-seeding is poor to achieve the same length of micelles from the same BCP. Moreover, as an alternative to temperature, the concentration of common solvent can also be used to realize a self-seeding process.[143] A certain amount of common solvent is first added to the seed micelles, followed by slow evaporation, and then elongated micelles with controlled length could be achieved. Similar to temperature, the amount of common solvent needs to be optimized.

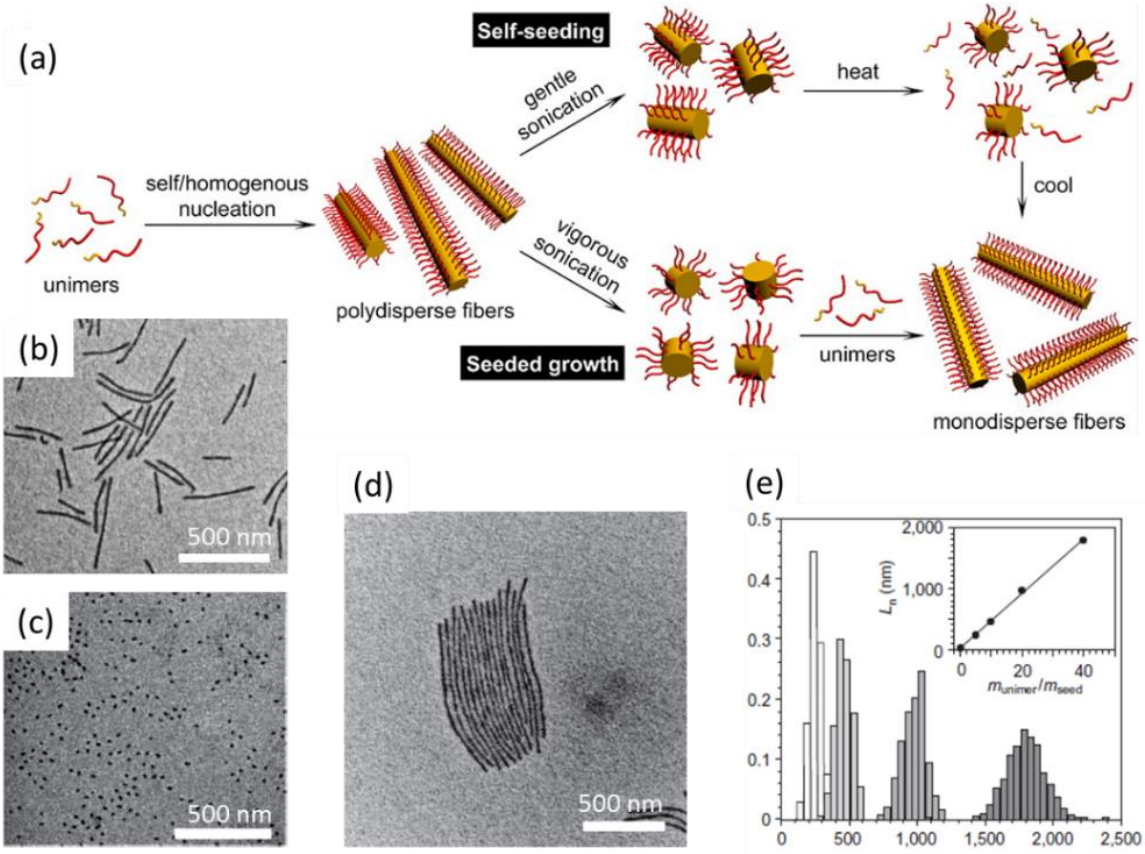

Figure 1.7. (a) Schematic representation of living CDSA by seeded-growth (bottom) and self-seeding (upper) methods, (b) TEM image of polydisperse micelles of PFS-*b*-PDMS, (c) PFS-*b*-PDMS seeds prepared by sonication, (d) uniform PFS-*b*-PDMS micelles by seeded-growth and (e) contour length histogram of the samples with different added unimers. Reproduced with permission from reference 140 and 146.

In addition to preparing uniform length fibre-like PFS micelles, living CDSA is also a powerful approach to prepare micelles with well-defined spatially segregated segments.[140, 146-148] This is achieved by adding the unimer of a second BCP with a corona having a different chemistry compared with that of the seed BCPs, which affords BAB triblock comicelles. By employing BCPs with different block ratios, (where low core-corona block ratio favours cylindrical morphology while high core-corona ratio favours platelet morphology) and adding the unimer in sequential order, scarf-like (Figure 1.8a) and spear-like (b) micelles can be achieved.[149] Multiple unimers can be added to the seeds at the same time. If the growth kinetics of the two added unimers are the same, elongated micelles with a uniform distribution of the two added BCPs can be obtained (Figure 1.8c), otherwise gradient block co-micelles

will be obtained (Figure 1.8d).[150-152] Additionally, functional molecules can also be incorporated into the BCPs to achieve block co-micelles with spatial functionalities. For example, by using a BCP with a cross-linkable corona, non-centrosymmetric AB diblock co-micelles can be achieved.[136] ABC triblock comicelles could be prepared by further adding a third BCP to the AB co-micelles. Moreover, many other functional groups can be incorporated into the micelles, such as phosphine-ligands,[153] photo- and thermal-responsive groups,[154, 155] fluorescent probes[146] and metal nanoparticles.[103, 104, 153]

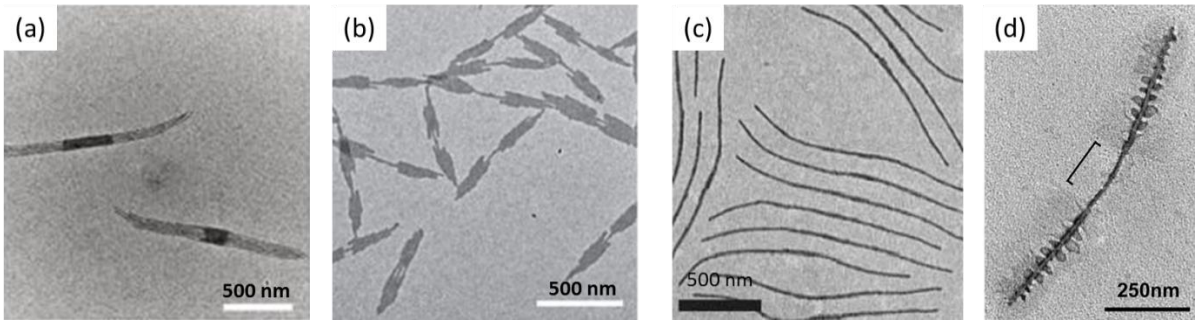

Figure 1.8. TEM images of (a) scarf-like micelles, (b) spear-like micelles, (c) cylindrical micelles with uniform distribution of two polymers with same epitaxial kinetics and (d) gradient micelles with polymers containing different coronal chemistry. Reproduced with permission from reference 148, 150, 151 and 153.

2D micelles with uniform area have also been prepared via living CDSA with three different types of PFS-containing BCPs.[147, 156, 157] The first reported 2D PFS micelles were obtained by using a diblock copolymer with a block ratio at ca. 1 : 1 (Figure 1.9a). By adding different amount of unimers to the 1D cylindrical seeds, lenticular platelet micelles with controlled area were achieved. By incorporating dye functionalized BCPs, block co-platelet micelles with spatially-defined areas of different fluorescence could be observed by confocal laser scanning microscopy (CLSM).[147] In another study, selected-area electron diffraction (SAED) analysis showed a polycrystalline structure for the PFS-*b*-P2VP lenticular micelles.[138] The reason for the polycrystallinity is proposed as the defects on the crystal growth surface formed by the interference of the corona forming block, which will affect the further deposition of the core chains. The second method to fabricate uniform 2D micelles has been reported with a blend of PFS homopolymer and diblock copolymer (Figure 1.9b).[156] By introducing the homopolymer, the corona density decreased, which resulted in decreasing corona chain repulsion.

During the co-assembly, rectangular micelles with uniform area were achieved. Furthermore, SAED analysis showed that the rectangular micelles had a core that was single crystalline. The defects induced by the corona can also be eliminated by using a charge-terminated homopolymer.[157] Unlike the corona-forming blocks, steric repulsions from the charge group could be neglected, which contributes the formation of well-defined platelet micelles (rectangular or hexagonal).

Interestingly, a micellar shape memory effect was observed by using different seed micelles in preparation of 2D micelles (Figure 1.9c and d). If the seed micelles were prepared from sonication of rectangular micelles, the obtained uniform 2D micelles were rectangular. If the seed micelles were formed from hexagonal micelles, the resulting micelles were hexagonal. SAED analysis confirmed that these micelles possessed a single crystalline PFS core.

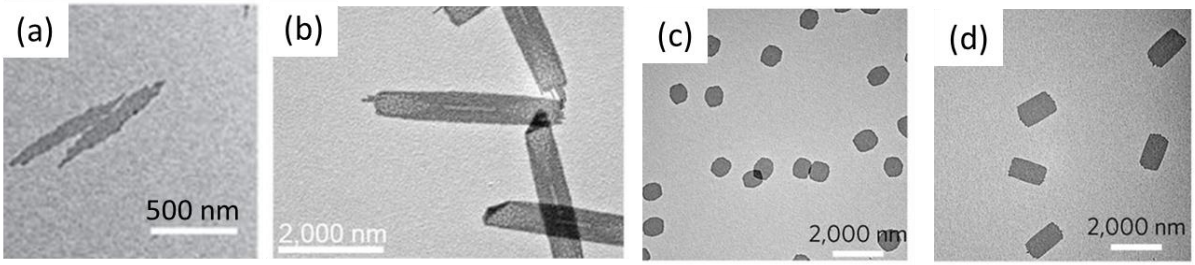

Figure 1.9. TEM images of 2D PFS micelles prepared by (a) PFS_{114}-*b*-$PDMS_{81}$, (b) blend of PFS_{36}-*b*-$P2VP_{502}$/PFS_{20}, (c and d) $PFS_{20}(PPh_2Me)I$ from different seed precursors. Reproduced with permission from reference 147, 156 and 157.

1.4.2. Hierarchical Self-Assembly of PFS Micelles via Living CDSA

Living CDSA has also shown the ability to create complex higher order structures.[148, 158-164] 1D PFS micelles with well-controlled dimensions and spatial functionalities could be assembled in solution in a controlled fashion under appropriate conditions. A good example to illustrate the hierarchical system prepared by living CDSA would be the train-track supermicelles (Figure 1.10a) prepared by carefully adjusting the hydrophobic interactions in the system.[148, 159] The primary level of the structure is the BCPs used for 1D micelle preparation: PFS-*b*-P2VP (polar segment) and PFS-*b*-PDMS (non-polar segment). The second level is the multi-step self-assembly of each diblock copolymer into uniform B-

A-B triblock co-micelles with non-polar PFS-*b*-PDMS middle segment and polar PFS-*b*-P2VP outer segments. The third level is the supermicelles prepared by the side-by-side self-assembly of B-A-B triblock co-micelles driven by the amphiphilicity. By altering the solvent, the BAB triblock co-micelles went through end-to-end self-assembly to form 3D superstructures (Figure 1.10b). Similar to examples of self-assembly in nature, H-bonding interactions could also be used to produce hierarchical self-assembled structures.[160] Cross-windmill supermicelles (Figure 1.10c) were observed in solution by self-assembly of B-A-B triblock co-micelles containing H-bonding donor (hydroxyl-functionalised poly(methylvinylsiloxane) (PMVS-OH)) and acceptor (P2VP) groups in the A and B blocks, respectively.

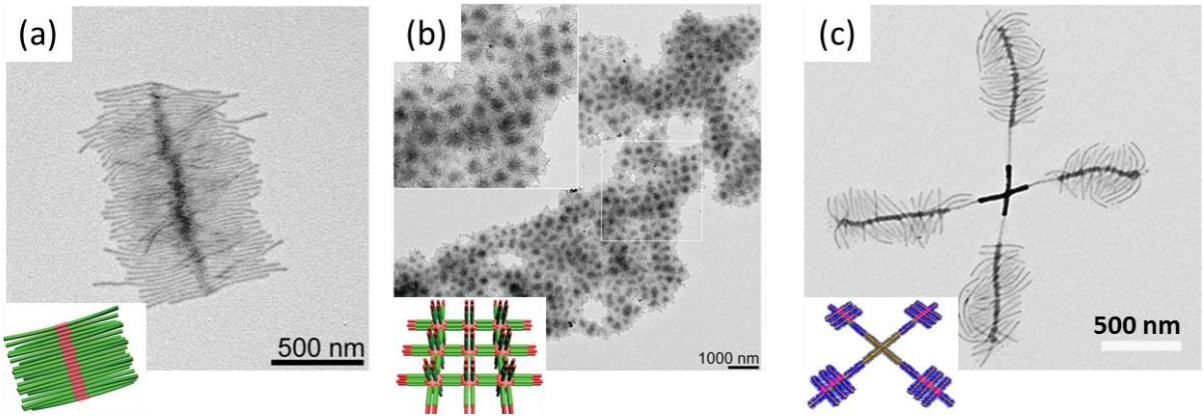

Figure 1.10. TEM images and schematic representations of supermicelles. (a) Side-by-side self-assembly of B-A-B cylindrical micelles consist of PFS-*b*-P2VP (green) and PFS-*b*-PDMS (red), (b) end-to-end self-assembly of B-A-B cylindrical micelles consist of PFS-*b*-P2VP (green) and PFS-*b*-PDMS (red) and (c) cross-windmill super micelles prepared by H-bonding interactions between P2VP (green, cross centre) and PMVS-OH (purple). Reproduced with permission from reference 148 and 160.

Controlled PFS micelle growth could be achieved not only by self-assembly in solution, but also by templating with different surfaces. PFS-*b*-P2VP seed micelles were templated by silica beads with the H-bonding interactions between P2VP and silica-coated PS beads (Figure 1.11a). By adding more unimers to the beads, the micelle growth was observed from the seeds on the silica bead surface. After P2VP cross-linking, the micelle-bead structure was dissolved in DCM to remove silica to afford a 'nanofibrous colloidosome'.[161, 162] Another example was the templated micellar growth from water-in-

oil (W/O) colloidosomes. The colloidosomes were first prepared with PFS-*b*-PMVS micelles on the surface of W/O emulsion droplets (Figure 1.11b). By adding BCPs with fluorescent tags to the micelle stabilized droplets, the elongation of the micelles was observed and the colloidosomes were found to possess fluorescent arms.[163] Generally, living CDSA could be used as a promising strategy for fabricating well-defined complex and hierarchical structures for a variety of applications by carefully introducing functional groups and adjusting self-assembly conditions.

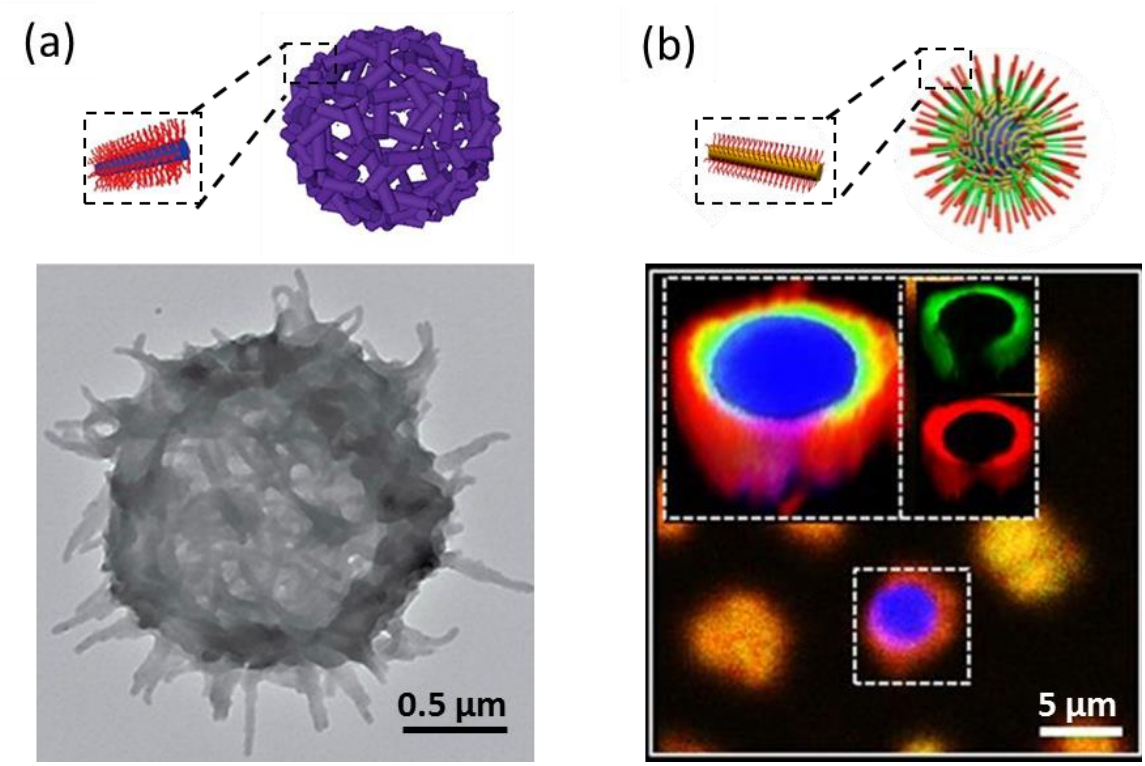

Figure 1.11. (a) Schematic representation and TEM image of a hollow basket-like nanofibrous colloidosome prepared by coordination of PFS-*b*-P2VP on silica bead surface after bead removal and (b) schematic representation and CLSM images of growth of PFS-*b*-PMVS micelles on water-in-oil emulsion droplets in solution. Reproduced with permission from reference 161 and 163.

1.4.3. Living CDSA of BCPs with Non-PFS Core-Forming Blocks

As discussed above, many crystallisable polymers have been reported to form nanostructures by CDSA. However, only a few of them have been reported to achieve controlled micelle dimensions via living CDSA. Early reports on PS-*b*-PE-*b*-PS showed that fibre-like micelle length has been controlled up to

500 nm. By adding a second triblock terpolymer, PS-*b*-PE-*b*-PMMA, fibre-like micelles with uniform lengths and patchy segments have been prepared.[165] CDSA behaviours of biodegradable PCL have been widely studied in a variety of solvents. Very recently, near monodisperse 1D fibres of PCL-*b*-PDMA with controlled length up to 800 nm and low length distributions ($L_w/L_n < 1.12$) have been reported via seeded-growth in organic solvent.[166] After optimization of the polymer architecture and solvent conditions, living CDSA of PCL-containing BCPs has been conducted directly in aqueous media. In addition, a modified polycarbonate, another biodegradable and crystallisable polymer, has been reported to undergo living CDSA to achieve uniform fibre-like micelles with controlled length (up to 1.6 μm) with narrow length distributions ($L_w/L_n < 1.07$).[167]

Another class of important crystallisable polymers are π-conjugated polymers, such as P3HT, polyfluorene (PF) and poly(phenylenevinylene) (PPV), which are widely used in the field of electronic devices and bioimaging, due to the advantages in semi-conductivity, quantum yield, photostability, fast emission rates and low cytotoxicity.[168, 169] However, the reports on the preparation of non-spherical morphologies of the π-conjugated polymers are scarce, and even less with dimensional control. This might be due to the hydrophobicity of the π-conjugated polymers which results in arduous processing. In the past decades, progress has been made with P3HT-containg BCPs. Uniform fibre-like micelles with controlled length have been achieved via both seeded-growth and self-seeding.[170-173] For the π-conjugated polymer OPV, 1D micelle length has been achieved by seeded-growth method and 2D OPV-based micelles were prepared via self-seeding method.[121, 155, 174] More recently, length control of B-A-B fibre-like triblock co-micelles of PF-containing BCPs has been achieved by living CDSA.[175] In addition, exciton energy transfer with very long diffusion lengths (> 200 nm) was observed from the luminescent core to the quencher corona on the terminal blocks of the triblock co-micelle. Dimensional control of fibre-like micelles containing these biodegradable and π-conjugated core-forming blocks, proves promising in the goal to achieve further progress in optoelectronic and biomedical applications.

1.5. Biomedical Applications of Fibre-like Micelles with a Crystalline Core

Therapeutic agents, such as doxorubicin (DOX) and paclitaxel (PTX) for cancer treatment, generally have a poor bioavailability due to the limited molecular weight, hydrophobicity and cytotoxicity.[176] Drug delivery systems (DDS) have been designed to overcome these limitations to assist drugs to pass various biological barriers.[177-179] Polymeric micelles have been employed as one of the delivery platforms and have been studied for decades.[51, 178, 180-185] Spherical micelles are the most enormously studied drug delivery vector with optimized cellular uptake, stability, blood circulation, cell toxicity and targeting.[51, 178, 185] Non-spherical micelles, especially fibre-like micelles (or filomicelles, worm-like and cylindrical micelles) have exhibited improved benefits in delivering therapeutic cargos.[186-190] In this section, fibre-like micelles with crystalline core will be mainly discussed, before which a brief description will be introduced on designing polymeric nanoparticles.

1.5.1. Polymeric Micelles as Drug Delivery Vectors (DDVs)

Some general principles have been established for designing and optimising polymeric nanoparticles for use as DDVs to achieve better efficiency and less side effects. Size is one of the most important factors for the delivery efficiency.[178, 190-192] Nanoparticle size smaller than ca. 10 nm will have a fast renal clearance. Particles over 1 μm in size will accumulate in the liver and spleen and trigger quick removal. Most cancer cells have blood vessels with ca. 200 nm diameter, while normal vascular diameters are 5-40 μm. It has been suggested that ca. 200 nm is the optimal size for nanoparticle DDVs, which is large enough to have a longer retention time in the body circulation and small enough to cause fast removal by the immune system. Due to the leaky vasculature, particles around 100 nm will prefer to aggregate at cancer cells due to the enhanced permeation and retention (EPR) effect (passive cancer cell targeting).[192, 193] In addition, surface chemistry of the micelles have been shown as another factor contributing to the drug delivery efficacy.[194-196] Further functionalization of the micelle surface with smart ingredients, such as cell-recognition groups, subcellular targeting molecules and stimuli-responsive groups, would introduce functionalities such as active targeting and improved drug release efficiency.[197] In addition to the size and surface modification, the morphology of nanoparticles has been

reported to have a great influence on the delivery efficiency by affecting the circulation time, biodistribution, cellular internalization and active targeting.[191, 196, 198]

1.5.2. Fibre-Like Micelle as DDVs

In recent reports, higher therapeutic efficacy and less side effects have been reported in cancer drug delivery with fibre-like micelles compared to traditional spherical micelles,[199-203] and this is suggested to be caused by the advantages of fibre morphologies, such as long length, high surface area and flexibility. The improvement in circulation time, high cancer cell accumulation, deep penetration in tumours and enhanced active targeting have been achieved with many types of fibre-like structures, such as polymeric micelles with amorphous cores,[204-207] modified virus,[208] inorganic particles[209, 210] and synthetic carbon nanotubes.[211, 212] Herein, polymeric micelles with crystalline cores will be the focus. Poly(butadiene) (PB) and poly(ethylethylene) (PEE) fibre-like micelles containing crystalline cores were the first micelles transferred into an aqueous environment and served as models for evaluating fundamental indices in drug delivery.[91, 205, 213, 214] Since the onset of the potential of being DDVs with these micelles, crystalline biodegradable PCL and poly(ethylene) (PE) were co-employed as core-forming blocks to prepare fibre-like micelles for drug delivery studies. Longer circulation times were observed *in vivo* with (PCL-*b*-PE)-*b*-PEG fibre-like micelles (ca. 18 μm) compared to PCL-*b*-PE-*b*-PEG spherical micelles. Similarly, longer fibre-like micelles of (PCL-*b*-PE)-*b*-PEG (ca. 18 μm) possessed longer circulation time than the shorter ones (< ca. 4 μm).[215] The elongated structure and prolonged circulation time provide fibre-like micelles with a higher probability of reaching the targeted cancer cells in body circulation. PCL-based micelles have been reported to accumulate quickly in tumors in rats.[216] After 10 mins of intravenous administration of PCL fibres functionalized with a near infrared fluorophore (NIF), the tumor in a rat showed strong luminescence with a high contrast to the dark regions. Improved specific targeting had also been reported for fibre-like micelles. With biotin labelled PE fibre-like micelles, a higher affinity to avidin-coated cell surface and smooth muscle cells was observed compared with spherical micelles that displayed a lower affinity.[205] These results suggest that fibre-like micelles could provide significant advantages compared with spherical micelles in DDS.

1.5.3. Fibre-Like Micelles with Uniform Length for Biomedicine

We have discussed the many advantages of fibre-like micelles, however most fibre-like micelles studied previously had issues like that of uncontrolled length or non-pure morphologies (mixed with spherical and platelet micelles). Therefore, fibre-like micelles with controlled length and narrow distributions are desirable for future studies.

Living CDSA of BCPs with a crystallisable core can efficiently afford morphologically pure micelles with controlled dimensions. Water-soluble PFS-based micelles with uniform length have been reported recently.[217] By using a water-soluble corona-forming block, the micelles with controlled length were prepared in organic solvents and transferred in aqueous media by dialysis. In further studies, charged B-A-B triblock-comicelles (with charge segments on two termini) were prepared and shown to interact with DNA strands. These results suggest that these micelles could be potentially used as gene delivery vectors. More recently, uniform fibre-like micelles of PCL-*b*-PMMA-*b*-PDMA with controlled length have been achieved directly in aqueous media by living CDSA.[166] Interestingly, during the process of adding unimer, a robust hydrogel was obtained with an overall solid content of 15 wt%, and the micelles grew up to 2 μm in length. Further cellular studies showed a high stability and biocompatibility for this hydrogel. In addition, another biodegradable polycarbonate based diblock copolymer was reported to form uniform 1D fibres with controlled length via living CDSA.[167] Micelles with length of ca. 120 nm showed stability in H_2O after dialysis and no cytotoxicity to a series of cell lines, which implies they could have potential applications as DDVs.

1.6. Poly(*L*-lactide) (PLLA) and Self-Assembled Structures

Polylactide (PLA), a renewable aliphatic polyester based on hydroxyalkanoic acid, is an important synthetic biorelevant polymer in both academia and industry.[218-220] Due to the unique biodegradable and biocompatibility properties, PLA has been approved for clinical use by FDA and is widely used as an alternative material to traditional petrochemically derived polymers in biomedicine.[219, 221, 222] Two synthetic methods have been used for PLA production: polycondensation of polylactic acid and ring-

opening polymerization (ROP) of lactide.[218, 219] Due to the lower control over the molecular characteristics by the first method, ROP has been widely preferred and can afford PLLA with high molecular weight, narrowed polydispersity and efficient end-group capping.

1.6.1. PLLA Structures and Properties

With the chiral centre in lactic acid, the monomer, lactide (LA), for ROP has three different stereoisomers: enantiopure *L*- and *D*-lactide (*L*-LA and *D*-LA) and *meso*-lactide (*meso*-LA). Commercial-grade lactide has a racemic form as *rac*-lactide (*rac*-LA). Under non-epimerization conditions, ROP of enantiopure monomers provides isotactic polymers; ROP of *rac*-LA can obtain PLA with isotactic multiblock backbones; and ROP of *meso*-LA can achieve heterotactic and syndiotactic backbones (Figure 1.12). The physical properties are related to the PLA chain microstructure. [218, 219, 223, 224]

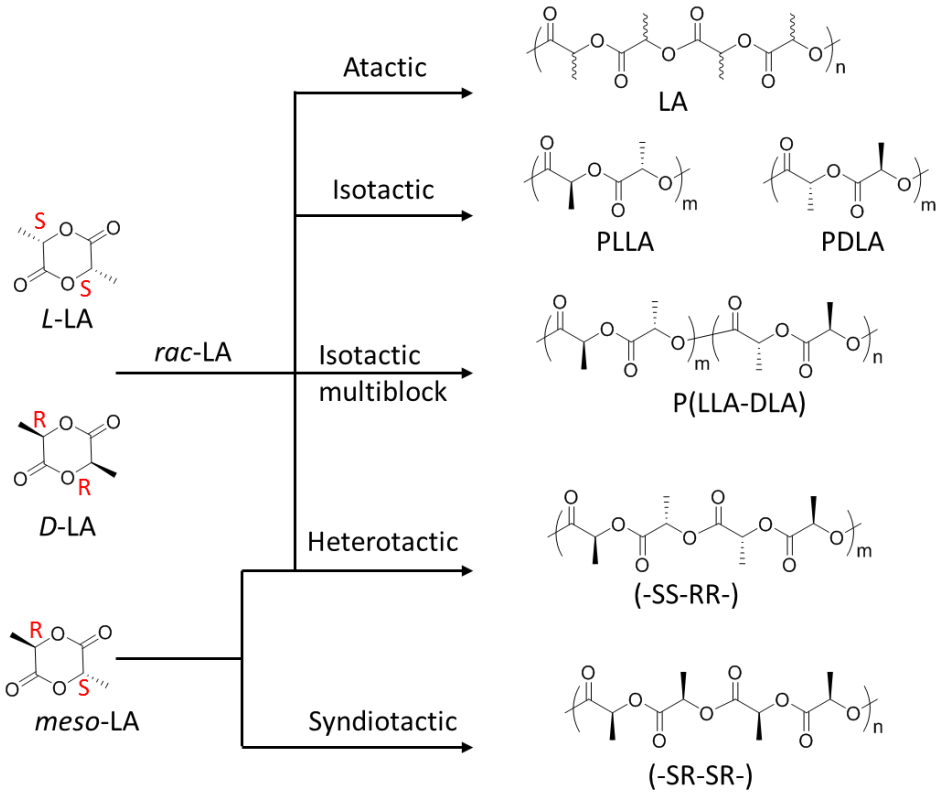

Figure 1.12. Ring-opening polymerization of lactides with different enantiomers. Reproduced with permission from reference [223].

Due to the chiral centre on the polymer backbone, PLA with different stereochemistries has different physical properties. PLA polymers obtained from *meso*-LA and *rac*-LA are amorphous due to the random distribution of *S*- and *R*- chiral centres. PLLA and PDLA prepared with enantiopure monomers possess crystallinity. Crystalline PLLA (or PDLA) exhibits a higher melting temperature (T_m: ca. 170 °C) and glass transition temperature (T_g: ca. 60 °C) compared with that of amorphous PLA (T_m: ca. 130 °C, no T_g observed). A stereocomplex has been prepared by mixing PLLA and PDLA with 1:1 mass ratio, which shows improved crystallinity and increased T_m (ca. 230 °C). The thermal properties vary with the crystallinity and molecular weight of prepared PLA polymers.[218, 225]

1.6.2. Crystalline PLLA

The hydrophobicity and crystallinity of PLLA is of interest to this thesis work due to the potential of producing uniform PLLA-based nanoparticles with controlled dimensions via living CDSA. The crystallisation behaviour of PLLA has been studied and four crystalline forms (α, α', β and γ, with different chain conformations and cell symmetries) have been reported for PLLA by preparation under different conditions.[225, 226] The α form (Figure 1.13) can be obtained by melt or cold crystallisation, and also by solution spinning processes at low drawing temperatures. The unit cell was characterized as a packing of left-handed 10_3 helix chains in an orthorhombic unit cell with a = 1.06 nm, b = 1.737 nm and c = 2.88 nm.[227-229] Upon applying mechanical stretching to an α-form PLLA, or using high temperature solution-spinning processes, an α'-form was suggested with polymer chains packing with left-handed 3_1 helix in an orthorhombic unit cell with a = 1.031 nm, b = 1.821 nm and c = 0.90 nm.[225, 228]. The β form was found as a frustrated structure of three three-fold helices in a trigonal unit cell with a = b = 1.052 nm and c = 0.88 nm.[230, 231] The γ form of PLLA was found during the epitaxial growth from a hexamethylbenzene substrate. Two antiparallel helices packed in an orthorhombic unit cell with a = 0.995 nm, b = 0.625 nm and c = 0.88 nm.[232]

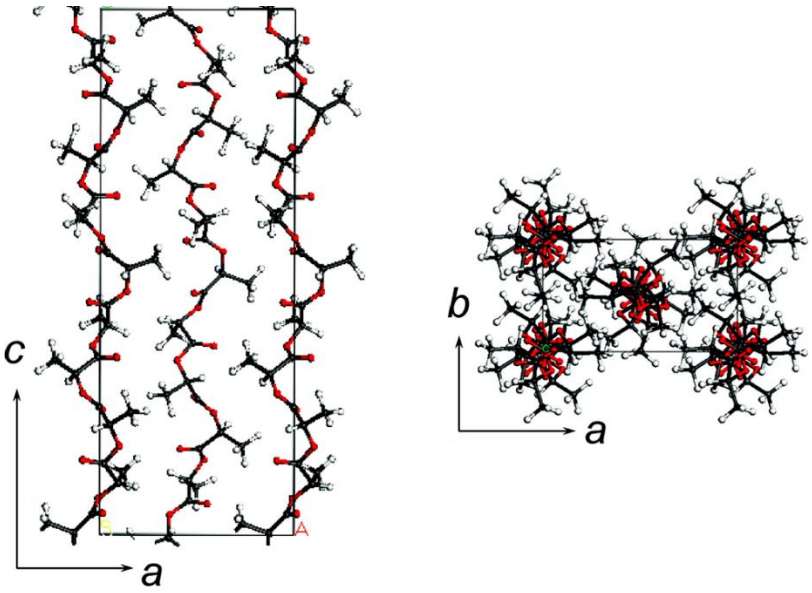

Figure 1.13. Schematic represents of the crystal structure of PLLA α-form. Reproduced with permission from reference 227.

1.6.3. Synthesis of PLLA Homopolymers by ROP

ROP has allowed the preparation of PLA polymers with well-defined molecular weight, stereo-control and functional chain ends.[218, 219] Many mechanisms have been proposed for lactide ROP, such as anionic, cationic, coordination-insertion and monomer-activated. A variety of catalysts have been studied for these reactions, such as organic acid and base, enzymes, Lewis acid and base and metal reagents.[233-240] In this thesis, semi-crystalline PLLA with well-defined molecular characteristics is desired for living CDSA studies. Therefore, in this section, ROP of *L*-lactide with a metal catalyst and a metal-free catalytic system will be discussed, as they are employed for PLLA homopolymer preparation in Chapter 3 and 4.

The most widely used reaction for *L*-lactide ROP in industry has a mechanism of metal coordination-insertion with tin(II) bis(2-ethylhexanoate) ($Sn(Oct)_2$) as catalyst (Figure 1.14a).[241-243] The first step of the reaction is the coordination of *L*-lactide to the tin(II) centre. The second step is the attack by an alkoxide initiator on the activated carbonyl carbon, which then triggers ring-opening via acyl-oxygen cleavage. This yields a new chain-extended metal alkoxide species for further ring-opening, which is suggested to be stabilized by the vicinal carbonyl group. The last step involves the hydrolysis of the

active metal-alkoxide bonds resulting in a hydroxyl end group. This tin catalyst could provide high molecular weight PLLA with narrow distributions without epimerization and transesterifications.[244, 245] However, the reaction requires a high temperature, concentrated system (or bulk system) and long reaction time. Moreover, the toxicity of tin(II) residue in the product would have concerns in biological applications.

Recently a metal-free catalytic system with a thiourea and a tertiary amine for *L*-lactide ROP by primary alcohols has been reported (Figure 1.14b)[240, 246] with high levels of control over the polymerization. The key step is the monomer activation with hydrogen bonding interactions between the monomer carbonyl group and catalyst thiourea group. The ring-opening was triggered by the activated alcohol species with the tertiary amine reagent. The reaction with this organocatalytic system can be carried out at ambient conditions with fast kinetic profile (with optimized combination of thiourea species and organic base). This polymerization exhibited 'living' characteristics due to the linear relationship between molecular weight and monomer conversion, however, this catalytic system is only limited to initiators with a primary alcohol.

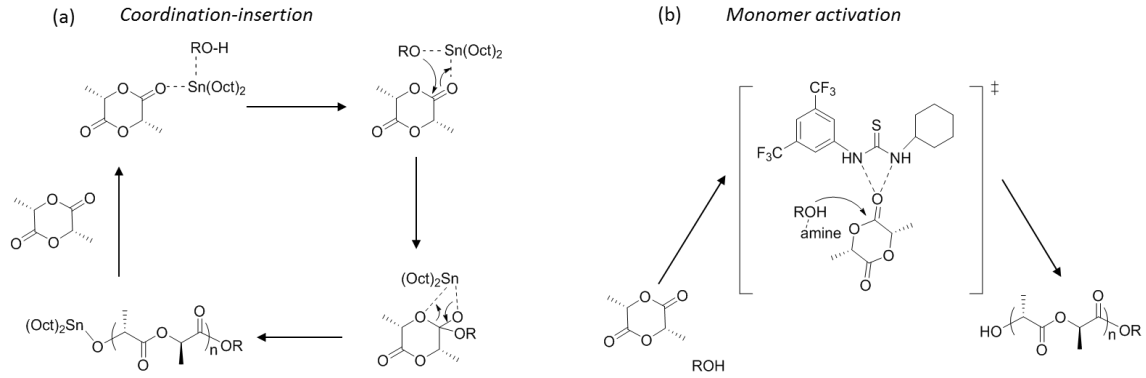

Figure 1.14. Mechanistic schemes of *L*-lactide ROP by a alcohol with (a) tin(II) catalyst and (b) a thiourea-amine catalyst system.

1.6.4. Synthesis of PLLA-Based Diblock Copolymers

This thesis aims to explore the biological applications of PLLA-based nanoparticles. Therefore, PLLA-containing BCPs need to be prepared with hydrophilic corona-forming blocks to achieve water

solubility. Most functional and hydrophilic polymers are acrylate- or methacrylate-based. However, these polymers are generally prepared via controlled radical polymerizations (CRP), such as atom transfer radical polymerization (ATRP), nitroxide mediated polymerization (NMP) and reversible addition fragmentation chain transfer (RAFT) polymerization. Therefore, a strategy of combining ROP and CRP is suggested to prepare PLLA-based diblock copolymers in this thesis. To achieve the target polymers, a dual-function initiator is introduced with a hydroxyl group for *L*-lactide ROP and a chain transfer agent (CTA) for corona block RAFT polymerization. Similar strategies have been well developed to prepare PLLA-based diblock and triblock copolymers, branched polymers, grafted polymers, dendrimers and polymers with higher level complexity.[39, 247]

1.6.5. PLLA-Based Micelles by CDSA

Due to the attractive biodegradability and biocompatibility, PLA-based micelles have been extensively studied in biomedical applications,[218, 248-250] however, most micelles have spherical morphologies. The CDSA approach offers clear advantages in that non-spherical micelles of PLLA can be readily accessed. Both fibre-like and platelet like micelles of PLLA have been prepared via CDSA, either by direct morphology formation in controlled solvent conditions or by morphology transformation with the addition of H-bonding parameters[251] or thermal annealing.[252] An interesting morphology transition was observed with PLLA- and PDLA-based diblock copolymers.[111] The rod-to-sphere morphology transition was triggered by the formation of a stereocomplex between PLLA and PDLA. However, all these non-spherical micelles were not morphologically pure (mixture of fibres and spheres or fibres and platelets) and there was no control over dimensions.

Significant progress has been made with PLLA-based micelles with size control recently. PLLA-*b*-PAA micelles were reported to achieve a length control up to 300 nm by a solvent and temperature changing procedure.[253] Moderate control of the length of these micelles was shown ($L_w/L_n < 1.3$) by adjusting the PLLA block length.[254] Further studies demonstrated that the PLLA-*b*-PAA micelles (both spherical and fibre-like morphologies) can undergo spontaneous cavitation to afford hollow micelles (hollow spheres and nanotubes, respectively). The cavity diameter can be varied by controlling drying conditions.

PLLA-based non-spherical micelles have also been reported with multiple corona-forming blocks, such as PDMA and PEG.[112] By careful selection of the self-assembly conditions (solvent compositions and temperatures) and precise control over BCP compositions, uniform 2D platelets of PLLA-*b*-PDMA with tuneable area could be achieved directly by CDSA, which can be considered as a self-seeding process with seeds generated *in situ*.[137]

Studies on macrophage cell immune response were carried out with mannose functionalized PLLA-*b*-PAA cylindrical micelles with controlled lengths ($L_w/L_n < 1.20$). Good cell compatibility was observed with all micelles.[255] Longer fibre-like micelles (L_n: ca. 215 nm) were more efficient at inducing immune response than that of shorter ones (L_n: ca. 99 nm). In addition, uniform 2D PLLA platelets with controlled area prepared via *in situ* self-seeding method have been used to stabilize water-in-water emulsions (Figure 1.15).[256] Platelet micelles with larger areas retained better stability to the emulsion droplets compared with smaller area micelles, despite the modification of the platelet surface (cationic, zwitterionic or neutral). Similarly, 2D PLLA micelles have been used to prepare crystalsomes with an extended blood circulation time,[257] however, no area characteristics of the platelets were discussed.

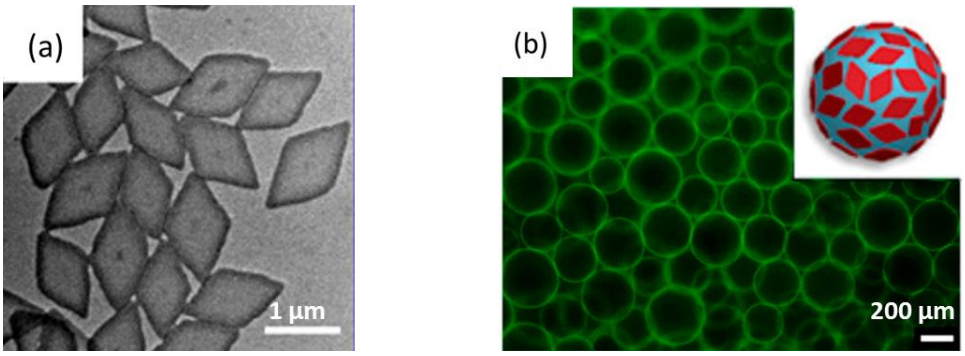

Figure 1.15. (a) TEM images of uniform 2D PLLA platelets prepared by *in situ* self-seeding and (b) Schematic representation and CLSM images of water-in-water emulsion droplets with 2D PLLA platelets on the surface. Reproduced with permission from reference 256.

Generally, the formation of PLLA-based non-spherical micelles with controlled length has not been reported. It is desirable that micelles with uniform length based on PLLA diblock copolymers could be achieved by living CDSA at ambient conditions.

1.7. Thesis Aims

The introduction of this thesis so far has mainly discussed the basic principles and recent advances in BCP solution self-assembly. Living CDSA has been used as an effective method to prepare non-spherical micelles with controlled dimensions. Moreover, higher level self-assembly of well-controlled 1D micelles via living CDSA has allowed the construction of hierarchical systems. By precisely controlling the synthesis techniques, living CDSA has also been used to fabricate functional materials. However, most of the nanostructures are focused on PFS-based BCPs. Therefore, the goal of this thesis is to expand living CDSA to other semi-crystalline polymers and to explore the applications of these micelles with well-defined dimensions.

1.7.1. Exploration of the Biomedical Applications of PFS Based Micelles

Fibre-like micelles by BCP self-assembly have shown advantages as drug delivery vectors. However, the length of most fibre-like polymeric micelles used in biological tests are not well controlled. It is desirable to achieve micelles with uniform length for biomedical applications. On the other hand, reports of well-controlled properties, water-soluble PFS-based micelles with well-controlled morphologies, dimensions and functionalities are limited. One of the aims of this thesis is to prepare water-soluble PFS micelles with controlled length for cellular uptake studies.

1.7.2. Expansion of the Living CDSA to a Biodegradable Polymer

Biodegradable and biocompatible PLLA-based materials have attracted attention in biomedical applications over the years. However, most micelles being used have a spherical morphology. With the advantages of 1D fibre morphologies, uniform 1D PLLA micelles with controlled lengths are highly desirable but remain challenging to obtain. Living CDSA has been applied to PLLA BCPs to achieve length control. However, only limited length control has been reported ($L_n \leq 300$ nm) via intricate procedures of tuning solvent compositions and self-assembly temperatures. Therefore, this thesis will describe attempts to achieve micelle length control of PLLA-based BCPs via epitaxial growth by living CDSA under mild conditions.

1.7.3. Controlling the Dimensions and Functionalities of The Micelles with a Biodegradable Core

With the advancement in polymer synthesis, PLLA-containing BCPs could be prepared with precisely controlled compositions, designed architectures and molecular weight characteristics. These finely tuned BCPs allow a better understanding of solution self-assembly of PLLA BCPs. 2D micelles with defined diamond shapes and tuneable areas could be achieved by carefully adjusting the self-assembly conditions. However, compared with the convenient epitaxial growth by living CDSA, the restrictive requirements on synthesis and self-assembly conditions have limited the wider accessibility of these 2D micelles. Therefore, the thesis will describe attempts to achieve well-defined 2D materials via a more easily applied method at mild conditions.

1.8. Thesis Summary and Collaborator Acknowledgements

Under the guideline of the research group policy of Prof. Ian Manners, the thesis consists of three self-contained chapters which are in forms similar to manuscripts intended for publication and peer-review. This thesis contains three results chapters in addition to a final conclusions and future work chapter. In accordance with the interdisciplinary research philosophy of the Manners group, research projects are generally under collaborations with colleagues. Collaborator contributions to this thesis are outlined below.

Chapter 2 explores the potential biomedical applications of the PFS cylindrical micelles and the attempt to achieve aqueous living CDSA. Uniform 1D PFS micelles have been prepared for biological tests and the results showed the cellular uptake with these length-controlled micelles. Dr. Holly Baum carried out cellular uptake experiments of PFS micelles. Diego Garcia Hernandez carried out the preliminary cellular uptake of PF micelles. Dr. Xuhui Jin synthesized the PF homopolymer.

Chapter 3 discusses the limitations or obstacles in epitaxial growth of PLLA diblock copolymers. Uniform 1D fibre-like micelles of PLLA-based diblock copolymers have been prepared via living CDSA and the core structure of these micelles has been characterized in detail. Spatial multi-block co-

micelles have also been prepared by using PLLA-based BCPs with different corona-forming blocks. X-ray diffraction and scattering experiments were carried out in collaboration with Dr. George R. Whittell and Prof. Robert M. Richardson. AFM measurements were carried out by Dr Robert L. Harniman. SAED characterization was carried out by Dr. Jean-Charls Eloi.

Chapter 4 expands the scope of living CDSA with PLLA BCPs by preparing 2D platelet micelles in addition to previously discussed 1D fibre-like mcielles. A series of complex and hierarchical 2D structures have been prepared by a blend of homopolymer and diblock copolymer with different functionalities. Applications in templating these platelets have been shown with inorganic nanoparticles. Synthesis and self-assembly of charge-terminated PLLA polymer were carried out in collaboration with Dr. Xiaoming He. AFM characterization was carried out by Dr. Robert L. Harniman. SAED characterization was carried out by Dr. Ming-Siao Hsiao and Dr. Jean-Charles Eloi.

Chapter 5 describes how the work in this thesis could be developed further.

Chapter 2 **Functional Water-Soluble Fibre-Like Micelles for Biological Applications via Living Crystallisation-Driven Self-Assembly**

Abstract

Fibre-like micelles comprised of self-assembled block copolymers (BCPs) exhibit promising potential for biomedical applications. 'Living' crystallisation-driven self-assembly (CDSA) is an effective method for fabrication of uniform 1D and 2D nanoparticles from amphiphilic BCPs with a crystallisable core-forming block. The self-assembly of poly(ferrocenyldimethylsilane) (PFS)-based diblock copolymers in solution has been studied extensively as a route to nanostructures with controlled morphologies and dimensions. Poly(di-*n*-hexylfluorene) (PF) has been widely used in applications such as bioimaging due to its intrinsic fluorescence and optical properties. However, there has been limited exploration of the biological applications of PFS- and PF-based micelles due to the poor colloidal stability in aqueous media.

Herein, to provide a foundation for subsequent bioapplication studies, we report the preparation of uniform water-soluble PFS-and PF-based fibre-like micelles. The cellular uptake behavior of PFS-based micelles of controlled lengths was probed by incubation of these micelles with HeLa cells. The results suggest that the micelle cellular uptake is concentration dependent. PF-based micelles have been modified with functional molecules, such as fluorescent probes and folic acid (FA). The aggregation behavior of these micelles in both aqueous and cell media have been studied. The results suggest that the micelles are well-suited for cellular uptake studies, which ongoing work will be focused on. Furthermore, our attempts to perform living CDSA in aqueous media failed to give control over PFS fibre-like micelle length. However, the micelles resulting from living CDSA in organic solvents were successfully transferred into H_2O by dialysis.Introduction

Polymeric micelles prepared by block copolymer (BCP) self-assembly have promising potential applications in biomedicine,[191, 258, 259] particularly in drug delivery and bioimaging. Many issues and

problems, such as low drug loading capacity, drug hydrophobicity, fast renal clearance and cytotoxicity have been tackled by micelle design and engineering.[259-261] Spherical micelles have been widely studied as they are the most prevalent morphology accessible by diblock copolymer self-assembly.[38, 39, 67] Unlike spherical micelles, the study of elongated one-dimensional (1D) fibre-like micelles in drug delivery has only been reported in the last decade.[63, 262] Worm-like micelles were reported to facilitate higher drug loadings,[263, 264] displayed prolonged blood circulation times and enhanced tumour penetration,[215, 216] and exhibit improved tumour cell internalisation.[211, 265]

Most studies to date have focused on the self-assembly of BCPs with an amorphous core-forming block whereby the most significant factors influencing the observed morphology are core and corona block ratio, solvent system, and temperature.[63, 266, 267] Unfortunately, 1D fibre-like morphologies are only favoured in a relatively narrow region of phase space.[268] Several synthetic unimolecular micelles and bottle brush copolymers have been reported to possess a core-shell cylindrical morphology.[269-272] However, these methods require long and complicated synthetic procedures which restrict the variety of molecules that can be used as building blocks. Therefore, it is challenging to obtain morphologically pure fibre-like micelles via solution self-assembly of amorphous core-containing BCPs.

However, fibre-like morphologies have been shown to be preferentially formed by the self-assembly of BCPs with a crystallisable core-forming block and long solvophilic corona-forming block, this process is termed crystallisation-driven self-assembly (CDSA).[70, 92, 97, 155, 173, 273, 274] Moreover, seeded-growth and self-seeding methods (Scheme 2.1) have been developed to access fibre-like micelles of controlled length and low length dispersity.[140, 142-144, 158, 174, 273, 275] Polydisperse fibre-like micelles were first prepared by CDSA via a nucleation-elongation process. These fibres could be subjected to sonication to form small fragments which are termed ‘seeds’. The termini of the seeds are active for subsequent epitaxial growth of additional BCPs (unimers). The seeded-growth method enables the formation of uniform fibre-like micelles of controlled length by adding unimers into a solution of seeds. When using the thermal self-seeding method, upon heating, a proportion of the seeds dissolve to form unimers, which can then epitaxially grow from the surviving seeds upon cooling to afford fibres with uniform

length. Due to the analogies with living covalent polymerisations of organic monomers, these two process are termed 'Living CDSA'.[92]

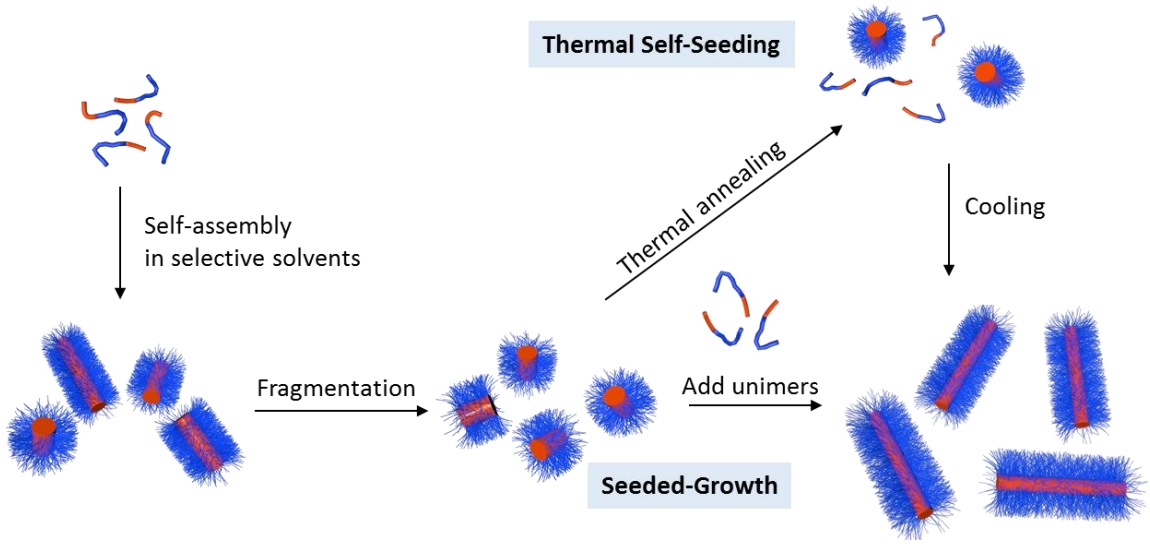

Scheme 2.1. Schematic representation of living CDSA by seeded-growth and self-seeding method.[158]

The living CDSA methods have been studied extensively with a crystallisable poly(ferrocenyldimethylsilane) (PFS) core-forming block and organic soluble corona-forming block.[70, 92] The lengths of PFS-based cylindrical micelles have been controlled from 20 nm to 5 μm.[140, 146] By modifying the corona-forming block with different functional groups, 1D fluorescent barcode micelles,[146, 276] patchy micelles[152, 277] and non-centrosymmetric micelles[136] can be prepared with controlled lengths with low length dispersity.

More recently, controlled epitaxial growth by living CDSA has been reported with BCPs containing other crystallisable core-forming blocks, such as π-conjugated poly(3-hexylthiophene) (P3HT),[170, 172, 173] poly(di-*n*-hexylfluorene) (PF),[175] polyselenophene,[278] biodegradable poly(*L*-lactide) (PLLA)[137, 253], poly(ε-caprolactone) (PCL)[166] and polycarbonate.[167] In addition, instead of using a solvophilic corona-forming block, charge-terminated homopolymers could also achieve micelle morphologies with controlled dimensions via living CDSA.[157] Furthermore, analogously to the living CDSA observed with BCPs, controlled supramolecular polymerisations of perylene diimide[279] and amphiphilic platinum (II) complexes[280, 281] were reported to lead to fibre-like micelles with controlled dimensions.

To further explore the biological applications, fibre-like micelles with controlled dimensions need to be prepared in, or transferred into, biologically relevant solvents. Early studies on fibre-like micelles in aqueous environments were shown with poly(butadiene)-*block*-poly(ethylene glycol) (PB-*b*-PEG), which possessed PEG weight fractions of ca. 45-55%. By controlling amount of cross-linking of the vinyl group in the PB block, these micelles could be used as a stiffness-tuneable materials.[91, 205, 262, 282] In studies on poly(styrene)-*b*-poly(acrylic acid) (PS-*b*-PAA) in water (H_2O), the block compositions and the processing conditions were found to be important to control the dimensions of the fibre-like micelles.[283, 284] Short fibre-like micelles (ca. 20 nm) were obtained with a PS:PAA block ratio of 1:2, while long fibre-like micelles were observed with a ratio of 1:3. By controlling the cross-linking of the PAA block, a sphere-to-fibre morphology transition was observed and the intermediate morphologies could be kinetically trapped and isolated. Furthermore, these prepared fibre-like micelles were successfully labelled with functional groups, such as folate and cell-penetrating peptides.[285]

In addition to simple diblock copolymers, ABC miktoarm star polymers have also been used to prepared fibre-like micelles in H_2O.[286, 287] These micelles were loaded with two different hydrophobic molecules to study their ability to act as multi-payload drug delivery vectors.[67, 288] PCL-based fibre-like micelles have also been studied for drug delivery applications due to their biocompatibility and biodegradability.[106, 213, 289, 290] Fibre-like micelles ca. 1 μm in length formed in H_2O has been reported by undergoing a sphere-to-worm morphology transition after 3 weeks aging.[290] Furthermore, elongation of PCL-*b*-PEG fibre-like micelles was observed by unimer addition and end-to-end coupling of the short micelles.[106] However, all of the fibre-like micelles mentioned were not subject to length control and the final micelles prepared sometimes contained other morphologies such as spherical micelles.

More recently, water-soluble fibre-like micelles of PFS-*b*-poly(allyl glycidyl ether-*graft*-triethylene glycol) (PFS-*b*-P(AGE-*g*-TEG)), with controlled length and narrow length dispersity, were successfully prepared and transferred into aqueous media by dialysis from dimethylformamide (DMF).[217] These micelles also have been shown to have potential as DNA delivery vectors. Although this strategy provides a good platform for preparing uniform water-soluble fibre-like micelles, the process contains

post-polymerisation modification and solvent transfer steps. A significant advancement in aqueous living CDSA was reported with PCL-*b*-poly(methyl methacrylate)-*b*-poly(*N*,*N*-dimethylacrylamide) (PCL-*b*-PMMA-*b*-PDMA) triblock copolymers.[166] Uniform fibre-like micelles were successfully prepared directly in aqueous media, with a short glassy hydrophobic PMMA central block protecting the crystalline PCL core from fragmentation (caused by the corona swelling). Very recently near monodisperse water-soluble fibre-like micelles with biodegradable polycarbonate cores were prepared in methanol (MeOH), followed by dialysis into H_2O.[167] The toxicity evaluation showed no discernible cytotoxicity to either healthy or cancer cells.

Conjugated polymers have been widely studied as fluorescent probes in bioimaging due to their strong fluorescence intensity, high photostability and low cytotoxicity.[168, 169, 291] Conjugated polymers with absorption and emission properties in the near infra-red (NIR) region are desirable and attractive for bioimaging. The radiation in the NIR wavelength range is non-destructive to tissues and can permit deep penetration.[292, 293] Polyfluorene is one of the commonly used conjugated polymers for fluorescent probes, since it can be easily modified to access NIR absorption and emission by copolymerisation with other conjugated moieties.[169]

Poor solubility in H_2O is the main obstacle limiting the biological applications of conjugated polymers.[168] Several methods have helped to develop the bioapplications of these materials such as chemical functionalisation of the polymer with hydrophilic moieties[168, 291, 294, 295] and nanoprecipitation via a solvent exchange technique.[296-301]

The nanoparticles accessed are generally spherical; no studies have been reported on the non-spherical particles in bioimaging. By utilizing living CDSA of PF-based diblock copolymers,[175] uniform fibre-like micelles with controlled length can be achieved. This could allow access to nanoparticles which provide an opportunity to better understanding the cellular behaviour of conjugated polymers and 1D fibre-like micelles. Furthermore, chemical modification of corona-forming blocks could also provide access to NIR micelles for bioimaging.

In this chapter, we aim to achieve the living CDSA of PFS-based diblock copolymers directly in aqueous media to widen the platform of preparing biologically applicable micelles under mild conditions. Moreover, cellular uptake of uniform 1D fibre-like micelles has been studied. Both water-soluble PFS-based and PF-based fibre-like micelles are discussed. Functional groups are introduced to modify the uniform micelles. This work aims to advance fundamental understanding of the cellular behaviour of 1D fibre-like micelles.

2.1. Results and Discussion

In this chapter, different hydrophilic polymers were employed as corona-forming blocks for the preparation of PFS- and PF-containing diblock copolymers, such as polyethylene glycol (PEG), TEG functionalised PAGE and poly(*N*-isopropylacrylamide) (PNIPAm).

2.1.1. Synthesis and characterisation of BCPs and precursors

To prepare water-soluble micelles, different amphiphilic diblock copolymers were synthesised as shown in Figure 2.1 and detailed strategies are outlined in the supplementary information (Scheme S2.1-S2.3). In general, PFS-OH was first prepared via an anionic ring-opening polymerisation (ROP) which was terminated with chloro(dimethyl)vinylsilane, followed by a thiol-ene click reaction with 2-mercaptoethanol. PFS-*b*-PAGE was synthesised using PFS-OH as a macroinitiator for the ROP of AGE. The water-soluble PFS-*b*-P(AGE-*g*-TEG) was obtained after a post-polymerisation functionalisation with TEG. PNIPAm- (and PMMA-) containing diblock copolymers were prepared by a reversible addition-fragmentation chain transfer (RAFT) polymerisation with a PFS macroinitiator, which is first prepared by modifying the chain end of PFS-OH with a chain transfer agent (CTA). PFS-*b*-PEG diblock copolymers were synthesised via a Steglich esterification with PFS-OH and a carboxylic acid terminated commercialised PEG, MeO-PEG-COOH. In the synthesis of PF-containing diblock copolymers, alkyne-terminated PF was first prepared via a Grignard metathesis chain-growth polymerisation, followed by an azide-alkyne click reaction with an azide group terminated PEG (N_3-

PEG-OH). Further modification of the terminal hydroxyl group can afford the diblock copolymers attached with functional molecules, such as fluorescent dyes or folic acid (FA).

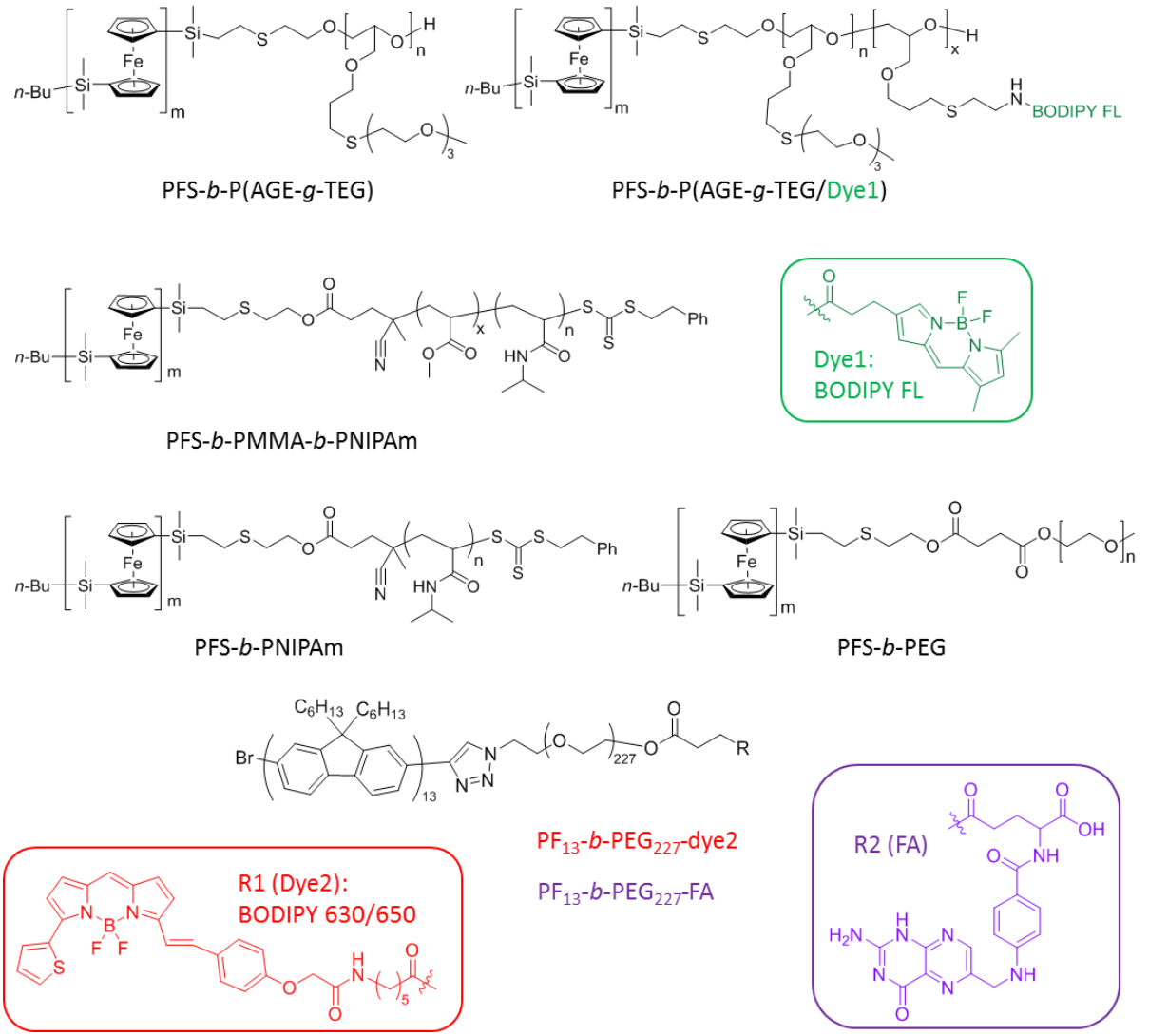

Figure 2.1. Structures of prepared PFS- and PF-containing BCPs.

The characterisation of polymer molecular weight was carried out by different techniques: gel permeation chromatography (GPC) analysis was used to obtain the number average molecular weight (M_n) and molar-mass dispersity ($Đ_M$) (Figure S2.1-S2.3); matrix assisted laser desorption ionization time-of-flight mass spectrometry (MALDI-TOF MS) was used to obtain the weight average molecular weight (M_w) of PFS, PF and PEG homopolymers (Figure S2.4-S2.6); and nuclear magnetic resonance (NMR) spectroscopic analysis was used to obtain the block ratio of the block copolymers corresponding

to the degree of polymerisation (DP_n) of core and corona blocks (Figure S2.7-S2.14). All characterisation data is summarised in Table 2.1 and S2.1.

Table 2.1. Molecular weight characterisation of PFS- and PF-based diblock copolymers.

Polymer	M_n (kg·mol^{-1})[a]	M_n (kg·mol^{-1})[b]	$Đ_M$[b]	Block ratio (Core:Corona)[a]
PFS_8-*b*-P(AGE-*g*-TEG)$_{115}$	35.7	22.9	1.54	1:14
PFS_{10}-*b*-P(AGE-*g*-TEG)$_{104}$	33.1	17.5	1.17	1:10
PFS_{28}-*b*-P(AGE-*g*-TEG)$_{259}$	82.9	75.9	1.35	1:9.3
PFS_{53}-*b*-P(AGE-*g*-TEG)$_{155}$	56.1	51.7	1.13	1:3
PFS_{27}-*b*-P(AGE-*g*-TEG/Dye1)$_{100}$	35.9	27.8	1.56	1:3.7
PFS_{28}-*b*-$PNIPAm_{494}$	62.6	112.5	1.28	1:17.6
PFS_{28}-*b*-$PMMA_6$-*b*-$PNIPAm_{496}$	63.8	198.8	1.35	1:0.2:17
PFS_{28}-*b*-PEG_{120}	12.1	17.1	1.08	1:4.2
PFS_{28}-*b*-PEG_{251}	16.8	22.9	1.08	1:8.9
PF_{13}-*b*-PEG_{227}-OH	14.3	29.9	1.12	1:17
PF_{13}-*b*-PEG_{227}-Dye2[c]	14.9	-	-	1:17
PF_{13}-*b*-PEG_{227}-FA[c]	14.8	-	-	1:17

[a] determined by ^{1}H NMR spectroscopy, [b] determined by GPC relative to polystyrene (PS) standards in *n*-Bu_4NBr/THF, [c] no GPC characterization due to the poor solubility of functional molecules in THF.

In the synthesis of functional PF-*b*-PEG, a key challenge is the preparation of the corona-forming block. This involved the use of monosubstituted HO-PEG-N_3, which is derived from HO-PEG-OH. The synthesis consists of two steps (Scheme S2.3): a substitution reaction of HO-PEG-OH with tosyl choride (TsCl) to prepare HO-PEG-OTs, followed by the azide substitution to afford HO-PEG-N_3. It is important to assure in the first step that only the monosubstituted product is formed and not the di-substituted by-product (TsO-PEG-OTs), which may generate by-product (N_3-PEG-N_3) and cause triblock copolymer formation in the later synthesis. MALDI-TOF MS was used to confirm that the prepared polymer contains only unsubstituted PEG and monosubstituted PEG (Figure 2.2). In terms of attempting to obtain pure monosubstituted PEG (HO-PEG-N_3), polymeric PEG cannot be easily purified by silica chromatography unlike oligomeric PEG. The strategy used here (Scheme S2.3) is to prepare a mixture of unsubstituted PEG (HO-PEG-OH) and monosubstituted PEG (HO-PEG-N_3) and then use the mixture directly for PF-*b*-PEG preparation. After the formation of diblock copolymer, the

purification was carried out to remove the PEG homopolymer by precipitation in MeOH. Due to the different dissolution behaviour of PF-*b*-PEG and PEG homopolymer, PF-*b*-PEG was collected as a pellet after high speed centrifuge (14000 rpm) while PEG stayed in the supernatant and could be decanted.

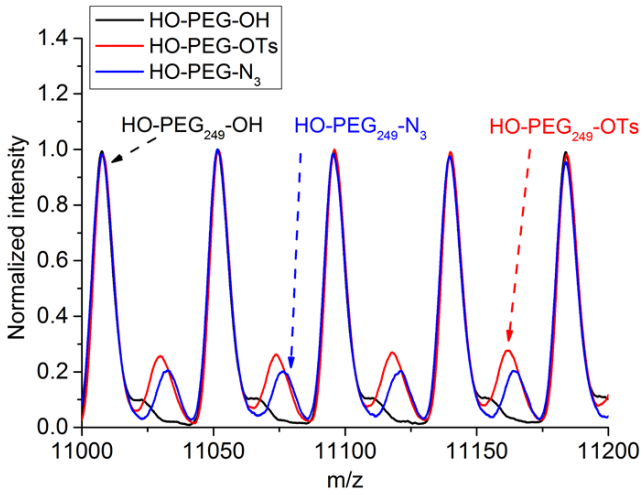

Figure 2.2. Overlaid MALDI-TOF MS spectra showed the mixture of monosubstituted PEG and unsubstituted PEG. No observation of the presence of di-substituted by-product.

2.1.2. Attempted use of seeded-growth to prepare PFS-based micelles in aqueous media

In a previously published work, direct seeded-growth experiments in H_2O were carried with PFS_{56}-*b*-P(AGE-*g*-TEG)$_{156}$.[217] Most of the resulting micelles were of very similar length to the seeds, which indicated that no apparent epitaxial growth was observed. Elongation was observed with a small number of micelles, but the length was not controlled. Some of the micelles showed an uneven growth (Figure S2.15). The elongated sections have a different electron contrast from the central seeds (blue circle in Figure S2.15). These differences in contrast may be due to the differences in PFS core crystallinity or height of the grown sections and the seeds. Some new individual micelles with less electron density than the seeds also formed, which suggested that self-nucleation also occurred (red circle in Figure S2.15). It appears that as H2O is an extremely poor solvent for the hydrophobic PFS core-forming block in PFS56-b-P(AGE-g-TEG)156, controlled epitaxial growth is disfavoured compared to in the case of organic solvents.

Self-assembly of PFS_{53}-*b*-P(AGE-*g*-TEG)$_{155}$ in H_2O. To perform further studies of aqueous living CDSA of PFS micelles, a PFS-containing polymer PFS_{53}-*b*-P(AGE-*g*-TEG)$_{155}$ was synthesised with a core-corona block ratio of 1:3 (possessing a similar block ratio as PFS_{56}-*b*-P(AGE-*g*-TEG)$_{156}$). To examine the possibility of fibre formation in aqueous media, self-assembly of PFS_{53}-*b*-P(AGE-*g*-TEG)$_{155}$ direct in H_2O was carried out via a heating-cooling process. The polymer was dissolved in H_2O at different concentrations at 85 °C and the resulting solution was slowly cooled (over 3 h from 85 to 23 °C). After aging for 24 h, macroscopic precipitation was observed in all samples (Figure S2.16). These results suggest that PFS_{53}-*b*-P(AGE-*g*-TEG)$_{155}$ cannot form colloidally stable micelles in H_2O directly which may be due to the fast precipitation of the relatively long hydrophobic PFS core-forming block or the short corona-forming block being unable to provide sufficient colloidal stability. On the contrary, colloidal stability could be achieve by a reported strategy of transferring the micelles from the organic solvent to H_2O via dialysis.[217] Fibres of PFS_{53}-*b*-P(AGE-*g*-TEG)$_{155}$ were first prepared in DMF and seed micelles (L_n = 23, L_w/L_n = 1.06) were achieved after being subjected to sonication (Figure S2.17). Following dialysis against H_2O, the seed micelles were colloidally stable in H_2O and no macroscopic precipitation was observed over several weeks. The difference in colloidal stability in H_2O and DMF may be derived from the hydrophobicity of PFS core block, which resulting in fast precipitation in H_2O.

Seeded-growth of PFS_{28}-*b*-P(AGE-*g*-TEG)$_{259}$. According to the results of macroscopic precipitation of PFS_{53}-*b*-P(AGE-*g*-TEG)$_{155}$ (core:corona = 1:3) in H_2O, it was expected that a diblock copolymer with a shorter core-forming block and a longer corona-forming block would be desirable for further aqueous living CDSA studies. Therefore, PFS_{28}-*b*-P(AGE-*g*-TEG)$_{259}$ (core:corona = 1:9) was synthesised for aqueous self-assembly studies. The direct self-assembly of PFS_{28}-*b*-P(AGE-*g*-TEG)$_{259}$ in H_2O was carried out via a heating-cooling process (the solution was kept at 85 °C for 2 h and slowly cooled to 23 °C over 3 h). After aging for 24 h, long and polydisperse fibres were observed by TEM images (Figure 2.3a). Dynamic light scattering (DLS) analysis (Figure 2.3c) showed the presence of assemblies with apparent hydrodynamic radii ($R_{h,\,app}$) of 325 and 2000 nm. Sonication was then used to

fragment the polydisperse fibres to afford seeds. However, no seed-like micelles were observed by TEM (**Figure S2.18**Figure S2.18) despite the use of a series of different sonication time (40, 30 and 10 min).

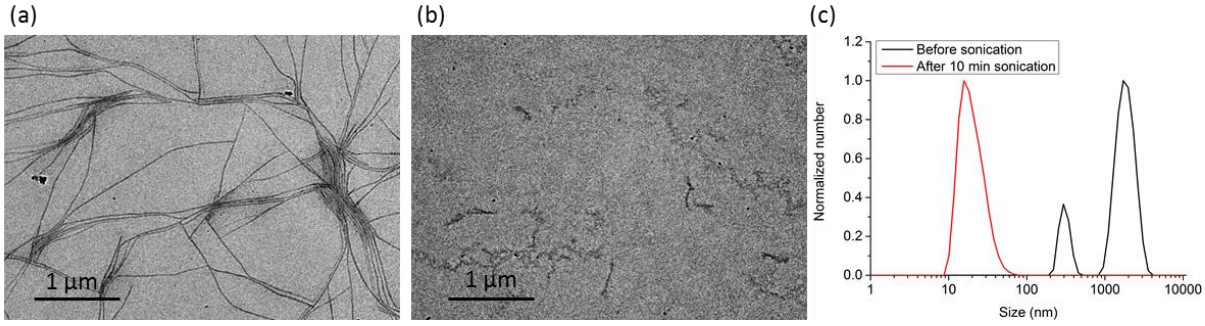

Figure 2.3. (a) TEM images of PFS_{28}-*b*-P(AGE-*g*-TEG)$_{259}$ fibres directly formed in H_2O (0.1 mg/mL, by heating-cooling method), (b) TEM images after 10 min sonication of fibre solution in H_2O, and (c) DLS analysis of fibre solutions before sonication (black) and after 10 min sonication (red).

Even after sonication for 10 min, the sample showed nanoparticles in the solution possessing a $R_{h,\,app}$ value of 18 nm by DLS (Figure 2.3c), which is similar to a unimer state of polymers in the solution.[277] If a polymer sample shows an apparent hydrodynamic radius of ca. 10 nm in a solvent by DLS, it is most likely in a unimer state in this solvent. This suggests that fibre dissolution occurs by sonication, which might be the result of the low crystallinity of the micelles formed directly in H_2O.

The strategy was then changed to prepare the seed micelles in organic solvents and then to transfer them into H_2O. PFS_{28}-*b*-P(AGE-*g*-TEG)$_{259}$ was directly dissolved in MeOH at 65 °C and the solution was heated for 2 h, followed by slowly cooling to room temperature (over 2 h from 65 °C to 23 °C). The polydisperse fibres were sonicated for 1 h at 0 °C to afford uniform seed micelles (L_n = 73 nm, L_w/L_n = 1.07) as shown by TEM images (Figure S2.19b). After dialysed into H_2O, the seeds (L_n = 67 nm, L_w/L_n = 1.08) appeared to be colloidally stable (Figure S2.19c).

Seeded-growth experiments were carried out by diluting the seeds (PFS_{28}-*b*-P(AGE-*g*-TEG)$_{259}$, in MeOH) into H_2O (MeOH:H_2O = 1:99), followed by the addition of PFS_{28}-*b*-P(AGE-*g*-TEG)$_{259}$ unimers (in tetrahydrofuran (THF), with m_{unimer}:m_{seed} = 5) with a small volume fraction of THF (THF:H_2O = 3:97) in the final solution. After aging for 24 h, no apparent epitaxial growth was observed. Most micelles were much shorter than the length of the seed micelles (Figure 2.4a and c). This suggests that

the occurrence of self-nucleation of the added unimers, which aggregated immediately and then crystallised to form new nuclei. Another seeded-growth experiment was carried out with a increased THF volume fraction in the final aqueous solution (THF:H_2O = 10:90). After aging for 24 h, elongated polydisperse micelles and seed micelles were both observed in TEM images (Figure 2.4b). The elongated micelles might be formed by either self-nucleation or the epitaxial growth from the seed termini surfaces of the added unimers. However, the presence of seed micelles suggests that under these conditions unimer addition to the active faces of the seeds is not possible. It appears that fast self-nucleation and relative inactivity of seeds are competing with the epitaxial growth of PFS_{28}-*b*-P(AGE-*g*-TEG)$_{259}$ from the seed termini in aqueous media.

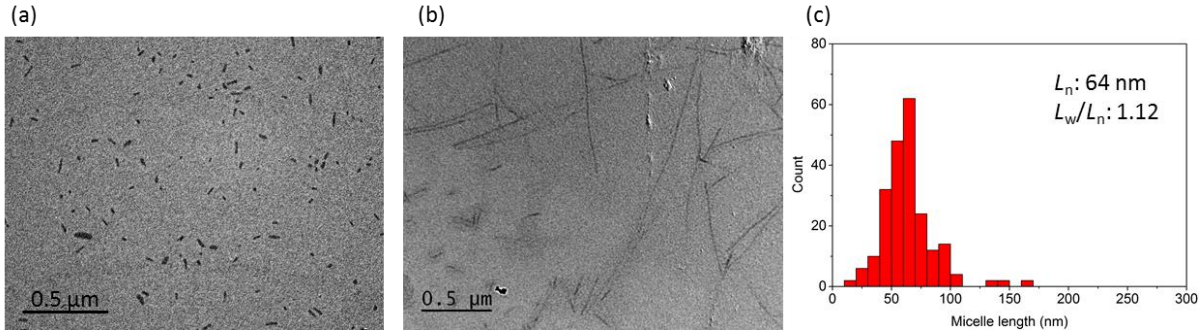

Figure 2.4. Seeded-growth of PFS_{28}-*b*-P(AGE-*g*-TEG)$_{259}$ micelles by adding unimer (in THF, with m_{unimer}:m_{seed} = 5) into seeds (L_n = 73 nm, L_w/L_n = 1.07, in MeOH) after dilution with H_2O. TEM images of (a) samples in THF/H_2O (3:97), (b) samples in THF/H_2O (10:90) and (c) contour length histogram of micelles in the samples in THF/H_2O (3:97).

Attempts to minimise self-nucleation. The spontaneous self-nucleation leading to an uncontrolled seeded-growth may be a result of the long hydrophobic PFS core-forming block in PFS_{28}-*b*-P(AGE-*g*-TEG)$_{259}$. Another water-soluble PFS diblock copolymer with an even shorter core forming block, PFS_8-*b*-P(AGE-*g*-TEG)$_{115}$, was therefore prepared for self-assembly studies. The self-assembly behaviour of PFS_8-*b*-P(AGE-*g*-TEG)$_{115}$ was studied in various solvents: MeOH, ethanol (EtOH), isopropanol (*i*-PrOH) and H_2O. After aging samples for 36 h, no micelle was observed by TEM in all four solvents (Figure S2.20). This may be due to the relatively high corona-core block ratio (14:1), which improves the solvation of PFS in H_2O. Seeded growth experiments were carried out with PFS_8-*b*-P(AGE-*g*-

TEG)$_{115}$. The unimer (PFS$_8$-*b*-P(AGE-*g*-TEG)$_{115}$ (in THF) was added to the seed (PFS$_{28}$-*b*-P(AGE-*g*-TEG)$_{259}$, L_n = 73 nm, L_w/L_n = 1.07, in H_2O) in THF/H_2O mixture (*v*:*v* = 1:9). After aging for 48 h, TEM images (Figure S2.21a) after solvent evaporation showed only a unimer film and seed micelles. After aging for 20 days, a small number of elongated micelles with uncontrolled length and unimer film were observed (Figure S2.21b). This result suggests that PFS$_8$-*b*-P(AGE-*g*-TEG)$_{115}$ is not suitable for self-assembly studies due to the short core-forming block.

Subsequently, another diblock copolymer, PFS$_{10}$-*b*-P(AGE-*g*-TEG)$_{104}$, with a slightly longer PFS core-forming block was prepared in an effort to aid self-assembly. The self-assembly of PFS$_{10}$-*b*-P(AGE-*g*-TEG)$_{104}$ directly in H_2O was first investigated by the heating-cooling method. The self-assembly results were analysed by TEM (Figure S2.22). No micelle was observed after aging for 1 and 3 days, the TEM images instead showed a film of unimer (Figure 2.5a and S2.22a and b). DLS analysis (Figure 2.5b) of the sample being aged for 1 day showed particles (ca. 150 nm in diameter) presenting in the solution, which indicated that PFS$_{10}$-*b*-P(AGE-*g*-TEG)$_{104}$ was in an aggregated state in H_2O after the heating-cooling process. After aging for 7 days, polydisperse micelles with significantly less unimer film were observed by TEM imaging (Figure S2.22c). After aging for 12 days, only polydisperse fibres were detected (Figure S2.22d). These results suggest a slow self-nucleation process for PFS$_{10}$-*b*-P(AGE-*g*-TEG)$_{104}$ in H_2O.

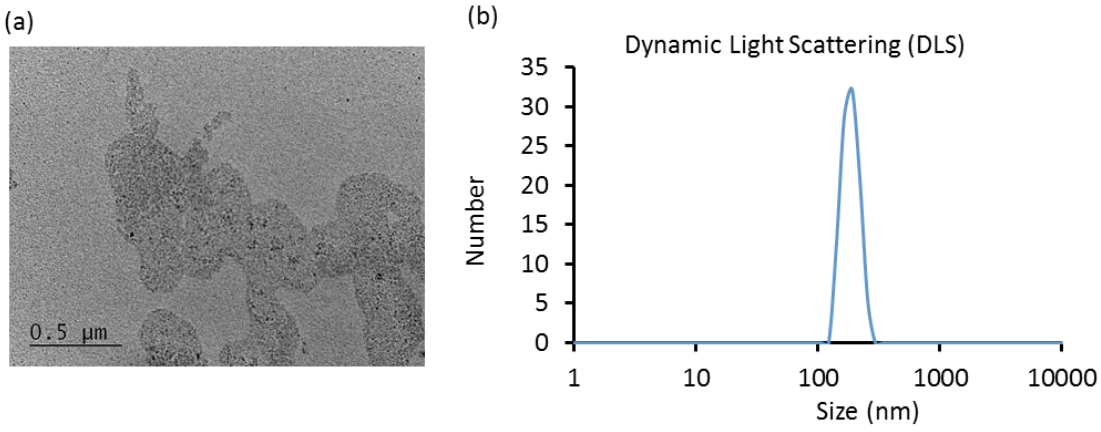

Figure 2.5. (a) TEM and (b) DLS analysis of solution state of PFS$_{10}$-*b*-P(AGE-*g*-TEG)$_{104}$ by direct self-assembly in H_2O via a heating-cooling method after aging for 1 day with a concentration at 0.1 mg/mL.

Attempts to perform seeded-growth of PFS_{10}-*b*-P(AGE-*g*-TEG)$_{104}$ were carried out by adding unimer (PFS_{10}-*b*-P(AGE-*g*-TEG)$_{104}$, in THF) to the seed solutions (PFS_{28}-*b*-P(AGE-*g*-TEG)$_{259}$, L_n = 73 nm, L_w/L_n = 1.07, in MeOH, Figure S2.19) after dilution with H_2O (THF:H_2O = 1:10). After aging the sample for 48 h, TEM images (Figure 2.6) showed co-existence of elongated micelles with uncontrolled growth and seed micelles. This result indicates the occurrence of self-nucleation. It seems that the added unimer being trapped quickly by H_2O to form aggregates and the THF helps the aggregates to crystallise to form new nuclei.

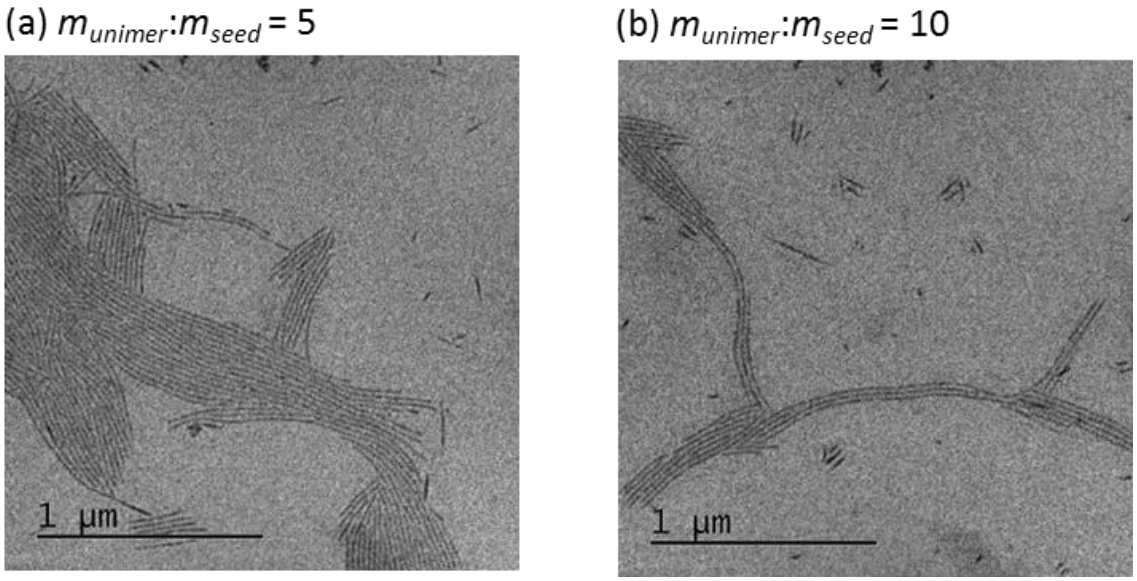

Figure 2.6. TEM images of seeded-growth of adding unimer (PFS_{10}-*b*-P(AGE-*g*-TEG)$_{104}$, in THF) to seeds (PFS_{28}-*b*-P(AGE-*g*-TEG)$_{259}$, diluted in H_2O) with unimer-to-seed mass ratios of (a) 5 and (b) 10 in THF/H_2O (*v*:*v* = 1:9).

Another seeded-growth experiment was carried out by using the PFS_{10}-*b*-P(AGE-*g*-TEG)$_{104}$ unimer in H_2O instead of in THF, as THF facilitates self-nucleation. Based on the slow fibre formation process of PFS_{10}-*b*-P(AGE-*g*-TEG)$_{104}$ observed above (Figure 2.5 and S2.22)), the polymer could be regarded as being in an unimer-like state in H_2O before the 24 h aging after the heating-cooling process. The seeded-growth experiment was carried out by adding the unimer-like PFS_{10}-*b*-P(AGE-*g*-TEG)$_{104}$ (in H_2O) to the seed solutions (PFS_{28}-*b*-P(AGE-*g*-TEG)$_{259}$, diluted in H_2O) at 23 °C. However, TEM images (Figure S2.23) showed no apparent growth of the added unimer was observed after sample aging for 1 day. On

further aging for another 2 days, still only unimer films and seed micelles were observed. This result indicates that the added unimers are trapped and not capable of undergoing epitaxial growth from the pre-existing seed termini.

Experiments at elevated temperature. Other than self-nucleation, inactivity of seed micelles as a consequence of coverage of seed surfaces by corona forming block in H_2O at 23 °C may also result in uncontrolled epitaxial growth. According to previous studies, elevated temperatures have been employed to improve living CDSA of π-conjugated polymers, such as P3HT and PPV.[121, 142, 143] Herein, thermal self-seeding experiments on PFS_{28}-*b*-P(AGE-*g*-TEG)$_{259}$ seeds were carried out and attempted to improve the living CDSA. The seeds (PFS_{28}-*b*-P(AGE-*g*-TEG)$_{259}$, in MeOH) were diluted in H_2O (MeOH:H_2O = 1:99) and then heated at different temperatures for 30 min followed by slowly cooled down. With samples that were heated at 40 °C, TEM images (Figure 2.7a) showed polydisperse fibre formation (L_w/L_n = 1.23) in solution and these fibres had a shorter measured length (L_n = 50 nm) than that of seed micelles (L_n = 73 nm). This result suggests that self-nucleation occurs under the self-seeding conditions. With samples heated at 50 and 60 °C (Figure 2.7b and c), spherical micelles were mainly observed. Generally, the elevated temperature may cause the dissolution of pre-existing seeds, and spherical micelles formed by fast aggregation upon cooling.

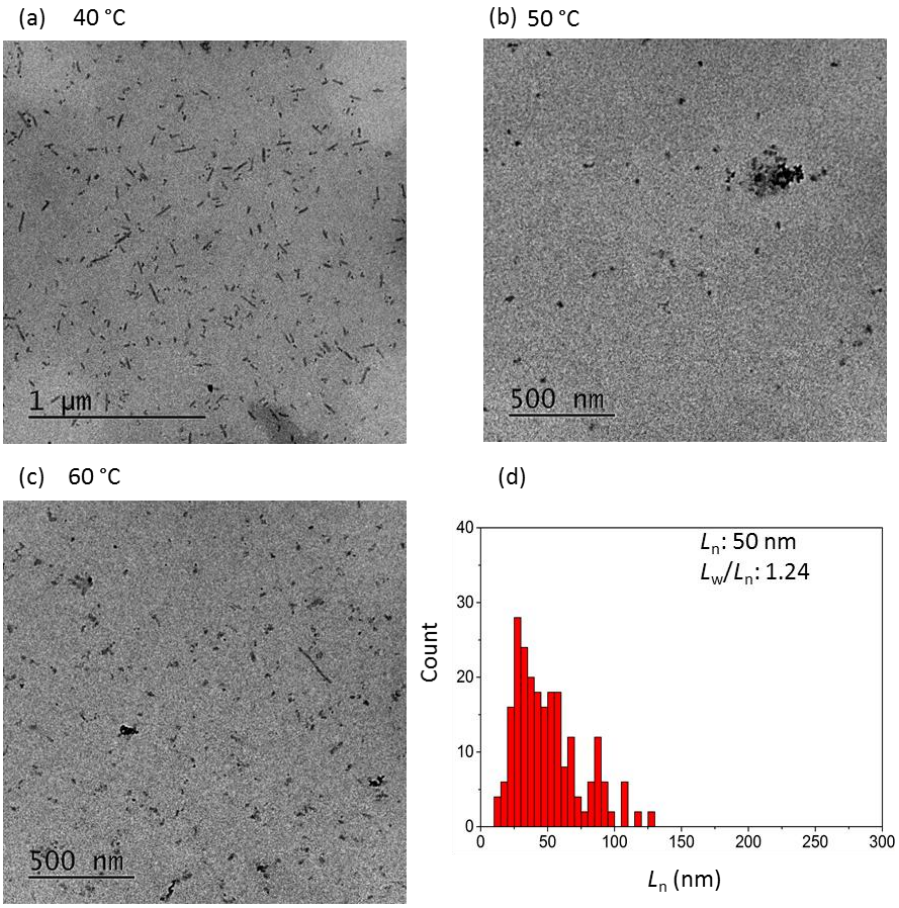

Figure 2.7. TEM images of self-seeding experiments of PFS_{28}-*b*-P(AGE-*g*-TEG)$_{259}$ seed micelles (diluted in H_2O, MeOH:H_2O = 1:99) at (a) 40, (b) 50 and (c) 60 °C. (d) Contour length histogram of micelles prepared by self-seeding at 40 °C.

Another elevated temperature experiment was carried out with seeded-growth of PFS_{10}-*b*-P(AGE-*g*-TEG)$_{104}$. The unimer (PFS_{10}-*b*-P(AGE-*g*-TEG)$_{104}$, in H_2O) was added to the seed (PFS_{28}-*b*-P(AGE-*g*-TEG)$_{259}$, L_n = 67 nm, L_w/L_n = 1.08, in H_2O) solutions at elevated temperatures (40, 45, 50 and 55 °C, respectively) for 30 min and slowly cooled down to 23 °C. Heating at 40, 45 and 50 °C resulted in only seed micelles and small aggregates being observed. With samples heated at 55 °C, only aggregates and unimer film were observed (Figure S2.24). These results indicate that thermal self-seeding does not resolve the problems associated with controlled growth of the PFS BCP in aqueous media which is primarily a result if the highly hydrophobic core-forming block.

Seeded-growth in organic solvents in the presence of H_2O. To further study the influence of H_2O on the seeded-growth of PFS-containing diblock copolymers, experiments were carried out in a mixture of H_2O and organic solvents. As control experiments, seeded-growth of PFS_{10}-*b*-P(AGE-*g*-TEG)$_{104}$ unimer was first carried out in MeOH and DMF. Typically, the PFS_{28}-*b*-P(AGE-*g*-TEG)$_{259}$ seeds (in DMF) were diluted in MeOH (or DMF) and PFS_{10}-*b*-P(AGE-*g*-TEG)$_{104}$ unimers (in THF) were added at 23 °C. After aging for 24 h, TEM images (Figure S2.25 and S2.26) showed elongated micelles with controlled lengths and low length dispersity (< 1.05). When seeded-growth experiments were conducted in mixed solvents of H_2O/MeOH or H_2O/DMF (with v_{water}:$v_{organic}$ of 10:90, 20:80 and 30:70), TEM analysis showed (Figure S2.27 and S2.28) no length control of micelles was achieved irrespective of the low volume fractions of H_2O (down to 10%).

In summary, controlled epitaxial growth of PFS-containing BCPs directly in aqueous media has not been achieved. We believe this is due to H_2O being an extremely poor solvent for the hydrophobic PFS core-forming block resulting in rapid self-nucleation of the added unimer and effective coverage of the high energy surface on seed micelle termini by the coronal block.

Stability studies on PFS-based micelles directly formed in H_2O. A stability study on PFS-based micelles in H_2O was carried and the results were assessed by TEM. The self-assembly of PFS_{10}-*b*-P(AGE-*g*-TEG)$_{104}$ and PFS_{28}-*b*-P(AGE-*g*-TEG)$_{259}$ directly in H_2O was carried out via a heating-cooling process and the morphologies formed in solutions were characterised by TEM (Figure 2.3a and S2.22d). Both PFS_{10}-*b*-P(AGE-*g*-TEG)$_{104}$ and PFS_{28}-*b*-P(AGE-*g*-TEG)$_{259}$ formed long fibres in H_2O after 12 days aging. But after aging for 30 days, no fibre micelles (Figure S2.29a and b) but only small aggregates and unimer films were observed. As control experiments, the self-assembly of PFS_{10}-*b*-P(AGE-*g*-TEG)$_{104}$ and PFS_{28}-*b*-P(AGE-*g*-TEG)$_{259}$ were carried out in MeOH via a similar heating-cooling process, with a heating temperature of 65 °C. After aging for 30 days, long fibres were still observed (Figure S2.29c and d). These results suggest that the micelles formed directly in H_2O may have a low core crystallinity leading to instability.

2.1.3. 1D PFS-based micelles for cellular uptake studies

Although no controlled micelle growth has been achieved directly in aqueous media with PFS-based micelles, the uniform PFS fibre-like micelles could be prepared in organic solvents and transferred into H_2O by dialysis. Due to the reported colloidal stability in H_2O after dialysis, PFS-*b*-P(AGE-*g*-TEG) was used to prepare uniform fibre-like micelles for cellular uptake studies.

Preliminary cellular uptake results of PFS-*b*-(PAGE-*g*-TEG) micelles. In order to study the cellular behaviour of micelles, a fluorescent dye (BODIPY FL, emission at 512 nm, Scheme S2.1) functionalised PFS-based diblock copolymer, PFS_{27}-*b*-P(AGE-*g*-TEG/Dye1)$_{100}$, was prepared (Figure 2.8a and b). Initially fluorescent micelles were prepared by adding PFS_{27}-*b*-P(AGE-*g*-TEG/Dye1)$_{100}$ unimer (in THF) to the seed micelles (PFS_{53}-*b*-P(AGE-*g*-TEG)$_{155}$, in DMF, L_n = 23 nm, L_w/L_n = 1.06, Figure S2.17) after being diluted in MeOH (DMF:MeOH = 1:99). After aging for 48 h, the micelles were dialysed into H_2O for another 48 h to remove MeOH and THF. TEM images (Figure 2.8b) showed the cylindrical micelles had a uniform length (L_n = 78 nm, L_w/L_n = 1.06). According to the previous research on size effects of nanoparticles in cell internalisation, particle sizes smaller than 200 nm showed satisfactory internalisation by cells.[178] The cellular uptake investigations of these micelles were then carried out with cell culture from the HeLa cell line. The micelles were incubated with the cells in serum-containing Dulbecco's Modified Eagle's media (DMEM) for 8 h. Confocal laser scanning microscopy (CLSM) analysis (Figure 2.8c) showed limited apparent uptake of the cylindrical micelles by the cells. Only a very small number of green puncta were observed with the stained HeLa cells, while most cells showed no green fluorescent signal. Further studies showed extensive aggregation of these micelles in serum-containing and serum-free cell media (Figure S2.30), which may be the reason for the limited cellular uptake observed.

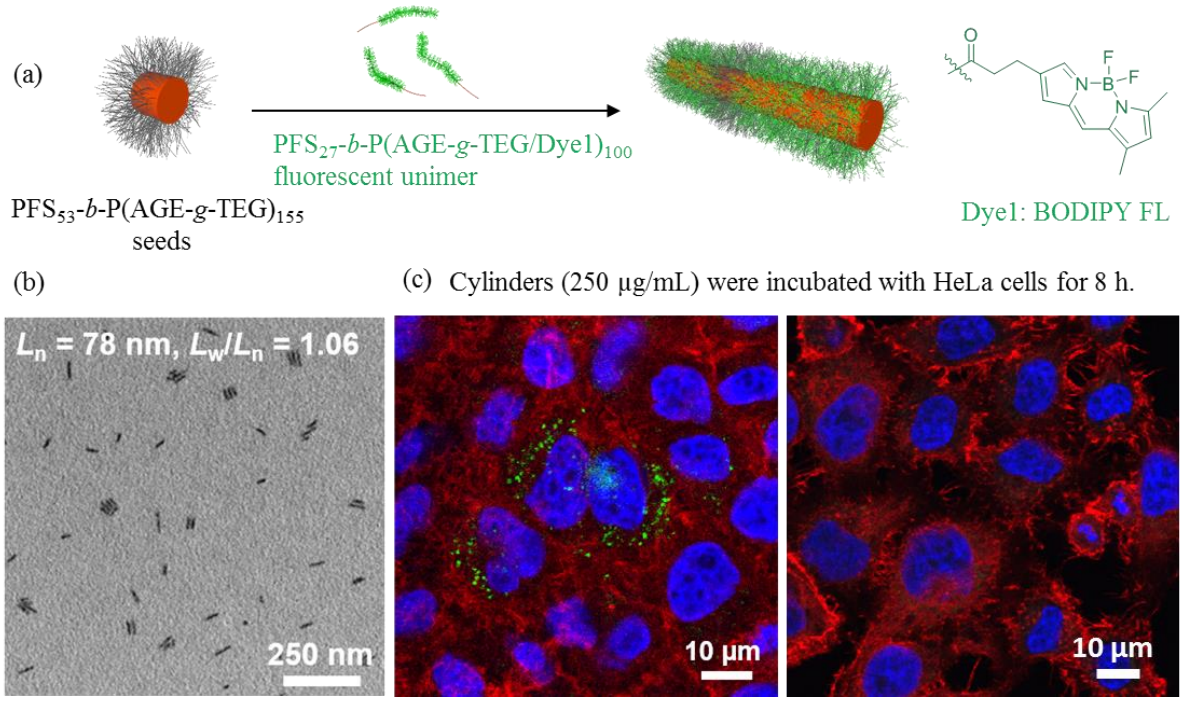

Figure 2.8. Fluorescent cylindrical micelles for cellular uptake experiments. (a) Schematic representation of preparation of fluorescent cylindrical micelles and BODIPY FL structure, (b) TEM images of uniform cylindrical micelles (L_n = 78 nm, L_w/L_n = 1.06) and (c) preliminary results of cellular uptake experiments of cylindrical micelles by HeLa cells. Red indicates phalloidin-594 stained actin filaments in cytoplasm. Blue indicates DAPI stained cell nuclei and green puncta indicate cylindrical micelles. Cells and micelles were incubated in Dulbecco's Modified Eagle Medium (DMEM) with 10% Foetal Bovine Serum.

Charged species generally show better solubility behaviour in cell media possibly since aggregation is hindered by electrostatic repulsion. It is envisioned that the introduction of positively charged compartments into the cylindrical micelles will not only minimize their aggregation but will also enhance their interaction with negatively charged cell surface. A reported water-soluble B-A-B triblock co-micelle with two terminal positively-charged segments (B block: PFS-*b*-P2VP/Me) and a neutral central segment (A block: PFS-*b*-P(AGE-*g*-TEG/Dye1)) was prepared for the cellular uptake studies.[217] PFS-*b*-P2VP (unimer in THF) was added to the uniform fluorescent micelles (L_n = 78 nm, L_w/L_n = 1.06, in MeOH, Figure 2.8b) in MeOH/*i*-PrOH (1:1). Me_2SO_4 (molar ratio at 5:1 of Me_2SO_4 to 2VP) was added to the resulting triblock comicelles (L_n = 142 nm, L_w/L_n = 1.05, in MeOH/*i*-PrOH, Figure 2.9b) for P2VP methylation, followed by dialysis to afford water-soluble charged triblock co-micelles. The

detailed preparation method has been included in the supplementary information. These triblock co-micelles were incubated with HeLa cells for cellular uptake studies. These results showed extensive uptake of the charged triblock co-micelles by HeLa cells (green puncta in cells) after 3 h incubation (Figure 2.9c). After 8 h incubation, a shape change in the cytoskeleton was observed (Figure 2.9d). These results suggest three possible reasons for the cytotoxicity: one is the inherent properties of PFS, which is not biocompatible; the second is the high percentage of charged terminal segments; and the third reason is the high concentration of the micelles. To investigate the cellular uptake behaviour of these micelles further, optimizations in micelle structures and cellular uptake concentrations have been carried out.

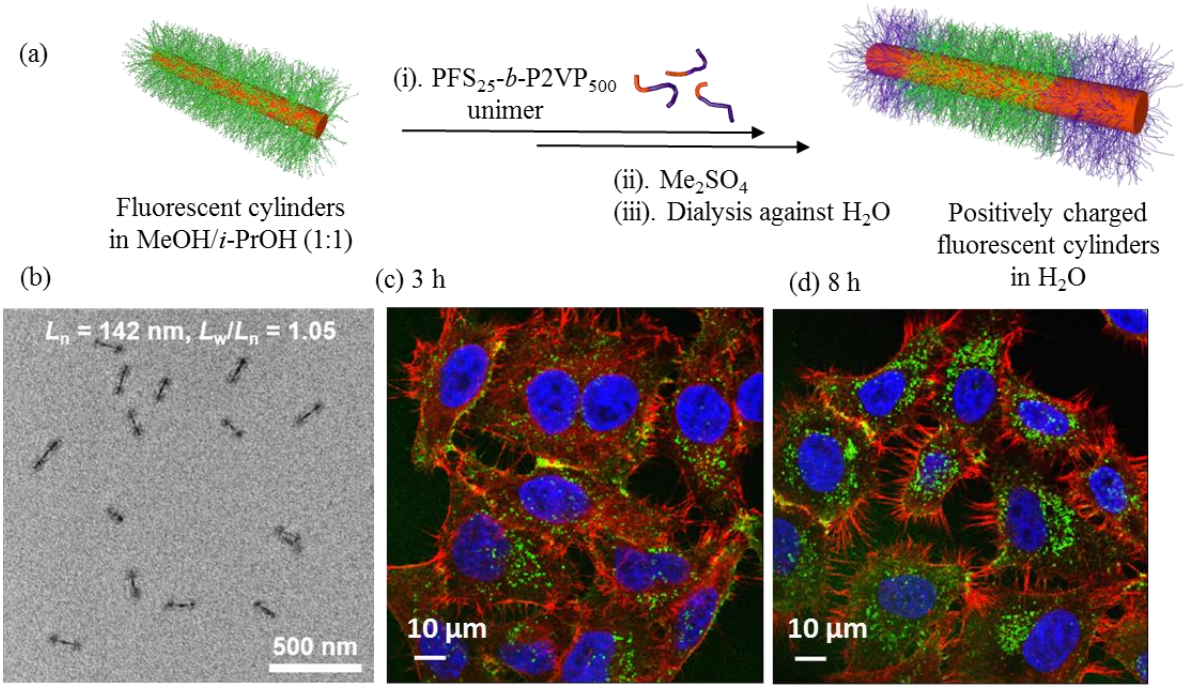

Figure 2.9. Triblock co-micelles with charged terminal segments for cellular uptake experiments. (a) Schematic representation of preparation of triblock co-micelles, (b) TEM image of uniform triblock micelles (L_n = 142 nm, L_w/L_n = 1.05) and (c) preliminary results of cellular uptake experiments of charged triblock co-micelles by HeLa cells. Red indicates phalloidin-594 stained actin filaments in cytoplasm. Blue indicates DAPI stained cell nuclei and green puncta indicate cylindrical micelles. Cells and micelles were incubated in DMEM with 10% Foetal Bovine Serum.

Optimization of the charged-segment length of PFS-based triblock comicelles. According to the preliminary cellular uptake results with PFS-based triblock comicelles (L_n = 142 nm), B-A-B triblock co-micelles with a target length of ca.150 nm with different length fractions (b) of charged-segments were targeted for further cellular uptake studies (Figure S2.31a). By adding the fluorescent unimer (PFS$_{27}$-*b*-P(AGE-*g*-TEG/Dye)$_{100}$, in THF) into the seeds (PFS$_{53}$-*b*-P(AGE-*g*-TEG)$_{155}$, in MeOH), uniform fluorescent micelles with controlled lengths and narrow length distribution ($L_w/L_n < 1.05$) were obtained (Figure S2.31b and S2.32). As we targeted the same overall micelle length but with different charged segment lengths (b) (Figure 2.10e), the central block fluorescent micelles were varied in length. PFS$_{25}$-*b*-P2VP$_{500}$ was used as the polymer for the charged segments. After diluting the fluorescent micelles in *i*-PrOH, PFS$_{25}$-*b*-P2VP$_{500}$ unimer (in THF) was added into the solution. After aging for 4 days, TEM images (Figure 2.10a-d) showed spatially-defined triblock comicelles formation. Due to the delocalised lone pair electrons on the nitrogen atom in the pyridine ring, an obvious electron density contrast can be observed from the central segment (PAGE) and the terminal segments (P2VP). According to the measured average length of triblock comicelles, the length fractions of P2VP segments were found as 7, 9, 27 and 50% (Figure S2.31b).

After diluting the micelles with H_2O, Me_2SO_4 (molar ratio at 5:1 of Me_2SO_4 to 2VP) was added to the micelle solution and the samples were aged for 1 day for methylation. Dialysis was then carried out in H_2O for 2 days with multiple dialysate changes. The micelles having a charged-segment length fraction of 50% (b = 50%) were found to be heavily aggregated by TEM characterisation (Figure S2.33a-d). DLS was used to study the aggregation of the prepared triblock co-micelles in H_2O. Based on the DLS number-averaged intensity (Figure S2.33e), samples with b = 50% showed an apparent hydrodynamic radius ($R_{h,\,app}$) of ca. 1000 nm, which suggested the occurrence of micelle aggregation. Samples with b = 7% showed a $R_{h,\,app}$ value of ca. 100 and ca. 1000 nm, which suggested co-existence of aggregates and dispersed micelles; samples with 9 and 27% length fractions of charged-segments showed $R_{h,\,app}$ of ca. 100 nm, which suggests colloidally-dispersed micelles. Due to the high content of charged species

in the sample with 50% length fraction of charged-segment, the micelles were supposed to be dispersed by electrostatic repulsion in solution. The cause of aggregation is under investigation.

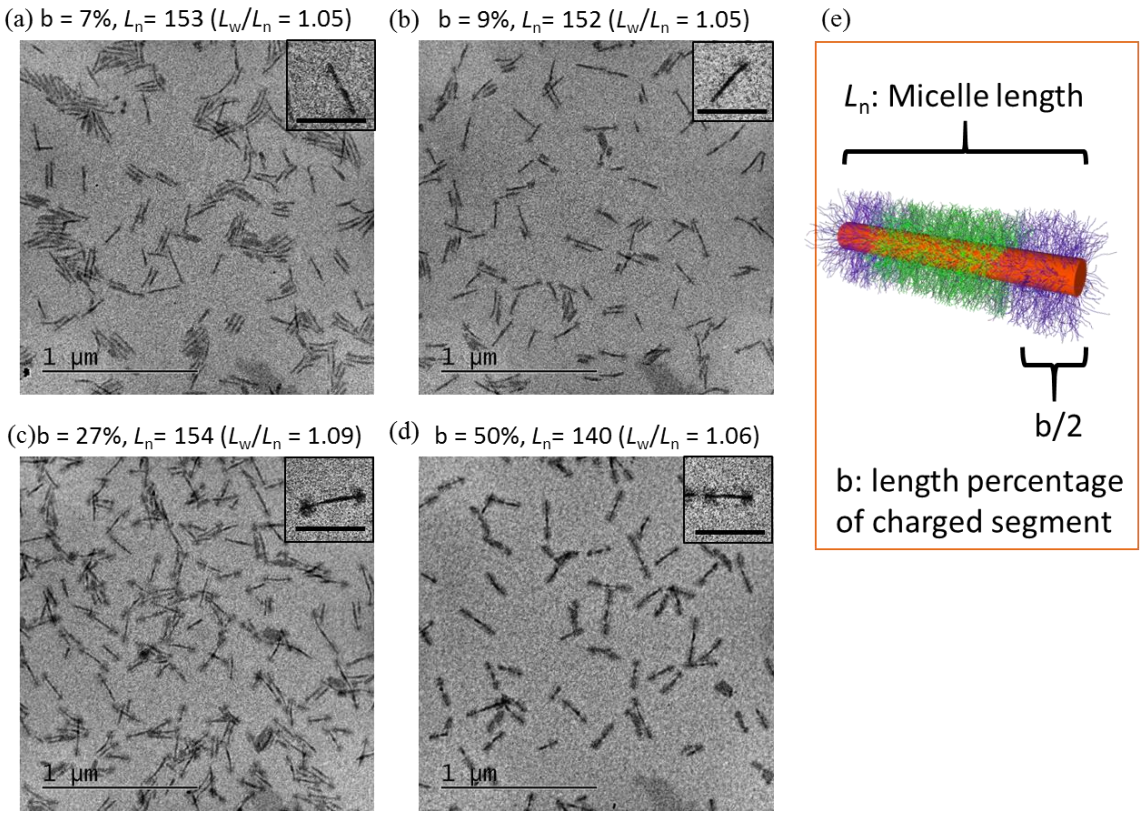

Figure 2.10. TEM images of triblock comicelles prepared by addition of PFS_{25}-*b*-$P2VP_{500}$ (unimer in THF) to PFS_{27}-*b*-P(AGE-*g*-TEG/Dye)$_{100}$ micelles (different lengths, in MeOH) in MeOH/*i*-PrOH (1:1) at 23 °C with charged-segment length fractions of (a) b = 7%, (b) b = 9%, (c) b = 27%, (d) b = 50%. Inset scale bars: 200 nm.

Aggregation studies were also carried out by CLSM of the prepared triblock co-micelles in H_2O and in cell media. As shown in the CLSM images (Figure S2.34), micelles with b = 7, 9, 27 and 50% (individual small light spot, ca. 150 nm, inaccurate measurement due to the limited resolution of CLSM) showed a dispersed state in H_2O. However, in the samples diluted in cell medium, aggregated micelles were observed in samples of b = 7, 9 and 50% (large bright green spot, ca. 400 nm by approximate measurement), while no apparent aggregation was observed of sample with b= 27%.

Cellular uptake experiments were carried out with all micelles (samples with different charged-segment length fractions) by incubation of micelles and HeLa cells for 8 h. The CLSM images (Figure 2.11)

showed that only samples with 27% length fractions of charged-segments exhibited a detectable uptake into cells (green puncta in cells). It is suggested that aggregation in other samples would be the main reason of unsuccessful uptake of these micelles into cells.

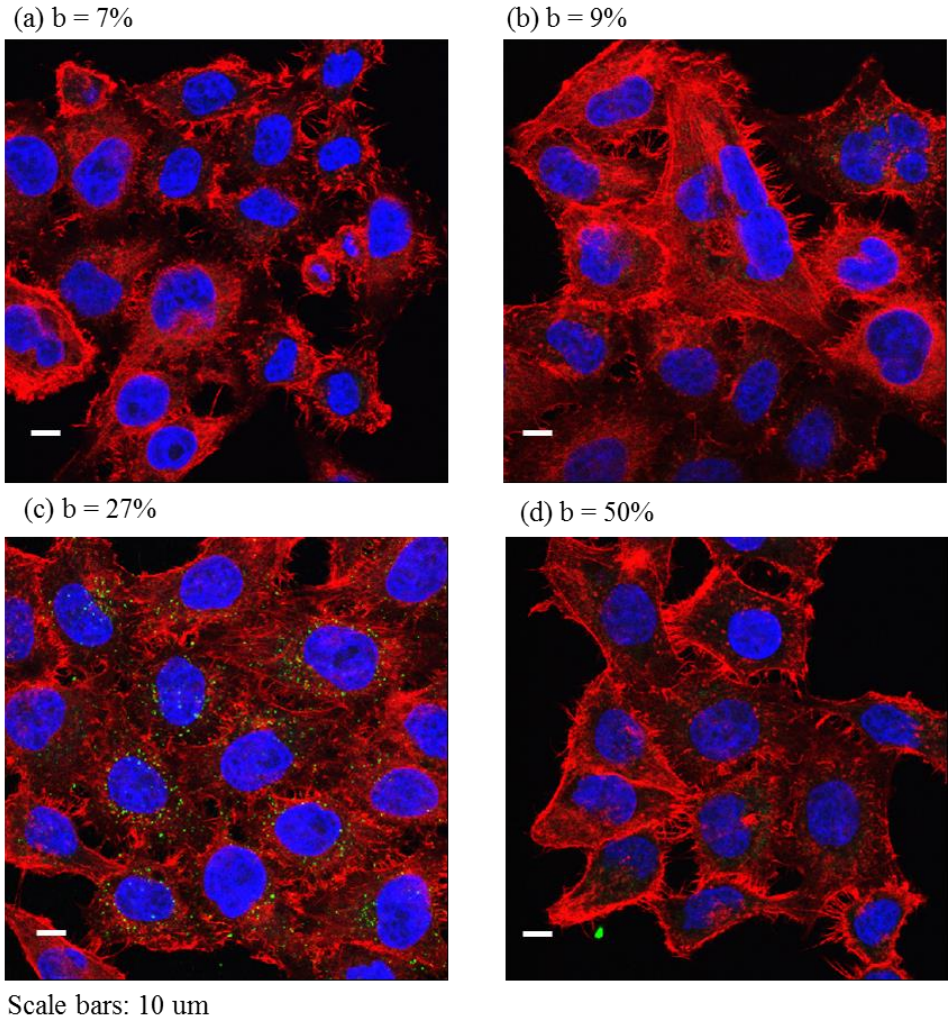

Figure 2.11. CLSM images of cellular uptake of triblock comicelles based on PFS_{27}-*b*-P(AGE-*g*-TEG/Dye)$_{100}$ with different charged segment lengths (a) b = 7%, (b) b = 9%, (c) b = 27%, and (d) b = 50% by HeLa cells with an incubation concentration at 50 μg/ml. Red indicates phalloidin-594 stained actin filaments in cytoplasm. Blue indicates DAPI stained cell nuclei and green puncta indicate cylindrical micelles.

With the successful cellular uptake of micelles where b = 27%, further studies on micelle internalisation with different concentrations were carried out. With 8 h incubation, the CLSM images (Figure 2.12) showed that samples with a concentration of 50 μg/mL showed the most cellular uptake (Figure 2.12c),

while green puncta were observed mostly outside of cells in the samples with a concentration of 10 μg/mL (Figure 2.12a). These results suggest that the rate of cellular uptake of prepared triblock co-micelles is concentration dependent. In addition, Z-stacks of the images taken from the bottom to the top of cells showed that the prepared cylindrical micelles were internalised into the cells rather than lying on the cell surface (Figure S2.35).

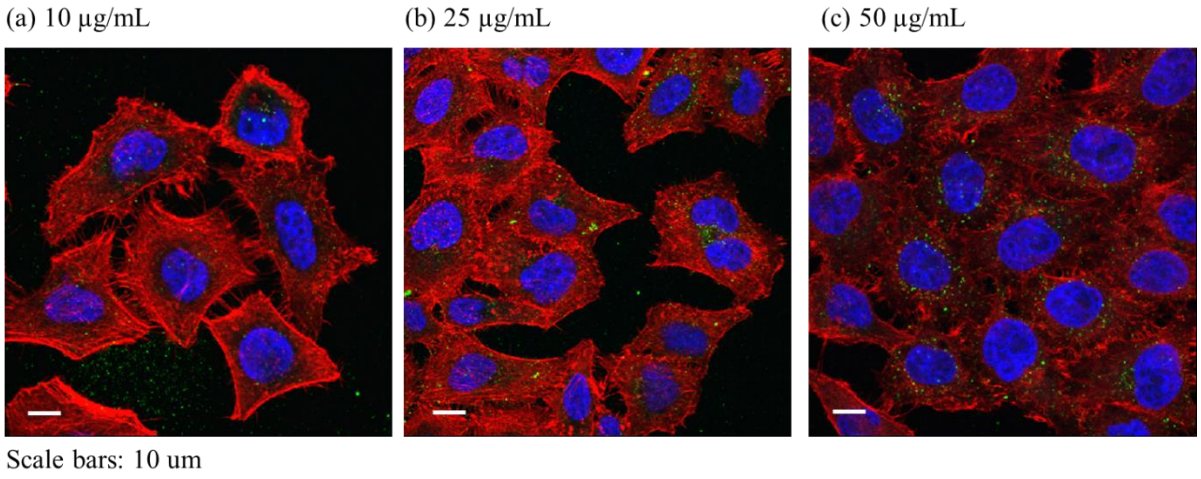

Figure 2.12. Concentration studies on cellular uptake experiments of triblock comicelles based on PFS_{27}-*b*-P(AGE-*g*-TEG/Dye)$_{100}$ with charged segment of b = 27%: (a)10, (b)25, and (c) 50μg/mL. Red indicates phalloidin-594 stained actin filaments in cytoplasm. Blue indicates DAPI stained cell nuclei and green puncta indicate cylindrical micelles.

Water-soluble PFS-based micelles with PNIPAm corona-forming block. Considering the aggregation issues of PFS-*b*-P(AGE-*g*-TEG) micelles, PNIPAm was employed as an alternative corona-forming block for the micelle preparation. PNIPAm is a biocompatible and water-soluble polymer and displays thermoresponsive behaviour which has been widely studied in gels, sensors and drug discovery.[302-304]

The strategy for preparing charged B-A-B triblock co-micelles was applied to PFS_{28}-*b*-$PNIPAm_{494}$ based micelles, where we aimed to form micelles with a consistent overall length, but with different charged-segment length fractions (b) (b aimed for 5, 10, 25 and 50%, respectively). PFS_{25}-*b*-$P2VP_{500}$ was used to prepare the charged terminal segments (B-block). To introduce fluorescence into the micelle, the central neutral segment was formed by seeded-growth of a blend of PFS_{28}-*b*-$PNIPAm_{494}$

and PFS_{27}-*b*-P(AGE-*g*-TEG/Dye)$_{100}$ in a 1:1 mass ratio unimer (in THF) from PFS_{53}-*b*-P(AGE-*g*-TEG)$_{155}$ seeds in MeOH. After aging for 3 days, TEM images (Figure S2.36) showed uniform micelles with controlled length and low length dispersity (L_w/L_n < 1.03). After diluting the samples with *i*-PrOH, PFS_{25}-*b*-$P2VP_{500}$ was added and the samples were aged for 4 days. TEM images (Figure 2.13) showed the well-defined triblock comicelles with controlled length (L_n ca. 170 nm) and low length dispersity (L_w/L_n < 1.04). Methylation of P2VP was carried out by adding Me_2SO_4 (molar ratio at 5:1 of Me_2SO_4 to 2VP) after diluting the samples into H_2O. After dialysis into H_2O, the samples were analysed by TEM. However, fragmentation of micelles was observed (Figure S2.37).

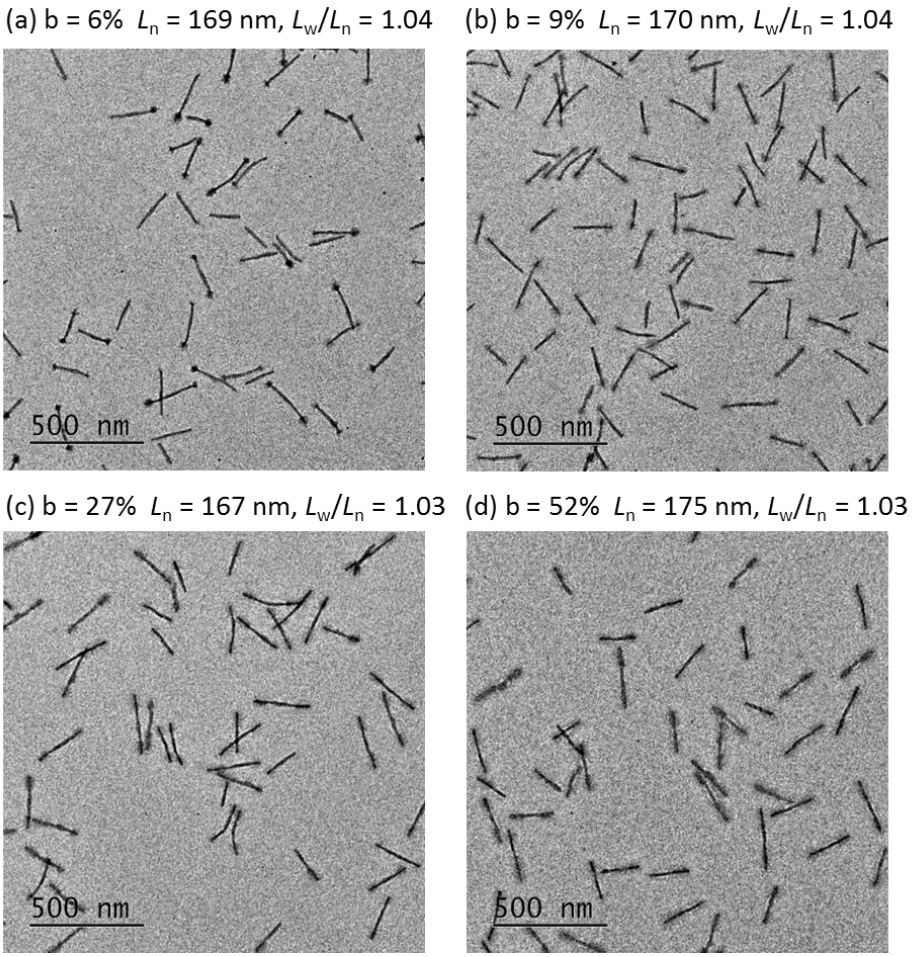

Figure 2.13. TEM images of triblock comicelles prepared by addition of PFS_{25}-*b*-$P2VP_{500}$ (unimer in THF) to central micelles (blend of PFS_{28}-*b*-$PNIPAm_{494}$ and PFS_{27}-*b*-P(AGE-*g*-TEG/Dye)$_{100}$ in a 1:1 mass ratio, in MeOH) in MeOH/*i*-PrOH (1:1) at 23 °C with charged-segment length fractions of (a) b = 6%, (b) b = 9%, (c) b = 27%, (d) b = 52%.

The fragmentation of elongated fibre-like micelles has been reported under various conditions. Swelling of the corona has been proposed as a reason for micelle fragmentation.[166, 305] In a recent study of PCL-*b*-PEG micelles in H_2O, micelle fragmentation was proposed to be caused by PEG swelling and phenol was added into the solution to provide additional insight as a H-bonding promotor.[305] The results suggested that the H-bonding interactions between phenol and PEG caused the swelling of PEG corona, and this stress could be transferred to the PCL core resulting in fragmentation. In another study,[166] when transferring the PCL-*b*-PDMA micelles into H_2O, micelle fragmentation was observed, which was proposed to be a consequence of the swelling of the PDMA corona, which similarly applies stress to the crystalline core and its subsequent fracture. However, in the case of fragmentation of PFS-*b*-PNIPAm micelles in mixture of *i*-PrOH/H_2O (*v*:*v* = 5:95), corona swelling was not suggested as the reason.[306] The authors argued that the corona should contract rather than swell in *i*-PrOH/H_2O due to the cononsolvency effects, where PNIPAm became less solvated in a mixture of *i*-PrOH/H_2O compared with in each individual solvent.[307-309] Thus far the reasons are still under investigation. In our case, fragmentation of micelles was observed upon dialysis, which is similar to the previous reported work.[306]

To prevent the fragmentation, a triblock copolymer was prepared according to a previously reported work.[166] A short block of glassy and hydrophobic polymer (PMMA) was incorporated in between the PFS and PNIPAm blocks to protect the PFS core from the forces caused by coronal swelling. Similar to the preparation mentioned above, the central fluorescent segments were prepared by adding unimer (a blend of PFS_{28}-*b*-$PMMA_6$-*b*-$PNIPAm_{496}$ and PFS_{27}-*b*-P(AGE-*g*-TEG/Dye)$_{100}$ with a mass ratio of 1:1, in THF) to PFS_{53}-*b*-P(AGE-*g*-TEG)$_{155}$ seeds (in MeOH). After aging for 3 days, TEM showed monodispersed cylindrical micelles with controlled length and low length dispersities (L_w/L_n < 1.02) (Figure S2.38). The triblock micelles were prepared by adding PFS_{25}-*b*-$P2VP_{500}$ to the prepared fluorescent micelles. After 4 days aging, TEM image (Figure 2.14) showed the well-defined triblock comicelles with controlled length (L_n ca. 140 nm) and low length dispersity (L_w/L_n < 1.03). After P2VP methylation and dialysis against H_2O, the samples were analysed by TEM. However, fragmentation of micelles was still observed (Figure S2.39). Two reasons are suggested for the fragmentation. One would

be the length of PMMA block, which is too short to provide sufficient protection to the core-forming PFS block. The other one may be the high corona core block length ratio. The long corona-forming block results in a strong force caused by swelling which may lead to fragmentation. The reason for fragmentation has not been fully understood and the phenomenon is still under investigation.

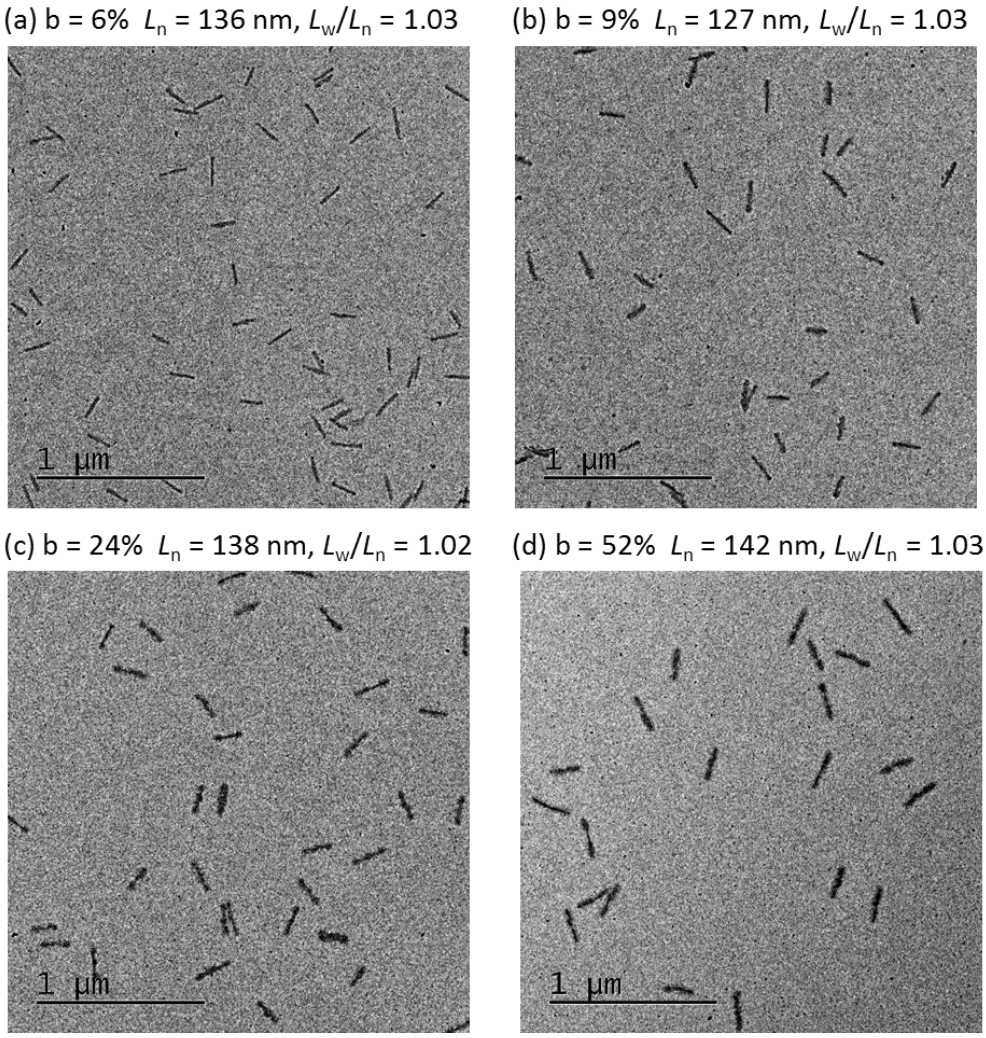

Figure 2.14. TEM images of triblock comicelles prepared by addition of PFS_{25}-*b*-$P2VP_{500}$ (unimer in THF) to central micelles (blend of PFS_{28}-*b*-$PMMA_6$-*b*-$PNIPAm_{496}$ and PFS_{27}-*b*-$P(AGE\text{-}g\text{-}TEG/Dye)_{100}$ in a 1:1 mass ratio, in MeOH) in MeOH/*i*-PrOH (1:1) at 23 °C with charged-segment length fractions of (a) b = 6%, (b) b = 9%, (c) b = 24%, (d) b = 52%.

Water-soluble PFS-*b*-PEG micelles. Following on from the results of PFS-*b*-P(AGE-*g*-TEG) and PFS-*b*-PNIPAm micelles, to prevent the observed aggregation and fragmentation, PEG was employed as water-soluble corona-forming block for micelle preparation. Commercially available methoxy

terminated PEG samples (M_n: 5 and 10 kg/mol) were first modified with a carboxylic acid terminal group and then coupled with hydroxy terminated PFS (PFS-OH) via Steglich esterification reaction to afford PFS-*b*-PEG diblock copolymers, PFS_{28}-*b*-PEG_{120} and PFS_{28}-*b*-PEG_{251} (Scheme S2.2). In the initial preparation of micelles, after adding the unimers (in THF) to PFS_{53}-*b*-P(AGE-*g*-TEG)$_{155}$ seed in MeOH, PFS_{28}-*b*-PEG_{120} showed 2D platelet micelle formation, while PFS_{28}-*b*-PEG_{251} showed uniform 1D micelles (Figure S2.40). The short PEG chains swelled less, resulting in less inter-coronal repulsion compared with the longer chains, which may be the reason for the formation of 2D-like micelles. Therefore, PFS_{28}-*b*-PEG_{251} was used for further micelle preparation for cellular uptake studies. Similar to the previous methods for triblock comicelles preparation, the fluorescent middle segment was prepared by the addition of unimer (a blend of PFS_{28}-*b*-PEG_{251} and PFS_{27}-*b*-P(AGE-*g*-TEG/Dye)$_{100}$ with a mass ratio of 1:1, in THF) to PFS_{53}-*b*-P(AGE-*g*-TEG)$_{155}$ seeds in MeOH (Figure S2.41). After the addition of PFS_{25}-*b*-$P2VP_{500}$ unimers to the central segment micelle solutions, well-defined triblock co-micelles were prepared and shown by TEM (Figure 2.15). After methylation of P2VP, the micelles were dialysed into H_2O with multiple dialysate changes. However, macroscopic precipitation of micelles was observed. The result suggests that PEG_{251} may not be able to provide sufficient colloidally stability for the PFS_{28}-*b*-PEG_{251} micelles in H_2O.

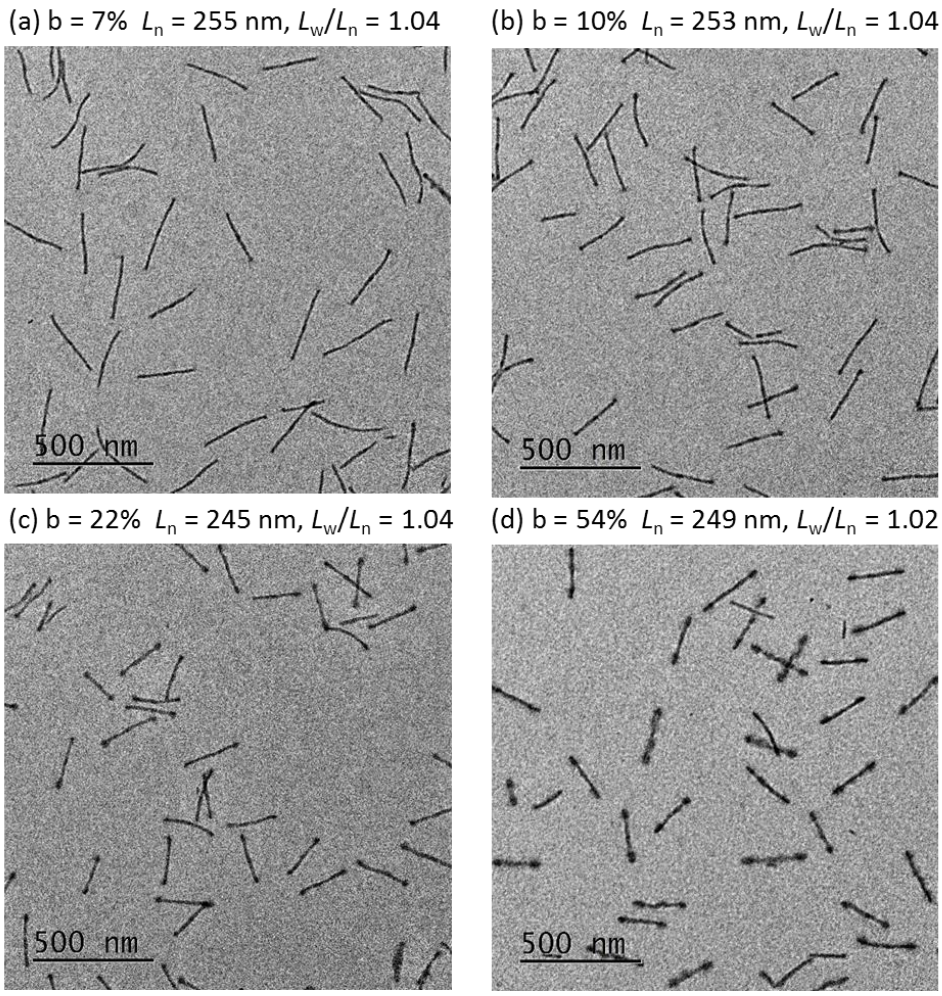

Figure 2.15. TEM images of triblock comicelles prepared by addition of PFS_{25}-*b*-$P2VP_{500}$ (unimer in THF) to central micelles (blend of PFS_{28}-*b*-PEG_{251} and PFS_{27}-*b*-$P(AGE\text{-}g\text{-}TEG/Dye)_{100}$ in a 1:1 mass ratio, in MeOH) in MeOH/*i*-PrOH (1:1) at 23 °C with charged-segment length fractions of (a) b = 7%, (b) b = 10%, (c) b = 22%, (d) b = 54%.

In general, PFS-based micelles have been observed being internalised into HeLa cells, but aggregation issues have not been resolved. More investigations on corona:core block length ratios and appropriate hydrophilic corona-forming blocks are essential to prepare well-dispersed and colloidally stable PFS-based micelles.

2.1.4. 1D PF-based micelles for cellular uptake studies

Preliminary cellular uptake results of PF-*b*-PEG micelles. Due to the inherent fluorescence emission, PF-based micelles are promising for cellular uptake experiments without the need of functionalisation with a fluorescent dye. PF_{13}-*b*-PEG_{227} diblock copolymer was prepared by an azide-alkyne 'click' reaction between an azide terminated PEG and alkyne terminated PF (Scheme S2.3). PF_{13}-*b*-PEG_{227} micelles with an average length of 100 nm were prepared by living CDSA in a mixture of MeOH/THF (1:1) and transferred into H_2O. No fragmentation of the micelles was observed by TEM characterisation. The micelles were than incubated with HeLa cells for 8 hours. The Z-cross images (Figure S2.42) by CLSM showed the micelles were present outside of cells and were not internalised. This may be caused by the neutral surface of PF_{13}-*b*-PEG_{227} micelles, which cannot be easily attached on the negative charged surface of HeLa cells.

Monofunctional PEG for water-soluble micelle preparation. Based on the preliminary results, functionalisation of the PF-*b*-PEG micelle surface with targeting moieties is desirable, which may facilitate the cellular uptake of the micelles. FA and a fluorescent dye (BODIPY 630/650, emission at 650 nm) were employed as functional molecules for micelle surface modification. The PEG chain was functionalised at the terminus with an amine group for the coupling reaction with the *N*-hydroxysuccinimide (NHS) group modified FA and fluorescent dye (Scheme S2.3). FA has been widely studied as a targeting group for cancer cells.[198, 310, 311] If a fluorescent dye molecule (with a different emission wavelength) is attached, the micelle would be dual-fluorescent. Dual-colour fluorescent probes have widespread applications in studying complex biological process (such as tumour angiogenesis and cellular fusion) with improved sensitivity and resolution.[312, 313] The dye functionalised micelles were prepared by adding the unimer (PF_{13}-*b*-PEG_{227}-Dye2, in THF) to the PF_{13}-*b*-PEG_{227}-OH seeds (L_n: 21 nm, L_w/L_n: 1.05, Figure S2.43) in MeOH:THF (*v*:*v* = 6:8) with L_n of 105 nm and L_w/L_n of 1.06 (Figure 2.16a). The FA functionalised micelles were prepared as triblock comicelles. The central segment was prepared by adding unimer (PF_{13}-*b*-PEG_{227}-OH, in THF) to seeds (PF_{13}-*b*-PEG_{227}-OH, in MeOH:THF = 1:1) in MeOH:THF (*v*:*v* = 1:1) (L_n = 21 nm, L_w/L_n = 1.05, Figure 2.16b) After adding

12% DMSO (for FA solubility), PF_{13}-*b*-PEG_{227}-FA unimers (in THF) were added in to afford triblock co-micelles (L_n = 100 nm, L_w/L_n = 1.08) (Figure 2.16c).

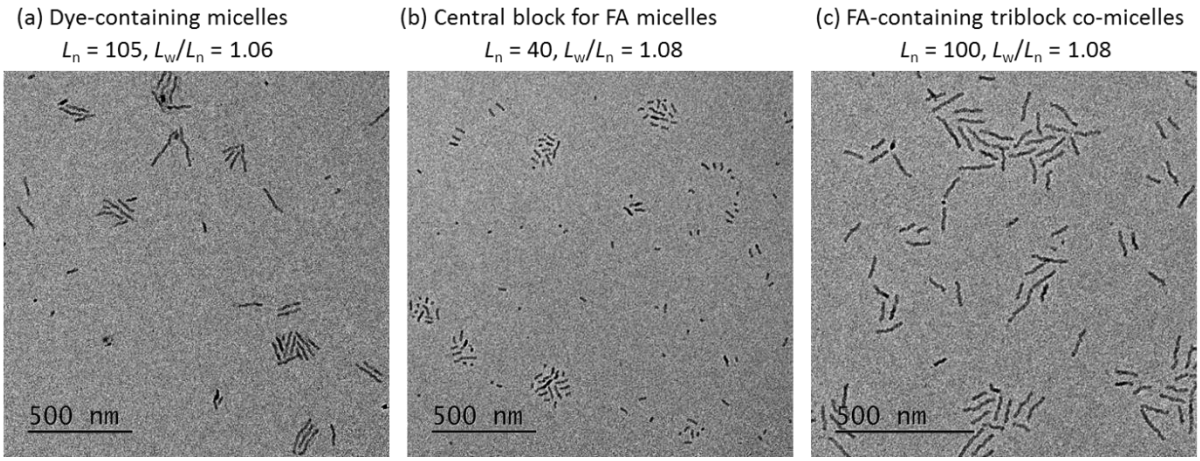

Figure 2.16. TEM images of uniform (a) PF_{13}-*b*-PEG_{227}-Dye2 micelles (L_n = 105 nm, L_w/L_n = 1.06) prepared by addition of PF_{13}-*b*-PEG_{227}-dye2 (unimer in THF) to PF_{13}-*b*-PEG_{227}-OH seed micelles (L_n = 21 nm, L_w/L_n = 1.05, in THF/MeOH (1:1)) in THF/MeOH (5:4) at 23 °C and (b) PF_{13}-*b*-PEG_{227}-FA micelles prepared by addition of PF_{13}-*b*-PEG_{227}-OH (unimer in THF) to PF_{13}-*b*-PEG_{227}-OH seed micelles (L_n = 21 nm, L_w/L_n = 1.05, in THF/MeOH (1:1)) in THF/MeOH (1:1) at 23 °C and followed by addition of PF_{13}-*b*-PEG_{227}-FA (unimer in THF) to PF_{13}-*b*-PEG_{227}-OH micelles (L_n = 21 nm, L_w/L_n = 1.05, in THF/MeOH (1:1)) in THF/MeOH/DMSO (5:4:1) at 23 °C.

The prepared functional micelles were then dialyzed into H_2O and dispersed in cell media. Aggregation studies were carried out by CLSM (Figure S2.44). With the sample containing folic acid, no aggregation of micelles was observed in both H_2O and cell media, which suggested that they could be appropriate for cellular uptake experiments. However, with the sample containing dye molecules, aggregated micelles were observed in both H_2O and cell media. The aggregation of the micelles may be caused by the hydrophobic properties of the dye molecule, or the interactions with the species (such as amino acid) in cell media.

2.2. Summary

We have studied the preparation and applications of 1D fibre-like micelles with PFS- and PF-based diblock copolymers in aqueous media. In the first section, living CDSA of PFS-*b*-P(AGE-*g*-TEG) polymer directly in H_2O was studied. Different factors, such as the weight fractions of the hydrophobic PFS block, common solvent content and temperature were investigated. However, no controlled epitaxial growth of PFS-*b*-P(AGE-*g*-TEG) micelles directly in H_2O has been achieved. Self-nucleation of the unimer and the 'inactivity' of the seeds have been proposed as the reasons for uncontrolled epitaxial growth in H_2O. In general, PFS maybe too hydrophobic to produce well-controlled micelles directly in aqueous media. Controlled living CDSA directly in H_2O might be achieved with other BCPs containing less hydrophobic core-forming blocks.

In the second section, uniform 1D triblock co-micelles based on PFS-*b*-P(AGE-*g*-TEG) with different charged segment lengths based on PFS-*b*-P2VP were prepared, and subsequently transferred into aqueous media. Preliminary cellular uptake experiments showed the internalisation of the cylindrical micelles into HeLa cells. The aggregation of the micelles in H_2O and cell media was proposed as a reason for limited cellular uptake. Moreover, PNIPAm and PEG were employed as water-soluble corona-forming blocks for the micelle preparation. However, fragmentation of PFS-*b*-PNIPAm micelles and precipitation of PFS-*b*-PEG micelles was observed after dialysis of these micelles into H_2O. Furthermore, functional water-soluble PF-based micelles have been prepared with fluorescence dye and folic acid targeting group attached on the surface of the coronal shell (at the termini of the corona-forming block). FA functionalised micelles were well-suited for further biological studies, which are currently ongoing. In addition, dye-containing micelles showed aggregation in both H_2O and cell media. Further studies to target the preparation of well dispersed PFS-based micelles in H_2O with other hydrophilic corona-forming blocks, as well as biomedical applications of functional PF-based 1D fibre-like micelles will be explored.

2.3. Chapter 2 Supplementary Material

2.3.1. Materials and Methods

All reactions were carried out in an MBraun MB150B-G glove box under nitrogen atmosphere or using standard Schlenk line techniques. Glassware were dried in an oven (200 °C) for 16 hours before used for air and H_2O sensitive reactions. Solvents for self-assembly were purchased at HPLC grade and filtered through a PTFE membrane with pore size of 450 nm. Solvents for reactions were obtained from a Grubbs type solvent purification system. All reagents and solvents were purchased from Sigma-Aldrich (UK), Acros, Fluka, Fisher Chemical and Alfa Aesar, and used as received unless otherwise noted. PEG polymer (M_n: 5 and 10 kg/mol) were purified by azeotropic distillation from toluene, followed by drying at 50 °C under reduced pressure over night prior to use. *N*-Isopropylacrylamide (NIPAm) was recrystallised twice from methanol before use. Dioxane and Methyl methacrylate (MMA) were purified by passing through a basic alumina column before use. Naphthalene and AIBN were recrystallised twice from methanol and stored in the dark at 4 °C. Allyl glycidyl ether was dried with CaH_2 and distilled under reduced pressure before use. Benzyl alcohol was dried with Mg at 90 °C, following by distillation before use.

^1H and ^{13}C NMR spectra were obtained using a Varian 400 MHz spectrometer with $CDCl_3$ (^1H NMR: δ = 7.26 ppm; ^{13}C NMR δ = 77.16 ppm) as solvents. and integrations of all peaks were against to TMS standard in NMR solvents.

Gel Permeation Chromatography (GPC) was conducted on a Viscotek VE2001 GPCmax chromatograph equipped with a refractive indices (RI) and a UV detector array. *n*-Bu_4NBr/THF (0.1 w/w %) was used as the eluent, with the flow rate set at 1 mL/min. The columns used were of grade GP5000HHR followed by GP2500HHR (Viscotek) at a constant temperature of 30 °C. The calibration of RI detector was carried out using polystyrene standards (Viscotek). Samples were prepared at 2 mg/mL in eluent and filtered through a Ministart SRP 15 filter (polytetrafluorethylene membrane, pore size = 0.45 µm).

Infrared spectra (IR) were recorded on a Perkin Elmer Spectrum One Fourier Transform Infrared Spectrometer (FT-IR).

Dynamic light scattering (DLS) was employed to determine the size of micelles formed in selective solvents. The measurements were performed on a Malvern Instruments Zetasizer Nano S using a 5 mW He−Ne laser (633 nm) at 25 °C. Samples (1 mL) were measured in an optical glass cuvette (10.0 mm path length) with a concentration of 0.05 mg/mL.

Transmission Electron Microscopy **(**TEM**)** images were obtained on a JEOL 1400 microscope with a SIS MegaViewIII digital camera, which was operated at 120 kV. Samples were prepared by drop casting 4 μL of the micelle solution onto a carbon coated copper grid. Copper grids (400 mesh) were purchased from Agar Scientific and carbon films were prepared on mica sheets by carbon sputtering with an Agar TEM Turbo Carbon Coater. The carbon films were deposited onto the copper grids by floatation on H2O and the carbon coated grids were allowed to dry in air. Samples were stained with uranyl acetate solution (2% wt in EtOH).

For micelle contour lengths analysis, ca. 200 micelles in several images were traced manually using the ImageJ software package developed at the US National Institute of Health. The number average micelle length (L_n) and weight average micelle length (L_w) were calculated using eq. S1 from measurements of the contour lengths (L_i) of individual micelles, where N_i is the number of micelles of length L_i, and n is the number of micelles examined in each sample. The distribution of micelle lengths is characterised by both L_w/L_n.

$$L_n = \frac{\sum_{i=1}^{n} N_i L_i}{\sum_{i=1}^{n} Ni} \qquad L_w = \frac{\sum_{i=1}^{n} N_i L_i^2}{\sum_{i=1}^{n} Ni} \qquad \text{(eq. S1)}$$

Confocal Laser Scanning Microscopy (CLSM). Confocal imaging was performed using a Leica SP5-AOBS confocal laser scanning microscope, using a 63× oil-immersion lens. Excitation lasers were operated at 488 nm for BODIPY FL, 635 nm for BODIPY 630/650 and 405 nm for PF. Confocal images were obtained using digital detectors with observation windows of 500-570 nm for BODIPY FL, 645-750 nm for BODIPY 630/650 and 415-470 nm for PF.

2.3.2. Synthesis Procedures

Synthesis of Potassium Naphthalenide (ca. 1M in THF)

In an oven-dried Schlenk flask, Potassium metal (3.9 g, 100 mmol) was added to a solution of naphthalene (11 g, 85 mmol) in dry THF (100 mL) under N_2 atmosphere. After stirred for 16 h, the potassium naphthalenide solution (dark green, ca. 1M) was ready and kept in the freezer under N_2 for further reactions.

Synthesis of 2-(2-(2-methoxyethoxy)ethoxy)ethyl 4-methylbenzenesulfonate (TEG-Ts).

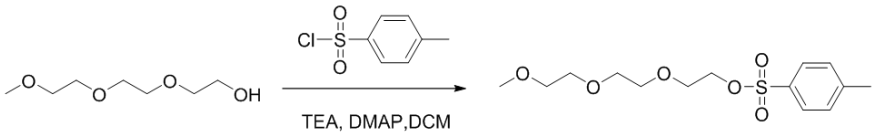

Triethylene glycol monomethyl ether (5 mL, 31 mmol), triethylamine (TEA) (8.7 mL, 62 mmol) and 4-dimethylaminopyridine (DMAP) (0.76 g, 6.2 mmol) were dissolved in dry DCM (100 mL) in a Schlenk flask. The solution was kept stirring at 0 °C for 1 hour before the addition of 4-toluenesulfonyl chloride (6.5 g, 34 mmol). The reaction was stirred for another 16 h before washed with H2O and dried over $MgSO_4$. The organic phase was concentrated to afford the TEG-Ts as a yellow oil (8 g, 82%). ^{1}H NMR ($CDCl_3$, 400 MHz): δ (ppm) 7.77 (m, 2H, Ar), 7.32 (m, 2H, Ar), 4.13 (t, 2H, C$\underline{H_2}$-OTs), 3.67-3.49 (m, 10H, CH_3O-(C$\underline{H_2}$C$\underline{H_2}$O)$_2$-C$\underline{H_2}$-), 3.34 (s, 3H, C$\underline{H_3}$O), 2.42 (s, 3H, Ar-C$\underline{H_3}$). ^{13}C NMR ($CDCl_3$, 100 MHz): δ (ppm) 144.8, 133.1, 129.9 and 128.0 (Ar), 17.9, 70.7, 70.5, 69.3 and 68.7 (C$\underline{H_2}$C$\underline{H_2}$O), 59.1 (C$\underline{H_3}$O), 21.7(Ar-C$\underline{H_3}$). ESI *m/z* ($C_{14}H_{22}O_6S$): $[M]^+$ found 318.11, calc. 318.11.

Synthesis of S-(2-(2-(2-methoxyethoxy)ethoxy)ethyl) ethanethioate (TEG-Thioate).

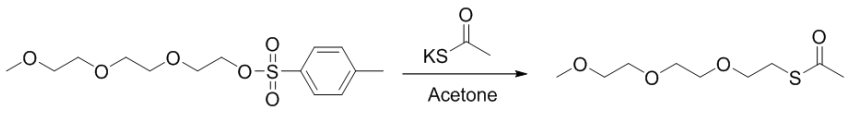

TEG-Ts (7.5 g, 23.6 mmol) was dissolved in acetone (100 mL) in a 250 mL round bottom flask. Potassium thioacetate (3.3 g, 28.3mmol) was added. The reaction was stirred at 50 °C for 16h. After acetone was removed under reduced pressure, the product was diluted in DCM (50 mL) and washed

with brine (3 × 30 mL). The organic phase was dried over $MgSO_4$ and concentrated to give TEG-thioate as a light yellow oil (5.2 g, 99%). ^{1}H NMR ($CDCl_3$, 400 MHz): δ (ppm) 3.65-3.55 (m, 10H, CH_3O-($C\underline{H_2}C\underline{H_2}O)_2$-$C\underline{H_2}$-), 3.38 (s, 3H, $C\underline{H_3}O$), 3.09 (t, 2H, $C\underline{H_2}$-S), 2.33 (s, 3H, S-C(O)-$C\underline{H_3}$). ^{13}C NMR ($CDCl_3$, 100 MHz): δ (ppm) 195.7 (CO), 72.1, 70.7, 70.6, 70.4 and 69.9 ($\underline{C}H_2\underline{C}H_2O$), 59.2 ($\underline{C}H_3O$), 30.7 ($\underline{C}H_2$-S), 28.9 (S-C(O)-$\underline{C}H_3$). ESI *m/z* ($C_9H_{18}O_4S$): $[M]^+$ found 222.09, calc. 222.09.

Synthesis of 2-(2-(2-methoxyethoxy)ethoxy)ethane-1-thiol (TEG-SH).

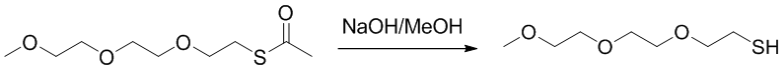

It is recommended to prepare the thiol immediately before its use otherwise it could react to form disulfides. In a 50 mL Schlenk flask, NaOH (0.6 g, mmol) was dissolved in MeOH (15 mL) to give a solution (1M) of NaOMe. TEG-thioate (1g, 4.5 mmol) was dissolved in 10 ml of MeOH in another 100 ml round bottom flask with a stirrer bar. Both flasks were sealed with septum and purged with N_2 for 30 min. NaOMe solution (10 mL) was transferred to the TEG-thioate solution via a cannula. The reaction was stirred for 45 min. In the meantime, a HCl solution (10 mL, 1M) was purged with N_2 in a third 50 ml Schlenk flask sealed with a septum. After 45 minutes the HCl solution was transferred to the reaction mixture using a cannula. The reaction solution was further stirred for 10 min before extracted with DCM. The organic phase was combined, dried over Mg_2SO_4 and concentrated to give TEG-SH as a clear oil (0.77 g, 95%). ^{1}H NMR ($CDCl_3$, 400 MHz): δ (ppm) 3.64-3.55 (m, 10H, CH_3O-($C\underline{H_2}C\underline{H_2}O)_2$-$C\underline{H_2}$-), 3.37 (s, 3H, $C\underline{H_3}O$), 2.69 (q, 2H, $C\underline{H_2}$-SH), 1.58 (t, 3H, SH). ^{13}C NMR ($CDCl_3$, 100 MHz): δ (ppm) 73.1, 72.1, 70.7, 70.6 and 70.4 ($\underline{C}H_2\underline{C}H_2O$), 59.2 ($\underline{C}H_3O$), 34.4 ($\underline{C}H_2$-S). ESI *m/z* ($C_9H_{18}O_4S$): $[M]^+$ found 180.08, calc. 180.08.

Synthesis of 4-cyano-4-(((phenethylthio)carbonothioyl)thio)pentanoic acid (CTA-COOH). Following previously reported procedures, in an oven-dried round bottom flask, 2-Phenylethanethiol (4.0 mL, 29.86 mmol) was added dropwise to a stirred suspension of K_3PO_4 (8.0 g, 37.69 mmol) in acetone (20 mL) and stirred for 1 h. CS_2 (5.5 mL, 91.45 mmol) was added and the solution turned bright yellow. After stirring for 16 h, the suspension was filtered, and the cake was washed with acetone

(2 × 20 mL). After removing the solvents from the filtrate under reduced pressure, the resulting yellow solid was suspended in diethyl ether (100 mL). Solid iodine (3.2 g, 12.61 mmol) was gradually added and then stirred at room temperature for 1 h, and the insoluble white precipitate was removed by filtration. The yellow-brown filtrate was washed with an aqueous solution of sodium thiosulfate, dried over magnesium sulfate, and then evaporated to yield yellow solid. 4,4'-azobis(4-cyanopentanoic acid) (ACVA) (5.1 g, 17.90 mmol) was added to a solution of the solid in ethyl acetate (50 mL). The solution was degassed by nitrogen bubbling for 30 min and heated at reflux under nitrogen for 16 h. After removal of the solvents under reduced pressure, the crude product was washed with H_2O (5 × 100 mL). The organic phase was concentrated and purified by silica chromatography using a mixed eluent (hexane: ethyl acetate = 4:1, gradually increasing to 1:1) to afford CTA-COOH as an orange oil (4.3 g, 44%). ^{1}H NMR (400 MHz, $CDCl_3$, 298 K): δ (ppm) 7.4-7.2 (m, 5H, Ph), 3.60 (t, 2H, $PhCH_2C\underline{H_2}$), 3.00 (t, 2H, $PhC\underline{H_2}$), 2.70 (t, 2H, $C\underline{H_2}COOH$), 2.6-2.4 (m, 2H, $CNCC\underline{H_2}$), 1.90 (s, 3H, CH_3). ^{13}C NMR (125 MHz, $CDCl_3$, 298 K): δ (ppm) 216.5 ($\underline{C}$=S), 177.2 ($\underline{C}$=O), 139.2, 128.9, 128.6, and 126.9 (Ph), 118.9 (CN), 46.4 ($\underline{C}CN$), 38.1 ($\underline{C}H_2CS$), 34.2 ($Ph\underline{C}H_2$), 33.6 ($CNC\underline{C}H_2$), 29.6 ($\underline{C}H_2COOH$), 24.9 ($\underline{C}H_3$).

Synthesis of FA-NHS ester. To a solution of FA (1 g, 2.3 mmol) in degassed DMSO (4 mL), NHS (800 mg, 6.9 mmol), DCC (523 mg, 2.3 mmol) and DMAP (28 mg, 0.23 mmol) were added. The reaction mixture was stirred at 23 °C for 36 h in dark. Following the filtration, the reaction solution was poured into a mixture of acetone/diethyl ether (3:7) and stirred for 1 h. The yellow precipitate was collected and washed with acetone/diethyl ether solution to afford the product as a yellow solid (1.5 g, 88%). ^{1}H NMR (400 MHz, DMSO-d_6, 298 K): δ (ppm) 8.6 (s, 1H, Ar), 7.61 (d, 2H, Ar), 6.60 (d, 2H, Ar), 4.45-4.26 (m, 3H, $C\underline{H_2}$-NH and C$\underline{H}$-NH), 2.46 (m, 4H, $C\underline{H_2}$ of NHS), 2.28 (m, 2H, $C\underline{H_2}$-COOH), 2.03-1.83 (m, 2H, $C\underline{H_2}CH_2$-COOH).

Synthesis of PFS-vinyl homopolymers. PFS_{28}-vinyl was used as an example for the typical procedure of preparing PFS homopolymers. In a glove box, to a vigorously stirred solution of dimethylsila[1]ferrocenophane (400 mg, 1.65 mmol) in dry THF (3 mL) in a Schlenk flask, 1.6 M *n*-butyllithium (*n*-BuLi) in hexane (36.8 µL, 59 µmol) was added in one portion. The reaction mixture

was stirred for 1 h and removed from the glove box. After setting up the reaction flask under a nitrogen atmosphere with a Schlenk line, the reaction was quenched with an excess of chlorodimethylvinylsilane. The reaction solution was precipitated in methanol (3 × 30 mL) and dried in vacuo to afford the polymer as an orange solid (390 mg, 97%, 82% end group functionalisation by ^{1}H NMR).^{1}H NMR (400 MHz; CD_2Cl_2): δ (ppm) 6.29 (dd, 1H, C<u>H</u>=CH_2), 5.99 (dd, 1H, CH=CH<u>H</u>-cis), 5.70 (dd, 1H, CH=CH<u>H</u>trans), 4.23 (m, 112H, Cp), 4.03 (m, 112H, Cp), 0.47 (s, 162H, FcSi(C<u>H</u>$_3$)$_2$), 0.29 (s, 6H, Si(C<u>H</u>$_3$)$_2$), 0.21 (s, 6H, Si(C<u>H</u>$_3$)$_2$). MALDI *m/z*: $[M]^+$ found: 6902.11, DP_n: 28. GPC (*n*-Bu_4NBr/THF, PS standard): M_n = 5942 g/mol, $Đ_m$ = 1.13.

For PFS_8-vinyl: 368 mg, 92%. (92% end group functionalisation). ^{1}H NMR (400 MHz; CD_2Cl_2): δ (ppm) 6.29 (dd, 0.92H, C<u>H</u>=CH_2), 5.99 (dd, 0.98H, CH=CH<u>H</u>-cis), 5.70 (dd, 0.97H, CH=CH<u>H</u>trans), 4.23 (m, 32H, Cp), 4.03 (m, 32H, Cp), 1.32 (m, 4H, $CH_3C\underline{H}_2C\underline{H}_2CH_2$-Si), 0.88 (t, 3H, C<u>H</u>$_3$-CH_2), 0.65 (m, 2H, $CH_3CH_2CH_2C\underline{H}_2$-Si), 0.47 (s, 42H, FcSi(C<u>H</u>$_3$)$_2$), 0.29 (s, 6H, Si(C<u>H</u>$_3$)$_2$), 0.21 (s, 6H, Si(C<u>H</u>$_3$)$_2$). MALDI *m/z*: $[M]^+$ found: 2083.25, DP_n: 8.

For PFS_{10}-vinyl: 387 mg, 97%. (98% end group functionalisation). ^{1}H NMR (400 MHz; CD_2Cl_2): δ (ppm) 6.29 (dd, 0.98H, C<u>H</u>=CH_2), 5.99 (dd, 1.03H, CH=CH<u>H</u>-cis), 5.70 (dd, 1.02H, CH=CH<u>H</u>trans), 4.23 (m, 40H, Cp), 4.03 (m, 40H, Cp), 0.47 (s, 53H, FcSi(C<u>H</u>$_3$)$_2$), 0.29 (s, 6H, Si(C<u>H</u>$_3$)$_2$), 0.21 (s, 6H, Si(C<u>H</u>$_3$)$_2$). MALDI *m/z*: $[M]^+$ found: 2564.15, DP_n: 10. GPC (*n*-Bu_4NBr/THF, PS standard): M_n = 3017 g/mol, $Đ_m$ =1.13.

For PFS_{27}-vinyl: 392 mg, 98%. (91% end group functionalisation). ^{1}H NMR (400 MHz; CD_2Cl_2): δ (ppm) 6.29 (dd, 0.91H, C<u>H</u>=CH_2), 5.99 (dd, 1.14H, CH=CH<u>H</u>-cis), 5.70 (dd, 0.95H, CH=CH<u>H</u>trans), 4.23 (m, 108H, Cp), 4.03 (m, 108H, Cp), 0.47 (s, 164H, FcSi(C<u>H</u>$_3$)$_2$), 0.29 (s, 6H, Si(C<u>H</u>$_3$)$_2$), 0.21 (s, 6H, Si(C<u>H</u>$_3$)$_2$). MALDI *m/z*: $[M]^+$ found: 6742.91, DP_n: 27. GPC (*n*-Bu_4NBr/THF, PS standard): M_n = 6915 g/mol, $Đ_m$ =1.12.

For PFS_{53}-vinyl: 397 mg, 99%. (70% end group functionalisation). ^{1}H NMR (400 MHz; CD_2Cl_2): δ (ppm) 6.29 (dd, 0.70H, C<u>H</u>=CH_2), 5.99 (dd, 0.89H, CH=CH<u>H</u>-cis), 5.70 (dd, 0.74H, CH=CH<u>H</u>trans), 4.23 (m, 212H, Cp), 4.03 (m, 212H, Cp), 0.47 (s, 313H, FcSi(C<u>H</u>$_3$)$_2$), 0.29 (s, 6H, Si(C<u>H</u>$_3$)$_2$), 0.21 (s,

6H, Si(C$\underline{H}_3$)$_2$). MALDI *m/z*: $[M]^+$ found: 12939.35, DP_n: 53. GPC (*n*-Bu_4NBr/THF, PS standard): M_n = 10694 g/mol, $Đ_m$ =1.08.

Synthesis of PFS-OH homopolymers. PFS_{28}-OH is used here as an example for the typical procedure of preparing PFS-OH homopolymers. To a solution of PFS_{28}-vinyl (300 mg, 43 μmol) in dry THF (3 mL) in a Schleck flask, 2,2-dimethoxy-2-phenylacetophenone (DMPA) (1.0 mg, 3.9 μmol) and 2-mercaptoethanol (50 μL, 700 μmol, approx. 15 equiv.) was added under N_2 atmosphere. After freeze-pump-thaw three times, the reaction mixture was irradiated 3 cm away from a mercury lamp for 1 h at 23 °C. The reaction solution was precipitated in methanol (3 × 30 mL) and dried in vacuo to afford the polymer as an orange solid (289 mg, 96%). ^{1}H NMR (400 MHz; CD_2Cl_2): δ (ppm) 4.23 (m, 112H, Cp), 4.03 (m, 112H, Cp), 0.47 (s, 163H, FcSi(C$\underline{H}_3$)$_2$), 0.29 (s, 6H, Si(C$\underline{H}_3$)$_2$), 0.21 (s, 6H, Si(C$\underline{H}_3$)$_2$). MALDI *m/z*: $[M]^+$ found: 6978.19, DP_n: 28. GPC (*n*-Bu_4NBr/THF, PS standard): M_n = 6432 g/mol, $Đ_m$ = 1.14.

For PFS_8-OH: 276 mg, 92%. ^{1}H NMR (400 MHz; CD_2Cl_2): δ (ppm) 4.23 (m, 32H, Cp), 4.03 (m, 32H, Cp), 3.64 (t, 2H, C$\underline{H}_2$-OH), 2.68 (t, 2H, CH_2-S-C$\underline{H}_2$), 2.55 (t, 2H, C$\underline{H}_2$-S-CH_2), 1.32 (m, 4H, $CH_3C\underline{H}_2C\underline{H}_2CH_2$-Si), 0.88 (t, 3H, C$\underline{H}_3$-$CH_2$), 0.65 (m, 2H, $CH_3CH_2CH_2C\underline{H}_2$-Si), 0.47 (s, 42H, FcSi(C$\underline{H}_3$)$_2$), 0.29 (s, 6H, Si(C$\underline{H}_3$)$_2$), 0.21 (s, 6H, Si(C$\underline{H}_3$)$_2$). MALDI *m/z*: $[M]^+$ found: 2079.29, DP_n: 8. GPC (*n*-Bu_4NBr/THF, PS standard): M_n = 1759 g/mol, $Đ_m$ =1.09.

For PFS_{10}-OH: 273 mg, 91%. ^{1}H NMR (400 MHz; CD_2Cl_2): δ (ppm) 4.23 (m, 40H, Cp), 4.03 (m, 40H, Cp), 3.64 (t, 2H, C$\underline{H}_2$-OH), 2.68 (t, 2H, CH_2-S-C$\underline{H}_2$), 2.55 (t, 2H, C$\underline{H}_2$-S-CH_2), 1.32 (m, 4H, $CH_3C\underline{H}_2C\underline{H}_2CH_2$-Si), 0.88 (t, 3H, C$\underline{H}_3$-$CH_2$), 0.65 (m, 2H, $CH_3CH_2CH_2C\underline{H}_2$-Si), 0.47 (s, 54H, FcSi(C$\underline{H}_3$)$_2$), 0.29 (s, 6H, Si(C$\underline{H}_3$)$_2$), 0.21 (s, 6H, Si(C$\underline{H}_3$)$_2$). MALDI *m/z*: $[M]^+$ found: 2641.45, DP_n: 10. GPC (*n*-Bu_4NBr/THF, PS standard): M_n = 3259 g/mol, $Đ_m$ =1.16.

For PFS_{27}-OH: 285 mg, 95%. (91% end group functionalisation). ^{1}H NMR (400 MHz; CD_2Cl_2): δ (ppm) 4.23 (m, 108H, Cp), 4.03 (m, 108H, Cp), 0.47 (s, 164H, FcSi(C$\underline{H}_3$)$_2$), 0.29 (s, 6H, Si(C$\underline{H}_3$)$_2$), 0.21 (s, 6H, Si(C$\underline{H}_3$)$_2$). MALDI *m/z*: $[M]^+$ found: 6665.01, DP_n: 27. GPC (*n*-Bu_4NBr/THF, PS standard): M_n = 7150 g/mol, $Đ_m$ =1.12.

For PFS_{53}-OH: 298 mg, 99%. (70% end group functionalisation). ^{1}H NMR (400 MHz; CD_2Cl_2): δ (ppm) 4.23 (m, 212H, Cp), 4.03 (m, 212H, Cp), 0.47 (s, 313H, FcSi($C\underline{H}_3$)$_2$), 0.29 (s, 6H, Si($C\underline{H}_3$)$_2$), 0.21 (s, 6H, Si($C\underline{H}_3$)$_2$). MALDI *m/z*: $[M]^+$ found: 13017.28, DP_n: 53. GPC (*n*-Bu_4NBr/THF, PS standard): M_n = 10840 g/mol, $Đ_m$ =1.11.

Synthesis of PFS-*b*-PAGE diblock polymers. PFS_{28}-*b*-$PAGE_{259}$ is used here as an example for the typical procedure of preparing PFS-*b*-PAGE diblock polymers. In a glove box, to a solution of PFS_{28}-OH (80 mg, 11.8 μmol) in dry THF (3 mL) in a Schlenk flask, potassium naphthalendie solution (prepared as ca. 1M in THF) was added dropwise until the solution turned dark green and the colour did not fade after 30 s. Allyl glycidyl ether (500 μl, 4.2 mmol) was added into the dark green solution and after which the colour faded immediately. The reaction mixture was then removed from the glove box and stirred at 37 °C for 24 hours under N_2, followed by precipitation in hexane (3 × 30 mL). The crude product was purified by silica chromatograph using a mixed eluent (DCM:MeOH = 10:0, gradually increasing to 9:1) to afford pure PFS_{28}-*b*-$PAGE_{259}$ as a waxy orange oil (312 mg, 65%). ^{1}H NMR (400 MHz; CD_2Cl_2): δ (ppm) 5.96-5.87 (m, 259 H, C$\underline{H}$=CH_2 of PAGE), 5.25-5.15 (m, 509 H, CH=C$\underline{H}_2$ of PAGE), 4.23 (m, 112H, Cp), 4.03 (m, 112H, Cp), 3.99 (d, 521 H, C$\underline{H}_2$-CH=CH_2 of PAGE), 3.63-3.46 (m, 1327 H, C$\underline{H}_2$-C$\underline{H}$(O)-C$\underline{H}_2$ of PAGE backbone), 0.47 (s, 160H, FcSi($C\underline{H}_3$)$_2$), 0.29 (s, 6H, Si($C\underline{H}_3$)$_2$), 0.21 (s, 6H, Si($C\underline{H}_3$)$_2$). M_n = 36343 g/mol. GPC (*n*-Bu_4NBr/THF, PS standard): M_n = 19489 g/mol, $Đ_m$ = 1.13.

For PFS_8-*b*-$PAGE_{115}$: 105 mg, 55%. ^{1}H NMR (400 MHz; CD_2Cl_2): δ (ppm) 5.95-5.85 (m, 115 H, C$\underline{H}$=CH_2 of PAGE), 5.28-5.13 (m, 291 H, CH=C$\underline{H}_2$ of PAGE), 4.23 (m, 32H, Cp), 4.03-3.97 (m, 266H, Cp and C$\underline{H}_2$-CH=CH_2 of PAGE), 3.58-3.45 (m, 634 H, C$\underline{H}_2$-C$\underline{H}$(O)-C$\underline{H}_2$ of PAGE backbone), 0.47 (s, 43H, FcSi($C\underline{H}_3$)$_2$), 0.29 (s, 6H, Si($C\underline{H}_3$)$_2$), 0.21 (s, 6H, Si($C\underline{H}_3$)$_2$). M_n = 15063 g/mol. GPC (*n*-Bu_4NBr/THF, PS standard): M_n = 11005 g/mol, $Đ_m$ = 1.11.

For PFS_{10}-*b*-$PAGE_{104}$: 111 mg, 69%. ^{1}H NMR (400 MHz; CD_2Cl_2): δ (ppm) 5.95-5.85 (m, 104 H, C$\underline{H}$=CH_2 of PAGE), 5.28-5.13 (m, 274 H, CH=C$\underline{H}_2$ of PAGE), 4.23 (m, 40H, Cp), 4.03-3.97 (m, 247H, Cp and C$\underline{H}_2$-CH=CH_2 of PAGE), 3.58-3.45 (m, 524 H, C$\underline{H}_2$-C$\underline{H}$(O)-C$\underline{H}_2$ of PAGE backbone), 0.47 (s,

53 H, FcSi(C$\underline{H}_3$)$_2$), 0.29 (s, 6H, Si(C$\underline{H}_3$)$_2$), 0.21 (s, 6H, Si(C$\underline{H}_3$)$_2$). M_n = 14292 g/mol. GPC (*n*-Bu$_4$NBr/THF, PS standard): M_n = 9470 g/mol, $Đ_m$ =1.16.

For PFS$_{27}$-*b*-PAGE$_{100}$: 120 mg, 67%. ^{1}H NMR (400 MHz; CD_2Cl_2): δ (ppm) 5.95-5.85 (m, 100 H, C$\underline{H}$=CH$_2$ of PAGE), 5.28-5.13 (m, 200 H, CH=C$\underline{H}_2$ of PAGE), 4.23 (m, 108H, Cp), 4.03-3.97 (m, 303H, Cp and C$\underline{H}_2$-CH=CH$_2$ of PAGE), 3.58-3.45 (m, 524 H, C$\underline{H}_2$-C$\underline{H}$(O)-C$\underline{H}_2$ of PAGE backbone), 0.47 (s, 152 H, FcSi(C$\underline{H}_3$)$_2$), 0.29 (s, 6H, Si(C$\underline{H}_3$)$_2$), 0.21 (s, 6H, Si(C$\underline{H}_3$)$_2$). M_n = 17952 g/mol. GPC (*n*-Bu$_4$NBr/THF, PS standard): M_n = 8666 g/mol, $Đ_m$ =1.24.

For PFS$_{53}$-*b*-PAGE$_{155}$: 144 mg, 52%. ^{1}H NMR (400 MHz; CD_2Cl_2): δ (ppm) 5.95-5.85 (m, 155 H, C$\underline{H}$=CH$_2$ of PAGE), 5.28-5.13 (m, 310 H, CH=C$\underline{H}_2$ of PAGE), 4.23 (m, 212H, Cp), 4.03-3.97 (m, 524H, Cp and C$\underline{H}_2$-CH=CH$_2$ of PAGE), 3.58-3.45 (m, 776 H, C$\underline{H}_2$-C$\underline{H}$(O)-C$\underline{H}_2$ of PAGE backbone), 0.47 (s, 310H, FcSi(C$\underline{H}_3$)$_2$), 0.29 (s, 6H, Si(C$\underline{H}_3$)$_2$), 0.21 (s, 6H, Si(C$\underline{H}_3$)$_2$). M_n = 30562 g/mol. GPC (*n*-Bu$_4$NBr/THF, PS standard): M_n = 24698 g/mol, $Đ_m$ =1.13.

Synthesis of PFS-*b*-PAGE/TEG diblock polymers. PFS$_{28}$-*b*-P(AGE/TEG)$_{259}$ is used here as an example for the typical procedure of preparing PFS-*b*-P(AGE/TEG) diblock polymers. To a solution of PFS$_{28}$-*b*-PAGE$_{259}$ (20 mg, 0.55 μmol, 0.143 mmol vinyl group) in dry THF (3 mL) in a Schleck flask, 2,2-dimethoxy-2-phenylacetophenone (DMPA) (1.0 mg, 3.9 μmol) and TEG-SH (320 μL, 1.78 mmol, approx. 5 equiv. per vinyl group) was added under N_2 atmosphere. After freeze-pump-thaw three times, the reaction mixture was irradiated 3 cm away from a mercury lamp for 1 h at 23 °C. The reaction solution was precipitated in hexane (3 × 30 mL) and dried in vacuo to afford the polymer as an orange solid (35 mg, 75%). ^{1}H NMR (400 MHz; CD_2Cl_2): δ (ppm) 4.23 (m, 112H, Cp), 4.03 (m, 112H, Cp), 3.63-3.49 (m, 4403 H SCH$_2$C$\underline{H}_2$O(C$\underline{H}_2$C$\underline{H}_2$O)$_2$CH$_3$ of TEG and C$\underline{H}_2$OC$\underline{H}_2$C$\underline{H}$(O)C$\underline{H}_2$O of PAGE), 3.34 (s, 777 H, OC$\underline{H}_3$), 2.70-2.60 (m, 964 H, C$\underline{H}_2$SC$\underline{H}_2$), 1.85 (t, 482 H, C$\underline{H}_2$CH$_2$S) 0.47 (s, 162H, FcSi(C$\underline{H}_3$)$_2$), 0.29 (s, 6H, Si(C$\underline{H}_3$)$_2$), 0.21 (s, 6H, Si(C$\underline{H}_3$)$_2$). M_n = 82970 g/mol. GPC (*n*-Bu$_4$NBr/THF, PS standard): M_n = 75963 g/mol, $Đ_m$ =1.35.

For PFS$_8$-*b*-P(AGE/TEG)$_{115}$: 105 mg, 55%. ^{1}H NMR (400 MHz; CD_2Cl_2): δ (ppm) 4.23 (m, 32H, Cp), 4.03 (m, 32H, Cp), 3.63-3.49 (m, 1955 H SCH$_2$C$\underline{H}_2$O(C$\underline{H}_2$C$\underline{H}_2$O)$_2$CH$_3$ of TEG and

$C\underline{H_2}OC\underline{H_2}C\underline{H}(O)C\underline{H_2}O$ of PAGE), 3.34 (s, 345 H, $OC\underline{H_3}$), 2.70-2.60 (m, 460 H, $C\underline{H_2}SC\underline{H_2}$), 1.85 (t, 230 H, $C\underline{H_2}CH_2S$) 0.47 (s, 42H, $FcSi(C\underline{H_3})_2$), 0.29 (s, 6H, $Si(C\underline{H_3})_2$), 0.21 (s, 6H, $Si(C\underline{H_3})_2$). M_n = 35763 g/mol. GPC (*n*-Bu_4NBr/THF, PS standard): M_n = 22908 g/mol, $Đ_m$ = 1.54.

For PFS_{10}-*b*-$P(AGE/TEG)_{104}$: 111 mg, 69%. ^1H NMR (400 MHz; CD_2Cl_2): δ (ppm) 4.23 (m, 40H, Cp), 4.03 (m, 40H, Cp), 3.63-3.46 (m, 1768 H $SCH_2C\underline{H_2}O(C\underline{H_2}C\underline{H_2}O)_2CH_3$ of TEG and $C\underline{H_2}OC\underline{H_2}C\underline{H}(O)C\underline{H_2}O$ of PAGE), 3.34 (s, 312 H, $OC\underline{H_3}$), 2.70-2.60 (m, 392 H, $C\underline{H_2}SC\underline{H_2}$), 1.85 (t, 190 H, $C\underline{H_2}CH_2S$) 0.47 (s, 54H, $FcSi(C\underline{H_3})_2$), 0.29 (s, 6H, $Si(C\underline{H_3})_2$), 0.21 (s, 6H, $Si(C\underline{H_3})_2$). M_n = 33012 g/mol. GPC (*n*-Bu_4NBr/THF, PS standard): M_n = 17546 g/mol, $Đ_m$ = 1.17.

For PFS_{53}-*b*-$P(AGE/TEG)_{155}$: 144 mg, 52%. ^1H NMR (400 MHz; CD_2Cl_2): δ (ppm) 4.23 (m, 212H, Cp), 4.03 (m, 212H, Cp), 3.63-3.46 (m, 2635 H $SCH_2C\underline{H_2}O(C\underline{H_2}C\underline{H_2}O)_2CH_3$ of TEG and $C\underline{H_2}OC\underline{H_2}C\underline{H}(O)C\underline{H_2}O$ of PAGE), 3.34 (s, 645 H, $OC\underline{H_3}$), 2.70-2.60 (m, 620 H, $C\underline{H_2}SC\underline{H_2}$), 1.85 (t, 310 H, $C\underline{H_2}CH_2S$) 0.47 (s, 278 H, $FcSi(C\underline{H_3})_2$), 0.29 (s, 6H, $Si(C\underline{H_3})_2$), 0.21 (s, 6H, $Si(C\underline{H_3})_2$). M_n = 56079 g/mol. GPC (*n*-Bu_4NBr/THF, PS standard): M_n = 51744 g/mol, $Đ_m$ = 1.13.

Synthesis of PFS_{27}-*b*-$P(AGE/TEG/NH_2)_{100}$. To a solution of PFS_{27}-*b*-$PAGE_{100}$ (20 mg, 1.1 μmol, 0.1 mmol vinyl group) in dry THF (3 mL) in a Schleck flask, 2,2-dimethoxy-2-phenylacetophenone (DMPA) (1.0 mg, 3.9 μmol), TEG-SH (89 μL, 0.49 mmol, 5eq. per 98% vinyl group) and cysteamine hydrochloride (1.1 mg, 0.01 mmol, 5 eq. per 2% vinyl group) were added under N_2 atmosphere. After freeze-pump-thaw three times, the reaction mixture was irradiated 3 cm away from a mercury lamp for 1 h at 23 °C. The mixture was then precipitated once in *n*-hexanes with 10% triethylamine and twice more in *n*-hexanes, then dried *in vacuo* to afford pure block copolymer (31 mg, 76%). After the confirmation of full conversion of vinyl groups by ^1H NMR, the product was directly used for next step. At this step, no determination of the percentage incorporation of aminoethanol groups was carried out, due to the signals coalescing with the much greater signals corresponding to the TEG-SH. ^1H NMR (400 MHz; CD_2Cl_2): δ (ppm) 4.23 (m, 108H, Cp), 4.02 (m, 108H, Cp), 3.63-3.49 (m, 1477 H $SCH_2C\underline{H_2}O(C\underline{H_2}C\underline{H_2}O)_2CH_3$ of TEG and $C\underline{H_2}OC\underline{H_2}C\underline{H}(O)C\underline{H_2}O$ of PAGE), 3.34 (s, 255 H, $OC\underline{H_3}$),

2.70-2.60 (m, 329 H, C$\underline{H_2}$SC$\underline{H_2}$), 1.85 (t, 258 H, C$\underline{H_2}$CH$_2$S) 0.47 (s, 162H, FcSi(C$\underline{H_3}$)$_2$), 0.29 (s, 6H, Si(C$\underline{H_3}$)$_2$), 0.21 (s, 6H, Si(C$\underline{H_3}$)$_2$).

Synthesis of PFS$_{27}$-*b*-P(AGE/TEG/Dye)$_{100}$. To a solution of PFS$_{27}$-*b*-P(AGE/TEG/NH$_2$)$_{100}$ (25 mg, 0.7 μmol) in dry THF (3 mL) in a Schleck flask, BODIPY FL NHS ester (1 mg, 2.5 μmol) was added under N_2 atmosphere. The reaction was stirred at 23 °C for 16 h, followed by precipitation in n-hexanes. Until no fluorescent can be detected under UV light in the supernatant, the polymer was dried in vacuo to afford pure block copolymer (20 mg, 80%). ^{1}H NMR (400 MHz; CD_2Cl_2): δ (ppm) 7.12 (s, 3H, Ar*H*), 6.90 (s, 3H, Ar*H*), 6.27 (s, 3H, Ar*H*), 6.14 (s, 3H, Ar*H*), 4.23 (m, 108H, Cp), 4.02 (m, 108H, Cp), 3.63-3.49 (m, 1670 H SCH$_2$C$\underline{H_2}$O(C$\underline{H_2}$C$\underline{H_2}$O)$_2$CH$_3$ of TEG and C$\underline{H_2}$OC$\underline{H_2}$C$\underline{H}$(O)C$\underline{H_2}$O of PAGE), 3.34 (s, 291 H, OC$\underline{H_3}$), 2.71-2.59 (m, 385 H, C$\underline{H_2}$SC$\underline{H_2}$ of TEG and SCH$_2$C$\underline{H_2}$NH$_2$ of cysteamine), 1.85 (t, 200 H, C$\underline{H_2}$CH$_2$S of) 0.47 (s, 162H, FcSi(C$\underline{H_3}$)$_2$), 0.29 (s, 6H, Si(C$\underline{H_3}$)$_2$), 0.21 (s, 6H, Si(C$\underline{H_3}$)$_2$). M_n = 35951 g/mol. GPC (*n*-Bu$_4$NBr/THF, PS standard): M_n = 27800 g/mol, $Đ_m$ = 1.56.

Synthesis of PFS$_{28}$-CTA macroinitiator. To a solution of PFS$_{28}$-OH (100 mg, 14.7 μmol) in dry DCM (3 mL) in a Schleck flask, CTA-COOH (20 mg, 47 μmol), DCC (10 mg, 48 μmol) and DMAP (3 mg, 24 μmol) were added. The reaction mixture was stirred at 23 °C for 36 h. The reaction solution was precipitated in MeOH (3 × 30 mL) and dried under vacuum for 16h to afford the product as an orange solid (95 mg, 89%, 40% end-capped with CTA). ^{1}H NMR (400 MHz; CD_2Cl_2): δ (ppm) 7.31-7.21 (m, 5H, Ar), 4.23 (m, 112H, Cp), 4.02 (m, 112H, Cp), 3.07-3.00 (m, 2H, PhC$\underline{H_2}$), 2.70-2.56 (m, 4H, C$\underline{H_2}$COOH and CNCC$\underline{H_2}$), 1.90 (s, 3H, C$\underline{H_3}$), 0.47 (s, 162H, FcSi(C$\underline{H_3}$)$_2$), 0.29 (s, 6H, Si(C$\underline{H_3}$)$_2$), 0.21 (s, 6H, Si(C$\underline{H_3}$)$_2$). MALDI *m/z*: $[M]^+$ found: 7240.69, DP_n: 28. GPC (*n*-Bu$_4$NBr/THF, PS standard): M_n = 8986 g/mol, $Đ_m$ = 1.16.

Synthesis of PFS$_{28}$-*b*-PNIPAm$_{494}$. PFS$_{28}$-CTA (50 mg, 7 μmol), NIPAm (200 mg, 1.77mmol) and AIBN (0.23 mg, 0.35 mmol) were dissolved in dry THF (3 mL) in a Schlenk flask. The solution was then freeze-pump-thawed four times and heated for 3.5 h at 70 ˚C. The reaction was quenched by immersion of the Schlenk flask in liquid nitrogen and the polymer was precipitated in hexane three times, followed by being dried under vacuum and characterised (180 mg, 72%). ^{1}H NMR (400 MHz,

$CDCl_3$): δ (ppm) 7.0-5.6 (br, 455H, N<u>H</u>-CH-$(CH_3)_2$), 4.23 (s, 112H, Cp), 4.02-3.98 (m, 606H, Cp and NH-C<u>H</u>-$(CH_3)_2$ from PNIPAm), 2.28-0.89 (5883 H, m, C<u>H</u>$_3$ and C<u>H</u>C<u>H</u>$_2$ from PNIPAm), 0.47 (s, 162H, FcSi(C<u>H</u>$_3$)$_2$), 0.29 (s, 6H, Si(C<u>H</u>$_3$)$_2$), 0.21 (s, 6H, Si(C<u>H</u>$_3$)$_2$). M_n = 62681 g/mol. GPC (*n*-Bu_4NBr/THF, PS standard): M_n = 112512 g·mol^{-1}, $Đ_m$ = 1.28.

Synthesis of PFS_{28}-*b*-$PMMA_6$. PFS_{28}-CTA (100 mg, 15 μmol), MMA (18 μL, 150 μmol) and AIBN (0.5 mg, 3 μmol) were dissolved in dry THF (3 mL) in a Schlenk flask. The solution was then freeze-pump-thawed four times and heated for 2 h at 70 ˚C. The reaction was quenched by immersion of the Schlenk flask in liquid nitrogen and the polymer was precipitated in hexane three times, followed by being dried under vacuum and characterised (55 mg, 45%). ^{1}H NMR (400 MHz, $CDCl_3$): δ (ppm) 7.32-7.22 (m, 5H, Ar), 4.23 (m, 112H, Cp), 4.02 (m, 112H, Cp), 3.58 (s, 18H, OC<u>H</u>$_3$ of PMMA), 1.86 (m, 18H, CHC<u>H</u>$_3$ of PMMA), 0.47 (s, 162H, FcSi(C<u>H</u>$_3$)$_2$), 0.29 (s, 6H, Si(C<u>H</u>$_3$)$_2$), 0.21 (s, 6H, Si(C<u>H</u>$_3$)$_2$). M_n = 7380 g/mol. GPC (*n*-Bu_4NBr/THF, PS standard): M_n = 12358 g·mol^{-1}, $Đ_m$ = 1.21.

Synthesis of PFS_{28}-*b*-$PMMA_6$-*b*-$PNIPAm_{496}$. PFS_{28}-*b*-$PMMA_6$ (50 mg, 7 μmol), NIPAm (400 mg, 3.5 mmol) and AIBN (0.23 mg, 1.4 μmol) were dissolved in dry THF (3 mL) in a Schlenk flask. The solution was then freeze-pump-thawed four times and heated for 3.5 h at 70 ˚C. The reaction was quenched by immersion of the Schlenk flask in liquid nitrogen and the polymer was precipitated in hexane three times, followed by being dried under vacuum and characterised (270 mg, 60%). ^{1}H NMR (400 MHz, $CDCl_3$): δ (ppm) 7.0-5.6 (br, 487H, N<u>H</u>-CH-$(CH_3)_2$), 4.23 (m, 112H, Cp), 4.02-3.98 (m, 606H, Cp and NH-C<u>H</u>-$(CH_3)_2$ from PNIPAm), 3.58 (s, 18H, OC<u>H</u>$_3$ of PMMA), 2.28-0.89 (5469 H, m, C<u>H</u>$_3$, CHC<u>H</u>$_3$ of PMMA and C<u>H</u>C<u>H</u>$_2$ from PNIPAm), 0.47 (s, 162H, FcSi(C<u>H</u>$_3$)$_2$), 0.29 (s, 6H, Si(C<u>H</u>$_3$)$_2$), 0.21 (s, 6H, Si(C<u>H</u>$_3$)$_2$). M_n = 63808 g/mol. GPC (*n*-Bu_4NBr/THF, PS standard): M_n = 198838 g·mol^{-1}, $Đ_m$ = 1.35.

Synthesis of PEG-COOH homopolymers. PEG-COOH (M_n: 5 kg/mol) was used as an example for the typical procedure of preparing PEG-COOH homopolymers. PEG-OH (M_n: 5 kg/mol, 1 g, 0.2 mmol) and succinic anhydride (30 mg, 0.3 mmol) were dissolved in dry DCM (100 mL). The reaction was cooled to 0 °C and kept for 30 min. TEA (41 μL, 0.3 mmol) was added in slowly. The reaction mixture

was stirred for 24 h with a gradually temperature raise to 23 °C. The reaction solution was precipitated in hexane (3 × 30 mL) and dried under vacuum for 16 h to afford the product as white solid (950 mg, 95%). ^{1}H NMR (400 MHz; CD_2Cl_2): δ (ppm) 3.64 (s, 390H, OC$\underline{H}_2$C$\underline{H}_2$), 3.34 (s, 3H, OC$\underline{H}_3$), 2.65 (m, 4H, C(O)OC$\underline{H}_2$C$\underline{H}_2$COOH. MALDI *m/z*: $[M]^+$ found: 5177.35, DP_n: 116. GPC (*n*-Bu_4NBr/THF, PS standard): M_n = 6886 g/mol, $Đ_m$ = 1.09.

For PEG-COOH (M_n: 10 kg/mol): 970 mg, 97%. ^{1}H NMR (400 MHz; CD_2Cl_2): δ (ppm) 3.64 (s, 850H, OC$\underline{H}_2$C$\underline{H}_2$), 3.34 (s, 3H, OC$\underline{H}_3$), 2.65 (m, 4H, C(O)OC$\underline{H}_2$C$\underline{H}_2$COOH. MALDI *m/z*: $[M]^+$ found: 9850.50, DP_n: 220. GPC (*n*-Bu_4NBr/THF, PS standard): M_n = 13197 g/mol, $Đ_m$ = 1.14.

Synthesis of PFS-*b*-PEG diblock copolymers. PFS_{28}-*b*-PEG_{120} is used here as an example for the typical procedure of preparing PFS-*b*-PEG diblock polymers. PFS_{28}-OH (100 mg, 15 μmol), PEG-COOH (M_n: 5 kg/mol, 75 mg, 15 mmol), DCC (10 mg, 48 μmol) and DMAP (3 mg, 24 μmol) were dissolved in dry DCM (2 mL). The reaction mixture was stirred at 23 °C for 48 h. The reaction solution was precipitated in hexane (3 × 30 mL) and dried under vacuum for 16 h to afford the product as a light orange solid (150 mg, 85%). ^{1}H NMR (400 MHz; CD_2Cl_2): δ (ppm) 4.23 (m, 112H, Cp), 4.02 (m, 112H, Cp), 3.60 (s, 483H, OC$\underline{H}_2$C$\underline{H}_2$), 3.34 (s, 3H, OC$\underline{H}_3$), 0.47 (s, 162H, FcSi(C$\underline{H}_3$)$_2$), 0.29 (s, 6H, Si(C$\underline{H}_3$)$_2$), 0.21 (s, 6H, Si(C$\underline{H}_3$)$_2$). M_n = 12060 g/mol. GPC (*n*-Bu_4NBr/THF, PS standard): M_n = 17139 g/mol, $Đ_m$ = 1.08.

For PFS_{28}-*b*-PEG_{251}: 140 mg, 70%. ^{1}H NMR (400 MHz; CD_2Cl_2): δ (ppm) 4.23 (m, 112H, Cp), 4.02 (m, 112H, Cp), 3.60 (s, 1006H, OC$\underline{H}_2$C$\underline{H}_2$), 3.34 (s, 3H, OC$\underline{H}_3$), 0.47 (s, 162H, FcSi(C$\underline{H}_3$)$_2$), 0.29 (s, 6H, Si(C$\underline{H}_3$)$_2$), 0.21 (s, 6H, Si(C$\underline{H}_3$)$_2$). M_n = 16780 g/mol. GPC (*n*-Bu_4NBr/THF, PS standard): M_n = 22903 g/mol, $Đ_m$ = 1.08.

Synthesis of alkyne-terminated poly(di-*n*-hexylfluorene) (PF_{13}-alkyne). The alkyne-terminated PF_{13} was synthesised according to a reported procedure.[175] To a solution of 2-Bromo-7-iodo-9,9-bis-n-hexylfluorene (1.00 g, 1.85 mmol) in dry THF, *i*-PrMgCl/LiCl (1:1) (1.45 ml, 1.89 mmol, 1.3 M) was added dropwise at -20 °C. The reaction mixture was stirred for 70 min and warmed up to 23 °C, followed by quickly transfer to a solution of Ni(dppp)Cl_2 (56 mg, 0.103 mmol) in dry THF (100 mL) at 0 °C.

After 10 min, the reaction mixture was quenched with excess of ethynylmagnesium chloride (0.5 M in THF, 3 ml) and stirred for another 60 min. The reaction solution was precipitated in MeOH to afford the PF_{13}-alkyne as a yellow green solid (282 mg, 46%). ^{1}H NMR (400 MHz; CD_2Cl_2): δ (ppm) 7.86-7.84 (m, 26H, Ar), 7.71-7.68 (m, 52H, Ar), 2.14-2.08 (m, 52H, alkyl chain), 1.14-0.78 (m, 260H, alkyl chain). MALDI *m/z*: $[M]^+$ found: 4425.76, DP_n: 13. GPC (*n*-Bu_4NBr/THF, PS standard): M_n = 8470 g/mol, $Đ_m$ = 1.22.

Synthesis of monosubstituted PEG homopolymer (HO-PEG$_{249}$-OTs). Under N_2 atmosphere, PEG (HO-PEG_{249}-OH) (5 g, 0.5 mmol) and TEA (210 uL, 1.5 mmol) was dissolved in dry DCM (100 mL) in a Schlenk flask and cooled to 0 °C. 4-Toluenesulfonyl chloride (TsCl, 40 mg, 0.2 mmol) was dissolved in dry DCM (50 mL) in another Schlenk flask under N_2. The TsCl solution was transferred dropwise into the HO-PEG_{249}-OH solution at 0 °C. The reaction was stirred for 16 h, followed by precipitation in cold diethyl ether. The product was collected as a white powder of a mixture of HO-PEG-OH and HO-PEG-OTs (5 g, 99%). MALDI *m/z*: $[M]^+$ found: 11162.12 (OH-PEG_{249}-OTs), 11007.58 (OH-PEG_{249}-OH). MALDI-TOF MS confirmed the presence of monosubstituted HO-PEG_{249}-OTs and absence of di-substituted OTs-PEG-OTs.

Synthesis of monosubstituted PEG homopolymer (HO-PEG$_{249}$-N$_3$). HO-PEG_{249}-OTs (HO-PEG_{249}-OH) (5 g, 0.5 mmol, ca. 0.1 mmol of OTs) was dissolved in DMF, followed by addition of NaN_3 (32 mg, 0.5 mmol). The reaction was stirred at 80 °C for 16 h. The reaction was precipitated in cold diethyl ether and dried under vacuum. The product was collected as a white powder of a mixture of HO-PEG-OH and HO-PEG-N_3 (5 g, 99%). MALDI *m/z*: $[M]^+$ found: 11077.27 (OH-PEG_{249}-N_3), 11007.58 (OH-PEG_{249}-OH). MALDI-TOF MS confirmed the presence of monosubstituted HO-PEG_{249}-N_3 and absence of di-substituted TsO-PEG_{249}-OTs and monosubstituted HO-PEG_{249}-OTs.

Synthesis of PF$_{13}$-*b*-PEG$_{227}$-OH. To a solution of PF_{13}-alkyne (20 mg, 5 μmol) and PEG-N_3 (mixed with HO-PEG-OH, 500 mg, 50 μmol) in dry THF (3 mL) in a Schlenk flask, a pre-mixed solution (1 mL, in THF) of CuBr (10 mg, 0.07 mmol) and pentamethyldiethylenetriamine (PMDETA, 15 μL, 0.07 mmol) was added in under N_2 atmosphere. The reaction mixture was stirred at 40 °C for 48 h.

Copper/PMDETA complex was removed by passing a basic alumina column. The cured product was precipitated in cold diethyl ether to afford the white solid. The white solid was washed with MeOH to remove excessive HO-PEG-OH. The final product was collected by precipitation in cold diethyl ether as a light yellow solid (35 mg, 50%). ^{1}H NMR (400 MHz; CD_2Cl_2): δ (ppm) 7.86-7.84 (m, 26H, Ar), 7.71-7.68 (m, 52H, Ar), 3.64 (s, 910H, C$\underline{H_2}$C$\underline{H_2}$O of PEG), 2.14-2.08 (m, 52H, alkyl chain), 1.14-0.78 (m, 260H, alkyl chain). M_n = 14316 g/mol. GPC (*n*-Bu_4NBr/THF, PS standard): M_n = 29927 g/mol, $Đ_m$ = 1.12.

Synthesis of PF_{13}-*b*-PEG_{227}-NHBoc. PF_{13}-*b*-PEG_{227}-OH (30 mg, 2.1 μmol), Boc-β-alanine (5 mg, 26 μmol), DCC (10 mg, 21 μmol) and DMAP (3 mg, 24 μmol) were dissolved in dry dry THF (3 mL) in a Schlenk flask. The reaction mixture was stirred at 23 °C for 48 h. The reaction solution was precipitated in hexane (3 × 30 mL) and dried under vacuum for 16h to afford the product as a light yellow solid (30 mg, 99%). ^{1}H NMR (400 MHz; CD_2Cl_2): δ (ppm) 7.86-7.84 (m, 26H, Ar), 7.71-7.68 (m, 52H, Ar), 3.64 (s, 910H, C$\underline{H_2}$C$\underline{H_2}$O of PEG), 2.14-2.08 (m, 52H, alkyl chain), 1.44 (s, 9H, Boc), 1.14-0.78 (m, 260H, alkyl chain). After the confirmation of presence of Boc, the product was used for next step immediately.

Synthesis of PF_{13}-*b*-PEG_{227}-NH_2. To a solution of PF_{13}-*b*-PEG_{227}-NHBoc (30 mg, 2.1 μmol) in dry THF (3 mL) in a Schlenk flask, iodotrimethylsilane (TMSI,) was added under N_2 atmosphere. The reaction mixture was stirred at 23 °C for 2 h. The reaction solution was precipitated in hexane (3 × 30 mL) and then dried under vacuum for 16h to afford a yellow solid (30 mg, 99%). ^{1}H NMR (400 MHz; CD_2Cl_2): δ (ppm) 7.86-7.84 (m, 26H, Ar), 7.71-7.68 (m, 52H, Ar), 3.64 (s, 910H, C$\underline{H_2}$C$\underline{H_2}$O of PEG), 2.14-2.08 (m, 52H, alkyl chain), 1.14-0.78 (m, 260H, alkyl chain). After the confirmation of absence of Boc, the product was used for next step immediately.

Synthesis of functional PF_{13}-*b*-PEG_{227}. PF_{13}-*b*-PEG_{227}-Dye was used as an example for the typical procedure of preparing functional PF-*b*-PEG diblock polymers. PF_{13}-*b*-PEG_{227}-NH_2 (10 mg, 7 μmol) and BODIPY 630/650 NHS ester (5 mg, 7.1 μmol) were dissolved in dry DCM (1 mL). The mixture was stirred at 23 °C for 16 h. The reaction solution was precipitated in hexane until no fluorescent can

be detected under UV light in the supernatant. The polymer was dried in vacuo to afford product as a blue solid (10 mg, 60%). ^{1}H NMR (400 MHz; CD_2Cl_2): δ (ppm) 6.79 (m, 1H, Ar of dye). 6.62 (m, 1H, Ar of dye), 6.39 (m, 1H, Ar of dye), 6.18 (m, 1H, Ar of dye), 7.86-7.84 (m, 26H, Ar), 7.71-7.68 (m, 52H, Ar), 3.64 (s, 910H, C$\underline{H_2}$C$\underline{H_2}$O of PEG), 2.14-2.08 (m, 52H, alkyl chain), 1.14-0.78 (m, 260H, alkyl chain).

For PF_{13}-*b*-PEG_{227}-Folic acid (FA): 10 mg, 77%. ^{1}H NMR (400 MHz; DMSO-d_6): δ (ppm) 8.64 (s, 1H, NH), 7.64 (m, 1H, Ar of FA), 6.63 (m, 1H, Ar of dye), 3.53 (s, 910H, C$\underline{H_2}$C$\underline{H_2}$O of PEG).

2.3.3. Self-Assembly Procedures of PFS-Based Polymers

All solvent compositions are given as volume ratio (*v*:*v*). All micelle length measurements were carried out with 200 micelles. Self-nucleation to form polydisperse micelles were carried out by direct dissolution with heating-cooling method with a heating temperature lower than the solvent boiling point (65 °C for MeOH, 70 °C for DMF, EtOH and *i*-PrOH, and 85 °C for H_2O). Seeded-growth experiments were carried out at 23 °C.

Self-nucleation of PFS-*b*-P(AGE-g-TEG) polymers. Self-assembly of PFS_{53}-*b*-P(AGE-*g*-TEG)$_{155}$ in DMF was used as an example. PFS_{53}-*b*-P(AGE-*g*-TEG)$_{155}$ solid (0.5 mg) was weighed into a vial and directly dissolved in DMF (1 mL) with a concentration at 0.5 mg/mL. The vial was sealed and heated at 70 °C for 2 h, followed by slowly cooling to 23 °C over 2.5 h. The solution was aged for 24 h. The formed polydisperse fibre-like micelles were characterised by TEM.

Similar procedures were used for self-assembly of PFS_{53}-*b*-P(AGE-*g*-TEG)$_{155}$, PFS_{28}-*b*-P(AGE-*g*-TEG)$_{259}$, PFS_{10}-*b*-P(AGE-*g*-TEG)$_{104}$ and PFS_8-*b*-P(AGE-*g*-TEG)$_{115}$ in various solvents. For self-assembly in organic solvents, the concentrations were 0.5 mg/mL, while for H_2O, lower concentrations (0.1 or 0.05 mg/mL) were applied.

Preparation of seed micelles. All seed micelle solutions were prepared by sonication of the polydisperse micelle solutions from self-nucleation of polymer in selective solvents and characterised by TEM.

For PFS_{53}-*b*-P(AGE-*g*-TEG)$_{155}$ seeds (L_n = 23 nm, L_w/L_n = 1.06) in DMF: sonication of PFS_{53}-*b*-P(AGE-*g*-TEG)$_{155}$ polydisperse micelles in DMF was carried out for 2 h in a H_2O sonication bath cooled with ice.

For PFS_{28}-*b*-P(AGE-*g*-TEG)$_{259}$ seeds (L_n = 73 nm, L_w/L_n = 1.07) in MeOH: sonication of PFS_{28}-*b*-P(AGE-*g*-TEG)$_{259}$ polydisperse micelles in MeOH was carried out for 1 h in a dry ice/acetone bath with a ltrasonication probe.

Seeded-growth of PFS-based micelles at 23 °C. Seeded-growth of PFS_{28}-*b*-P(AGE-*g*-TEG)$_{259}$ from PFS_{53}-*b*-P(AGE-*g*-TEG)$_{155}$ seeds was used as an example. PFS_{53}-*b*-P(AGE-g-TEG)$_{155}$ seed micelle solution (10 μL, 0.5 mg/mL, DMF) was diluted in H_2O (200 μL) to which was added PFS_{28}-*b*-P(AGE-*g*-TEG)$_{259}$ unimer (2.5 μL, 10 mg/mL in THF, m_{unimer}:m_{seed} = 5). The resulting solution was then manually shaken for 10 s and aged for 24 h at 23 °C before TEM characterisation. THF content in final solution is less than 3%. To the samples with THF content of 10%, the seed was diluted in THF/H_2O (1:9) directly.

Similar procedures were used for seeded-growth of PFS_{10}-*b*-P(AGE-*g*-TEG)$_{104}$ and PFS_8-*b*-P(AGE-*g*-TEG)$_{115}$ from PFS_{28}-*b*-P(AGE-*g*-TEG)$_{259}$ seed micelles in various solvents.

Seeded-growth of PFS-based micelles at elevated temperatures. The procedure of seeded-growth of PFS_{10}-*b*-P(AGE-*g*-TEG)$_{104}$ from PFS_{28}-*b*-P(AGE-*g*-TEG)$_{259}$ seeds was used as an example. Both the PFS_{10}-*b*-P(AGE-*g*-TEG)$_{104}$ unimer solution (10 mg/mL in THF) and PFS_{28}-*b*-P(AGE-*g*-TEG)$_{259}$ seed micelle solution (10 μL, 0.5 mg/mL, diluted in 200 μL H_2O) were kept at 40 °C for 30 min. The unimer (2.5 μL, m_{unimer}:m_{seed} = 5) was added to the seed solution at 40 °C. After being kept for another 30 min, the solution was allowed slowly cooling to 23 °C over 1 h. The sample was further aged for 24 h at 23 °C before TEM characterisation. Similar procedure was used for seeded-growth at 50 and 60 °C.

Self-seeding of PFS_{28}-*b*-P(AGE-g-TEG)$_{259}$ micelles. PFS_{28}-*b*-P(AGE-*g*-TEG)$_{259}$ seed micelle solution (10 μL, 0.5 mg/mL, diluted in 200 μL H_2O) were kept at 40 °C for 30 min, followed by slowly cooled

to 23 °C over 1 h. The sample was further aged for 24 h at 23 °C before TEM characterisation. Similar procedure was used for self-seeding at 45, 50 and 55 °C.

Preparation of triblock co-micelles for cellular uptake studies. Procedure of preparing triblock co-micelles with PFS_{27}-*b*-P(AGE-*g*-TEG/Dye)$_{100}$ was used as an example. PFS_{53}-*b*-P(AGE-g-TEG)$_{155}$ seed micelle solution (100 μL, 0.5 mg/mL, DMF) was diluted in MeOH (2 mL) to which was added PFS_{27}-*b*-P(AGE-*g*-TEG/Dye)$_{100}$ unimer (26 μL, 10 mg/mL in THF, m_{unimer}:m_{seed} = 5.2, for aimed b = 5%). The resulting solution was then manually shaken for 10 s and aged for 3 d at 23 °C before TEM characterisation. For aimed b = 10%, 24.5 μL unimer (m_{unimer}:m_{seed} = 4.9) was added; for aimed b =25%, 19.5 μL unimer (m_{unimer}:m_{seed} = 3.9) was added; and for aimed b = 50%, 11.5 μL unimer (m_{unimer}:m_{seed} = 2.3) was added. The calculation was based on the aimed total length of 150 nm and the seed length (L_n = 23 nm).

After adding *i*-PrOH (1 mL) to the prepared fluorescent micelles, PFS_{25}-*b*-$P2VP_{500}$ unimer (3.3 μL, 5 mg/mL in THF, m_{unimer}:m_{seed} = 0.33) was added in. The resulting solution was then manually shaken for 10 s and aged for 3 d at 23 °C before TEM characterisation. For aimed b = 10%, 6.6 μL unimer (m_{unimer}:m_{seed} = 0.66) was added; for aimed b =25%, 16.3 μL unimer (m_{unimer}:m_{seed} = 1.63) was added; and for aimed b = 50%, 32.6 μL unimer(m_{unimer}:m_{seed} = 3.26) was added.

The prepared triblock co-micelle solutions were then diluted with H_2O (2 mL), followed by dialysis against H_2O (resistance 18.2 MΩ·cm at 25 °C) for 2 days with multiple dialysate changes. The solution was concentrated to 660 μL under a stream of N_2 gas to afford triblock comicelles in H_2O with a concentration at ca. 0.5 mg/mL.

Similar procedures were applied to preparation of triblock co-micelles with PFS_{28}-*b*-PEG_{251}, PFS_{28}-*b*-$PNIPAm_{494}$ and PFS_{28}-*b*-$PMMA_6$-*b*-$PNIPAm_{496}$.

2.3.4. Self-Assembly Procedures for PF-Based Micelles.

Self-nucleation of PF_{13}-*b*-PEG_{227}. PF_{13}-*b*-PEG_{227} (100 μL, 10 mg/mL in THF) was diluted in THF (900 μL) and MeOH (1 mL) was added slowly to the THF solution over 10 min at 23 °C. The resulting

solution with a solid concentration of 0.5 mg/mL was manually shaken for 10 s and aged at 23 °C for another 24 h. The formed polydisperse fibre-like micelles were characterised by TEM.

Preparation of PF_{13}-*b*-PEG_{227} seed micelles. PF_{13}-*b*-PEG_{227} polydisperse micelles (in MeOH/THF, 1:1) was sonicated for 3 h in a H_2O sonication bath cooled with ice. The resulting micelle solution was characterised by TEM.

Preparation of dual fluorescent functional PF_{13}-*b*-PEG_{227} micelles. PF_{13}-*b*-PEG_{227} seed micelle solution (400 μL, 0.5 mg/mL, in MeOH/THF, *v*:*v* = 1:1) was diluted in MeOH (600 μL) to which was added THF (720 μL). PF_{13}-*b*-PEG_{227}-dye unimer (80 μL, 10 mg/mL in THF, m_{unimer}:m_{seed} = 4) was added to the diluted seed solution. The resulting solution in MeOH/THF (10:8) was then manually shaken for 10 s and aged for 1 d at 23 °C before TEM characterisation. The prepared micelle solutions were then diluted with H_2O (2 mL), followed by dialysis against H_2O (resistance 18.2 MΩ·cm at 25 °C) for 2 days with multiple dialysate changes. The solution was then concentrated to 1 mL under a stream of N_2 gas to afford dual fluorescent micelles in H_2O with a concentration at ca. 1 mg/mL. The prepared micelles were characterised by TEM and CLSM.

Preparation of FA functionalised PF_{13}-*b*-PEG_{227} micelles.

PF_{13}-*b*-PEG_{227} seed micelle solution (400 μL, 0.5 mg/mL, in MeOH/THF, *v*:*v* = 1:1) was diluted in MeOH (600 μL) to which was added THF (720 μL). PF_{13}-*b*-PEG_{227} unimer (40 μL, 10 mg/mL in THF, m_{unimer}:m_{seed} = 2) was added to the diluted seed solution. The resulting solution in MeOH/THF (10:8) was then manually shaken for 10 s and aged for 24 h at 23 °C. DMSO (200 μL) was then added to the prepared micelle solutions, followed by adding PF_{13}-*b*-PEG_{227}-FA unimers (40 uL, 10mg/mL in DMSO/THF, 1:9). After aging for another 24 h, the prepared micelle solutions were then diluted with H_2O (2 mL), followed by dialysis against H_2O (resistance 18.2 MΩ·cm at 25 °C) for 2 days with multiple dialysate changes. The solution was then concentrated to 1 mL by N_2 blowing to afford dual fluorescent micelles in H_2O with a concentration at 1 mg/mL. The prepared micelles were characterised by TEM and CLSM.

2.3.5. Cellular Uptake Experiments.

HeLa cells were cultured in Dulbecco's Modified Eagle Medium (DMEM; Sigma-Aldrich) supplemented with 10% Foetal Bovine Serum (FBS; Sigma-Aldrich) in a humidified 5% CO_2 incubator at 37°C. Cells were seeded onto glass coverslips in 48-well tissue culture plates at a density of 2×10^4 cells per well and incubated for 24 hours before use. PFS-based cylindrical micelles were diluted to a concentration of 250 μg/mL in DMEM/FBS (10:90). Cells were incubated with diluted micelles for periods of 0.5-8 h as indicated in the figure legends. At the end of the incubation period cells were transferred to ice to prevent further endocytosis of the micelles. Cells were washed twice with ice-cold Phosphate Buffered Saline (PBS) to remove any residual micelles and fixed on ice in 4% paraformaldehyde (PFA) in PBS. All subsequent steps were conducted at room temperature. Following a further three washes with PBS, cell membranes were permeabilised with 0.1% Triton X-100 in PBS for 5 minutes, and non-specific binding blocked with a 30-minute incubation in 5% Bovine Serum Albumin (BSA) in PBS. Cells were incubated with DAPI (to stain the nuclei) and AlexaFluor594-phalloidin (to stain F-actin) in 5% BSA:PBS (5:95) for 1 hour. Unbound stain was removed with three PBS washes. Coverslips were washed in ddH_2O to remove any residual salt, dried, and mounted onto slides using Prolong Diamond anti-fade mountant (Invitrogen). Cells were characterised by CLSM.

2.3.6. Supplementary Figures

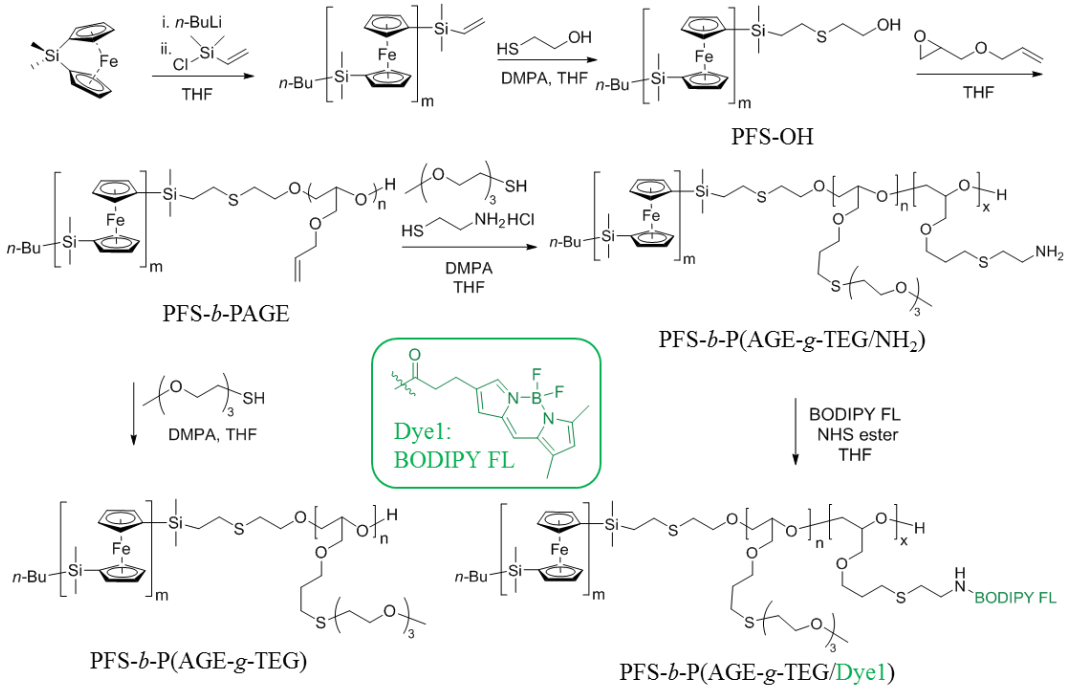

Scheme S2.1. Synthesis of PFS-*b*-P(AGE-*g*-TEG) and fluorescent dye functionalised PFS-*b*-P(AGE-*g*-TEG/dye) diblock copolymers.

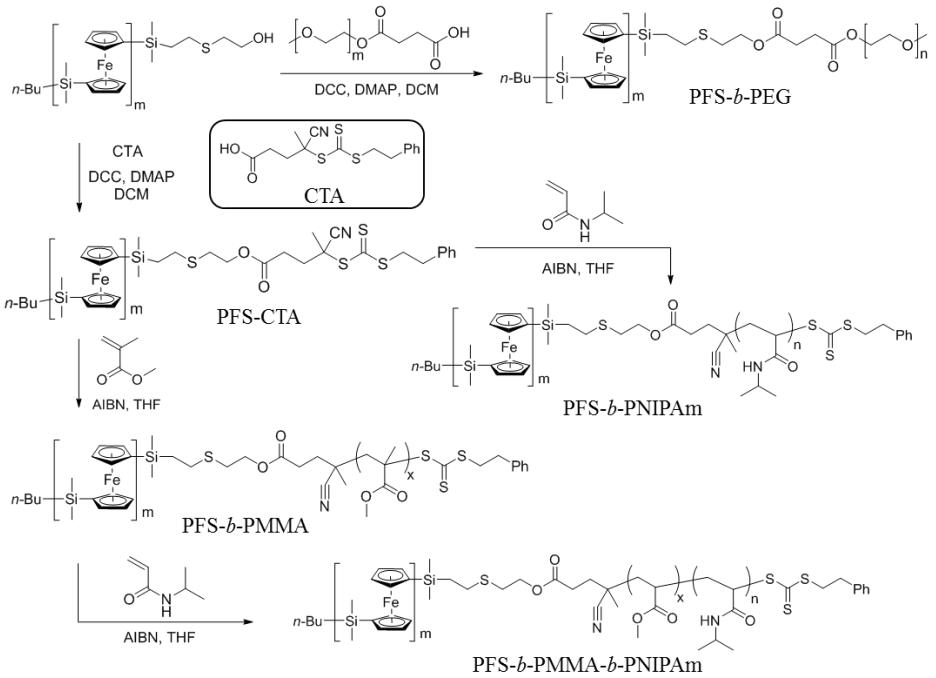

Scheme S2.2. Synthesis of PFS-containing block copolymers with PEG, PNIPAm or PMMA as corona-forming block.

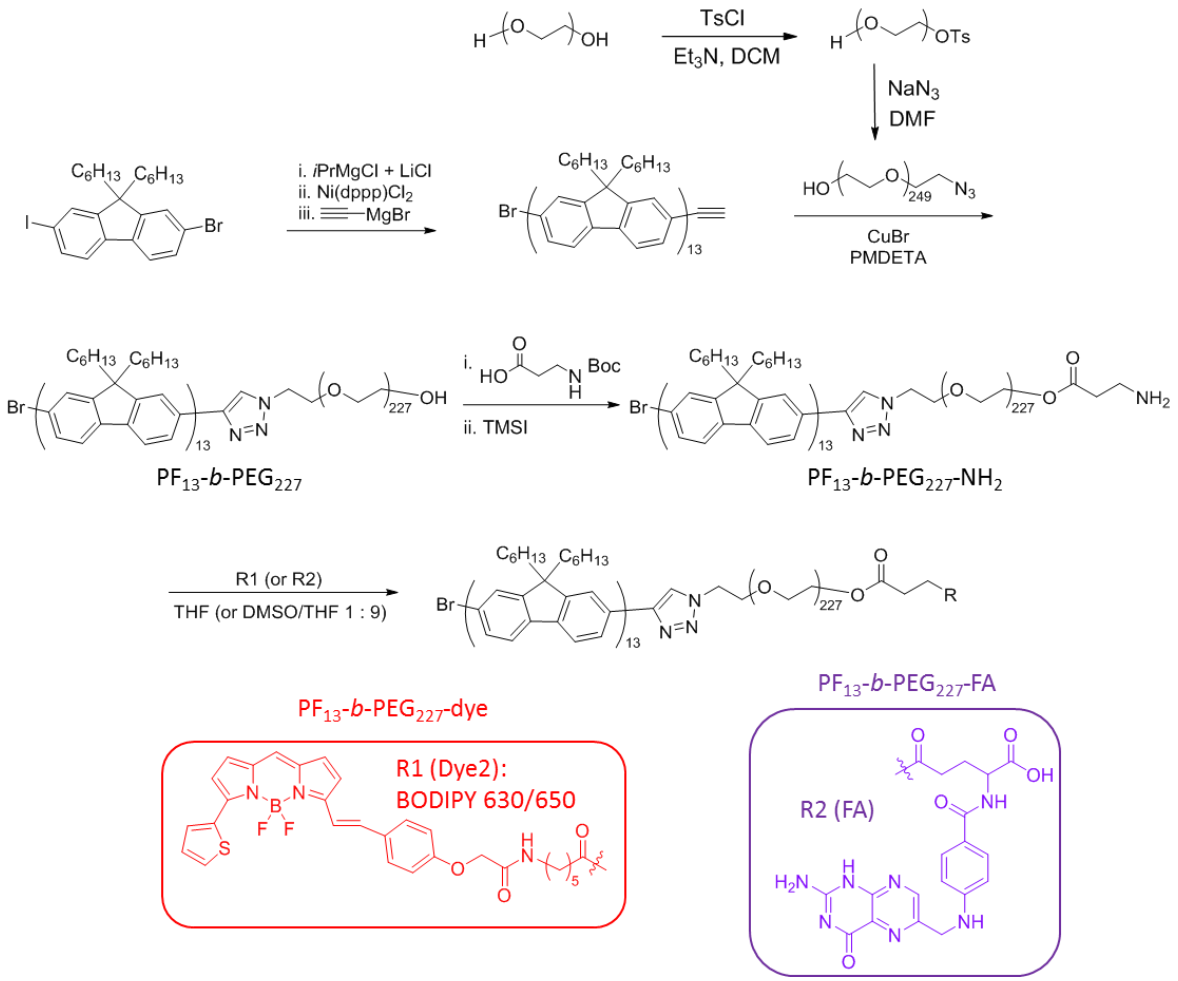

Scheme S2.3. Synthesis functionalised PF-based diblock copolymers.

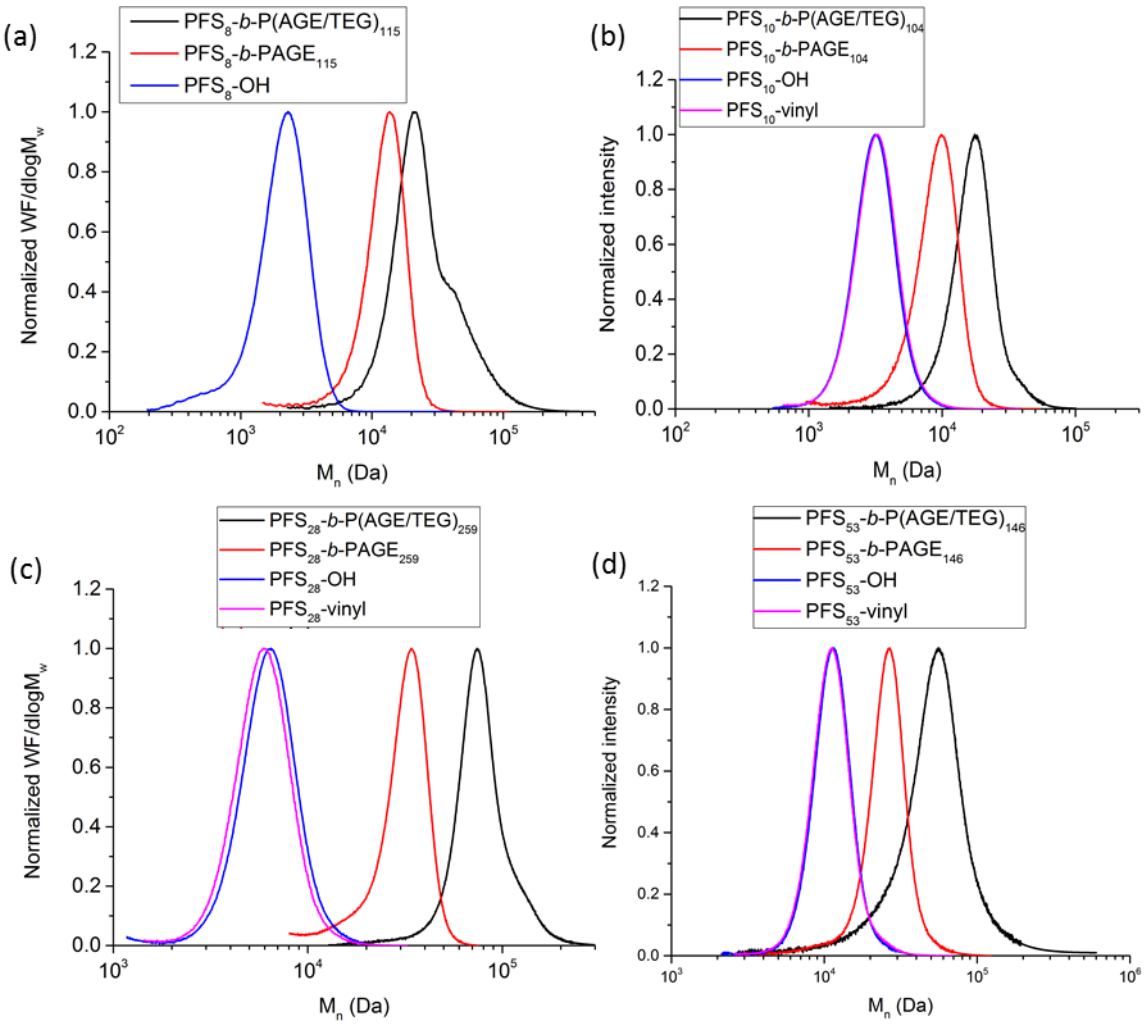

Figure S2.1. GPC chromatographs (refractive index trace) in *n*-Bu_4NBr/THF of PFS homopolymers and PFS-*b*-P(AGE-*g*-TEG) diblock copolymers.

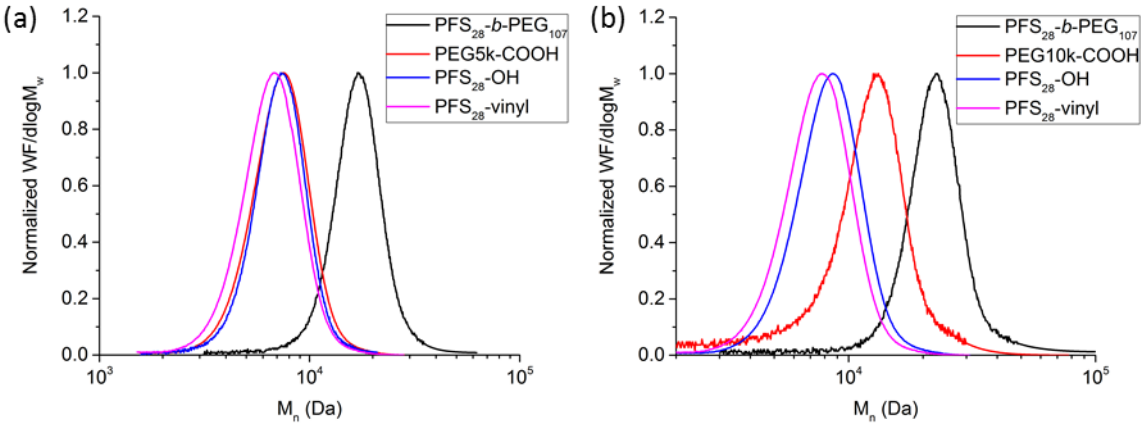

Figure S2.2. GPC chromatographs (refractive index trace) in *n*-Bu_4NBr/THF of PFS homopolymers and PFS-*b*-PEG diblock copolymers.

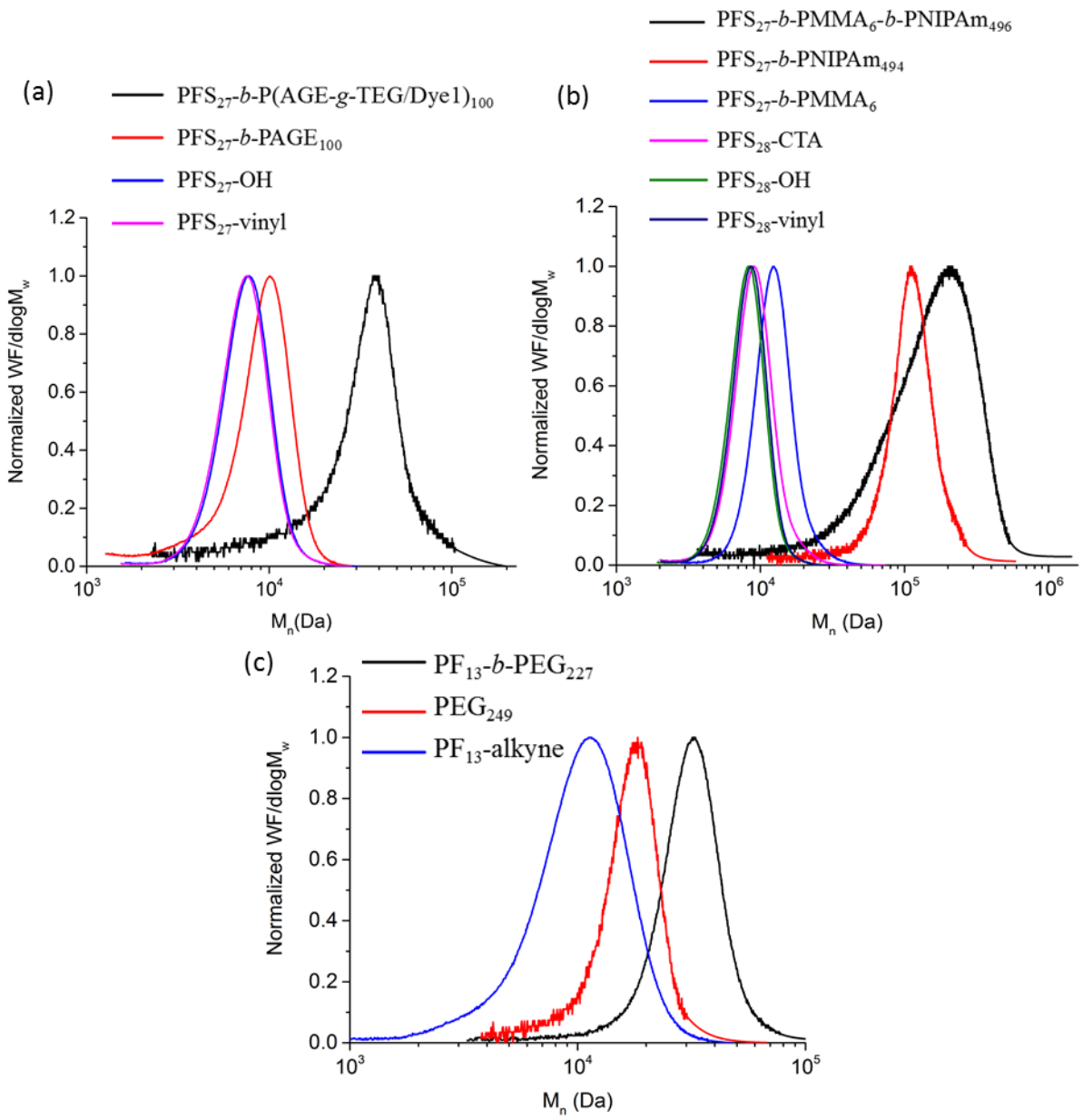

Figure S2.3. GPC chromatographs (refractive index trace) in *n*-Bu_4NBr/THF of PFS- and PF-containing polymers: (a) Dye functionalised PFS-*b*-P(AGE-*g*-TEG/dye) diblock copolymers and precursors;(b) PFS-*b*-PNIPAm diblock copolymers and precursors; (c) PF-*b*-PEG diblock copolymers and precursors.

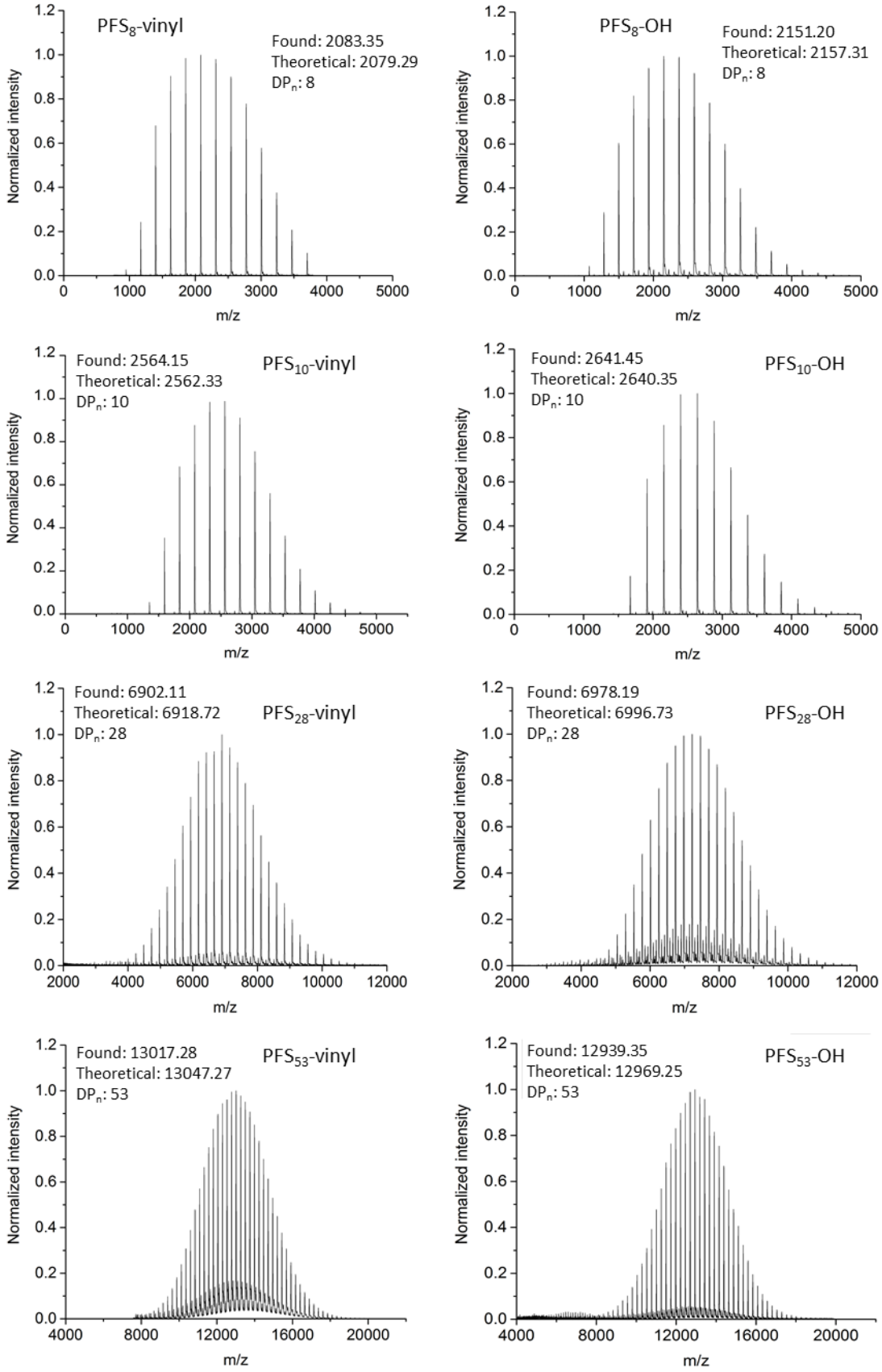

Figure S2.4. MALDI-TOF mass spectra of PFS-vinyl and PFS-OH homopolymers.

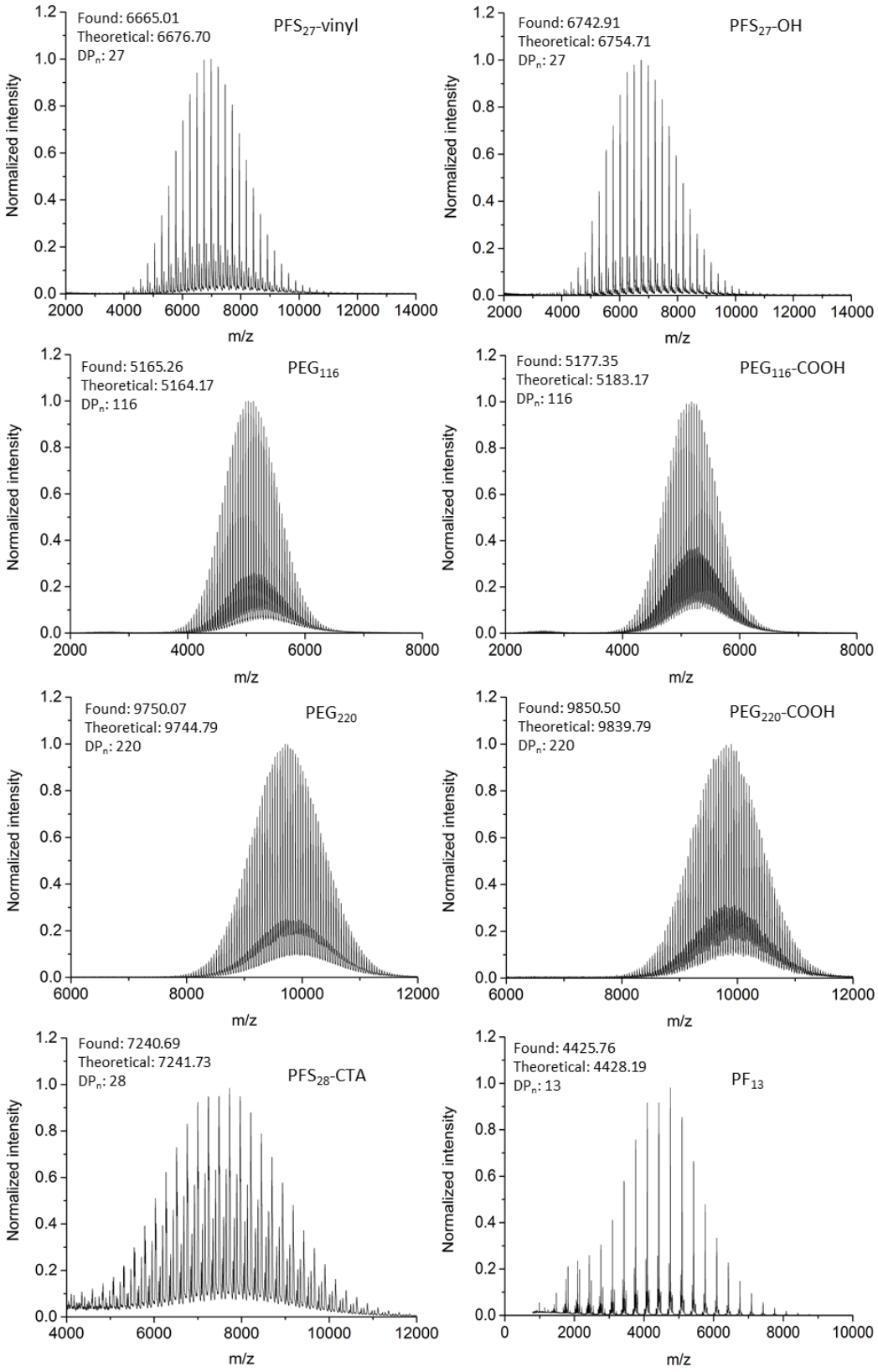

Figure S2.5. MALDI-TOF mass spectra of PFS, PEG and PF homopolymers.

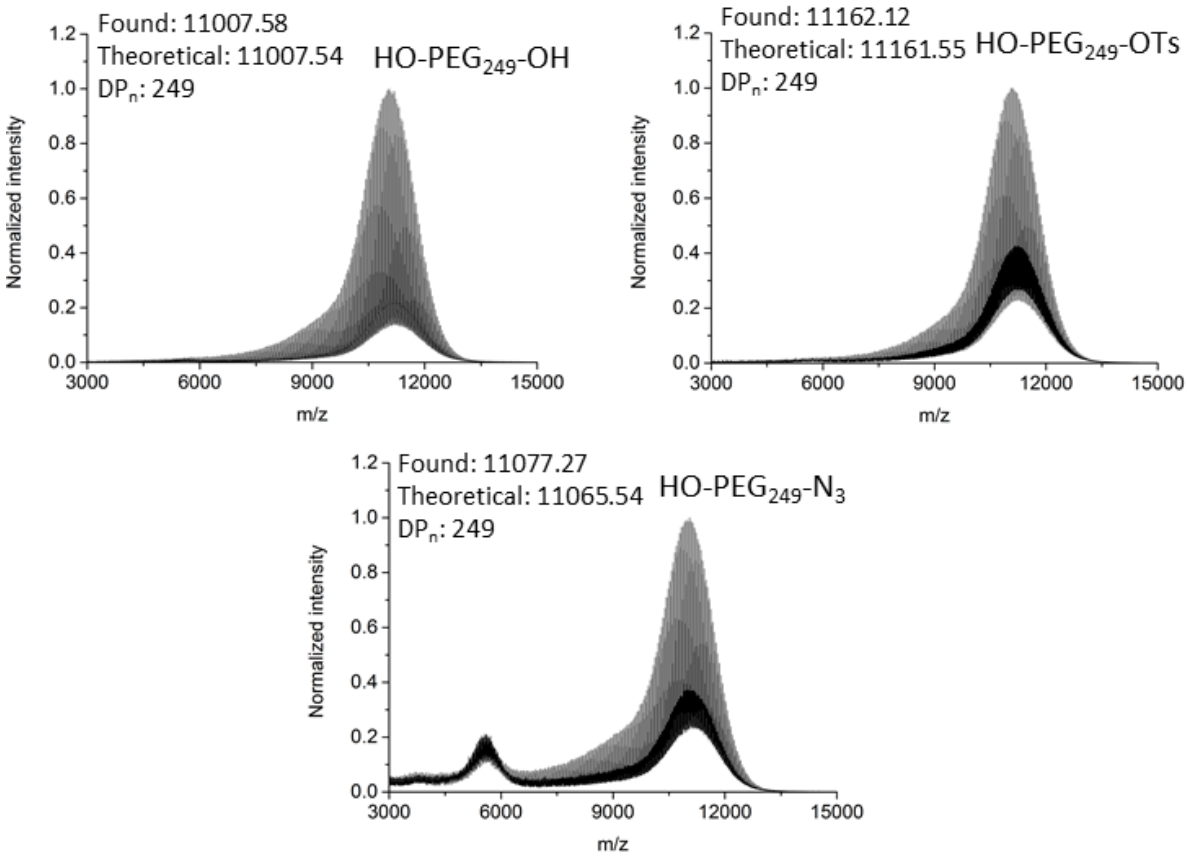

Figure S2.6. MALDI-TOF mass spectra of functionalisesd PEG homopolymers.

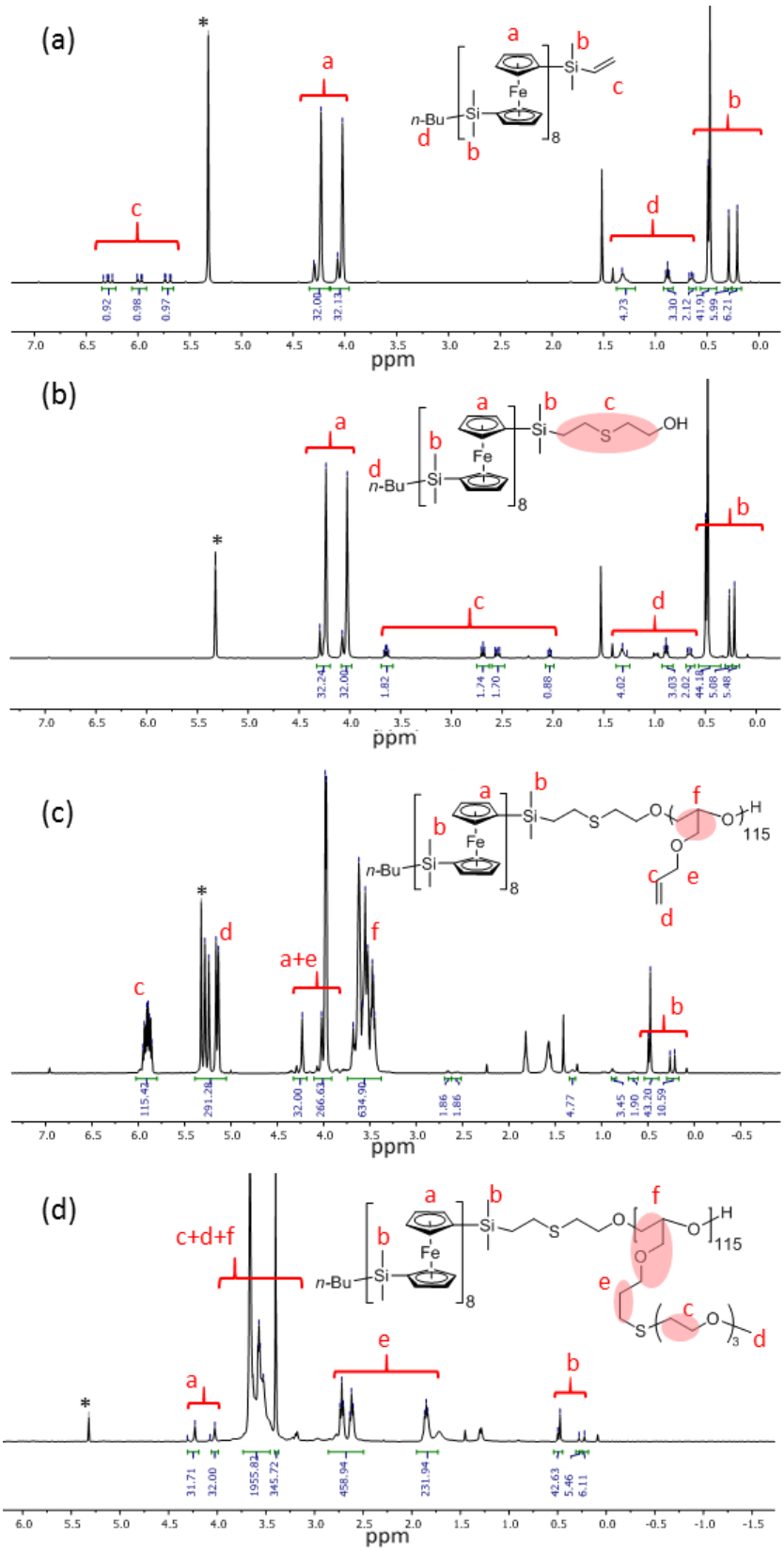

Figure S2.7. ^{1}H NMR spectra (in CD_2Cl_2) of (a)PFS_8-vinyl, (b)PFS_8-OH, (c)PFS_8-*b*-$PAGE_{115}$ and (d) PFS_8-*b*-P(AGE-*g*-TEG)$_{115}$.

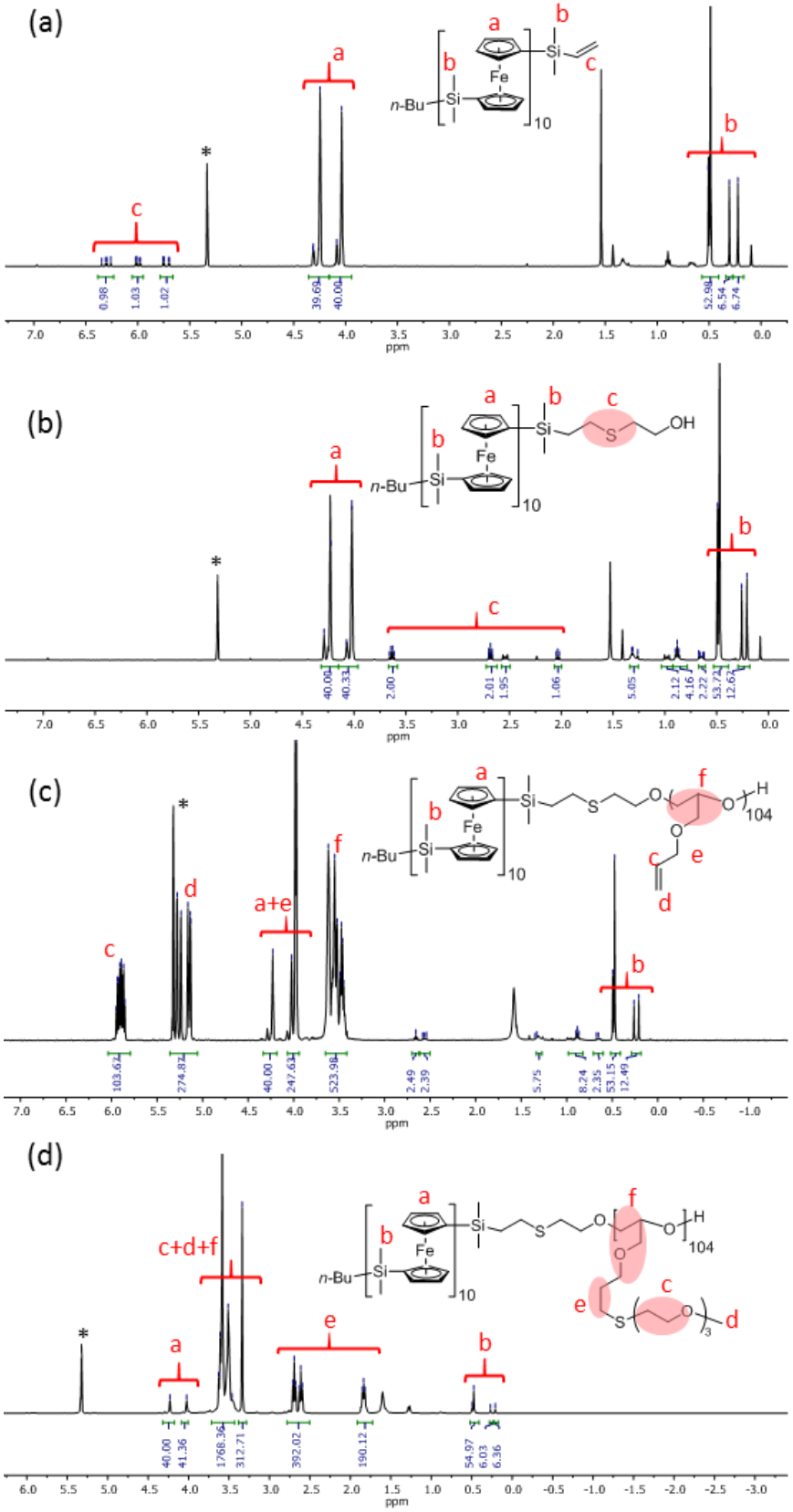

Figure S2.8. ^{1}H NMR spectra (in CD_2Cl_2) of (a)PFS_{10}-vinyl, (b)PFS_{10}-OH, (c)PFS_{10}-*b*-$PAGE_{104}$ and (d) PFS_{10}-*b*-P(AGE-*g*-TEG)$_{104}$.

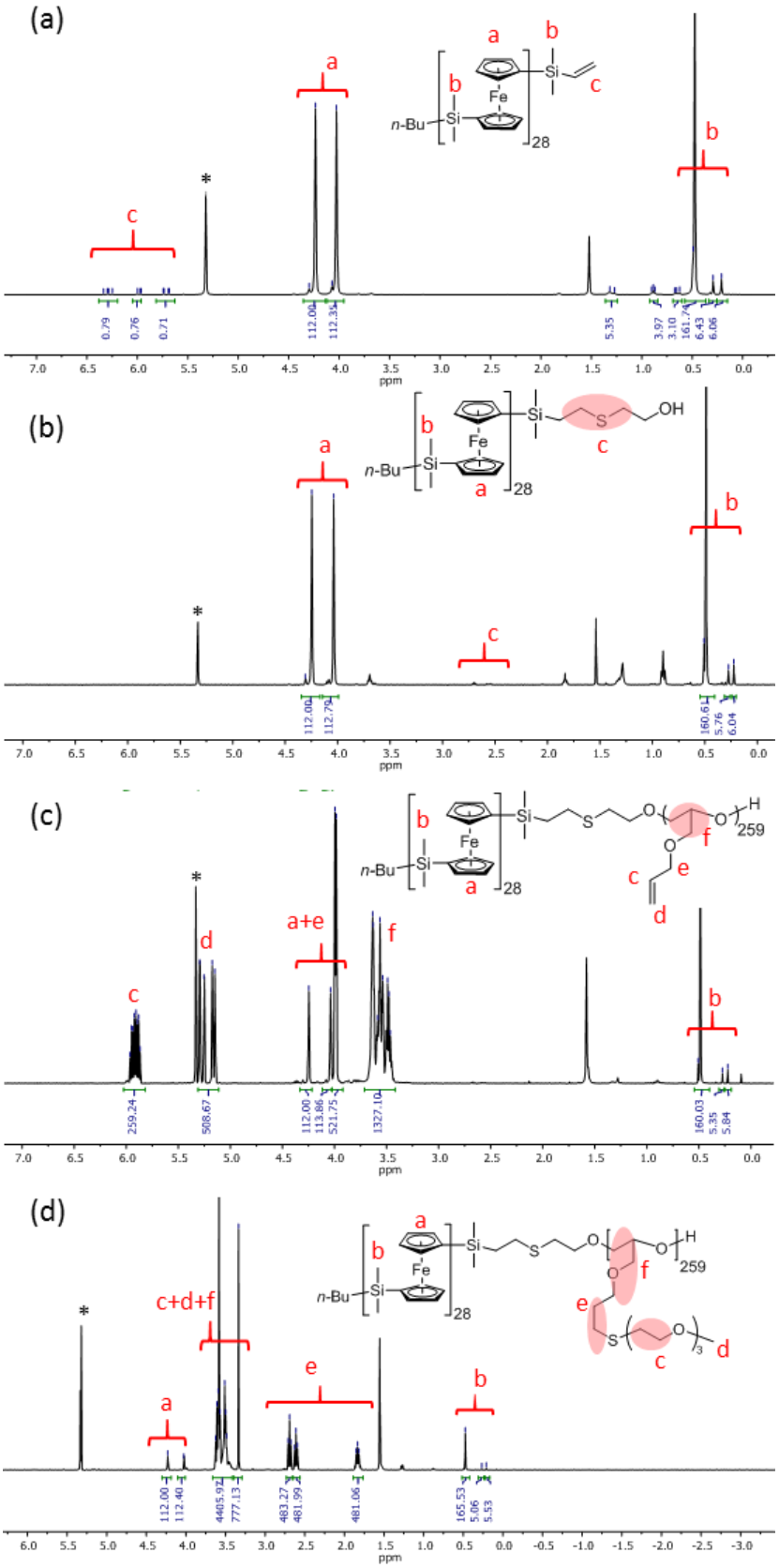

Figure S2.9. ^{1}H NMR spectra (in CD_2Cl_2) of (a)PFS_{28}-vinyl, (b)PFS_{28}-OH, (c)PFS_{28}-*b*-$PAGE_{259}$ and (d) PFS_{28}-*b*-P(AGE-*g*-TEG)$_{259}$.

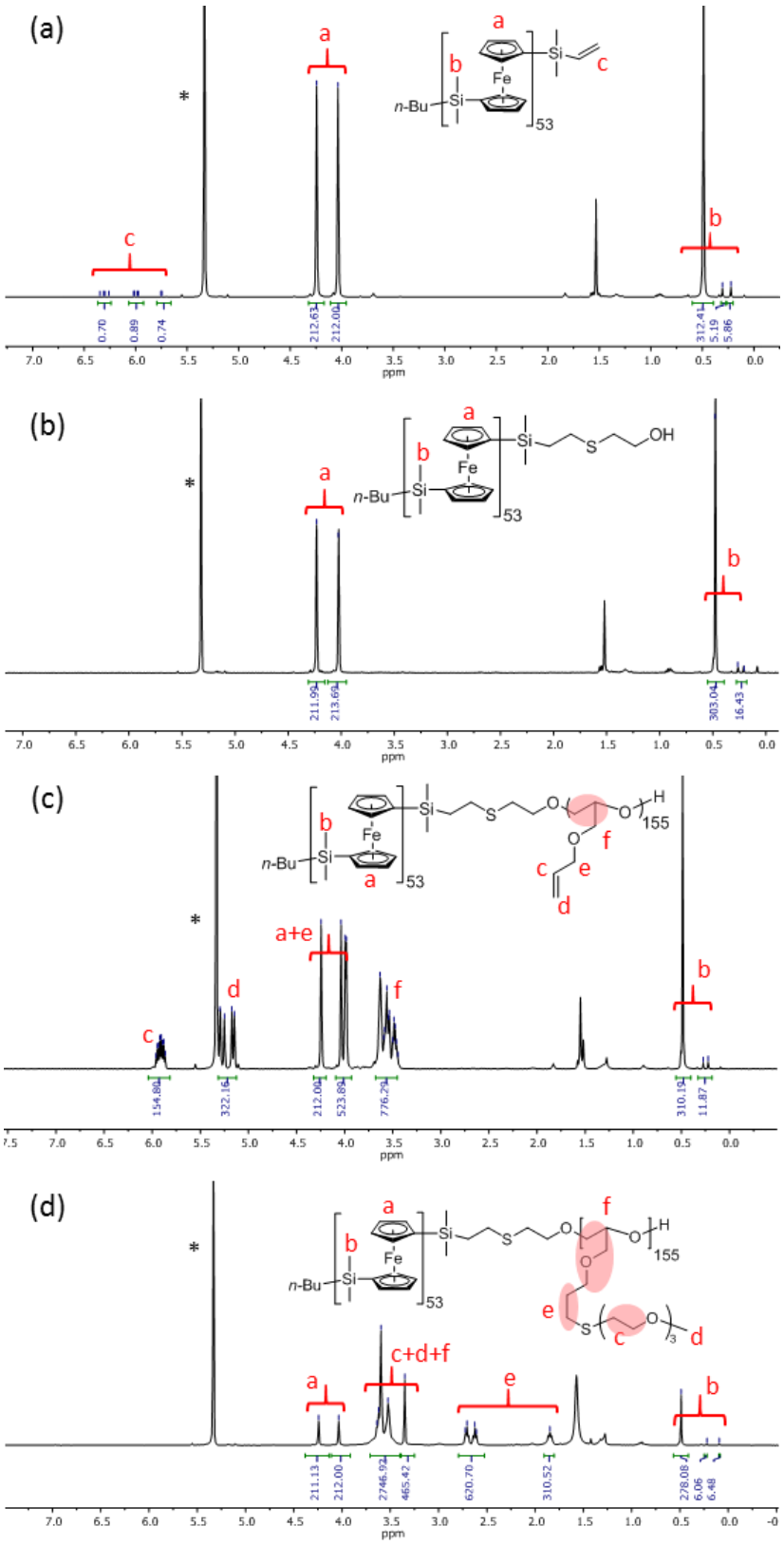

Figure S2.10. ^{1}H NMR spectra (in CD_2Cl_2) of (a)PFS_{53}-vinyl, (b)PFS_{53}-OH, (c)PFS_{53}-*b*-$PAGE_{155}$ and (d) PFS_{53}-*b*-P(AGE-*g*-TEG)$_{155}$.

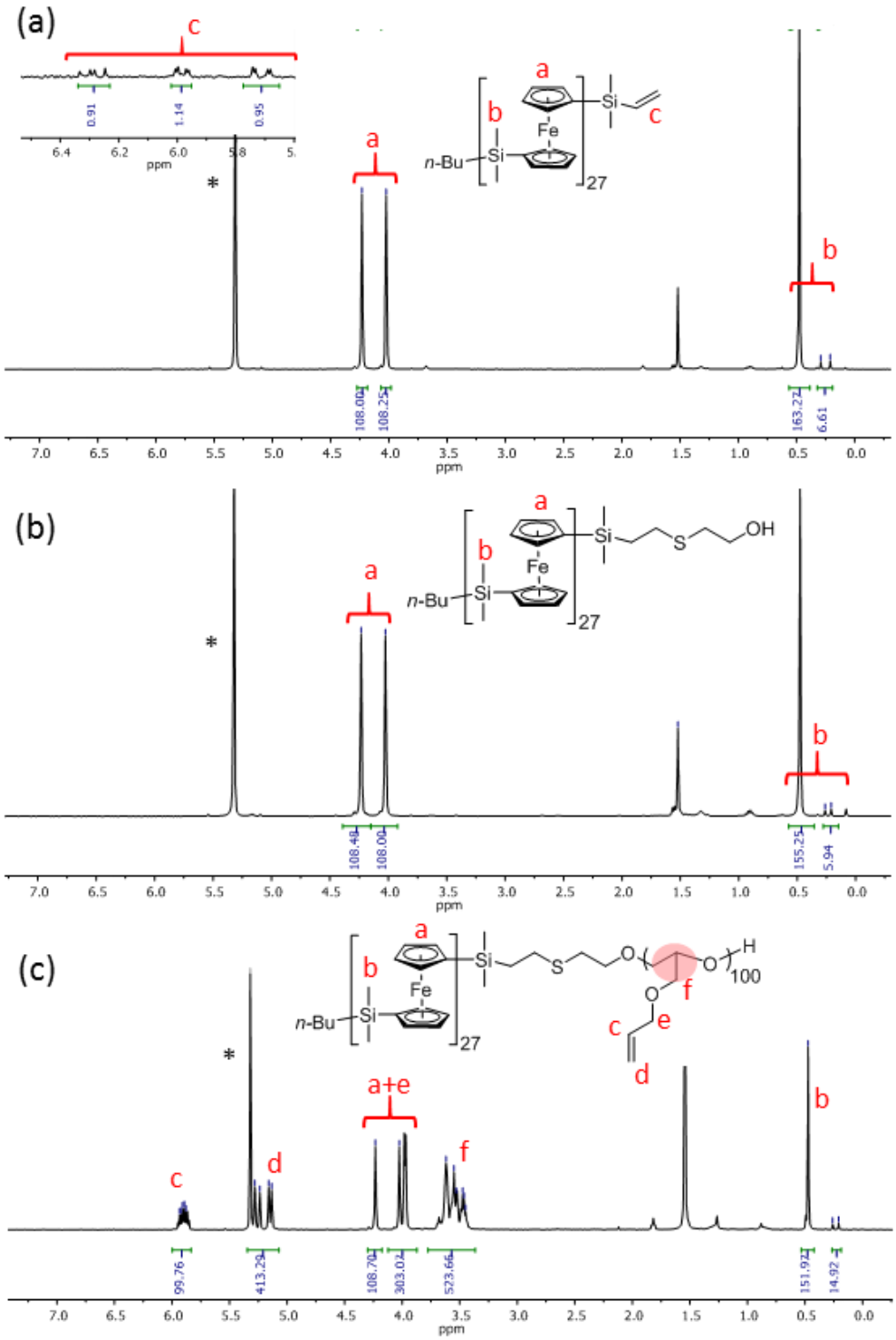
(a)
c
a
b
n-Bu
Si
Fe
27
OH
S
(b)
(c)
a+e
d
f
ppm

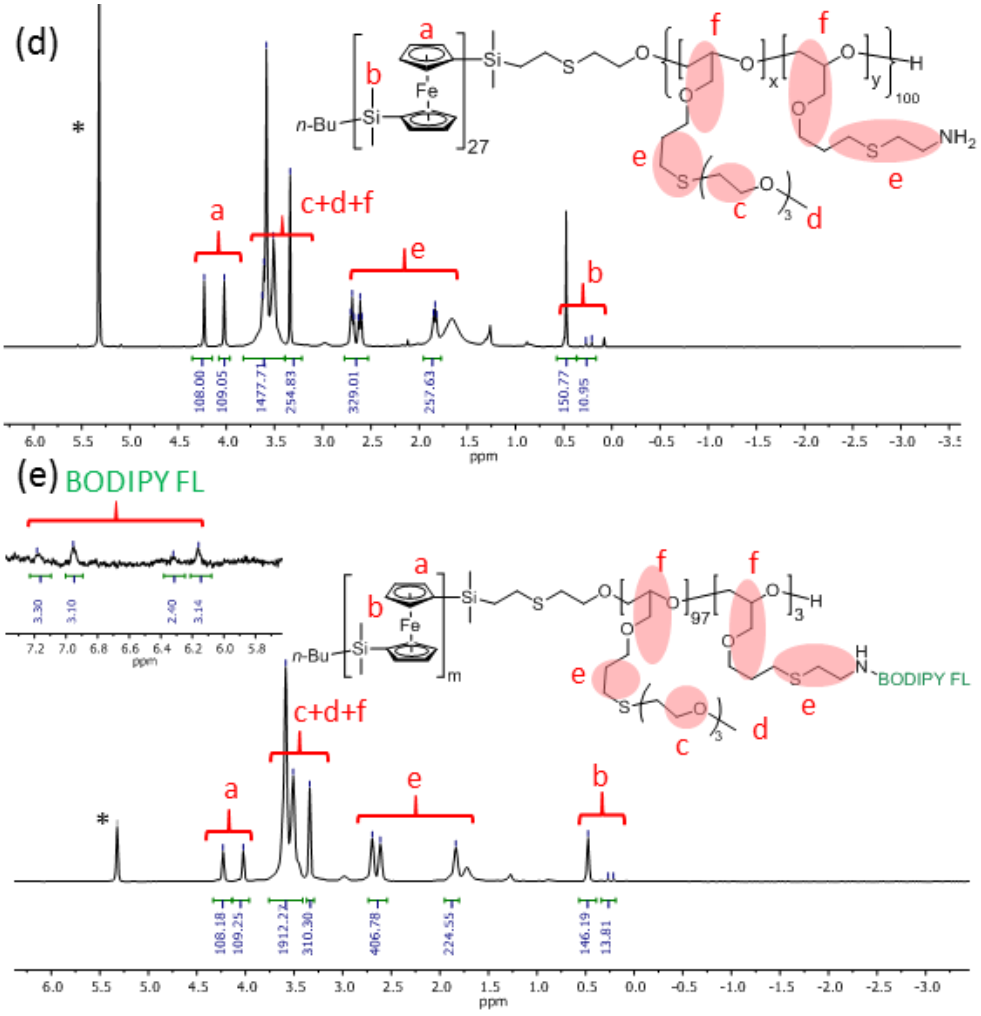

Figure S2.11. ^{1}H NMR spectra (in CD_2Cl_2) of (a)PFS_{53}-vinyl, (b)PFS_{53}-OH, (c)PFS_{53}-*b*-$PAGE_{155}$, (d) PFS_{53}-*b*-$P(AGE\text{-}g\text{-}TEG/NH_2)_{155}$ and (e) PFS_{53}-*b*-$P(AGE\text{-}g\text{-}TEG/Dye1)_{155}$.

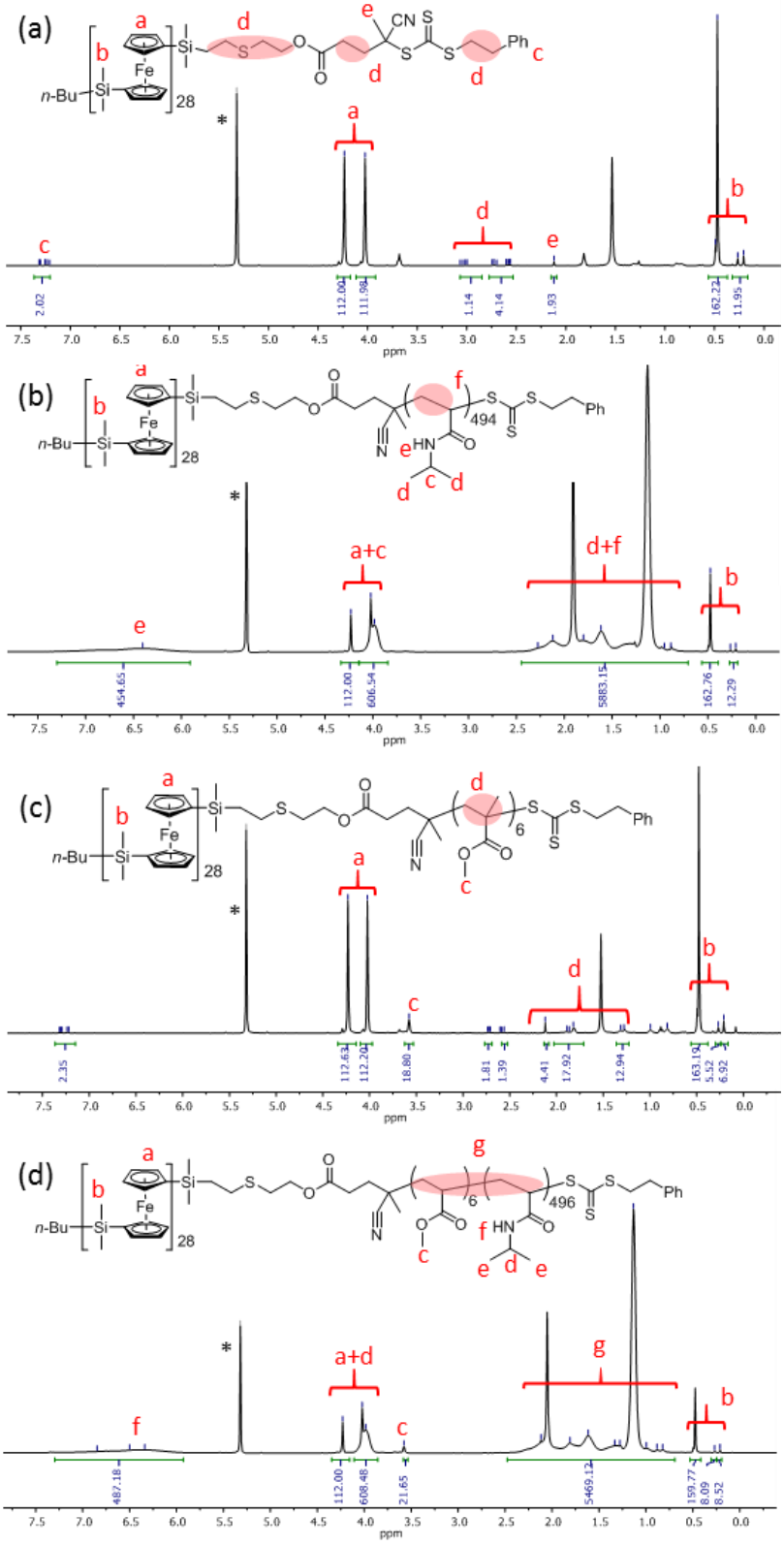

Figure S2.12. ^{1}H NMR spectra (in CD_2Cl_2) of (a)PFS_{28}-CTA, (b)PFS_{28}-*b*-$PNIPAm_{494}$, (c)PFS_{28}-*b*-$PMMA_6$, (d) PFS_{28}-*b*-$PMMA_6$-*b*-$PNIPAm_{496}$.

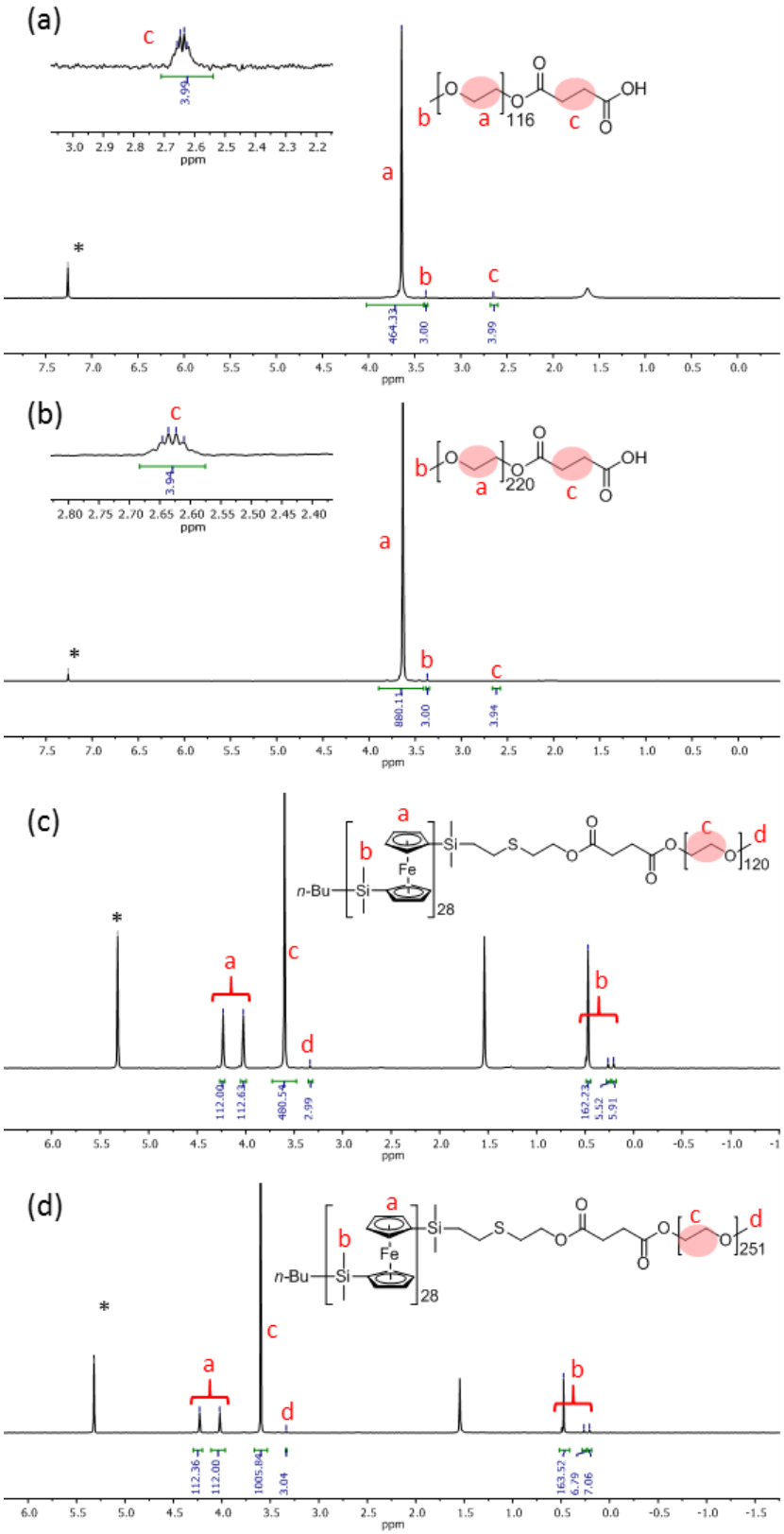

Figure S2.13. ^{1}H NMR spectra of (a)PEG-COOH (M_n = 5 kg/mol) (in $CDCl_3$), (b)PEG-COOH (M_n = 10 kg/mol) (in $CDCl_3$), (c)PFS_{28}-*b*-PEG_{120} (in CD_2Cl_2), (d) PFS_{28}-*b*-PEG_{251} (in CD_2Cl_2).

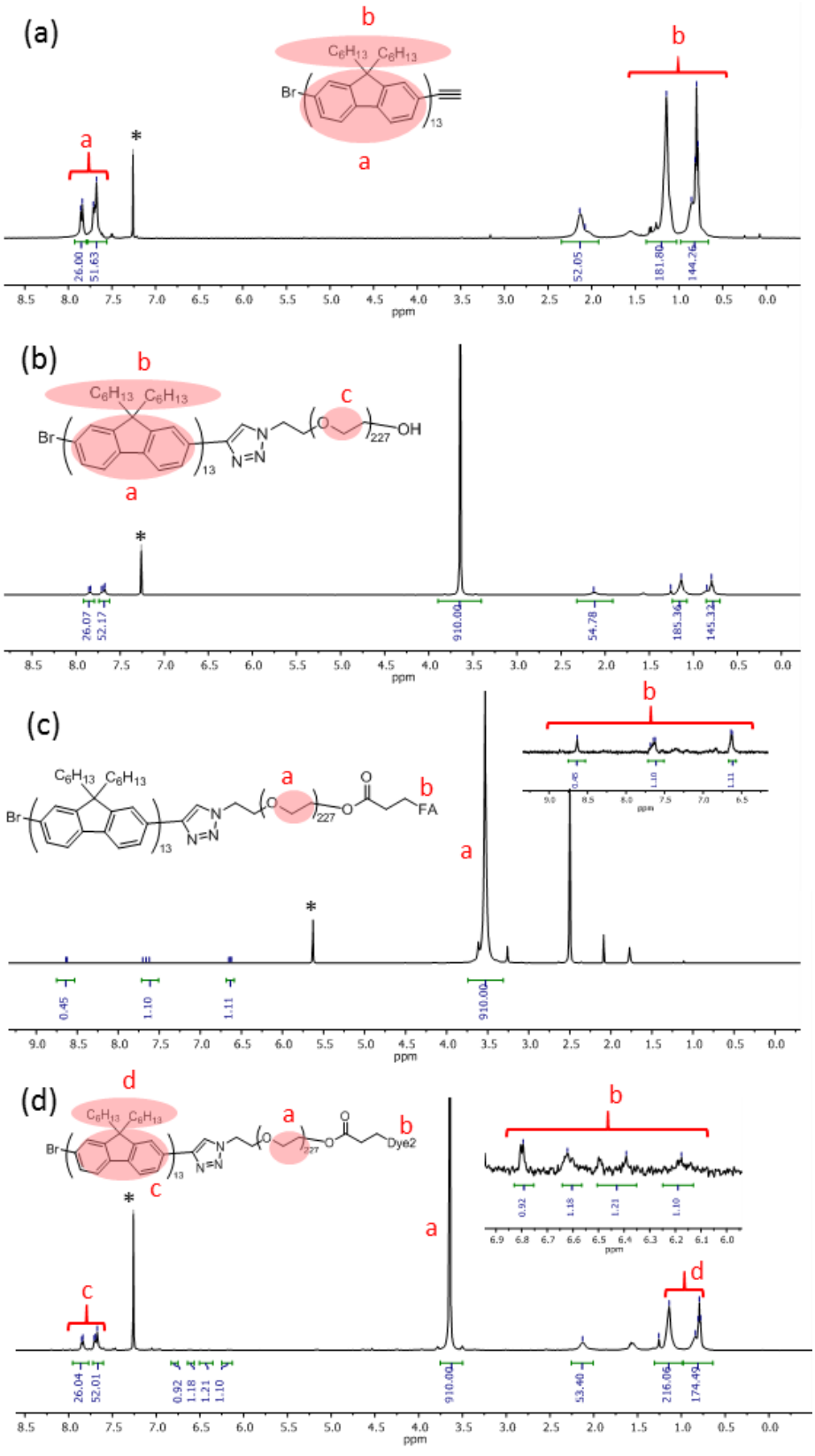

Figure S2.14. ^{1}H NMR spectra (in $CDCl_3$) of (a)PF_{13}, (b)PF_{13}-*b*-PEG_{227}, (c)PF_{13}-*b*-PEG_{227}-FA, (d) PF_{13}-*b*-PEG_{227}-Dye2.

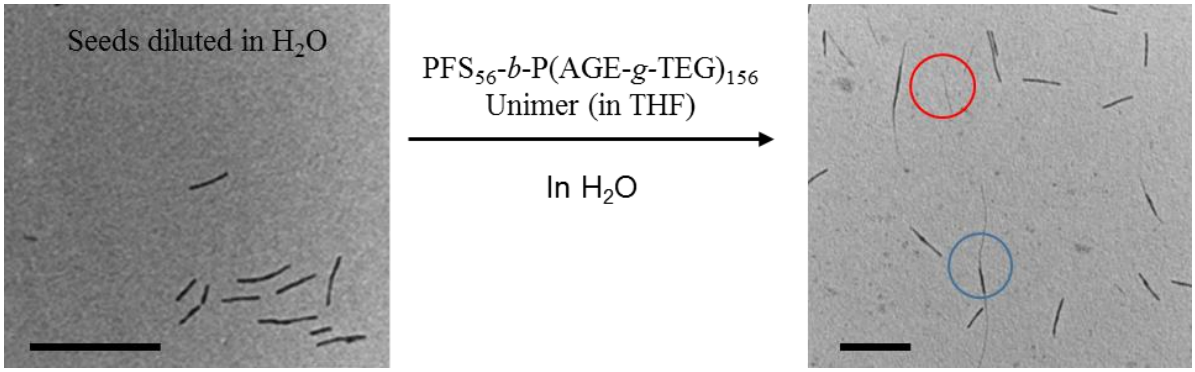

Figure S2.15. TEM images of seeded-growth of PFS_{53}-*b*-P(AGE-*g*-TEG)$_{155}$ in H_2O. Scale bars: 200 nm. Reproduced from reference 67. Blue circle: the contrast between the seed (dark) and the grown section (light). Red circle: individual new micelles formed via self-nucleation.

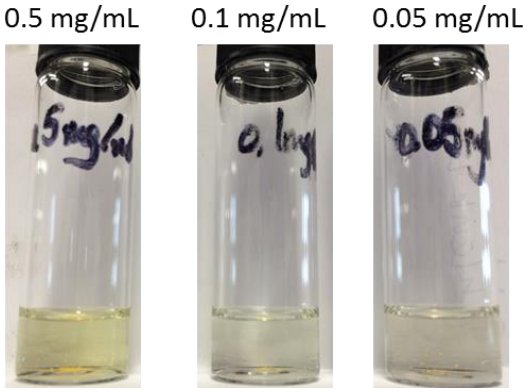

Figure S2.16. Visualized precipitation of PFS_{53}-*b*-P(AGE-*g*-TEG)$_{155}$ in H_2O by direct dissolution.

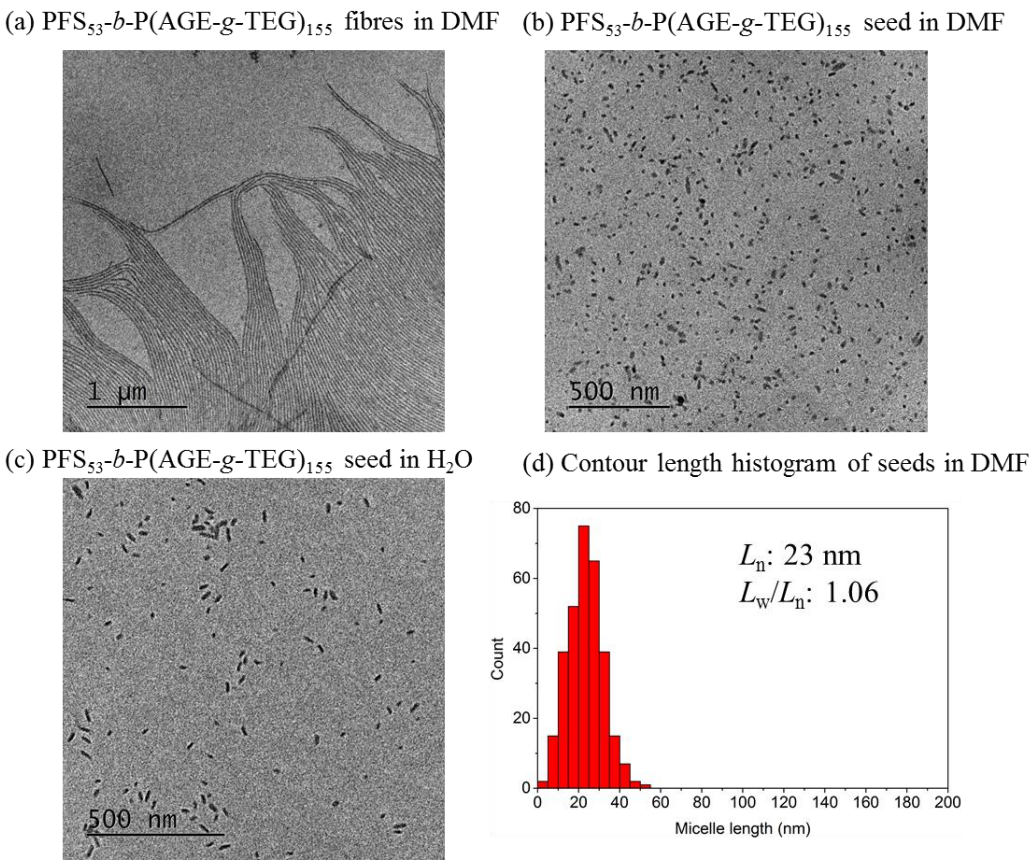

Figure S2.17. TEM images of (a) PFS_{53}-*b*-P(AGE-*g*-TEG)$_{155}$ in DMF (0.5 mg/mL, by direct dissolution with a heating-cooling process), (b) PFS_{53}-*b*-P(AGE-*g*-TEG)$_{155}$ seed micelles in DMF prepared by sonication of polydisperse fibre solution for 1 h with a ultrasonicate probe at 0 °C and (c) PFS_{53}-*b*-P(AGE-*g*-TEG)$_{155}$ seed micelles in H_2O by dialysis and (d) contour length histograms of PFS_{53}-*b*-P(AGE-*g*-TEG)$_{155}$ seed micelles in DMF.

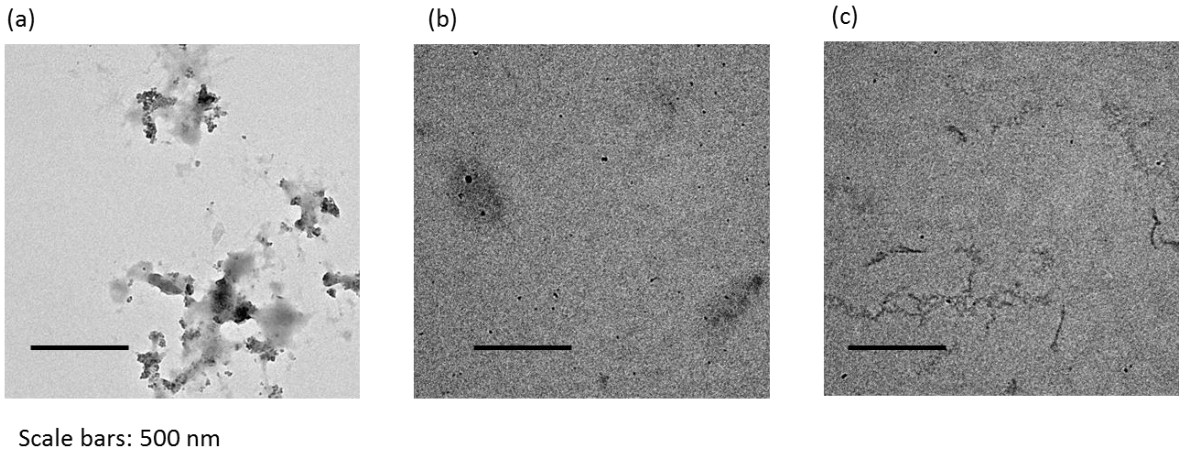

Figure S2.18. TEM images of PFS_{28}-*b*-P(AGE-*g*-TEG)$_{259}$ fibre solutions prepared in H_2O sonicated in an ultrasonic bath at 0 °C for (a) 40, (b) 30 and (c) 10 min.

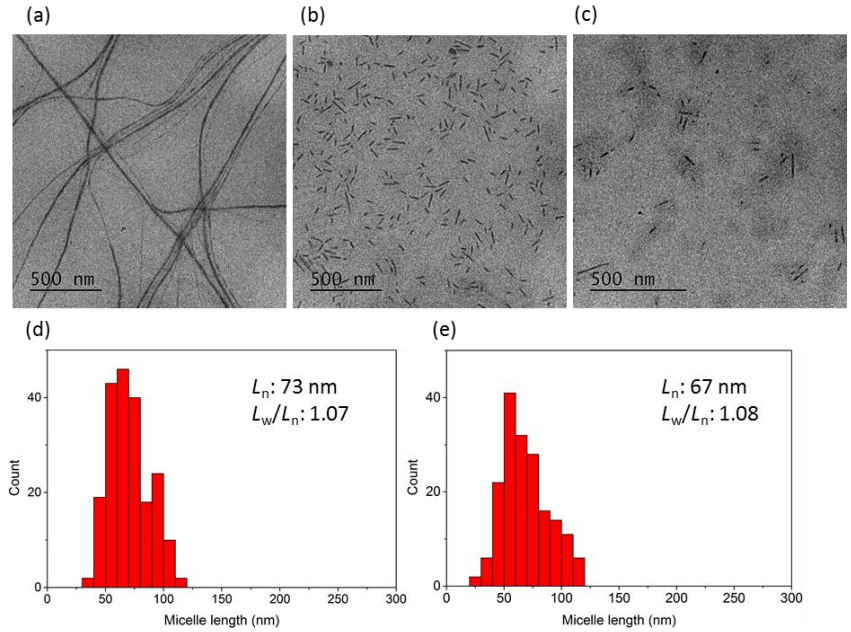

Figure S2.19. TEM images of (a) PFS_{28}-*b*-P(AGE-*g*-TEG)$_{259}$ in MeOH (0.5 mg/mL, by direct dissolution with a heating-cooling process), (b) PFS_{28}-*b*-P(AGE-*g*-TEG)$_{259}$ seed micelles in MeOH prepared by sonication of polydisperse fibre solution for 1 h with a ultrasonic probe at 0 °C and (c) PFS_{28}-*b*-P(AGE-*g*-TEG)$_{259}$ seed micelles in H_2O by 10-fold dilution. Contour length histogram of (d) PFS_{28}-*b*-P(AGE-*g*-TEG)$_{259}$ seed micelles in MeOH and (e) PFS_{28}-*b*-P(AGE-*g*-TEG)$_{259}$ seed micelles in H_2O.

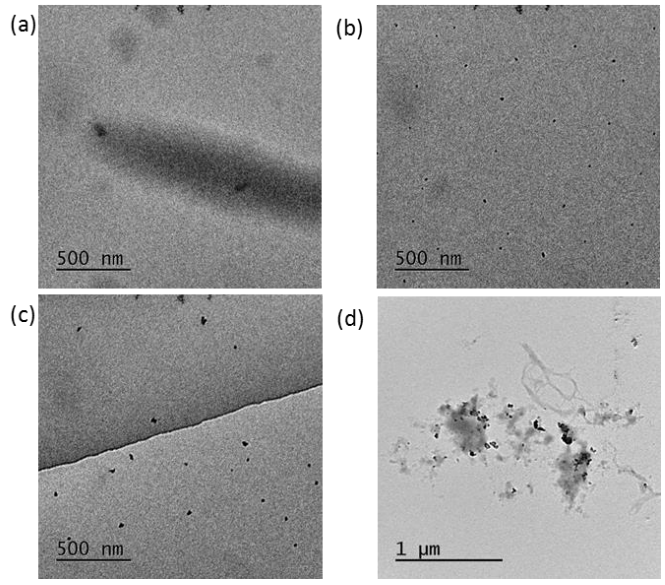

Figure S2.20. TEM images of self-assembly of PFS_8-*b*-P(AGE-*g*-TEG)$_{115}$ in (a) MeOH, (b) EtOH, (c) *i*-PrOH and (d) H_2O via a heating-cooling method (0.5 mg/mL) after aging at 23 °C for 36 h.

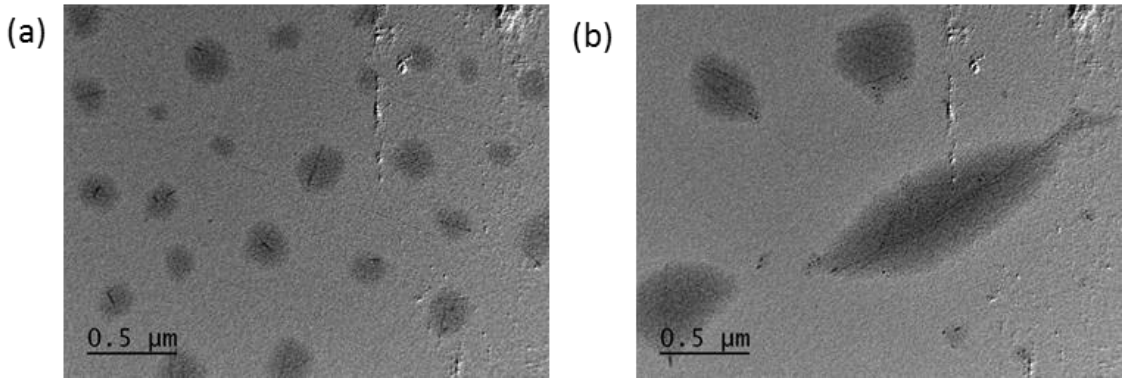

Figure S2.21. TEM images of seeded-growth of adding PFS_8-*b*-P(AGE-*g*-TEG)$_{115}$ (in THF) to PFS_{28}-*b*-P(AGE-*g*-TEG)$_{259}$ seeds (in MeOH, diluted in H_2O) in THF/H_2O (*v*:*v* = 1:9) after aging for (a) 2 days and (b) 20 days.

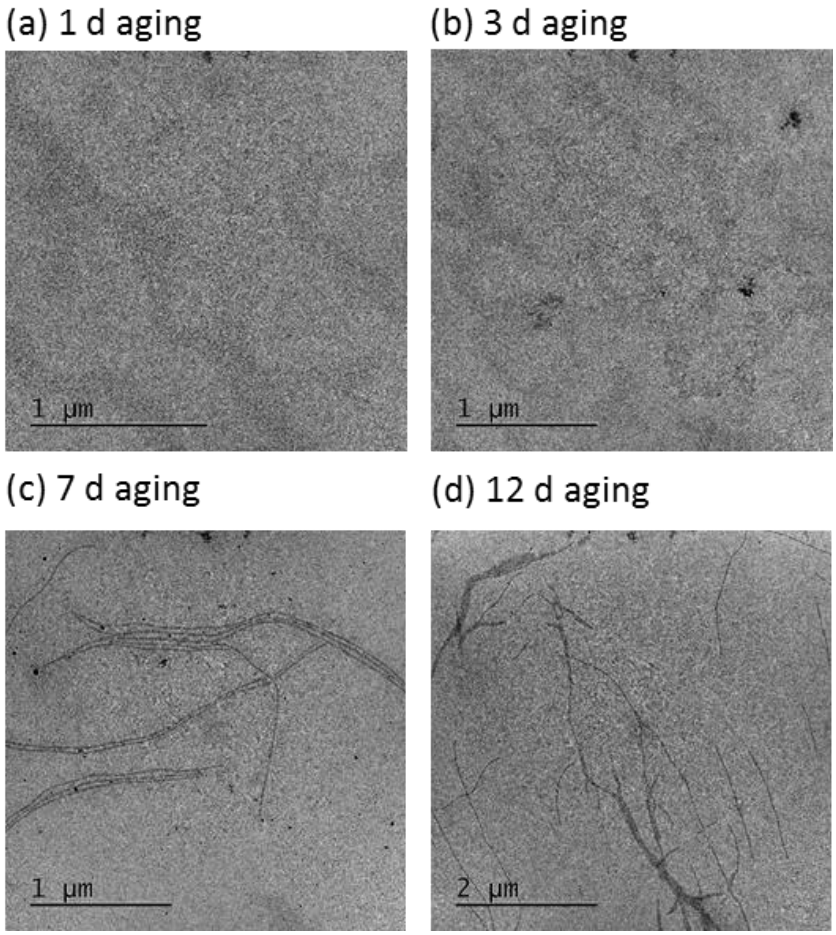

Figure S2.22. TEM images of self-assembly of PFS_{10}-*b*-P(AGE-*g*-TEG)$_{104}$ direct in H_2O via a heating-cooling method (0.1 mg/mL) after aging for (a) 1, (b) 3, (c) 7 and (d) 12 days at 23 °C

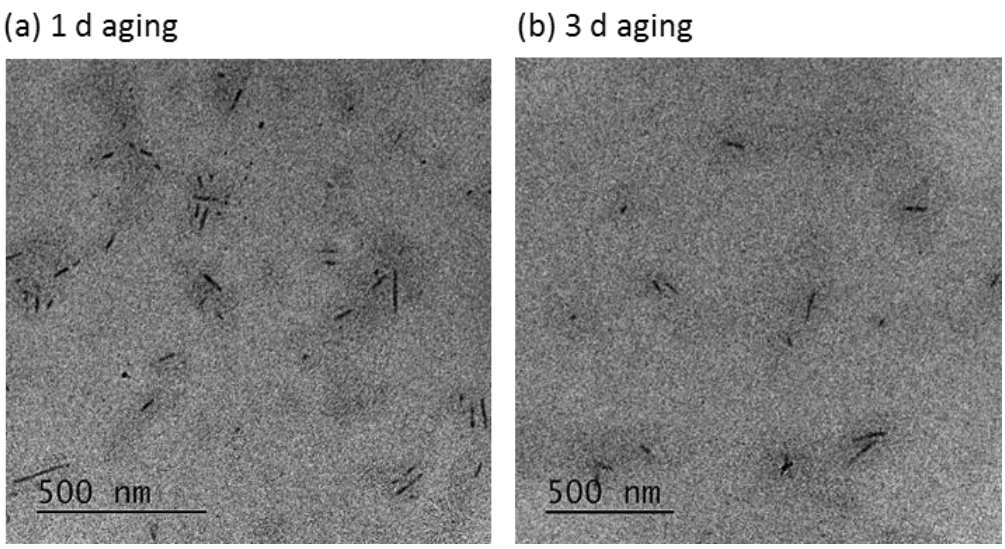

Figure S2.23. TEM images of seeded growth by addition of PFS_{10}-*b*-P(AGE-*g*-TEG)$_{104}$ (in H_2O, before 24 h aging after heating-cooling process, with m_{unimer}:m_{seed} = 5) into the seed solutions (PFS_{28}-*b*-P(AGE-*g*-TEG)$_{259,}$ diluted in H_2O) at 23 °C after aging for (a) 1 and (b) 3 days.

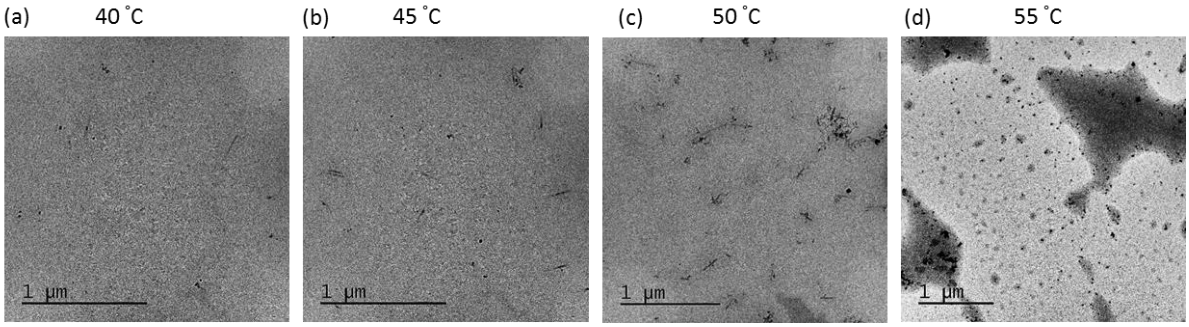

Figure S2.24. TEM images of seeded-growth of adding PFS_{10}-*b*-P(AGE-*g*-TEG)$_{104}$ (in trapped state in H_2O, with m_{unimer}:m_{seed} = 5) into the seed solutions (PFS_{28}-*b*-P(AGE-*g*-TEG)$_{259,}$ diluted in H_2O) at (a) 40, (b) 45, (c) 50 and (d)55 °C after aging for 1 day.

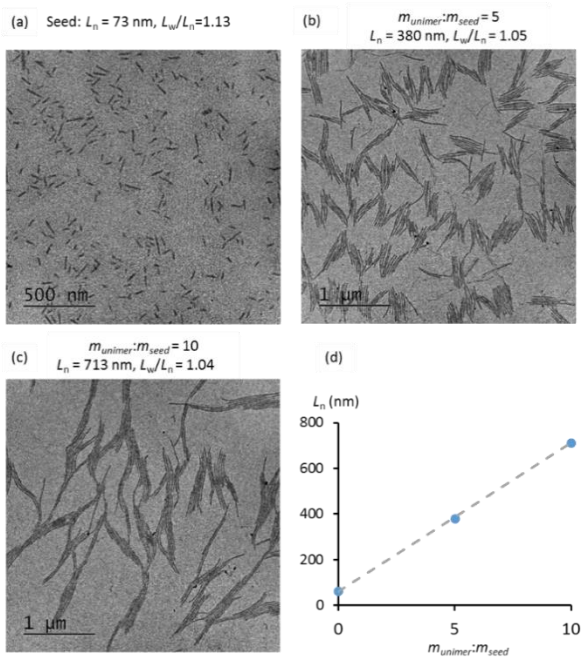

Figure S2.25. Seeded-growth of PFS_{10}-*b*-P(AGE-*g*-TEG)$_{104}$ in DMF by adding unimers (in THF) into (a) seeds (PFS_{28}-*b*-P(AGE-*g*-TEG)$_{259}$, diluted in DMF) with unimer-to-seed mass ratios of (b) 5 and (c) 10. (d) Linear plot of micelle length L_n versus unimer-to-seed mass ratios.

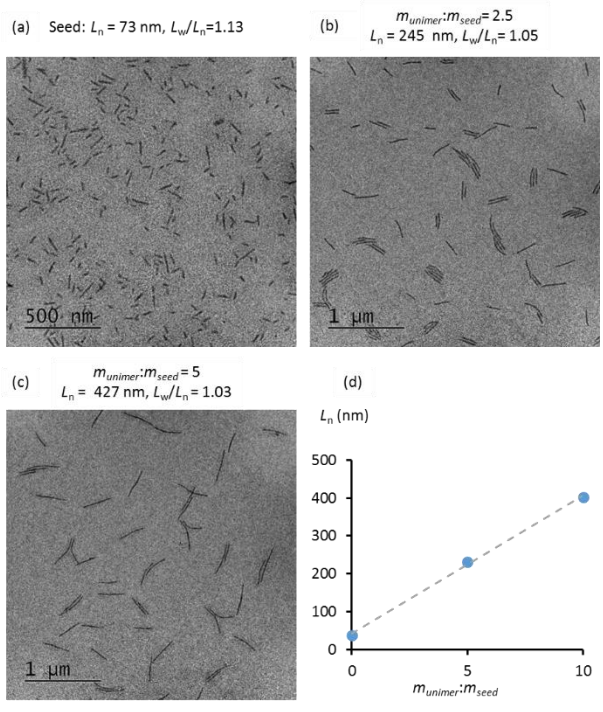

Figure S2.26. Seeded-growth of PFS_{10}-*b*-P(AGE-*g*-TEG)$_{104}$ in MeOH by adding unimers (in THF) into (a) seeds (PFS_{28}-*b*-P(AGE-*g*-TEG)$_{259}$, in MeOH) with unimer-to-seed mass ratios of (b) 2.5 and (c) 5. (d) Linear plot of micelle length L_n versus unimer-to-seed mass ratios.

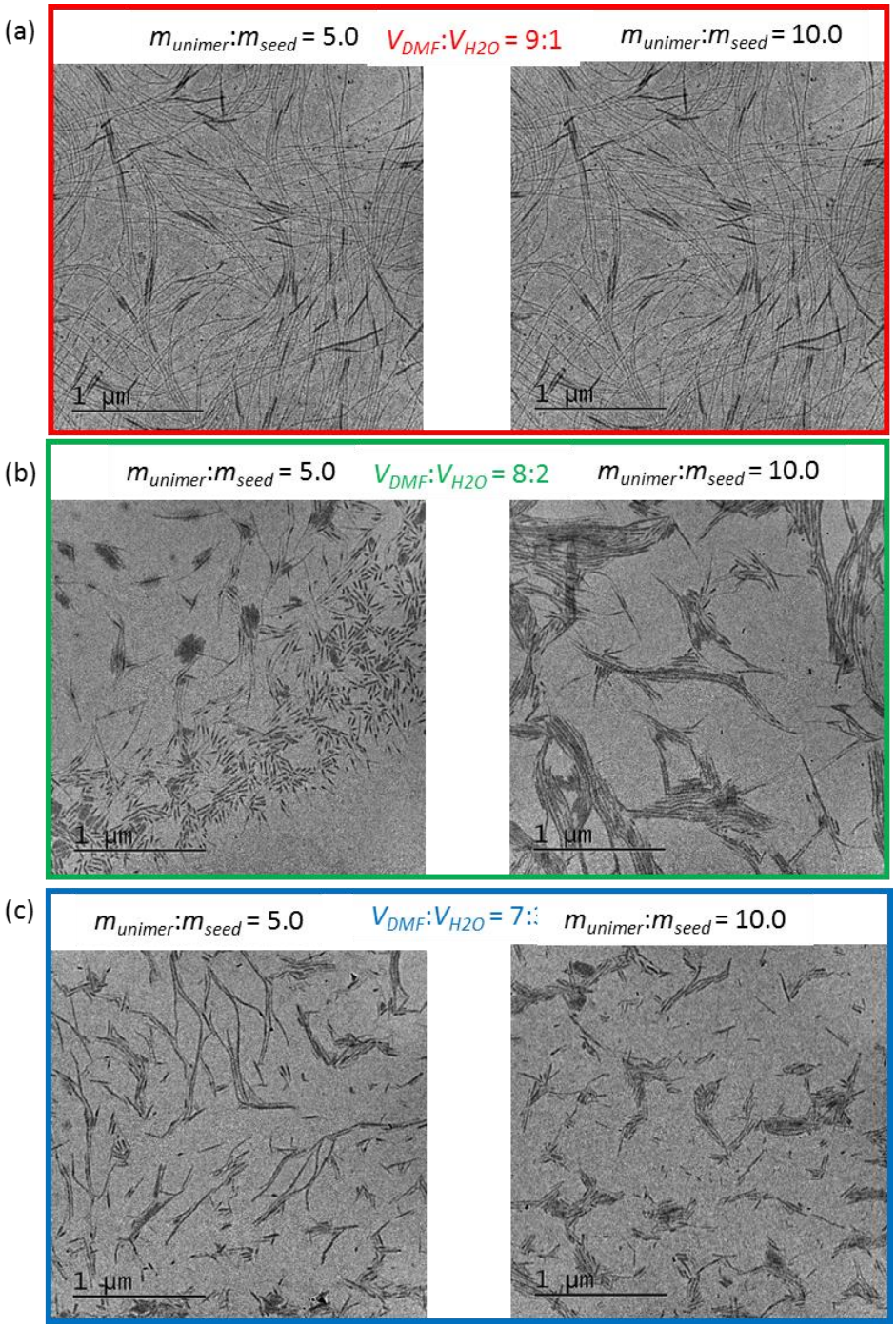

Figure S2.27. Seeded-growth of PFS_{10}-*b*-P(AGE-*g*-TEG)$_{104}$ in DMF/H_2O with volume ratios of (a) 9:1, (b) 8:2 and (c) 7:3 by adding unimers (in THF) into seeds (PFS_{28}-*b*-P(AGE-*g*-TEG)$_{259}$, in DMF) with unimer-to-seed mass ratios of 5 and 10.

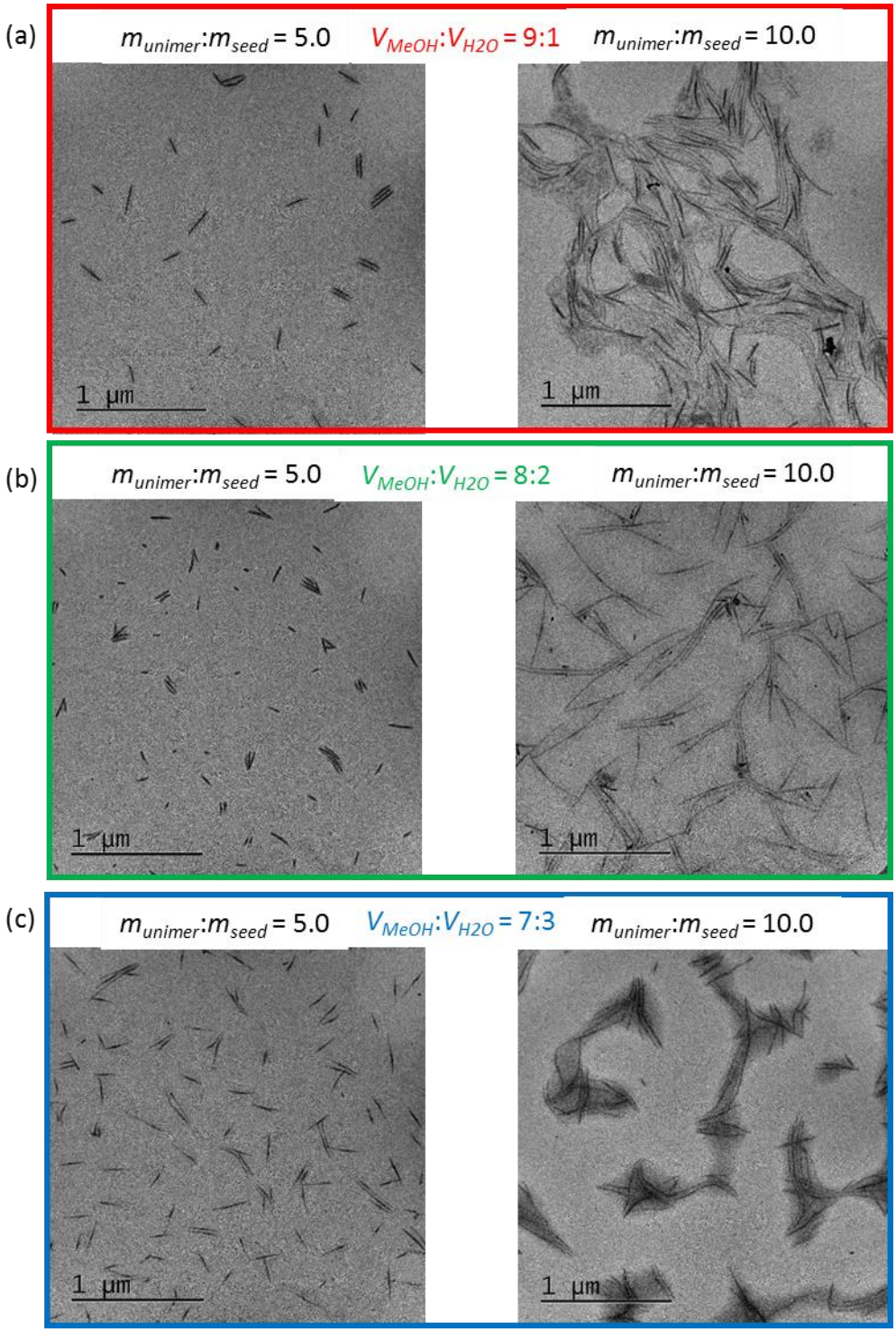

Figure S2.28. Seeded-growth of PFS_{10}-*b*-P(AGE-*g*-TEG)$_{104}$ in MeOH/H_2O with volume ratios of (a) 9:1, (b) 8:2 and (c) 7:3 by adding unimers (in THF) into seeds (PFS_{28}-*b*-P(AGE-*g*-TEG)$_{259}$, in MeOH) with unimer-to-seed mass ratios of 5 and 10.

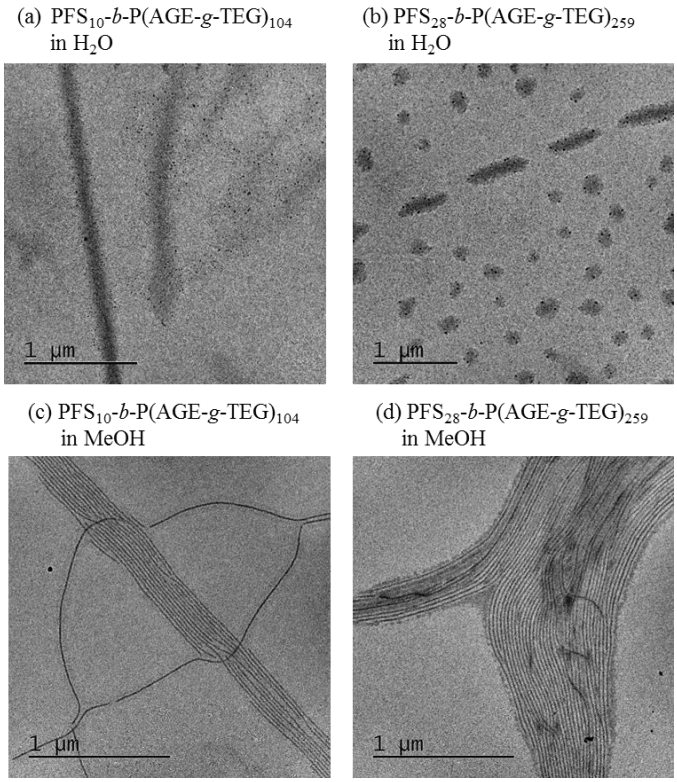

Figure S2.29. TEM images of (30 days aging) self-assembly solutions of (a) PFS_{10}-*b*-P(AGE-*g*-TEG)$_{104}$ in H_2O, (b) PFS_{28}-*b*-P(AGE-*g*-TEG)$_{259}$ in H_2O, (c) PFS_{10}-*b*-P(AGE-*g*-TEG)$_{104}$ in MeOH and (d) PFS_{28}-*b*-P(AGE-*g*-TEG)$_{259}$ in MeOH.

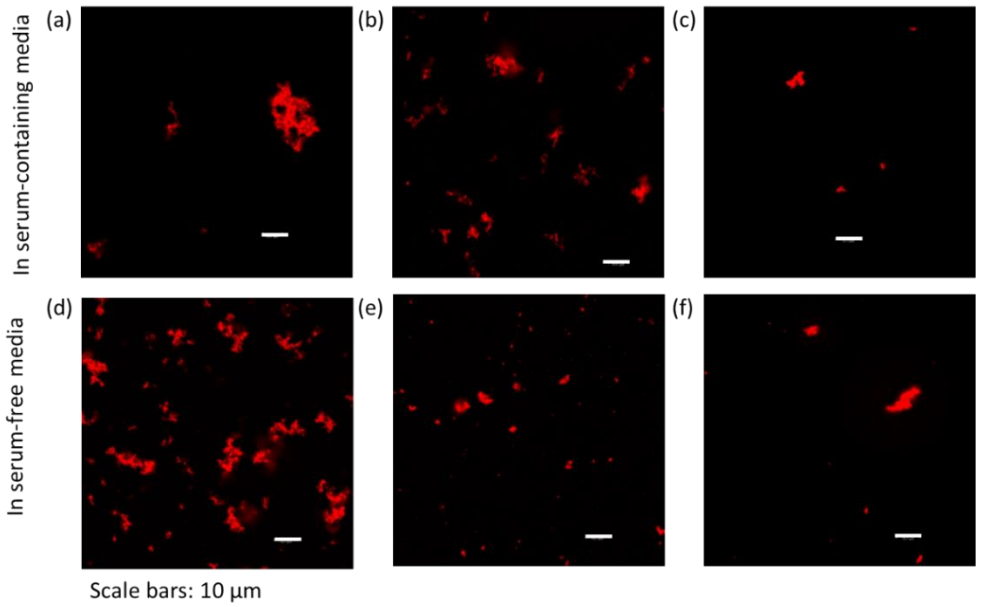

Figure S2.30. Aggregation studies of cylindrical micelles in (a-c) serum-containing and (d-f) serum-free cell media with concentrations of (a and d) 0.5, (b and e) 0.25 and (c and f) 0.06 mg/mL.

(a)

Aimed micelle				
Item	b percentage (%)	Total length (nm)	Central segment (nm)	Charged segment (nm)
1	5	150	142.5	7.5
2	10	150	135	15
3	25	150	112.5	37.5
4	50	150	75	75

(b)

Prepared micelle				
Item	Total length (nm)	Central segment (nm)	Charged segment (nm)	b percentage (%)
1	153	142	11	7
2	152	138	14	9
3	154	111	43	27
4	140	69	70	50

(c)

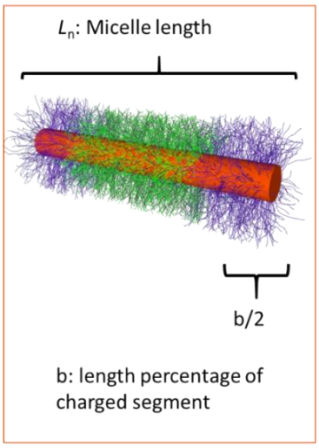

Figure S2.31. Preparation of triblock co-micelles with charged segments. (a) Designed triblock co-micelles based on PFS$_{27}$-*b*-P(AGE-*g*-TEG/dye1)$_{100}$, (b) prepared triblock co-micelles based on PFS$_{27}$-*b*-P(AGE-*g*-TEG/dye)$_{100}$ with varied charged segment lengths and (c) schematic representation of charged triblock co-micelles.

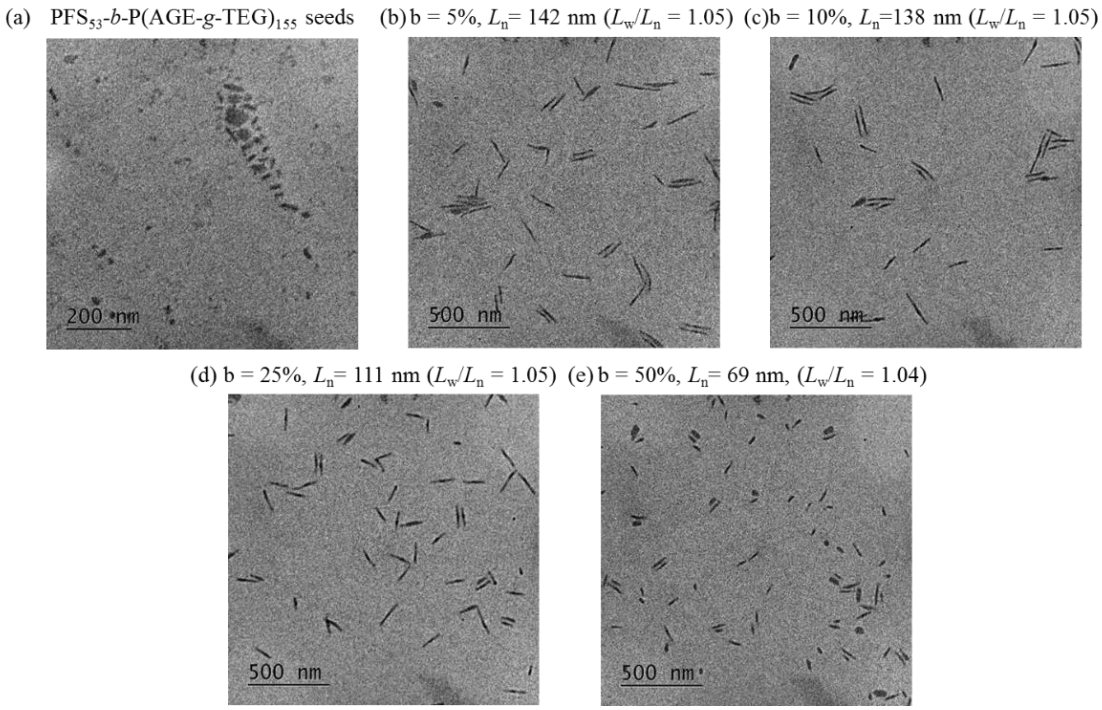

Figure S2.32. TEM images of central segments for triblock co-micelles by addition of PFS$_{27}$-*b*-P(AGE-*g*-TEG/dye1)$_{100}$ (unimer in THF) to (a) PFS$_{53}$-*b*-P(AGE-*g*-TEG)$_{155}$ seed (L_n = 23, L_w/L_n = 1.06, in DMF) in MeOH; (b) central segment for aimed b = 5%; (c) central segment for aimed b = 10%; (d) central segment for aimed b = 25% and (e) central segment for aimed b = 50%.

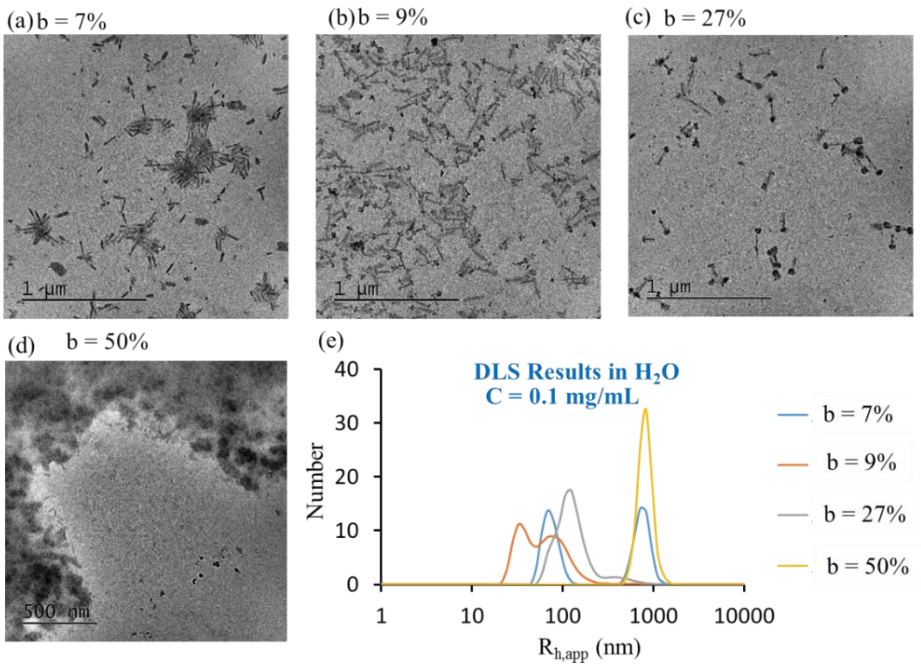

Figure S2.33. Evaluation of prepared triblock co-micelles based on PFS_{27}-*b*-P(AGE-*g*-TEG/dye1)$_{100}$ after dialysis into H_2O. TEM images of triblock comicelles with (a) b = 7%, (b) b = 9%, (c) b = 27% and (d) b = 50%. (e) DLS analysis of micelles in H_2O.

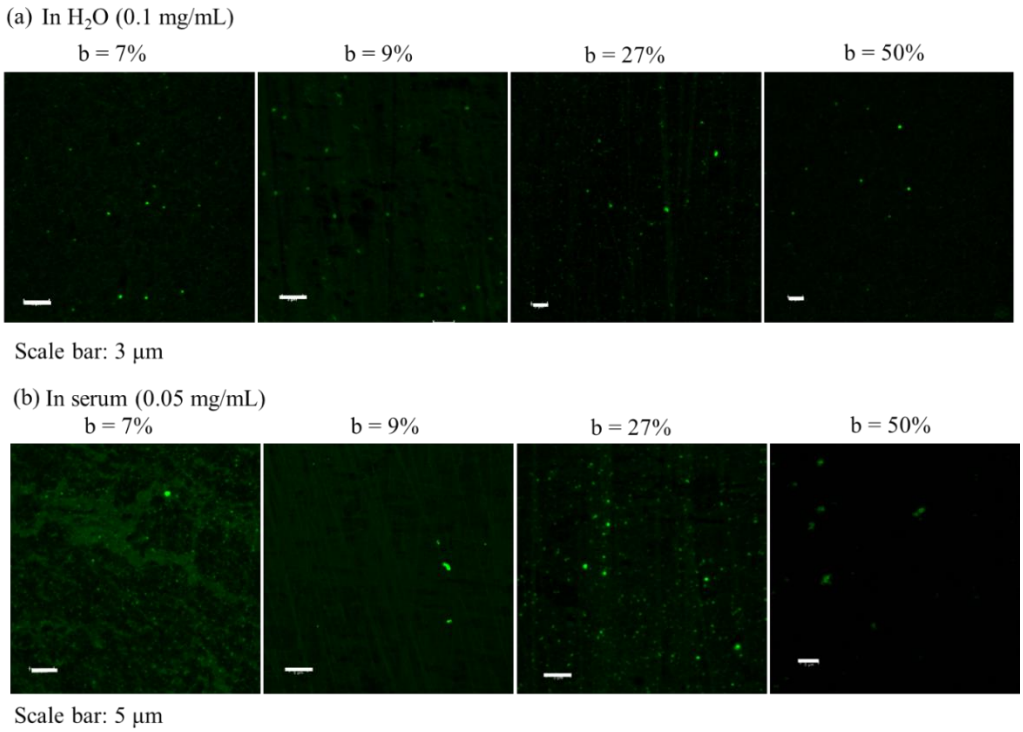

Figure S2.34. CLSM images of aggregation studies on triblock comicelles based on PFS_{27}-*b*-P(AGE-*g*-TEG/dye1)$_{100}$ in (a) H_2O and (b) cell media.

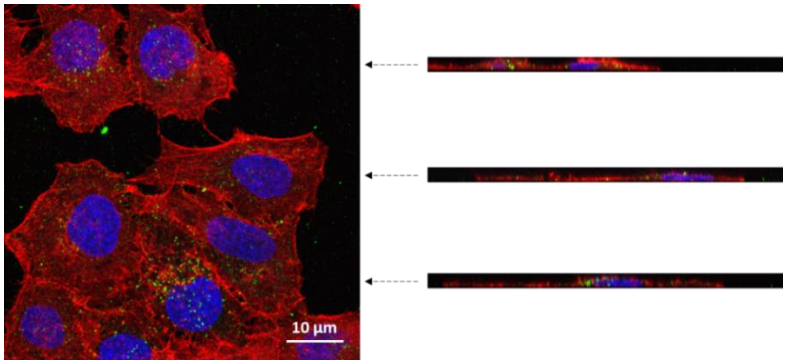

Figure S2.35. CLSM Z-cross section images of cellular uptake of PFS_{27}-*b*-P(AGE-g-TEG/dye1)$_{100}$ micelles by HeLa cells with 8 h incubation with a concentration at 0.05 mg/mL. Dotted arrows indicate xz cross section through the cells at that point. Green puncta within red boundary indicates micelles within the cell not stuck to the surface. Red shows phalloidin-594 stained actin filaments in cytoplasm. Blue indicates DAPI stained cell nuclei.

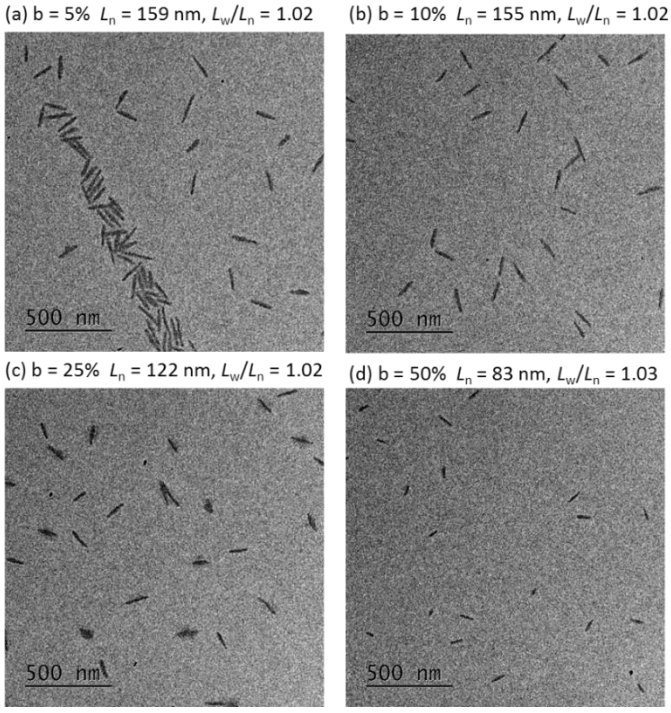

Figure S2.36. TEM images of central segments for triblock co-micelles by addition of blend unimer (PFS_{28}-*b*-$PNIPAm_{494}$ and PFS_{27}-*b*-P(AGE-*g*-TEG/dye1)$_{100}$ in 1: 1 mass ratio, in THF) to PFS_{53}-*b*-P(AGE-*g*-TEG)$_{155}$ seed (L_n = 23, L_w/L_n = 1.06, in DMF) in MeOH with different aimed length: (a) central segment for aimed b = 5%; (b) central segment for aimed b = 10%;(c) central segment for aimed b = 25% and (d) central segment for aimed b = 50%.

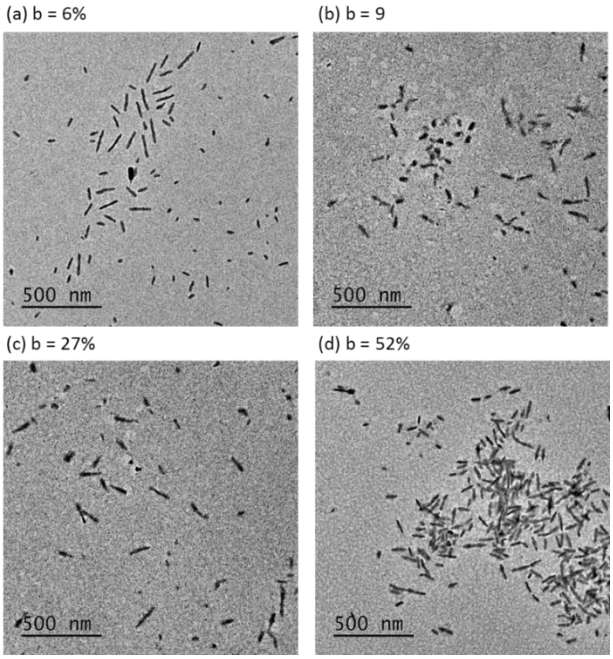

Figure S2.37. TEM images showed the fragmentation of PFS_{28}-*b*-$PNIPAm_{494}$ micelles after dialysis into H_2O.

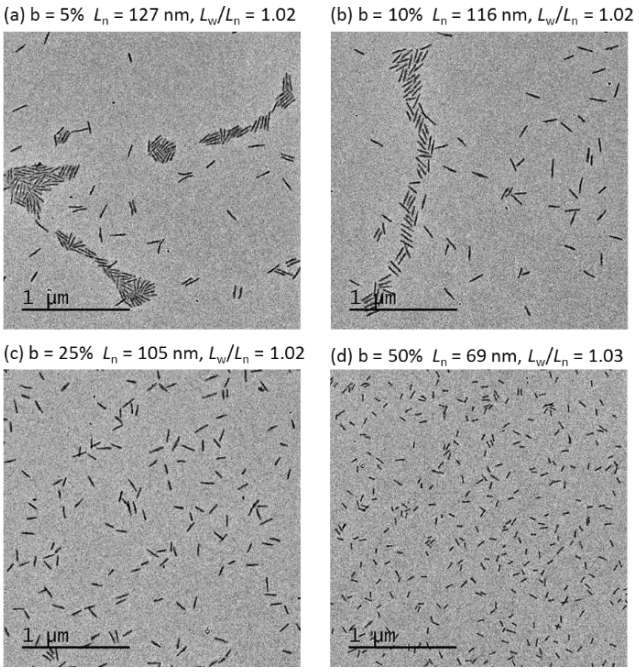

Figure S2.38. TEM images of central segments for triblock co-micelles by addition of blend unimer (PFS_{28}-*b*-$PMMA_6$-*b*-$PNIPAm_{496}$ and PFS_{27}-*b*-P(AGE-*g*-TEG/dye1)$_{100}$ in 1: 1 mass ratio, in THF) to PFS_{53}-*b*-P(AGE-*g*-TEG)$_{155}$ seed (L_n = 23, L_w/L_n = 1.06, in DMF) in MeOH with different aimed length: (a) central segment for aimed b = 5%; (b) central segment for aimed b = 10%;(c) central segment for aimed b = 25% and (d) central segment for aimed b = 50%.

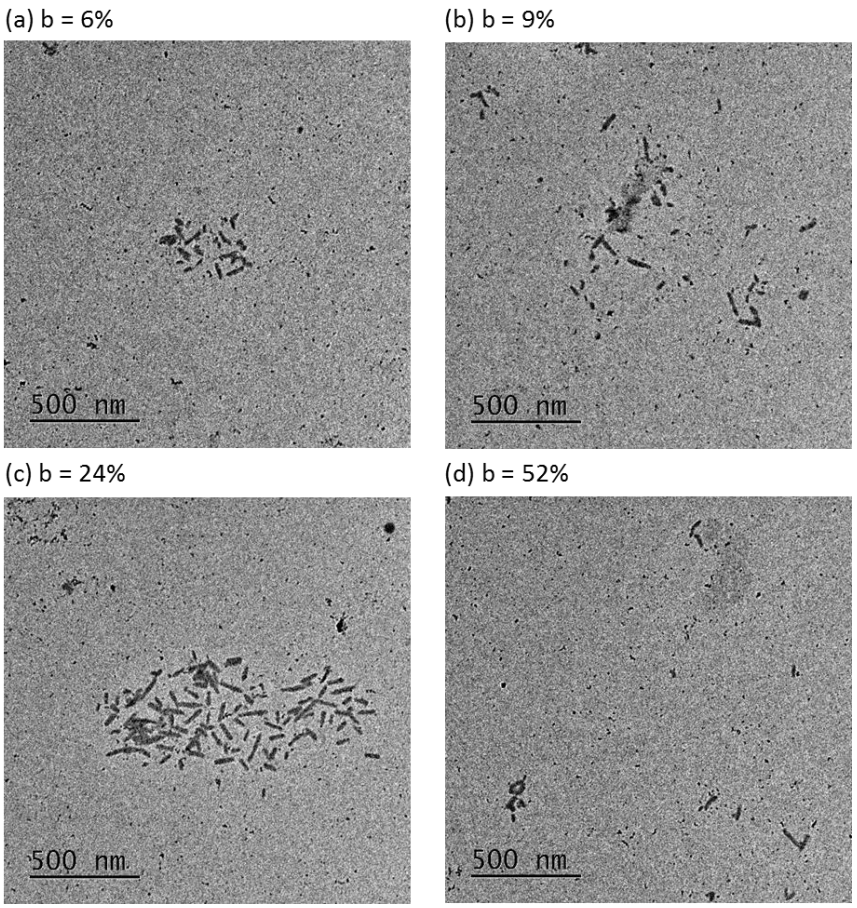

Figure S2.39. TEM images showed the fragmentation of PFS_{28}-*b*-$PMMA_6$-*b*-$PNIPAm_{496}$ micelles after dialysis into H_2O.

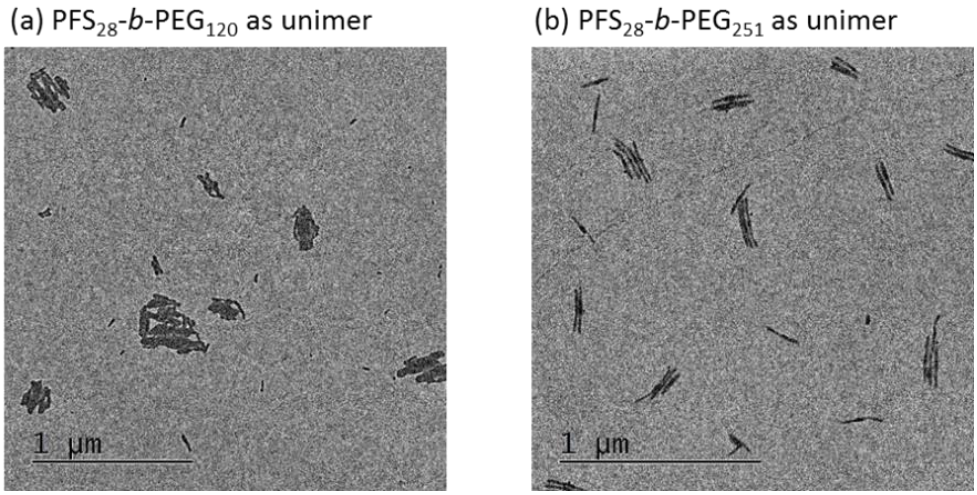

Figure S2.40. TEM images of seeded-growth samples (3 days aging) of adding unimers (a) PFS_{28}-*b*-PEG_{120} (in THF) and (b) PFS_{28}-*b*-PEG_{251} (in THF) with m_{unimer}:m_{seed} = 5 to PFS_{53}-*b*-P(AGE-*g*-TEG)$_{155}$ seed (L_n = 23, L_w/L_n = 1.06, in DMF) in MeOH.

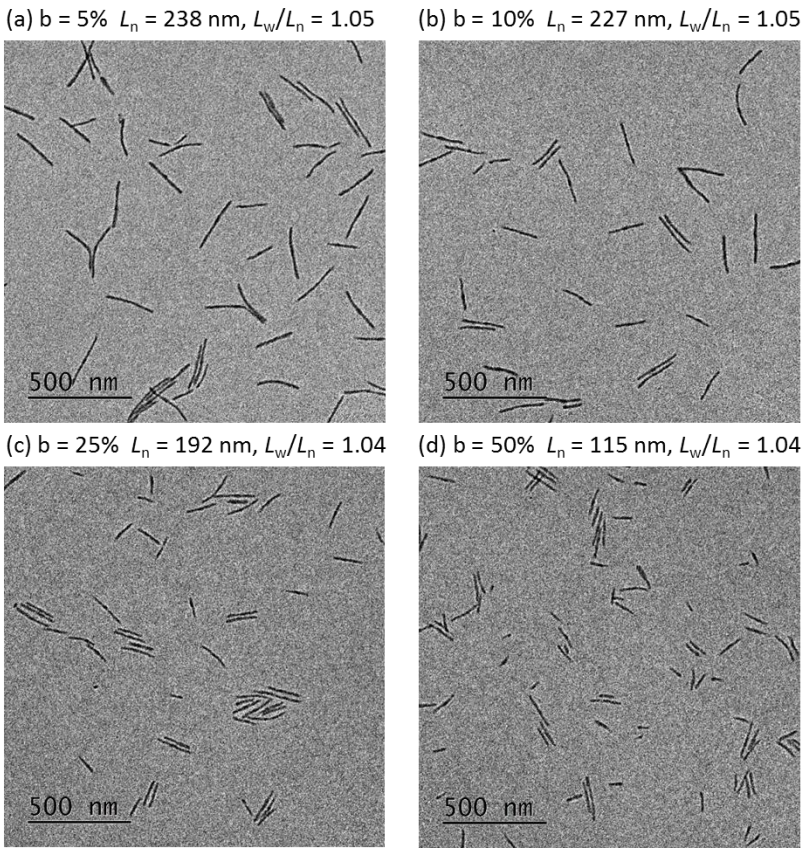

Figure S2.41. TEM images of central segments for triblock co-micelles by addition of blend unimer (PFS_{28}-*b*-PEG_{251} and PFS_{27}-*b*-P(AGE-*g*-TEG/dye1)$_{100}$ in 1: 1 mass ratio, in THF) to PFS_{53}-*b*-P(AGE-*g*-TEG)$_{155}$ seed (L_n = 23, L_w/L_n = 1.06, in DMF) in MeOH with different aimed length: (a) central segment for aimed b = 5%; (b) central segment for aimed b = 10%;(c) central segment for aimed b = 25% and (d) central segment for aimed b = 50%.

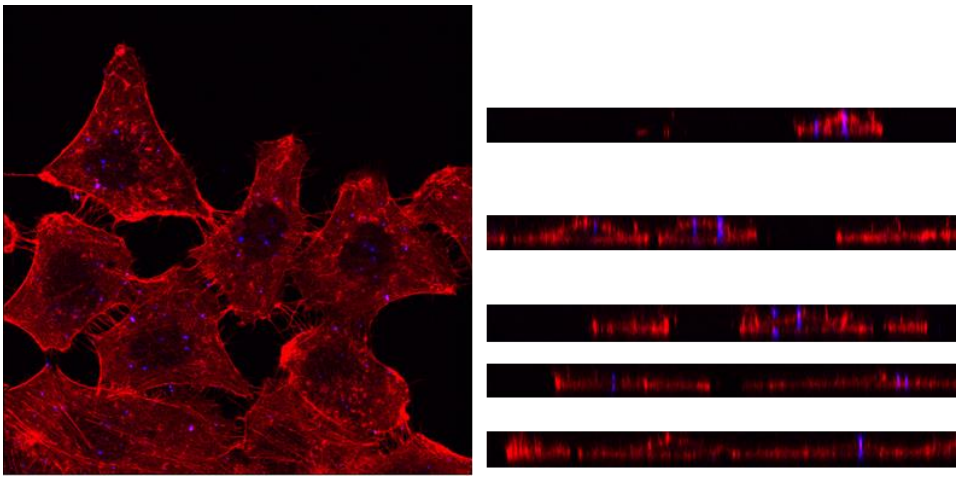

Figure S2.42. CLSM Z-cross section images of cellular uptake of PF_{13}-*b*-PEG_{227} micelles by HeLa cells with 8 h incubation with a concentration at 0.06 mg/mL. Red indicates phalloidin-594 stained actin filaments in cytoplasm and blue puncta indicate PF-*b*-PEG fibre-like micelles.

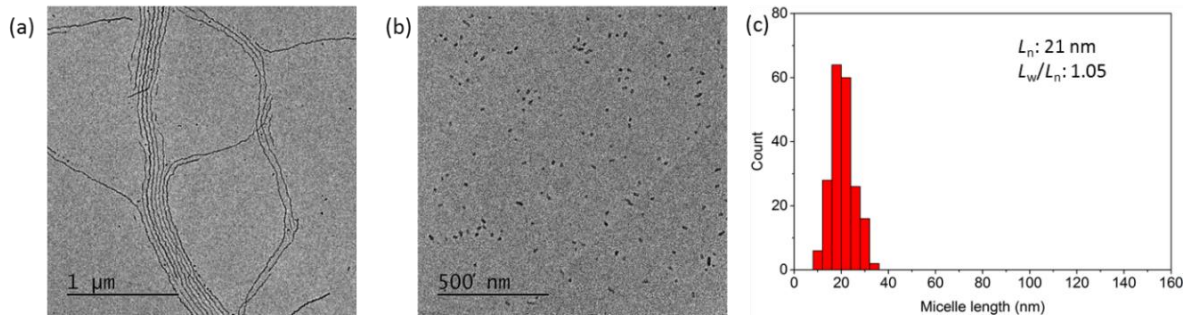

Figure S2.43. Preparation of PF_{13}-*b*-PEG_{227} seed micelles. (a) Polydisperse fibres of PF_{13}-*b*-PEG_{227} by direct dissolution in MeOH/THF (*v*:*v* = 1:1) at 0.5 mg/mL at 23 °C, (b) seed micelles prepared by sonication at 0 °C in a ultrasonic bath for 3 h (L_n: 21 nm, L_w/L_n: 1.05) and (c) contour length histogram of seed micelles.

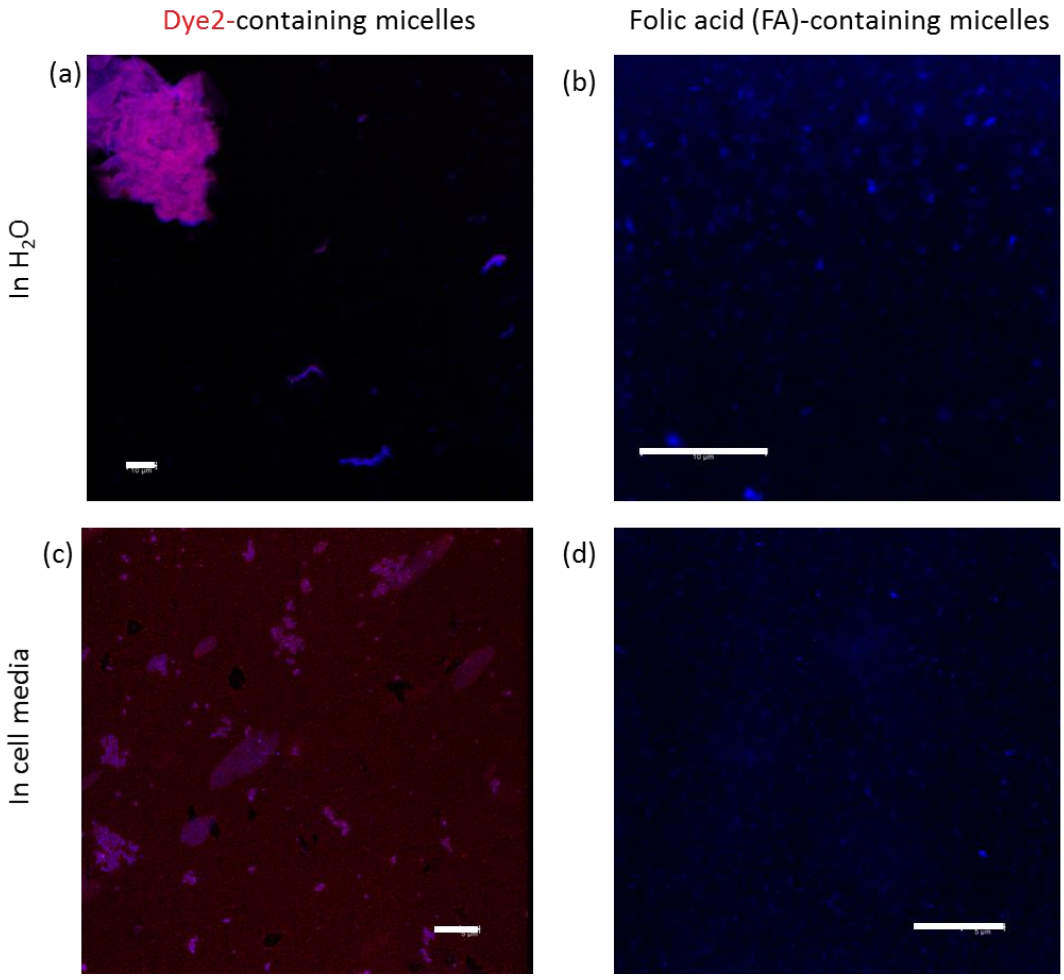

Figure S2.44. CLSM images of aggregation studies of (a and c) PF_{13}-*b*-PEG_{227}-Dye2 and (b and d) PF_{13}-*b*-PEG_{227}-FA micelles in (a and b) H_2O and (c and d) cell media. Scale bar: 10 μm.

Table S2.1. Molecular weight characterisation of homopolymers and diblock copolymers.

Polymer	M_w (g·mol^{-1})[a]	M_n (kg·mol^{-1})[b]	M_n (kg·mol^{-1})[c]	$Đ_M$[c]	Block ratio (Core:Corona)[b]
PFS_8-vinyl	2,083	-	-	-	-
PFS_8-OH	2,079	-	1.7	1.09	-
PFS_8-*b*-$PAGE_{115}$	-	15.1	11.1	1.11	1:14
PFS_{10}-vinyl	2,564	-	3.1	1.13	-
PFS_{10}-OH	2,641	-	3.2	1.16	-
PFS_{10}-*b*-$PAGE_{104}$	-	14.3	9.5	1.16	1:10
PFS_{27}-vinyl	6,742	-	6.9	1.12	-
PFS_{27}-OH	6,665	-	7.2	1.12	-
PFS_{27}-*b*-$PAGE_{100}$	-	17.9	86.7	1.24	1:3.7
PFS_{28}-vinyl		-			-
PFS_{28}-OH	6,978	-	6.4	1.14	-
PFS_{28}-*b*-$PAGE_{259}$	-	36.3	19.5	1.13	1:9
PFS_{53}-vinyl	12,939	-	10.7	1.08	-
PFS_{53}-OH	13,017	-	10.8	1.11	-
PFS_{53}-*b*-$PAGE_{155}$	-	30.5	24.7	1.13	1:2.9
PFS_{28}-CTA	7,240	-	8.9	1.16	-
PFS_{28}-*b*-$PMMA_6$	-	7.4	12.4	1.21	1:0.2
PEG_{116}-COOH	5,177	-	6.8	1.09	-
PEG_{220}-COOH	9,762	-	13.2	1.14	-
HO-PEG_{249}-OTs	11,029	-	-	-	-
HO-PEG_{249}-N_3	10,988	-	-	-	-
PF_{13}	4,425	-	8.5	1.22	-

[a] determined by MALDI-TOF MS [b] determined by ^{1}H NMR spectroscopy, [c] determined by GPC relative to polystyrene (PS) standards in *n*-Bu_4NBr/THF.

Chapter 3 **Optimizing the 'Living' Crystallisation-Driven Self-Assembly of Poly(*L*-lactide) Block Copolymers: Uniform Fibre-Like Micelles and Block Co-micelles via Solvent Quality Modulation**

Abstract

Fibre-like micelles based on biodegradable and biocompatible polymers exhibit considerable promise for applications in nanomedicine, but until recently no methods were easily available to prepare samples with controllable, uniform dimensions and spatial control functionality. 'Living' crystallisation-driven self-assembly (CDSA) is a promising, recently developed seeded-growth method for the preparation of uniform 1D and 2D nanoparticles from crystallisable polymeric amphiphiles. Poly(*L*-lactide) (PLLA) is a crystalline biodegradable polymer which has been widely studied in biomedicine. However, the creation of uniform PLLA-based fibre-like structures by 'living' CDSA has been a major challenge. Herein, we report the successful formation of uniform fibre-like nanoparticles of PLLA block copolymers with controlled lengths up to 1 μm by 'living' CDSA through modulation of solvent quality. This likely improves solvation of the unimers at least partly by reducing hydrogen bonding interactions among PLLA chains. We propose that this minimises unwanted unimer aggregation which otherwise favours undesirable self-nucleation that competes with epitaxial crystallisation from seed termini. The same approach has also allowed the formation of well-defined segmented block co-micelles with PLLA cores via the sequential seeded-growth of different PLLA block copolymers.

3.1. Introduction

The solution self-assembly of amphiphilic block copolymers (BCPs) with amorphous core-forming blocks has been widely studied as a method of fabricating nanoparticles with morphologies such as spheres, cylinders/worms or 'fibre-like' micelles, platelets and vesicles.[38, 314-316] Cylinders or fibre-like micelles are attracting much interest particularly in biomedicine, due to the advantages of extended in vivo circulation times and improved cellular uptake behaviour compared with spherical particles.[215, 317, 318] However, morphologically pure samples of fibre-like micelles with amorphous core-forming blocks

are challenge to access by BCP self-assembly as they correspond to a restricted region of phase space.[268] Furthermore, length control and access to low dispersity samples has not been possible.[63, 262, 266, 267, 271, 272, 319]

Recent work has demonstrated that BCPs and related amphiphiles with a crystalline core-forming block readily form 1D fibres via a process termed crystallisation-driven self-assembly (CDSA).[70, 97, 274] Moreover, seeded-growth methods have been developed which allow length control, and access to low length dispersity samples. This process is analogous to living covalent polymerisations, and has been termed 'living CDSA' (Scheme 3.1).[139, 140, 158] In the most common form of living CDSA, polydisperse fibre-like micelles are prepared first in solution and are then fragmented by sonication to form small fragments or 'seeds'. The termini of these seeds are active to epitaxial growth of additional BCP and adjustment of the ratio of the added BCP to the seeds yields fibre-like micelles of controlled length and a low length dispersity.

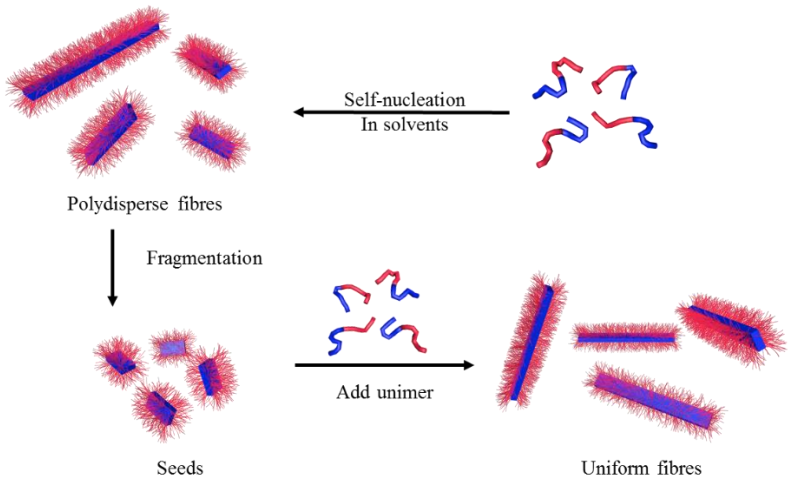

Scheme 3.1. Schematic representation of uniform fibres prepared by seeded-growth method of living CDSA.

The living CDSA method was initially developed using BCPs with crystallisable poly(ferrocenyldimethylsilane) (PFS)[92] core-forming block. Cylinders can be formed with a wide range of corona-core block ratios from 6:1 to 22:1,[97, 136] and using living CDSA with lengths from ca. 20 nm to > 5 μm.[140, 146] The sequential addition of PFS BCPs with different corona-forming blocks yields

segmented block co-micelles.[139] The formation of 1D block co-micelles that possess spatially-defined coronal regions with complementary hydrogen-bonding (H-bonding) groups allows access to supermicelles via hierarchical self-assembly.[158, 159] In addition, 2D platelets with controlled size have been prepared from diblock copolymers with low corona-core block ratios,[320] blends of diblock copolymer and homopolymer,[156] and charge-terminated homopolymers.[157] The properties and applications of PFS-based micelles and supermicelles have also been explored, such as their lyotropic liquid crystalline phase behaviour,[321] use in surface patterning,[322] and behaviour in aqueous media[217] such as interface stabilisation to form colloidosomes.[163]

Studies on fibre-like micelle formation with crystalline-coil BCPs have been extended to other materials, such as polyethylene[102, 103, 165, 323] and π-conjugated polymers.[120, 121, 170, 172, 173, 175, 278, 324-330] In order to develop applications in nanomedicine, well-defined 1D micelles based on crystalline biodegradable and biocompatible polymers are highly desirable. Polyesters such as Poly(*L*-lactide) (PLLA) and poly(ε-caprolactone) (PCL) as well as polycarbonates fulfil these requirements, and the exploration of living CDSA approaches to yield well-defined 1D and 2D assemblies derived from these materials as core-forming blocks has attracted much attention.[106, 107, 111, 113, 127, 137, 183, 253, 254, 290, 331-334] Examples of length control of up to ca. 800 nm have been described for PCL-b-poly(*N*,*N*-dimethylacrylamide) (PCL-*b*-PDMA) fibre-like micelles in ethanol. After transferring seeds into water by dialysis, living CDSA was carried out directly in aqueous media.[166] In addition, a recent report[167] described the successful extension of seeded-growth methods to polycarbonate-based fibre-like micelles.

In contrast, the efficient use of living CDSA methods for PLLA BCPs has been a substantial challenge. Initial studies in 2011 demonstrated that fine-tuning the self-assembly solvent composition and temperature allowed the formation of uniform fibre-like micelles with length up to 300 nm.[253, 254] By altering the solvation of the PLLA core-forming block, transitions between spheres (with kinetically-trapped amorphous cores) and cylinders (with crystalline cores) have been reported.[331] Further studies revealed a remarkable reverse morphology cylinder-to-sphere transition triggered by the stereocomplexation of two enantiomeric BCPs with PLLA and poly(*D*-lactide) (PDLA) core-forming

blocks.[111] More recently, the solubility of PLLA-*b*-PDMA diblock copolymers has been found to have another interesting and unexpected effect on the morphology formation.[137] A high corona-core block ratio (20:1) leads to a preference for the formation of 2D platelet micelles, while a low ratio (3:1) was found to lead to 1D cylindrical micelles. This behaviour is the opposite to that usually observed for self-assembled BCPs with crystallisable core-forming blocks predicted by packing parameter (*p*) considerations. The CDSA of PLLA-based diblock and triblock copolymers has also been characterised in detail by establishment of a phase diagram showing the morphology formed versus hydrophobic fraction.[113] Significantly, uniform 2D platelets with PLLA cores can be obtained under thermal self-seeding conditions in which seed formation is controlled by temperature.[256] In addition, 2D platelets with controlled dimensions and block co-platelets with spatially segmented structures have been reported using seeded-growth of a charge-terminated PLLA homopolymers.[157] However, to date no uniform 1D fibre-like micelles of PLLA-based diblock copolymers with length control over a wide range have been reported via a seeded-growth process under mild conditions.

Herein, we discuss a detailed collaborative exploration of the 'living' CDSA of PLLA-containing diblock copolymers in an attempt to improve the length control of PLLA fibre-like micelles formed. In addition, we have attempted to develop a new and efficient approach to allow access to currently unknow complex assemblies such as PLLA-based block co-micelles.

3.2. Results and Discussion

3.2.1. PLLA BCP Synthesis and Characterisation.

In this work, we have focused our studies on two PLLA BCPs, PLLA-*b*-Poly(*N*-isopropylacrylamide) (PLLA-*b*-PNIPAm) and PLLA-*b*-Poly(2-vinylpyridine) (PLLA-*b*-P2VP). In order to favour 1D fibre-like micelles formation, block ratios were targeted in which the degree of polymerisation (DP_n) of the corona-forming block was substantially larger than that of PLLA segment.

PLLA-*b*-PNIPAm and PLLA-*b*-P2VP BCPs were synthesised via a combination of ring-opening polymerisation (ROP) and reversible addition-fragmentation chain transfer (RAFT) polymerisation. PLLA homopolymer was first prepared by ROP with a dual-headed chain transfer agent (CTA) containing a terminal alcohol in the presence of a catalyst, 1,8-diazabicyclo[5.4.0]undec-7-ene (DBU). Subsequent RAFT polymerisation was conducted with the CTA-PLLA macroinitiators to prepare diblock copolymers (Scheme 3.2). The polymers can be obtained with predictable average molecular weights and relatively low molar mass distribution ($Đ_M$) according to different characterisation techniques (Table 3.1): gel permeation chromatography (GPC) analysis was used to determine the number average molecular weight (M_n) and $Đ_M$ (Figure S3.1); matrix assisted laser desorption ionization-time of flight mass spectrometry (MALDI-TOF MS) was employed to confirm the weight average molecular weight (M_w) of CTA-PLLA(Figure S3.2); and nuclear magnetic resonance (NMR) spectroscopy was used to confirm the block ratio of the diblock copolymer according to the molecular weight of PLLA homopolymer from MALDI-TOF MS characterisation (Figure S3.3).

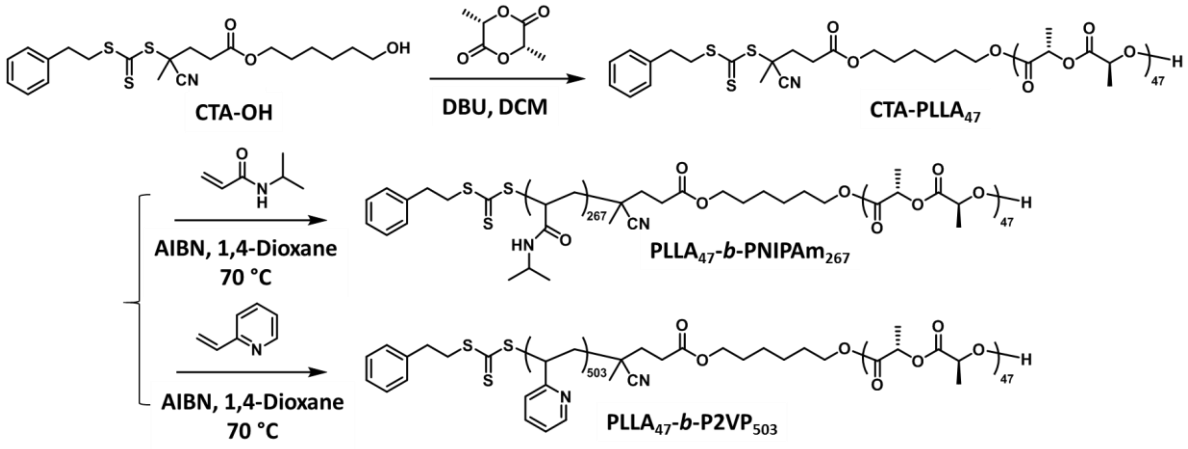

Scheme 3.2. Synthesis of $PLLA_{47}$-containing diblock copolymers.

PLLA homopolymer, formed by transesterification during the ROP or water initiation,[335] may exist as an impurity in the final PLLA-*b*-PNIPAm diblock copolymer after RAFT polymerisation of NIPAm. The presence of homopolymer may change the morphology during the self-assembly process.[336] Therefore, confirmation of the lack of homopolymer in the prepared diblock copolymer is of key importance. To confirm the purity of the diblock copolymer, DOSY NMR spectroscopic analysis was employed to complement GPC characterisation. In the ^{1}H NMR spectrum of PLLA$_{47}$-*b*-PNIPAm$_{267}$ (Figure S3.3b), the peaks at δ = 6.50, 4.00, 2.01 and 1.15 ppm were assigned to PNIPAm and δ = 5.15 and 1.56 ppm were assigned to PLLA, while in the ^{1}H NMR spectrum of PLLA$_{47}$-*b*-P2VP$_{502}$ (Figure S3.3c), the peaks at δ = 8.31, 7.04, 6.80, 6.30, 2.28 and 1.89 ppm were assigned to P2VP. In the DOSY spectra of the PLLA$_{47}$-*b*-PNIPAm$_{267}$ and PLLA$_{47}$-*b*-P2VP$_{502}$ (Figure S3.4b and c), all the signals appeared with a singular diffusion coefficient of $D = 1.31 \times 10^{-6}$ and 7.26×10^{-6} cm^2·s^{-1}, respectively. CTA-PLLA$_{47}$ homopolymer was also analysed by DOSY NMR spectrum, and the diffusion coefficient was found as $D = 9.16 \times 10^{-6}$ cm^2·s^{-1}. No signals can be detected above $D = 9.16 \times 10^{-6}$ cm^2·s^{-1} in either DOSY spectra, therefore, the PLLA$_{47}$-*b*-PNIPAm$_{267}$ and PLLA$_{47}$-*b*-P2VP$_{502}$ were successfully prepared as essentially pure diblock copolymers devoid of homopolymer impurities.

Table 3.1. Summary of PLLA-containing polymers characterisation data.

Polymer	M_w (g·mol^{-1})[a]	M_n (kg·mol^{-1})[b]	M_n (kg·mol^{-1})[c]	$Đ_M$[c]	Block ratio (Core:Corona)[b]
PLLA$_{47}$	7232	7.6	10.2	1.09	-
PLLA$_{47}$-*b*-PNIPAm$_{267}$	-	37.4	180	1.11	1:5
PLLA$_{47}$-*b*-P2VP$_{503}$	-	59.7	63.2	1.25	1:10

[a] determined by MALDI-TOF MS, [b] determined by ^{1}H NMR spectroscopy, [c] determined by GPC relative to PS standards in *n*-Bu$_4$NBr/THF.

The prepared polymers were also characterised by Fourier-transform infrared spectroscopy (FT-IR) (Figure S3.5) and thermogravimetric analysis (TGA) was carried out on the diblock copolymers (Figure S3.6). The latter showed that the decomposition temperatures (defined as the temperatures of 5% mass loss) of $PLLA_{47}$-*b*-$PNIPAm_{267}$ and $PLLA_{47}$-*b*-$P2VP_{503}$ were determined to be 245 and 295 °C, respectively.

3.2.2. Living CDSA Studies for $PLLA_{47}$-*b*-$PNIPAm_{267}$ in EtOH

Our initial attempts to perform controlled self-assembly of PLLA-containing diblock copolymers was carried out using the seeded-growth, living CDSA method.[139, 337] First seed micelles were prepared based on previously reported procedures.[158] Polydisperse $PLLA_{47}$-*b*-$PNIPAm_{267}$ micelles were prepared by heating the solution of polymer in a mixture of dimethyl sulfoxide (DMSO) and ethanol (EtOH) (*v*:*v* = 1:9) at 70 °C for 2 h followed by slow cooling to 23 °C over 2.5 h (Figure 3.1a). DMSO was used as a common solvent in the self-assembly. Although the solubility parameters for the polymer and solvent are significantly different (δ_{PLLA} = 20.2 $MPa^{1/2}$, δ_{DMSO} = 26.4 $MPa^{1/2}$), the formation of molecularly dissolved unimers and the absence of detectable aggregates was demonstrated by dynamic light scattering (DLS, Figure 3.10). EtOH was used as the selective solvent for self-assembly due to the similar solubility parameters of PNIPAm and EtOH (δ_{PNIPAm} = 24.8 $MPa^{1/2}$ and δ_{EtOH} = 26.2 $MPa^{1/2}$). Seed micelles were prepared by sonication of the polydisperse $PLLA_{47}$-*b*-$PNIPAm_{267}$ micelle solution in an ultrasonic bath for 2 h at 0 °C (Figure 3.1b). The prepared seed micelles had a measured number average length (L_n) of 36 nm and a length dispersity (L_w/L_n) of 1.10 (Figure 3.1c).

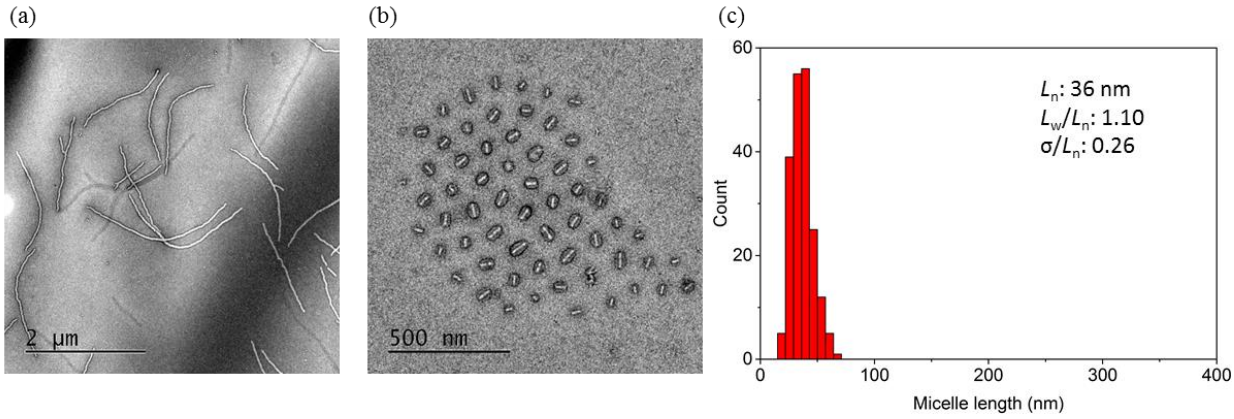

Figure 3.1. TEM images of (a) polydisperse $PLLA_{47}$-*b*-$PNIPAm_{267}$ micelles prepared by heating the polymer in DMSO/EtOH (1:9) at a concentration of 0.5 mg/mL at 70 °C for 2 h followed by slow cooling down to 23 °C ; (b) seeds prepared by sonication of polydisperse micelles at 0 °C for 2 h in a sonic cleaning bath; (c) contour length histogram of measured seeds length, L_n = 36 nm, L_w/L_n = 1.10, σ/L_n: 0.26. TEM samples were stained with a 2 wt% solution of uranyl acetate in EtOH.

Elongated micelles were obtained by adding unimers ($PLLA_{47}$-*b*-$PNIPAm_{267}$ in DMSO) to the seed solutions in EtOH. By varying the volume of unimer solution added to the seed solutions, different unimer-to-seed mass ratios (m_{unimer}:m_{seed}) were obtained. After aging for 5 days, samples were analysed by TEM. The images (Figure 3.2a-f) showed that elongated micelles had measured L_n values from ca. 100 - 800 nm, with $L_w/L_n \geq 1.06$ depending on the unimer-to-seed mass ratios. If the epitaxial growth of the micelles is controlled in manner akin to a living covalent polymerisation, a linear relationship of the measured average length versus the unimer-to-seed mass ratio should be observed. However, although elongated micelles and a linear growth trend of micelle length were obtained, the lengths were found to be significantly shorter than theoretical values (Figure 3.2g). The theoretical average length can be calculated from $L_n = (m_{unimer}/m_{seed} + 1) \times L_{n\ seed}$. Furthermore, at the higher unimer-to-seed mass ratios (m_{unimer}:m_{seed} = 20.0 and 30.0), the micelle length dispersity increased significantly (L_w/L_n = 1.12 and 1.15, respectively) which is reflected in the respective contour length histograms (Figure S3.7).

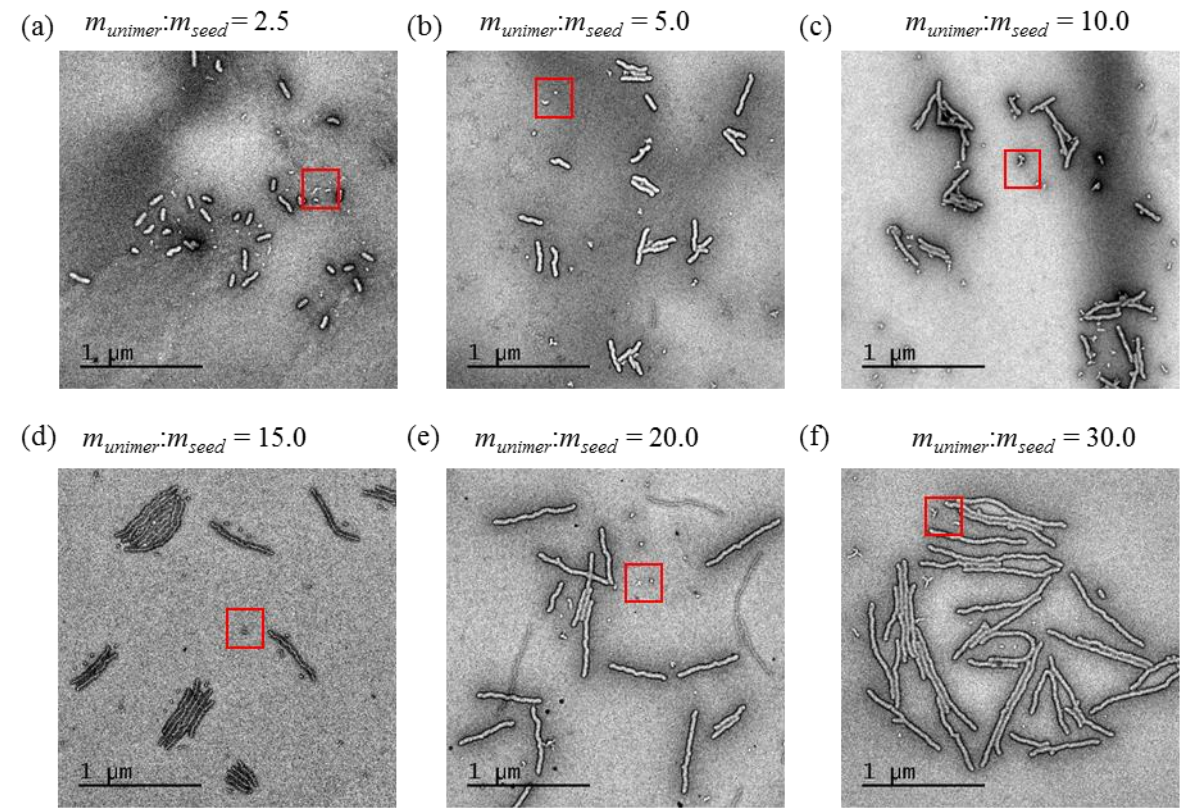

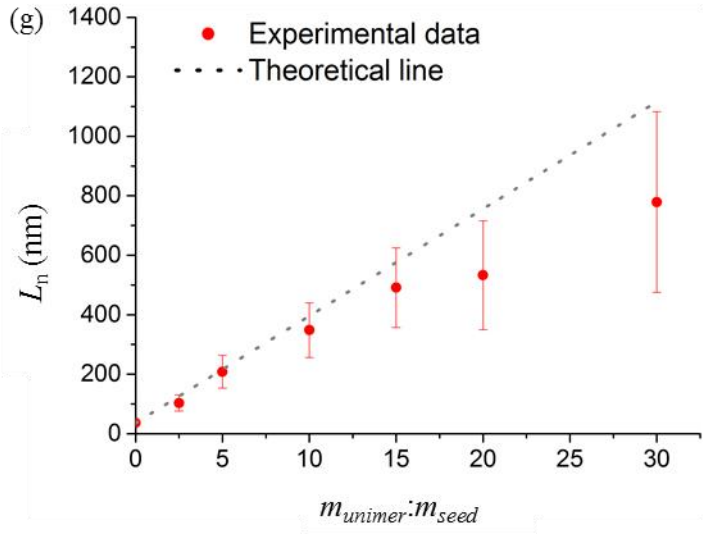

(h)

m_{unimer} :m_{seed}	L_n (nm)	L_w/L_n	σ/L_n
2.5	103	1.06	0.25
5.0	208	1.08	0.28
10.0	348	1.06	0.26
15.0	491	1.07	0.26
20.0	533	1.12	0.30
30.0	779	1.15	0.35

Figure 3.2. TEM images of samples (aging for 5 days) of elongated $PLLA_{47}$-*b*-$PNIPAm_{267}$ micelles prepared by seeded-growth from seed micelles (L_n = 36 nm, L_w/L_n = 1.10, σ/L_n: 0.26) in EtOH after addition of unimers (in DMSO) with unimer-to-seed mass ratios of (a) 2.5, (b) 5.0, (c) 10.0, (d) 15.0, (e) 20.0 and (f) 30.0; (g) plot of micelle number average length versus unimer-to-seed ratios; (h) measured length data summary. Red rectangles highlight spherical micelles. TEM samples were stained with a 2 wt% solution of uranyl acetate in EtOH.

Analysis of the results suggests that two factors could explain the results obtained. Firstly, the observation of small amounts of spherical micelles in the TEM at low unimer-to-seed mass ratios (red rectangles in Figure 3.2a-e) indicated that rapid aggregation of unimers competing with seeded-growth. This would reduce the amount of unimer available for seeded-growth and lower L_n values compared to those predicted based on the unimer-to-seed mass ratios. Secondly, the TEM data indicates that, especially at high unimer-to-seed mass ratios, an appreciable fraction of short fibre-like micelles was formed with an L_n value much lower than the theoretical value. This is illustrated in the contour length histograms where overlapping peaks were detected in lower micelle length regions when unimer-to-seed mass ratios were over 15 (Figure S3.7d-f). Significantly, the shortest micelles lengths measured in each sample were significantly longer than the length of seed (36 nm), which indicates that the presence of seed defects could not be the reason for the uncontrolled growth. The most likely explanation for the observed results is self-nucleation of added unimer, which results in the formation of new seeds is a problem.

Moreover, the self-nucleation effect would be expected to be amplified at high unimer-to-seed mass ratios due to the substantial increase in unimer concentration under these conditions resulting from the addition of relatively large amount of unimers to the seed solution. This is supported by the length distribution data in the contour length histograms (Figure S3.7).

3.2.3. Living CDSA Studies for PLLA$_{47}$-*b*-PNIPAm$_{267}$ in EtOH in the Presence of Trifluoroethanol (TFE) as a H-bond Disruptor

For living CDSA to be efficient, all or virtually all the added unimer needs to grow from the seed micelle termini. In the case of PLLA$_{47}$-*b*-PNIPAm$_{267}$ additional, undesirable unimer aggregation was detected to yield spherical micelles and there was also evidence for self-nucleation to generate new nuclei. One possible explanation for the facile unimer aggregation could be the formation of C−H···O hydrogen bonds (H-bonds) between the protons of a methyl group and the carbonyl oxygen on another polymer chain.

Hydrogen bonding (H-bonding) is an important non-covalent interaction in small molecules and biological macromolecules where it plays an important role in the formation of three-dimensional (3D) structures.[26, 338, 339] In block copolymer self-assembly, the morphologies formed can be altered by the presence of H-bonding moieties.[27, 251, 340, 341] The C−H···O bond is an example of a weak interaction that has been probed by computational calculations[342, 343] and FT-IR spectrometry.[344, 345] The bond energy of a C−H···O interaction has been calculated as 4.2-8.4 kJ/mol, significantly smaller than that of a well-known N−H···O or O−H···O bonds, at 16-21 kJ/mol. The significance of C−H···O bond has been recognized in structural and conformational determination of small molecules, nucleic acids, proteins and carbohydrates.[33, 346-348] PLA has a simple polyester backbone structure, which is expected to contain only weak interactions arising from H-bonding, dipole-dipole interactions, and van der Waals forces. The weak C−H···O bonds between PDLA and PLLA chains have been studied previously by real time IR spectroscopy, and have been shown to drive the formation of the PLLA/PDLA stereocomplex.[50, 349, 350] Hence, it is possible that H-bonding plays an important role in both PLLA BCP unimer aggregation and self-nucleation. This led us to explore the use of additives to mitigate this potential problem.

To prevent the fast self-nucleation when adding the unimer to seed solutions, trifluoroethanol (TFE), a reagent often used as a H-bond disruption agent,[351] was added into the solvent system. After optimisation the seeded-growth conditions, the amount of added TFE was increased with the increase of the unimer-to-seed ratio. Unimer with unimer-to-seed mass ratios of 2.5, 5.0, 10.0, 15.0, 20.0, and 30.0 was added to seed solutions in TFE/EtOH with volume ratio of 3:97, 3:97, 5:95, 8:92, 10:90 and 15:85, respectively. After aging for 5 days, the samples were analysed by TEM (Figure 3.3a-f). In contrast to the seeded-growth experiments performed in the absence of TFE, the measured micelle lengths possessed L_n values of up to 1103 nm, close to the theoretical values, with low dispersity ($L_w/L_n \leq 1.06$) even at high unimer-to-seed mass ratios (Figure 3.3h). A linear plot of the measured length versus the unimer-to-seed mass ratio was obtained (Figure 3.3g), with data points located on the theoretical line indicative of the controlled epitaxial growth of $PLLA_{47}$-*b*-$PNIPAm_{267}$ micelles by living CDSA. Significantly, the micelle contour length histograms showed narrow distributions for each

sample (Figure S3.8), which demonstrated a narrow length distribution and no overlapping peaks at low L_n values suggestive of a contribution from a self-nucleation event.

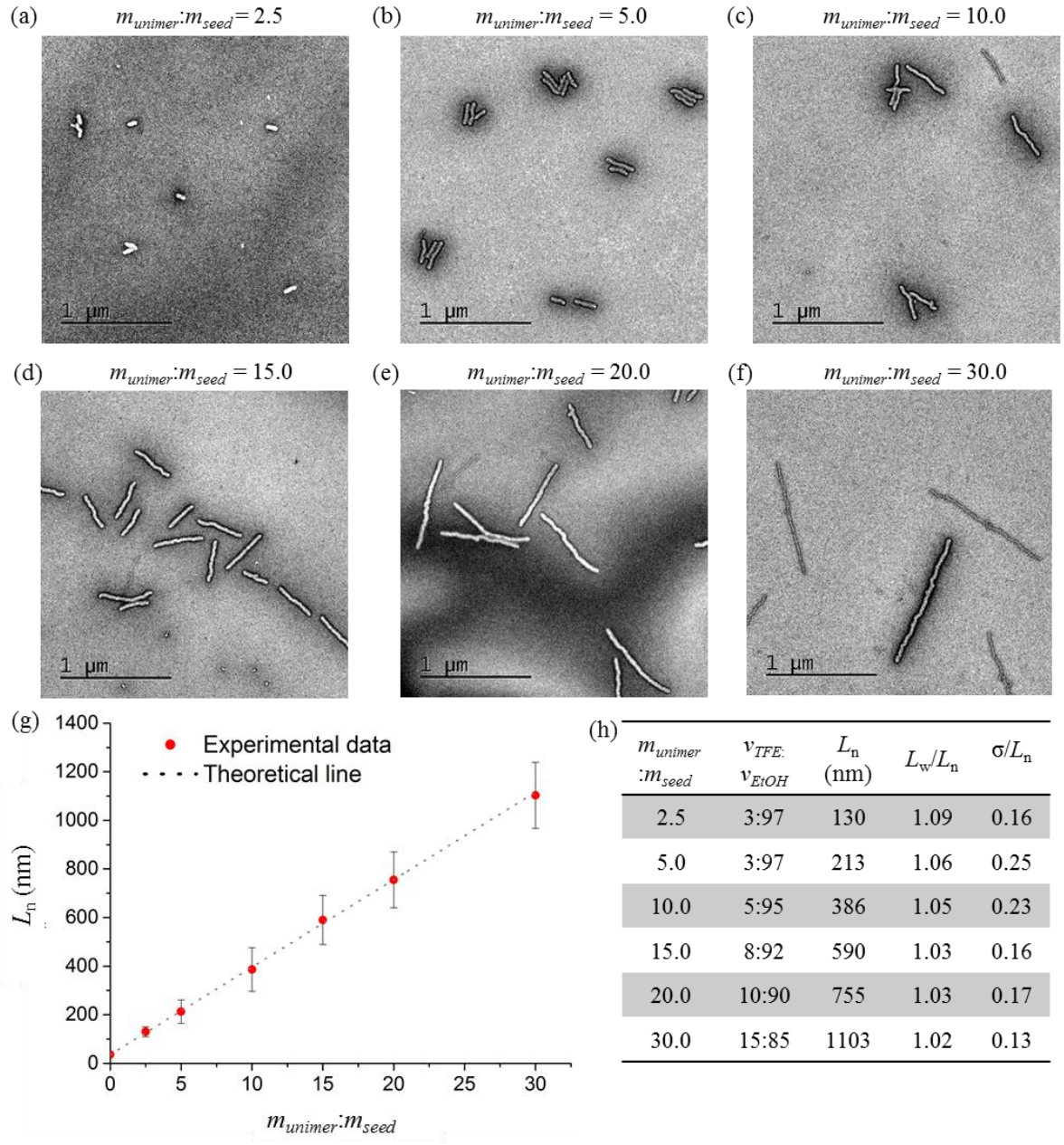

(h)

m_{unimer} :m_{seed}	v_{TFE}: v_{EtOH}	L_n (nm)	L_w/L_n	σ/L_n
2.5	3:97	130	1.09	0.16
5.0	3:97	213	1.06	0.25
10.0	5:95	386	1.05	0.23
15.0	8:92	590	1.03	0.16
20.0	10:90	755	1.03	0.17
30.0	15:85	1103	1.02	0.13

Figure 3.3. TEM images of samples (5 days aging) of uniform $PLLA_{47}$-*b*-$PNIPAm_{267}$ micelles prepared by seeded-growth from seed micelles (L_n = 36 nm, L_w/L_n = 1.10, σ/L_n: 0.26) in TFE/EtOH with volume ratios of (a) 3:97, (b) 3:97, (c) 5:95, (d) 8:92, (e) 10:90 and (f) 15:85 after the addition of unimers (in DMSO) with unimer-to-seed mass ratios of (a) 2.5, (b) 5.0, (c) 10.0, (d) 15.0, (e) 20.0 and (f) 30.0, respectively; (g) plot of number average micelle length vs m_{unimer}:m_{seed}; (h) summary of measured length and solvent compositions; TEM samples were stained with a 2 wt% solution of uranyl acetate in EtOH.

3.2.4. Characterisation of Fibre-Like PLLA$_{47}$-*b*-PNIPAm$_{267}$ Micelles

As living CDSA proceeds via an epitaxial growth mechanism the resulting crystalline micelle cores are highly ordered, and their structure has been likened to that of a single crystal.[138, 157] The ability to prepare fibre-like PLLA$_{47}$-*b*-PNIPAm$_{267}$ micelles via living CDSA in the presence of TFE facilitated detailed studies of the structure of the PLLA core using scattering experiments. We therefore took advantage of living CDSA under the aforementioned conditions to prepare a sample with L_n = 1040 nm and L_w/L_n = 1.04 (Figure S3.9). The fibres were analysed by atomic force microscopy (AFM), scanning transmission electron microscopy (STEM), selected area electron diffraction (SAED), powder X-ray diffraction (PXRD) and X-ray scattering techniques.

AFM measurements showed that the micelles possess a uniform height of 14 nm (Figure 3.4a and S3.10a and). The adhesion profile (Figure 3.4b) provided a detailed information such as the core width, and the width of the corona flanking each side of the core, giving values of 36 and 16 nm, respectively (Figure 3.4c). Due to the low electron density of PLLA$_{47}$-*b*-PNIPAm$_{267}$, TEM grids were negatively-stained with uranyl acetate (2% in EtOH), which resulted in a difficulty in terms of observing the corona forming block in conventional TEM images. Dark field STEM was used to characterise the micelle without the negative staining. The micrographs (Figure S3.11) illustrate the contrast between the core (dark) and the corona (bright). Measurements of core width ($W_{n,\,core}$) and corona width ($W_{n,\,corona}$) gave values of 24 and 18 nm, respectively. Based on the core height and width, the cross-section appears to be rectangular or a distorted oval or ellipse rather than circular.

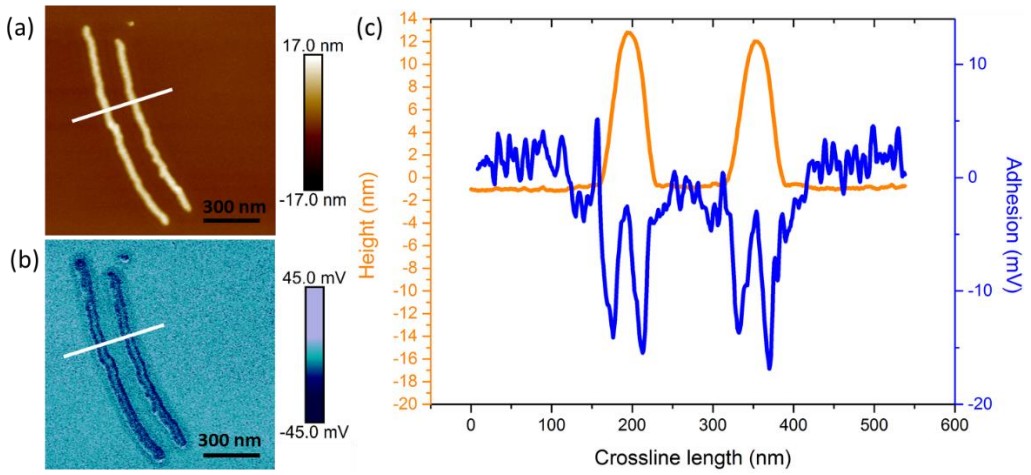

Figure 3.4. AFM images of $PLLA_{47}$-*b*-$PNIPAm_{267}$ micelles with controlled length. (a) Height image of micelles; (b) adhesion image of micelles; (c) linear height (orange) and adhesion (blue) profiles from (a) and (b).

To probe more details on the core structure, PXRD was carried out by drop-casting the micelle solution on a silicon substrate. The results showed weak broad Bragg peaks at 2θ = 16.7°, 19.0° and 23.0°, and a sharp peak at 28.9° (Figure 3.5a). This is in a good agreement with the α-form crystalline PLLA.[352] These angles correspond to the crystal planes with Miller index of (200/110), (203/113), (210) and (310/020) with d-spacing of 5.37, 4.66, 3.86 and 3.08 Å, respectively. The weak intensity of these peaks due to the small weight fractions of PLLA in $PLLA_{47}$-*b*-$PNIPAm_{267}$.

SAED was also employed to analyse the internal structure of micelles. Due to the rapid destruction of the micelles during irradiation by the electron beam, a video record was taken during the SAED experiment instead of a single image. The SAED image was a screenshot of the video recording when the beam was irradiating the micelles. A *quasi*-hexagonal pattern was obtained by SAED (Figure 3.5b and c). The diffraction pattern was shown as short lines (or stretched dots) rather than single dots, which presumably results from the aggregated and slightly misaligned micelles in the irradiation area on the TEM grid. The d-spacing was calculated as d = 5.43 Å, which is in a good agreement with the d-spacing of the 200/110 plane. From a combination of the PXRD and SAED results, the prepared micelles have a crystalline PLLA core with the same structure of PLLA α-form single crystal, which has an orthorhombic unit cell consisting of 10_3 helix PLLA chains with a = 10.7 Å, b = 6.2 Å, and c = 28.8 Å.[229]

To explore the orientation of the PLLA chains in the core, the fully extended PLLA chain length was calculated according to the reported PLLA α-form crystal unit cell data. In a PLLA unit cell, a 10_3 helix chain has a length of 28.8 nm (which is the length of c), which means a single repeat unit of *L*-lactide has a length of 5.76 nm. In the prepared $PLLA_{47}$-*b*-$PNIPAm_{267}$, a fully extended PLLA chain should have a length of 27.5 nm. Based on the AFM (core width of 36 nm and core height of 14 nm), PLLA chains appear to fold once and to pack parallel to the shortest axis of the core in the micelle (Figure 3.5d).

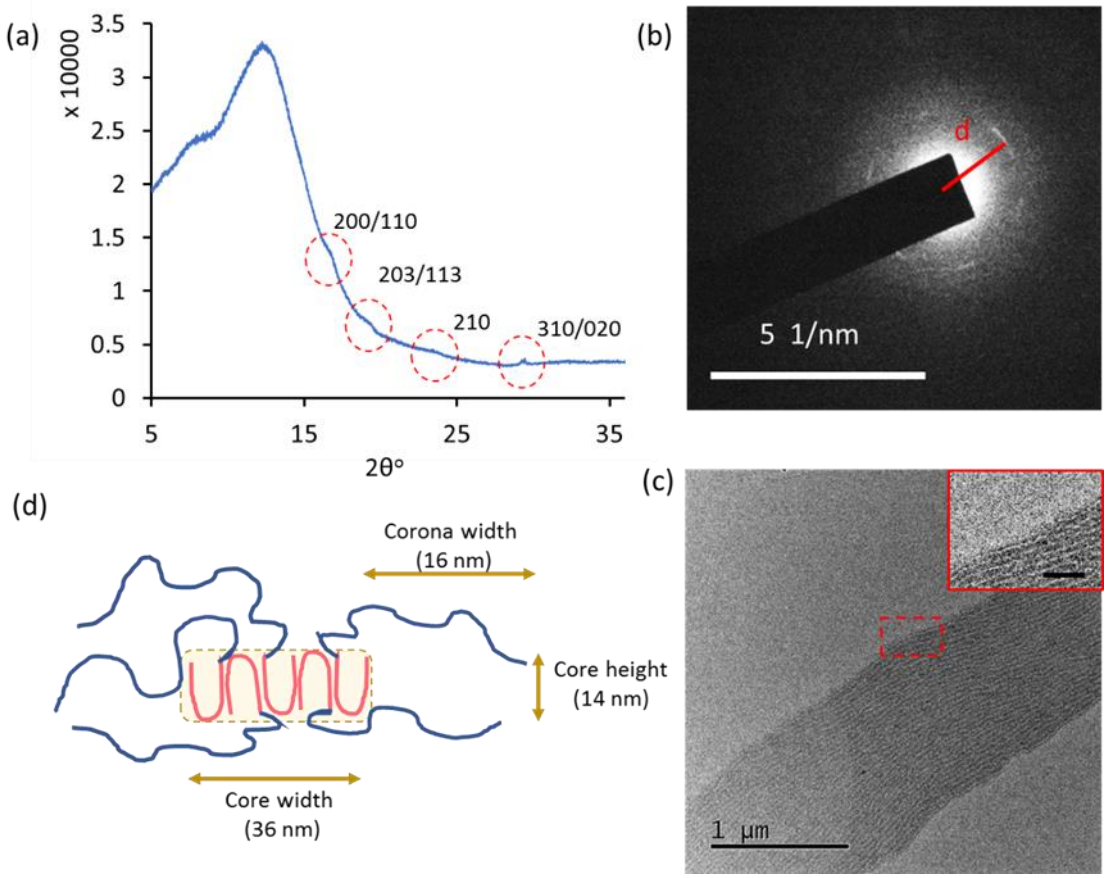

Figure 3.5. Micelle characterisation by PXRD and SAED. (a) PXRD profile of $PLLA_{47}$-*b*-$PNIPAm_{267}$ micelles; red circle showed the Bragg peaks; (b) SAED pattern of $PLLA_{47}$-*b*-$PNIPAm_{267}$ micelles; (c) TEM images of micelles in the area for SAED pattern record; aggregated and slight misaligned fibre-like micelles; inset scale bar: 200 nm; (d) Schematic representation of micelle cross-section by AFM characterisation. Pink: folded core chains; blue: collapsed corona chains.

To better understand the core structure of the $PLLA_{47}$-*b*-$PNIPAm_{267}$ micelles and to probe the shape of the core cross-section, small-angle X-ray scattering (SAXS) was employed to analyse solutions of

PLLA$_{47}$-*b*-PNIPAm$_{267}$ micelles, which have concentrations of 4, 20 and 30 mg/mL. To probe the cross-section of the micelle core, the analysis of SAXS data focused on the sample of 4 mg/mL. This concentration has been found low enough for the scattering intensity (S(*Q*)) to be regarded as constant.[167, 321]

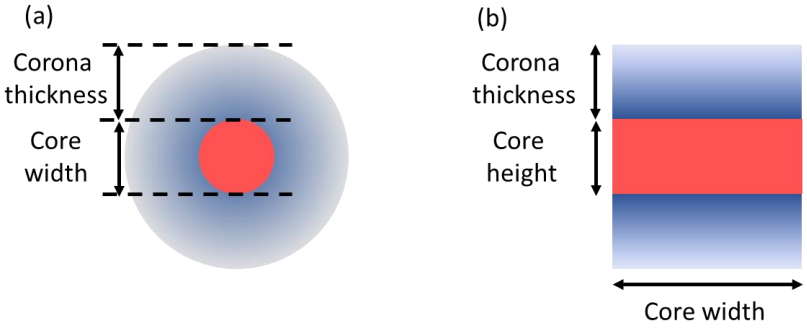

Figure 3.6. Schematic representation of the models used to fit SAXS data. (a) Model 1 has a homogeneous circular cross-section core (red) and a surrounding corona (blue) with decaying density; (b) Model 2 has a homogeneous rectangular cross-section core (red) with a decaying density corona (blue) attached on the long core edges.

Two models (Figure 3.6) were employed to analyse and fit the scattering intensity. Model 1 involved long core-shell rods containing a circular homogeneous density core and surrounded by a symmetrical shell with a decaying density. This model has been reported to fit the scattering intensity of PFS-*b*-PI cylindrical micelles in solution.[321] Model 2 (Figure S3.27) describes a long rod-like structure containing a homogeneous density core with a rectangular cross-section, and decaying density corona attached on the two long core edges. This model has been reported to fit the scattering intensity for P3HT-containing fibre-like structures in solution.[353] Fitting was conducted with a non-linear least-squares method to allow for the scaling factor, background, core and corona dimensions, scattering-length density (SLD) of the corona, and polydispersity of core and corona to refine.

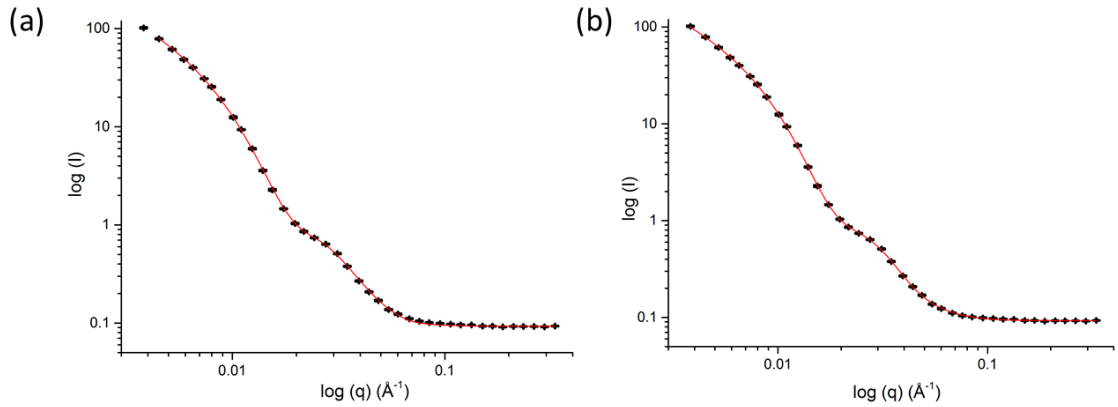

Figure 3.7. Plot of log (I) vs log (*q*) from SAXS data of a 4 mg/mL suspension of $PLLA_{47}$-*b*-$PNIPAm_{267}$ micelles (black in a and b) and fitting from Model 1 (red in a) and Model 2 (red in b).

Both the models give good fits for the measured scattering intensity of the sample solutions in the whole experimental *q* range (Figure 3.7). Model 1 predicts that the fibre-like micelles have a cylindrical core with a diameter of 4 nm and a corona with a width of 22 nm. The values for the core width, core height and corona thickness corresponding to the best fit for model 2 were 32, 7, and 19 nm, respectively. Although the scattering intensity fits well, the scattering intensity residuals from Model 1 scattered randomly away from zero in an unsymmetrical pattern and with a large amplitude (ca. 4, while a good fitting would have an amplitude around 1) (Figure S3.12). This result suggests that cylindrical rods with a circular cross-section may not provide a perfect fit for the micelles. To better probe the structure of micelle cross-section, AFM and STEM results were taken into consideration. The fitting results have been summarized in Table 3.2. The data from the model 2 fitting agrees well with the AFM measurements except in core height, which may be due to the collapsed corona on the core surface which results in an increased height. The difference in core width measured by STEM may be caused by the low resolution of core and corona boundary due to the low electron density of $PLLA_{47}$-*b*-$PNIPAm_{267}$. In general, model 2 with a rectangular cross-section fits well with $PLLA_{47}$-*b*-$PNIPAm_{267}$ micelles. However, the possibility of an elliptical cross-section cannot be excluded.

Table 3.2. Summary of size characterisation by TEM, AFM and SAXS of $PLLA_{47}$-*b*-PEG_{267} micelles prepared at 4 mg/mL in EtOH.

Technique	Length (nm)	Core height (nm)	Core width (nm)	Corona thickness (nm)
AFM	–	14	36	16
STEM	1040	–	24	18
SAXS (Model 1)	-	-	4	22
SAXS (Model 2)	–	7	32	19

In addition, the number of BCP molecules in a single micelle and the corona volume was extracted from the fitting to model 2. According to the density of core block (PLLA: 1.29 g/cm^3),[354] the fitted volume data for the core block, the number of polymer chains contained in a single micelle was calculated as 27,040, which corresponds to 26 PLLA chains per nanometer. As the Model 2 shows a decaying density for the corona block, the fitted corona SLD value should have a range between the SLD of pure corona and that of pure solvent. The SLD of corona at core-corona interface possess a higher value than that at the other end of corona. The fitted corona SLD data is between 7.73×10^{-6} and 8.77×10^{-6} Å^{-2} for a thickness of 19 nm. This corresponds to a PNIPAm volume fraction of 0.03 - 0.42.

Micelle solutions with higher concentrations (20 and 30 mg/mL) were analysed by WAXS. A similar result was obtained with that of PXRD experiments. In both samples, a weak Bragg peaks at *q* values of 1.18 Å^{-1} can be observed (Figure 3.8). This is consistent with the strong (110/200) reflections in the crystalline PLLA domains.[352] Therefore, the PLLA chains in the prepared fibre-like micelles adopt a α-form packing (10_3 helix chains).

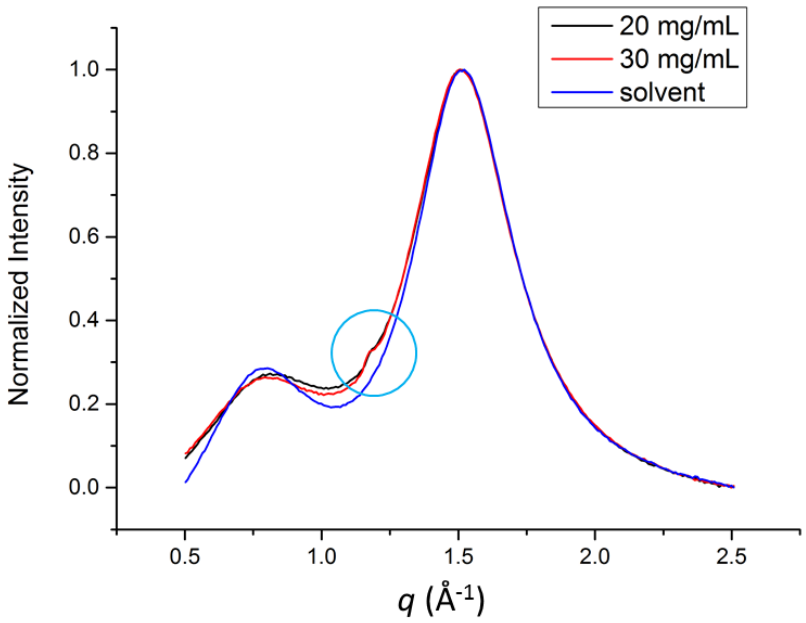

Figure 3.8. Normalized intensity by WAXS for PLLA$_{47}$-*b*-PEG$_{267}$ micelles in EtOH with various concentration, 20 (black), 30 (red) mg/mL, and solvent (blue). The blue circle identifies the Bragg peak.

3.2.5. Kinetic Studies on Living CDSA of PLLA$_{47}$-*b*-PNIPAm$_{267}$

In order to better understand the role of TFE in the living CDSA of PLLA$_{47}$-*b*-PNIPAm$_{267}$, kinetic studies were performed. According to the previous kinetic studies on the living CDSA of PFS-*b*-PDMS diblock copolymers, in some cases it took several days for the micelles to reach the final expected length at room temperature.[355] We therefore aged the samples for 5 days after the unimer addition in seeded-growth experiments before characterisation. Unimers (in DMSO) with varied unimer-to-seed mass ratios (m_{unimer}:m_{seed} = 2.5, 5.0, 10.0, 15.0, 20.0 and 30.0) were added into seeds (0.5 mg/mL, L_n = 36, L_w/L_n = 1.10, σ/L_n: 0.26) in EtOH or TFE/EtOH (with varied volume ratios, 3:97, 3:97, 5:95, 10:90 and 15:85 for unimer-to-seed mass ratios of 2.5, 5.0, 10.0, 15.0, 20.0 and 30.0, respectively). Aliquots were taken from the solutions at set time points, and the micelles were characterised by TEM after solvent evaporation (Figure S3.13 and S3.15). This allowed the micelle length to be monitored throughout the seeded-growth experiments (Figure S3.14, S3.16, S3.18, Table S3.1 and S3.2).

When seeded-growth experiments were conducted in EtOH, micelles obtained after aging for 1 d had shorter lengths than that expected. Micelle length showed a slight increase with the extension of the

aging time (Figure 3.9a). After aging for 5 days, micelles obtained with samples of low unimer-to-seed mass ratios (m_{unimer}:m_{seed} ≤ 5.0) possessed lengths close to the expected values, while micelles obtained with samples of high unimer-to-seed mass ratios (m_{unimer}:m_{seed} ≥ 10.0) possessed lengths much shorter than the theoretical lengths. In addition, all the samples of micelles showed relatively high length dispersity values for living CDSA processes (L_w/L_n ≥ 1.10) (Figure 3.9a, S3.13, S3.14 and S3.18a).

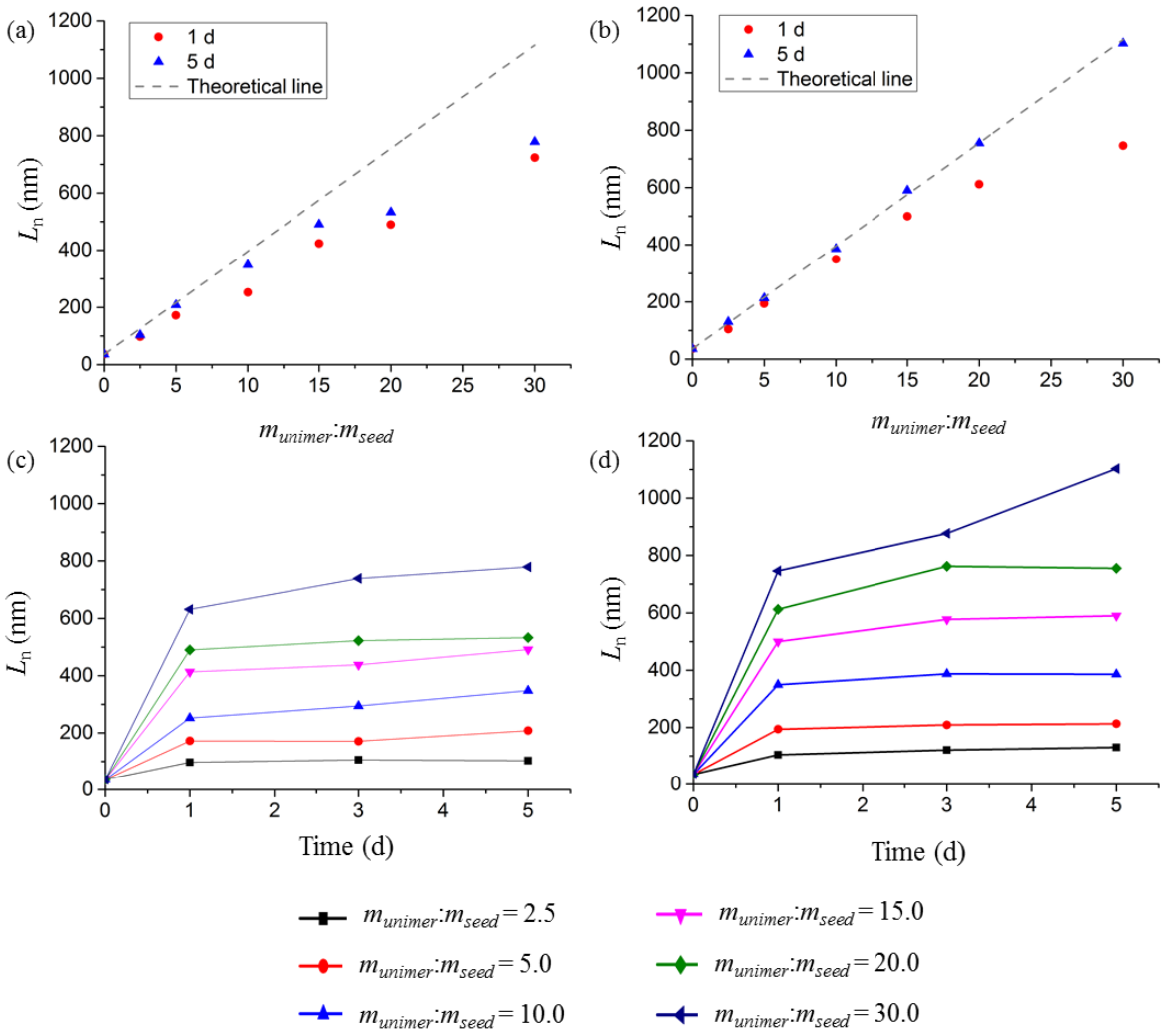

Figure 3.9. Kinetic studies on seeded-growth of $PLLA_{47}$-*b*-$PNIPAm_{267}$ unimers (in DMSO) from seed micelles (0.5 mg/mL in EtOH, L_n = 36 nm, L_w/L_n = 1.10) in (a and c) EtOH and in (b and d) TFE/EtOH (*v*:*v* = 3:97, 3:97, 5:95, 8:92, 10:90 and 15:85 for m_{unimer}:m_{seed} = 2.5, 5.0, 10.0, 15.0, 20.0 and 30.0, respectively). (a and b) Plots of micelle lengths versus unimer-to-seed mass ratios; (c and d) plots of micelle lengths as a function of time.

When TFE was introduced into the seeded-growth experiments, after aging samples for 1 day fibre-like micelles obtained also had lengths shorter than the expected values. However, the length dispersity was significantly lower ($L_w/L_n \leq 1.07$) compared with those prepared in the absence of TFE ($L_w/L_n \geq 1.07$, except $L_w/L_n = 1.05$ for m_{unimer}:m_{seed} = 2.5 and 5.0) (Figure S3.18b). Moreover, after aging the samples for 5 days the lengths of the fibre-like micelles prepared in the presence of TFE increased up to the predicted lengths with low length dispersity values ($L_w/L_n \leq 1.09$) (Figure 3.9b, S3.15, S3.16 and S3.18b).

After aging samples for 1 day, the fibre-like micelles obtained in both the absence and the presence of TFE possessed similar lengths. This suggested that the PLLA$_{47}$-*b*-PNIPAm$_{267}$ micelles exhibit a similar seeded-growth kinetics in both two solvent media, and that the presence of TFE does not significantly affect the micelle growth rate (Figure 3.9c and d).

The increase in micelle lengths after 1 day indicates that the unimer is still present. After ageing samples for 5 days, only a slight length increase was detected for samples prepared without TFE, while in the presence of TFE lengths increased substantially and reached the theoretical value based on the unimer to seed ratio. These results suggest that unimers have been consumed after 5-day ageing in the presence of TFE.

From the TEM analysis results (Figure S3.13), the samples prepared in the absence of TFE showed the presence of spherical micelles. These existed in all samples aged from 1 day to 5 days, but fewer were observed in TFE/EtOH. As noted previously, the formation of a small percentage of spherical micelles would help explain why the final micelles obtained after 5 days had shorter lengths compared with the values predicted theoretically based on unimer-to-seed mass ratios. Also, as noted previously, shoulder peaks in the short length range were present in micelle contour length histograms in the absence of TFE, especially in cases of high unimer-to-seed mass ratios and longer self-assembly times (3-5 days) (Figure S3.14). This provides further evidence of the additional problem of seed formation by self-nucleation which would also lead to shorter micelles than predicted.

In contrast, for the fibres formed in the presence of TFE, few spherical micelles were detected by TEM after 1 day and none after aging for 5 days (Figure S3.15). This indicates that in this case no unimer is trapped as spherical micelles after 5 days and therefore the fibres grew up to the theoretical length. Also, there was no evidence for self-nucleation in the fibre histograms (Figure S3.16). Although other explanations need to be considered (see the next section), the propensity for $PLLA_{47}$-*b*-$PNIPAm_{267}$ to undergo aggregation to form spherical micelles and to undergo self-nucleation in the absence of H-bond disruption agents but not in the presence of TFE is consistent with our postulate that a key role is played by intermolecular H-bonds among PLLA chains in promoting these events.

3.2.6. Investigation of the Potential Protonation of the PNIPAm Corona

Next, we considered other possible explanations for the role of TFE as a promoter for the efficient living CDSA of $PLLA_{47}$-*b*-$PNIPAm_{267}$ BCP. TFE has been widely used as a H-bond disruption agent in protein structure characterisations as a replacement of trifluoroacetic acid (TFA) (pKa = 0.23).[351, 356, 357] However, TFE is still weakly acidic (pKa = 12.5)[358], PNIPAm could potentially be protonated. If the corona-forming block is protonated, the self-assembly behaviour could be modified and this might, in principle, explain the improved living CDSA characteristics.[217, 256, 359-361] ^{1}H NMR experiments were conducted to explore the potential protonation of the PNIPAm corona. PNIPAm, mixture of PNIPAm and TFE (1:400 mole ratio, similar to that for seeded-growth experiments), and a mixture of PNIPAM and TFA (1:400 mole ratio) were separately dissolved in $CDCl_3$ for subsequent NMR characterisation.

If the amide groups in PNIPAm are protonated, the resonance for the amide proton would shift downfield due to the de-shielding effects. As shown in Figure S3.17, the chemical shift of the amide proton is at 6.50 ppm in neutral PNIPAm. When TFA was introduced, the resonance signal shifted downfield to 7.0 ppm. However, when TFE was introduced, no obvious shift of resonance signal of amide proton was observed. This indicates that PNIPAm is not protonated by TFE to any significant extent.

3.2.7. Influence of TFE and Other Solvent Additives on Polymer Solubility and Solvent Polarity

The quality of the solvent medium plays a crucial role in BCP self-assembly. On addition of a small amount of TFE, the polarity of the solvent medium is changed, which may further affect the solubility of the polymers in the solvents. Such effects may, in principle, explain the improved living CDSA behaviour for $PLLA_{47}$-*b*-$PNIPAm_{267}$ in the presence of TFE. To elucidate the effects of altering solvent polarity and polymer solubility, a selection of different solvents was introduced individually as a replacement of TFE in the seeded-growth of $PLLA_{47}$-*b*-$PNIPAm_{267}$. Detailed information on the solvent polarity and solubility parameters is listed in Table 3.3.[358, 362, 363] Dielectric constant values were employed as an indication of solvent polarity and Hildebrand solubility parameters were employed as an indication of the interactions between the solvent and the polymer.

Table 3.3. Table of dielectric constants and solubility parameters for selected solvents and polymers.

Solvents	DMSO	DMF	MeOH	EtOH	Acetone	TFE	THF	Dioxane	PLLA	PNIPAm
Dielectric constants	49	37	33	24.5	21	26.6	7.6	2.25	-	-
Solubility parameters ($MPa^{1/2}$)	26.4	24.7	29.7	26.2	19.7	23.9	18.5	20.5	20.2	24.8

The dissolution of $PLLA_{47}$-*b*-$PNIPAm_{267}$ in different selected solvents was analysed by DLS at a polymer concentration of 2 mg/mL. DLS analysis leads to apparent hydrodynamic radii ($R_{h,\,app}$) values of around 3-10 nm for the molecularly dissolved unimer state.[364] The BCP $PLLA_{47}$-*b*-$PNIPAm_{267}$ showed the formation of unimers in all solvents studied except for the case of methanol (MeOH) which gave a $R_{h,\,app}$ value of ca. 55 nm (Figure 3.10) as might be predicted by the large difference in solubility parameter from that of PLLA (29.7 $MPa^{1/2}$ of MeOH vs 20.2 $MPa^{1/2}$ of PLLA, Table 3.3). Therefore, most of the selected solvents, such as DMSO, dimethylformamide (DMF), acetone, TFE, THF and 1, 4-dioxane (dioxane), can be considered as common solvents for $PLLA_{47}$-*b*-$PNIPAm_{267}$.

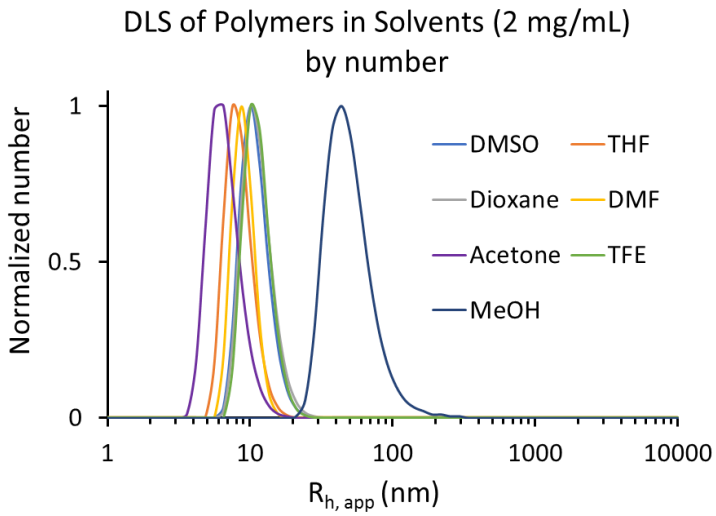

Figure 3.10. Solutions of $PLLA_{47}$-*b*-$PNIPAm_{267}$ in various solvents (2 mg/mL) characterised by DLS.

In order to explore the influence of different solvents on the living CDSA process, seeded-growth experiments were conducted by adding unimers (in DMSO) corresponding to a single unimer-to-seed mass ratio (m_{unimer}:m_{seed} = 15.0) to seeds (L_n = 33 nm, L_w/L_n = 1.13, in EtOH) in a mixture of a selected solvent and EtOH with varied volume ratios. For each selected solvent, three volume fractions (5, 10 and 15%) were applied. After aging for 5 days, the fibre-like micelle samples were characterised by TEM (Figure S3.19-S3.21). Based on the seed length and unimer-to-seed ratio, the theoretical length of the fibre-like micelles was 528 nm.

With a volume fraction of 5% of the added solvent in EtOH uniform fibres with L_n (and L_w/L_n) of 504 (1.04), 525 (1.04) and 512 (1.02) nm were obtained, close to the theoretical value for the cases of DMF (5% vol), DMSO (5% vol), Acetone (5% vol). In the case of 5% vol TFE in EtOH and L_n value of only 428 nm (L_w/L_n = 1.03) was apparent after 5 days, and larger volume fractions were required to obtain L_n values (L_n = 527 nm, L_w/L_n = 1.03 at 10% vol, Figure S3.19) close to the theoretical length consistent with the previously described experiments (Figure 3.3).

When the volume fraction of selected solvents increased to 15%, the fibre-like micelle samples with high volume fractions of DMSO, DMF, acetone and TFE possessed shorter fibre lengths than theoretical

length (Figure S3.19 and S3.20). This suggested that micelle dissolution is caused by the high content of common solvent. [143]

In the case of the addition of THF, dioxane and MeOH, the elongated fibres had lengths significantly shorter than the theoretical length ($L_n \leq 454$ nm) under all conditions with some evidence for the occurrence of self-nucleation as indicated by a shoulder on the length corresponding to lower micelle lengths (Figure 3.19 and S3.20).

In summary, these experiments indicate that efficient living CDSA $PLLA_{47}$-*b*-$PNIPAm_{267}$ can be achieved in the mixture of EtOH and selected solvents (5% DMSO, DMF, acetone or 10% TFE). It is likely that this is the result of generally improved unimer solubility in these cases which minimises aggregation to yield spherical micelles and the formation of new seed nuclei (self-nucleation). It is likely that the disruption of hydrogen bonds formed by PLLA by these additives plays a significant role as DMF, DMSO and acetone can be considered as weak H-bond acceptors[365] and TFE is considered as a H-bond donor. THF and dioxane, which are very weak H-bond acceptors[366, 367] were not found to promote living CDSA.

3.2.8. Role of H-bonds in the Crystalline PLLA Core

A model (Figure 3.11) of the PLLA crystalline core was employed to check for potential intermolecular H-bond formation. To construct the PLLA crystalline model, the crystal unit cell form needs to be determined. The $PLLA_{47}$-*b*-$PNIPAm_{267}$ micelles were characterised by PXRD and WAXS, and the results showed that the PLLA core adopted α-form crystallisation, which is consistent with the data reported previously.[227, 352] Therefore, the crystal structure data reported by Kanamoto[227] was used to build the crystal unit model of PLLA (Figure 3.10). The distance between the proton of methyl group and the oxygen atom of a carbonyl group on an adjacent chain was measured. The average length is 3.4 Å, which is in the range of weak H-bond formation. The formation of this type of weak H-bonds have been reported in the PLLA-PDLA stereocomplex and many protein structures.[350] This result suggests the possibility of H-bonding formation among the PLLA chains when the unimers are added

to a selective solvent, which is proposed to cause fast aggregation and self-nucleation in the seeded-growth of $PLLA_{47}$-*b*-$PNIPAm_{267}$.

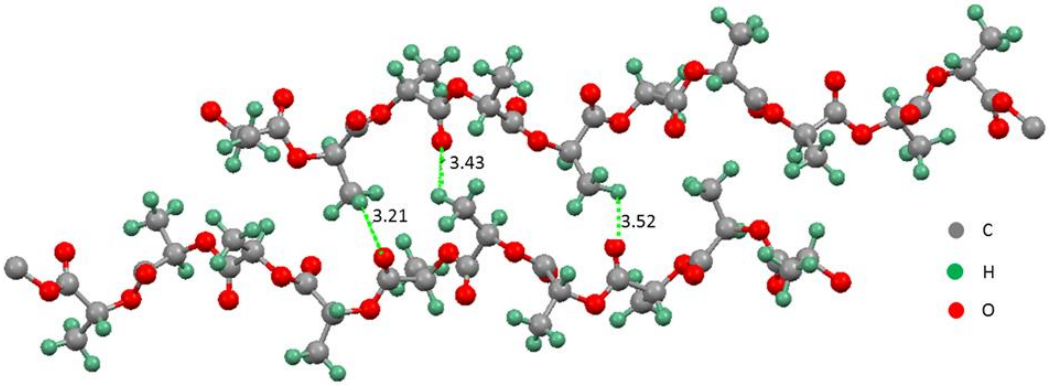

Figure 3.11. Measurement of O···H distance between two adjacent chains in a model of PLLA α-form crystal cell unit.

3.2.9. Extension of the Strategy to PLLA-*b*-P2VP

As a result of the access to efficient living CDSA of PLLA BCP, $PLLA_{47}$-*b*-$PNIPAm_{267}$, we attempted to explore the generality of the approach. We therefore transposed a similar approach to $PLLA_{47}$-*b*-$P2VP_{502}$.

(i) Uniform fibre-like micelles via living CDSA. $PLLA_{47}$-*b*-$P2VP_{502}$ fibres were prepared by heating the diblock copolymer at 0.5 mg/mL in solvents at 70 °C for 4 hours before slow cooling to 23 °C. The morphology of the micelles formed in the solutions were characterised by TEM (Figure S3.22a). Seed micelles were prepared by sonicating the polydisperse $PLLA_{47}$-*b*-$P2VP_{502}$ fibre solution (in DMSO:EtOH = 1:9) in a sonic cleaning bath for 2 h at 0 °C (Figure S3.22b). The prepared seed micelles have a measured number average length (L_n) of 29 nm, and a dispersity of L_w/L_n = 1.11 (Figure S3.22c).

Typical seeded-growth experiments were carried out at room temperature by adding unimer with different unimer-to-seed mass ratios to seed solutions in TFE/EtOH with different volume ratios, respectively (Figure 3.12). After aging for 5 days, the samples were analysed by TEM (Figure 3.12a-f). The measured micelle lengths had L_n from ca. 100 nm to ca. 900 nm with $L_w/L_n \leq 1.05$ (Figure 3.12h and S3.23). A linear plot of the measured length versus the unimer-to-seed mass ratio was obtained

(Figure 3.12g) and the length increased along the theoretical line, which showed a living epitaxial growth of $PLLA_{47}$-*b*-$P2VP_{502}$ micelles.

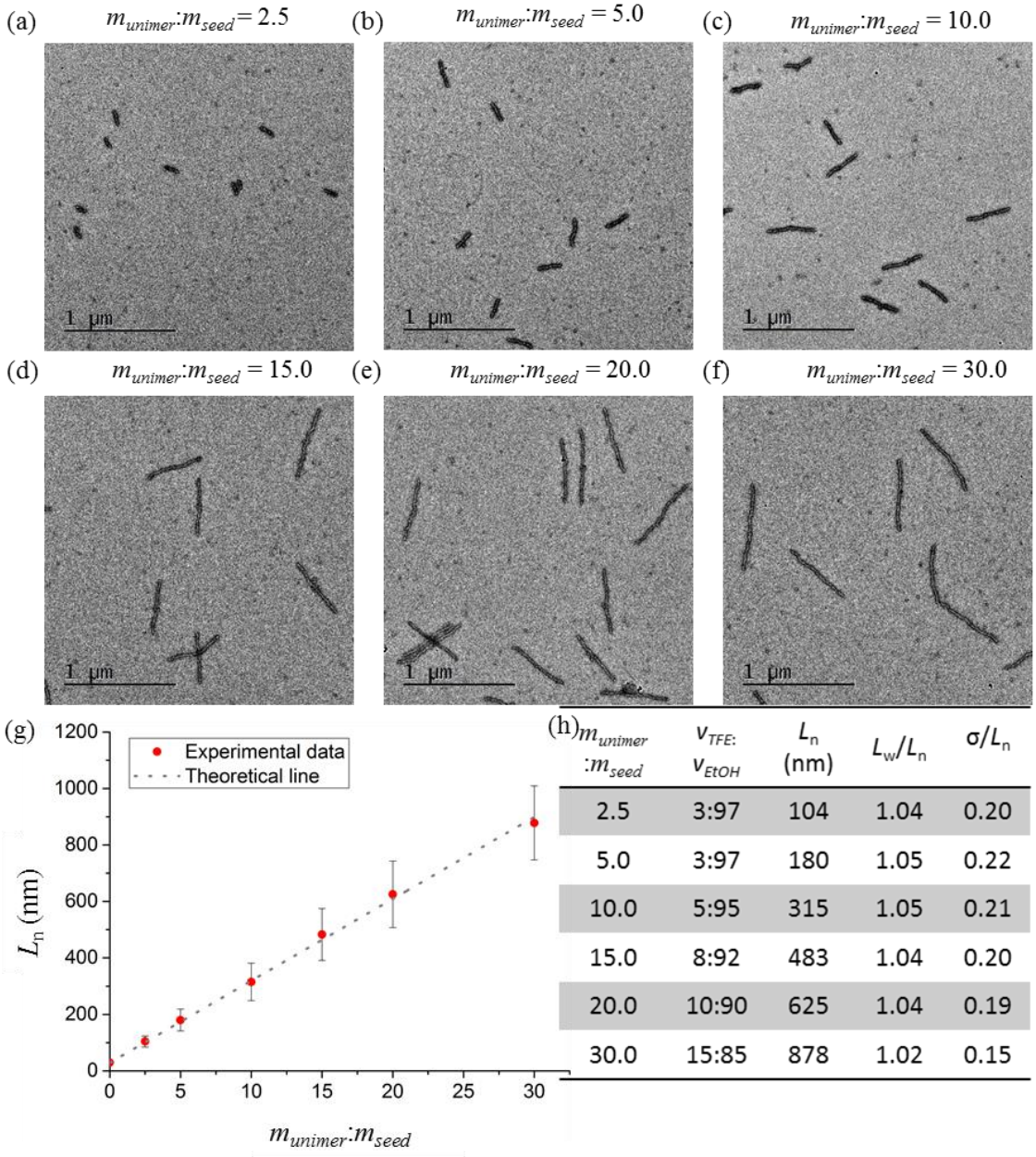

(h)

m_{unimer} :m_{seed}	v_{TFE}: v_{EtOH}	L_n (nm)	L_w/L_n	σ/L_n
2.5	3:97	104	1.04	0.20
5.0	3:97	180	1.05	0.22
10.0	5:95	315	1.05	0.21
15.0	8:92	483	1.04	0.20
20.0	10:90	625	1.04	0.19
30.0	15:85	878	1.02	0.15

Figure 3.12. TEM images of samples (aging for 5 days) of uniform $PLLA_{47}$-*b*-$P2VP_{502}$ micelles prepared by seeded-growth off seed micelles (L_n = 29 nm, L_w/L_n = 1.11, σ/L_n: 0.34) in TFE/EtOH with volume ratios of (a) 3:97, (b) 3:97, (c) 5:95, (d) 8:92, (e) 10:90 and (f) 15:85 after the addition of unimers (in DMSO) with unimer-to-seed mass ratios of (a) 2.5, (b) 5.0, (c) 10.0, (d) 15.0, (e) 20.0 and (f) 30.0, respectively; (g) plot of number average micelle length vs m_{unimer}:m_{seed}; (h) summary of measured length and solvent compositions.

Seeded-growth experiments in EtOH were conducted as control experiments. Unimers with various unimer-to-seed mass ratios were added into seeds in EtOH. After being aged for 5 days, the samples were analysed by TEM (Figure S3.24a-f). The measured micelle lengths had L_n values from ca. 90 to ca. 550 nm with $L_w/L_n \geq 1.05$ (Figure S3.25). The obtained micelles had shorter lengths compared with those predicted theoretically. With the increase of unimer-to-seed mass ratios, the micelle length dispersity indices increased greatly. Although the micelle was elongated, the epitaxial growth was not controlled. Therefore, the strategy for using TFE as H-bond disruption agent has been successfully extended to PLLA$_{47}$-*b*-P2VP$_{502}$ micelles.

(ii) Preparation of block co-micelles. Living CDSA allows for the preparation of complex micelle structures such as block co-micelles with well-defined segments of different control chemistry. PLLA-based pentablock co-micelles were prepared with PLLA$_{47}$-*b*-PNIPAm$_{267}$ and PLLA$_{47}$-*b*-P2VP$_{502}$ diblock copolymers, which showed the fabrication of PLLA-based complex nanostructures. As a result of the hydrophilicity of P2VP and biocompatibility of PNIPAm and PLLA, the prepared block co-micelles are of interest for applications in biomedicine.

Two pentablock co-micelles (pentablock 1 and pentablock 2, Figure 3.13c and f) with narrow length dispersities were prepared by alternating growth using PLLA$_{47}$-*b*-PNIPAm$_{267}$ and PLLA$_{47}$-*b*-P2VP$_{502}$ as unimers. The preparation of pentablock 1 started from the central segments (central block 1) comprising PLLA$_{47}$-*b*-PNIPAm$_{267}$ micelles. The central block 1 (Figure 3.13a) was prepared by adding unimers of PLLA$_{47}$-*b*-PNIPAm$_{267}$ (in DMSO, with a unimer-to-seed mass ratio of 9.0) to PLLA$_{47}$-*b*-PNIPAm$_{267}$ seed micelles (0.5 mg/mL, L_n = 33 nm) in TFE/EtOH (10:90) and aged at room temperature for 3 days. TEM characterisation showed that the elongated micelles had a L_n of 325 nm and L_w/L_n of 1.03. The triblock co-micelles (triblock 1) were prepared by adding PLLA$_{47}$-*b*-P2VP$_{502}$ unimers (10 mg/mL in DMSO) into the prepared PLLA$_{47}$-*b*-PNIPAm$_{267}$ micelles. After aging for 3 days, the micelles were characterised by TEM and the results showed triblock co-micelle formation (L_n = 549 nm, L_w/L_n =1.05) (Figure 3.13b). A clear segmented structure was observed as the difference in electron contrast between PNIPAm and P2VP. The pentablock co-micelle (pentablock 1) were prepared by adding

$PLLA_{47}$-*b*-$PNIPAm_{267}$ unimers (10 mg/mL in DMSO) into the triblock co-micelle solutions (L_n = 716 nm, L_w/L_n =1.03). The micelles were characterised by TEM after aging for 3 days at room temperature. The TEM images (Figure 3.13c) showed five-segmented micelles with clear boundaries. The dark and light segments correspond to P2VP and PNIPAm, respectively. Another pentablock co-micelles (pentablock 2) were prepared following the similar procedures but started with the central segments comprising $PLLA_{47}$-*b*-$P2VP_{502}$ micelles (Figure 3.13d-f and Figure S3.26d-f).

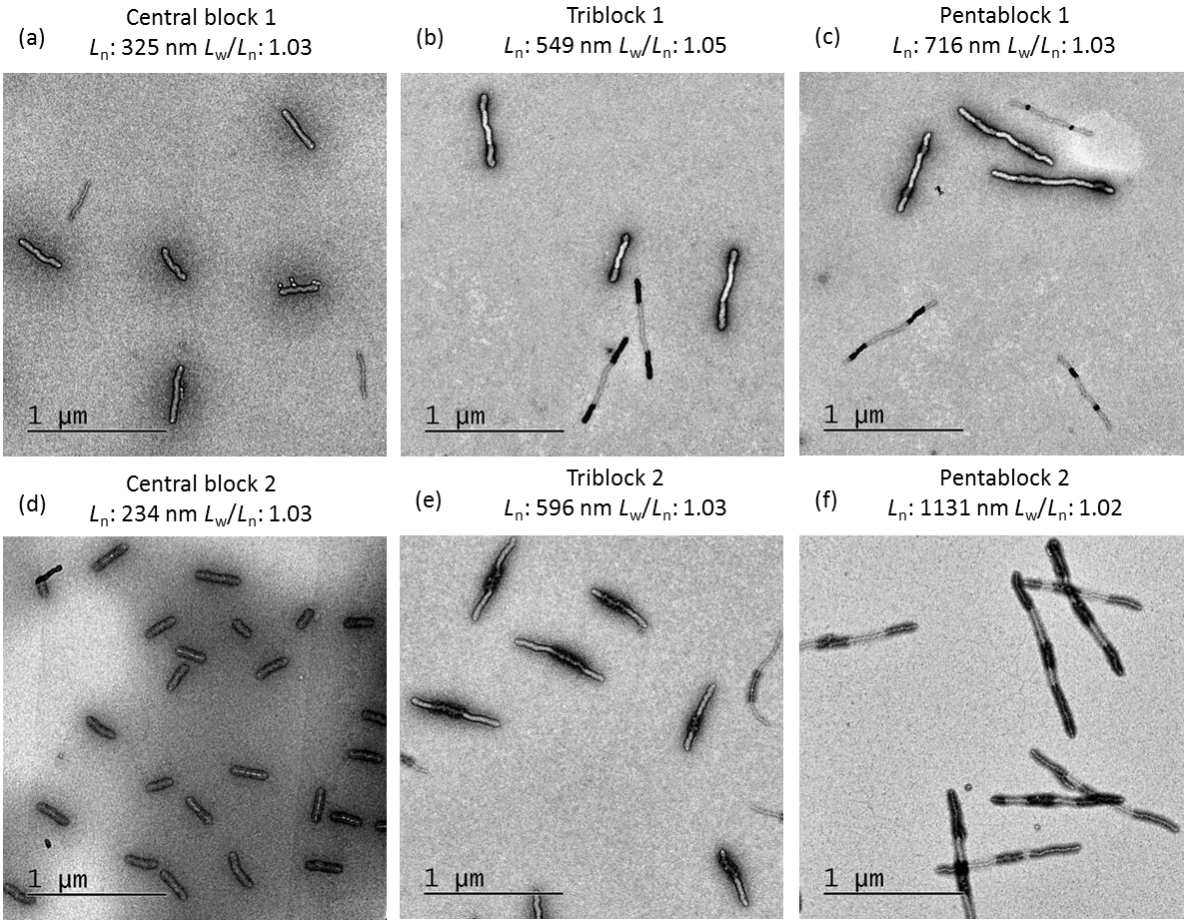

Figure 3.13. Preparation of pentablock co-micelles with $PLLA_{47}$-*b*-$PNIPAm_{267}$ and $PLLA_{47}$-*b*-$P2VP_{502}$ diblock copolymers. TEM images of (a) central block 1 ($PLLA_{47}$-*b*-$PNIPAm_{267}$), (b) triblock co-micelles 1, (c) pentablock co-micelles 1, (d) central block 2 ($PLLA_{47}$-*b*-$P2VP_{502}$), (e) triblock co-micelles 2 and (f) pentablock co-micelles 2. TEM samples were stained with a 2 wt% solution of uranyl acetate in EtOH. Light segments: consist of $PLLA_{47}$-*b*-$PNIPAm_{267}$; dark segments: consist of $PLLA_{47}$-*b*-$P2VP_{502}$.

3.3. Discussion

3.3.1. The Development of Efficient Living CDSA for PLLA BCPs.

Initial seeded-growth experiments with $PLLA_{47}$-*b*-$PNIPAm_{267}$ in EtOH were unsuccessful. Although elongated fibre-like micelles were obtained, micelle lengths were shorter than those predicted based on the unimer-to-seed mass ratios. In addition, competitive aggregation of spherical micelles was observed by TEM and, from the contour length histogram, shoulder peaks in the low micelle length region suggested that unimers undergo self-nucleation to form new seeds which generate fibre-like micelles with lower L_n values. Similar results were also observed for the seeded-growth of $PLLA_{47}$-*b*-$P2VP_{502}$ in EtOH. In contrast, seeded-growth of $PLLA_{47}$-*b*-$PNIPAm_{267}$ in TFE/EtOH can afford uniform fibres with close to theoretical lengths. Further studies indicated that other solvent additives, such as DMF, DMSO and acetone also lead to a substantial increase in the efficiency of the living CDSA growth process.

An explanation for the improved efficiency of living CDSA in the presence of solvent additives is at this point speculative. TFE, DMF, DMSO and acetone are all capable of disrupting hydrogen bonds and it is likely that this plays a significant role in improving the unimer solubility sufficiently such that competitive aggregation to form spherical micelles does not occur and that unimer addition to the seeds is promoted. It is also likely that the formation of new nuclei by self-nucleation is mitigated (Figrue 3.14)

However, although probably significant, the H-bonding disruption effect may well be part of a generally improved solvation of unimers in the presence of these solvent additives. For examples, the successful solvent additives are all characterised by higher dielectric constraints (Table 3.3) as well as competitive H-bonding capabilities.

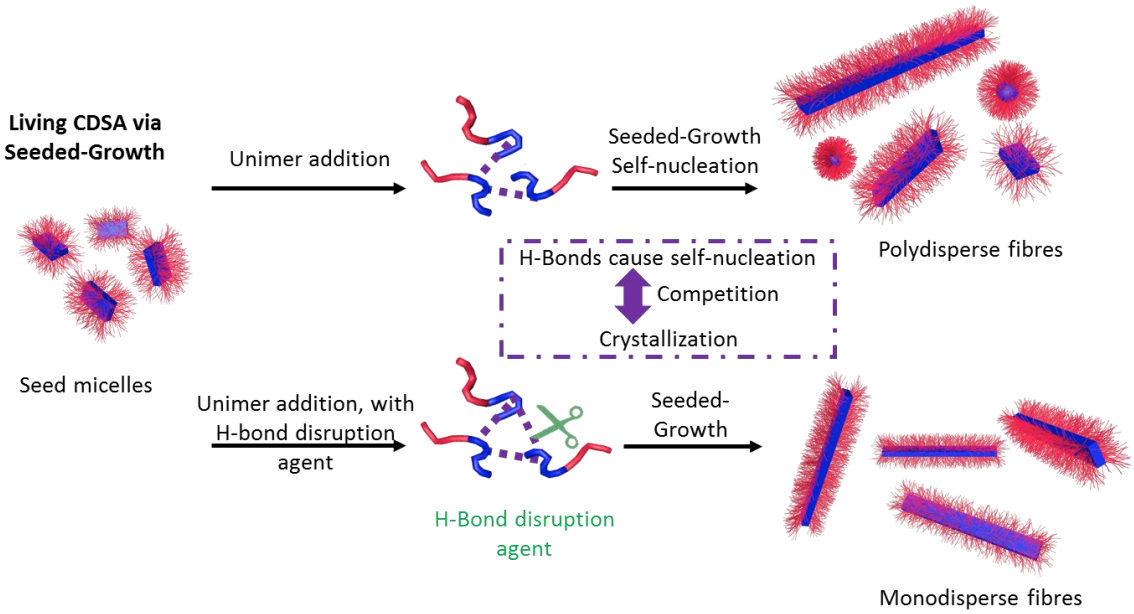

Figure 3.14. Schematic of regulation of PLLA seeded-growth with H-bond disruption agents.

3.3.2. Defects in Pentablock Co-Micelles Formation.

Triblock co-micelles and pentablock co-micelles were successfully prepared by alternatively seeded-growth of $PLLA_{47}$-*b*-$PNIPAm_{267}$ and $PLLA_{47}$-*b*-$P2VP_{502}$ unimers. One of the features of these block co-micelles was that the grown segments were not equivalent in length as would be expected for a controlled living CDSA process (Figure 3.13).

This is proposed to be caused by the different addition rates of BCPs with different corona-forming block lengths as previously reported.[151, 152, 355] In a typical experiment of preparing triblock co-micelles, the initial growth of $PLLA_{47}$-*b*-$PNIPAm_{267}$ unimer from $PLLA_{47}$-*b*-$P2VP_{502}$ seed micelles is suggested to be a slow step as a consequence of unfavourable corona-corona interactions between PNIPAm (δ = 24.8 $MPa^{1/2}$) and P2VP (δ = 20.8 $MPa^{1/2}$). Once the first unimer from $PLLA_{47}$-*b*-$PNIPAm_{267}$ has been added in this slow step, further unimers can deposit more rapidly. This might result in different lengths in the newly grown outer segments. In the preparation of pentablock co-micelles, the non-equivalent growth would be amplified by the same reason of switching to a different unimers.

3.4. Summary

In summary, we have reported the controlled epitaxial growth of 1D fibre-like micelles based on $PLLA_{47}$-*b*-$PNIPAm_{267}$ and $PLLA_{47}$-*b*-$P2VP_{502}$ diblock copolymers. We have also provided detailed $PLLA_{47}$-*b*-$PNIPAm_{267}$ micelle characterisation by AFM, SAED and SAXS. The results showed that the micelle has a crystalline PLLA core with a rectangular or elliptical cross-section, and a solvent swollen PNIPAm corona. In addition, we proposed that the fast aggregation to form spherical micelles and self-nucleation to form new fibres are two main factors competing with the epitaxial crystallisation of PLLA BCPs. This unwanted competing aggregation is suggested to be partly caused by H-bonding among PLLA chains. By using different solvent additives, which improve the BCP solvation and disrupt the H-bonds, efficient epitaxial growth of PLLA-containing diblock copolymers could be achieved. A similar strategy has been successfully extended to $PLLA_{47}$-*b*-$P2VP_{502}$ micelles. By employing subsequent and alternating addition of $PLLA_{47}$-*b*-$PNIPAm_{267}$ and $PLLA_{47}$-*b*-$P2VP_{502}$ unimers, uniform pentablock co micelles with well-defined special segments were achieved. This work provides an approach towards PLLA-containing complex functional nanostructures.

3.5. Chapter 3 Supplementary Material

3.5.1. Materials and Methods

All reactions were carried out in an MBraun MB150B-G glove box under nitrogen atmosphere or using standard Schlenk line techniques. Solvents for self-assembly were purchased at HPLC grade and filtered through a PTFE membrane with pore size of 450 nm. Solvents for reactions were obtained from a Grubbs type solvent purification system. All reagents and solvents were purchased from Sigma-Aldrich (UK), Acros, Fluka, Fisher Chemical and Alfa Aesar, and used as received unless otherwise noted. PEG and *L*-Lactide were purified by azeotropic distillation or recrystallisation respectively from toluene, followed by drying at 50 °C under reduced pressure over night prior to use. *N*-Isopropylacrylamide (NIPAm) was recrystallised twice from methanol before use. AIBN was recrystallised twice from methanol and stored in the dark at 4 °C. 2-Vinylpyridine (2VP) was passed through a basic aluminium oxide column before use. DBU were dried over CaH_2 and distilled under vacuum before use.

^{1}H and ^{13}C NMR spectra were obtained using a Varian 400 MHz spectrometer with $CDCl_3$ (^{1}H NMR: δ = 7.26 ppm; ^{13}C NMR δ = 77.16 ppm) as solvents and integrations of all peaks were against to TMSCl standard in NMR solvents. DOSY NMR spectra were obtained using a Varian 500 MHz spectrometer with $CDCl_3$ as solvents.

Matrix-assisted laser desorption/ionization time of flight (MALDI-TOF) mass spectrometry measurements were performed using a Bruker Ultraflextreme running in linear mode. Samples were prepared using a *trans*-2-[3-(4-*tert*-butylphenyl)-2-methyl-2-propenylidene]malononitrile matrix (20 mg/mL in THF) and the polymer sample (2 mg/mL in THF), mixed in a 10:1 (*v*/*v*) ratio. Approximately 1 μL of the mixed solution was deposited onto a stainless steel sample plate and allowed to dry in air.

Infrared spectra (IR) were recorded on a Perkin Elmer Spectrum One Fourier Transform Infrared Spectrometer (FT-IR).

Thermogravimetric analysis (TGA) was performed on a TA Instruments Q100 calorimeter at a scan rate of 10 °C/min under nitrogen.

Gel Permeation Chromatography (GPC) was conducted on a Viscotek VE2001 GPCmax chromatograph equipped with a refractive indices (RI) and a UV detector array. *n*-Bu_4NBr/THF (0.1 w/w %) was used as the eluent, with the flow rate set at 1 mL/min. The columns used were of grade GP5000HHR followed by GP2500HHR (Viscotek) at a constant temperature of 30 °C. The calibration of RI detector was carried out using polystyrene standards (Viscotek). Samples were prepared at 2 mg/mL in eluent and filtered through a Ministart SRP 15 filter (polytetrafluorethylene membrane, pore size = 0.45 μm).

Dynamic light scattering (DLS) was employed to determine the size of micelles formed in selective solvents. The measurements were performed at 25 °C on a Malvern Instruments Zetasizer Nano S using a 5 mW He−Ne laser (633 nm) and a detector oriented at 173°. Samples (1 mL) were measured in an optical glass cuvette (10.0 mm path length) with a concentration of 0.05 mg/mL. The results of DLS studies are reported as apparent hydrodynamic radii ($R_{h,\,app}$), acknowledging that the particles have been modelled as spheres in the experiments conducted.

Transmission electron microscopy **(**TEM) images were obtained on a JEOL 1400 microscope with a SIS MegaViewIII digital camera, which was operated at 120 kV. Selected area electron diffraction (SAED) data and scanning transmission election microscopy (STEM) images were obtained on a JEOL JEM-2100F field emission TEM equipped with an Oxford Instruments X-Max 80 mm2 X-ray detector WITH Aztec software from Oxford Instruments. STEM was operated in high angle annular dark field imaging (HAADF) mode. Samples were prepared by drop casting 4 μL of the micelle solution onto a carbon coated copper grid. Copper grids (400 mesh) were purchased from Agar Scientific and carbon films were prepared on mica sheets by carbon sputtering with an Agar TEM Turbo Carbon Coater. The carbon films were deposited onto the copper grids by floatation on water and the carbon coated grids were allowed to dry in air. For TEM images, samples were stained with uranyl acetate solution (2% wt in EtOH). For STEM and SAED data, no staining was applied.

For micelle contour lengths analysis, ca. 200 micelles in several images were traced manually using the ImageJ software package developed at the US National Institute of Health. The number average micelle

length (L_n) and weight average micelle length (L_w) were calculated using eq. S1 from measurements of the contour lengths (L_i) of individual micelles, where N_i is the number of micelles of length L_i, and n is the number of micelles examined in each sample. The distribution of micelle lengths is characterised by both L_w/L_n and the ratio σ/L_n.

$$L_n = \frac{\sum_{i=1}^{n} N_i L_i}{\sum_{i=1}^{n} Ni} \qquad L_w = \frac{\sum_{i=1}^{n} N_i L_i^2}{\sum_{i=1}^{n} Ni} \qquad \text{(eq.S1)}$$

Atomic force microscopy (AFM) analyses were performed in ambient conditions using a Bruker Multimode VIII atomic force microscope equipped with a ScanAsyst-HR fast scanning module and a ScanAsyst-Air-HR probe (tip radius, 2 nm), utilising peak force feedback control. Samples for AFM were prepared by drop casting 6 μL of micelle colloidal solution onto freshly cleaved mica before drying with a gentle stream of nitrogen.

X-ray scattering measurements (small- and wide-angle, SAXS and WAXS, respectively) were performed in transmission geometry using a Ganesha small angle X-ray scattering apparatus (SAXSLAB, Denmark). Solution samples were sealed into 1.5 mm diameter quartz capillary tubes (Capillary Tube Supplies, Cornwall, UK) and solid-state samples were drop cast onto mica or Kapton film (4,4'-oxydiphenylene-pyromellitimide, DuPont). The capillary or film was then secured in position, perpendicular to the X-ray beam and the detector was positioned at a distance of 1050 mm and 100 mm for the SAXS and WAXS measurements respectively. All measurements were recorded after evacuating the chamber to reduce air scattering. All the SAXS data was analysed after applying corrections for the scattering from the solvents and the empty capillary tube. SAXGUI (from SAXSLAB) was used for empty cell correction and SIMPLE SUBTRACT (in-house) for solvent.

3.5.2. Synthesis Procedures

Synthesis of 4-cyano-4-(((phenethylthio)carbonothioyl)thio)pentanoic acid (CTA-COOH). Following previously reported procedures,[368, 369] in an oven-dried round bottom flask, 2-Phenylethanethiol (4.0 mL, 29.86 mmol) was added dropwise to a stirred suspension of K_3PO_4 (8.0 g, 37.69 mmol) in acetone (20 mL) and stirring for 1 h. CS_2 (5.5 mL, 91.45 mmol) was added and the

solution turned bright yellow. After stirring for 16 h, the suspension was filtered, and the cake was washed with acetone (2 x 20 mL). After removing the solvents from the filtrate under reduced pressure, the resulting yellow solid was suspended in diethyl ether (100 mL). Solid iodine (3.2 g, 12.61 mmol) was gradually added and then stirred at room temperature for 1 h, and the insoluble white precipitate was removed by filtration. The yellow-brown filtrate was washed with an aqueous solution of sodium thiosulfate, dried over magnesium sulfate, and then evaporated to yield yellow solid. 4,4′-azobis(4-cyanopentanoic acid) (ACVA) (5.1 g, 17.90 mmol) was added to a solution of the solid in ethyl acetate (50 mL). The solution was degassed by nitrogen bubbling for 30 min and heated at reflux under nitrogen for 16 h. After removal of the solvents under reduced pressure, the crude product was washed with water (5 × 100 mL). The organic phase was concentrated and purified by silica chromatography using a mixed eluent (hexane: ethyl acetate = 4:1, gradually increasing to 1:1) to afford CTA-COOH as an orange oil (4.3 g, 44%). ^{1}H NMR (400 MHz, $CDCl_3$, 298 K): δ (ppm) 7.4-7.2 (m, 5H, Ph), 3.60 (t, 2H, $PhCH_2C\underline{H_2}$), 3.00 (t, 2H, $PhC\underline{H_2}$), 2.70 (t, 2H, $C\underline{H_2}COOH$), 2.6-2.4 (m, 2H, $CNCC\underline{H_2}$), 1.90 (s, 3H, CH_3). ^{13}C NMR (125 MHz, $CDCl_3$, 298 K): δ (ppm) 216.5 ($\underline{C}$=S), 177.2 ($\underline{C}$=O), 139.2, 128.9, 128.6, and 126.9 (Ph), 118.9 (CN), 46.4 ($\underline{C}CN$), 38.1 ($\underline{C}H_2CS$), 34.2 ($Ph\underline{C}H_2$), 33.6 ($CN\underline{C}CH_2$), 29.6 ($\underline{C}H_2COOH$), 24.9 ($\underline{C}H_3$).

Synthesis of 6-hydroxyhexyl 4-cyano-4(((phenethylthio)carbonothioyl)thio)pentanoate (CTA-OH). In an oven-dried Schlenk flask, CTA-COOH (1.0 g, 3.24 mmol) and 1,6-hexanediol (3.0 g, 25.92 mmol) were dissolved in dry $CHCl_3$ (50 mL). EDC·HCl (0.95 g, 4.87 mmol) and DMAP (59 mg, 0.487 mmol) were dissolved in dry $CHCl_3$ (15 mL) in another oven-dried Schlenk flask at ambient temperature, followed by adding into the reaction flask via a syringe. The reaction mixture was stirred under reflux for 48 h, filtered and concentrated to yield orange oil residue. The crude product was purified by silica chromatography (hexane: ethyl acetate = 3:1 as eluent) to afford CTA-OH as an orange oil (870 mg, 61%). ^{1}H NMR (400 MHz, $CDCl_3$, 298 K): δ (ppm) 7.4-7.2 (m, 5H, Ph), 4.12 (t, 2H, $COOC\underline{H_2}$), 3.66 (t, 2H, $C\underline{H_2}OH$), 3.59 (t, 2H, $PhC\underline{H_2}CH_2$), 3.00 (t, 2H, $Ph\text{-}C\underline{H_2}$), 2.64 (t, 2H, $C\underline{H_2}\text{-}COOH$), 2.6-2.4 (m, 2H, $CN\text{-}C\text{-}C\underline{H_2}$), 1.90 (s, 3H, $C\underline{H_3}$), 1.7-1.4 (m, 8H, $C\underline{H_2}C\underline{H_2}C\underline{H_2}C\underline{H_2}CH_2OH$). ^{13}C NMR (125 MHz,

$CDCl_3$, 298 K): δ (ppm) 216.5 (C=S), 171.6 (C=O), 139.2, 128.9, 128.6, and 126.9 (Ph), 118.9 (CN), 65.3 ($COO\underline{C}H_2$), 62.9 ($\underline{C}H_2OH$), 46.4 ($\underline{C}CN$), 38.1 ($\underline{C}H_2CS$), 34.2 ($Ph\underline{C}H_2$), 34.1 ($CN\underline{C}CH_2$), 32.7 ($\underline{C}H_2CH_2OH$), 30.6 ($\underline{C}H_2COOH$), 28.7 ($COOCH_2\underline{C}H_2$), 25.8 ($COOCH_2CH_2\underline{C}H_2$), 25.5 ($\underline{C}H_2CH_2CH_2OH$), 24.9 ($\underline{C}H_3$).

Synthesis of $PLLA_{47}$. In a nitrogen-filled glove box, solutions of DBU (11.2 uL, 0.18 mmol) and CTA-OH (28 mg, 0.062 mmol) in dry DCM (2 mL) were added to solution of *L*-lactide (400 mg, 2.78 mmol) in dry DCM (1mL). After stirring for 1 min at room temperature, the solution was quenched with benzoic acid and stirred for 30 min. After removed from the glove box, the reaction solution was precipitated three times into MeOH and collected by centrifugation. Polymers were further dried in a vacuum oven for 16 h before characterisation (367 mg, 92%). ^{1}H NMR (400 MHz, $CDCl_3$) δ (ppm): 5.17 (q, 102H, $C\underline{H}CH_3$), 1.57 (d, 306H, $CHC\underline{H}_3$). M_n (NMR): 7698 g·mol^{-1}. MALDI: m/z=7232. GPC (*n*-Bu_4NBr/THF, PS standard): M_n: 9800 g·mol^{-1}, $Đ_m$ = 1.09. ν_{max} (neat)/cm^{-1}: 3000-2880 (C-H); 1755, 1044 (C=O); 1456 (CH3); 1210-1163 (C(O)-O); 1088 (C-O).

Synthesis of $PLLA_{47}$-*b*-$PNIPAm_{267}$. $PLLA_{47}$ (100 mg, 0.015 mmol), NIPAm (355 mg, 3.2 mmol) and AIBN (0.47 mg, 0.003 mmol) were dissolved in 1,4-dioxane (3 mL) in a Schlenk flask. The solution was then freeze-pump-thawed four times and heated for 3.5 h at 70 ˚C. The reaction was quenched by immersion of the ampoule in liquid nitrogen and the polymer was precipitated in hexane three times, followed by being dried under vacuum and characterised (403 mg, 88%). ^{1}H NMR (400 MHz, $CDCl_3$) δ (ppm): 7.0-5.6 (br, 244H, $N\underline{H}$-CH-$(CH_3)_2$), 5.16 (q, 94H, $C\underline{H}(CH_3)$ from PLLA), 4.00 (br, 267H, NH-$C\underline{H}$-$(CH_3)_2$ from PNIPAm), 2.3-0.7 (3673 H, m, $C\underline{H}_3$ from PNIPAm, $CH(C\underline{H}_3)$ from PLLA, $C\underline{H}C\underline{H}_2$ from PNIPAm). GPC (*n*-Bu_4NBr/THF, PS standard): M_n = 180,600 g·mol^{-1}, $Đ_m$ = 1.11. ν_{max} (neat)/cm^{-1}: 3510-3313 (N-H); 3000-2880 (C-H); 1755 (C=O); 1644 (NH-C=O); 1458 (CH3); 1386-1367 (C-H), 1276-1185 (C-O); 1130,1088 (C-O).

Synthesis of $PLLA_{47}$-*b*-$P2VP_{502}$. $PLLA_{47}$ (100 mg, 0.015 mmol), 2VP (886 μL, 8.25 mmol) and AIBN (0.47 mg, 0.003 mmol) were dissolved in 1,4-dioxane (2 mL) in a Schlenk flask. The solution was then freeze-pump-thawed four times and heated for 16 h at 70 ˚C. The reaction was quenched by immersion

of the ampoule in liquid nitrogen and the polymer was precipitated in hexane three times, followed by being dried under vacuum and characterised (403 mg, 88%). ^{1}H NMR (400 MHz, $CDCl_3$) δ (ppm): 8.41-8.07 (m, 502H, Ar from P2VP), 7.20-6.30 (m, 1510H, Ar from P2VP), 5.16 (q, 94H, C<u>H</u>(CH_3) from PLLA), 2.28-1.48 (1940H, m, CH(C<u>H</u>$_3$) from PLLA, C<u>H</u>C<u>H</u>$_2$ from P2VP). GPC (*n*-Bu_4NBr/THF, PS standard): M_n = 63,245 g·mol^{-1}, $Đ_m$ = 1.25. ν_{max} (neat)/cm^{-1}: 3000-2880 (C-H); 1755, 1044 (C=O); 1590, 1585 (Ar); 1472, 1433 (Ar-C-N); 1088 (C-O); 745 (Ar).

3.5.3. Self-Assembly Procedures

All solvent compositions are given as volume ratio (*v*:*v*). All micelle length measurements were carried out with ca. 200 micelles. Self-nucleation to form polydisperse micelles were carried out by direct dissolution with heating-cooling method. Seeded-growth experiments were carried out at 23 °C.

Self-nucleation of PLLA$_{47}$-*b*-PNIPAm$_{267}$. 100 μL of PLLA$_{47}$-*b*-PNIPAm$_{267}$ solution (10 mg/mL in DMSO) was added to a vial with 100 μL DMSO and 1800 μL EtOH resulting a polymer solution of 0.5 mg/mL. The vial was sealed and heated at 70 °C for 4 h, followed by slowly cooling to 23 °C. And the solution was carried on aging for 24 h. The formed polydisperse fibre-like micelles were characterised by TEM.

Self-nucleation of PLLA$_{47}$-*b*-P2VP$_{502}$. 100 μL of PLLA$_{47}$-*b*-P2VP$_{502}$ solution (10 mg/mL in DMSO) was added to a vial with 100 μL DMSO and 1800 μL EtOH resulting a polymer solution of 0.5 mg/mL. The vial was sealed and heated at 70 °C for 4 h, followed by slowly cooling to 23 °C. And the solution was carried on aging for 24 h. The formed polydisperse fibre-like micelles were characterised by TEM.

3.5.4. Preparation of Seed Micelles.

All seed micelle solutions were prepared by sonication of the polydisperse micelle solutions from self-nucleation of polymer in selective solvents and characterised by TEM.

For $PLLA_{47}$-*b*-$PNIPAm_{267}$ seeds (L_n = 36 nm, L_w/L_n = 1.10, σ/L_n: 0.26): sonication of $PLLA_{47}$-*b*-$PNIPAm_{267}$ polydisperse micelles in DMSO/EtOH (1:9) was carried out for 2 h in a water sonication bath cooled with ice.

For $PLLA_{47}$-*b*-$PNIPAm_{267}$ seeds (L_n = 33 nm, L_w/L_n = 1.13, σ/L_n: 0.38): sonication of $PLLA_{47}$-*b*-$PNIPAm_{267}$ polydisperse micelles in DMSO/EtOH (1:9) was carried out for 2 h in a dry ice/acetone bath with a Ultrasonication probe.

For $PLLA_{47}$-*b*-$P2VP_{502}$ seeds (L_n = 29 nm, L_w/L_n = 1.11, σ/L_n: 0.34): sonication of $PLLA_{47}$-*b*-$PNIPAm_{267}$ polydisperse micelles in DMSO/EtOH (1:9) was carried out for 2 h in a in a water sonication bath cooled with ice.

3.5.5. Procedures of Seeded-Growth

Seeded-growth of $PLLA_{47}$-b-$PNIPAm_{267}$.

For seeded-growth without H-bond disruption reagents: 20 μL (for m_{unimer}:$m_{seed} \leq 10.0$) or 10 μL (for m_{unimer}:$m_{seed} > 10.0$) of seed micelle solution (0.5 mg/mL, DMSO/EtOH = 1:9) was diluted in 400 μL EtOH to which was added $PLLA_{47}$-*b*-$PNIPAm_{267}$ unimer (10 mg/mL in DMSO). The volumes of unimer added in were 2.5, 5, 10, 7.5, 10 and 15 μL corresponds to unimer-to-seed mass ratios of 2.5, 5, 10, 15, 20 and 30, respectively. And the resulting solution was then manually shaken for 10 s and aged for 5 days at 23 °C before TEM characterisation.

For seeded-growth with H-bond disruption reagent: 20 μL (for m_{unimer}:$m_{seed} \leq 10.0$) or 10 μL (for m_{unimer}:$m_{seed} > 10.0$) of seed micelle solution (0.5 mg/mL, DMSO/EtOH = 1:9) was diluted in 400 μL TFE/EtOH with volume ratio of 3:97, 3:97, 5:95, 8:92, 10:90 and 15:85 corresponds to unimer-to-seed mass ratios of 2.5, 5, 10, 15, 20 and 30, respectively, and to which solution was added $PLLA_{47}$-*b*-$PNIPAm_{267}$ unimer (10 mg/mL in DMSO) with volumes of 2.5, 5, 10, 7.5, 10 and 15 μL respectively. And the resulting solution was then manually shaken for 10 s and aged for 5 days at 23 °C before TEM characterisation.

Seeded-growth of $PLLA_{47}$-*b*-$PNIPAm_{267}$ for kinetic studies.

Same procedures were adopted with seeded-growth experiments of $PLLA_{47}$-*b*-$PNIPAm_{267}$. After unimer addition, aliquots were taken after samples aged for 1, 3, and 5 days for TEM characterisation.

Seeded-growth of $PLLA_{47}$-*b*-$PNIPAm_{267}$ for solvent effects studies.

10 μL of seed micelle solution (0.5 mg/mL, DMSO/EtOH = 1:9) was diluted in 400 μL solution of EtOH and selected solvents (MeOH, THF, Dioxane, DMF, DMSO, Acetone and TFE) individually with volume ratio of 5:95, 10:90 and 15:85, respectively. Similar procedures of unimer addition were adopted with seeded-growth experiments of $PLLA_{47}$-*b*-$PNIPAm_{267}$. And the resulting solution was then manually shaken for 10 s and aged for 5 days at 23 °C before TEM characterisation.

Seeded-growth of $PLLA_{47}$-b-$P2VP_{502}$.

Same procedures were adopted with seeded-growth experiments of $PLLA_{47}$-*b*-$PNIPAm_{267}$ in both EtOH and TFE/EtOH. After the unimer addition, samples were manually shaken for 10 s and aged for 5 days at 23 °C before TEM characterisation.

3.5.6. Preparation of Samples for SAXS Analysis.

To obtain quality data from SAXS experiments, micelles were prepared at higher concentrations compare with the method mentioned above. Polydisperse micelles of $PLLA_{47}$-*b*-$PNIPAm_{267}$ was prepared at a polymer concentration of 1 mg/mL by adding 200 μL of unimer solution (10 mg/mL in THF) to 1800 μL of EtOH. THF was employed as the common solvent in this preparation due to the large volatility compared with that of DMSO, which allowing the micelle solutions to be concentrated by applying nitrogen flow and resulting micelles suspended in TFE/EtOH. The solution was heated at 70 °C for 4 hours and slowly cool to 23 °C. The solution was further aged for 5 days and then characterised by TEM. The formed polydisperse micelles were sonicated at -78 °C in a dry ice/acetone bath for 1 h with a Ultrasonicate probe. TEM images showed that the seed micelles had a L_n (and L_w/L_n) of 36 (1.05) nm. 260 μL seed solution was diluted in 1 mL TFE/EtOH (1:9). To the seed solution, 94 μL

of unimer (50 mg/mL in THF) was added and the solution was manually shaken for 10 s. The final solution had a polymer concentration of 4.6 mg/mL. After ageing for 24 h, the micelle was determined a L_n (and L_w/L_n) value of 1040 (1.04) by TEM. The sample with a concentration of 4 mg/mL was prepared by adding 50 μL TFE/EtOH (1:9) to the micelle solution (100 μL). The rest micelle solution was concentrated by applying nitrogen flow to ~120 μL. The concentrated micelle solution had a concentration of 30 mg/mL. Samples with 20 mg/mL was prepared by adding 25 uL TFE/EtOH (1:9) to the concentrated micelle solution (50 μL). The micelle solution prepared for SAXS had been used in other characterisations (AFM, SAED and PXRD).

3.5.7. Preparation of pentablock co-micelles

For central block 1 micelles: 20 μL of $PLLA_{47}$-*b*-$PNIPAm_{267}$ seed micelle solution (L_n = 33 nm, 0.5 mg/mL, DMSO/EtOH = 1:9) was diluted in 400 μL TFE/EtOH (1:9) to which was added $PLLA_{47}$-*b*-$PNIPAm_{267}$ unimer (9 μL, 10 mg/mL in DMSO). And the resulting solution was then manually shaken for 10 s and aged for 3 days at 23 °C before TEM characterisation.

For triblock 1 co-micelles: $PLLA_{47}$-*b*-$P2VP_{502}$ unimer (3 uL, 10 mg/mL in DMSO) was then added into the central block 1 micelle solution (200 uL). The resulting solution was then manually shaken for 10 s and aged for 3 days at 23 °C before TEM characterisation.

For pentablock 1 co-micelles: $PLLA_{47}$-*b*-$PNIPAm_{267}$ unimer (3 μL, 10 mg/mL in DMSO) was then added into the triblock 1 co-micelle solution (100 uL). The resulting solution was then manually shaken for 10 s and aged for 3 days at 23 °C before TEM characterisation.

For central block 2 micelles: 20 μL of $PLLA_{47}$-*b*-$P2VP_{502}$ seed micelle solution (L_n = 29 nm, 0.5 mg/mL, DMSO/EtOH = 1:9) was diluted in 400 μL TFE/EtOH (1:9) to which was added $PLLA_{47}$-*b*-$P2VP_{502}$ unimer (9 μL, 10 mg/mL in DMSO). And the resulting solution was then manually shaken for 10 s and aged for 3 days at 23 °C before TEM characterisation.

For triblock 2 co-micelles: $PLLA_{47}$-*b*-$PNIPAm_{267}$ unimer (5 uL, 10 mg/mL in DMSO) was then added into the central block 2 micelle solution (200 uL). The resulting solution was then manually shaken for 10 s and aged for 3 days at 23 °C before TEM characterisation.

For pentablock 2 co-micelles: $PLLA_{47}$-*b*-$P2VP_{502}$ unimer (5 μL, 10 mg/mL in DMSO) was then added into the triblock 2 co-micelle solution (100 uL). The resulting solution was then manually shaken for 10 s and aged for 3 days at 23 °C before TEM characterisation.

3.5.8. Supplementary Figures

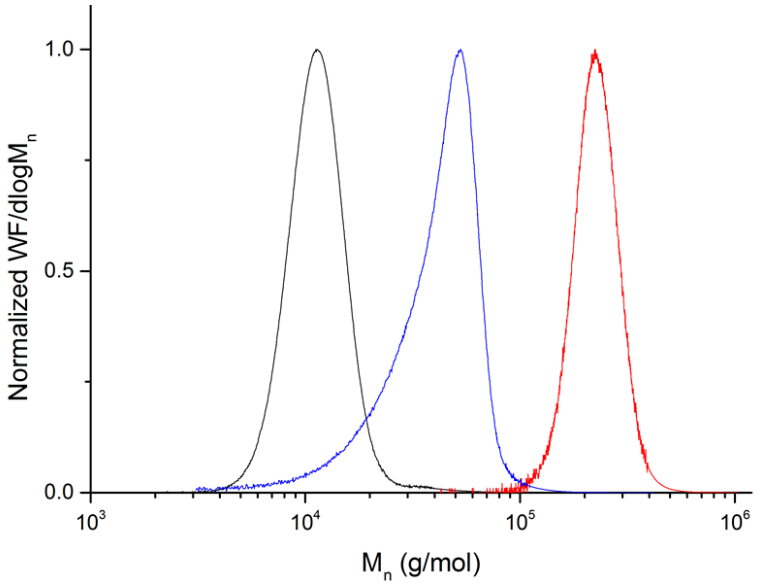

Figure S3.1. GPC chromatographs (refractive index trace) in *n*-Bu_4NBr/THF of $PLLA_{47}$ (black, $Đ_M$ = 1.09), $PLLA_{47}$-*b*-$P2VP_{502}$ (blue, $Đ_M$ = 1.25), $PLLA_{47}$-*b*-$PNIPAm_{267}$ (red, $Đ_M$ = 1.11).

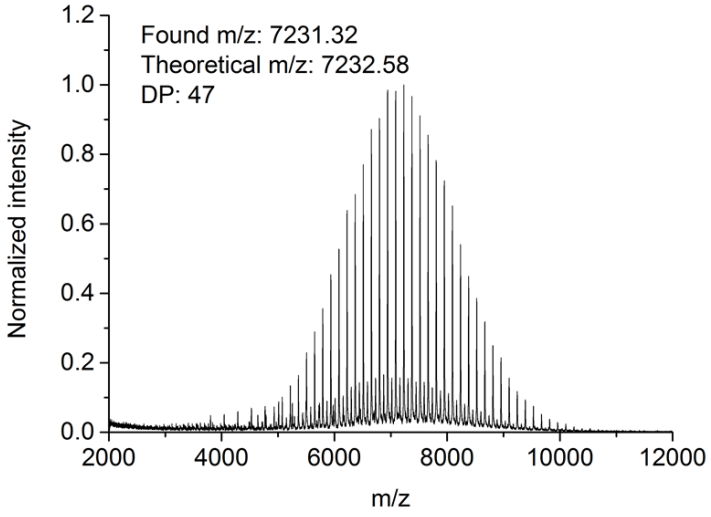

Figure S3.2. MALDI-TOF MS of CTA-$PLLA_{47}$.

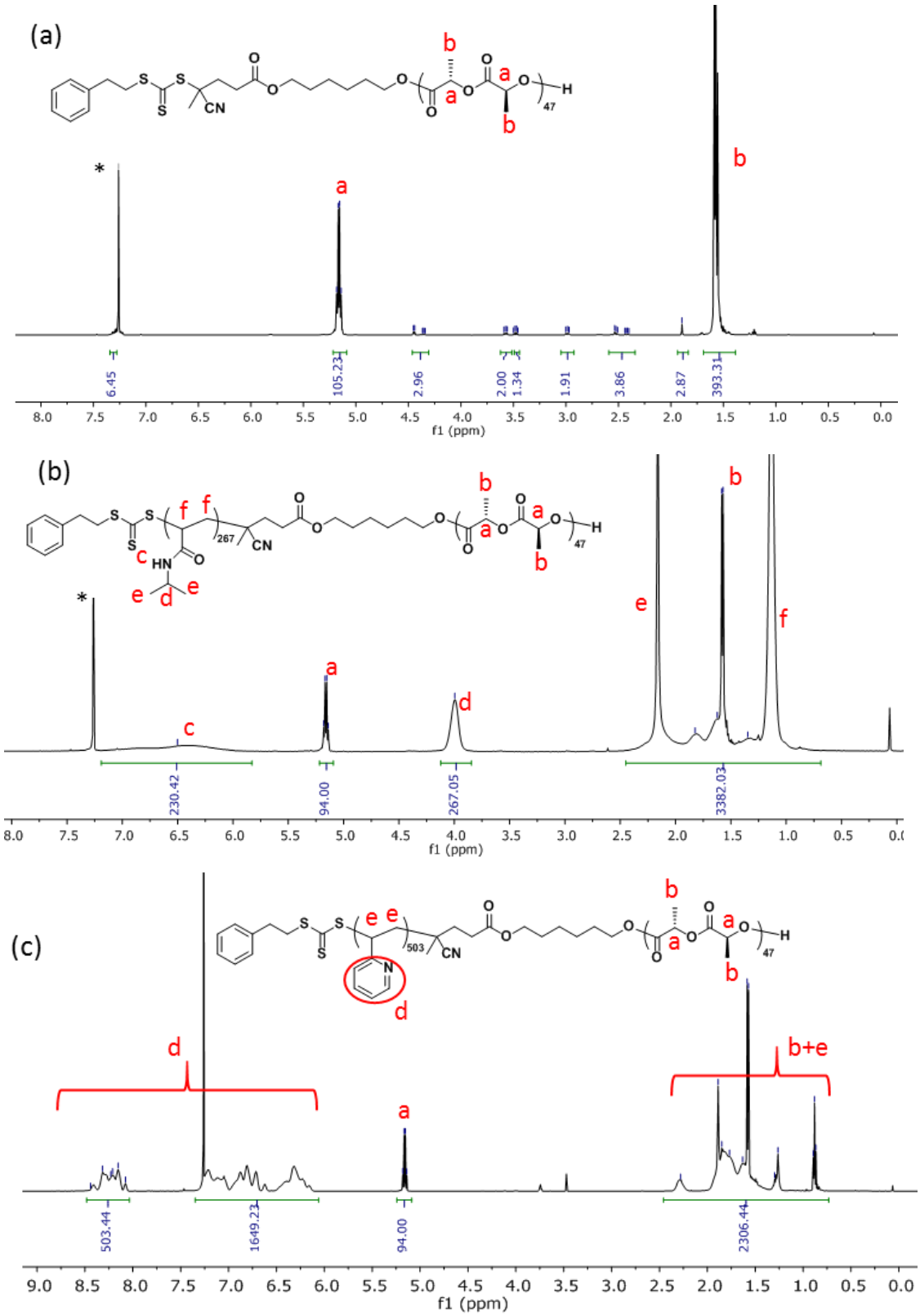

Figure S3.3. ^{1}H NMR (400 MHz, $CDCl_3$) spectra of (a) CTA-PLLA$_{47}$, (b) PLLA$_{47}$-*b*-PNIPAm$_{267}$ and (c) PLLA$_{47}$-*b*-P2VP$_{502}$.

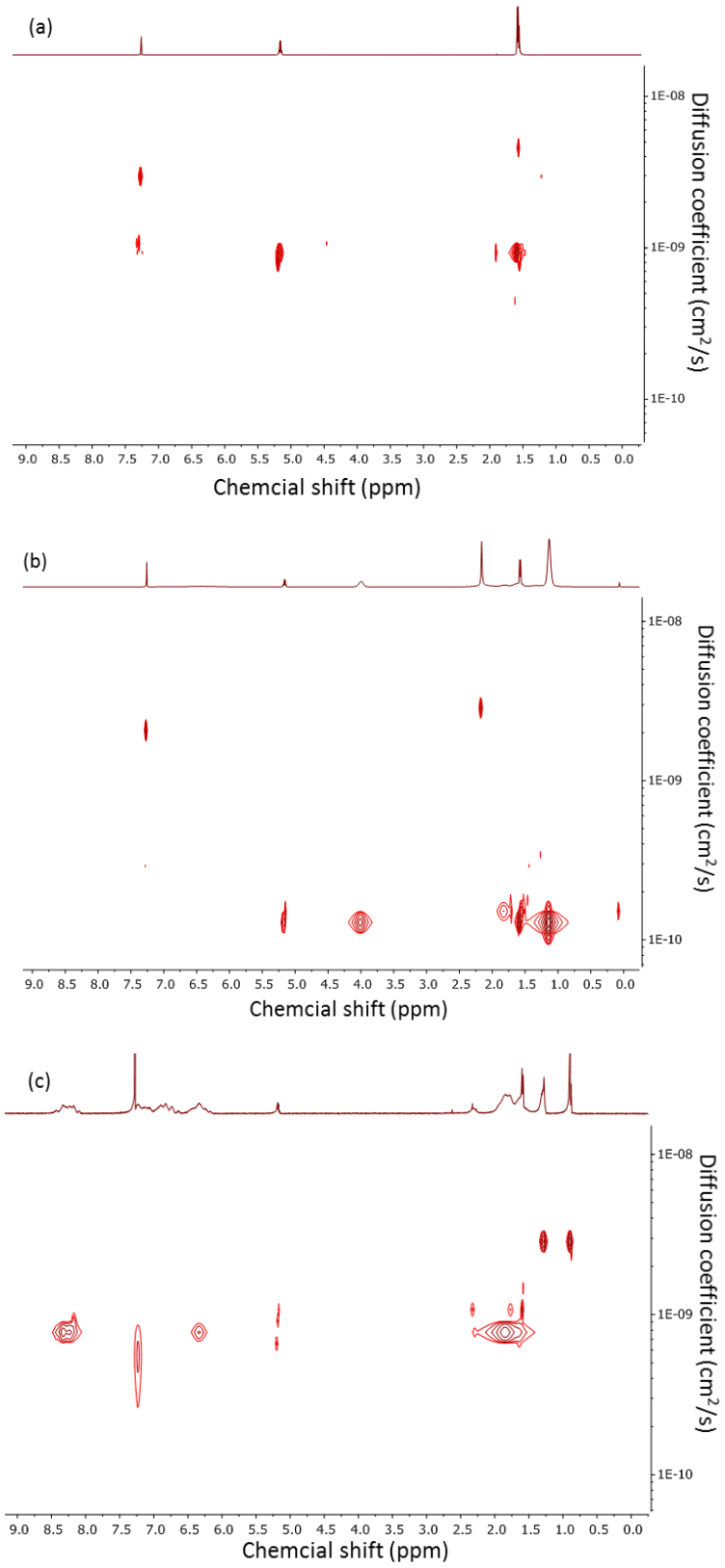

Figure S3.4. ^{1}H DOSY NMR (500 MHz, $CDCl_3$) spectra: (a) $PLLA_{47}$ and (b) $PLLA_{47}$-*b*-$PNIPAm_{267}$ and (c) $PLLA_{47}$-*b*-$P2VP_{502}$.

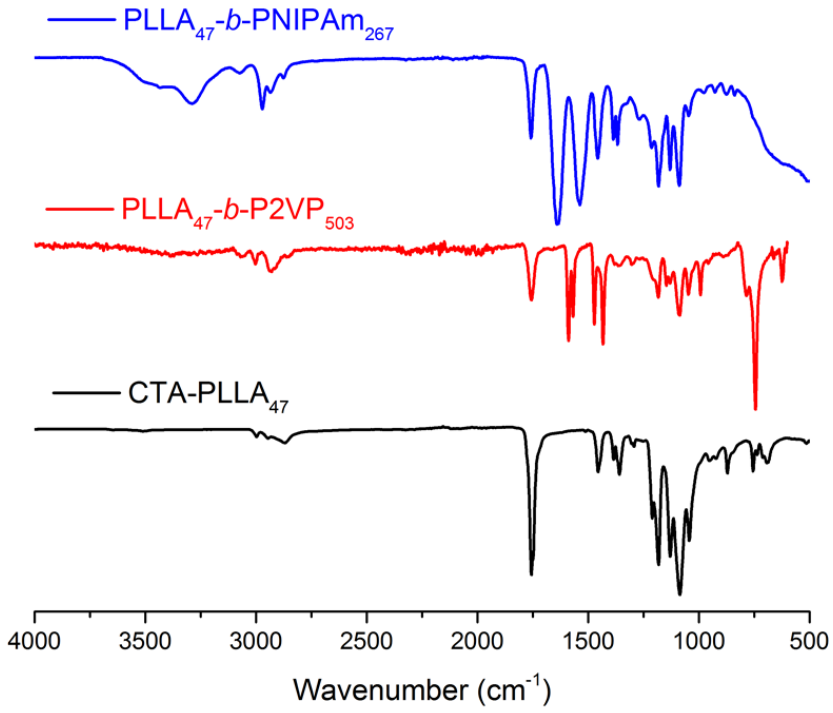

Figure S3.5. FT-IR characterisation of PLLA-containing polymers.

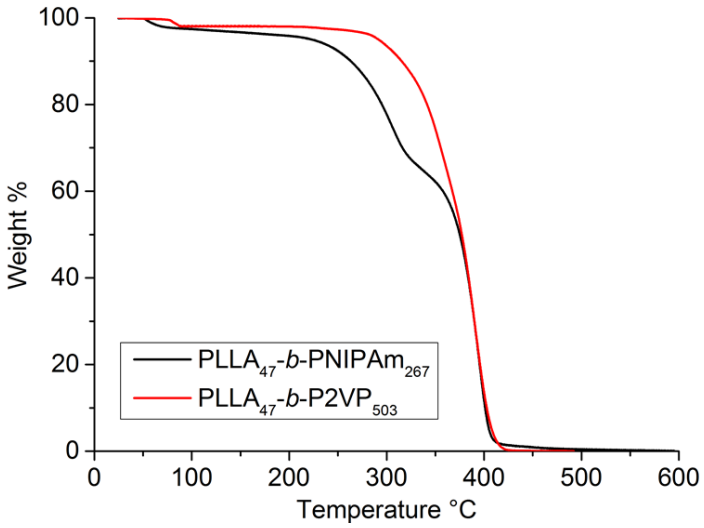

Figure S3.6. Thermogravimetric analysis (TGA) for PLLA$_{47}$-*b*-PNIPAm$_{267}$ (black) and PLLA$_{47}$-*b*-P2VP$_{503}$ (red). TGA was performed at a scan rate of 10 °C/min under nitrogen.

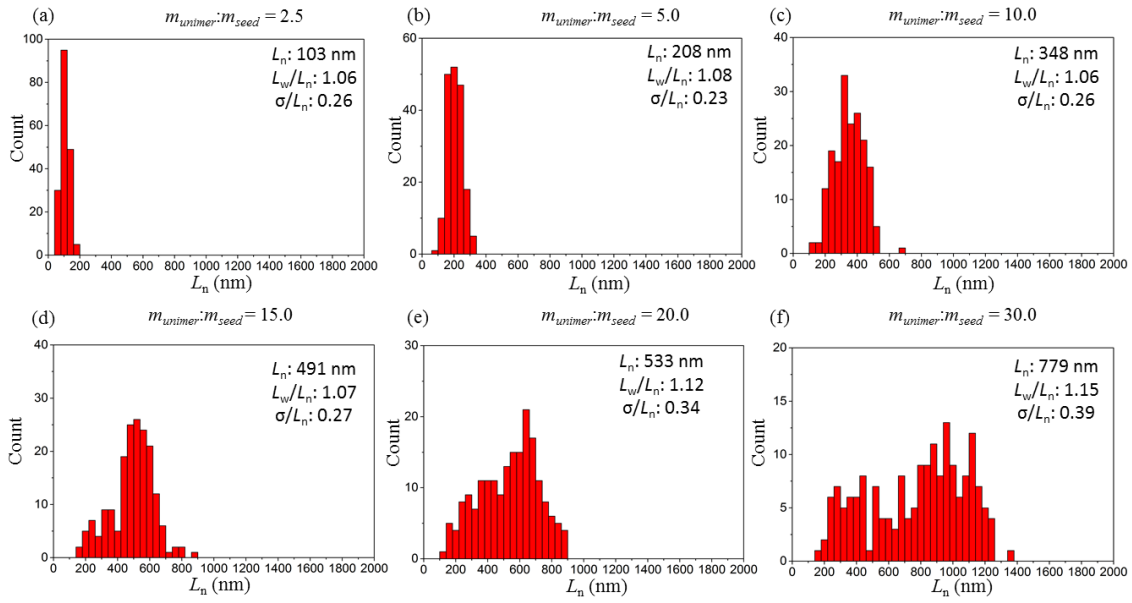

Figure S3.7. Contour length histogram of samples (aging for 5 days) of elongated $PLLA_{47}$-*b*-$PNIPAm_{267}$ micelles prepared by seeded-growth off seed micelles (L_n = 36 nm, L_w/L_n = 1.10, σ/L_n: 0.26) in EtOH after the addition of unimers (in DMSO) with unimer-to-seed mass ratios of (a) 2.5, (b) 5.0, (c) 10.0, (d) 15.0, (e) 20.0 and (f) 30.0.

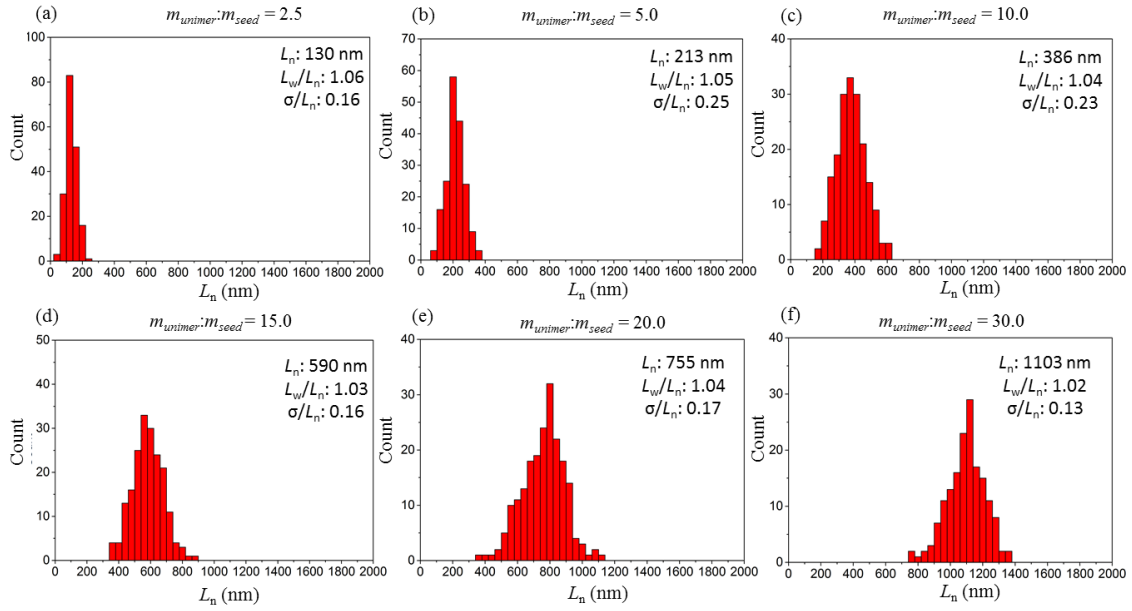

Figure S3.8. Contour length histogram of samples (aging for 5 days) of uniform $PLLA_{47}$-*b*-$PNIPAm_{267}$ micelles prepared by seeded-growth off seed micelles (L_n = 36 nm, L_w/L_n = 1.10, σ/L_n: 0.26) in TFE/EtOH with volume ratios of (a) 3:97, (b) 3:97, (c) 5:95, (d) 8:92, (e) 10:90 and (f) 15:85 after the addition of unimers (in DMSO) with unimer-to-seed mass ratios of (a) 2.5, (b) 5.0, (c) 10.0, (d) 15.0, (e) 20.0 and (f) 30.0, respectively.

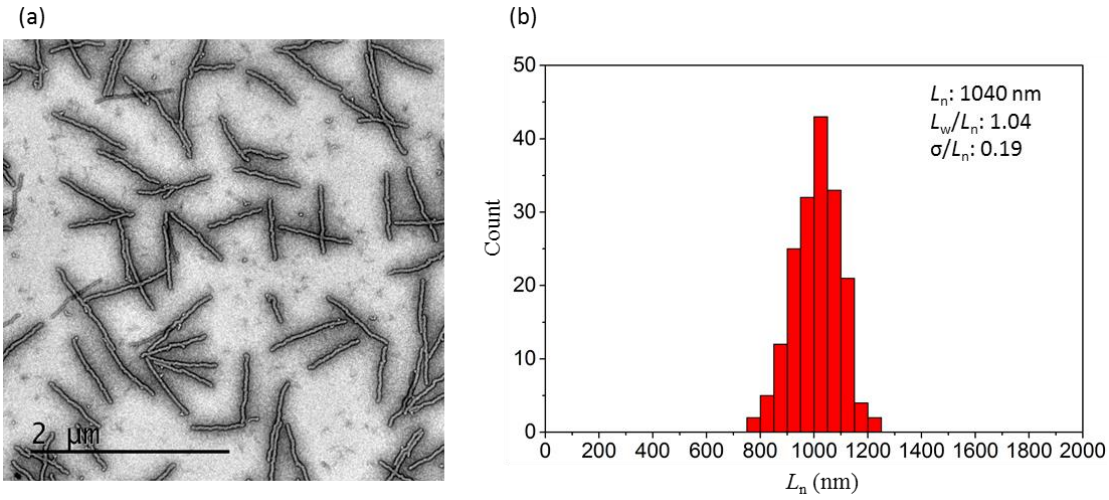

Figure S3.9. (a) TEM images of PLLA$_{47}$-*b*-PNIPAm$_{267}$ micelles prepared for characterisation experiments with length of L_n = 1040 nm (L_w/L_n = 1.04); (b) contour length histogram of measured length data. TEM image was stained with uranyl acetate solution (2% in EtOH).

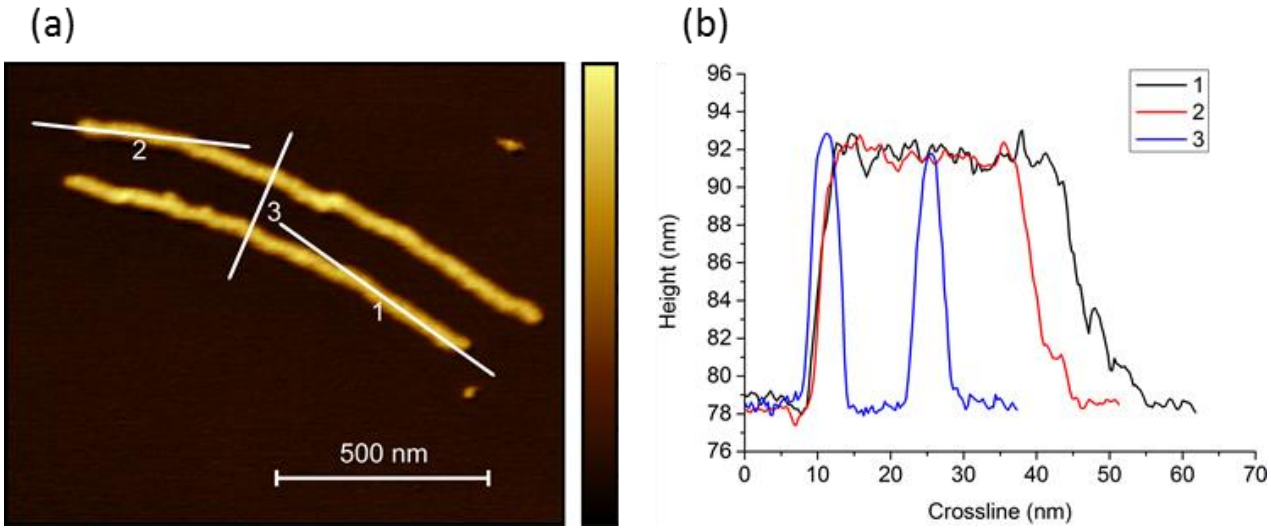

Figure S3.10. AFM images of PLLA$_{47}$-*b*-PNIPAm$_{267}$ micelles with controlled length. (a) Height image of micelles; (b) height profile by crossline measurements.

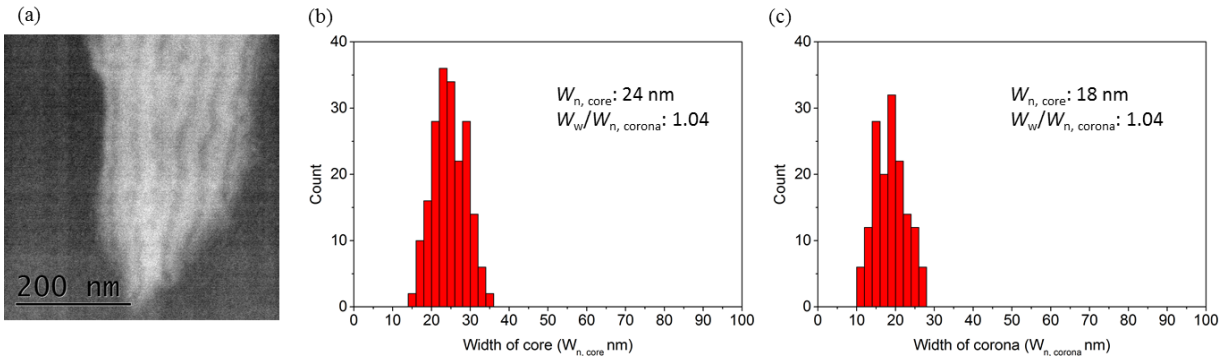

Figure S3.11. (a) STEM images of $PLLA_{47}$-*b*-$PNIPAm_{267}$ micelles in dark-field (white area is corona while dark area is core), (b) contour width histograms of core width measurement, and (c) contour width histograms of corona width measurement.

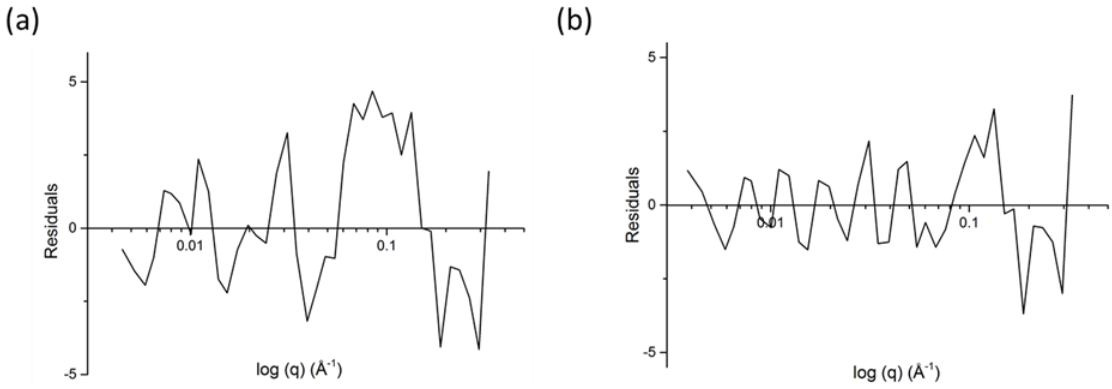

Figure S3.12. Plot of residual vs log (q) from Model 1 fitting data (a) and Model 2 fitting data (b).

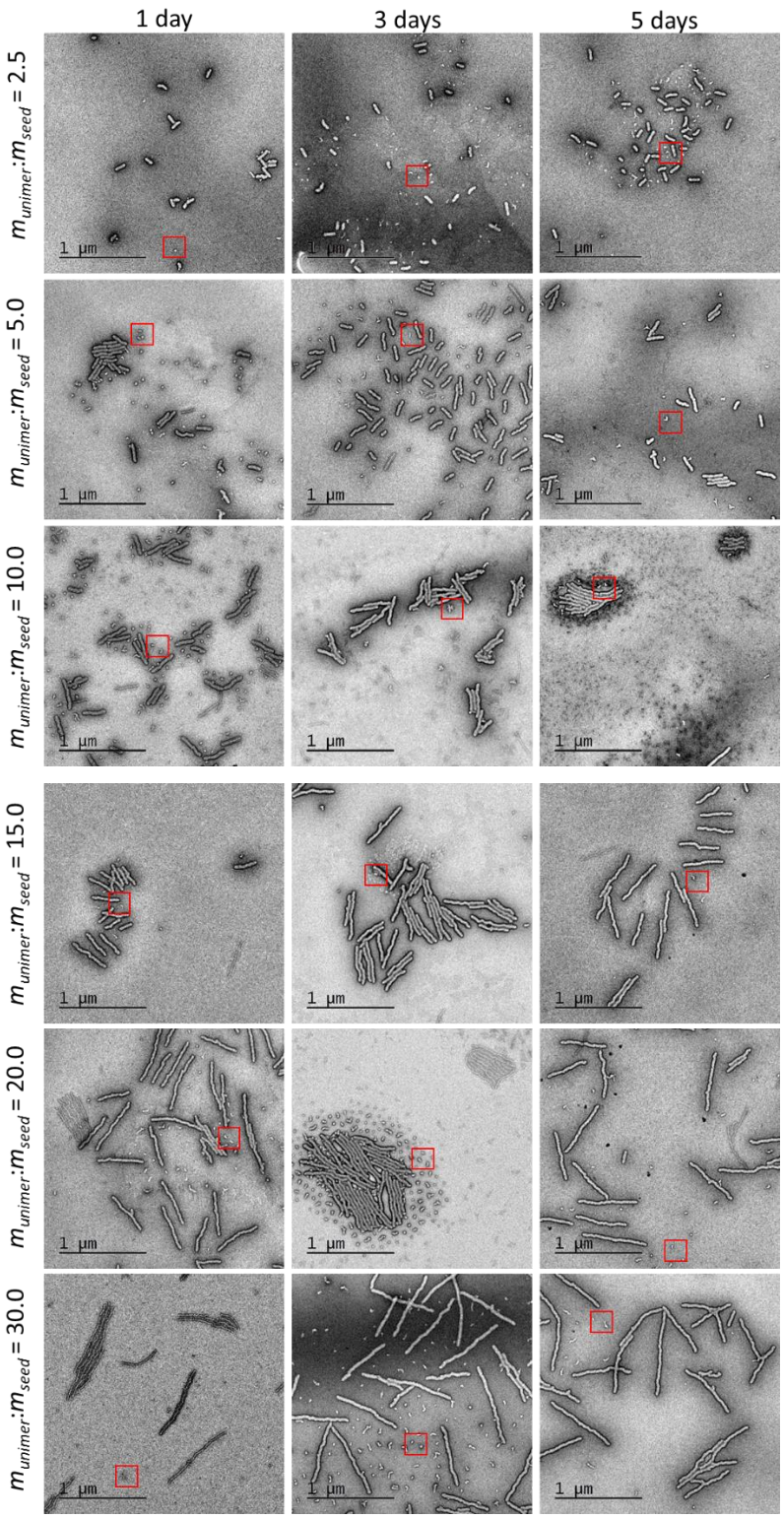

Figure S3.13. TEM images of elongated $PLLA_{47}$-*b*-$PNIPAm_{267}$ micelles in kinetic studies prepared by seeded-growth off seed micelles (L_n = 36 nm, L_w/L_n = 1.10, σ/L_n: 0.26) in EtOH after addition of unimers (in DMSO) with unimer-to-seed mass ratios of 2.5, 5.0, 10.0, 15.0, 20.0 and 30.0; TEM samples were stained with a 2 wt% solution of uranyl acetate in EtOH.

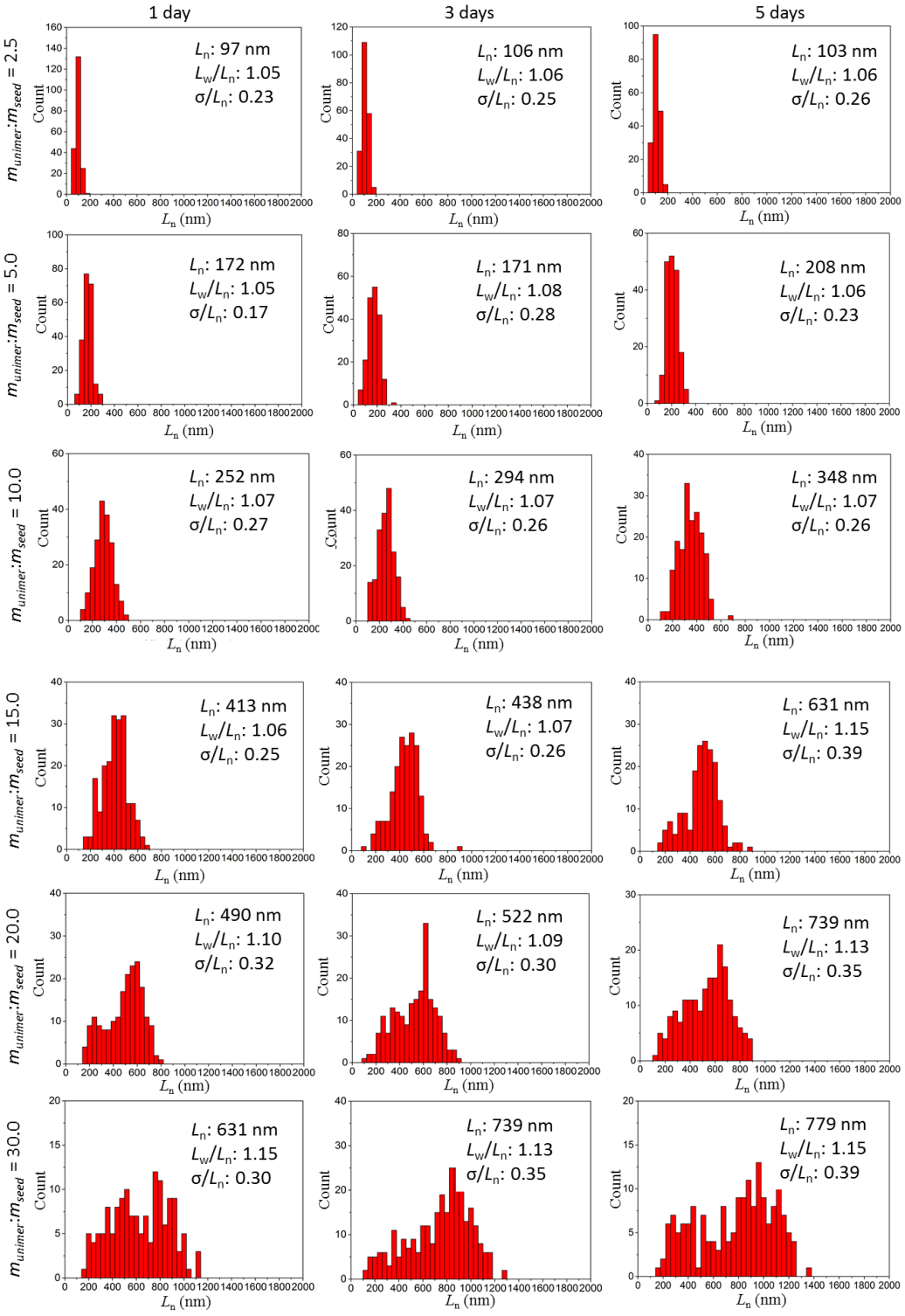

Figure S3.14. Contour length histograms of elongated PLLA$_{47}$-*b*-PNIPAm$_{267}$ micelles in kinetic studies prepared by seeded-growth off seed micelles (L_n = 36 nm, L_w/L_n = 1.10, σ/L_n: 0.26) in EtOH after addition of unimers (in DMSO) with unimer-to-seed mass ratios of 2.5, 5.0, 10.0, 15.0, 20.0 and 30.0.

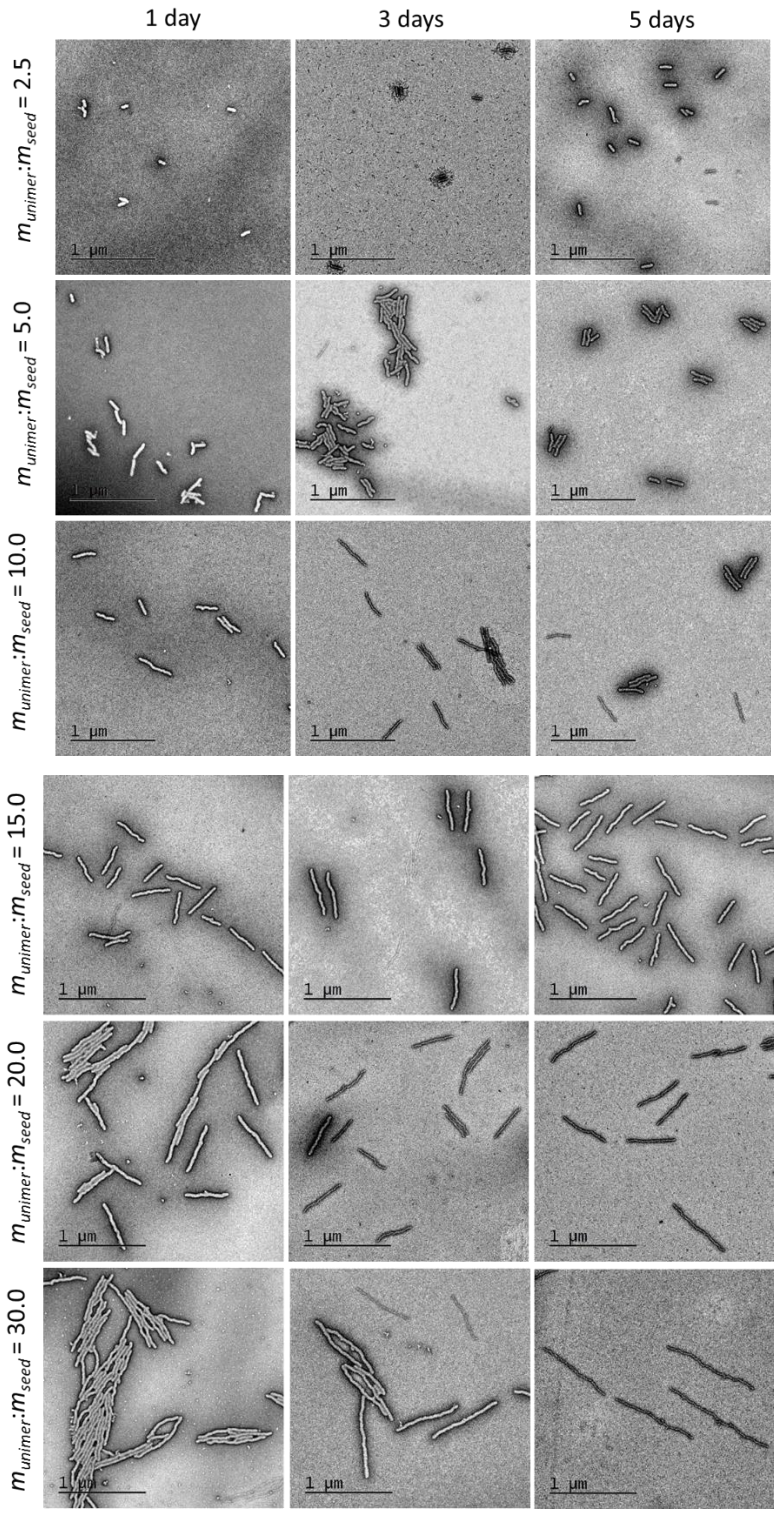

Figure S3.15. TEM images of uniform $PLLA_{47}$-*b*-$PNIPAm_{267}$ micelles in kinetic studies prepared by seeded-growth off seed micelles (L_n = 36 nm, L_w/L_n = 1.10, σ/L_n: 0.26) in TFE/EtOH with volume ratios of 3:97, 3:97, 5:95, 8:92, 10:90 and 15:85 after addition of unimers (in DMSO) with unimer-to-seed mass ratios of 2.5, 5.0, 10.0, 15.0, 20.0 and 30.0, respectively; TEM samples were stained with a 2 wt% solution of uranyl acetate in EtOH.

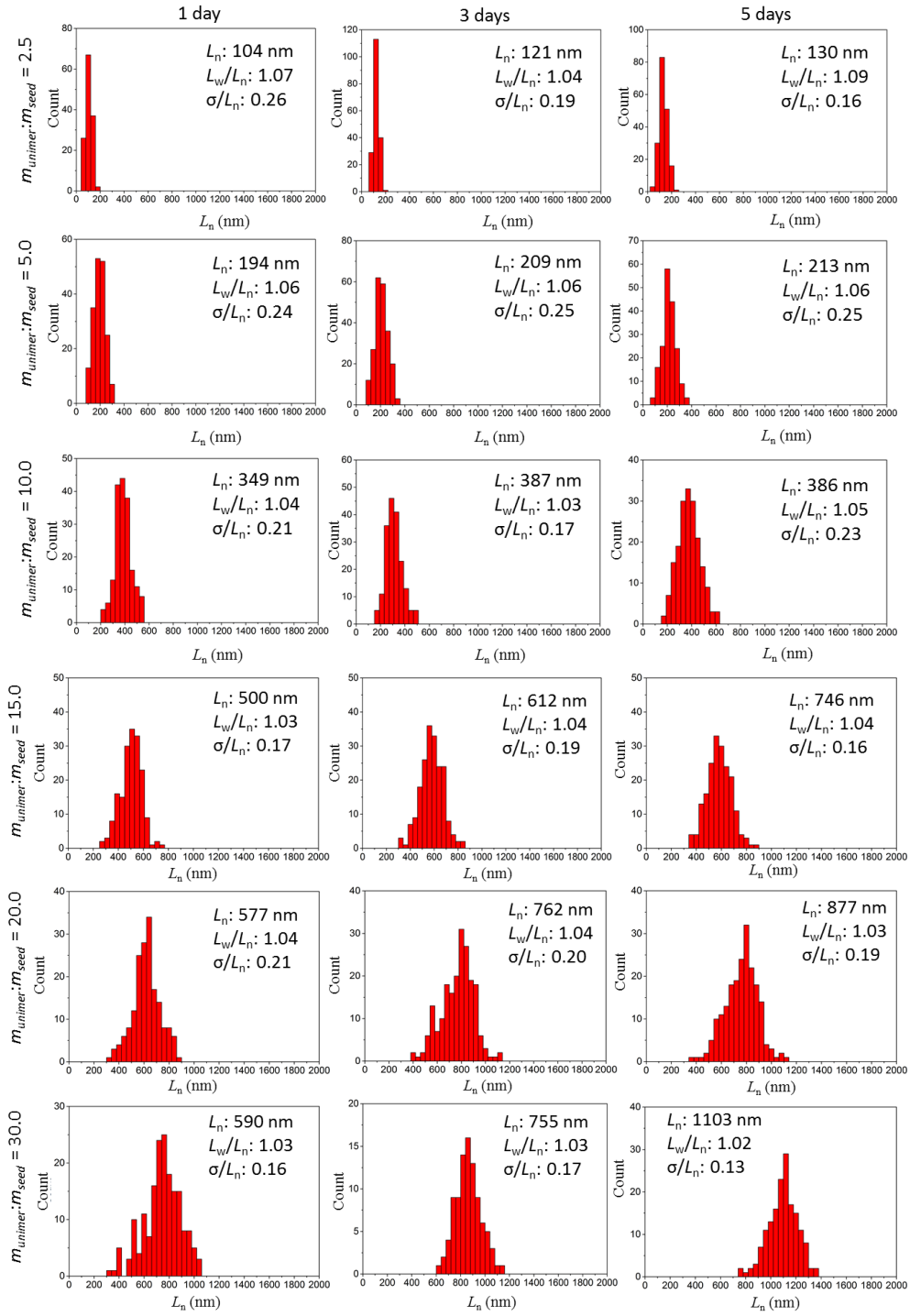

Figure S3.16. Contour length histograms of uniform PLLA$_{47}$-*b*-PNIPAm$_{267}$ micelles in kinetic studies prepared by seeded-growth off seed micelles (L_n = 36 nm, L_w/L_n = 1.10, σ/L_n: 0.26) in TFE/EtOH with volume ratios of 3:97, 3:97, 5:95, 8:92, 10:90 and 15:85 after addition of unimers (in DMSO) with unimer-to-seed mass ratios of 2.5, 5.0, 10.0, 15.0, 20.0 and 30.0, respectively.

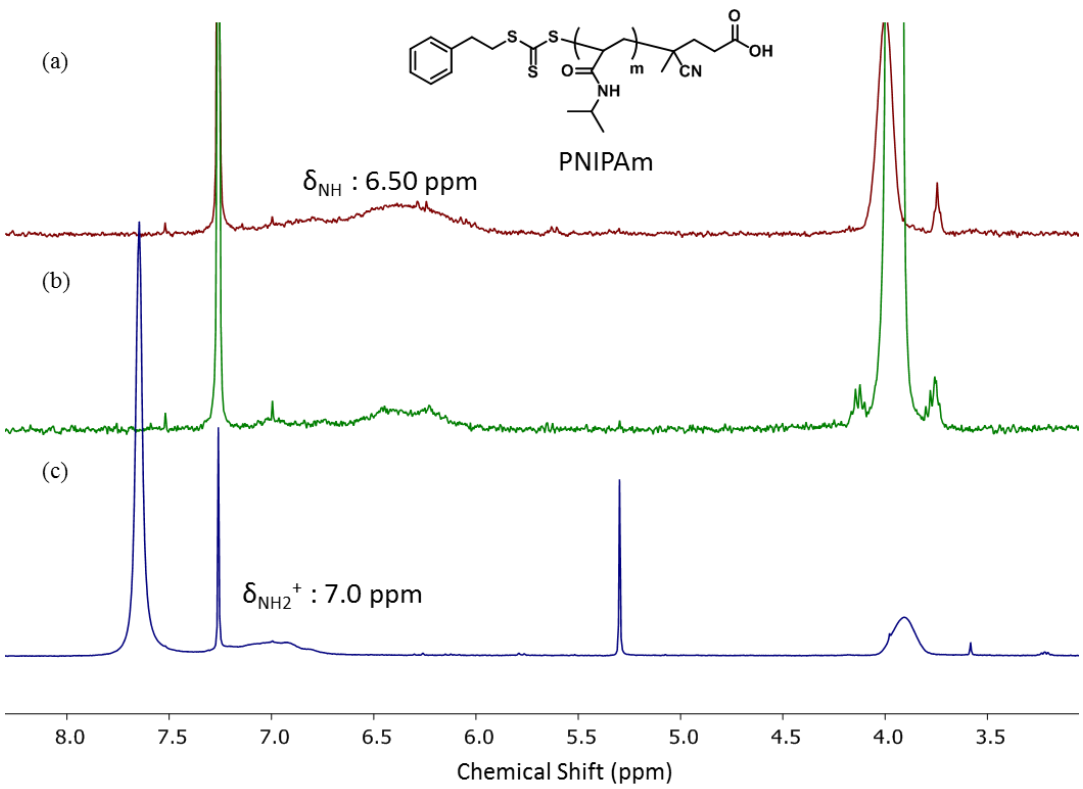

Figure S3.17. ^{1}H NMR in $CDCl_3$ of (a) PNIPAm, (b) PNIPAm and TFE and (c) PNIPAm and TFA.

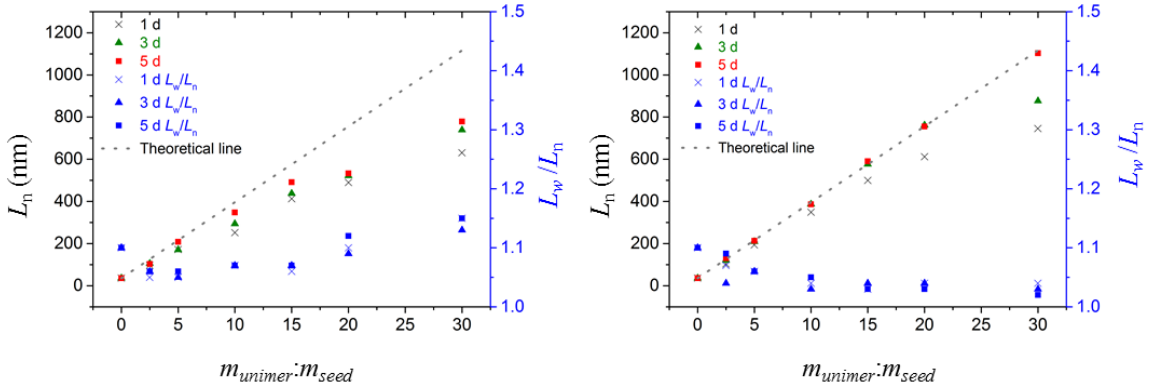

Figure S3.18. Plots of micelle lengths as a function of time monitored over 5 days. Unimers (in DMSO) was added to seed solutions (0.5 mg/mL, L_n = 36 nm) in (a) and in (b)EtOH TFE/EtOH (*v*:*v* = 3:97, 3:97, 5:95, 8:92, 10:90 and 15:85 for m_{unimer}:m_{seed} = 2.5, 5.0, 10.0, 15.0, 20.0 and 30.0, respectively). Black label - micelle average length; blue label - L_w/L_n.

Table S3.1. Data summary of kinetic studies on seeded-growth of $PLLA_{47}$-*b*-$PNIPAm_{267}$ micelles in EtOH over 5 days.

In EtOH		$m_{unimer}:m_{seed}$						
		0 (seed)	2.5	5.0	10.0	15.0	20.0	30.0
1 d	L_n	36	97	172	252	413	490	631
	L_w	40	102	180	271	439	540	728
	L_w/L_n	1.1	1.05	1.05	1.07	1.06	1.10	1.15
	σ	9.4	22.5	36.7	68.2	104.7	157.2	246.6
	L_n/eq	-	27	29	23	26	23	20
	σ/L_n	0.26	0.23	0.17	0.27	0.25	0.32	0.39
3 d	L_n	36	106	171	294	438	522	739
	L_w	40	113	184	300	468	570	830
	L_w/L_n	1.1	1.06	1.08	1.07	1.07	1.09	1.13
	σ	9.4	26.7	48.2	75.9	113.8	155.8	258.5
	L_n/eq	-	30	28	27	27	25	24
	σ/L_n	0.26	0.25	0.28	0.26	0.26	0.30	0.35
5 d	L_n	36	103	208	348	491	533	779
	L_w	40	109	221	373	527	596	899
	L_w/L_n	1.1	1.06	1.06	1.07	1.07	1.12	1.15
	σ	9.4	26.6	47.9	92.2	133.9	183.5	304.1
	L_n/eq	-	29	35	32	31	25	26
	σ/L_n	0.26	0.26	0.23	0.26	0.27	0.34	0.39

Table S3.2. Data summary of kinetic studies over 5 days on seeded-growth of $PLLA_{47}$-*b*-$PNIPAm_{267}$ micelles in TFE/EtOH with volume ratios of 3:97, 3:97, 5:95, 8:92, 10:90 and 15:85 after the addition of unimers (in DMSO) with unimer-to-seed mass ratios of 2.5, 5.0, 10.0, 15.0, 20.0 and 30.0, respectively.

In TFE/EtOH		$m_{unimer}:m_{seed}$						
		0 (seed)	2.5	5.0	10.0	15.0	20.0	30.0
1 d	L_n	36	104	194	349	500	612	746
	L_w	40	111	205	365	515	636	778
	L_w/L_n	1.1	1.07	1.06	1.04	1.03	1.04	1.04
	σ	9.4	27.3	47.5	73.6	85.1	120.4	155.3
	L_n/eq	-	30	32	31	31	29	24
	σ/L_n	0.26	0.26	0.24	0.21	0.17	0.19	0.16
3 d	L_n	36	121	209	387	577	762	877
	L_w	40	125	222	399	600	795	908
	L_w/L_n	1.1	1.04	1.06	1.03	1.04	1.04	1.03
	σ	9.4	22.5	51.8	67.6	122.7	157.9	165.1
	L_n/eq	-	34	34	35	36	36	28
	σ/L_n	0.26	0.19	0.25	0.17	0.21	0.20	0.19
5 d	L_n	36	130	213	386	590	755	1103
	L_w	40	142	228	406	606	779	1122
	L_w/L_n	1.1	1.09	1.06	1.05	1.03	1.03	1.02
	σ	9.4	20.4	55.1	90.1	95.7	133.6	138.2
	L_n/eq	-	37	36	35	37	36	35
	σ/L_n	0.26	0.16	0.25	0.23	0.16	0.17	0.13

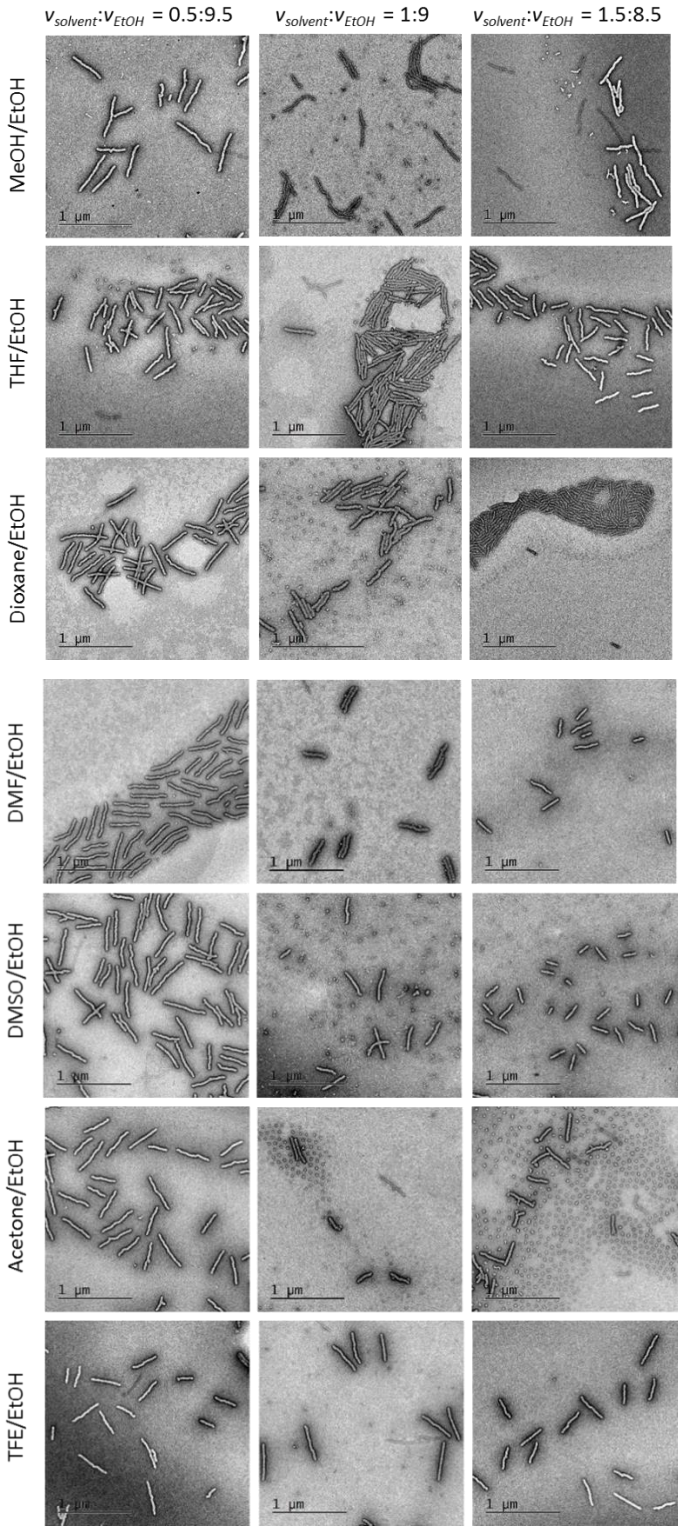

Figure S3.19. TEM images of uniform $PLLA_{47}$-*b*-$PNIPAm_{267}$ micelles in solvent effect studies prepared by adding unimers (m_{unimer}:m_{seed} = 15.0, in DMSO) to seed micelles (L_n = 36 nm, L_w/L_n = 1.10, σ/L_n: 0.26) in TFE/EtOH (*v*:*v* = 0.5:9.5, 1:9 and 1.5:8.5); TEM samples were stained with a 2 wt% solution of uranyl acetate in EtOH. Red circles show the presence of spherical micelles. Inset: 100 nm.

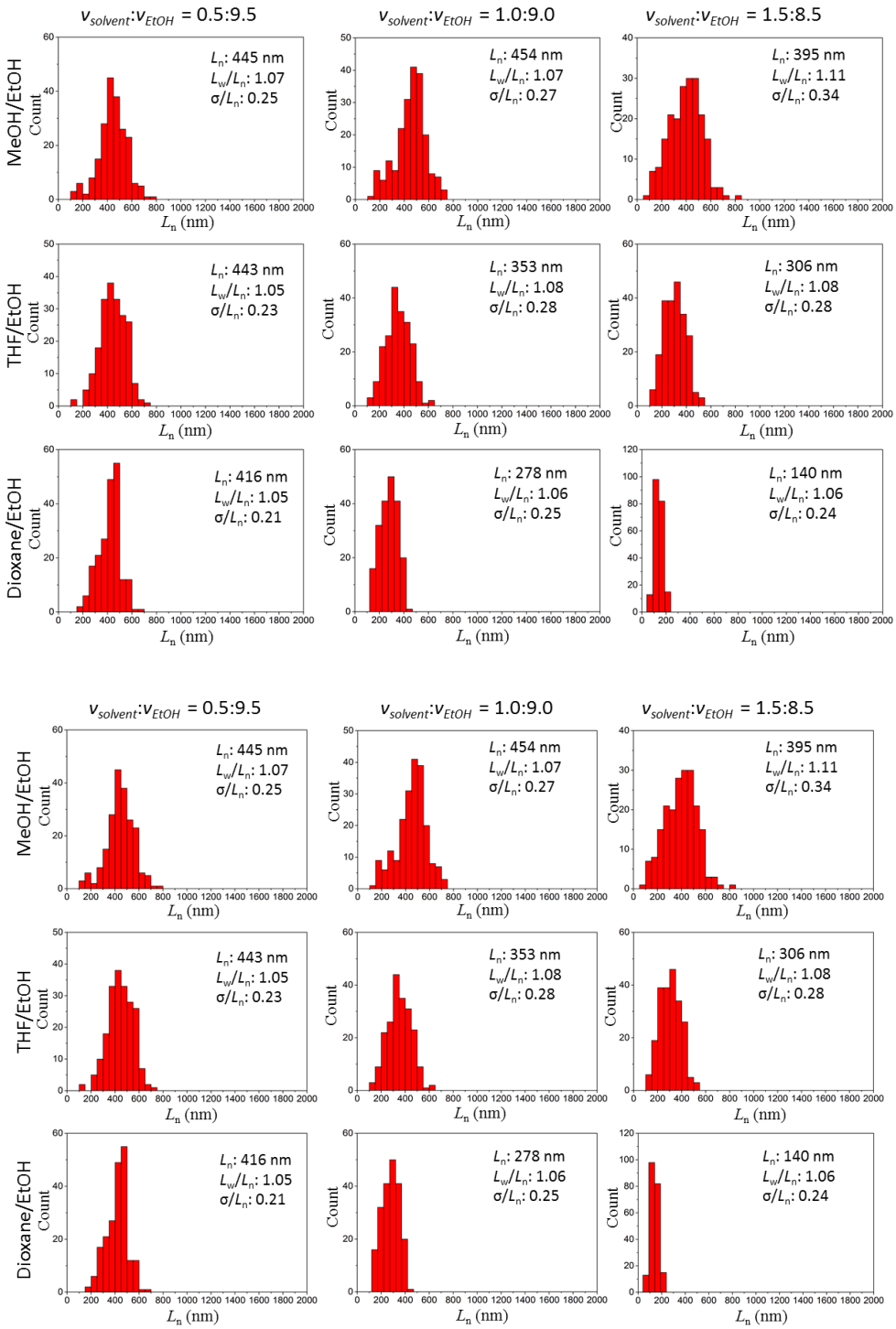

Figure S3.20. Contour length histograms of uniform PLLA$_{47}$-*b*-PNIPAm$_{267}$ micelles in solvent effect studies prepared by adding unimers (m_{unimer}:m_{seed} = 15.0, in DMSO) to seed micelles (L_n = 36 nm, L_w/L_n = 1.10, σ/L_n: 0.26) in TFE/EtOH (*v*:*v* = 0.5:9.5, 1.0:9.0 and 1.5:8.5).

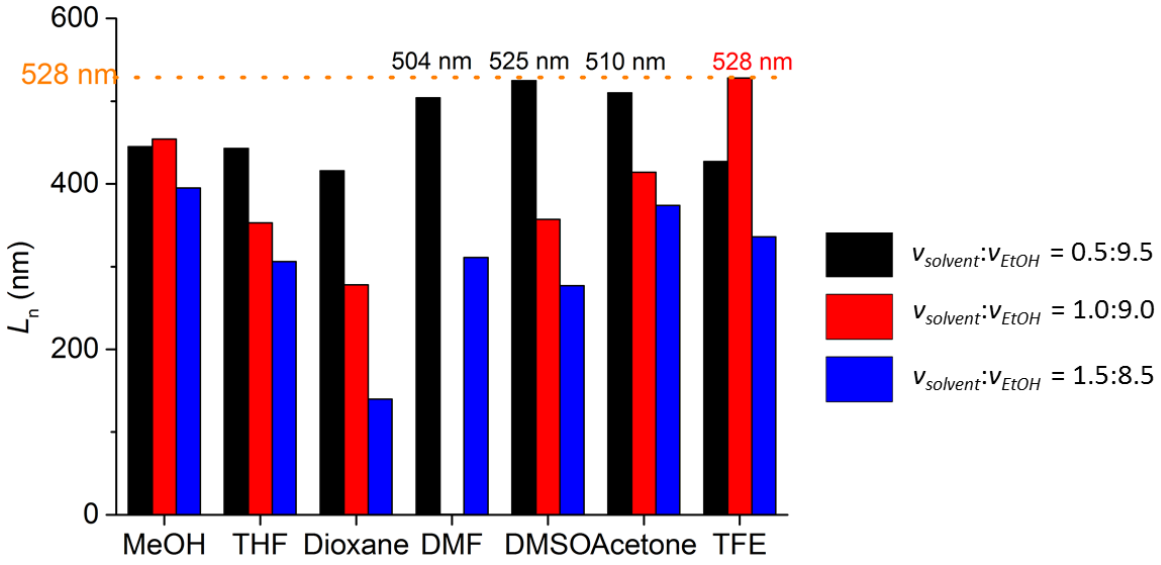

Figure S3.21. Lengths of elongated $PLLA_{47}$-*b*-$PNIPAm_{267}$ micelles obtained after 5 days aging by addition of unimer (m_{unimer}:m_{seed} = 15.0, in DMSO) into seeds (0.5 mg/mL, L_n = 33 nm, L_w/L_n = 1.13) in mixture of EtOH and various other solvents.

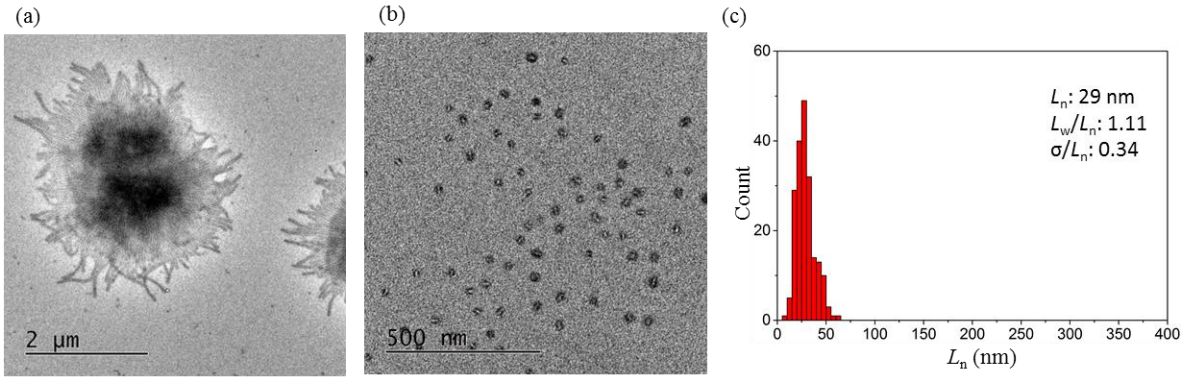

Figure S3.22. (a) Polydisperse $PLLA_{47}$-*b*-$P2VP_{502}$ micelles in DMSO/EtOH (1:9) with a concentration of 0.5 mg/ml prepared by heating the polymer in DMSO/EtOH (1:9) at 70 °C for 2 h followed by slow cooling down; (b) seeds prepared by sonication of polydisperse micelles at 0 °C for 2 h in a sonic cleaning bath; (c) contour length histogram of measured seeds length, L_n = 29 nm, L_w/L_n = 1.11.

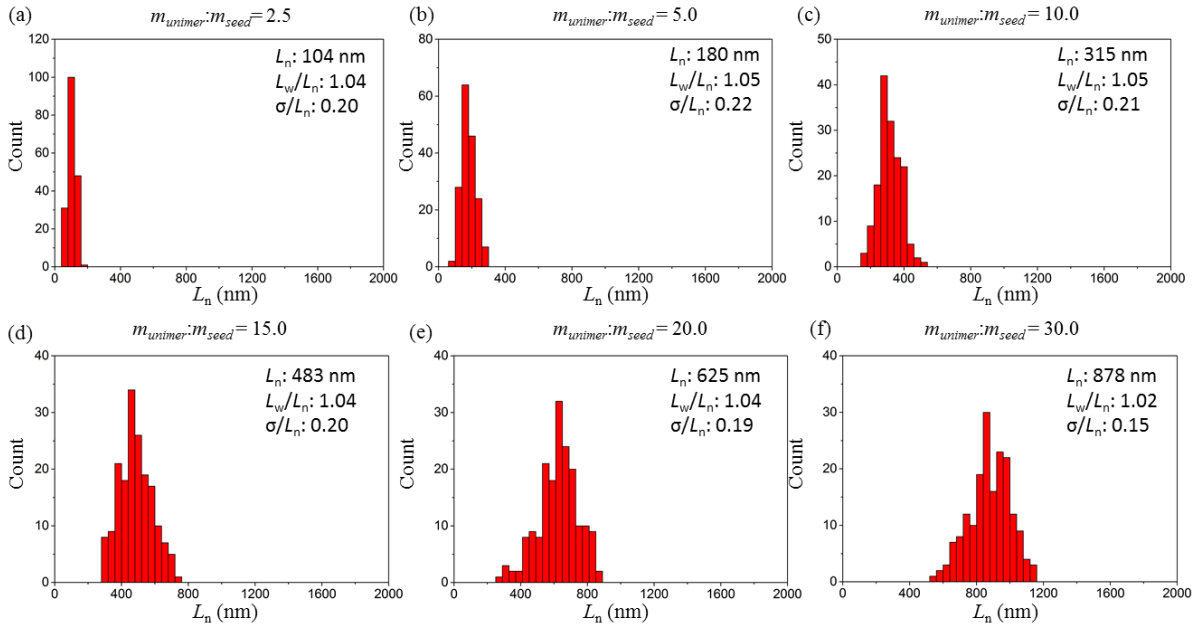

Figure S3.23. Contour length histogram of 5 days aged uniform $PLLA_{47}$-*b*-$P2VP_{502}$ micelles prepared by seeded-growth off seed micelles (L_n = 29 nm, L_w/L_n = 1.11, σ/L_n: 0.34) in TFE/EtOH with volume ratios of (a) 3:97, (b) 3:97, (c) 5:95, (d) 8:92, (e) 10:90 and (f) 15:85 after the addition of unimers (in DMSO) with unimer-to-seed mass ratios of (a) 2.5, (b) 5.0, (c) 10.0, (d) 15.0, (e) 20.0 and (f) 30.0, respectively.

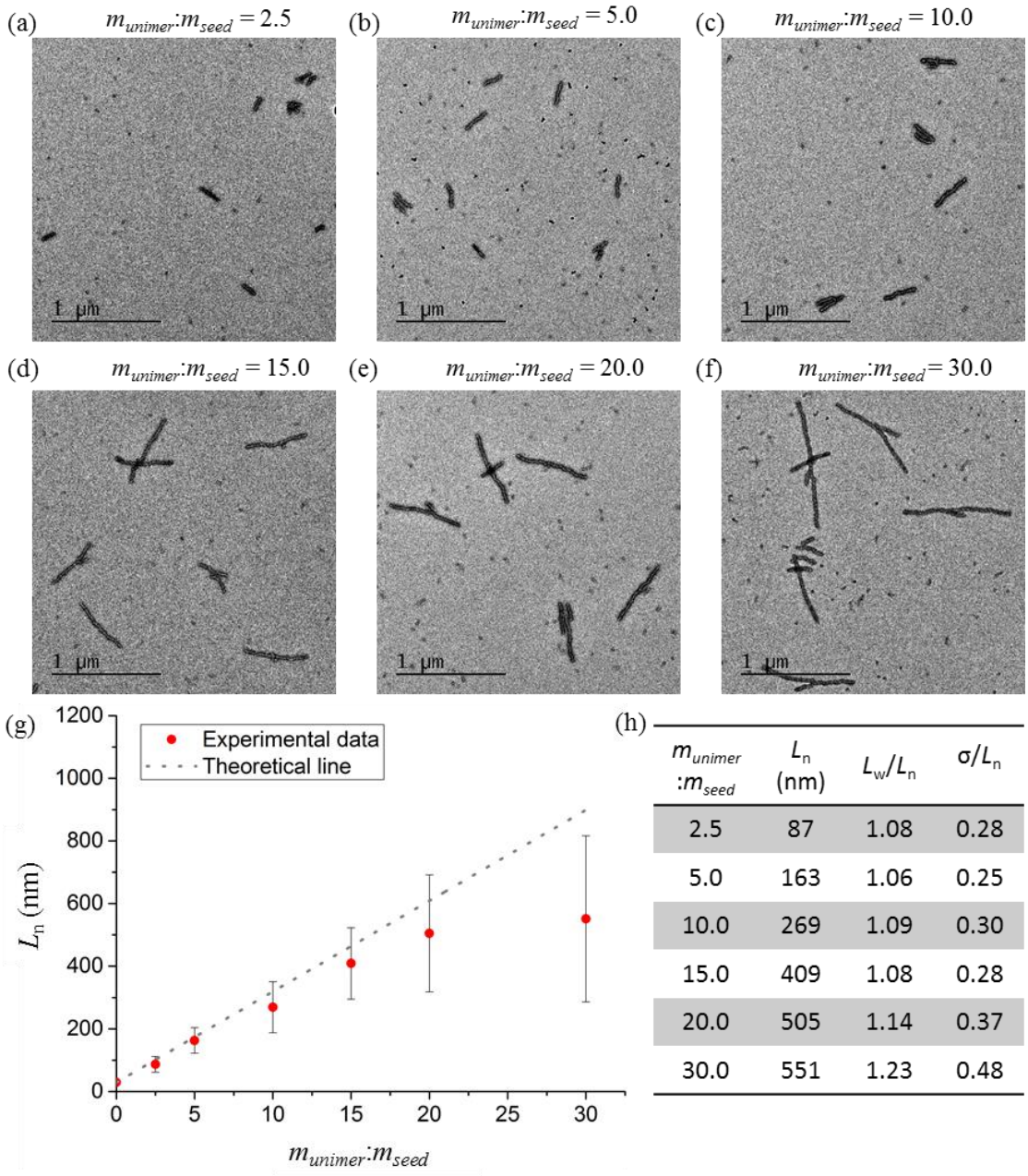

(h)

m_{unimer} :m_{seed}	L_n (nm)	L_w/L_n	σ/L_n
2.5	87	1.08	0.28
5.0	163	1.06	0.25
10.0	269	1.09	0.30
15.0	409	1.08	0.28
20.0	505	1.14	0.37
30.0	551	1.23	0.48

Figure S3.24. TEM images of 5 days aged samples of uniform $PLLA_{47}$-*b*-$P2VP_{502}$ micelles prepared by seeded-growth off seed micelles (L_n = 29 nm, L_w/L_n = 1.11, σ/L_n: 0.34) in EtOH after the addition of unimers (in DMSO) with unimer-to-seed mass ratios of (a) 2.5, (b) 5.0, (c) 10.0, (d) 15.0, (e) 20.0 and (f) 30.0; (g) plot of number average micelle length vs m_{unimer}:m_{seed}; (h) summary of measured lengths and solvent compositions.

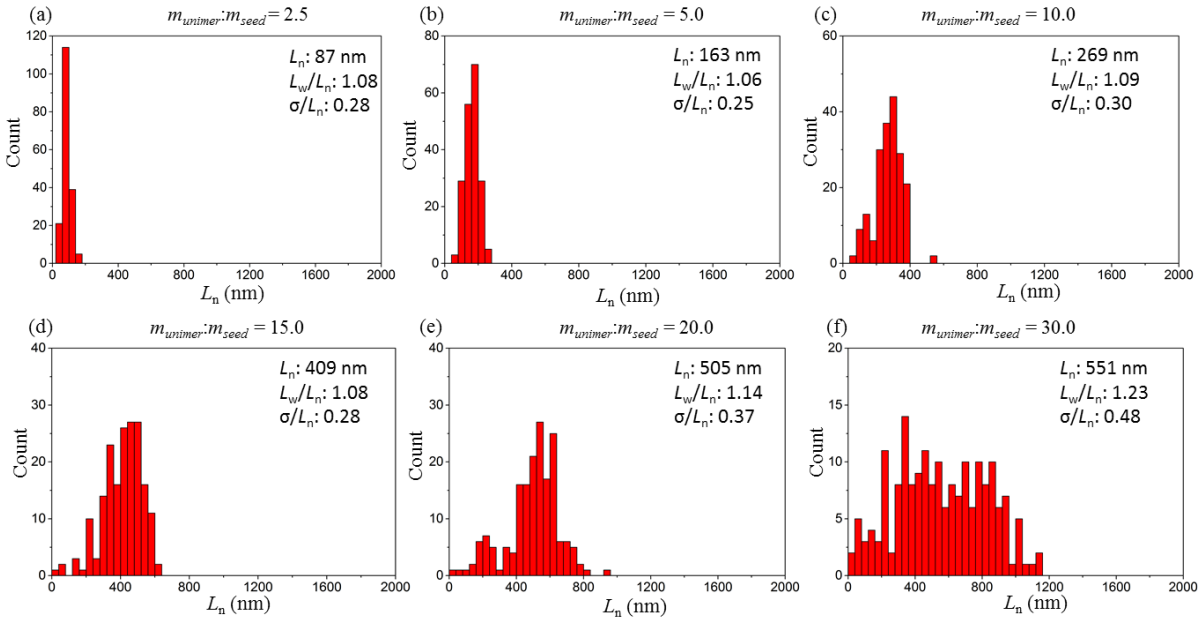

Figure S3.25. Contour length histogram of 5 days aged uniform $PLLA_{47}$-*b*-$P2VP_{502}$ micelles prepared by seeded-growth off seed micelles (L_n = 29 nm, L_w/L_n = 1.11, σ/L_n: 0.34) in EtOH after the addition of unimers (in DMSO) with unimer-to-seed mass ratios of (a) 2.5, (b) 5.0, (c) 10.0, (d) 15.0, (e) 20.0 and (f) 30.0.

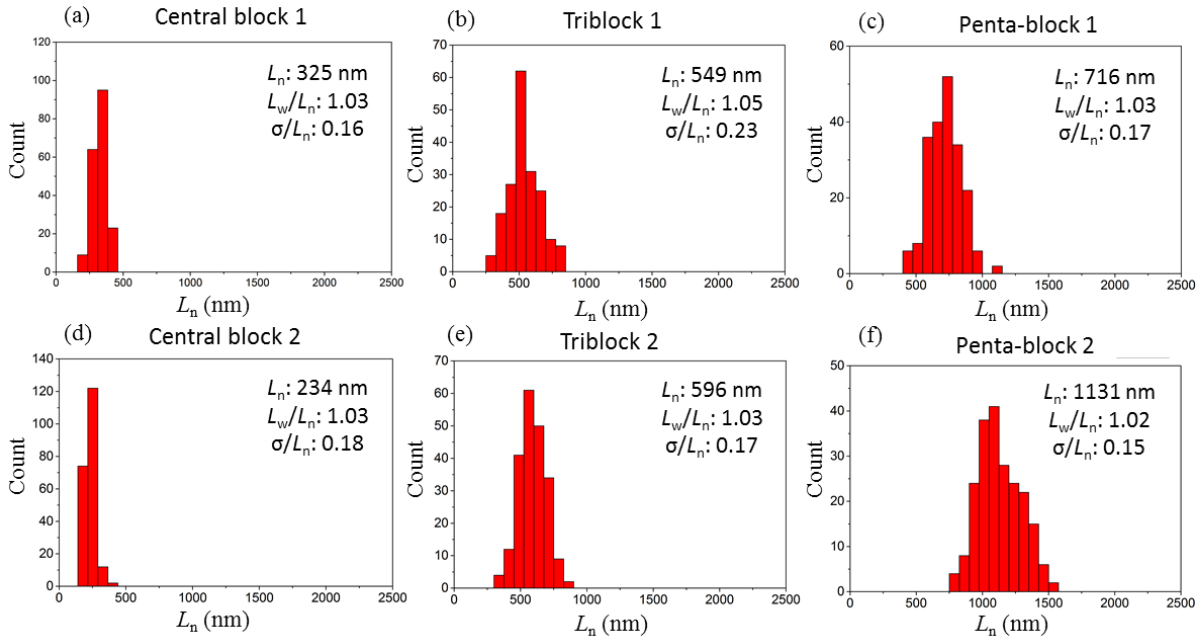

Figure S3.26. Contour length histograms of prepared block co-micelles: (a) central block 1, (b) triblock co-micelles 1, (c) pentablock co-micelles 1, (d) central 2, (e) triblock co-micelles 2 and (f) pentablock co-micelles 2.

Formula for SAXS Data Fitting with Model 2

Model 2 (Figure S3.27) describes a long rigid micelle with a rectangular cross-section (2*a* by 2*b*) core covered by corona on two faces perpendicular to the *a* direction. The core has a uniform scattering length density, ρ_{core}. The coronas have a rectangular cross-section (2*b* by *c*) with a linear decaying scattering intensity from the inner, ρ_{in}, to outer side, ρ_{out}. For the fitting process, the long rods approximation is used by considering the micelle length (2*l*) is significantly greater than the reciprocal of the minimum *q*. The scattering intensity (I(*q*)) from long rods solution can be described as:

$$I(q) = \frac{2\pi l}{q}\langle F_a(Qsin\phi)F_{bd}(qcos\phi)\rangle_\phi$$

where the angle brackets represent an average over the azimuthal angle of *q* with respect to the long micelle axis. The structure factors for the cross-section are defined as follows:

$$F_b(q) = 2bsinc(qb)$$

$$F_a(q) = 2\sum_{j=1,N}(\rho_j + \rho_{j+1})d_j sinc(qd_j)$$

where $\rho_j = \rho_{core}$ for $j = 1$, $\rho_j = \rho_{solvent}$ for $j = 1 + N$, and $\rho_j = \rho_{in} + (\rho_{out} - \rho_{in})[(j - 1.5)/(N - 1)]$ otherwise, while $d_j = a$ for $j = 1$ and $d_j = a + c(j - 1)/(N - 1)$ otherwise. The three dimensions, *a*, *b*, and *c* were assumed to have Schultz distributions and the expression was averaged numerically over these distributions.

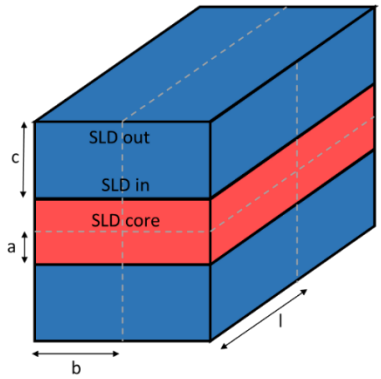

Figure S3.27. Schematic representation of Model 2 used in SAXS data fitting. Distances *a*, *b*, *c* and *l* represent half the core thickness, half the micelle width, the corona thickness and the micelle length respectively. SLD = scattering length density.

Calculation of Corona Volume Fraction in PLLA$_{47}$-*b*-PNIPAm$_{267}$ Micelles

The SLD of the core was held constant at the value of the pure PLLA. The literature values of the densities (PNIPAm: 1.10 g/cm^3; PLLA: 1.29 g/cm^3)[354, 370] were used to calculate the SLD of the materials in their pure state. In our solvated micelle system, it can be considered as a PNIPAm polymer (p) in solvent EtOH (s). For a simple mixture system of two materials, the volume fraction ($\emptyset$) is related to the SLD of the system (S_m), the pure polymer (S_p) and the solvent (S_s), which follows the equation:

$$S_m = S_p^0\,\phi + S_s^0\,(1-\emptyset) = S_s^0 + \emptyset\,(S_p^0 - S_s^0)$$

The system SLD (S_m) is obtained from fitting data. The SLD of a pure material (S^0) is calculated from the product of the number density, n_i, and atomic number, z_i, summed over the different types of atom.

$$S^0 = r_e \sum_i n_i z_i$$

where r_e is the Thompson scattering length of an electron. The number density is related to the chemical formula and mass density of the material.

$$n_i = \frac{f_i N_A A_i}{D}$$

where f_i is the number of atoms in the formula, N_A is Avagadro's Number, A_i is the atomic mass of atom i and D is the mass density.

$$S^0 = \frac{r_e N_A}{D} \sum_i F_i A_i z_i$$

Therefore, S_p^0 is calculated as 1.035×10^{-5}, S_s^0 is calculated as 7.65×10^{-6}. Calculation of the volume fraction of PNIPAm follows the bellowing equations:

$$\emptyset = \frac{S_m - S_s^0}{S_p^0 - S_s^0}$$

$$\emptyset_{PNIPAm} = \frac{S_m - S_{EtOH}}{S^0_{PNIPAm} - S_{EtOH}} = \frac{(7.73\text{–}8.77) \times 10^{-6} - 7.65 \times 10^{-6}}{1.035 \times 10^{-5} - 7.65\ \times 10^{-6}} = 0.03\text{–}0.42$$

Chapter 4 Complex and Hierarchical 2D Assemblies via Crystallisation-Driven Self-Assembly of Poly(*L*-lactide)

Sections of this chapter have been reproduced from:

Xiaoming He, **Yunxiang He**, Ming-Siao Hsiao, Robert L. Harniman, Sam Pearce, Mitchell A. Winnik, and Ian Manners. *Journal of the American Chemical Society*, **2017,** *139*, 9221-9228.

Abstract

Poly(*L*-lactide) (PLLA)-based nanoparticles have attracted much attention with respect to applications in drug delivery and nanomedicine as a result of their biocompatibility and biodegradability. Nevertheless, the ability to prepare PLLA assemblies with well-defined shape and dimensions is limited and represents a key challenge. Herein we report access to a series of monodisperse complex and hierarchical colloidally stable 2D structures based on PLLA cores using the seeded growth, "living-crystallisation-driven self-assembly" method. Specifically, we describe the formation of diamond-shaped platelet micelles and concentric 'patchy' block co-micelles by using seeds of the charge-terminated homopolymer $PLLA_{24}[PPh_2Me]I$ to initiate the sequential growth of either additional charge-terminated homopolymer or a crystallisable blend of the latter with the diblock copolymer, respectively. Moreover, uniform 2D platelet micelles have also been prepared by seeded-growth of a blend unimer of charge-neutral $PLLA_{26}$ homopolymer and diblock copolymer. The epitaxial nature of the growth processes used for the creation of the 2D block co-micelles was confirmed by selected area electron diffraction (SAED) analysis. Crosslinking the peripheral block and subsequent dissolution the interior block of the 'patchy' platelet co-micelles results in the formation of hollow diamond-shaped assemblies. We also demonstrate that, in contrast to the aforementioned results, seeded growth of the unsymmetrical PLLA diblock copolymers alone from 2D platelets leads to the formation of diamond-fiber hybrid structures.

4.1. Introduction

Two-dimensional (2D) planar nanostructures have received extensive recent attention due to their unique properties that originate from their ultrathin and flat morphology.[371-373] Representative examples include graphene,[374, 375] transition metal dichalcogenide nanosheets,[376] boron nitride,[377, 378] and clay nanoplatelets,[379-382] which have found applications in electronics, photonics, spintronics, and composite reinforcement. Such materials are generally prepared from bulk layered materials through a "top-down" approach. In contrast, the use of "bottom-up" routes to discrete 2D nanostructures are much less explored.[373, 383, 384]

The self-assembly of block copolymers (BCPs) is, in principle a potential route to 2D materials. However, although amorphous block copolymers have been extensively investigated and yield a wide range of micellar nanostructures including spheres, cylindrical or wormlike micelles, and kinetically trapped morphologies of remarkable complexity, the formation of 2D lamellar platelets is relatively rare.[38, 385-388] Generally, bilayer structures with flexible cores tend to undergo spontaneous closure to form vesicles.

Self-assembly of crystalline homopolymers and BCPs, however, has recently emerged as a promising route to generate analogous functional 2D materials due to their relative structural rigidity.[97, 107, 320, 389-401] Generally, crystalline homopolymers form thin lamellae in poor solvents which are not colloidally stable due to the absence of solvophilic substituents. However, previous work has demonstrated that the use of thiol-terminated crystalline homopolymers poly(ethylene glycol) (PEG) and polycaprolactone (PCL) allows peripheral nanoparticle patterning on 2D platelets.[390, 391] Fabrication of alternate rings of a homopolymer and BCP has also been reported, and fluorescent nanosheets have been recently described for π-conjugated homopolymers.[394] In addition, colloidally stable 2D platelets are commonly formed from crystallisable BCPs with short complementary corona-forming block,[97, 320, 393, 395, 396, 398 400, 401] whereas 1D cylindrical micelles are usually favoured for BCPs with long corona-

forming blocks due to the significant corona-corona repulsions which promote curvature of the core-corona interface.[96, 100, 105, 106, 128, 165, 325, 402-404]

Precise control of nanoparticle dimensions and their surface chemistry, together with access to uniform samples, are highly desirable in order to tailor their material properties. The use of crystallisation-driven, seeded growth strategies provides a recently established route for the preparation of near monodisperse fibre-like micelles and segmented 1D assemblies of controlled length from BCPs with a crystallisable core-forming block. This has been extensively developed for polyferrocenylsilane (PFS) BCPs[92] over the past decade where sonication of polydisperse fibre-like micelles leads to small seeds which are active to further growth on addition of dissolved BCP (unimer) in a process termed living crystallisation-driven self-assembly (CDSA).[139, 140, 146, 405] Similar approaches have been demonstrated for the preparation of analogous 1D materials with crystallisable organic cores based on polyethylene,[100, 165] polyesters,[166, 253] polycarbonate,[167] π-conjugated polymers,[170, 172, 175, 278] planar π-stacking molecules,[406-411] and other self-assembling molecular species.[280, 412, 413] Furthermore, the utility of the living CDSA strategy has been expanded to create uniform 2D structures with well-controlled dimensions.[146, 156, 397] For example, nanosheets formed by the crystallisation of precursors containing hyperbranched poly(ether amine) capped with a polyhedral oligomeric silsesquioxane can be fragmented into seeds by sonication, and these seeds can be used to control the growth of 2D platelets on subsequent precursor addition.[397] Manners and coworkers[146, 156, 414, 415] have demonstrated that precisely defined 2D lenticular and rectangular platelet micelles can be prepared by seeded growth of PFS BCPs and homopolymer/BCP blends, respectively. More recently, an efficient approach was also reported to the preparation of uniform, colloidally stable 2D platelets using PFS homopolymers with charged phosphonium cations as termini (e.g., $PFS_{20}[PPh_2Me]I$) in combination with seeded growth.[157] In this case, the presence of the charged termini hinders platelet stacking as a result of electrostatic repulsion and provides colloidal stability.

In this chapter we focus on the extension of seeded growth, living CDSA processes to the fabrication of well-controlled and unprecedented hierarchical 2D structures based on crystalline poly(*L*-lactide)

(PLLA). PLLA is a crystallisable polymer and promising for making nanostructures of substantial interest for biomedical applications due to the biocompatibility and biodegradability.[248] Early work on the micellisation of PLLA BCPs demonstrated the formation of spheres, cylinders, platelets, and in most cases, mixed morphologies.[333, 393, 416-422] The first studies of the use of living CDSA methods to prepare 1D PLLA-based micelles were carried out by the Dove and O'Reilly groups.[112, 253, 254, 423, 424] In contrast to the substantial efforts concerning 1D PLLA-based materials, nanoscale 2D platelet structures derived from PLLA BCPs are considerably less explored. Cheng and coworkers reported the growth of single crystalline PLLA from single crystals of PLLA-*b*-polystyrene (PLLA-*b*-PS) BCP.[393] In recent work, Xie and Wang and co-workers reported the formation of 2D platelets of PLLA-*b*-PEG via a morphological transition from spheres.[183] In addition, O'Reilly, Dove and co-workers[137] have further examined the factors that influence the formation of 1D and 2D morphologies by PLLA BCPs and have described the formation of well-defined platelet micelles as well as routes to hierarchical assemblies from 1D and 2D components by the use of BCP blends. Moreover, well-defined 2D platelets with controlled areas have been prepared by fine tuning the self-assembly conditions, and these micelles have been shown to stabilize the water-water emulsion droplets.[256] Manners and coworkers[157] extended the charge-terminated homopolymer strategies developed with PFS segments to PLLA homopolymers, $PLLA_m[PPh_2Me]I$ (m = 24 and 34), to obtain monodisperse colloidally stable diamond-shaped 2D platelets of controlled area. Such a morphology is well-established for PLLA single crystals.[137, 393, 401] Furthermore, preliminary details of functional PLLA 2D platelet micelles have been reported,[157] for example, the formation of segmented 2D platelets via the sequential addition of further $PLLA_m[PPh_2Me]I$ together with PLLA homopolymer with a terminal fluorescent dye. Herein, we report the fabrication of well-controlled and unprecedented hierarchical PLLA-based structures, including diamond-shaped 'patchy' platelet block co-micelles, hollow platelet micelles, and diamond-fibre hybrid structures using seeded growth and post-assembly processing approaches. In this chapter, we demonstrate that the use of seeded growth, living CDSA methods represents a powerful approach not only to PFS-based 2D materials but also to those based on other functional organic polymers.

4.2. Results and Discussion

In this chapter, we aim to extend the 'living' CDSA of PLLA-containing polymers to prepare 2D structures. Well-defined 2D platelets with controlled area and narrow dispersity will be prepared by seeded-growth method with charge-terminated PLLA homopolymer, uncharged PLLA homopolymer and a blend of PLLA homopolymer and diblock copolymer. Complex and hierarchical structures will be prepared by combining with PLLA 1D fibre like micelles and 2D platelet micelles. Functional 2D platelet micelles will be explored by uploading inorganic nanoparticles.

4.2.1. Synthesis and Characterisation of PLLA BCP building blocks

To perform the targeted living CDSA experiments we prepared several PLLA-based materials as building blocks (Scheme 4.1). The PLLA homopolymers were generally prepared via ring-opening polymerisations (ROP) of *L*-lactide with initiators in the presence of 1,8-Diazabicyclo[5.4.0]undec-7-ene (DBU) or thiourea catalyst according to the previous report.[425] The charge-neutral $PLLA_{26}$ (the subscript refers to the number average degree of polymerisation, DP_n) was prepared by ROP using a benzyl alcohol initiator. Charge-terminated $PLLA_{24}[PPh_2Me]I$ homopolymer was prepared with a phosphine-substituted alcohol initiator followed by quaternisation with methyl iodide (MeI).[157] Synthesis of $PLLA_{42}$-*b*-poly(2-vinylpyridine)$_{464}$ ($PLLA_{42}$-*b*-$P2VP_{464}$) and $PLLA_{47}$-*b*-poly(N-isopropylacrylamide)$_{267}$ ($PLLA_{47}$-*b*-$PNIPAm_{267}$) was carried out by combining ROP techniques and reversible addition-fragmentation chain transfer (RAFT) polymerisation.[253, 425] PLLA homopolymers were first prepared by ROP with an alcohol functionalised chain transfer agent initiator before being used as macroinitiators for 2VP polymerisations. In contrast, $PLLA_{20}$-*b*-poly(allyl glycidyl ether)$_{80}$ ($PLLA_{20}$-*b*-$PAGE_{80}$) was prepared according to a reported procedure.[426] $PAGE_{80}$-OH was first prepared followed by ROP of *L*-lactide to afford $PLLA_{20}$-*b*-$PAGE_{80}$. Poly(ethylene glycol)$_{45}$-*b*-$PLLA_{23}$ (PEG_{45}-*b*-$PLLA_{23}$) was synthesised by ROP of *L*-lactide with commercialised MeO-PEG-OH (M_n = 2000 g/mol) as the macroinitiator. The characterisation of polymer molecular weight was carried out by different techniques: gel permeation chromatography (GPC) analysis was used to obtain the number average

molecular weight (M_n) and molar-mass dispersity ($Đ_M$) (Figure S4.1-S4.3); matrix-assisted laser desorption ionisation time-of-flight mass spectrometry (MALDI-TOF MS) was used to obtain the weight average molecular weight (M_w) of PLLA and PAGE homopolymers (Figure S4.4-S4.5); and nuclear magnetic resonance (NMR) spectroscopic analysis was used to obtain the block ratio of the block copolymers corresponding to DP_n of core and corona blocks (Figure S4.6-S4.11). All characterisation data is summarised in Table 4.1.

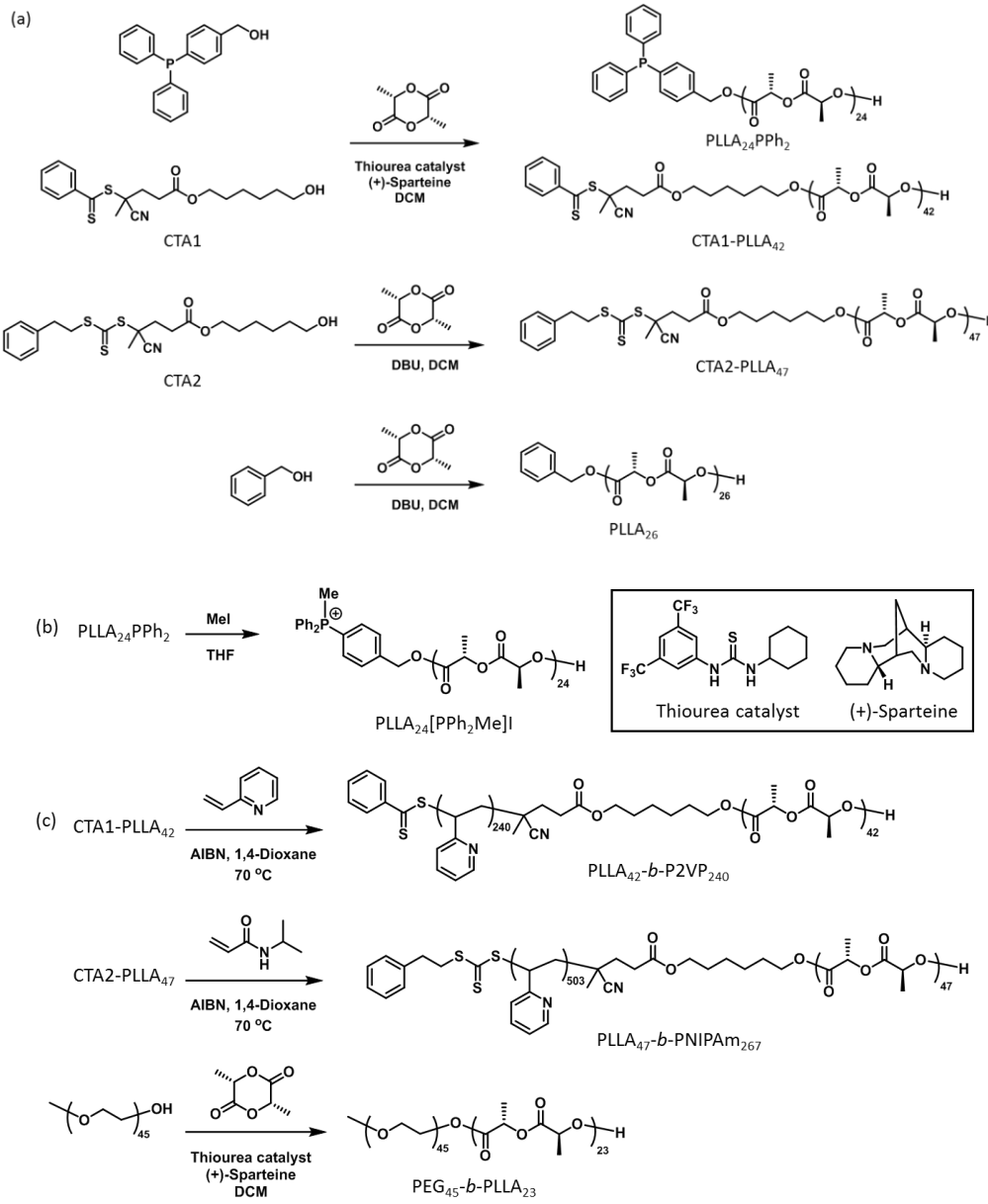

Scheme 4.1. Schemes of polymer synthesis. (a) Synthesis of PLLA homopolymers; (b) synthesis of charge-terminated PLLA by methylation; (c) synthesis of PLLA diblock copolymers.

The prepared polymers were also analysed by Fourier-transform infrared spectroscopy (FT-IR) (Figure S4.12). Thermal gravimetric analysis (TGA) was carried out on all the prepared polymers and the results are summarised in (Figure S4.13). All the diblock copolymers exhibited good thermal stability. The decomposition temperatures (defined as the temperatures of 5% mass loss) of $PLLA_{24}PPh_2MeI$, $PLLA_{42}$-*b*-$P2VP_{464}$, $PLLA_{20}$-*b*-$PAGE_{80}$, $PLLA_{47}$-*b*-$PNIPAm_{267}$ and PEG_{45}-*b*-$PLLA_{23}$ were determined to be 215, 295, 235, 245 and 275 °C, respectively.

Table 4.1. Polymer molecular weight characterisation.

Polymer	M_w (g·mol^{-1})[a]	M_n (kg·mol^{-1})[b]	M_n (kg·mol^{-1})[c]	$Đ_M$[c]	Block ratio (Corona: Core)[b]
$PLLA_{24}PPh_2$	3670	-	5.9	1.06	-
$PLLA_{24}[PPh_2Me]I$	3774	-	3.3	1.07	-
CTA1-$PLLA_{42}$	6460	7.6	10.6	1.20	-
CTA2-$PLLA_{47}$	7231	7.9	10.2	1.09	-
$PLLA_{26}$	3917	-	8.1	1.14.3	-
$PAGE_{80}$	9250	9.2	10.8	1.13	-
$PLLA_{42}$-*b*-$P2VP_{464}$	-	31.3	40.3	1.21	5:1
$PLLA_{47}$-*b*-$PNIPAm_{267}$	-	37.4	180	1.11	5:1
$PLLA_{20}$-*b*-$PAGE_{80}$	-	12.1	14.3	1.20	4:1
$PLLA_{23}$-*b*-PEG_{45}	-	5.3	9.1	1.09	2:1

[a] Determined by MALDI-TOF MS, [b] block ratios (DP_n ratios) are determined by ^{1}H NMR spectroscopy, [c] determined by GPC analysis relative to polystyrene (PS) standards in *n*-Bu_4NBr/THF.

4.2.2. Diamond-Shaped Platelet Micelles from Blends of Charge-Terminated Homopolymer and Diblock Copolymer

In addition to the self-assembly studies for amorphous blends of BCP and homopolymer,[414, 415] similar experiments have been performed for crystallisable analogues in the absence of seeds. For example, Eisenberg and van de Ven and coworkers previously reported the preparation for non-uniform 2D assemblies based on crystalline poly(ε-caprolactone) (PCL) cores by blending PCL-*b*-PEG BCP and

PCL homopolymer.[108, 427] Analogous polydisperse platelets have been reported for crystallisable blends of PFS BCPs and homopolymer.[428] Recently, we have shown that the seeded growth of crystallisable blends of BCP and homopolymer, or of a crystallisable charge-terminated homopolymer, allows the formation of uniform 2D platelet micelles and block comicelles with controlled dimensions at or near ambient temperature.[156, 157] Herein, we explore the use of the latter strategy for the fabrication of well-controlled, complex, and hierarchical PLLA-based assemblies.

In our initial experiments we examined the growth of the blend of $PLLA_{42}$-*b*-$P2VP_{464}$ and charge-terminated $PLLA_{24}[PPh_2Me]I$ from *quasi*-1D seeds[157] of $PLLA_{24}[PPh_2Me]I$ (L_n = 200 nm, L_w/L_n = 1.09, where L_w is the weight-average length and L_n is the number-average length). The seeds were prepared by sonication of 2D platelets of $PLLA_{24}[PPh_2Me]I$ (0.1 mg/mL) in a mixture of isopropanol (*i*-PrOH) and chloroform ($CHCl_3$) (*v*:*v* = 10:1), according to our previous report.[157] *i*-PrOH was chosen as a suitable selective solvent for the self-assembly experiments, because both the phosphonium moiety and the P2VP block are solvated in polar organic solvents such as *i*-PrOH, in which the PLLA block is insoluble.

As shown in Figure 4.1, addition of a solution of molecularly dissolved $PLLA_{42}$-*b*-$P2VP_{464}$/$PLLA_{24}[PPh_2Me]I$ blend (1:1, mass ratio) unimers in $CHCl_3$ to *quasi*-1D seed (L_n = 200 nm, L_w/L_n = 1.09) of $PLLA_{24}[PPh_2Me]I$ in *i*-PrOH led to uniform diamond-shaped platelet micelles, demonstrating the control implicit in this approach. The area (traced by hand with ImageJ) of the platelets was found to be linearly dependent on the unimer-to-seed mass ratio (m_{unimer}:m_{seed}) and the area dispersity was very low ($A_w/A_n \leq 1.02$, where A_w is the weight-average area and A_n is the number-average area). The contour areas for the platelets are summarised in Figure S4.14 and Table S4.1. Analysis of platelet height by atomic force microscopy (AFM) (Figure 4.1d and e) revealed an average value of 15 nm, and the height of the edge (17 nm) was higher than the centre (13 nm). One possible reason for the different heights of the centre and edge would be an uneven distribution of PLLA homopolymer and diblock copolymer on the platelet surface, where diblock copolymers grows slower than the homopolymer resulting a thicker edge with a collapsed corona-forming block.

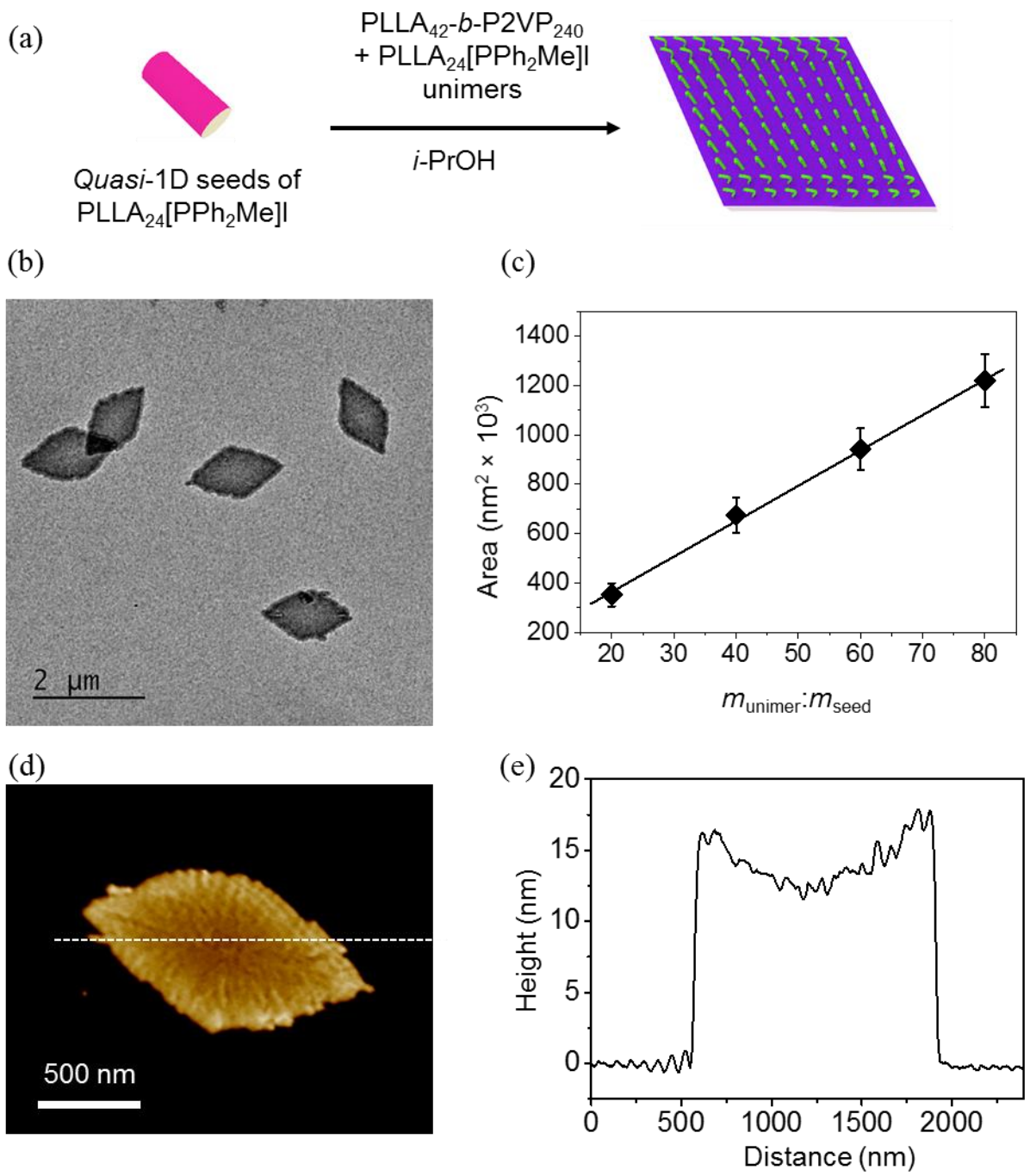

Figure 4.1. (a) Schematic representation for the formation of a 2D diamond-shaped platelet micelle through seeded growth of unimer of $PLLA_{42}$-*b*-$P2VP_{464}$/$PLLA_{24}[PPh_2Me]I$ (1:1, mass ratio) blend from *quasi*-1D seeds of $PLLA_{24}[PPh_2Me]I$ in *i*-PrOH; (b) its corresponding TEM image with m_{unimer}:m_{seed} of 80, the sample for TEM was not stained; (c) Linear dependence of micelle area on the m_{unimer}:m_{seed}. Error bars, standard deviation of measured areas; (d) AFM image with m_{unimer}:m_{seed} of 80; (e) the height profile of platelet comicelles.

4.2.3. Uniform Platelet Micelles from Blends of Neutral Homopolymer and Diblock Copolymer

Previously, PFS 2D platelet micelles have been prepared by blending of diblock copolymer and either neutral or charge-terminated homopolymer.[156, 157] The strategies for 2D micelle preparation have been extended to PLLA-based micelles. As noted previously, charge-terminated PLLA homopolymer can form diamond-shaped platelet micelles in solution and the size of such platelets can be controlled via a seeded-growth approach.[157] Blending of charge-terminated homopolymer and diblock copolymer can also afford platelet micelles with controlled area.[157] In both cases, the terminal charge is considered as a corona to stabilize the micelles in solution. To further explore the strategies for PLLA 2D micelle preparation, blends of neutral PLLA homopolymer and diblock copolymer were employed to study the self-assembly in solution. Based on the results of previous chapter, the additional solvation-promoting reagents, such as trifluoroethanol (TFE), were shown to improve the seeded-growth of PLLA diblock copolymers by improving the solvation of PLLA in solution, which helps to prevent problems associated with rapid self-nucleation. Therefore, TFE was introduced in the seeded-growth experiments in this section to assist the living CDSA. As control experiments, seeded-growth experiments were also carried out without the presence of TFE. As a comparison, the solvation-promoting reagents are not needed as the above results shown in preparation of uniform PLLA diamond shaped micelles by seeded-growth of charge-terminated PLLA homopolymer. This might be consequence of the repulsion of the charges on the polymer chain termini which could prevent rapid self-nucleation.

Self-nucleation of a $PLLA_{26}$/$PLLA_{47}$-*b*-$PNIPAm_{267}$ blend (1:1 mass ratio) was studied in a mixture of dimethyl sulfoxide (DMSO) and ethanol (EtOH) (*v*:*v* = 5:95) by heating at 70 °C for 2 h and slowly cooling down (2.5 h from 70 °C to 23 °C). After aging for 3 days, TEM analysis showed the presence of aggregated platelet micelles (Figure 4.2a), but the platelets were colloidally stable in solution. After 2 h sonication with an Ultrasonic probe, the aggregated platelets fragmented into small pieces (Figure 4.2b).

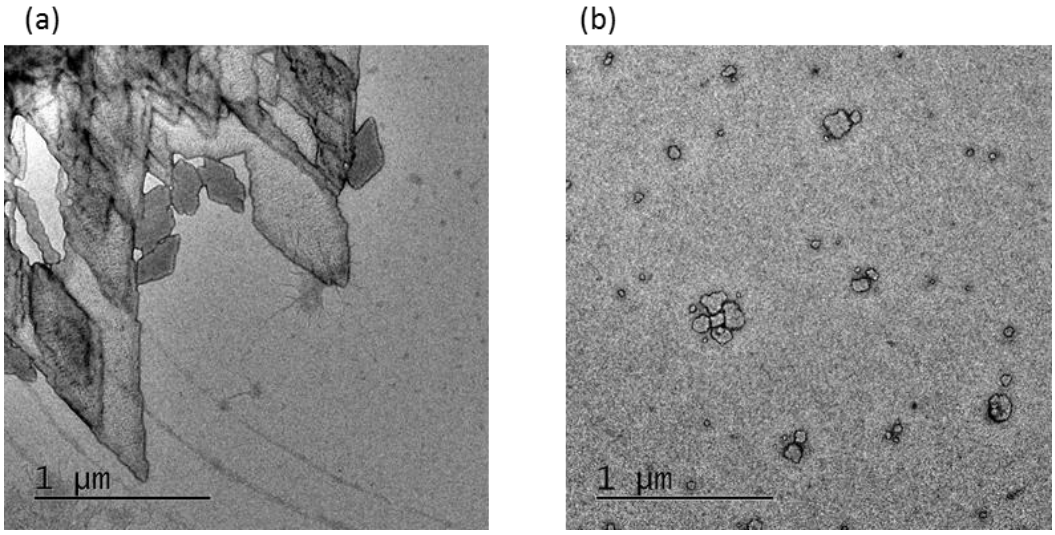

Figure 4.2. 2D Seed micelle for seeded-growth experiments: (a) Polydisperse 2D platelet micelles of $PLLA_{26}/PLLA_{47}$-*b*-$PNIPAm_{267}$ blends in DMSO/EtOH (1:9) with a concentration of 0.5 mg/mL; (b) seeds prepared by sonication of polydisperse micelles at 0 °C for 2 h in a sonic cleaning bath. TEM samples were stained with a 2 wt% solution of uranyl acetate in EtOH.

Seeded-growth experiments were carried out by addition of solutions of molecularly dissolved blend of $PLLA_{26}/PLLA_{47}$-*b*-$PNIPAm_{267}$ (1:1, mass ratio in DMSO, with varied m_{unimer}:m_{seed}) to 2D fragmented small platelet solutions in TFE/EtOH (with volume ratios of 5:95, 5:95, 10:90 and 15:85 to m_{unimer}:m_{seed} of 5.0, 10.0, 20.0 and 30.0, respectively). This led to platelet micelles with uniform measured areas with increased sizes compared to seed micelles (Figure 4.3a-d). The area of the platelets was found to be linearly dependent on the unimer-to-seed mass ratio (Figure 4.3e). The contour areas for the platelets are summarised in Figure S4.15. It is worth noting that the area dispersity of the grown 2D platelet micelles are relatively high ($A_w/A_n \leq 1.23$) and the shape of these platelets was not the near-perfect diamond-shaped morphology of the 2D micelles prepared in Figure 4.1. The reasons will be discussed later.

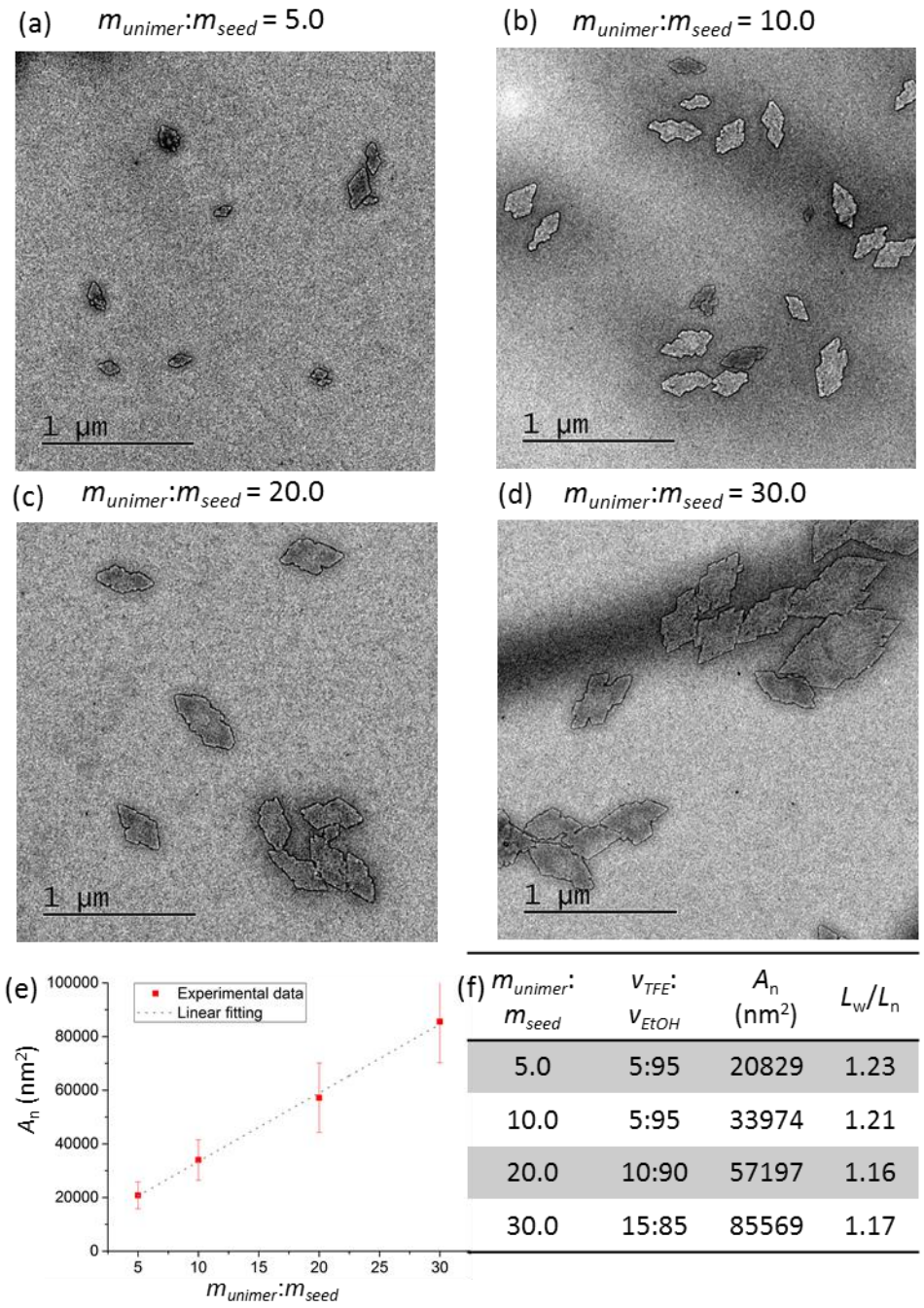

(f)

m_{unimer}: m_{seed}	v_{TFE}: v_{EtOH}	A_n (nm^2)	L_w/L_n
5.0	5:95	20829	1.23
10.0	5:95	33974	1.21
20.0	10:90	57197	1.16
30.0	15:85	85569	1.17

Figure 4.3. TEM images of samples of uniform micelles prepared by addition of unimers ($PLLA_{26}$/$PLLA_{47}$-*b*-$PNIPAm_{267}$ blend, 10 mg/mL in DMSO, aged for 5 days after unimer addition) with m_{unimer}:m_{seed} of (a) 5.0, (b) 10.0, (c) 20.0 and (d) 30.0 to 2D seed micelles in TFE/EtOH with volume ratios of (a) 5:95, (b) 5:95, (c) 10:90 and (d) 15:85, respectively; (e) plot of number average micelle area vs m_{unimer}:m_{seed}; (f) summary of seeded-growth solvent conditions and results. TEM samples were stained with a 2 wt% solution of uranyl acetate in EtOH.

As a control experiment, seeded-growth experiments were also conducted in the absence of TFE (in EtOH). To the 2D fragmented seed solutions in EtOH, solutions of $PLLA_{26}$/$PLLA_{47}$-*b*-$PNIPAm_{267}$ blend (1:1, mass ratio) in DMSO with m_{unimer}:m_{seed} of 5.0, 10.0, 20.0 and 30.0 were added, respectively. TEM images (Figure S4.16) showed polydisperse platelet micelles presence after aging the solution for 3 days: some platelets with increased area were observed, while small platelets were also present in the solution. These small platelets were likely formed by spontaneous nucleation of the added unimer. A comparison of seeded-growth TEM images with m_{unimer}:m_{seed} = 10.0 in TFE/EtOH and EtOH is shown in Figure 4.4.

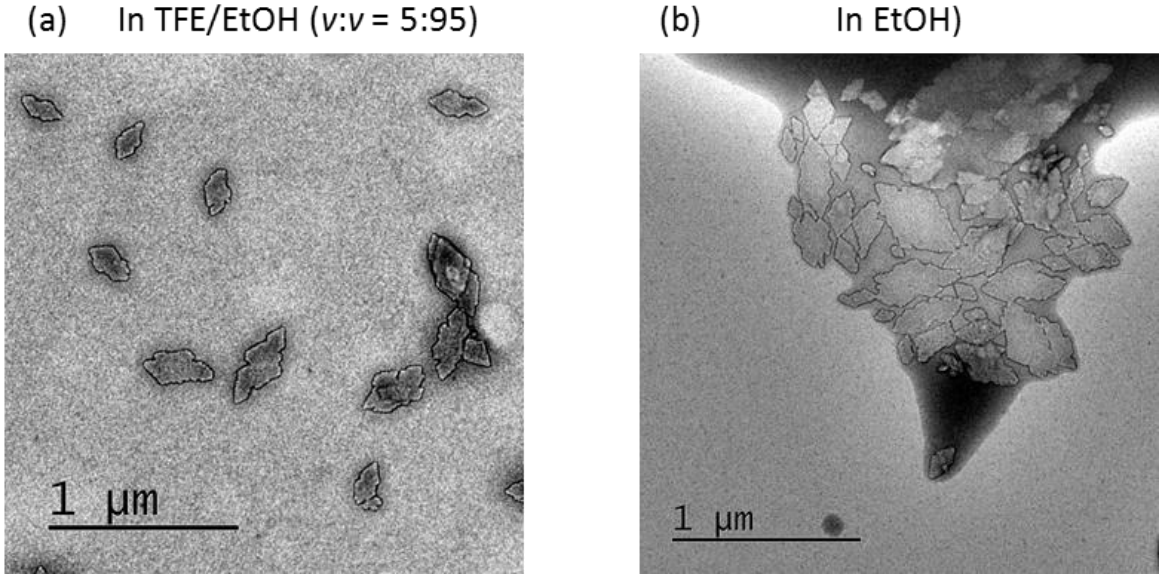

Figure 4.4. TEM images of seeded-growth of unimers (blend of $PLLA_{26}$/$PLLA_{47}$-*b*-$PNIPAm_{267}$, 10 mg/mL in DMSO, with m_{unimer}:m_{seed} = 10.0) from 2D seeds (in EtOH) in (a) TFE/EtOH and (b) EtOH.

In addition, 1D seeds were employed in the seeded-growth experiments with blends of $PLLA_{26}$/$PLLA_{47}$-*b*-$PNIPAm_{267}$ (1:1, mass ratio). To prepare the 1D seed, PEG_{45}-*b*-$PLLA_{23}$ (10 mg/mL in DMSO) was first added into methanol (MeOH) at 23 °C with a final polymer concentration at 0.5 mg/mL in DMSO/MeOH (5:95). After aging for 2 days, the polydisperse fibre (Figure 4.5a) solution was sonicated for 1 hour with an ultrasonic probe at 0 °C to give seed micelles (Figure 4.5b) (L_n = 200 nm, L_w/L_n = 1.09).

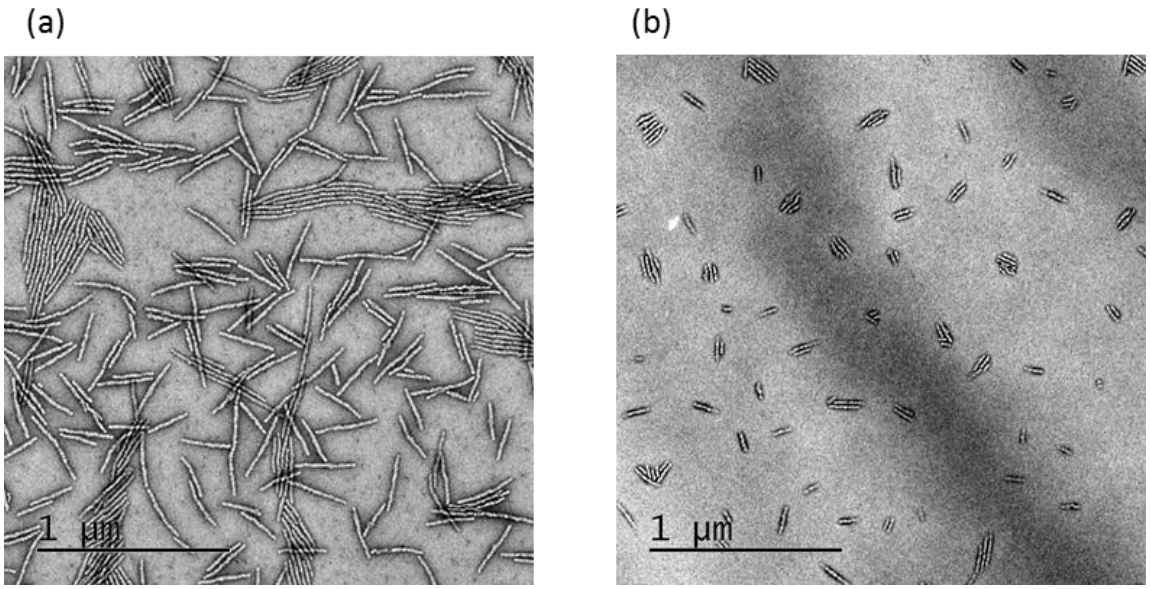

Figure 4.5. 1D Seed micelle for seeded-growth experiments: (a) Polydisperse 1D micelles of PEG_{45}-*b*-$PLLA_{23}$ in DMSO/MeOH (1:9) with a concentration of 0.5 mg/mL; (b) seeds prepared by sonication of polydisperse micelles at 0 °C for 2 h in a sonic cleaning bath (L_n = 200 nm, L_w/L_n = 1.09). TEM samples were stained with a 2 wt% solution of uranyl acetate in EtOH.

Solutions of $PLLA_{26}$/$PLLA_{47}$-*b*-$PNIPAm_{267}$ blend (1:1, mass ratio in DMSO) with different m_{unimer}:m_{seed} were added to the 1D seed solutions (PEG_{45}-*b*-$PLLA_{23}$, in MeOH) in TFE/EtOH (with volume ratios of 5:95, 5:95, 10:90 and 15:85 to m_{unimer}:m_{seed} of 5.0, 10.0, 20.0 and 30.0, respectively). After aging at 23 °C for 3 days, TEM images (Figure 4.6a-d) showed the formation of uniform platelets with 1D seed in the centre (white short rod structures) and a linear relationship between the area and the unimer-to-seed mass ratios (Figure 4.6e). The contour areas for the platelets are summarised in Figure S4.17. Similar to the seeded-growth results with 2D seeds mentioned above, the obtained 2D platelets possessed relative high distributions ($A_w/A_n \leq 1.20$) (Figure 4.6f and S4.17f) and the morphology observed consisted of irregular diamond-like platelets in TEM images.

In the seeded-growth of $PLLA_{26}$/$PLLA_{47}$-*b*-$PNIPAm_{267}$ blend from both 2D (Figure 4.2b) and 1D seed micelles (Figure 4.5b), the obtained 2D platelet micelles exhibited poorly-defined edges which were not smooth lines in TEM images. This may be due to the 'poison' effect of the long corona-forming block (core/corona block ratio: 1:5) as reported before.[320] In CDSA, the core crystallisation favours low curvature morphologies such as 2D platelet micelles while the corona repulsion favours high curvature morphologies such as spherical micelles. When a blend unimer ($PLLA_{26}$/$PLLA_{47}$-*b*-$PNIPAm_{267}$) is added, the crystal growth fronts of PLLA platelets are likely to be interfered by chain repulsion of PNIPAm resulting in the formation of defects. These defects could affect the epitaxial deposition of PLLA chains, further altering the growth directions of unimers to afford nondiamond-shaped morphologies. On the other hand, the 'poison' effect could also exist in the seeds. During the preparation of seeds (both 1D and 2D), diblock copolymer (PEG_{45}-*b*-$PLLA_{23}$ and $PLLA_{47}$-*b*-$PNIPAm_{267}$) were incorporated. Both 2D seed edge and 1D seed termini could be interfered with by the corona-forming blocks.

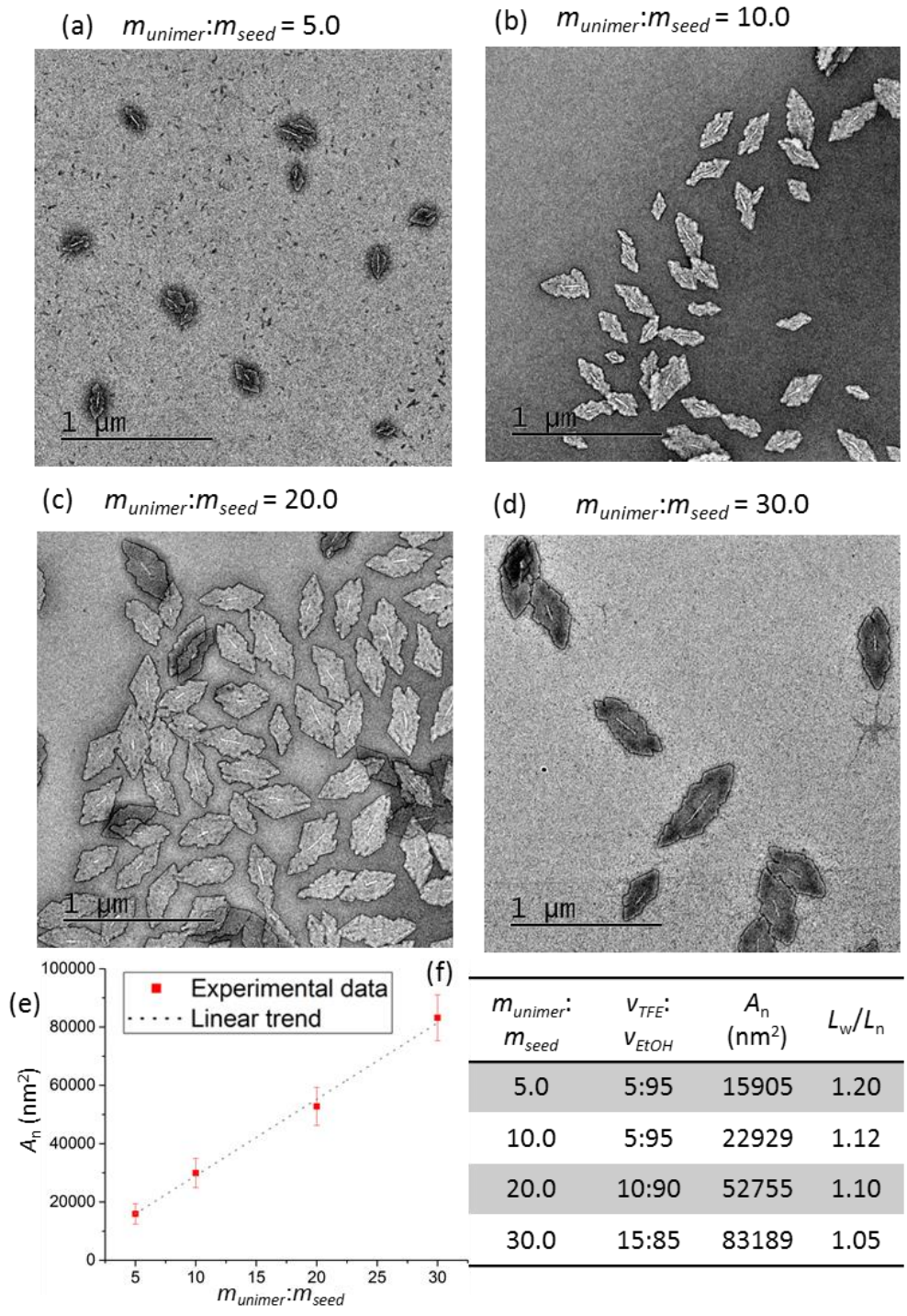

m_{unimer}: m_{seed}	v_{TFE}: v_{EtOH}	A_n (nm²)	L_w/L_n
5.0	5:95	15905	1.20
10.0	5:95	22929	1.12
20.0	10:90	52755	1.10
30.0	15:85	83189	1.05

Figure 4.6. TEM images of samples of uniform micelles prepared by addition of unimers ($PLLA_{26}$/$PLLA_{47}$-*b*-$PNIPAm_{267}$ blend, 10 mg/mL in DMSO, aged for 5 days after unimer addition) with unimer-to-seed mass ratios of (a) 5.0, (b) 10.0, (c) 20.0 and (d) 30.0 to 1D seed micelles (prepared with PEG_{45}-*b*-$PLLA_{23}$ in DMSO/MeOH (*v*:*v* = 5:95), 0.5 mg/mL, L_n = 200 nm, L_w/L_n = 1.09) in TFE/EtOH with volume ratios of (a) 5:95, (b) 5:95, (c) 10:90 and (d) 15:85, respectively; (e) plot of number average micelle area vs m_{unimer}:m_{seed}; TEM samples were stained with a 2 wt% solution of uranyl acetate in EtOH.

Again, as with the previous system, a control experiment involving seeded-growth in the absence of TFE (in EtOH) was performed. To the 1D solutions in EtOH (diluted the seeds in EtOH), a blend of $PLLA_{26}$/$PLLA_{47}$-*b*-$PNIPAm_{267}$ (1:1, mass ratio) solutions in DMSO (with m_{unimer}:m_{seed} = 5.0, 10.0, 20.0 and 30.0, respectively) were added. After aging for 3 days, TEM images (Figure S4.18) showed the polydisperse platelet micelles formation. A TEM analysis comparison of seeded-growth with m_{unimer}:m_{seed} = 10.0 in TFE/EtOH and EtOH is shown in Figure 4.7.

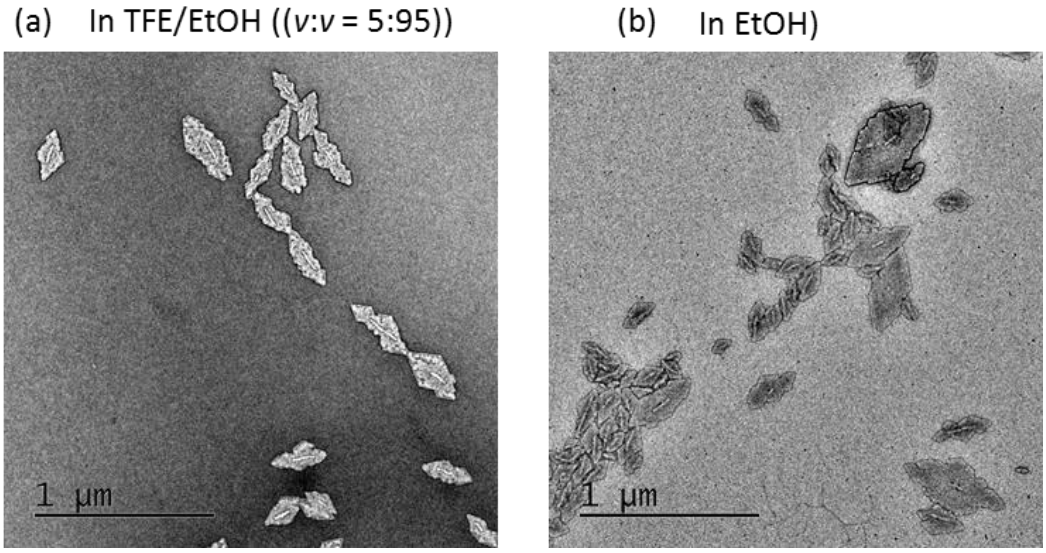

Figure 4.7. TEM images of seeded-growth of unimers ($PLLA_{26}$/$PLLA_{47}$-*b*-$PNIPAm_{267}$ blend, 10 mg/mL in DMSO, with m_{unimer}:m_{seed} of 10.0) from 1D seeds (prepared with PEG_{45}-*b*-$PLLA_{23}$ in DMSO/MeOH (5:95), L_n = 200 nm, L_w / L_n = 1.09) in (a) TFE/EtOH and (b) EtOH.

SAED was also employed to analyse the crystalline structure of the micelle core. Due to the rapid destruction of the micelles during irradiation by the electron beam, a video recording was taken during the SAED experiment instead of a single image. The SAED image was a screenshot of the video recording when the beam was irradiating the micelles. Hexagonal patterns (Figure S4.19a and b) were obtained by SAED for platelet micelles containing both 2D and 1D seeds. The d-spacings of the two patterns were calculated as d = 4.81 Å, which is in good agreement with the d-spacing of the (203/113) plane in an orthorhombic unit cell (α form) of PLLA, which also similar with the case of PLLA solution-grown crystals.[227, 352, 421]

4.2.4. Formation of "Patchy" Block Comicelles

Encouraged by the above results, we attempted to fabricate "patchy" diamond-shaped platelet block comicelles. Firstly, large diamond platelets (A_n = 3.94 × 10^5 nm^2, A_w/A_n = 1.04) were prepared by seeded growth of $PLLA_{24}[PPh_2Me]I$ unimers (5 mg/mL in $CHCl_3$) from small *quasi*-1D seed of $PLLA_{24}[PPh_2Me]I$ in *i*-PrOH. The second step was addition of the unimer of $PLLA_{42}$-*b*-$P2VP_{464}$/$PLLA_{24}[PPh_2Me]I$ blend in $CHCl_3$ to the well-formed, regular diamond-shaped platelets derived from $PLLA_{24}[PPh_2Me]I$ in *i*-PrOH, which yielded segmented block platelet comicelles, as shown in Figure 4.8 and S4.20.

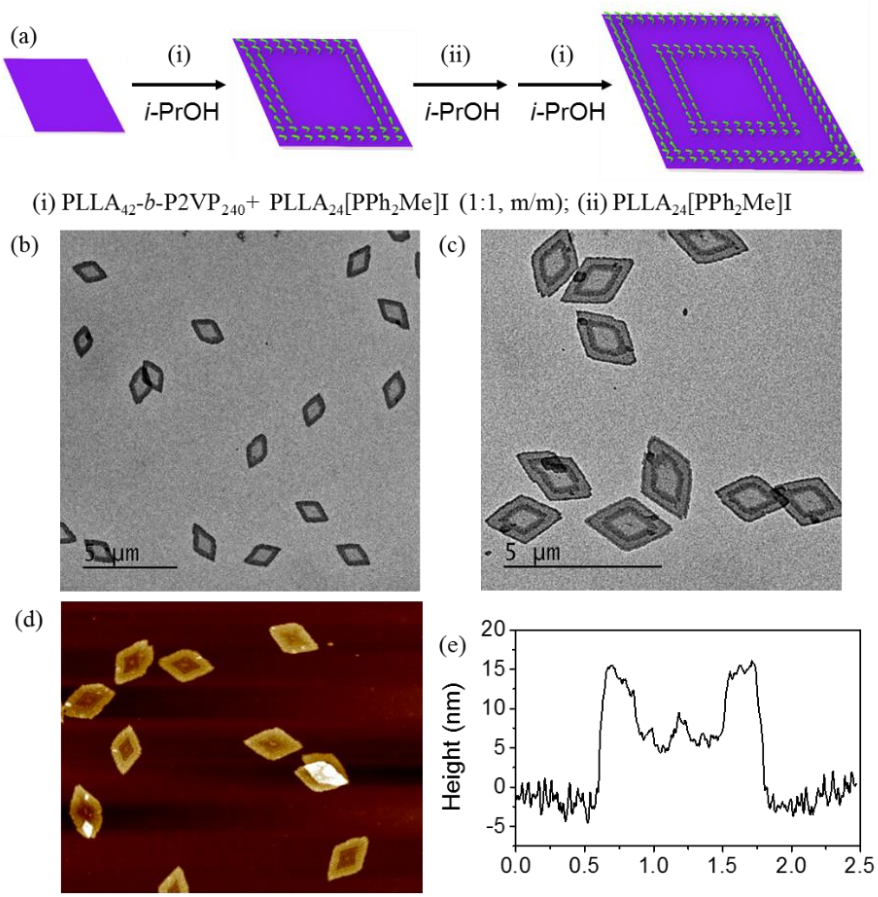

Figure 4.8. (a) Schematic representation of the formation of diamond-shaped 'patchy' platelet block comicelles through seeded growth. TEM images of (b) diblock and (c) tetra-block platelet comicelles. The samples for TEM were not stained. (d) AFM image and (e) the height profile of diblock platelet comicelle.

Different blend ratios of $PLLA_{42}$-*b*-$P2VP_{464}$/ $PLLA_{24}[PPh_2Me]I$ (1:4, 1:1 and 4:1, based on mass ratio) were all found to form platelet structures (Figure S4.20). A 1:1 mass ratio of BCP and homopolymer was found to give the most impressive control of the formation of 'patchy' diamond-shaped platelets, which were used in further work. The peripheral block was clearly observed as darker regions in TEM image, due to the higher electron density of the P2VP corona. AFM images showed a clear height difference between the two spatially distinct regions, with the second block formed by the $PLLA_{42}$-*b*-$P2VP_{464}$/$PLLA_{24}[PPh_2Me]I$ polymer blend (1:1, mass ratio) higher than the first block composed of $PLLA_{24}[PPh_2Me]I$ (18 nm vs. 9 nm, respectively). The higher peripheral region is a consequence of the presence of the long P2VP block. Further sequential alternating addition of unimers $PLLA_{24}[PPh_2Me]I$ and a $PLLA_{42}$-*b*-$P2VP_{464}$/$PLLA_{24}[PPh_2Me]I$ blend (1:1, mass ratio), resulted in concentric segmented platelet comicelles with four distinct regions of clear electron contrast based on TEM analysis (Figure 4.8c). These experiments demonstrated the formation of 2D platelets by the seeded growth of a crystallisable blend of BCP and homopolymer is not limited to PFS-based polymers, but also applicable for PLLA-based polymers.

In order to confirm that the growth of the platelets was driven by epitaxial growth, SAED analysis of a representative platelet micelle and block comicelle was carried out. As shown in Figure 4.9, both the platelet micelle precursor (Figure 4.9a and b) and block comicelle (Figure 4.9c-e) possess identical ED patterns with three pairs of diffraction spots, confirming that PLLA core in these two cases consists of a single crystalline layer and the growth of 2D block comicelle is driven by epitaxial crystallisation. These SAED patterns are assigned to be the [001] zone pattern of the orthorhombic (α) form of PLLA. ED analysis showed that the observed pattern contains four (110) planes with the d-spacing of 0.537 nm and two (200) planes having the d-spacing of 0.543 nm, which is consistent to the case of PLLA solution-grown crystals.[421] A similar platelet morphology and SAED pattern were also observed for lamellar single crystals of PLLA-*b*-PS by Cheng and coworkers.[393]

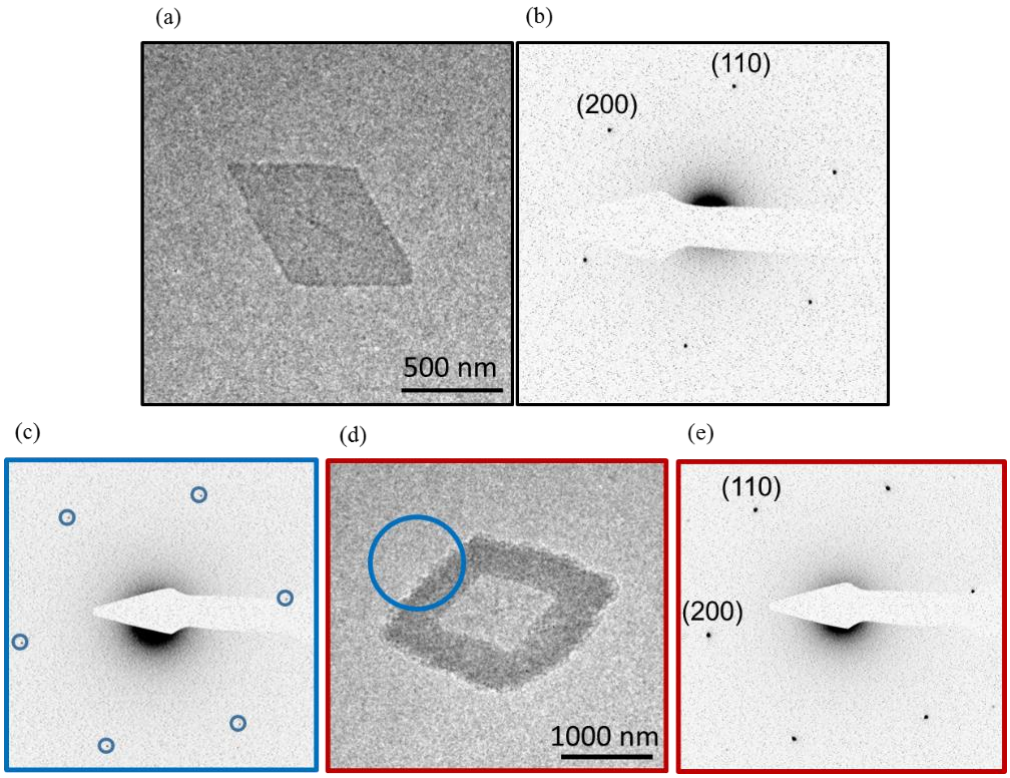

Figure 4.9. TEM images and selected area electron diffraction (SAED) patterns for platelet micelles (a and b) and comicelles (c-e). The black square in (a) and red square and blue circle in (d) represent the selected areas for the electron diffraction in (b), (c) and (e), in which the surrounding lines are labelled with the same colours. A relatively large area was used in (d) to maximize data quality. No diffraction from the surrounding carbon film was detected. The samples analysed by TEM were not stained.

4.2.5. Formation of Hollow Diamond-Shaped Platelet Micelles

Crosslinking of the core or corona/shell of micelles is a well-established method for the generation of micelles with improved stability.[429-432] The resulting micelles are resistant to dissolution and maintain their structure in good solvents. For instance, the P2VP coronas of the branched cylindrical micelles could be crosslinked by Karstedt's catalyst through the formation of small Pt nanoparticles with Pt coordination to the pyridyl groups on P2VP.[337] Although crosslinking has been widely used in a wide range of nanomaterials, its application in the fabrication of hollow platelet structures is very rare. This is a consequence of the limited methods for creating multicompartmental platelets. We have recently demonstrated that uniform hollow rectangular structures based on PFS systems could be prepared by controlling the crosslinking in a spatially selective manner, followed by dissolution of non-crossinked

regions in a good solvent for the core.[156, 430] However, analogous hollow structures derived from organic polymers have not been reported.

In order to fabricate hollow diamond-shaped platelets, we selected a concentric diamond-shaped platelet block comicelle, with the central block derived from $PLLA_{24}[PPh_2Me]I$ and peripheral block derived from $PLLA_{42}$-*b*-$P2VP_{464}$/ $PLLA_{24}[PPh_2Me]I$ blend (1:1, mass ratio) (Figure 4.8b and d). We found that Karstedt's catalyst can effectively *crosslink* the peripheral block consisting of $PLLA_{42}$-*b*-$P2VP_{464}$/ $PLLA_{24}[PPh_2Me]I$, by the formation of Pt nanoparticles (Figure 4.10, 4.11 and S4.21). By using scanning transmission electron microscopy energy-dispersive X-ray (STEM-EDX) in elemental mapping mode, the distribution of elemental Pt was directly revealed on the platelets (Figure 4.11c); their location matched well with the nanoparticle area, confirming that nanoparticles are mainly composed of Pt (Figure 4.11). A high-resolution TEM image of the Pt nanoparticles showed that they possess a diameter of 9-10 nm (Figure S4.21). The height of the crosslinked regions of the platelet was measured to be 5-10 nm higher than that of the non-crosslinked platelet (Figure S4.22a). By removing the *i*-PrOH and dispersing the crosslinked structure in THF, a diamond-shaped hollow structure was produced (Figure 4.10 and S4.22). The presence of a hollow interior was confirmed by AFM analysis, with the central height near to zero. In contrast to the use of Karstedt's catalyst alone, the combination of Karstedt's catalyst and 1,1,3,3-tetramethyldisiloxane (TMDS), which leads to *crosslink*ing via hydrosilylation,[139] was found to lead to severe aggregation (Figure S4.23).

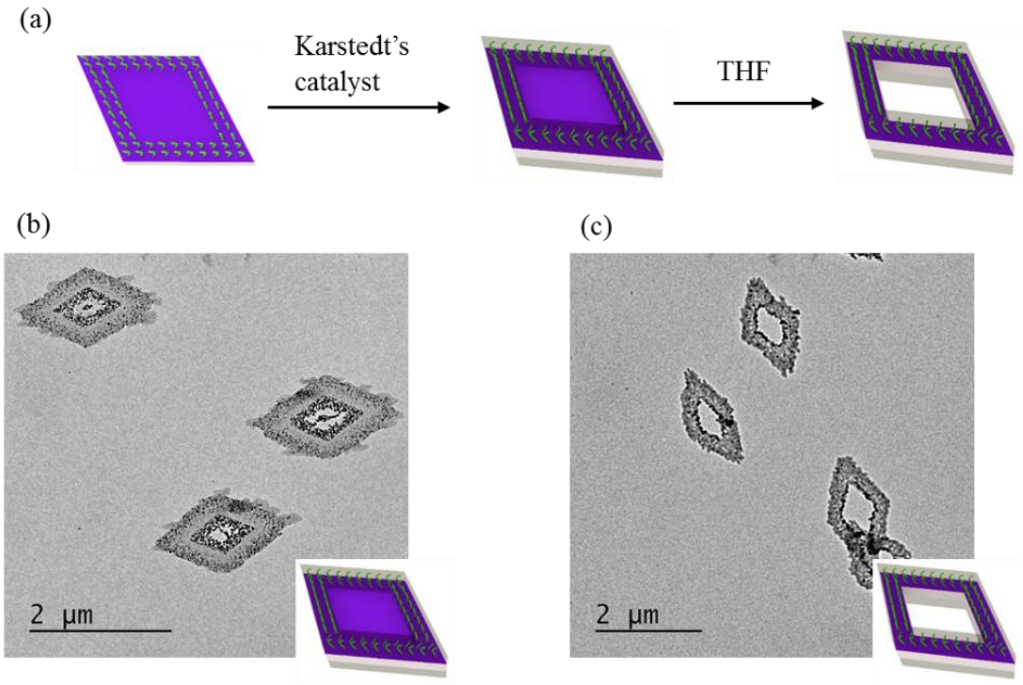

Figure 4.10. (a) Schematic representation for the formation of crosslinked platelet block comicelle and hollow micelles, and (b and c) their corresponding TEM images. The samples analysed by TEM were not stained.

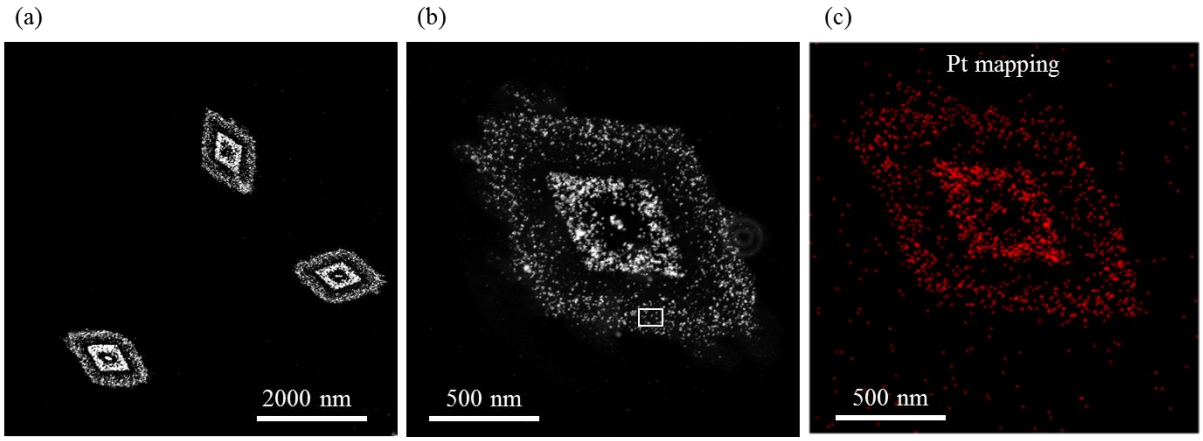

Figure 4.11. (a and b) Dark-field TEM image of crosslinked platelet comicelle. The central region is derived from $PLLA_{24}[PPh_2Me]I$ and the peripheral block is derived from $PLLA_{42}$-*b*-$P2VP_{464}$/ $PLLA_{24}[PPh_2Me]I$ (1:1, mass ratio). (c) STEM-EDX Pt element (red) mapping.

4.2.6. Formation of Diamond-Fibre Hybrid Structures.

We have demonstrated that seeded growth of either $PLLA_{24}[PPh_2Me]I$ homopolymer or a $PLLA_{42}$-*b*-$P2VP_{464}$/$PLLA_{24}[PPh_2Me]I$ blend from *quasi*-1D seeds or preformed 2D platelets leads to controlled formation of diamond-shaped platelets. Strikingly, addition of solely $PLLA_{42}$-*b*-$P2VP_{464}$ BCP in $CHCl_3$ to the $PLLA_{24}[PPh_2Me]I$ diamond platelet ($A_n = 3.94 \times 10^5$ nm^2, $A_w/A_n = 1.04$) in *i*-PrOH led to diamond-fibre hybrid structures (Figure 4.12b). The added $PLLA_{42}$-*b*-$P2VP_{464}$ BCP grew as fibres from the four edges of all the platelets. Similar hierarchical structures (Figure 4.12e) were also formed by addition of $PLLA_{20}$-*b*-$PAGE_{80}$ unimer in THF to the $PLLA_{24}[PPh_2Me]I$ platelets in *i*-PrOH, indicating that the formation of diamond-fibre hybrid structures is adaptable to other PLLA BCPs with a different corona. However, aggregation between the micelles was observed due to the relatively hydrophobic nature of the PAGE corona. In addition, the length of the $PLLA_{20}$-*b*-$PAGE_{80}$ fibres was found to be linearly dependent on the unimer-to-seed mass ratio, consistent with a living CDSA process (Figure S4.24).

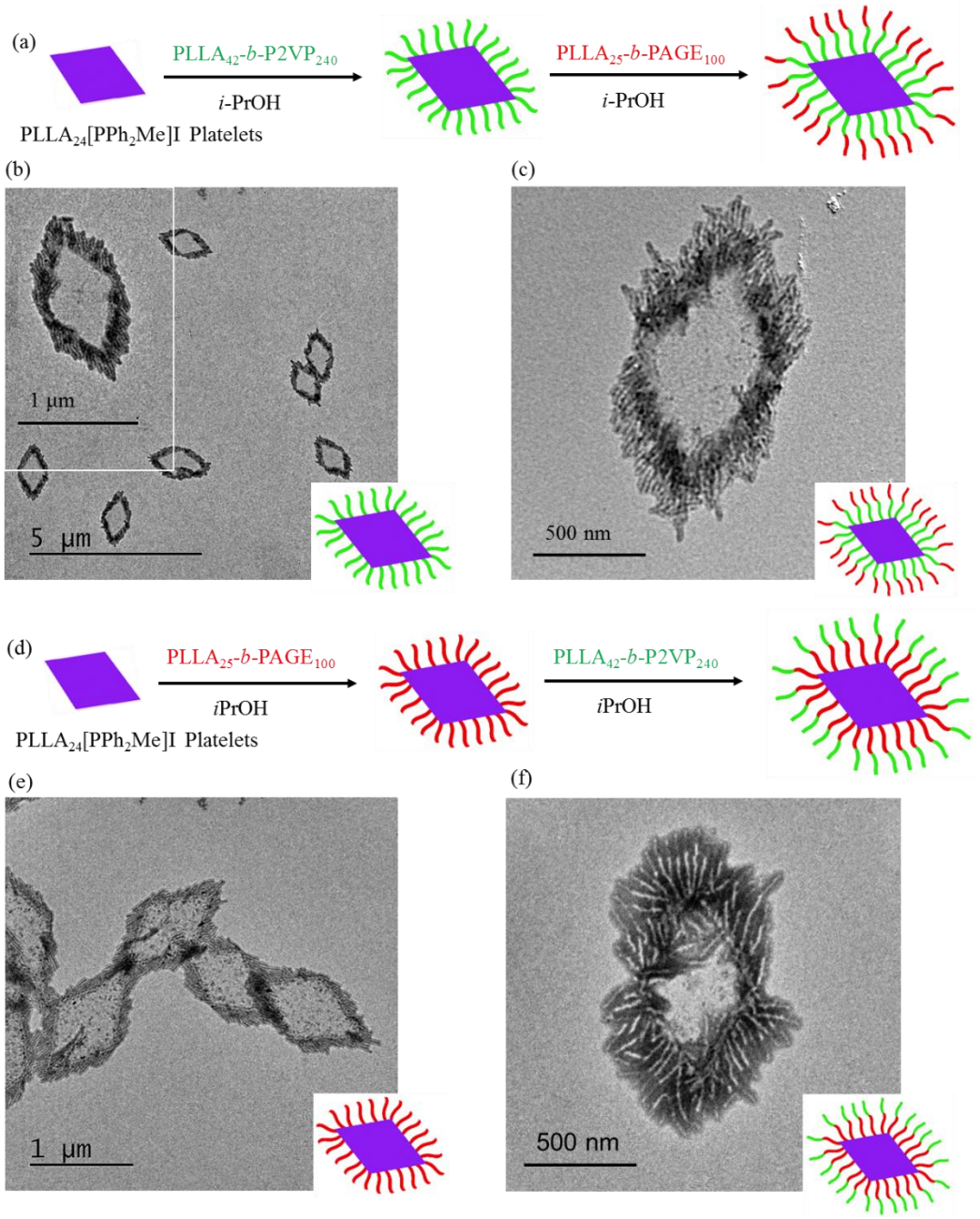

Figure 4.12. Schematic representation (a and d) and TEM images (b, c, e and f) of diamond-fibre hybrid structures (b) F(PLLA$_{42}$-*b*-P2VP$_{464}$)@D, (e) F(PLLA$_{20}$-*b*-PAGE$_{80}$)@D, and diamond-fibre(block)-like structures, (c) F(PLLA$_{20}$-*b*-PAGE$_{80}$)-*b*-F(PLLA$_{42}$-*b*-P2VP$_{464}$)@D, (f) F(PLLA$_{42}$-*b*-P2VP$_{464}$)-*b*-F(PLLA$_{20}$-*b*-PAGE$_{80}$)@D. F = fibre, D = diamond. The samples for TEM were not stained.

Moreover, diamond-fibre hybrid structures with fibres containing spatially segregated coronal chemistries could be prepared by further addition of different BCPs to the hybrid diamond-fibre structures (F@D). Thus, addition of PLLA$_{20}$-*b*-PAGE$_{80}$ unimer to diamond-fibre-hybrid structure F(PLLA$_{42}$-*b*-P2VP$_{464}$)@D, was found to afford the anticipated diamond-fibre block-like hybrid

structures F(PLLA$_{20}$-*b*-PAGE$_{80}$)-*b*-F(PLLA$_{42}$-*b*-P2VP$_{464}$)@D (Figure 4.12c). Similarly, addition of PLLA$_{42}$-*b*-P2VP$_{464}$ unimer to diamond-fibre hybrid structure F(PLLA$_{20}$-*b*-PAGE$_{80}$)@D, led to the formation of diamond-fibre block-like hybrid structures F(PLLA$_{42}$-*b*-P2VP$_{464}$)-*b*-F(PLLA$_{20}$-*b*-PAGE$_{80}$)@D. In the two diamond-fibre (block)-like structures mentioned above (Figure 4.12c and f), two blocks of fibres could be differentiated by the TEM due to their different contrast, and the second BCPs grows epitaxially at the end of the first block fibres. In our previous report, scarf-like micelles with cylindrical fibres selectively grown from the long-axis platelet end were formed by addition of PFS BCPs to rectangular platelets derived from PFS polymers.[149] The selective nature of the epitaxial growth in the PFS system was attributed to the preferred direction of crystal growth along the long axis (b axis, (010) direction).[138, 433] In contrast, the crystal growth of the diamond-shaped PLLA platelet is isotropic along all four (110) directions, therefore preferring the growth of fibres at four edges with similar growth rates.

4.2.7. Patterning of Diamond-Shaped Platelets with SiO_2 Nanoparticles (NPs)

Electrostatic interactions have been used for the controlled patterning of negatively-charged SiO_2 NPs on PFS-derived rectangular platelets with positive surfaces in a controlled manner.[157] It is expected that a choice of different shape of 2D platelet would tune the patterning mode of SiO_2 NPs with different shape, which might be important for tuning the property of materials. Here, we selected two different sizes of diamond-shaped platelets (A_n = 3.94× 10^5 nm^2, A_w/A_n = 1.04; A_n = 1.98× 10^6 nm^2, A_w/A_n = 1.03) derived from PLLA$_{24}$[PPh$_2$Me]I as templates to investigate the patterning mode of SiO_2 NPs.

A layer-by-layer approach was applied for the SiO_2 NPs patterning, similar to our previously reported procedure.[157] Platelet micelles derived from PLLA$_{24}$[PPh$_2$Me]I were drop-cast and dried on carbon-coated TEM grids in air. These grids were then immersed in the ethanol solution of SiO_2 NPs (diameter = 55 nm) for 30 min. Then *i*-PrOH was used to remove the free SiO_2 NPs on the grids after the incubation. Figure 4.13 shows the pattern of SiO_2 NPs loading on the PLLA$_{24}$[PPh$_2$Me]I platelets with two different sizes (Figure 4.13a: small size platelets; Figure 4.13b: large size platelets). All the plates were loaded with SiO_2 NPs, and no free platelets or SiO_2 NPs were found on the TEM grid, indicating

the specific loading due to the mutual electrostatic interaction. The SiO_2 NP loading density on the platelet edge was found to be slightly higher than that in the centre, perhaps as a consequence of the lower steric encumbrance at the platelet boundary.

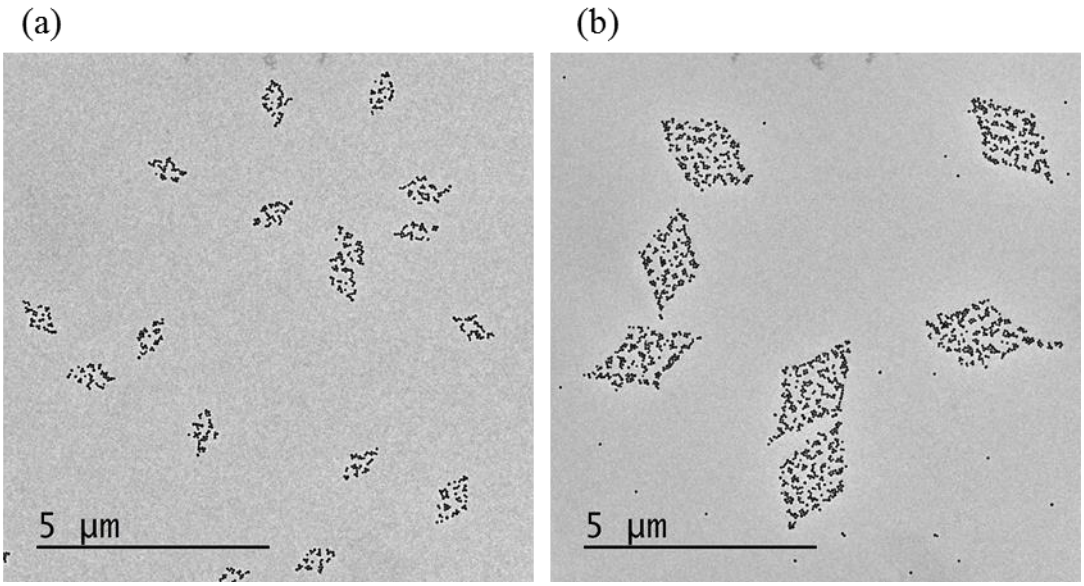

Figure 4.13. (a and b) TEM images showing the specific loading of negatively-charged SiO_2 NPs (diameter of SiO_2 NPs: 55 nm) on the positively charged diamond-shaped platelets. The platelets (A_n = 394,770 nm^2, A_w/A_n = 1.04) in (a) were prepared by seeded growth of $PLLA_{24}[PPh_2Me]I$ unimers in $CHCl_3$ using *quasi*-1D small seeds of $PLLA_{24}[PPh_2Me]I$ in *i*-PrOH. The platelets (A_n = 1985,400 nm^2, A_w/A_n = 1.03) in (b) were prepared by further addition of $PLLA_{24}[PPh_2Me]I$ unimers to the platelet in (a). The samples for TEM were not stained.

4.3. Summary

Soft matter-based nanoparticles are attractive for a broad range of applications. 2D assemblies are of particular current interest but the control of dimensions and spatial functionality represents a key challenge. In this chapter, by using seeded-growth method to blends of PLLA-based homopolymer and diblock copolymers, we have successfully demonstrated the formation of uniform 2D platelet micelles and a range of novel hierarchical platelet structures, such as 'patchy' platelet block comicelles, hollow platelets and diamond-fibre hybrid structures. The key to the preparation of these structures is the seeded growth living CDSA approach that allows precise control of the assembly process. Thus, uniform platelet micelles have been obtained by seeded growth of a blend unimer (charge-neutral $PLLA_{26}$ homopolymer and $PLLA_{47}$-*b*-$PNIPAm_{267}$ diblock copolymer) from both 2D and 1D seeds. Seeded growth of a $PLLA_{42}$-*b*-$P2VP_{464}$/$PLLA_{24}[PPh_2Me]I$ (diblock copolymer and charged homopolymer) polymer blend from both small *quasi*-1D seeds and large 2D diamond-shaped platelet micelles derived from $PLLA_{24}[PPh_2Me]I$ leads to the formation of well-defined diamond-shaped platelets and 'patchy' platelet block comicelles, respectively. This 2D living process is driven by an epitaxial growth mechanism, which was also confirmed by ED. Uniform hollow diamond-shaped structures could be produced by selectively crosslinking the peripheral block derived from $PLLA_{42}$-*b*-$P2VP_{464}$/ $PLLA_{24}[PPh_2Me]I$ of diamond-shaped platelet block comicelles with a central block derived from $PLLA_{24}[PPh_2Me]I$, followed by dissolution of the central block in a good solvent. On the other hand, addition solely of a cylinder-forming BCP led to the growth of fibres from four edges of the diamond-shaped platelet. Patterning of SiO_2 NPs on the diamond-shaped platelets has also been demonstrated.

Previous work has illustrated the promise of the living CDSA approach to 1D and 2D soft matter-based nanoparticles. However, the vast majority of the work to date has focused on PFS homopolymers and BCPs. In this chapter we have shown that this approach represents a powerful route to uniform, complex and hierarchical assemblies based on PLLA, a biodegradable organic polymer of considerable current interest for the development of release vehicles for pharmaceutical and other applications. Further studies directed towards these end-uses are currently underway.

4.4. Chapter 4 Supplementary Material

4.4.1. Materials and Instruments

All reactions were carried out in an MBraun MB150B-G glove box under argon or using standard Schlenk line techniques. All chemicals were purchased from Aldrich and were used as received unless otherwise stated. Solvents were dried using an MBraun solvent purification system prior to use. L-lactide was recrystallised twice from dry toluene and stored in the glove box. PEG was dried by azeotropic distillation in toluene before use. AIBN (2,2'-azo-bis(isobutyronitrile)) was recrystallised twice from methanol and stored in the dark at 4 °C. 2-vinyl pyridine was distilled over CaH_2 before use. CTA2-OH was prepared by **Chapter 3** procedure. All the self-assembly experiments were performed in HPLC grade solvents that were acquired from Fisher.

^{1}H and ^{13}C NMR spectra were obtained using a Varian 400 MHz spectrometer with $CDCl_3$ (^{1}H NMR: δ = 7.26 ppm; ^{13}C NMR δ = 77.16 ppm) as solvents and integrations of all peaks were against to TMSCl standard in NMR solvents.

Infrared spectra (IR) were recorded on a Perkin Elmer Spectrum One Fourier Transform Infrared Spectrometer (FT-IR).

Thermogravimetric analysis (TGA) was performed on a TA Instruments Q100 calorimeter at a scan rate of 10 °C/min under nitrogen.

Matrix-assisted laser desorption/ionization time of flight (MALDI-TOF) mass spectrometry measurements were performed using a Bruker Ultraflextreme running in linear mode. Samples were prepared using a *trans*-2-[3-(4-*tert*-butylphenyl)-2-methyl-2-propenylidene]malononitrile matrix (20 mg/mL in THF) and the polymer sample (2 mg/mL in THF), mixed in a 10:1 (*v*/*v*) ratio. Approximately 1 μL of the mixed solution was deposited onto a stainless steel sample plate and allowed to dry in air.

Molar mass dispersity ($Đ_M = M_w/M_n$) of all the polymers were obtained by Gel Permeation Chromatography (GPC) using a Viscotek VE 2001 Triple-Detector Gel Permeation Chromatograph equipped with automatic sampler, pump, injector, inline degasser, column oven (30 °C), and RI,

viscometry, and light scattering detectors. A flow rate of 1.0 mL/min was used with *n*Bu_4NBr/THF (0.1 wt% *n*Bu_4NBr) as the eluent. Samples were dissolved in the eluent (2 mg/mL) and filtered (PTFE membrane with 0.45 μm pore size) before analysis. Calibration of the detectors was performed using polystyrene standards (Viscotek).

Transmission electron microscopy (TEM). Copper grids from Agar Scientific, mesh 400, were coated with a carbon film. Carbon coating was done using an Agar TEM Turbo Carbon Coater in which carbon was sputtered onto mica sheets before deposition on the grids via flotation on water. The samples for electron microscopy were prepared by drop-casting one drop (10 μl) of the micelle colloidal solution onto a carbon-coated copper grid. Bright-field transmission electron microscopy (TEM) micrographs were obtained on a JEOL1200EX II microscope operating at 120 kV and equipped with an SIS MegaViewIII digital camera. As the micelles reported here are trapped kinetically because of crystallisation of the core block, the morphologies observed from dried samples by TEM are anticipated to match closely those observed in solution, as previously shown for 1D systems.

Selected area election diffraction (SAED) patterns for PFS based platelet micelle and comicelles were collected by Philips CM200 LaB6 TEM equipped with 4 pi imaging system with spot size of 8 nm at 200 kV (the diameter of selected area aperture is 200 nm). The d-spacings of SAED patterns were calibrated using gold nanoparticles standard. Elemental mapping from images of *quasi*-hexagonal disk-like platelet micelles and comicelles was performed on the FEI Talos F200X FEG TEM operating at 200 kV in STEM mode with spot size of 6.

Micelle area and length distributions were determined using the software program ImageJ from the National Institutes of Health. For the statistical analyses, more than 200 micelles in several images were traced by the software in order to obtain the area or length information. The number average micelle length (L_n) and weight average micelle length (L_w) (for 1D cylindrical micelles) or number average micelle area (A_n) and weight average micelle area (A_w) (for 2D platelets) were calculated as shown below (*L*, length of object; *N*, number; *A*, area of object).

$$(1) \qquad L_n = \frac{\sum_{i=1}^{n} N_i L_i}{\sum_{i=1}^{n} N_i} \qquad (2) \qquad L_w = \frac{\sum_{i=1}^{n} N_i L_i^2}{\sum_{i=1}^{n} N_i L_i}$$

$$(3) \qquad A_n = \frac{\sum_{i=1}^{n} N_i A_i}{\sum_{i=1}^{n} N_i} \qquad (4) \qquad A_w = \frac{\sum_{i=1}^{n} N_i A_i^2}{\sum_{i=1}^{n} N_i A_i}$$

The standard deviations (σ) of the measured lengths were calculated directly from the data set.

Atomic force microscopy (AFM). Samples for AFM were prepared by drop-casting 8 μL of the micelle solution onto a freshly cleaved mica substrate or carbon-coated mica substrate. Imaging was conducted under ambient conditions using a Bruker Multimode VIII atomic force microscope equipped with a ScanAsyst-HR fast scanning module and a ScanAsyst-Air-HR probe (tip radius, 2 nm), utilizing peak force feedback control. Images were analysed using Gwyddion or Nanoscope Analysis software program.

4.4.2. Synthesis Procedures

Synthesis of PLLA$_{24}$[PPh$_2$Me]I. This was prepared and characterised by previous report.[157, 253, 254]

Synthesis of PLLA$_{24}$PPh$_2$. This material was synthesised with a reported procedure. The initiator [4(diphenylphosphanyl)phenyl]methanol (55 mg, 0.18 mmol) and (-)-sparteine (33 μL, 0.14 mmol) were dissolved in dry DCM (1 mL) in a vial, while L-lactide (520 mg, 3.6 mmol) and 1-(3,5 bis(trifluoromethyl)phenyl)-3cyclohexyl-thiourea (101 mg, 0.27 mmol) were dissolved in dry DCM (2 ml) in another vial. The initiator solution was quickly added into the L-lactide solution under vigorous stirring and the mixture was stirred at room temperature for 3 h. The product was precipitated in MeOH three times before filtration and drying in vacuo to yield a white solid (466 mg, 90 %).

MALDI-MS: *m/z* 3760 $[M+Na]^+$ (DP_n = 24).

GPC (THF, PS standard): M_n = 5903 g·mol^{-1}, $Đ_M$ = 1.06.

^{31}P NMR (162 MHz, $CDCl_3$): δ (ppm) -5.19.

^{1}H NMR (400 MHz, $CDCl_3$): δ (ppm) 7.34-7.26 (m, 14 H; ArH), 5.15 (q, 48 H; C<u>H</u>CH_3), 1.57 (d, 144 H; CHC<u>H</u>$_3$).

Synthesis of PLLA$_{24}$PPh$_2$MeI. To 8 mL THF solution of PLLA24PPh2 (400 mg) was added excess MeI (0.4 mL), and the resulting mixture was allowed to stir for 2 hours at room temperature. The product was precipitated into *n*-hexane three times from THF before filtration and drying *in vacuo* to yield a white solid (361 mg, 90%).

MALDI-MS: *m/z* 3774 $[M]^+$ (DP_n = 24).

GPC (THF, PS standard): M_n = 3321 g·mol^{-1}, $Đ_M$ = 1.07.

^{31}P NMR (162 MHz, CDCl3): *δ* (ppm) + 22.38.

^{1}H NMR (400 MHz, CDCl3): *δ* (ppm) 7.83-7.60 (m, 14 H; Ar*H*), 5.15 (q, 48 H; C<u>H</u>CH3), 3.25 (d, 3 H; C<u>H3</u>), 1.56 (d, 144 H; CHC<u>H3</u>).

ν_{max} (neat)/cm^{-1}: 3000-2880 (C-H); 1755, 1044 (C=O); 1456 (CH_3); 1210-1163 (C(O)-O); 1088 (C-O).

Synthesis of PLLA$_{26}$. In a nitrogen-filled glove box, solutions of DBU (12.5 uL, 0.083 mmol) and benzyl alcohol (7.5 mg, 0.069 mmol) in dry DCM (2 mL) were added to solution of *L*-lactide (300 mg, 2.08 mmol) in dry DCM (1mL). After stirring for 1 min at room temperature, the solution was quenched with benzoic acid and stirred for 30 min. After removed from the glove box, the reaction solution was precipitated three times into MeOH and collected by centrifugation. Polymers were further dried in a vacuum oven for 16 h before characterisation (271 mg, 92%).

MALDI: *m/z*=3917 $[M+Na]^+$ (DP_n = 26).

GPC (*n*-Bu_4NBr/THF, PS standard): M_n = 8132 g·mol^{-1}, $Đ_M$ = 1.13.

^{1}H NMR (400 MHz, $CDCl_3$): δ (ppm) 5.17 (q, 52 H, C<u>H</u>CH_3), 1.57 (d, 185 H, CHC<u>H</u>$_3$). M_n = 7698 g·mol^{-1}.

ν_{max} (neat)/cm^{-1}: 3000-2880 (C-H); 1755, 1044 (C=O); 1456 (CH_3); 1210-1163 (C(O)-O); 1088 (C-O).

Synthesis of PEG$_{45}$-*b*-PLLA$_{23}$. PEG2K (200.0 mg, 0.10 mmol) and (-)-sparteine (23.2 μL, 0.1 mmol) were dissolved in dry DCM (1 mL) in a vial with a stirbar. In a second vial, *L*-lactide (290.2 mg, 2 mmol) and 1-(3,5-bis(trifluoromethyl)phenyl)-3-cyclohexyl-thiourea (74.0 mg, 0.2 mmol) were dissolved in dry DCM (1 mL). The PEG solution was quickly injected into the lactide solution. The mixture was stirred at room temperature for 3 h. The product was precipitated in diethyl ether three times and dried under vacuum to yield a white solid (416 mg, 81%).

GPC (*n*-Bu_4NBr/THF, PS standard): M_n = 9103 g·mol^{-1}, $Đ_M$ = 1.09.

^{1}H NMR (400 MHz, $CDCl_3$): δ (ppm) 5.16 (q, 46 H; C<u>H</u>CH_3 of PLLA), 3.64 (s, 180 H, PEG), 3.38 (s, 3 H, C<u>H</u>$_3$-PEG), 1.60 (d, 138 H; CHC<u>H</u>$_3$ of PLLA), M_n = 5314 g·mol^{-1}.

ν_{max} (neat)/cm^{-1}: 3000-2880 (C-H); 1755, 1044 (C=O); 1456 (CH_3); 1210-1163 (C(O)-O); 1088 (C-O); 872, 756 (C-H).

Synthesis of PAGE$_{80}$. In an oven-dried Schlenk flask, benzyl alcohol (7.3 uL, 0.07 mmol) was dissolved in dry THF (20 mL). Potassium naphthalenide (1M in THF) was added in dropwise till the solution turned into dark green and the colour did not fade in 1 min. Allyl glycidyl ether (1 mL, 8.42 mmol) was added into the benzyl alcohol solution. The mixture was stirred at 40 °C for 36 h. The product was precipitated three times in hexane and dried under vacuum to yield clear oil (705 mg, 70%).

MALDI-MS: *m/z* 9250 $[M+Na]^+$ (DP_n = 80).

GPC (*n*-Bu_4NBr/THF, PS standard): M_n = 10825 g·mol^{-1}, $Đ_M$ = 1.13.

^{1}H NMR (400 MHz, CDCl3): δ (ppm) 7.32 (m, 5H, Ar), 5.93-5.83 (m, 80 H, C<u>H</u>=CH$_2$), 5.27-5.14 (m, 160 H, CH=C<u>H$_2$</u>), 4.54 (s, 2 H, Ar-C<u>H$_2$</u>-O), 3.98 (d, 162 H, CH$_2$=CH-C<u>H$_2$</u>-O), 3.63-3.44 (m, 405 H, C<u>H$_2$</u>-C<u>H</u>(O)-C<u>H$_2$</u>-O).

Synthesis of PLLA$_{20}$-*b*-PAGE$_{80}$. In an oven-dried Schlenk flask, PAGE (400 mg, 0.044 mmol), *L*-lactide (125 mg, 0.88 mmol) and tin(II) 2-ethylhexanoate (2 drops) were dissolved in dried dioxane (1 mL). The mixture was heated at 110 °C for 5 hours. The product was precipitated three times in hexane and dried under vacuum to yield while solid (500 mg, 95%).

GPC (*n*-Bu$_4$NBr/THF, PS standard): M_n = 14310 g·mol^{-1}, $Đ_M$ = 1.20.

^{1}H NMR (400 MHz, CDCl3): δ (ppm) 7.32 (m, 5H, Ar), 5.93-5.83 (m, 80 H, C<u>H</u>=CH$_2$), 5.27-5.14 (m, 205 H, C<u>H</u>CH$_3$ of PLLA and CH=C<u>H$_2$</u> of PAGE), 4.54 (s, 2 H, Ar-C<u>H$_2$</u>-O), 3.98 (d, 164 H, CH$_2$=CH-C<u>H$_2$</u>-O), 3.63-3.44 (m, 406 H, C<u>H$_2$</u>-C<u>H</u>(O)-C<u>H$_2$</u>-O), 1.58 (d, 120 H, CHC<u>H$_3$</u> of PLLA). M_n = 12100 g·mol^{-1}.

ν_{max} (neat)/cm^{-1}: 3084 (C=C); 3000-2880 (C-H); 1755, 1044 (C=O); 1456 (CH$_3$); 1210-1163 (C(O)-O); 1088 (C-O); 924 (C=C).

Synthesis of 6-hydroxyhexyl 4-cyano-4(((phenethylthio)carbonothioyl)thio)pentanoate (CTA1-OH). In an oven-dried Schlenk flask, 4-cyano-4-(phenylcarbonothioylthio)pentanoic acid (300 mg, 1.07 mmol) and 1,6-hexanediol (1.0 g, 8.64 mmol) were dissolved in dry CHCl$_3$ (20 mL). EDC·HCl (300 mg, 1.60 mmol) and DMAP (20 mg, 0.16 mmol) were dissolved in dry CHCl$_3$ (10 mL) in another oven-dried Schlenk flask at ambient temperature, followed by adding into the reaction flask via a syringe. The reaction mixture was stirred under reflux for 48 h, filtered and concentrated to yield pink oil residue. The crude product was purified by silica chromatography (hexane:ethyl acetate = 4:1 as eluent) to afford CTA-OH as pink oil (280 mg, 70%).

^{1}H NMR (400 MHz, CDCl$_3$, 298 K): δ (ppm) 7.9-7.4 (m, 5H, Ph), 4.11 (t, 2H, COOC<u>H$_2$</u>), 3.65 (t, 2H, C<u>H$_2$</u>OH), 2.6-2.4 (m, 4H, CN-C-C<u>H$_2$</u>C<u>H$_2$</u>), 1.94 (s, 3H, C<u>H$_3$</u>), 1.6-1.3 (m, 8H,

C$\underline{H_2}$C$\underline{H_2}$C$\underline{H_2}$C$\underline{H_2}$CH$_2$OH). ^{13}C NMR (125 MHz, $CDCl_3$, 298 K): δ (ppm) 222.4 (C=S), 171.7 (C=O), 144.7, 133.2, 128.7, and 126.8 (Ph), 118.7 (CN), 65.3 (COO$\underline{C}$H$_2$), 62.9 ($\underline{C}$H$_2$OH), 45.9 ($\underline{C}$CN), 33.6 (CNC$\underline{C}$H$_2$), 32.7 ($\underline{C}$H$_2$CH$_2$OH), 30.0 ($\underline{C}$H$_2$COO), 28.7 (COOCH$_2\underline{C}$H$_2$), 25.9 (COOCH$_2$CH$_2\underline{C}$H$_2$), 25.5 ($\underline{C}$H$_2$CH$_2$CH$_2$OH), 24.9 ($\underline{C}$H$_3$).

Synthesis of CTA1-PLLA$_{42}$. This material was synthesised according to a procedure reported by O'Reilly and Dove research groups.[253] In an N_2-filled glovebox at room temperature, initiator CTA1-OH (40 mg, 0.11 mmol) and (-)-sparteine (26 μL, 0.11 mmol) were combined in one vial with *L*-lactide (0.68 g, 4.7 mmol) and 1-(3,5-bis(trifluoromethyl)phenyl)-3-cyclohexyl-thiourea (82 mg, 0.22 mmol) in another. Dry dichloromethane (2 mL and 4 mL for each vial respectively) was then added to each of the vials, and then the initiator solution was quickly injected into another one. The mixture was stirred at room temperature for 3 h. The product was precipitated in *n*-hexane three times before filtration and drying *in vacuo* to yield a white solid. Yield: 90 %.

MALDI-MS: *m/z* 6460 (DP_n = 42).

GPC (*n*-Bu_4NBr/THF, PS standard): M_n = 10,660 g·mol^{-1}, $Đ_M$ = 1.20.

^{1}H NMR (400 MHz, $CDCl_3$): δ (ppm) 5.18 (q, 84 H; C$\underline{H}$CH$_3$ of PLLA), 1.60 (d, 252 H; CHC$\underline{H_3}$ of PLLA).

Synthesis of PLLA$_{42}$-*b*-P2VP$_{464}$. In a N_2-filled glove box at room temperature, CTA1-PLLA$_{42}$ (50 mg, 0.008 mmol), 2-vinyl pyridine (253 mg, 2.4 mmol), AIBN (0.33 mg, 0.002 mmol) and 1,4-dioxane (0.5 mL) were mixed in a Schlenk tube. The solution was heated to 70 °C in an oil bath with magnetic stirring for 24 h. Then the polymerisation was stopped by cooling to room temperature. The polymer was precipitated in *n*-hexane. Then the polymer was purified by dissolving the polymer in 5 mL THF followed by precipitation 3 times with 10 mL hexane to afford light pink solid (239 mg, 80%).

GPC (*n*-Bu_4NBr/THF, PS standard): M_n = 40,300, $Đ_M$ = 1.21.

^{1}H NMR (500MHz, CD_2Cl_2): δ (ppm) = 8.29 (m, 464 H; P2VP Ar), 7.30-6.20 (m, 1438 H; P2VP Ar), 5.18 (q, 84 H; C<u>H</u>CH_3 of PLLA), 2.34-1.60 (m, 1711 H; C<u>H_2</u>-C<u>H</u> of P2VP and C<u>H</u>CH_3 of PLLA). M_n = 31345 g·mol^{-1}.

ν_{max} (neat)/cm^{-1}: 3000-2880 (C-H); 1755, 1044 (C=O); 1590, 1585 (Ar); 1472, 1433 (Ar-C-N); 1088 (C-O); 745 (Ar).

Synthesis of CTA2-PLLA$_{47}$. In a nitrogen-filled glove box, solutions of DBU (11.2 uL, 0.18 mmol) and CTA2-OH (28 mg, 0.062 mmol) in dry DCM (2 mL) were added to solution of *L*-lactide (400 mg, 2.78 mmol) in dry DCM (1mL). After stirring for 1 min at room temperature, the solution was quenched with benzoic acid and stirred for 30 min. After removed from the glove box, the reaction solution was precipitated three times into MeOH and collected by centrifugation. Polymers were further dried in a vacuum oven for 16 h before characterisation (367 mg, 92%).

MALDI: *m/z*=7232 (DP_n = 47).

GPC (*n*-Bu_4NBr/THF, PS standard): M_n= 9800 g·mol^{-1}, $Đ_m$ = 1.09.

^{1}H NMR (400 MHz, $CDCl_3$): δ (ppm) 5.17 (q, 102H, C<u>H</u>CH_3), 1.57 (d, 306H, CHC<u>H_3</u>). M_n (NMR) = 7698 g·mol^{-1}.

Synthesis of PLLA$_{47}$-*b*-PNIPAm$_{267}$. PLLA$_{47}$ (100 mg, 0.015 mmol), NIPAm (355 mg, 3.2 mmol) and AIBN (0.47 mg, 0.003 mmol) were dissolved in 1,4-dioxane (3 mL) in a Schlenk flask. The solution was then freeze-pump-thawed four times and heated for 3.5 h at 70 ˚C. The reaction was quenched by immersion of the ampoule in liquid nitrogen and the polymer was precipitated in hexane three times, followed by being dried under vacuum and characterised (403 mg, 88%).

^{1}H NMR (400 MHz, $CDCl_3$): δ (ppm) 7.0-5.6 (br, 244H, N<u>H</u>-CH-$(CH_3)_2$), 5.16 (q, 94H, C<u>H</u>(CH_3) of PLLA), 4.00 (br, 267H, NH-C<u>H</u>-$(CH_3)_2$ of PNIPAm), 2.3-0.7 (3673 H, m, C<u>H_3</u> of PNIPAm, CH(C<u>H_3</u>) from PLLA, C<u>H</u>C<u>H_2</u> of PNIPAm), M_n = 36,987 g·mol^{-1}.

GPC (*n*-Bu_4NBr/THF, PS standard): M_n = 180,600 g·mol^{-1}, $Đ_m$ = 1.11.

ν_{max} (neat)/cm^{-1}: 3510-3313 (N-H); 3000-2880 (C-H); 1755 (C=O); 1644 (NH-C=O); 1458 (CH_3); 1386-1367 (C-H), 1276-1185 (C-O); 1130,1088 (C-O).

4.4.3. Self-assembly for Nanoparticle Morphology Preparation

All solvent compositions are given as volume ratio (*v*:*v*). All micelle length measurements were carried out with 200 micelles. Self-nucleation to form polydisperse micelles were carried out by direct dissolution with heating-cooling method. Seeded-growth experiments were carried out at 23 °C. All seed micelle solutions were prepared by sonication of the polydisperse micelle solutions from self-nucleation of polymer in selective solvents.

Formation of *quasi*-1D seeds of $PLLA_{24}[PPh_2Me]I$. To 4 mL *i*-PrOH was added 400 □L of $PLLA_{24}[PPh_2Me]I$ unimer as a 1 mg/mL $CHCl_3$ solution. The total solvent composition was *i*-PrOH/$CHCl_3$ (10:1). The solution was manually shaken for 10 s and aged for 24 h at 23 °C to prepare large 2D diamond-shape platelet aggregates from self-nucleation. The platelet aggregates were then fragmentized by sonication at 23 °C for 90 min using an ultrasonic bath to produce relatively small, *quasi*-1D platelet fragments of low dispersity that function as seeds (L_n = 200 nm, L_w/L_n = 1.09).

Seeded growth of $PLLA_{24}[PPh_2Me]I$ unimer from *quasi*-1D seeds of $PLLA_{24}[PPh_2Me]I$. To 1 mL *i*-PrOH solution was added 25 □L seed (0.1 mg/mL) of $PLLA_{24}[PPh_2Me]I$ in *i*-PrOH /$CHCl_3$ (10:1). Then a certain amount of concentrated unimer $PLLA_{24}[PPh_2Me]I$ as a 5 mg/mL $CHCl_3$ solution was added to the dilute seed solution. The solution was manually shaken for 10 s and aged for 24 h at 23 °C. Highly uniform 2D diamond platelets with controlled size were observed.

Seeded growth of $PLLA_{42}$-*b*-$P2VP_{464}$/$PLLA_{24}[PPh_2Me]I$ blend unimer from *quasi*-1D seeds of $PLLA_{24}[PPh_2Me]I$. To 1 mL *i*-PrOH solution was added 25 □L seed (0.1 mg/mL) of $PLLA_{24}[PPh_2Me]I$ in *i*-PrOH /$CHCl_3$ (10:1). Then a certain amount of concentrated $PLLA_{42}$-*b*-$P2VP_{464}$/$PLLA_{24}[PPh_2Me]I$ blend unimer with different mass ratio (4:1, 1:1 or 4:1) as a 5 mg/mL

(overall concentration) $CHCl_3$ solution was added to the dilute seed solution. The solution was manually shaken for 10 s and aged for 24 h at 23 °C.

Formation of 2D seeds of $PLLA_{26}$/$PLLA_{47}$-*b*-$PNIPAm_{267}$ blends. 100 μL of $PLLA_{26}$/$PLLA_{47}$-*b*-$PNIPAm_{267}$ solution (1:1 mass ratio, 10 mg/mL in DMSO) was added to a vial with 100 μL DMSO and 1800 μL EtOH resulting a polymer solution of 0.5 mg/mL. The vial was sealed and heated at 70 °C for 2 h, followed by slowly cooling to 23 °C, and the solution was carried on aging for 48 h. The formed polydisperse platelet micelles were characterised by TEM. Solutions of the polydisperse platelet micelles in DMSO/EtOH (1:9) was sonicated for 2 h in ice-cooled a sonic clean bath to afford 2D seed solutions.

Formation of 1D seeds of PEG_{45}-*b*-$PLLA_{23}$. 100 μL of PEG_{45}-*b*-$PLLA_{23}$ solution (10 mg/mL in DMSO) was added to a vial with 100 μL DMSO and 1800 μL EtOH resulting a polymer solution of 0.5 mg/mL. The vial was sealed and aged at 23 °C for 2 days for TEM characterisation. Solutions of the polydisperse micelles in DMSO/EtOH (1:9) was sonicated for 2 h in ice-cooled a sonic clean bath to afford 1D seed solutions.

Seeded growth of $PLLA_{26}$/$PLLA_{47}$-*b*-$PNIPAm_{267}$ blends from 2D/1D seeds.

Typical procedures for seeded-growth with 2D seeds in TFE/EtOH: 20 μL of seed micelle solution (0.5 mg/mL, DMSO/EtOH = 1:9) was diluted in 200 μL TFE/EtOH with volume ratio of 5:95, 5:95, 10:90 and 15:85 corresponds to unimer-to-seed mass ratios of 5, 10, 20 and 30, respectively, and to which solution was added $PLLA_{26}$/$PLLA_{47}$-*b*-$PNIPAm_{267}$ unimer (10 mg/mL in DMSO for m_{unimer}:m_{seed} ≤ 10.0; 20 mg/mL in DMSO for m_{unimer}:m_{seed} > 10.0) with volumes of 5, 10, 5 and 10 μL,

respectively. The resulting solution was then manually shaken for 10 s and aged for 5 days at 23 °C before TEM characterisation.

For seeded-growth in EtOH: typical procedure was followed but using EtOH as solvents.

For seeded-growth with 1D seeds: typical procedure was followed but using 1D seed solutions.

Formation of concentric 2D platelet block comicelles. Firstly, a large diamond platelets (A_n = 394,770 nm^2, A_w/A_n = 1.04) derived from $PLLA_{24}[PPh_2Me]I$ were prepared by seeded growth $PLLA_{24}[PPh_2Me]I$ unimer from *quasi*-1D seeds of $PLLA_{24}[PPh_2Me]I$ with unimer-to-seed mass ratio of 20. Then specified amounts of the $PLLA_{42}$-*b*-$P2VP_{464}$/$PLLA_{24}[PPh_2Me]I$ blend unimers (1:1, mass ratio) were added as 5 mg/mL (overall concentration) $CHCl_3$ solutions. The solution was manually shaken for 10 s and aged for 24 hours at 23 °C to get the desired diblock platelet comicelles. For the preparation of tetrablock platelet comicelles, specified amounts of $PLLA_{24}[PPh_2Me]I$ (5 mg/mL in $CHCl_3$) and $PLLA_{42}$-*b*-$P2VP_{464}$/$PLLA_{24}[PPh_2Me]I$ blend unimers (1:1 mass ratio, overall concentration of 5 mg/mL in $CHCl_3$) were further subsequently added.

Crosslinking of P2VP coronas and formation of hollow diamond-shaped platelet by removal of non-crosslinked central regions. To a 1.5 mL screw-cap vial was added 0.2 mL aliquot of a solution of the block comicelles. The vial was flushed with nitrogen and capped and transferred to glovebox. In the glovebox, 1 μL of Karstedt's catalyst (Platinumdivinyltetramethyldisiloxane complex in xylenes with a Pt mass% of 2.1-2.4, ABCR) was added and the solution was shaken for a few seconds and then allowed to age for 24 h. To remove the non-crosslinked regions, 50 μL of the solution was dried with nitrogen stream and then redispersed in 100 uL of THF. The samples were left in THF for at least 1 day prior to analysis.

Formation of diamond-fibre-like micelles. To $PLLA_{24}[PPh_2Me]I$ platelet micelles (0.025 mg/mL) in *i*-PrOH, was added certain amount of concentrated $PLLA_{42}$-*b*-$P2VP_{464}$ or $PLLA_{20}$-*b*-$PAGE_{80}$ unimer as a 2 mg/mL $CHCl_3$ solution. The solution was manually shaken for 10 s and aged for 24 h at 23 °C. To

prepare diamond-fibre(block)-like micelles, $PLLA_{42}$-*b*-$P2VP_{464}$ or $PLLA_{20}$-*b*-$PAGE_{80}$ unimers were added subsequently to $PLLA_{24}[PPh_2Me]I$ platelet micelles (0.025 mg/mL) in *i*-PrOH, with interval of 24 h.

4.4.4. Supplementary Figures

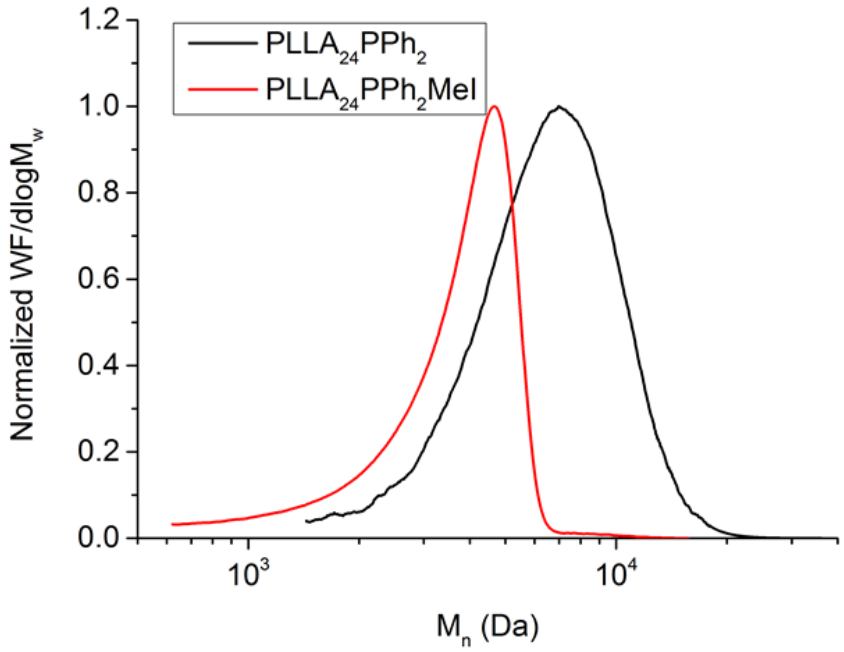

Figure S4.1. RI GPC curves of $PLLA_{24}PPh_2$ (black) and $PLLA_{24}PPh_2MeI$ (red). A flow rate of 1.0 mL/min was used with THF as the eluent.

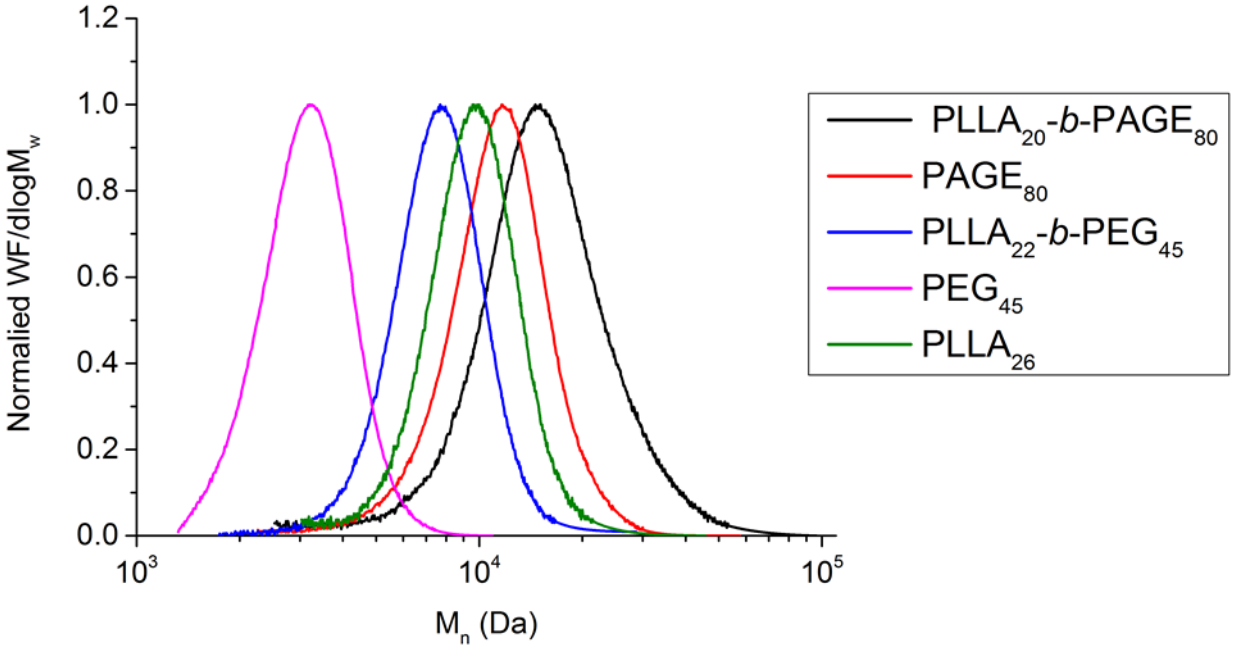

Figure S4.2. RI GPC curves of $PLLA_{20}$-*b*-$PAGE_{80}$ (black), $PAGE_{80}$ (red), PEG_{45}-*b*-$PLLA_{23}$ (blue) and PEG_{45} (pink). A flow rate of 1.0 mL/min was used with *n*Bu_4NBr/THF (0.1 wt% *n*Bu_4NBr) as the eluent.

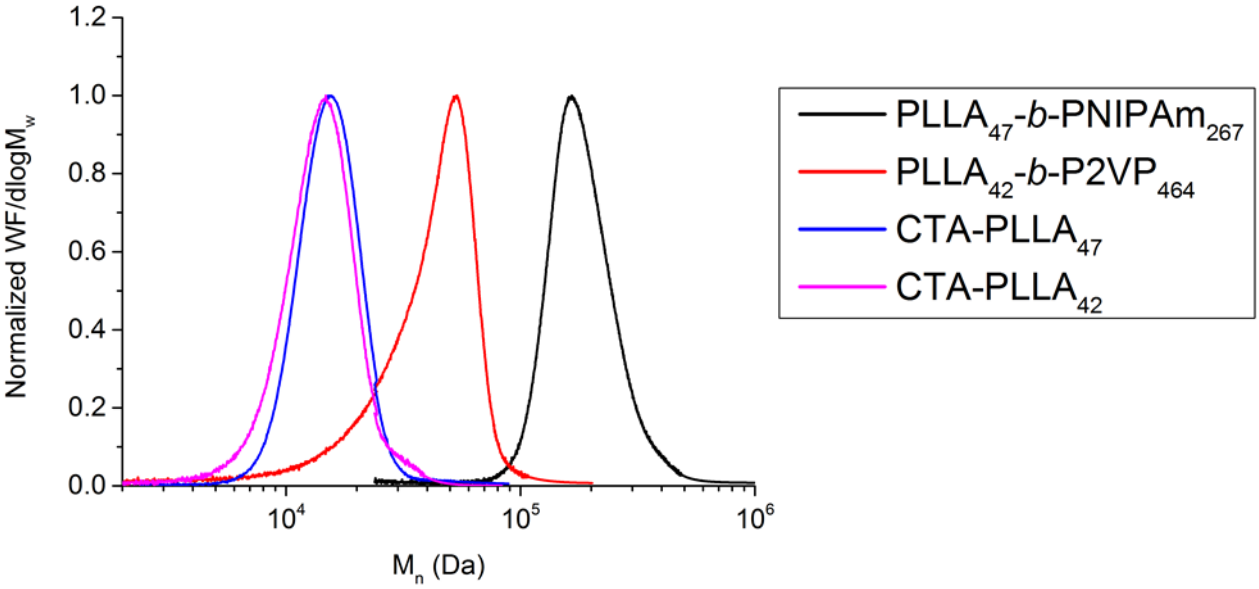

Figure S4.3. RI GPC curves of $CTA\text{-}PLLA_{42}$ (pink), $CTA\text{-}PLLA_{47}$ (blue), $PLLA_{42}$-*b*-$P2VP_{464}$, (red) and $PLLA_{47}$-*b*-$PNIPAm_{267}$ (black). A flow rate of 1.0 mL/min was used with *n*Bu_4NBr/THF (0.1 wt% *n*Bu_4NBr) as the eluent.

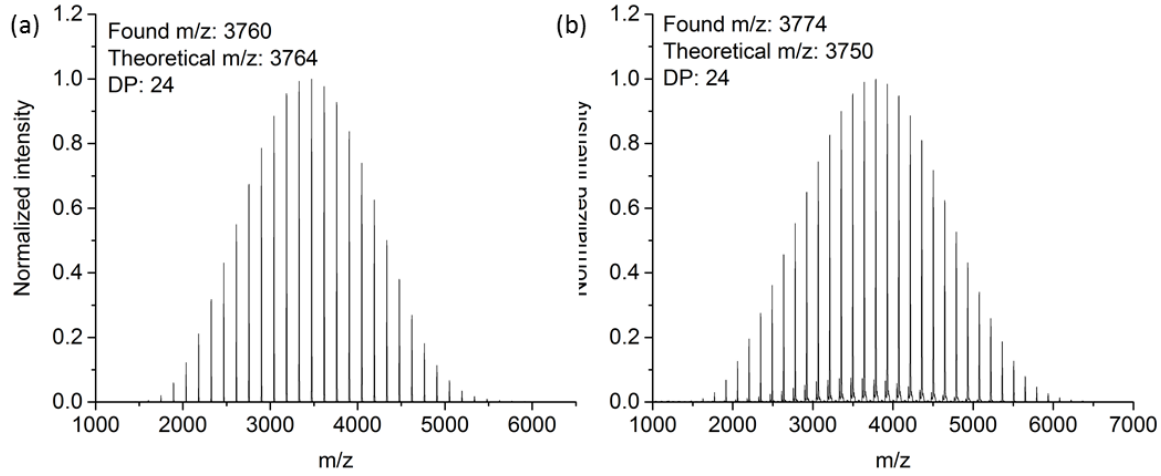

Figure S4.4. MALDI-TOF MS spectra of (a) $PLLA_{24}$-PPh_2 and (b) $PLLA_{24}PPh_2MeI$.

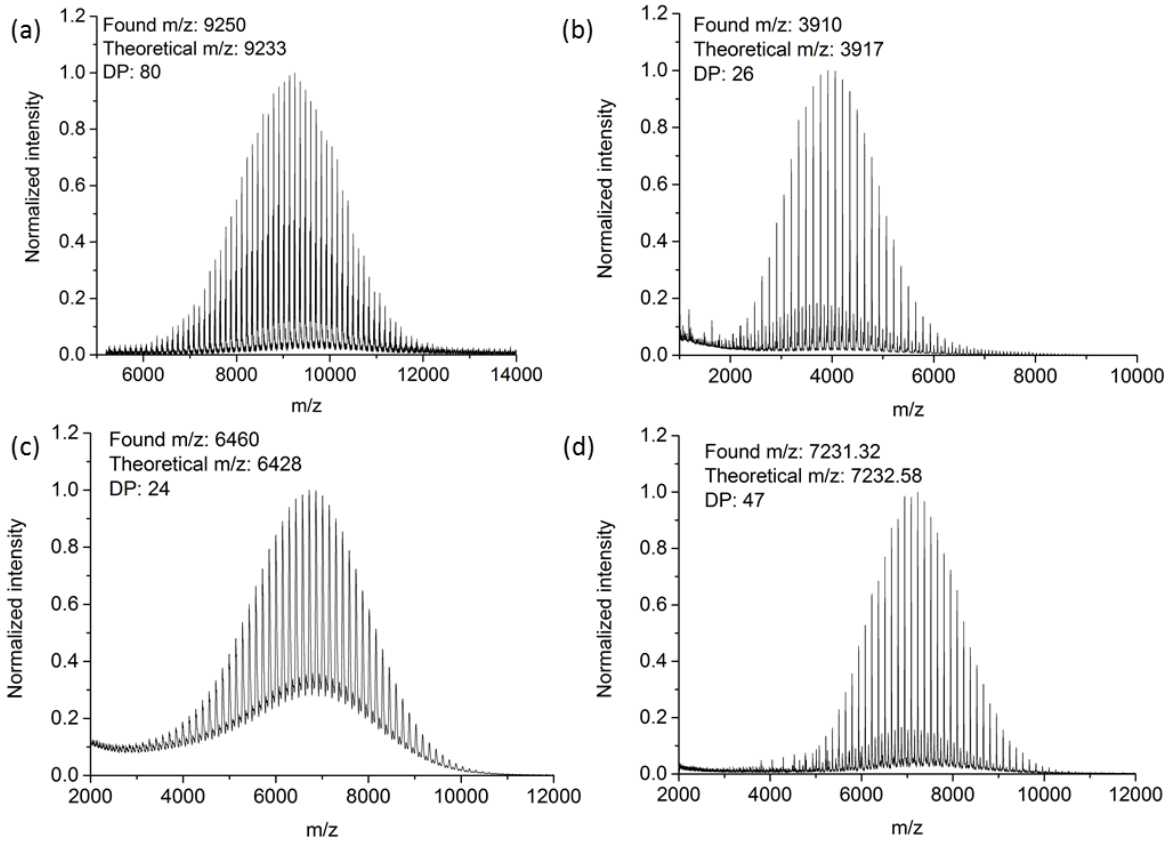

Figure S4.5. MALDI-TOF MS spectra of (a) $PAGE_{80}$, (b) $PLLA_{26}$, (c) CTA-$PLLA_{42}$, and (d) CTA-$PLLA_{47}$.

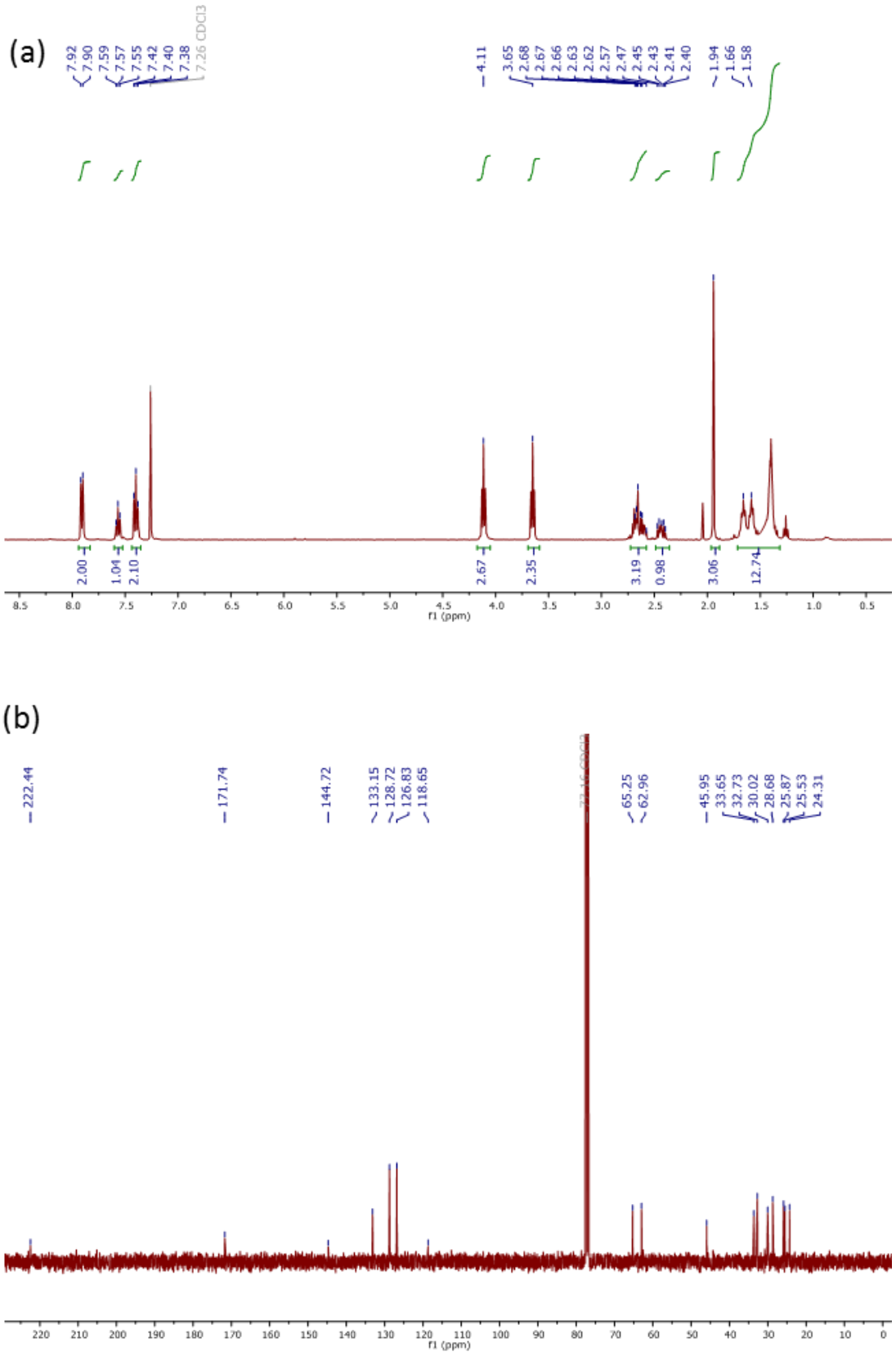

Figure S4.6. Characterisation of CTA1-OH: (a) ^{1}H NMR and (b) ^{13}C NMR spectra in $CDCl_3$.

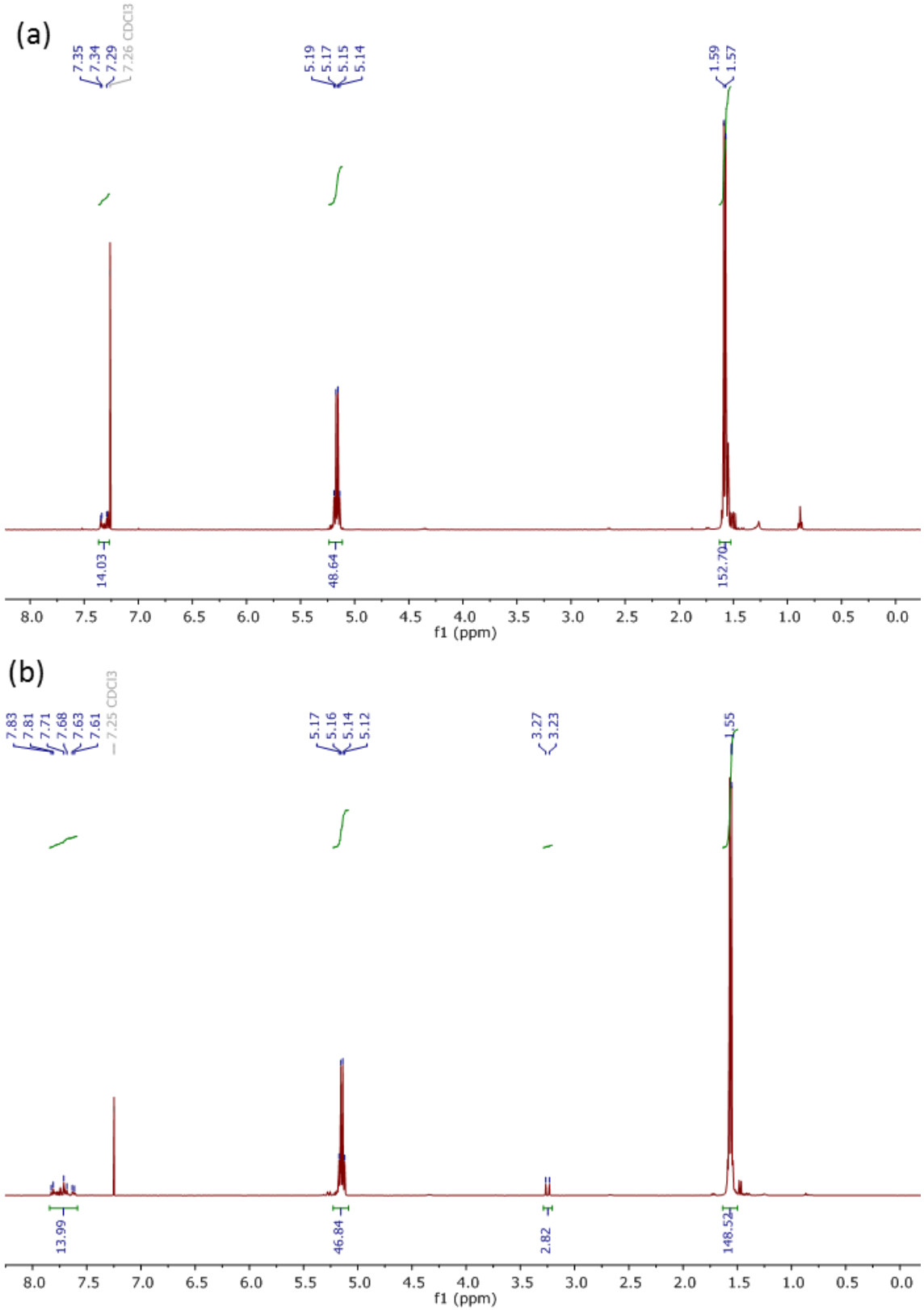

Figure S4.7. ^{1}H NMR spectra (in $CDCl_3$) of (a) $PLLA_{24}PPh_2$ and (b) $PLLA_{24}PPh_2MeI$.

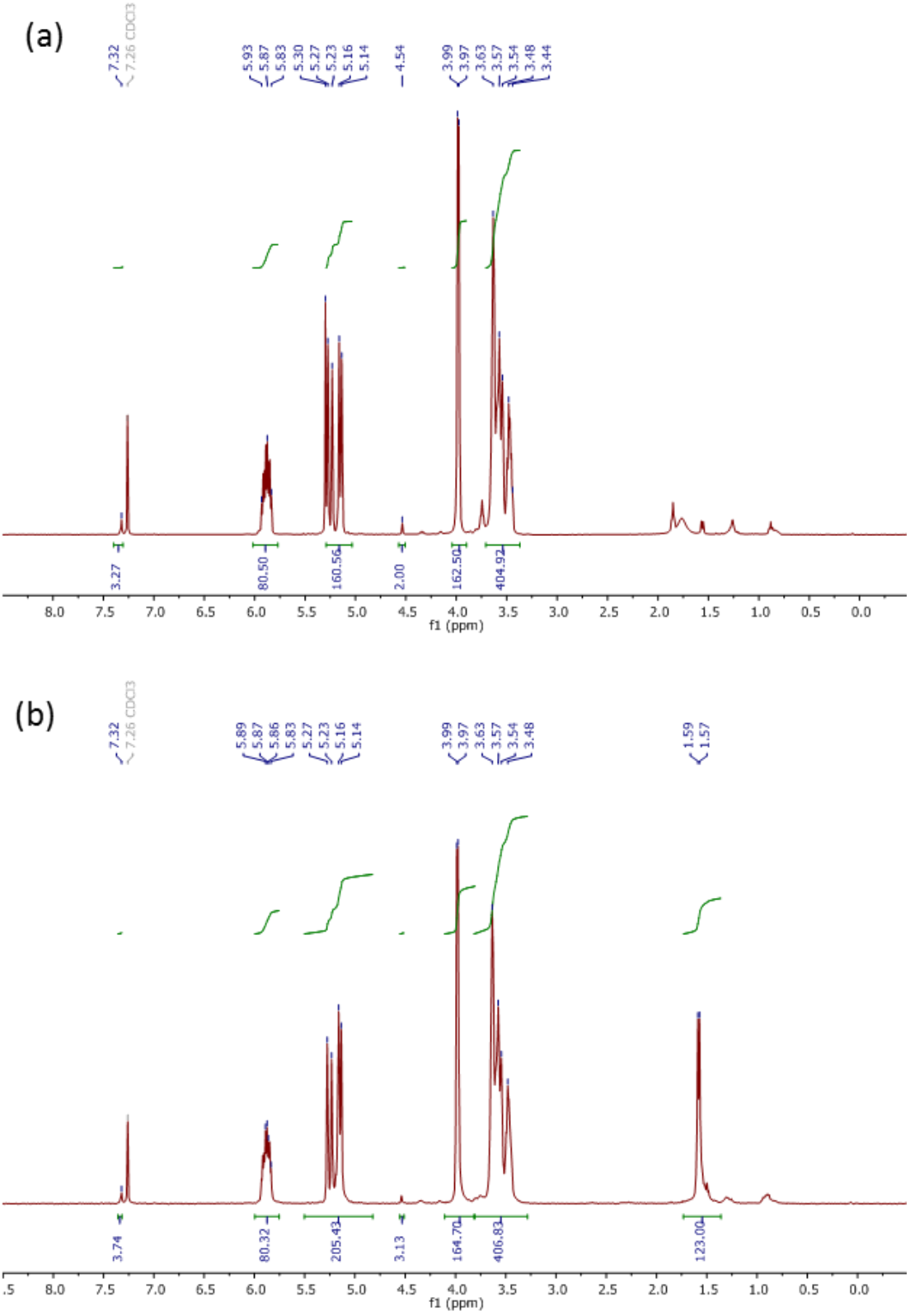

Figure S4.8. ^{1}H NMR spectra (in $CDCl_3$) of (a) $PAGE_{80}$ and (b) $PLLA_{20}$-*b*-$PAGE_{80}$.

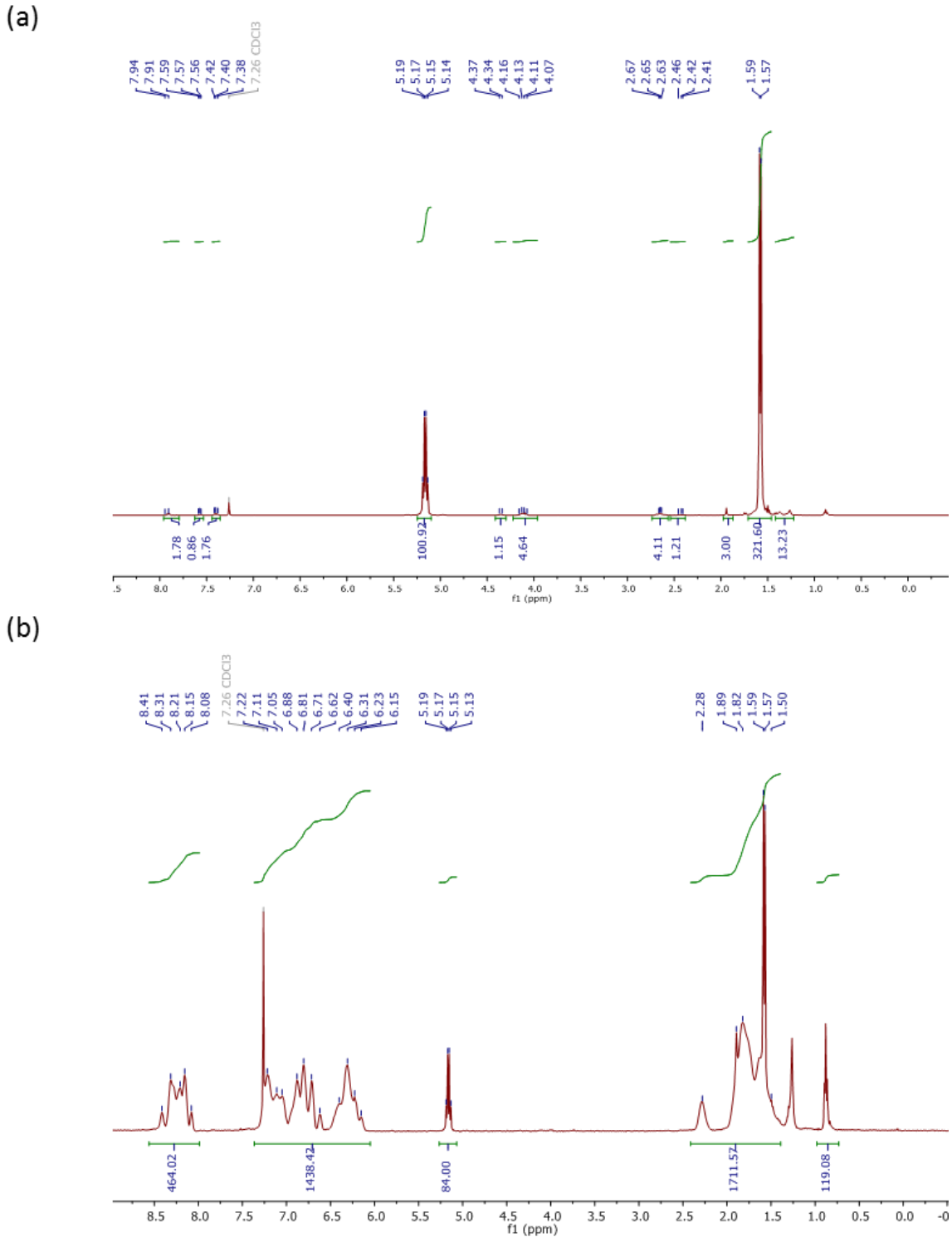

Figure S4.9. ^{1}H NMR spectra (in $CDCl_3$) of (a) $PLLA_{42}$ and (b) $PLLA_{42}$-*b*-$PAGE_{464}$.

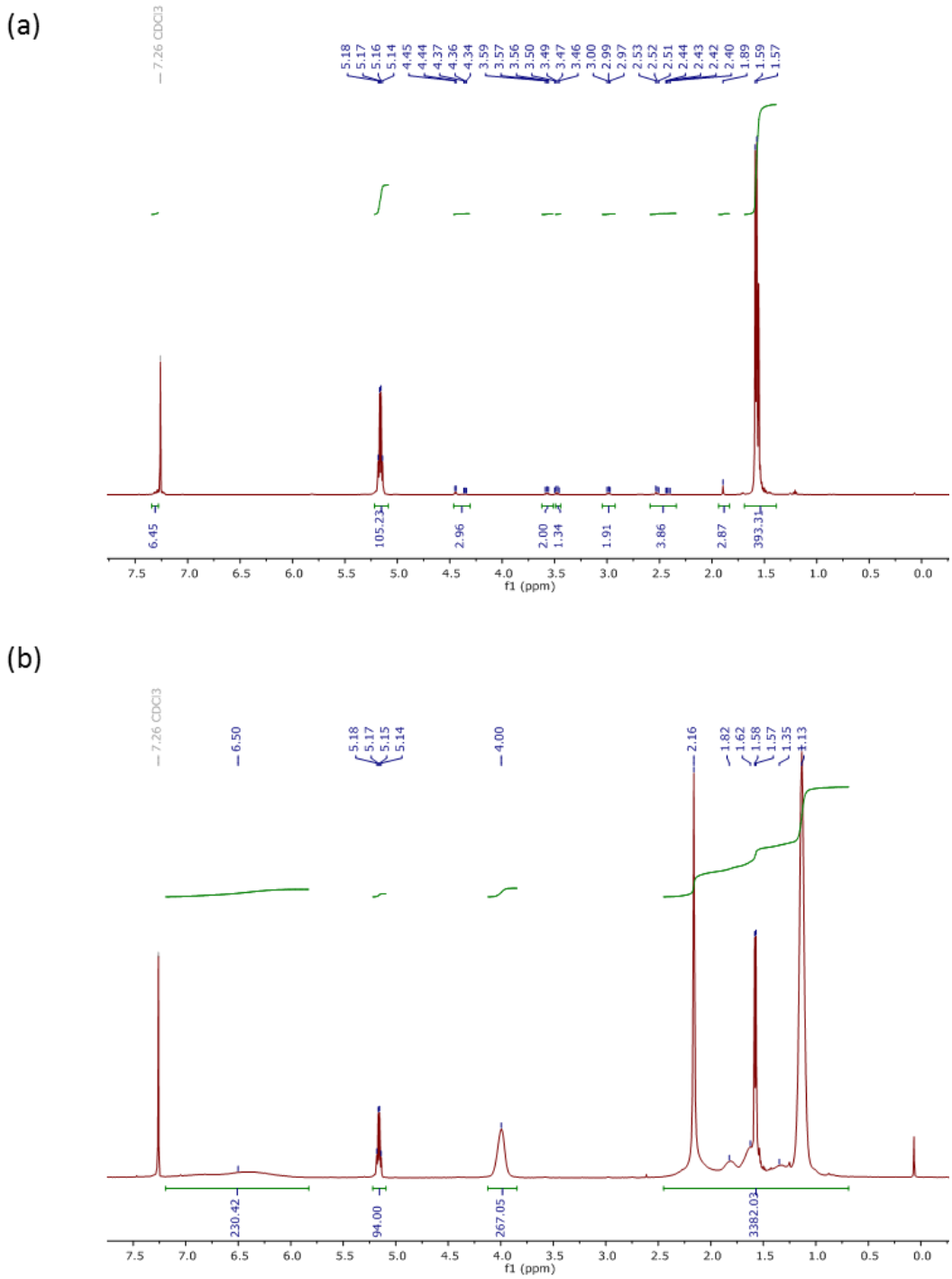

Figure S4.10. ^{1}H NMR spectra (in $CDCl_3$) of (a) $PLLA_{47}$ and (b) $PLLA_{47}$-*b*-$PNIPAm_{267}$.

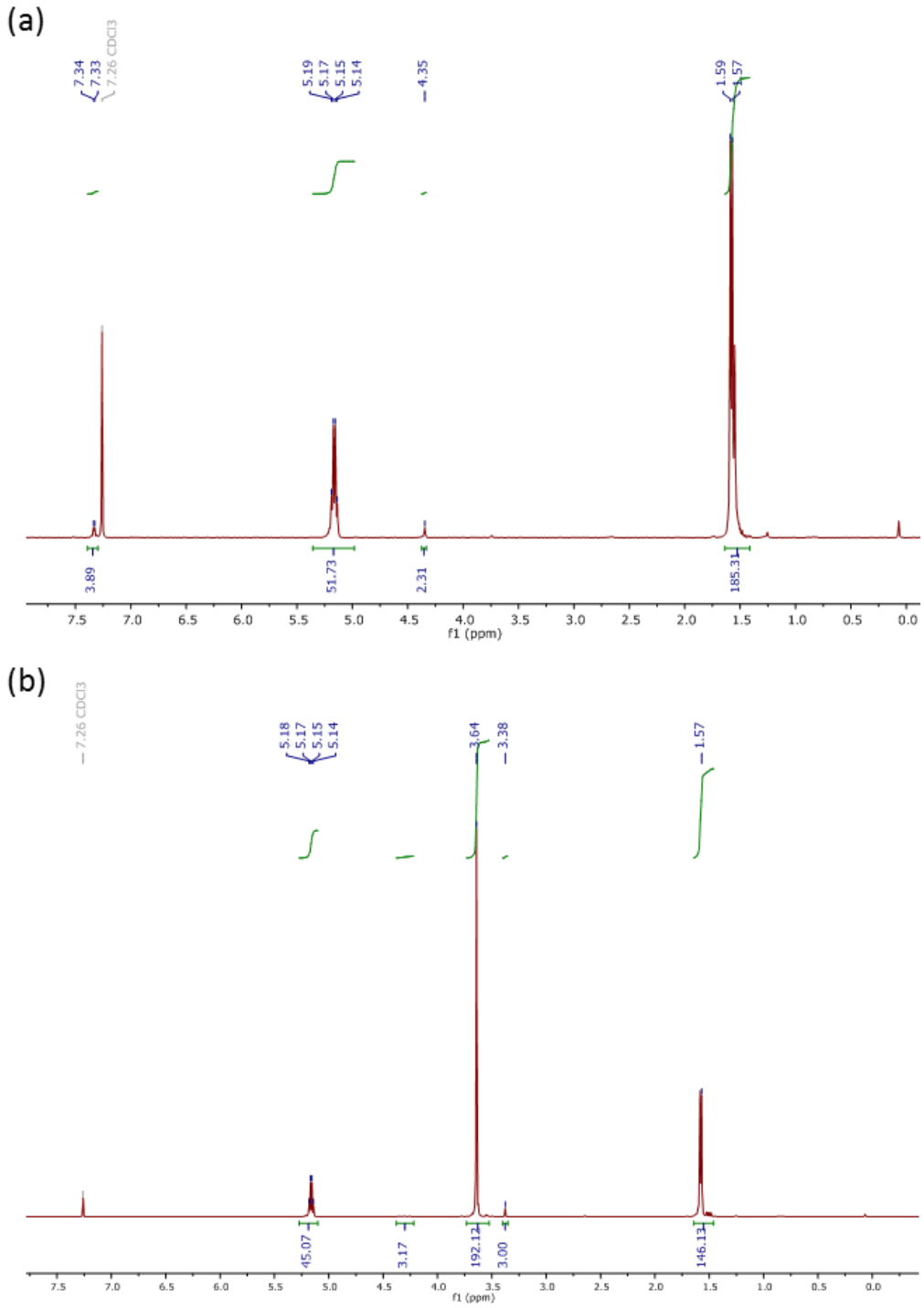

Figure S4.11. ^{1}H NMR spectra (in $CDCl_3$) of (a) $PLLA_{26}$ and (b) $PLLA_{23}$-*b*-PEG_{45}.

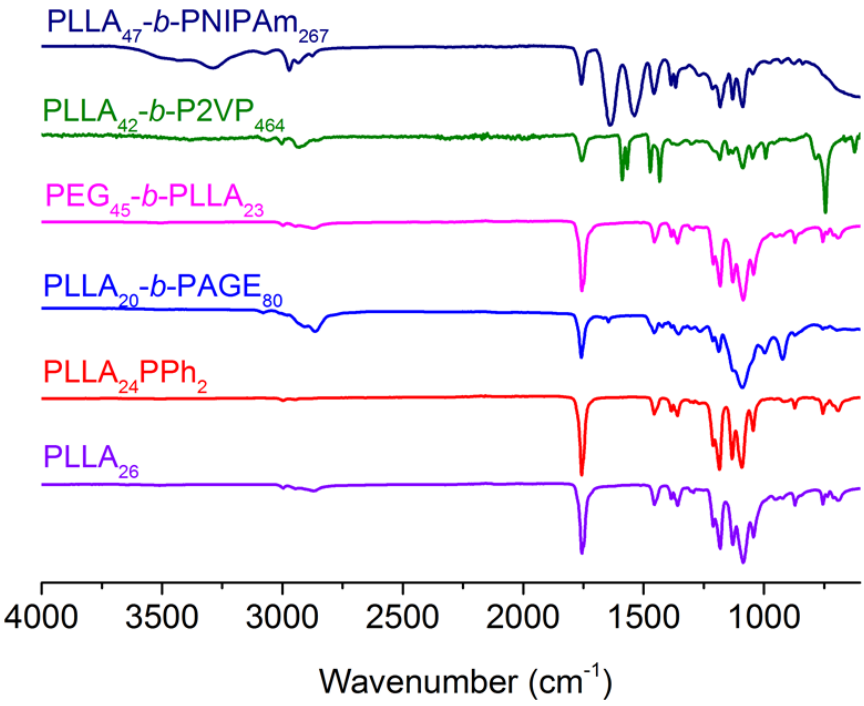

Figure S4.12. FT-IR characterisation of PLLA-containing polymers.

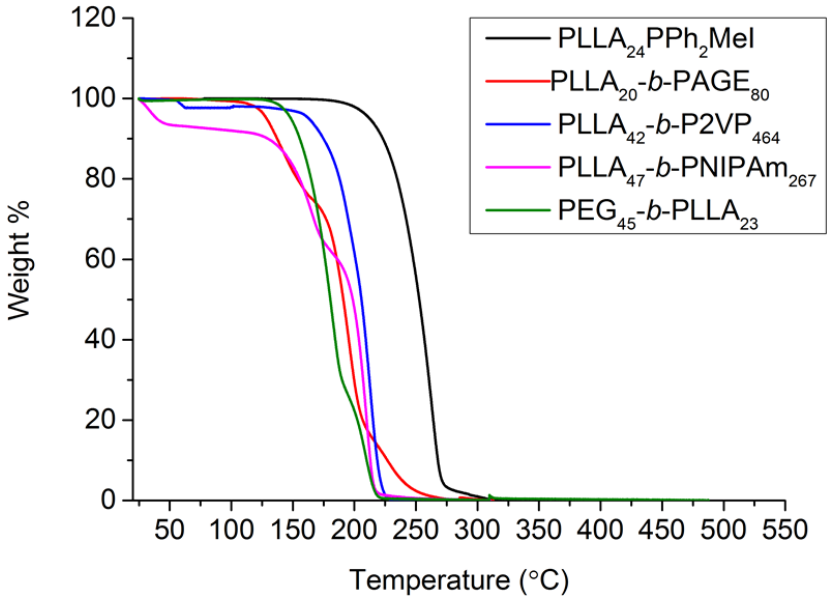

Figure S4.13. Thermogravimetric analysis (TGA) for $PLLA_{24}PPh_2MeI$ (black), $PLLA_{20}$-*b*-$PAGE_{80}$ (red), $PLLA_{42}$-*b*-$P2VP_{464}$ (blue), $PLLA_{47}$-*b*-$PNIPAm_{267}$ (pink) and PEG_{45}-*b*-$PLLA_{23}$ (green). TGA was performed at a scan rate of 10 °C/min under nitrogen.

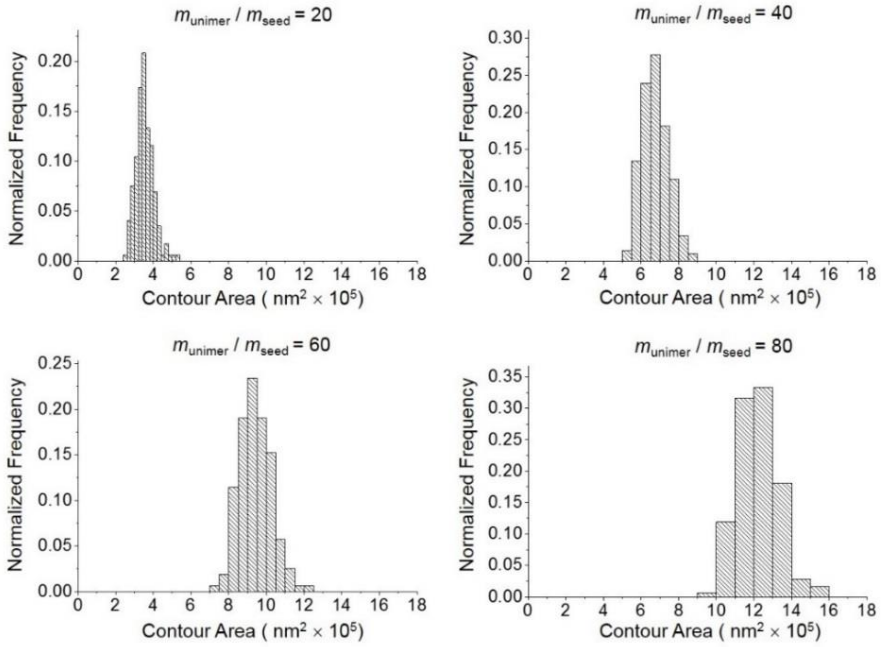

Figure S4.14. Contour area distributions of diamond-shaped platelet micelles by the seeded growth of unimer $PLLA_{24}[PPh_2Me]I$/ $PLLA_{42}$-*b*-$P2VP_{464}$ blend (1:1, mass ratio) in $CHCl_3$ from *quasi*-1D seed (L_n = 200 nm, L_w/L_n = 1.09) of $PLLA_{24}[PPh_2Me]I$ in *i*-PrOH at 23 °C.

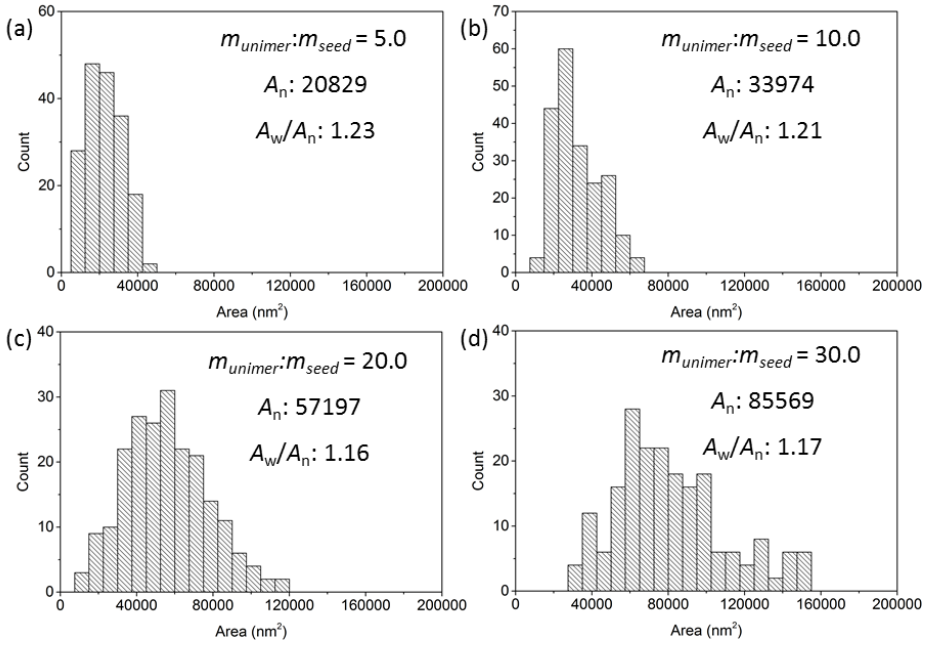

Figure S4.15. Contour length histogram of samples of uniform 2D platelet micelles prepared by addition of unimers ($PLLA_{26}$/$PLLA_{47}$-*b*-$PNIPAm_{267}$ blend, 10 mg/mL in DMSO) with m_{unimer}:m_{seed} of (a) 5.0, (b) 10.0, (c) 20.0 and (d) 30.0 to the 2D seed micelles in TFE/EtOH with volume ratios of (a) 5:95, (b) 5:95, (c) 10:90 and (d) 15:85, respectively.

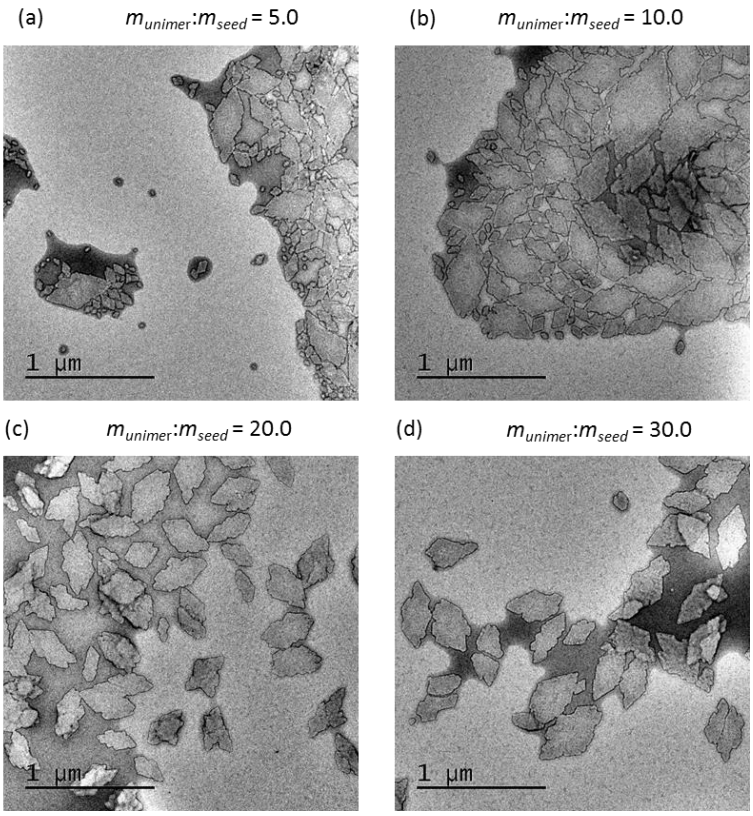

Figure S4.16. TEM images of samples of 2D platelet micelles prepared by seeded growth from 2D seed micelles in EtOH (in absence of TFE) with unimers ($PLLA_{26}$/$PLLA_{47}$-*b*-$PNIPAm_{267}$ blend, 10 mg/mL in DMSO) of m_{unimer}:m_{seed} ratios of (a) 5.0, (b) 10.0, (c) 20.0 and (d) 30.0, respectively.

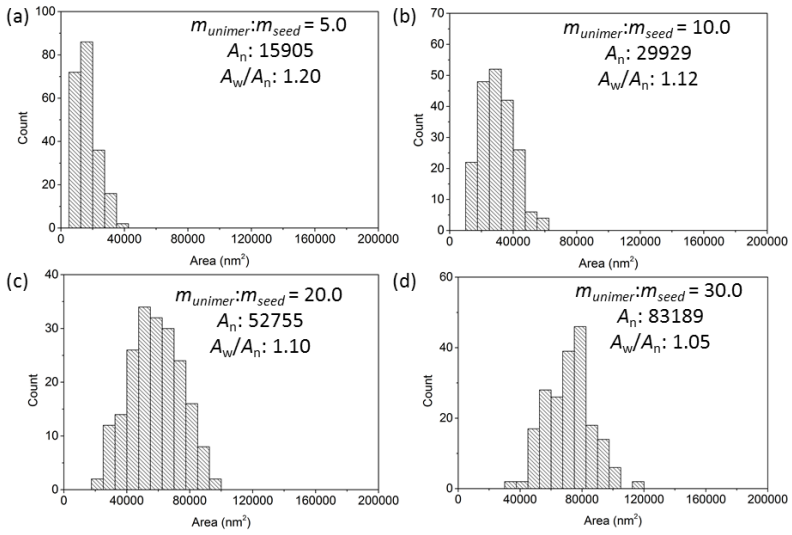

Figure S4.17. Contour length histogram of samples of uniform 2D platelet $PLLA_{47}$-*b*-$PNIPAm_{267}$ micelles prepared by addition of unimers ($PLLA_{26}$/$PLLA_{47}$-*b*-$PNIPAm_{267}$ blend, 10 mg/mL in DMSO) with m_{unimer}:m_{seed} of (a) 5.0, (b) 10.0, (c) 20.0 and (d) 30.0 to the 1D seed micelles (PEG_{45}-*b*-$PLLA_{23}$ micelles) in TFE/EtOH with volume ratios of (a) 5:95, (b) 5:95, (c) 10:90 and (d) 15:85, respectively.

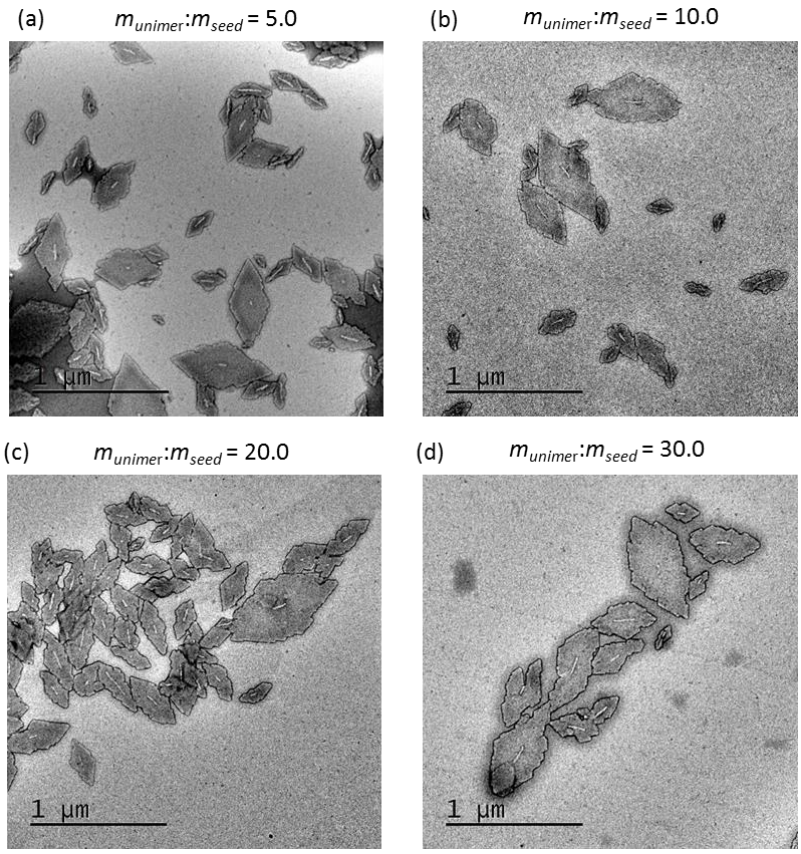

Figure S4.18. TEM images of samples of 2D platelet micelles prepared by seeded growth from 1D seed micelles (PEG_{45}-*b*-$PLLA_{23}$ micelles) in EtOH with unimers ($PLLA_{26}$/$PLLA_{47}$-*b*-$PNIPAm_{267}$ blend, 10 mg/mL in DMSO) of unimer-to-seed mass ratios of (a)5.0, (b) 10.0, (c) 20.0 and (d) 30.0, respectively.

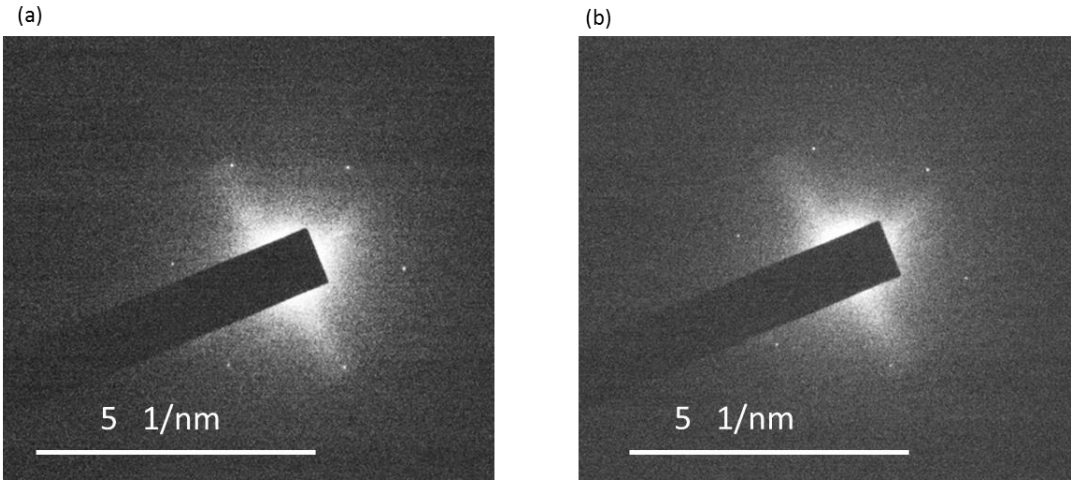

Figure S4.19. SAED patterns of platelet micelles with (a) 2D seed and (b) 1D seed.

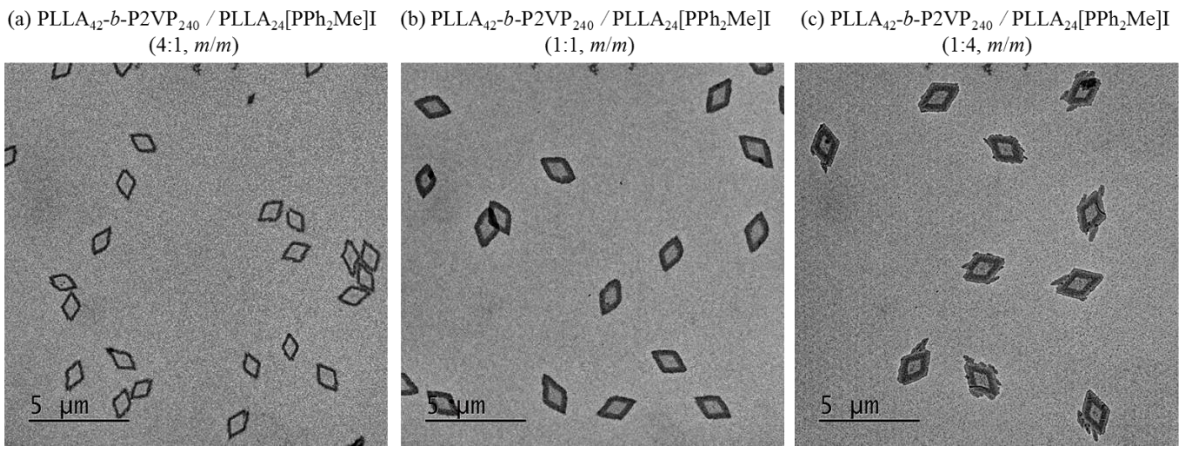

Figure S4.20. Effect of blend mass ratio of $PLLA_{42}$-*b*-$P2VP_{464}$ / $PLLA_{24}[PPh_2Me]I$ on the seeded growth. The samples for TEM were not stained.

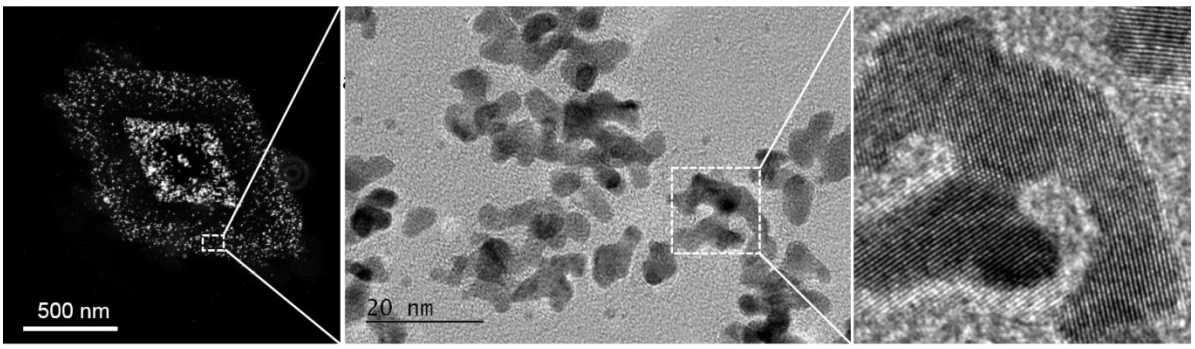

Figure S4.21. High-resolution TEM image of Pt nanoparticles on the surface of crosslinked platelet comicelles.

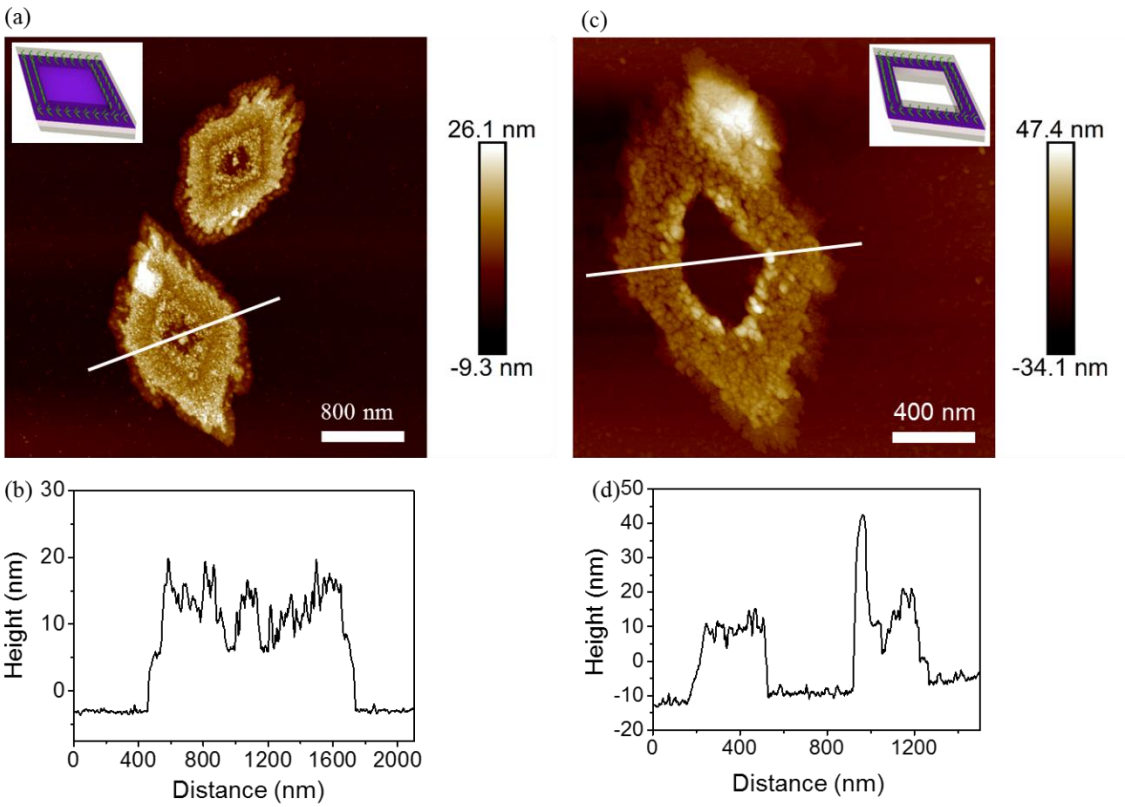

Figure S4.22. AFM images (a,b) and their height profiles (b,d) of platelet comicelles crosslinked with Karstedt's catalyst (a,c) and hollow micelles (b,d).

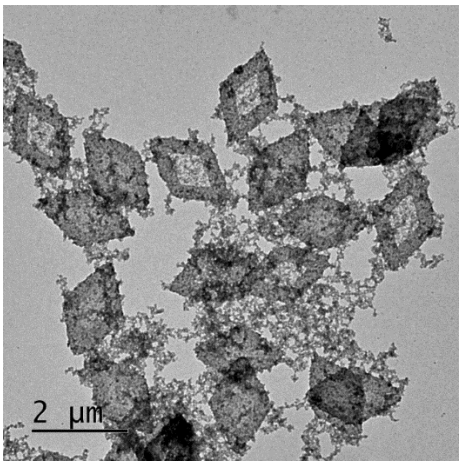

Figure S4.23. TEM image of platelet block comicelles crosslinked by Karstedt's catalyst and 1,1,3,3-tetramethyldisiloxane (TMDS). The sample for TEM was not stained.

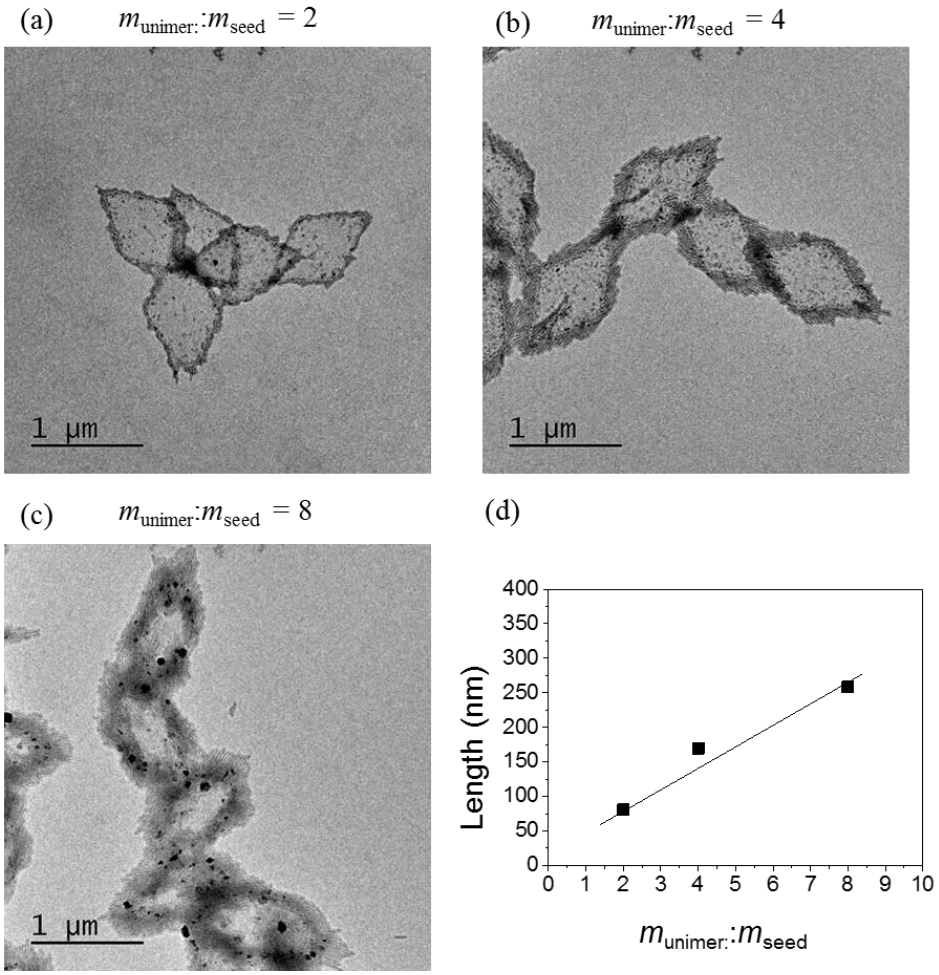

Figure S4.24. (a-c) TEM images of diamond fibre-like hybrid structures with different fibre lengths, prepared by addition of $PLLA_{20}$-*b*-$PAGE_{80}$ unimer in THF to diamond-shaped platelet of $PLLA_{24}[PPh_2Me]I$ in *i*-PrOH. (d) linear dependence of length of $PLLA_{20}$-*b*-$PAGE_{80}$ fibres on the m_{unimer}:m_{seed}. The samples for TEM were not stained. The black spot in TEM images was probably formation of spherical $PLLA_{20}$-*b*-$PAGE_{80}$ micelles. The reason is probably due to that severe aggregation of $PLLA_{20}$-*b*-$PAGE_{80}$ fibres inhibits the active site for further initiating the unimer efficiently.

Table S4.1. Contour area data for 2D diamond-shaped platelet micelles prepared by the seeded growth of unimers of a $PLLA_{24}[PPh_2Me]I/PLLA_{42}$-*b*-$P2VP_{464}$ blend (1:1, mass ratio) in $CHCl_3$ from *quasi*-1D seeds (L_n = 200 nm, L_w/L_n = 1.09) of $PLLA_{24}[PPh_2Me]I$ in *i*-PrOH at 23 °C.*

	$m_{unimer}:m_{seed}$			
	20	**40**	**60**	**80**
A_n (nm^2)	351,860	674,350	942,390	1,220,500
A_w (nm^2)	358,040	381,580	949,930	1,229,830
A_w / A_n	1.02	1.01	1.01	1.01
σ / A_n	0.13	0.10	0.90	0.09

* As measured from TEM micrographs of a minimum of 200 platelets. σ, standard deviation of measured areas.

Chapter 5 **Summary and Future Work**

In general, the aim of the work demonstrated in this thesis is to expand the living crystallization-driven self-assembly (CDSA) approaches to the biorelevant crystallizable organic polymer, poly(*L*-lactide) (PLLA). The investigations focus on preparing one- and two-dimensional (1D and 2D) morphologies of PLLA micelles and controlling the dimensions. The work in the thesis also provide a foundation for future studies on the applications of uniform fibre-like micelles prepared by living CDSA in biomedicine. This was achieved by studying the cellular uptake and aqueous solution behaviour of uniform fibre-like micelles composed of poly(ferrocenyldimethylsilane) (PFS)- or polyfluorene (PF)-based BCPs. In this chapter, future research directions related to this thesis have been outlined based on the results achieved.

5.1. Controlled Epitaxial Growth of 1D Fibre-like Micelles in Aqueous Media via Living CDSA

Chapter 2 presents the self-assembly behaviour of PFS-based BCPs directly in aqueous media. A variety of BCPs with different block ratios of PFS core-forming block and a hydrophilic bottle-brush polymer corona-forming block were prepared. Direct self-assembly of these BCPs in aqueous media was carried out and colloidally stable fibre-like micelles in H_2O were achieved with BCPs possessing suitable core-corona block ratios. The results suggest the core chain length is important for fibre-formation in H_2O. Self-assembly of BCPs containing long PFS chains leads to macroscopic precipitation while no self-assembled structures were attained with BCPs containing short PFS chains.

In addition, seeded-growth of prepared PFS-based BCPs were attempted directly in H_2O. Seed micelles were not accessible via the usual method of sonication,[92, 158] perhaps because they possess low crystallinity. However, the seed micelles could be prepared by sonication of the polydisperse fibres formed in organic solvents and transferred into H_2O by dialysis. After adding unimers to seed micelles in H_2O, both short micelles (micelle length either shorter or similar to the seed length) and elongated

polydisperse fibre-like micelles were detected. Strategies involving the use of more common solvent (THF) and raising the temperature to address the uncontrolled micelle growth issue were not successful. Moreover, seeded-growth of PFS BCPs was explored in a mixture of H_2O/organic solvents with various compositions. However, the results demonstrated that micelle growth became less controlled with the presence of even a small amount of H_2O (10%). Thus far, no uniform 1D fibre-like micelles of PFS-based BCPs have been achieved directly in H_2O by living CDSA.

We conclude that as a result of the hydrophobicity of PFS, which results in spontaneous aggregation of the PFS chains which then undergo self-nucleation to form new nuclei. Future work on direct living CDSA in aqueous media should focus on other crystallizable core forming blocks, which are more hydrophilic than PFS, such as polyesters and polycarbonates. It has been very recently shown that PCL-based diblock copolymers successfully undergo living CDSA directly in H_2O.[166]

5.2. Towards Biomedical Applications of Uniform 1D Fibre-like Micelles

Chapter 2 demonstrated the preliminary results of cellular uptake studies with uniform 1D fibre-like micelles with cores of PFS and PF. For these uniform fibre-like micelles, a variety of water-soluble polymers were employed as corona-forming blocks. Due to the difficulty in preparing micelles directly in H_2O, uniform fibre-like micelles were prepared in organic solvents and transferred into H_2O by dialysis.

Studies on cellular uptake of PFS-based micelles initially started with charge neutral micelles modified with fluorescent groups. Cellular uptake results showed limited number of micelles in the cells, which was suggested to be caused by the aggregation of these micelles in cell media. Charge-terminated B-A-B triblock co-micelles of PFS were prepared to address the aggregation issue (A: charge neutral segment; B: positively charged segments).[217] Successful cellular uptake of charged block co-micelles with a high concentration (250 μg/mL) were achieved, but cytotoxicity was also observed. The cytotoxicity was attributed to either the high concentration of charge or the intrinsic non-biocompatibility of PFS.

PFS B-A-B micelle structures were optimized by introducing different amounts of charge to the corona (varying the length of B). The resulting micelles showed a total length ca. 150 nm with varied charge segment length fractions (b = ca. 5%, 10%, 25% and 50%). Cellular uptake results were positive for micelles with b = 25%, while micelles with other x values were not found in the cells. Aggregation studies demonstrated that samples with b = 10 and 25% exhibited dispersion in both H_2O. With the presence of positive charge, micelles were supposed to disperse well in H_2O due to the repulsion among charges. But the micelles with b = 50% were found to aggregate heavily, for reasons that are currently under investigation. In addition, micelles were found to aggregate more exensively in cell media than in H_2O, and this might be the result of interactions between the positively charged fibre-like micelles and the negatively charged species in cell media. Furthermore, with the micelles of b = 25%, the cellular uptake was found to be concentration dependent with higher concentration exhibiting faster cellular uptake.

Poly(*N*-isopropylacrylamide) (PNIPAm) and poly(ethylene glycol) (PEG) were employed as corona-forming blocks in order to obtain water-soluble PFS micelles. B-A-B triblock comicelles were successfully prepared in organic solvents with both corona blocks. When transferring into H_2O, fragmentation of the micelles with PNIPAm was observed. Swelling of the corona was suggested as a reason for fragmentation, as observed in PCL-containing BCPs.[305] However, a reported fragmentation of PFS-*b*-PNIPAm micelles in mixture of H_2O/*i*-PrOH was suggested not to be caused by corona swelling, as the cononsolvency effect that the solvation of PINIPAm in the mixture was poorer than that in pure solvent individually (in H_2O or in *i*-PrOH).[306] The fragmentation is under investigation. In addition to the micelles with PEG as corona-forming block, the macroscopic precipitation of the micelles was observed. The short PEG chain was proposed as a reason for the precipitation.

PF-based uniform 1D fibre-like micelles were prepared with a PEG corona-forming block. The preliminary cellular uptake results showed that the micelles were on the cell surface rather than in the cells. Functionalization of the micelles were carried out with a fluorescent dye and folic acid (FA) to facilitate the cellular uptake.[285] Aggregation studies demonstrated that FA-functionalized micelles were

well-dispersed in both H_2O and cell media, while the dye-functionalized micelles aggregated significantly in cell media. Cellular uptake studies of PF-based micelles constitute ongoing work.

We concluded that with appropriate design of micelle structures and surface functionalization, successful cellular uptake would be achieved with these uniform 1D fibre-like micelles. Future work with these charged triblock co-micelles will look at elucidating the relationship between the amount of charge and the cellular uptake behaviour. To address issues with fragmentation, the effect of hydrophilic corona-forming polymers with different swelling behaviour in H_2O will be studied. In addition, dialysis in PBS buffers, other than H_2O, may prevent the fragmentation by reducing the corona swelling with salts. Cytotoxicity studies of these fibres will be carried out to examine the potential for future biological applications.

For PFS-based micelles, 2D platelets could be employed biological tests. These 2D micelles possess a high aspect ratio, which might potentially enhance the anti-tumour effects, such as deep cell penetration and enhanced cell adhesion. With the higher surface area of these 2D micelles, the enhanced cargo loading capability could be achieved, since cargos are normally loaded on the corona-forming block to minimise the interference with the core crystallisation. For PF-based micelles, cellular uptake tests will be conducted and multi-functional (multi-fluorescent, active targeting, and pH-responsive) uniform 1D fibre-like micelles will be prepared.

5.3. Extension of Living CDSA to PLLA

Chapter 3 and **Chapter 4** presents the living CDSA of homopolymers and BCPs containing and a crystallizable biodegradable and biocompatible PLLA core-forming block. In **Chapter 3,** PLLA-*b*-PNIPAm was prepared and used as the main polymer for self-assembly studies. The initial seeded-growth results showed an uncontrolled micelle growth which can be attributed to the spontaneous aggregation of the added unimer, which then undergoes self-nucleation, competing with the epitaxial growth from the pre-existing seeds in solution. With the addition of a certain portion (typically 5 - 10%) of solvent additives, uniform fibre-like micelles with controlled length and narrow length distributions

were attainable. These solvent additives behaved as common solvents which improved the PLLA solvation in solution, and probably also as H-bonding disruption agents, which would hinder the formation of intermolecular H-bonding interactions among the PLLA chains. Both of these factors could prevent the fast aggregation and subsequent self-nucleation of PLLA. This strategy has been successfully transferred to PLLA-*b*-P2VP BCPs to afford uniform fibre-like micelles via controlled micelle growth using the living CDSA.

In Chapter 4, a small positively charged-terminated phosphine group was used to replace a bulky polymer as the corona-forming block. This charged group offers less steric repulsion and the sufficient solvation in polar solvents, affording uniform 2D diamond-shaped platelet micelles of PLLA charged homopolymers. With the blend of diblock copolymer with either charged or charge-neutral homopolymers, uniform 2D platelet micelles, spatial segmented 2D platelet micelles and complex platelet scarf-like micelles were prepared with controlled dimensions.

Based on the results of controlled PLLA 1D fibre-like micelles in **Chapter 3** and studies on PFS micelles in aqueous media in **Chapter 2**, the future work will be focused on preparation of uniform water-soluble PLLA-based micelles for biomedical applications. Different hydrophilic polymers could be employed as corona-forming blocks for water-soluble PLLA fibre-like micelles, such as thermoresponsive poly(N,N-dimethylaminoethyl methacrylate) (PDMAEMA) and pH-responsive poly(acrylic acid) (PAA). In addition, the degradation of PLLA has been widely studied as bulk materials under various conditions.[434-437] Less study has been reported on the degradation of uniform PLLA-based micelles. It is important to understand the degradation rate and behavior of PLLA micelles under physical conditions to further rational design as drug delivery vectors.

Living CDSA has been shown to successfully fabricate 1D and 2D nanostructures with dimensional control with various crystalline polymers.[139, 140, 148, 156, 158, 175] PLLA and poly(*D*-lactide) (PDLA) have been reported to form crystalline spherical micelles, which is derived from the formation of a stereocomplex.[111, 438] In hence, living CDSA has the potential to fabricate crystalline spherical micelles composed of a PLLA/PDLA stereocomplex (Figure 5.1), to achieve nanostructure control in zero-

dimensions (0D) (crystalline spherical micelles). As previously reported,[139] sonication may fragment the crystalline spherical micelles to expose active surface for further epitaxial growth. The size of the grown spherical micelle might be limited by the core block length, but the morphology transition may occur to afford novel morphologies as in the case of BCPs with amorphous core.[63, 439]

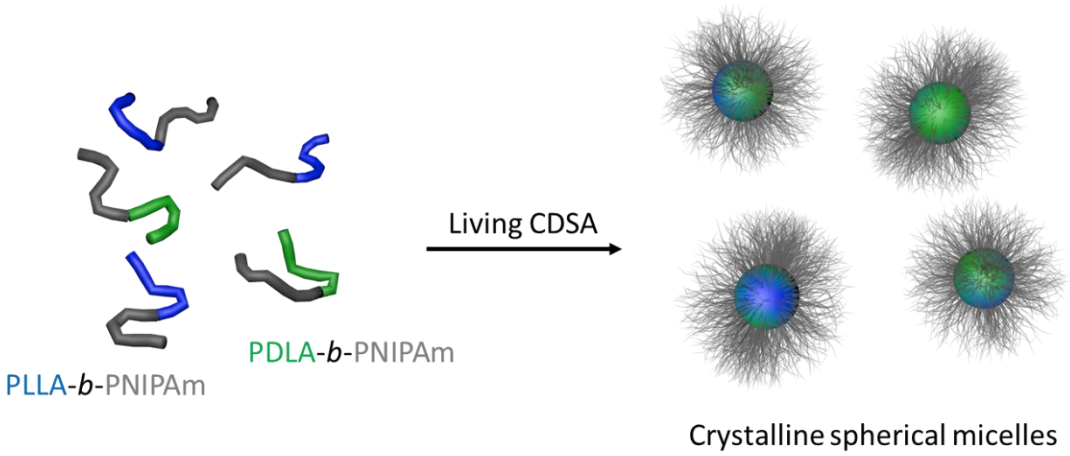

Figure 5.1. Schematic representation of preparation of uniform polymeric micelles in 0D by stereocomplexation of PLLA and PDLA.

5.4. Complex Nanostructures and Applications of PLLA-based Material

Chapter 3 has described the preparation of spatially segmented 1D fibre-like penta-block co-micelles by living CDSA with PLLA-*b*-PNIPAm and PLLA-*b*-P2VP BCPs. **Chapter 4** has presented the preparation of complex and hierarchical 2D platelet micelles with varied structures and functions. By blending of homopolymer and diblock copolymer with different functional corona-forming blocks, cross-linkable platelets, hollow platelets and multi-segmented block-coplatelets could be achieved. By sequentially adding homopolymer and diblock copolymer to the seed micelles, diamond-fibre hybrid micelles could be achieved. These uniform 2D platelets have also been used as templates for inorganic nanoparticles.

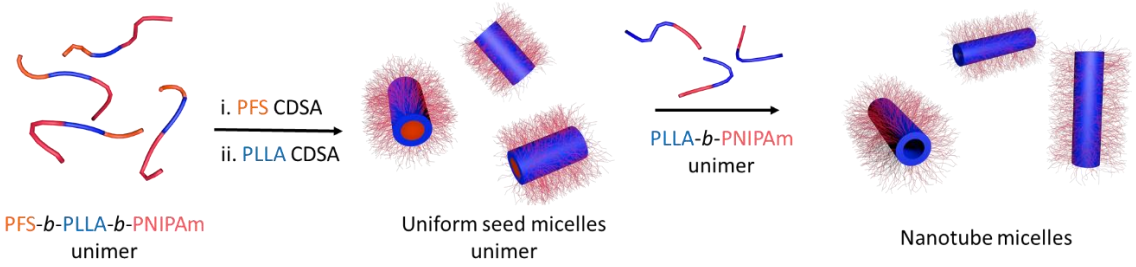

Figure 5.2. Schematic representation of fabrication of nanotube structures via living CDSA of a triblock copolymer containing two crystallizable core-forming blocks.

Future works on the preparation of complex structures will look at BCPs containing two crystallizable core-forming blocks, such as PFS-*b*-PLLA-*b*-corona. Due to the different solvation behaviour, a two-step crystallization strategy could be employed to give rise to complex structures by varying solvent conditions, such as nanotube structures (Figure 5.2) and higher ordered supermicelles (Figure 5.3a). The nanotube structure could be potentially used in selectively trapping ions or particles in solution, since the inner diameter of the tube could be adjusted by varying the PFS block length. The complex supermicelles have the potential to be templates for particles or construct complex patterns for lithography.

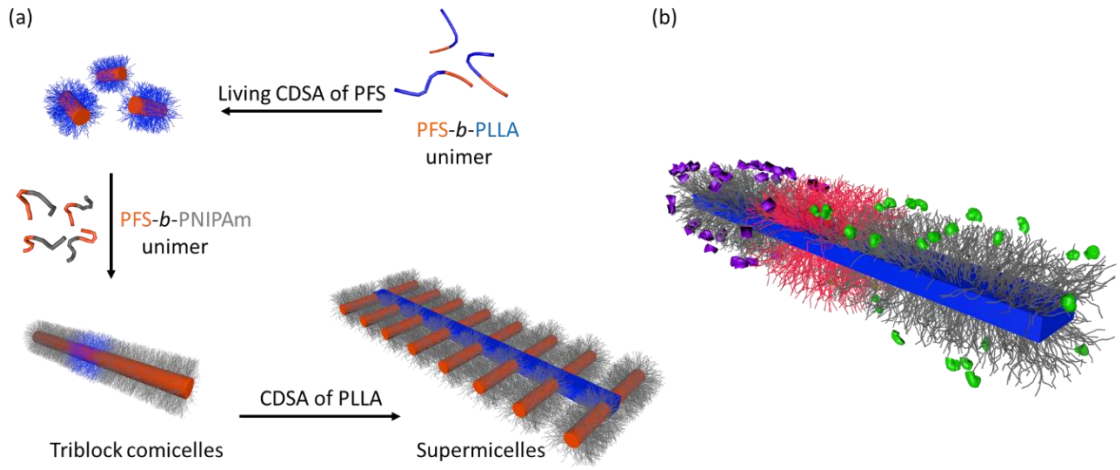

Figure 5.3. Schematic representation of (a) fabrication of supermicelles via two crystallization steps and (b) spatially functional 1D firbe-like micelles.

The preparation of functional micelles by introducing functional groups into BCPs can also be investigated further. With the preparation of spatially segmented micelles (such as the penta-block co-

micelles), different functional groups such as catalysts, enzymes and light-responsive molecules can be loaded into different segments to afford a multi-functional micelle (Figure 5.3b). Due to the biocompatibility of PLLA, these micelles could be used as biocatalysts in cellular environment. Reactions catalysed by enzymes are highly selective and efficient,[440-442] but the requirement of aqueous media limits the types of applicable starting materials. The designed multi-functional PLLA micelles could bring different species into aqueous media to contact with enzymes, which may result in products containing new bonding arrangements or highly selectivity under mild conditions.

References

1. Stupp, S. I., *Chemical Reviews* **2005,** *105*, 1023.
2. Blanco, E.; Shen, H.; Ferrari, M., *Nat Biotechnol* **2015,** *33*, 941.
3. Lu, W.; Lieber, C. M., *Nat Mater* **2007,** *6*, 841.
4. Liu, Y.; Mai, S.; Li, N.; Yiu, C. K.; Mao, J.; Pashley, D. H.; Tay, F. R., *Acta Biomater* **2011,** *7*, 1742.
5. Wallraff, G. M.; Hinsberg, W. D., *Chemical Reviews* **1999,** *99*, 1801.
6. Saifullah, M. S. M.; Subramanian, K. R. V.; Tapley, E.; Kang, D.-J.; Welland, M. E.; Butler, M., *Nano Letters* **2003,** *3*, 1587.
7. Grigorescu, A. E.; Hagen, C. W., *Nanotechnology* **2009,** *20*, 292001.
8. Lutz, J. F.; Ouchi, M.; Liu, D. R.; Sawamoto, M., *Science* **2013,** *341*, 1238149.
9. Whitesides, G. M.; Grzybowski, B., *Science* **2002,** *295*, 2418.
10. Lehn, J. M., *Science* **2002,** *295*, 2400.
11. Thorkelsson, K.; Bai, P.; Xu, T., *Nano Today* **2015,** *10*, 48.
12. Xu, Z.; Wang, L.; Fang, F.; Fu, Y.; Yin, Z., *Current Nanoscience* **2016,** *12*, 725.
13. Kortaberria, G., Nanostructured Morphologies by Self-Assembly of Diblock Copolymers: A Review. In *Molecular Self-assembly in Nanoscience and Nanotechnology*, 2017.
14. Chen, P.-Y.; McKittrick, J.; Meyers, M. A., *Progress in Materials Science* **2012,** *57*, 1492.
15. Liu, Z.; Meyers, M. A.; Zhang, Z.; Ritchie, R. O., *Progress in Materials Science* **2017,** *88*, 467.
16. Alberts, B.; Wilson, J.; Hunt, T., *Molecular biology of the cell. Reference edition*. 5th ed.; Garland Science: Abingdon, 2008.
17. Fratzl, P.; Weinkamer, R., *Progress in Materials Science* **2007,** *52*, 1263.
18. Lakes, R., *Nature* **1993,** *361*, 511.
19. Bhushan, B., *Philos Trans A Math Phys Eng Sci* **2009,** *367*, 1445.
20. Philp, D.; Stoddart, J. F., *Angewandte Chemie International Edition in English* **1996,** *35*, 1154.
21. Chen, Q.; Pugno, N. M., *J Mech Behav Biomed Mater* **2013,** *19*, 3.
22. Steed, J. W.; Turner, D. R.; Wallace, K. J., *Core concepts in supramolecular chemistry and nanochemistry*. John Wiley: Chichester, England ; Hoboken, NJ, 2007.
23. Hoeben, F. J.; Jonkheijm, P.; Meijer, E. W.; Schenning, A. P., *Chem Rev* **2005,** *105*, 1491.
24. Grzybowski, B. A.; Wilmer, C. E.; Kim, J.; Browne, K. P.; Bishop, K. J. M., *Soft Matter* **2009,** *5*.
25. Mendes, A. C.; Baran, E. T.; Reis, R. L.; Azevedo, H. S., *Wiley Interdiscip Rev Nanomed Nanobiotechnol* **2013,** *5*, 582.
26. Wahl, M., *Trends in Biochemical Sciences* **1997,** *22*, 97.
27. Zhu, Y.; Liu, L.; Du, J., *Macromolecules* **2012,** *46*, 194.
28. Sijbesma, R. P.; Meijer, E. W., *Current Opinion in Colloid & Interface Science* **1999,** *4*, 24.
29. Berg, J. M.; Tymoczko, J. L.; Stryer, L., *Biochemistry*. 5th ed ed.; W.H. Freeman: New York, 2002.
30. Brodsky, B.; Persikov, A. V., *Fibrous Proteins: Coiled-Coils, Collagen and Elastomers* **2005,** *70*, 301.
31. Berisio, R.; Vitagliano, L.; Mazzarella, L.; Zagari, A., *Protein Sci* **2002,** *11*, 262.
32. Bhattacharjee, A.; Bansal, M., *IUBMB Life* **2005,** *57*, 161.
33. Bella, J.; Berman, H. M., *J Mol Biol* **1996,** *264*, 734.
34. Klug, A., *Philos Trans R Soc Lond B Biol Sci* **1999,** *354*, 531.
35. Kegel, W. K.; van der Schoot, P., *Biophys J* **2006,** *91*, 1501.
36. Durham, A. C. H.; Klug, A., *Nature New Biology* **1971,** *229*, 42.
37. Haffner, H.; Appel, H.; Holmes, K. C., *European Biophysics Journal* **1986,** *14*.
38. Mai, Y.; Eisenberg, A., *Chem Soc Rev* **2012,** *41*, 5969.

39. Epps, I. I. I. T. H.; O'Reilly, R. K., *Chemical Science* **2016,** *7*, 1674.
40. Hamley, I. W., *The physics of block copolymers*. Oxford University Press: Oxford, 1998.
41. Bates, F. S.; Fredrickson, G. H., *Physics Today* **1999,** *52*, 32.
42. Nuyken, O.; Pask, S., *Polymers* **2013,** *5*, 361.
43. Benoit, D.; Chaplinski, V.; Braslau, R.; Hawker, C. J., *Journal of the American Chemical Society* **1999,** *121*, 3904.
44. Braunecker, W. A.; Matyjaszewski, K., *Progress in Polymer Science* **2007,** *32*, 93.
45. Schacher, F. H.; Rupar, P. A.; Manners, I., *Angew Chem Int Ed Engl* **2012,** *51*, 7898.
46. Brendel, J. C.; Schacher, F. H., *Chem Asian J* **2018,** *13*, 230.
47. Bates, F. S., *Science* **1991,** *251*, 898.
48. Bates, F. S.; Hillmyer, M. A.; Lodge, T. P.; Bates, C. M.; Delaney, K. T.; Fredrickson, G. H., *Science* **2012,** *336*, 434.
49. Förster, S.; Plantenberg, T., *Angewandte Chemie International Edition* **2002,** *41*.
50. Guo, Z.; Zhang, G.; Qiu, F.; Zhang, H.; Yang, Y.; Shi, A. C., *Phys Rev Lett* **2008,** *101*, 028301.
51. Lim, E. K.; Kim, T.; Paik, S.; Haam, S.; Huh, Y. M.; Lee, K., *Chem Rev* **2015,** *115*, 327.
52. Feng, H.; Lu, X.; Wang, W.; Kang, N.-G.; Mays, J., *Polymers* **2017,** *9*.
53. Matsen, M. W.; Schick, M., *Phys Rev Lett* **1994,** *72*, 2660.
54. Castelletto, V.; Hamley, I. W., *Current Opinion in Solid State and Materials Science* **2004,** *8*, 426.
55. Zheng, W.; Wang, Z.-G., *Macromolecules* **1995,** *28*, 7215.
56. Tang, P.; Qiu, F.; Zhang, H.; Yang, Y., *Phys Rev E Stat Nonlin Soft Matter Phys* **2004,** *69*, 031803.
57. Hadjichristidis, N.; Iatrou, H.; Pitsikalis, M.; Pispas, S.; Avgeropoulos, A., *Progress in Polymer Science* **2005,** *30*, 725.
58. DeRouchey, J.; Thurn-Albrecht, T.; Russell, T. P.; Kolb, R., *Macromolecules* **2004,** *37*, 2538.
59. Honeker, C. C.; Thomas, E. L., *Chemistry of Materials* **1996,** *8*, 1702.
60. Hamley, I. W., *Progress in Polymer Science* **2009,** *34*, 1161.
61. Albert, J. N. L.; Epps, T. H., *Materials Today* **2010,** *13*, 24.
62. Cameron, N. S.; Corbierre, M. K.; Eisenberg, A., *Canadian Journal of Chemistry-Revue Canadienne De Chimie* **1999,** *77*, 1311.
63. Zhang, L.; Eisenberg, A., *Science* **1995,** *268*, 1728.
64. Zhang, L.; Yu, K.; Eisenberg, A., *Science* **1996,** *272*, 1777.
65. Zhang, L.; Eisenberg, A., *Journal of the American Chemical Society* **1996,** *118*, 3168.
66. Zhang, L. F.; Eisenberg, A., *Polymers for Advanced Technologies* **1998,** *9*, 677.
67. Cui, H.; Chen, Z.; Zhong, S.; Wooley, K. L.; Pochan, D. J., *Science* **2007,** *317*, 647.
68. Zhong, S.; Cui, H.; Chen, Z.; Wooley, K. L.; Pochan, D. J., *Soft Matter* **2008,** *4*, 90.
69. Hayward, R. C.; Pochan, D. J., *Macromolecules* **2010,** *43*, 3577.
70. Tritschler, U.; Pearce, S.; Gwyther, J.; Whittell, G. R.; Manners, I., *Macromolecules* **2017,** *50*, 3439.
71. Riess, G., *Progress in Polymer Science* **2003,** *28*, 1107.
72. Nyrkova, I. A.; Semenov, A. N., *Faraday Discuss.* **2005,** *128*, 113.
73. Israelachvili, J. N.; Mitchell, D. J.; Ninham, B. W., *Biochimica et Biophysica Acta (BBA) - Biomembranes* **1977,** *470*, 185.
74. Nagarajan, R., *Langmuir* **2002,** *18*, 31.
75. Lee, Y. S., *Self-assembly and nanotechnology : a force balance approach*. John Wiley & Sons: Hoboken, N.J., 2008.
76. Doncom, K. E. B.; Blackman, L. D.; Wright, D. B.; Gibson, M. I.; O'Reilly, R. K., *Chem Soc Rev* **2017,** *46*, 4119.
77. Zhang, L.; Eisenberg, A., *Macromolecules* **1999,** *32*, 2239.
78. Jain, S.; Bates, F. S., *Macromolecules* **2004,** *37*, 1511.

79. Dionzou, M.; Morere, A.; Roux, C.; Lonetti, B.; Marty, J. D.; Mingotaud, C.; Joseph, P.; Goudouneche, D.; Payre, B.; Leonetti, M.; Mingotaud, A. F., *Soft Matter* **2016,** *12*, 2166.
80. Zhang, L. F.; Eisenberg, A., *Abstracts of Papers of the American Chemical Society* **1998,** *216*, U18.
81. Kelley, E. G.; Albert, J. N.; Sullivan, M. O.; Epps, T. H., 3rd, *Chem Soc Rev* **2013,** *42*, 7057.
82. Welch, M. E.; Ober, C. K., *Journal of Polymer Science Part B: Polymer Physics* **2013,** *51*, 1457.
83. Lu, A.; O'Reilly, R. K., *Curr Opin Biotechnol* **2013,** *24*, 639.
84. Blanazs, A.; Madsen, J.; Battaglia, G.; Ryan, A. J.; Armes, S. P., *J Am Chem Soc* **2011,** *133*, 16581.
85. Charleux, B.; Delaittre, G.; Rieger, J.; D'Agosto, F., *Macromolecules* **2012,** *45*, 6753.
86. Canning, S. L.; Smith, G. N.; Armes, S. P., *Macromolecules* **2016,** *49*, 1985.
87. Warren, N. J.; Armes, S. P., *J Am Chem Soc* **2014,** *136*, 10174.
88. Groschel, A. H.; Schacher, F. H.; Schmalz, H.; Borisov, O. V.; Zhulina, E. B.; Walther, A.; Muller, A. H., *Nat Commun* **2012,** *3*, 710.
89. Groschel, A. H.; Muller, A. H., *Nanoscale* **2015,** *7*, 11841.
90. Lobling, T. I.; Borisov, O.; Haataja, J. S.; Ikkala, O.; Groschel, A. H.; Muller, A. H., *Nat Commun* **2016,** *7*, 12097.
91. Jain, S.; Bates, F. S., *Science* **2003,** *300*, 460.
92. Hailes, R. L.; Oliver, A. M.; Gwyther, J.; Whittell, G. R.; Manners, I., *Chem Soc Rev* **2016,** *45*, 5358.
93. Vilgis, T.; Halperin, A., *Macromolecules* **1991,** *24*, 2090.
94. Crassous, J. J.; Schurtenberger, P.; Ballauff, M.; Mihut, A. M., *Polymer* **2015,** *62*, A1.
95. Massey, J.; Power, K. N.; Manners, I.; Winnik, M. A., *Journal of the American Chemical Society* **1998,** *120*, 9533.
96. Massey, J. A.; Temple, K.; Cao, L.; Rharbi, Y.; Raez, J.; Winnik, M. A.; Manners, I., *Journal of the American Chemical Society* **2000,** *122*, 11577.
97. Cao, L.; Manners, I.; Winnik, M. A., *Macromolecules* **2002,** *35*, 8258.
98. Wang, X. S.; Winnik, M. A.; Manners, I., *Macromolecules* **2002,** *35*, 9146.
99. Guérin, G.; Raez, J.; Manners, I.; Winnik, M. A., *Macromolecules* **2005,** *38*, 7819.
100. Schmelz, J.; Karg, M.; Hellweg, T.; Schmalz, H., *ACS Nano* **2011,** *5*, 9523.
101. Yin, L. G.; Hillmyer, M. A., *Macromolecules* **2011,** *44*, 3021.
102. Yin, L.; Lodge, T. P.; Hillmyer, M. A., *Macromolecules* **2012,** *45*, 9460.
103. Schöbel, J.; Karg, M.; Rosenbach, D.; Krauss, G.; Greiner, A.; Schmalz, H., *Macromolecules* **2016,** *49*, 2761.
104. Schobel, J.; Burgard, M.; Hils, C.; Dersch, R.; Dulle, M.; Volk, K.; Karg, M.; Greiner, A.; Schmalz, H., *Angewandte Chemie-International Edition* **2017,** *56*, 405.
105. Du, Z.-X.; Xu, J.-T.; Fan, Z.-Q., *Macromolecules* **2007,** *40*, 7633.
106. He, W.-N.; Zhou, B.; Xu, J.-T.; Du, B.-Y.; Fan, Z.-Q., *Macromolecules* **2012,** *45*, 9768.
107. Wang, J.; Zhu, W.; Peng, B.; Chen, Y., *Polymer* **2013,** *54*, 6760.
108. Rizis, G.; van de Ven, T. G.; Eisenberg, A., *Angew Chem Int Ed Engl* **2014,** *53*, 9000.
109. Wang, X. Y.; Wang, R. Y.; Fan, B.; Xu, J. T.; Du, B. Y.; Fan, Z. Q., *Macromolecules* **2018,** *51*, 2138.
110. Fujiwara, T.; Miyamoto, M.; Kimura, Y.; Iwata, T.; Doi, Y., *Macromolecules* **2001,** *34*, 4043.
111. Sun, L.; Pitto-Barry, A.; Kirby, N.; Schiller, T. L.; Sanchez, A. M.; Dyson, M. A.; Sloan, J.; Wilson, N. R.; O'Reilly, R. K.; Dove, A. P., *Nat Commun* **2014,** *5*, 5746.
112. Pitto-Barry, A.; Kirby, N.; Dove, A. P.; O'Reilly, R. K., *Polym. Chem.* **2014,** *5*, 1427.
113. Yu, W.; Inam, M.; Jones, J. R.; Dove, A. P.; O'Reilly, R. K., *Polymer Chemistry* **2017,** *8*, 5504.
114. Song, Y.; Chen, Y. C.; Su, L.; Li, R. C.; Letteri, R. A.; Wooley, K. L., *Polymer* **2017,** *122*, 270.
115. Venkataraman, S.; Hedrick, J. L.; Yang, Y. Y., *Polym. Chem.* **2014,** *5*, 2035.

116. Vora, A.; Wojtecki, R. J.; Schmidt, K.; Chunder, A.; Cheng, J. Y.; Nelson, A.; Sanders, D. P., *Polymer Chemistry* **2016,** *7*, 940.
117. Lee, E.; Hammer, B.; Kim, J. K.; Page, Z.; Emrick, T.; Hayward, R. C., *Journal of the American Chemical Society* **2011,** *133*, 10390.
118. Kim, Y. J.; Cho, C. H.; Paek, K.; Jo, M.; Park, M. K.; Lee, N. E.; Kim, Y. J.; Kim, B. J.; Lee, E., *Journal of the American Chemical Society* **2014,** *136*, 2767.
119. Kynaston, E. L.; Gould, O. E. C.; Gwyther, J.; Whittell, G. R.; Winnik, M. A.; Manners, I., *Macromolecular Chemistry and Physics* **2015,** *216*, 685.
120. Feng, C.; Gonzalez-Alvarez, M. J.; Song, Y.; Li, I.; Zhao, G.; Molev, G.; Guerin, G.; Walker, G.; Scholes, G. D.; Manners, I.; Winnik, M. A., *Soft Matter* **2014,** *10*, 8875.
121. Han, L.; Wang, M.; Jia, X.; Chen, W.; Qian, H.; He, F., *Nat Commun* **2018,** *9*, 865.
122. Hamley, I. W., Crystallization in Block Copolymers. In *Interfaces Crystallization Viscoelasticity*, Springer Berlin Heidelberg: Berlin, Heidelberg, 1999.
123. Müller, A. J.; Balsamo, V.; Arnal, M. L., Nucleation and Crystallization in Diblock and Triblock Copolymers. In *Block Copolymers II*, 2005.
124. Blundell, D. J.; Keller, A.; Kovacs, A. J., *Journal of Polymer Science Part B: Polymer Letters* **1966,** *4*, 481.
125. John D. Hoffman, G. T. D., John I. Lauritzen. Jr, The Rate of Crystallization of Linear Polymers with Chain Folding. In *Treatise on Solid State Volume 3 Crystalline and Noncrystalline Solids*, Hannay, N. B., Ed. Springer US: US, 1976.
126. Zhang, M. C.; Guo, B. H.; Xu, J., *Crystals* **2017,** *7*.
127. Du, Z.-X.; Xu, J.-T.; Fan, Z.-Q., *Macromolecular Rapid Communications* **2008,** *29*, 467.
128. Mihut, A. M.; Drechsler, M.; Moller, M.; Ballauff, M., *Macromol Rapid Commun* **2010,** *31*, 449.
129. Yin, L. G.; Lodge, T. P.; Hillmyer, M. A., *Macromolecules* **2012,** *45*, 9460.
130. Mihut, A. M.; Crassous, J. J.; Schmalz, H.; Drechsler, M.; Ballauff, M., *Soft Matter* **2012,** *8*.
131. He, W. N.; Xu, J. T.; Du, B. Y.; Fan, Z. Q.; Sun, F. L., *Macromolecular Chemistry and Physics* **2012,** *213*, 952.
132. Raez, J.; Tomba, J. P.; Manners, I.; Winnik, M. A., *Journal of the American Chemical Society* **2003,** *125*, 9546.
133. Halperin, A., *Europhysics Letters* **1989,** *10*, 549.
134. Halperin, A., *Macromolecules* **1991,** *24*, 1418.
135. Vilgis, T.; Halperin, A., *Macromolecules* **1991,** *24*, 2090.
136. Rupar, P. A.; Chabanne, L.; Winnik, M. A.; Manners, I., *Science* **2012,** *337*, 559.
137. Inam, M.; Cambridge, G.; Pitto-Barry, A.; Laker, Z. P. L.; Wilson, N. R.; Mathers, R. T.; Dove, A. P.; O'Reilly, R. K., *Chem Sci* **2017,** *8*, 4223.
138. Hsiao, M.-S.; Yusoff, S. F. M.; Winnik, M. A.; Manners, I., *Macromolecules* **2014,** *47*, 2361.
139. Wang, X.; Guerin, G.; Wang, H.; Wang, Y.; Manners, I.; Winnik, M. A., *Science* **2007,** *317*, 644.
140. Gilroy, J. B.; Gadt, T.; Whittell, G. R.; Chabanne, L.; Mitchels, J. M.; Richardson, R. M.; Winnik, M. A.; Manners, I., *Nat Chem* **2010,** *2*, 566.
141. Guerin, G.; Wang, H.; Manners, I.; Winnik, M. A., *Journal of the American Chemical Society* **2008,** *130*, 14763.
142. Qian, J.; Guerin, G.; Lu, Y.; Cambridge, G.; Manners, I.; Winnik, M. A., *Angew Chem Int Ed Engl* **2011,** *50*, 1622.
143. Qian, J.; Lu, Y.; Chia, A.; Zhang, M.; Rupar, P. A.; Gunari, N.; Walker, G. C.; Cambridge, G.; He, F.; Guerin, G.; Manners, I.; Winnik, M. A., *ACS Nano* **2013,** *7*, 3754.
144. Guerin, G.; Rupar, P. A.; Manners, I.; Winnik, M. A., *Nat Commun* **2018,** *9*, 1158.
145. Whitmore, M. D.; Noolandi, J., *Macromolecules* **1988,** *21*, 1482.
146. Hudson, Z. M.; Lunn, D. J.; Winnik, M. A.; Manners, I., *Nat Commun* **2014,** *5*, 3372.
147. Hudson, Z. M.; Boott, C. E.; Robinson, M. E.; Rupar, P. A.; Winnik, M. A.; Manners, I., *Nat Chem* **2014,** *6*, 893.

148. Qiu, H. B.; Hudson, Z. M.; Winnik, M. A.; Manners, I., *Science* **2015,** *347*, 1329.
149. Gadt, T.; Ieong, N. S.; Cambridge, G.; Winnik, M. A.; Manners, I., *Nat Mater* **2009,** *8*, 144.
150. Cambridge, G.; Guerin, G.; Manners, I.; Winnik, M. A., *Macromolecular Rapid Communications* **2010,** *31*, 934.
151. Xu, J.; Zhou, H.; Yu, Q.; Manners, I.; Winnik, M. A., *J Am Chem Soc* **2018,** *140*, 2619.
152. Finnegan, J. R.; Lunn, D. J.; Gould, O. E.; Hudson, Z. M.; Whittell, G. R.; Winnik, M. A.; Manners, I., *J Am Chem Soc* **2014,** *136*, 13835.
153. Lunn, D. J.; Gould, O. E.; Whittell, G. R.; Armstrong, D. P.; Mineart, K. P.; Winnik, M. A.; Spontak, R. J.; Pringle, P. G.; Manners, I., *Nat Commun* **2016,** *7*, 12371.
154. Gao, Y.; Qiu, H. B.; Zhou, H.; Li, X. Y.; Harniman, R.; Winnik, M. A.; Manners, I., *Journal of the American Chemical Society* **2015,** *137*, 2203.
155. Tao, D.; Feng, C.; Cui, Y.; Yang, X.; Manners, I.; Winnik, M. A.; Huang, X., *J Am Chem Soc* **2017,** *139*, 7136.
156. Qiu, H.; Gao, Y.; Boott, C. E.; Gould, O. E.; Harniman, R. L.; Miles, M. J.; Webb, S. E.; Winnik, M. A.; Manners, I., *Science* **2016,** *352*, 697.
157. He, X.; Hsiao, M. S.; Boott, C. E.; Harniman, R. L.; Nazemi, A.; Li, X.; Winnik, M. A.; Manners, I., *Nat Mater* **2017,** *16*, 481.
158. Qiu, H.; Gao, Y.; Du, V. A.; Harniman, R.; Winnik, M. A.; Manners, I., *J Am Chem Soc* **2015,** *137*, 2375.
159. Li, X.; Gao, Y.; Boott, C. E.; Hayward, D. W.; Harniman, R.; Whittell, G. R.; Richardson, R. M.; Winnik, M. A.; Manners, I., *J Am Chem Soc* **2016,** *138*, 4087.
160. Li, X.; Gao, Y.; Harniman, R.; Winnik, M.; Manners, I., *J Am Chem Soc* **2016,** *138*, 12902.
161. Jia, L.; Zhao, G. Y.; Shi, W. Q.; Coombs, N.; Gourevich, I.; Walker, G. C.; Guerin, G.; Manners, I.; Winnik, M. A., *Nature Communications* **2014,** *5*.
162. Jia, L.; Tong, L.; Liang, Y.; Petretic, A.; Guerin, G.; Manners, I.; Winnik, M. A., *Journal of the American Chemical Society* **2014,** *136*, 16676.
163. Dou, H.; Li, M.; Qiao, Y.; Harniman, R.; Li, X.; Boott, C. E.; Mann, S.; Manners, I., *Nat Commun* **2017,** *8*, 426.
164. Jia, L.; Guerin, G.; Lu, Y.; Yu, Q.; Manners, I.; Winnik, M. A., *Angew Chem Int Ed Engl* **2018,** *57*, 17205.
165. Schmelz, J.; Schedl, A. E.; Steinlein, C.; Manners, I.; Schmalz, H., *J Am Chem Soc* **2012,** *134*, 14217.
166. Arno, M. C.; Inam, M.; Coe, Z.; Cambridge, G.; Macdougall, L. J.; Keogh, R.; Dove, A. P.; O'Reilly, R. K., *J Am Chem Soc* **2017,** *139*, 16980.
167. Finnegan, J. R.; He, X.; Street, S. T. G.; Garcia-Hernandez, J. D.; Hayward, D. W.; Harniman, R. L.; Richardson, R. M.; Whittell, G. R.; Manners, I., *J Am Chem Soc* **2018**.
168. Tuncel, D.; Demir, H. V., *Nanoscale* **2010,** *2*, 484.
169. Braeken, Y.; Cheruku, S.; Ethirajan, A.; Maes, W., *Materials (Basel)* **2017,** *10*.
170. Qian, J.; Li, X.; Lunn, D. J.; Gwyther, J.; Hudson, Z. M.; Kynaston, E.; Rupar, P. A.; Winnik, M. A.; Manners, I., *J Am Chem Soc* **2014,** *136*, 4121.
171. Li, X.; Wolanin, P. J.; MacFarlane, L. R.; Harniman, R. L.; Qian, J.; Gould, O. E. C.; Dane, T. G.; Rudin, J.; Cryan, M. J.; Schmaltz, T.; Frauenrath, H.; Winnik, M. A.; Faul, C. F. J.; Manners, I., *Nat Commun* **2017,** *8*, 15909.
172. Gwyther, J.; Gilroy, J. B.; Rupar, P. A.; Lunn, D. J.; Kynaston, E.; Patra, S. K.; Whittell, G. R.; Winnik, M. A.; Manners, I., *Chemistry* **2013,** *19*, 9186.
173. Patra, S. K.; Ahmed, R.; Whittell, G. R.; Lunn, D. J.; Dunphy, E. L.; Winnik, M. A.; Manners, I., *J Am Chem Soc* **2011,** *133*, 8842.
174. Tao, D.; Feng, C.; Lu, Y.; Cui, Y.; Yang, X.; Manners, I.; Winnik, M. A.; Huang, X., *Macromolecules* **2018,** *51*, 2065.

175. Jin, X. H.; Price, M. B.; Finnegan, J. R.; Boott, C. E.; Richter, J. M.; Rao, A.; Menke, S. M.; Friend, R. H.; Whittell, G. R.; Manners, I., *Science* **2018,** *360*, 897.
176. Lee, S. E.; Bairstow, S. F.; Werling, J. O.; Chaubal, M. V.; Lin, L.; Murphy, M. A.; DiOrio, J. P.; Gass, J.; Rabinow, B.; Wang, X. E.; Zhang, Y.; Yang, Z. J.; Hoffman, R. M., *Pharmaceutical Development and Technology* **2014,** *19*, 438.
177. de, J., *International Journal of Nanomedicine* **2008**.
178. Elsabahy, M.; Wooley, K. L., *Chem Soc Rev* **2012,** *41*, 2545.
179. Mitragotri, S.; Lahann, J., *Adv Mater* **2012,** *24*, 3717.
180. Parveen, S.; Misra, R.; Sahoo, S. K., *Nanomedicine* **2012,** *8*, 147.
181. Miyata, K.; Christie, R. J.; Kataoka, K., *Reactive and Functional Polymers* **2011,** *71*, 227.
182. Mitragotri, S.; Burke, P. A.; Langer, R., *Nat Rev Drug Discov* **2014,** *13*, 655.
183. Wang, Z.; Zhu, W.; Qiu, Y.; Yi, X.; von dem Bussche, A.; Kane, A.; Gao, H.; Koski, K.; Hurt, R., *Chem Soc Rev* **2016,** *45*, 1750.
184. Truong, N. P.; Quinn, J. F.; Whittaker, M. R.; Davis, T. P., *Polymer Chemistry* **2016,** *7*, 4295.
185. Tran, S.; DeGiovanni, P. J.; Piel, B.; Rai, P., *Clin Transl Med* **2017,** *6*, 44.
186. Venkataraman, S.; Hedrick, J. L.; Ong, Z. Y.; Yang, C.; Ee, P. L. R.; Hammond, P. T.; Yang, Y. Y., *Advanced Drug Delivery Reviews* **2011,** *63*, 1228.
187. Oltra, N. S.; Swift, J.; Mahmud, A.; Rajagopal, K.; Loverde, S. M.; Discher, D. E., *Journal of Materials Chemistry B* **2013,** *1*.
188. Oltra, N. S.; Nair, P.; Discher, D. E., *Annual Review of Chemical and Biomolecular Engineering, Vol 5* **2014,** *5*, 281.
189. Truong, N. P.; Whittaker, M. R.; Mak, C. W.; Davis, T. P., *Expert Opin Drug Deliv* **2015,** *12*, 129.
190. Banerjee, A.; Qi, J. P.; Gogoi, R.; Wong, J.; Mitragotri, S., *Journal of Controlled Release* **2016,** *238*, 176.
191. Venkataraman, S.; Hedrick, J. L.; Ong, Z. Y.; Yang, C.; Ee, P. L.; Hammond, P. T.; Yang, Y. Y., *Adv Drug Deliv Rev* **2011,** *63*, 1228.
192. Alexis, F.; Pridgen, E.; Molnar, L. K.; Farokhzad, O. C., *Molecular Pharmaceutics* **2008,** *5*, 505.
193. Matsumura, Y.; Maeda, H., *Cancer Res* **1986,** *46*, 6387.
194. Gref, R.; Minamitake, Y.; Peracchia, M. T.; Trubetskoy, V.; Torchilin, V.; Langer, R., *Science* **1994,** *263*, 1600.
195. Vllasaliu, D.; Fowler, R.; Stolnik, S., *Expert Opinion on Drug Delivery* **2014,** *11*, 139.
196. Champion, J. A.; Katare, Y. K.; Mitragotri, S., *Journal of Controlled Release* **2007,** *121*, 3.
197. Pasqualini, R.; Ruoslahti, E., *Nature* **1996,** *380*, 364.
198. Fernandez, M.; Javaid, F.; Chudasama, V., *Chem Sci* **2018,** *9*, 790.
199. Cai, S. S.; Vijayan, K.; Cheng, D.; Lima, E. M.; Discher, D. E., *Pharmaceutical Research* **2007,** *24*, 2099.
200. Yu, H. J.; Xu, Z. A.; Wang, D. G.; Chen, X. Z.; Zhang, Z. W.; Yin, Q.; Li, Y. P., *Polymer Chemistry* **2013,** *4*, 5052.
201. Barua, S.; Mitragotri, S., *Acs Nano* **2013,** *7*, 9558.
202. Elsabahy, M.; Shrestha, R.; Clark, C.; Taylor, S.; Leonard, J.; Wooley, K. L., *Nano Letters* **2013,** *13*, 2172.
203. Karagoz, B.; Boyer, C.; Davis, T. P., *Macromolecular Rapid Communications* **2014,** *35*, 417.
204. Howard, M.; Zern, B. J.; Anselmo, A. C.; Shuvaev, V. V.; Mitragotri, S.; Muzykantov, V., *Acs Nano* **2014,** *8*, 4100.
205. Dalhaimer, P.; Engler, A. J.; Parthasarathy, R.; Discher, D. E., *Biomacromolecules* **2004,** *5*, 1714.
206. Kolhar, P.; Anselmo, A. C.; Gupta, V.; Pant, K.; Prabhakarpandian, B.; Ruoslahti, E.; Mitragotri, S., *Proceedings of the National Academy of Sciences of the United States of America* **2013,** *110*, 10753.
207. Champion, J. A.; Mitragotri, S., *Pharmaceutical Research* **2009,** *26*, 244.
208. Bruckman, M. A.; Randolph, L. N.; VanMeter, A.; Hern, S.; Shoffstall, A. J.; Taurog, R. E.; Steinmetz, N. F., *Virology* **2014,** *449*, 163.

209. Yu, T.; Hubbard, D.; Ray, A.; Ghandehari, H., *Journal of Controlled Release* **2012,** *163*, 46.
210. Black, K. C. L.; Wang, Y. C.; Luehmann, H. P.; Cai, X.; Xing, W. X.; Pang, B.; Zhao, Y. F.; Cutler, C. S.; Wang, L. H. V.; Liu, Y. J.; Xia, Y. N., *Acs Nano* **2014,** *8*, 4385.
211. Park, J. H.; von Maltzahn, G.; Zhang, L.; Schwartz, M. P.; Ruoslahti, E.; Bhatia, S. N.; Sailor, M. J., *Adv Mater* **2008,** *20*, 1630.
212. Singh, R.; Pantarotto, D.; Lacerda, L.; Pastorin, G.; Klumpp, C.; Prato, M.; Bianco, A.; Kostarelos, K., *Proceedings of the National Academy of Sciences of the United States of America* **2006,** *103*, 3357.
213. Geng, Y.; Discher, D. E., *J Am Chem Soc* **2005,** *127*, 12780.
214. Dalhaimer, P.; Bates, F. S.; Discher, D. E., *Macromolecules* **2003,** *36*, 6873.
215. Geng, Y.; Dalhaimer, P.; Cai, S.; Tsai, R.; Tewari, M.; Minko, T.; Discher, D. E., *Nat Nanotechnol* **2007,** *2*, 249.
216. Christian, D. A.; Cai, S.; Garbuzenko, O. B.; Harada, T.; Zajac, A. L.; Minko, T.; Discher, D. E., *Mol Pharm* **2009,** *6*, 1343.
217. Nazemi, A.; Boott, C. E.; Lunn, D. J.; Gwyther, J.; Hayward, D. W.; Richardson, R. M.; Winnik, M. A.; Manners, I., *J Am Chem Soc* **2016,** *138*, 4484.
218. Dove, A. P., *Chem Commun (Camb)* **2008**, 6446.
219. Dechy-Cabaret, O.; Martin-Vaca, B.; Bourissou, D., *Chemical Reviews* **2004,** *104*, 6147.
220. Drumright, R. E.; Gruber, P. R.; Henton, D. E., *Advanced Materials* **2000,** *12*, 1841.
221. Uhrich, K. E.; Cannizzaro, S. M.; Langer, R. S.; Shakesheff, K. M., *Chemical Reviews* **1999,** *99*, 3181.
222. Jacobson, G. B.; Shinde, R.; Contag, C. H.; Zare, R. N., *Angewandte Chemie-International Edition* **2008,** *47*, 7880.
223. Stanford, M. J.; Dove, A. P., *Chem Soc Rev* **2010,** *39*, 486.
224. Kricheldorf, H. R., *Chemosphere* **2001,** *43*, 49.
225. Gupta, A. P.; Kumar, V., *European Polymer Journal* **2007,** *43*, 4053.
226. Di Lorenzo, M. L., *European Polymer Journal* **2005,** *41*, 569.
227. Wasanasuk, K.; Tashiro, K.; Hanesaka, M.; Ohhara, T.; Kurihara, K.; Kuroki, R.; Tamada, T.; Ozeki, T.; Kanamoto, T., *Macromolecules* **2011,** *44*, 6441.
228. Lim, L. T.; Auras, R.; Rubino, M., *Progress in Polymer Science* **2008,** *33*, 820.
229. Sasaki, S.; Asakura, T., *Macromolecules* **2003,** *36*, 8385.
230. Puiggali, J.; Ikada, Y.; Tsuji, H.; Cartier, L.; Okihara, T.; Lotz, B., *Polymer* **2000,** *41*, 8921.
231. Hoogsteen, W.; Postema, A. R.; Pennings, A. J.; Ten Brinke, G.; Zugenmaier, P., *Macromolecules* **1990,** *23*, 634.
232. Cartier, L.; Okihara, T.; Ikada, Y.; Tsuji, H.; Puiggali, J.; Lotz, B., *Polymer* **2000,** *41*, 8909.
233. Kricheldorf, H. R.; Kreiser, I., *Makromolekulare Chemie-Macromolecular Chemistry and Physics* **1987,** *188*, 1861.
234. Kricheldorf, H. R.; Berl, M.; Scharnagl, N., *Macromolecules* **1988,** *21*, 286.
235. Degee, P.; Dubois, P.; Jerome, R., *Macromolecular Symposia* **1997,** *123*, 67.
236. Matsumura, S.; Tsukada, K.; Toshima, K., *Macromolecules* **1997,** *30*, 3122.
237. Matsumura, S.; Tsukada, K.; Toshima, K., *International Journal of Biological Macromolecules* **1999,** *25*, 161.
238. Bhaw-Luximon, A.; Jhurry, D.; Spassky, N.; Pensec, S.; Belleney, J., *Polymer* **2001,** *42*, 9651.
239. Loeker, F. C.; Duxbury, C. J.; Kumar, R.; Gao, W.; Gross, R. A.; Howdle, S. M., *Macromolecules* **2004,** *37*, 2450.
240. Pratt, R. C.; Lohmeijer, B. G. G.; Long, D. A.; Lundberg, P. N. P.; Dove, A. P.; Li, H. B.; Wade, C. G.; Waymouth, R. M.; Hedrick, J. L., *Macromolecules* **2006,** *39*, 7863.
241. Kowalski, A.; Libiszowski, J.; Duda, A.; Penczek, S., *Macromolecules* **2000,** *33*, 1964.
242. Kasperczyk, J. E., *Macromolecules* **1995,** *28*, 3937.

243. Schwach, G.; Coudane, J.; Engel, R.; Vert, M., *Journal of Polymer Science Part a-Polymer Chemistry* **1997,** *35*, 3431.
244. Kricheldorf, H. R.; Boettcher, C.; Tonnes, K. U., *Polymer* **1992,** *33*, 2817.
245. Kricheldorf, H. R.; Kreisersaunders, I.; Boettcher, C., *Polymer* **1995,** *36*, 1253.
246. Dove, A. P.; Pratt, R. C.; Lohmeijer, B. G.; Waymouth, R. M.; Hedrick, J. L., *J Am Chem Soc* **2005,** *127*, 13798.
247. Yildirim, I.; Weber, C.; Schubert, U. S., *Progress in Polymer Science* **2018,** *76*, 111.
248. Oh, J. K., *Soft Matter* **2011,** *7*.
249. Saini, P.; Arora, M.; Kumar, M., *Adv Drug Deliv Rev* **2016,** *107*, 47.
250. Lee, B. K.; Yun, Y.; Park, K., *Adv Drug Deliv Rev* **2016,** *107*, 176.
251. Kim, S. H.; Nederberg, F.; Jakobs, R.; Tan, J. P.; Fukushima, K.; Nelson, A.; Meijer, E. W.; Yang, Y. Y.; Hedrick, J. L., *Angew Chem Int Ed Engl* **2009,** *48*, 4508.
252. Bhargava, P.; Tu, Y. F.; Zheng, J. X.; Xiong, H. M.; Quirk, R. P.; Cheng, S. Z. D., *Journal of the American Chemical Society* **2007,** *129*, 1113.
253. Petzetakis, N.; Dove, A. P.; O'Reilly, R. K., *Chem. Sci.* **2011,** *2*, 955.
254. Sun, L.; Petzetakis, N.; Pitto-Barry, A.; Schiller, T. L.; Kirby, N.; Keddie, D. J.; Boyd, B. J.; O'Reilly, R. K.; Dove, A. P., *Macromolecules* **2013,** *46*, 9074.
255. Li, Z.; Sun, L.; Zhang, Y.; Dove, A. P.; O'Reilly, R. K.; Chen, G., *ACS Macro Lett* **2016,** *5*, 1059.
256. Inam, M.; Jones, J. R.; Perez-Madrigal, M. M.; Arno, M. C.; Dove, A. P.; O'Reilly, R. K., *ACS Cent Sci* **2018,** *4*, 63.
257. Qi, H.; Zhou, H.; Tang, Q.; Lee, J. Y.; Fan, Z.; Kim, S.; Staub, M. C.; Zhou, T.; Mei, S.; Han, L.; Pochan, D. J.; Cheng, H.; Hu, W.; Li, C. Y., *Nat Commun* **2018,** *9*, 3005.
258. Hubbell, J. A.; Chilkoti, A., *Science* **2012,** *337*, 303.
259. Guo, X.; Wang, L.; Wei, X.; Zhou, S., *Journal of Polymer Science Part A: Polymer Chemistry* **2016,** *54*, 3525.
260. Matsumura, Y.; Kataoka, K., *Cancer Science* **2009,** *100*, 572.
261. Torchilin, V. P., *Pharm Res* **2007,** *24*, 1.
262. Won, Y. Y.; Davis, H. T.; Bates, F. S., *Science* **1999,** *283*, 960.
263. Crothers, M.; Zhou, Z.; Ricardo, N. M.; Yang, Z.; Taboada, P.; Chaibundit, C.; Attwood, D.; Booth, C., *Int J Pharm* **2005,** *293*, 91.
264. Geng, Y.; Ahmed, F.; Bhasin, N.; Discher, D. E., *J Phys Chem B* **2005,** *109*, 3772.
265. Park, J. H.; von Maltzahn, G.; Zhang, L.; Derfus, A. M.; Simberg, D.; Harris, T. J.; Ruoslahti, E.; Bhatia, S. N.; Sailor, M. J., *Small* **2009,** *5*, 694.
266. Grumelard, J.; Taubert, A.; Meier, W., *Chem Commun (Camb)* **2004**, 1462.
267. Hamley, I. W., *Soft Matter* **2005,** *1*.
268. Khandpur, A. K.; Foerster, S.; Bates, F. S.; Hamley, I. W.; Ryan, A. J.; Bras, W.; Almdal, K.; Mortensen, K., *Macromolecules* **1995,** *28*, 8796.
269. Ajiro, H.; Akashi, M., *Macromol Rapid Commun* **2010,** *31*, 714.
270. Chen, Q.; Zhao, H.; Ming, T.; Wang, J.; Wu, C., *J Am Chem Soc* **2009,** *131*, 16650.
271. Cheng, C.; Qi, K.; Germack, D. S.; Khoshdel, E.; Wooley, K. L., *Advanced Materials* **2007,** *19*, 2830.
272. Dreiss, C. c. A., *Soft Matter* **2007,** *3*.
273. Wang, H.; Lin, W.; Fritz, K. P.; Scholes, G. D.; Winnik, M. A.; Manners, I., *J Am Chem Soc* **2007,** *129*, 12924.
274. He, W.-N.; Xu, J.-T., *Progress in Polymer Science* **2012,** *37*, 1350.
275. Li, X.; Jin, B.; Gao, Y.; Hayward, D. W.; Winnik, M. A.; Luo, Y.; Manners, I., *Angew Chem Int Ed Engl* **2016,** *55*, 11392.
276. He, F.; Gadt, T.; Manners, I.; Winnik, M. A., *J Am Chem Soc* **2011,** *133*, 9095.
277. Oliver, A. M.; Gwyther, J.; Winnik, M. A.; Manners, I., *Macromolecules* **2017,** *51*, 222.

278. Kynaston, E. L.; Nazemi, A.; MacFarlane, L. R.; Whittell, G. R.; Faul, C. F. J.; Manners, I., *Macromolecules* **2018,** *51*, 1002.
279. Jarrett-Wilkins, C.; He, X.; Symons, H. E.; Harniman, R. L.; Faul, C. F. J.; Manners, I., *Chemistry* **2018,** *24*, 15556.
280. Robinson, M. E.; Lunn, D. J.; Nazemi, A.; Whittell, G. R.; De Cola, L.; Manners, I., *Chem Commun (Camb)* **2015,** *51*, 15921.
281. Robinson, M. E.; Nazemi, A.; Lunn, D. J.; Hayward, D. W.; Boott, C. E.; Hsiao, M. S.; Harniman, R. L.; Davis, S. A.; Whittell, G. R.; Richardson, R. M.; De Cola, L.; Manners, I., *ACS Nano* **2017,** *11*, 9162.
282. Kim, Y.; Dalhaimer, P.; Christian, D. A.; Discher, D. E., *Nanotechnology* **2005,** *16*, S484.
283. Zhang, K.; Fang, H.; Chen, Z.; Taylor, J. S.; Wooley, K. L., *Bioconjug Chem* **2008,** *19*, 1880.
284. Ma, Q. G.; Remsen, E. E.; Clark, C. G.; Kowalewski, T.; Wooley, K. L., *Proceedings of the National Academy of Sciences of the United States of America* **2002,** *99*, 5058.
285. Zhang, K.; Rossin, R.; Hagooly, A.; Chen, Z.; Welch, M. J.; Wooley, K. L., *J Polym Sci A Polym Chem* **2008,** *46*, 7578.
286. Li, Z.; Hillmyer, M. A.; Lodge, T. P., *Macromolecules* **2004,** *37*, 8933.
287. Li, Z.; Kesselman, E.; Talmon, Y.; Hillmyer, M. A.; Lodge, T. P., *Science* **2004,** *306*, 98.
288. Lodge, T. P.; Rasdal, A.; Li, Z.; Hillmyer, M. A., *J Am Chem Soc* **2005,** *127*, 17608.
289. Geng, Y.; Discher, D. E., *Polymer* **2006,** *47*, 2519.
290. Rizis, G.; van de Ven, T. G.; Eisenberg, A., *Soft Matter* **2014,** *10*, 2825.
291. Ahmad Khanbeigi, R.; Abelha, T. F.; Woods, A.; Rastoin, O.; Harvey, R. D.; Jones, M. C.; Forbes, B.; Green, M. A.; Collins, H.; Dailey, L. A., *Biomacromolecules* **2015,** *16*, 733.
292. Hemmer, E.; Benayas, A.; Légaré, F.; Vetrone, F., *Nanoscale Horizons* **2016,** *1*, 168.
293. Hong, G.; Zou, Y.; Antaris, A. L.; Diao, S.; Wu, D.; Cheng, K.; Zhang, X.; Chen, C.; Liu, B.; He, Y.; Wu, J. Z.; Yuan, J.; Zhang, B.; Tao, Z.; Fukunaga, C.; Dai, H., *Nat Commun* **2014,** *5*, 4206.
294. Pu, K.-Y.; Li, K.; Liu, B., *Advanced Functional Materials* **2010,** *20*, 2770.
295. Michalet, X.; Pinaud, F. F.; Bentolila, L. A.; Tsay, J. M.; Doose, S.; Li, J. J.; Sundaresan, G.; Wu, A. M.; Gambhir, S. S.; Weiss, S., *Science* **2005,** *307*, 538.
296. Joshi, H. S.; Jamshidi, R.; Tor, Y., *Angewandte Chemie International Edition* **1999,** *38*, 2721.
297. Wu, C.; Szymanski, C.; Cain, Z.; McNeill, J., *J Am Chem Soc* **2007,** *129*, 12904.
298. Kaeser, A.; Schenning, A. P., *Adv Mater* **2010,** *22*, 2985.
299. Howes, P.; Thorogate, R.; Green, M.; Jickells, S.; Daniel, B., *Chem Commun (Camb)* **2009**, 2490.
300. Howes, P.; Green, M.; Levitt, J.; Suhling, K.; Hughes, M., *J Am Chem Soc* **2010,** *132*, 3989.
301. Li, K.; Pan, J.; Feng, S.-S.; Wu, A. W.; Pu, K.-Y.; Liu, Y.; Liu, B., *Advanced Functional Materials* **2009,** *19*, 3535.
302. Guan, Y.; Zhang, Y., *Soft Matter* **2011,** *7*.
303. Gandhi, A.; Paul, A.; Sen, S. O.; Sen, K. K., *Asian Journal of Pharmaceutical Sciences* **2015,** *10*, 99.
304. Karimi, M.; Sahandi Zangabad, P.; Ghasemi, A.; Amiri, M.; Bahrami, M.; Malekzad, H.; Ghahramanzadeh Asl, H.; Mahdieh, Z.; Bozorgomid, M.; Ghasemi, A.; Rahmani Taji Boyuk, M. R.; Hamblin, M. R., *ACS Appl Mater Interfaces* **2016,** *8*, 21107.
305. Yang, J. X.; Fan, B.; Li, J. H.; Xu, J. T.; Du, B. Y.; Fan, Z. Q., *Macromolecules* **2016,** *49*, 367.
306. Zhou, H.; Lu, Y.; Zhang, M.; Guerin, G.; Manners, I.; Winnik, M. A., *Macromolecules* **2016,** *49*, 4265.
307. Schild, H. G.; Muthukumar, M.; Tirrell, D. A., *Macromolecules* **1991,** *24*, 948.
308. Winnik, F. M.; Ringsdorf, H.; Venzmer, J., *Macromolecules* **1990,** *23*, 2415.
309. Winnik, F. M.; Ottaviani, M. F.; Bossmann, S. H.; Garcia-Garibay, M.; Turro, N. J., *Macromolecules* **1992,** *25*, 6007.
310. Wang, S.; Low, P. S., *Journal of Controlled Release* **1998,** *53*, 39.

311. Lu, Y., *Journal of Controlled Release* **2003,** *91*, 17.
312. Shen, Y. T.; Zhang, Q. B.; Zhang, J. S.; Lu, Z. H.; Wang, A. D.; Fei, X. F.; Dai, X. L.; Wu, J. D.; Wang, Z. M.; Zhao, Y. D.; Tian, Y.; Dong, J.; Lan, Q.; Huang, Q., *Experimental and Therapeutic Medicine* **2015,** *10*, 2047.
313. Ma, T. C.; Hou, Y.; Zeng, J. F.; Liu, C. Y.; Zhang, P. S.; Jing, L. H.; Shangguan, D.; Gao, M. Y., *Journal of the American Chemical Society* **2018,** *140*, 211.
314. Fang, B.; Walther, A.; Wolf, A.; Xu, Y.; Yuan, J.; Muller, A. H., *Angew Chem Int Ed Engl* **2009,** *48*, 2877.
315. Yang, P.; Mykhaylyk, O. O.; Jones, E. R.; Armes, S. P., *Macromolecules* **2016,** *49*, 6731.
316. Ladmiral, V.; Semsarilar, M.; Canton, I.; Armes, S. P., *J Am Chem Soc* **2013,** *135*, 13574.
317. Gratton, S. E.; Ropp, P. A.; Pohlhaus, P. D.; Luft, J. C.; Madden, V. J.; Napier, M. E.; DeSimone, J. M., *Proc Natl Acad Sci U S A* **2008,** *105*, 11613.
318. Albanese, A.; Tang, P. S.; Chan, W. C., *Annu Rev Biomed Eng* **2012,** *14*, 1.
319. Huang, K.; Canterbury, D. P.; Rzayev, J., *Macromolecules* **2010,** *43*, 6632.
320. Mohd Yusoff, S. F.; Hsiao, M.-S.; Schacher, F. H.; Winnik, M. A.; Manners, I., *Macromolecules* **2012,** *45*, 3883.
321. Hayward, D. W.; Gilroy, J. B.; Rupar, P. A.; Chabanne, L.; Pizzey, C.; Winnik, M. A.; Whittell, G. R.; Manners, I.; Richardson, R. M., *Macromolecules* **2015,** *48*, 1579.
322. Gould, O. E.; Qiu, H.; Lunn, D. J.; Rowden, J.; Harniman, R. L.; Hudson, Z. M.; Winnik, M. A.; Miles, M. J.; Manners, I., *Nat Commun* **2015,** *6*, 10009.
323. Schmalz, H.; Schmelz, J.; Drechsler, M.; Yuan, J.; Walther, A.; Schweimer, K.; Mihut, A. M., *Macromolecules* **2008,** *41*, 3235.
324. Kamps, A. C.; Fryd, M.; Park, S. J., *ACS Nano* **2012,** *6*, 2844.
325. Lee, I. H.; Amaladass, P.; Yoon, K. Y.; Shin, S.; Kim, Y. J.; Kim, I.; Lee, E.; Choi, T. L., *J Am Chem Soc* **2013,** *135*, 17695.
326. Tung, Y.-C.; Wu, W.-C.; Chen, W.-C., *Macromolecular Rapid Communications* **2006,** *27*, 1838.
327. Tian, Y.; Chen, C.-Y.; Yip, H.-L.; Wu, W.-C.; Chen, W.-C.; Jen, A. K. Y., *Macromolecules* **2010,** *43*, 282.
328. Li, K.; Wang, Q., *Chem Commun (Camb)* **2005**, 4786.
329. Leclère, P.; Calderone, A.; Marsitzky, D.; Francke, V.; Geerts, Y.; Müllen, K.; Brédas, J. L.; Lazzaroni, R., *Advanced Materials* **2000,** *12*, 1042.
330. Wang, H.; Wang, H. H.; Urban, V. S.; Littrell, K. C.; Thiyagarajan, P.; Yu, L., *Journal of the American Chemical Society* **2000,** *122*, 6855.
331. Petzetakis, N.; Walker, D.; Dove, A. P.; O'Reilly, R. K., *Soft Matter* **2012,** *8*.
332. Dalhaimer, P.; Bermudez, H.; Discher, D. E., *Journal of Polymer Science Part B-Polymer Physics* **2004,** *42*, 168.
333. Zhang, J.; Wang, L. Q.; Wang, H.; Tu, K., *Biomacromolecules* **2006,** *7*, 2492.
334. Ganda, S.; Dulle, M.; Drechsler, M.; Förster, B.; Förster, S.; Stenzel, M. H., *Macromolecules* **2017,** *50*, 8544.
335. Dove, A. P., *ACS Macro Letters* **2012,** *1*, 1409.
336. Xu, G. K.; Feng, X. Q.; Li, Y., *Journal of Physical Chemistry B* **2010,** *114*, 1257.
337. Qiu, H.; Du, V. A.; Winnik, M. A.; Manners, I., *J Am Chem Soc* **2013,** *135*, 17739.
338. Cannon, C. G., *Spectrochimica Acta* **1958,** *10*, 341.
339. Seto, C. T.; Whitesides, G. M., *Journal of the American Chemical Society* **1993,** *115*, 905.
340. Venkataraman, S.; Chowdhury, Z. A.; Lee, A. L.; Tong, Y. W.; Akiba, I.; Yang, Y. Y., *Macromol Rapid Commun* **2013,** *34*, 652.
341. Jiang, S.; Göpfert, A.; Abetz, V., *Macromolecules* **2003,** *36*, 6171.
342. Kollman, P.; McKelvey, J.; Johansson, A.; Rothenberg, S., *Journal of the American Chemical Society* **1975,** *97*, 955.

343. Seiler, P.; Weisman, G. R.; Glendening, E. D.; Weinhold, F.; Johnson, V. B.; Dunitz, J. D., *Angewandte Chemie International Edition in English* **1987,** *26*, 1175.
344. Allerhand, A.; Von Rague Schleyer, P., *Journal of the American Chemical Society* **1963,** *85*, 1715.
345. Desiraju, G. R.; Steiner, T., *The weak hydrogen bond : in structural chemistry and biology*. Oxford University Press: Oxford ; New York, 1999.
346. Jeffrey, G. A.; Maluszynska, H., *International Journal of Biological Macromolecules* **1982,** *4*, 173.
347. Sussman, J. L.; Seeman, N. C.; Kim, S. H.; Berman, H. M., *Journal of Molecular Biology* **1972,** *66*, 403.
348. Steiner, T.; Saenger, W., *Journal of the American Chemical Society* **1992,** *114*, 10146.
349. Zhang, J.; Tsuji, H.; Noda, I.; Ozaki, Y., *Macromolecules* **2004,** *37*, 6433.
350. Zhang, J.; Sato, H.; Tsuji, H.; Noda, I.; Ozaki, Y., *Macromolecules* **2005,** *38*, 1822.
351. Starzyk, A.; Barber-Armstrong, W.; Sridharan, M.; Decatur, S. M., *Biochemistry* **2005,** *44*, 369.
352. Li, J.; Xiao, P.; Li, H.; Zhang, Y.; Xue, F.; Luo, B.; Huang, S.; Shang, Y.; Wen, H.; de Claville Christiansen, J.; Yu, D.; Jiang, S., *Polymer Chemistry* **2015,** *6*, 3988.
353. Hayward, D. W.; Lunn, D. J.; Seddon, A.; Finnegan, J. R.; Gould, O. E. C.; Magdysyuk, O.; Manners, I.; Whittell, G. R.; Richardson, R. M., *Macromolecules* **2018,** *51*, 3097.
354. Farah, S.; Anderson, D. G.; Langer, R., *Adv Drug Deliv Rev* **2016,** *107*, 367.
355. Boott, C. E.; Leitao, E. M.; Hayward, D. W.; Laine, R. F.; Mahou, P.; Guerin, G.; Winnik, M. A.; Richardson, R. M.; Kaminski, C. F.; Whittell, G. R.; Manners, I., *ACS Nano* **2018,** *12*, 8920.
356. Butterfield, S.; Hejjaoui, M.; Fauvet, B.; Awad, L.; Lashuel, H. A., *J Mol Biol* **2012,** *421*, 204.
357. Nagy, P. I., *Int J Mol Sci* **2014,** *15*, 19562.
358. Llinas, M.; Klein, M. P., *Journal of the American Chemical Society* **1975,** *97*, 4731.
359. Sturcova, A.; Dybal, J.; Zhigunov, A.; Kotov, N.; Braunova, A., *Soft Matter* **2014,** *10*, 8011.
360. Gonzalez, Y. I.; Nakanishi, H.; Stjerndahl, M.; Kaler, E. W., *J Phys Chem B* **2005,** *109*, 11675.
361. Gonzalez-Alvarez, M. J.; Jia, L.; Guerin, G.; Kim, K. S.; Du, V. A.; Walker, G.; Manners, I.; Winnik, M. A., *Macromolecules* **2016,** *49*, 7975.
362. Harwood, L. M.; Moody, C. J.; Percy, J. M., *Experimental organic chemistry : standard and microscale*. 2nd ed.; Blackwell Science: Oxford, 1999.
363. Marcus, Y., *Pure and Applied Chemistry* **1990,** *62*, 139.
364. Oliver, A. M.; Gwyther, J.; Winnik, M. A.; Manners, I., *Macromolecules* **2018,** *51*, 222.
365. Figueras, J., *Journal of the American Chemical Society* **1971,** *93*, 3255.
366. Lazzaroni, S.; Dondi, D.; Mezzetti, A.; Protti, S., *Photochem Photobiol Sci* **2018,** *17*, 923.
367. Chatterjee, T.; Mandal, M.; Mandal, P. K., *Phys Chem Chem Phys* **2016,** *18*, 24332.
368. Jones, E. R.; Semsarilar, M.; Blanazs, A.; Armes, S. P., *Macromolecules* **2012,** *45*, 5091.
369. Skey, J.; O'Reilly, R. K., *Chem Commun (Camb)* **2008**, 4183.
370. Cetintas, M.; Kamperman, M., *Polymer* **2016,** *107*, 387.
371. Zhang, X.; Xie, Y., *Chem Soc Rev* **2013,** *42*, 8187.
372. Zhuang, X.; Mai, Y.; Wu, D.; Zhang, F.; Feng, X., *Adv Mater* **2015,** *27*, 403.
373. Boott, C. E.; Nazemi, A.; Manners, I., *Angew Chem Int Ed Engl* **2015,** *54*, 13876.
374. Geim, A. K.; Novoselov, K. S., *Nat Mater* **2007,** *6*, 183.
375. Lin, Y. M.; Dimitrakopoulos, C.; Jenkins, K. A.; Farmer, D. B.; Chiu, H. Y.; Grill, A.; Avouris, P., *Science* **2010,** *327*, 662.
376. Splendiani, A.; Sun, L.; Zhang, Y.; Li, T.; Kim, J.; Chim, C. Y.; Galli, G.; Wang, F., *Nano Lett* **2010,** *10*, 1271.
377. Golberg, D.; Bando, Y.; Huang, Y.; Terao, T.; Mitome, M.; Tang, C.; Zhi, C., *ACS Nano* **2010,** *4*, 2979.
378. Gibb, A. L.; Alem, N.; Chen, J. H.; Erickson, K. J.; Ciston, J.; Gautam, A.; Linck, M.; Zettl, A., *J Am Chem Soc* **2013,** *135*, 6758.

379. Ras, R. H.; Umemura, Y.; Johnston, C. T.; Yamagishi, A.; Schoonheydt, R. A., *Phys Chem Chem Phys* **2007,** *9*, 918.
380. Takagi, S.; Shimada, T.; Ishida, Y.; Fujimura, T.; Masui, D.; Tachibana, H.; Eguchi, M.; Inoue, H., *Langmuir* **2013,** *29*, 2108.
381. Tamesue, S.; Ohtani, M.; Yamada, K.; Ishida, Y.; Spruell, J. M.; Lynd, N. A.; Hawker, C. J.; Aida, T., *J Am Chem Soc* **2013,** *135*, 15650.
382. Chen, Z.; Chan, Y. T.; Miyajima, D.; Kajitani, T.; Kosaka, A.; Fukushima, T.; Lobez, J. M.; Aida, T., *Nat Commun* **2016,** *7*, 13640.
383. Sakamoto, R.; Hoshiko, K.; Liu, Q.; Yagi, T.; Nagayama, T.; Kusaka, S.; Tsuchiya, M.; Kitagawa, Y.; Wong, W. Y.; Nishihara, H., *Nat Commun* **2015,** *6*, 6713.
384. Schluter, A. D.; Payamyar, P.; Ottinger, H. C., *Macromol Rapid Commun* **2016,** *37*, 1638.
385. Dupont, J.; Liu, G., *Soft Matter* **2010,** *6*.
386. Pochan, D. J.; Chen, Z.; Cui, H.; Hales, K.; Qi, K.; Wooley, K. L., *Science* **2004,** *306*, 94.
387. Groschel, A. H.; Walther, A.; Lobling, T. I.; Schacher, F. H.; Schmalz, H.; Muller, A. H., *Nature* **2013,** *503*, 247.
388. Jang, S. G.; Audus, D. J.; Klinger, D.; Krogstad, D. V.; Kim, B. J.; Cameron, A.; Kim, S. W.; Delaney, K. T.; Hur, S. M.; Killops, K. L.; Fredrickson, G. H.; Kramer, E. J.; Hawker, C. J., *J Am Chem Soc* **2013,** *135*, 6649.
389. Keller, A., *Polymer* **1962,** *3*, 393.
390. Li, B.; Li, C. Y., *J Am Chem Soc* **2007,** *129*, 12.
391. Dong, B.; Zhou, T.; Zhang, H.; Li, C. Y., *ACS Nano* **2013,** *7*, 5192.
392. Chen, W. Y.; Li, C. Y.; Zheng, J. X.; Huang, P.; Zhu, L.; Ge, Q.; Quirk, R. P.; Lotz, B.; Deng, L.; Wu, C.; Thomas, E. L.; Cheng, S. Z. D., *Macromolecules* **2004,** *37*, 5292.
393. Zheng, J. X.; Xiong, H.; Chen, W. Y.; Lee, K.; Van Horn, R. M.; Quirk, R. P.; Lotz, B.; Thomas, E. L.; Shi, A.-C.; Cheng, S. Z. D., *Macromolecules* **2006,** *39*, 641.
394. Yang, F.; Cheng, S.; Zhang, X.; Ren, X.; Li, R.; Dong, H.; Hu, W., *Adv Mater* **2018,** *30*.
395. Su, M.; Huang, H.; Ma, X.; Wang, Q.; Su, Z., *Macromol Rapid Commun* **2013,** *34*, 1067.
396. Tong, Z.; Li, Y.; Xu, H.; Chen, H.; Yu, W.; Zhuo, W.; Zhang, R.; Jiang, G., *ACS Macro Letters* **2016,** *5*, 867.
397. Yu, B.; Jiang, X.; Yin, J., *Macromolecules* **2014,** *47*, 4761.
398. Zhu, W.; Peng, B.; Wang, J.; Zhang, K.; Liu, L.; Chen, Y., *Macromol Biosci* **2014,** *14*, 1764.
399. Wu, J.; Weng, L.-T.; Qin, W.; Liang, G.; Tang, B. Z., *ACS Macro Letters* **2015,** *4*, 593.
400. Fan, B.; Wang, R.-Y.; Wang, X.-Y.; Xu, J.-T.; Du, B.-Y.; Fan, Z.-Q., *Macromolecules* **2017,** *50*, 2006.
401. Chiang, Y.-W.; Hu, Y.-Y.; Li, J.-N.; Huang, S.-H.; Kuo, S.-W., *Macromolecules* **2015,** *48*, 8526.
402. Lazzari, M.; Scalarone, D.; Vazquez-Vazquez, C.; López-Quintela, M. A., *Macromolecular Rapid Communications* **2008,** *29*, 352.
403. Brubaker, C. E.; Velluto, D.; Demurtas, D.; Phelps, E. A.; Hubbell, J. A., *ACS Nano* **2015,** *9*, 6872.
404. Lazzari, M.; Lopez-Quintela, M. A., *Macromol Rapid Commun* **2009,** *30*, 1785.
405. Boott, C. E.; Gwyther, J.; Harniman, R. L.; Hayward, D. W.; Manners, I., *Nat Chem* **2017,** *9*, 785.
406. Zhang, W.; Jin, W.; Fukushima, T.; Saeki, A.; Seki, S.; Aida, T., *Science* **2011,** *334*, 340.
407. Zhang, W.; Jin, W.; Fukushima, T.; Mori, T.; Aida, T., *J Am Chem Soc* **2015,** *137*, 13792.
408. Ma, X.; Zhang, Y.; Zhang, Y.; Liu, Y.; Che, Y.; Zhao, J., *Angew Chem Int Ed Engl* **2016,** *55*, 9539.
409. Ogi, S.; Sugiyasu, K.; Manna, S.; Samitsu, S.; Takeuchi, M., *Nat Chem* **2014,** *6*, 188.
410. Ogi, S.; Stepanenko, V.; Sugiyasu, K.; Takeuchi, M.; Wurthner, F., *J Am Chem Soc* **2015,** *137*, 3300.
411. Fukui, T.; Kawai, S.; Fujinuma, S.; Matsushita, Y.; Yasuda, T.; Sakurai, T.; Seki, S.; Takeuchi, M.; Sugiyasu, K., *Nat Chem* **2017,** *9*, 493.

412. Pal, A.; Malakoutikhah, M.; Leonetti, G.; Tezcan, M.; Colomb-Delsuc, M.; Nguyen, V. D.; van der Gucht, J.; Otto, S., *Angew Chem Int Ed Engl* **2015,** *54*, 7852.
413. Aliprandi, A.; Mauro, M.; De Cola, L., *Nat Chem* **2016,** *8*, 10.
414. Zhu, J.; Zhang, S.; Zhang, K.; Wang, X.; Mays, J. W.; Wooley, K. L.; Pochan, D. J., *Nat Commun* **2013,** *4*, 2297.
415. Wright, D. B.; Patterson, J. P.; Pitto-Barry, A.; Lu, A.; Kirby, N.; Gianneschi, N. C.; Chassenieux, C.; Colombani, O.; O'Reilly, R. K., *Macromolecules* **2015,** *48*, 6516.
416. Kang, N.; Perron, M. E.; Prud'homme, R. E.; Zhang, Y.; Gaucher, G.; Leroux, J. C., *Nano Lett* **2005,** *5*, 315.
417. Kim, S. H.; Tan, J. P. K.; Nederberg, F.; Fukushima, K.; Yang, Y. Y.; Waymouth, R. M.; Hedrick, J. L., *Macromolecules* **2009,** *42*, 25.
418. Nederberg, F.; Appel, E.; Tan, J. P.; Kim, S. H.; Fukushima, K.; Sly, J.; Miller, R. D.; Waymouth, R. M.; Yang, Y. Y.; Hedrick, J. L., *Biomacromolecules* **2009,** *10*, 1460.
419. Fu, J.; Luan, B.; Yu, X.; Cong, Y.; Li, J.; Pan, C.; Han, Y.; Yang, Y.; Li, B., *Macromolecules* **2004,** *37*, 976.
420. Chen, C.-K.; Lin, S.-C.; Ho, R.-M.; Chiang, Y.-W.; Lotz, B., *Macromolecules* **2010,** *43*, 7752.
421. Miyata, T.; Masuko, T., *Polymer* **1997,** *38*, 4003.
422. Iwata, T.; Doi, Y., *Macromolecules* **1998,** *31*, 2461.
423. Patterson, J. P.; Sanchez, A. M.; Petzetakis, N.; Smart, T. P.; Epps, T. H., 3rd; Portman, I.; Wilson, N. R.; O'Reilly, R. K., *Soft Matter* **2012,** *8*, 3322.
424. Sun, L.; Pitto-Barry, A.; Thomas, A. W.; Inam, M.; Doncom, K.; Dove, A. P.; O'Reilly, R. K., *Polym Chem* **2016,** *7*, 2337.
425. Pratt, R. C.; Lohmeijer, B. G. G.; Long, D. A.; Lundberg, P. N. P.; Dove, A. P.; Li, H.; Wade, C. G.; Waymouth, R. M.; Hedrick, J. L., *Macromolecules* **2006,** *39*, 7863.
426. Hu, Z.; Fan, X.; Wang, H.; Wang, J., *Polymer* **2009,** *50*, 4175.
427. Rizis, G.; van de Ven, T. G.; Eisenberg, A., *ACS Nano* **2015,** *9*, 3627.
428. Cambridge, G.; Gonzalez-Alvarez, M. J.; Guerin, G.; Manners, I.; Winnik, M. A., *Macromolecules* **2015,** *48*, 707.
429. O'Reilly, R. K.; Hawker, C. J.; Wooley, K. L., *Chem Soc Rev* **2006,** *35*, 1068.
430. Rupar, P. A.; Cambridge, G.; Winnik, M. A.; Manners, I., *J Am Chem Soc* **2011,** *133*, 16947.
431. Thurmond, K. B.; Kowalewski, T.; Wooley, K. L., *Journal of the American Chemical Society* **1997,** *119*, 6656.
432. Guo, A.; Liu, G.; Tao, J., *Macromolecules* **1996,** *29*, 2487.
433. Gilroy, J. B.; Rupar, P. A.; Whittell, G. R.; Chabanne, L.; Terrill, N. J.; Winnik, M. A.; Manners, I.; Richardson, R. M., *J Am Chem Soc* **2011,** *133*, 17056.
434. Paula, E. L. d.; Mano, V.; Duek, E. A. R.; Pereira, F. V., *Química Nova* **2015**.
435. Oyama, H. T.; Tanishima, D.; Ogawa, R., *Biomacromolecules* **2017,** *18*, 1281.
436. Tokiwa, Y.; Calabia, B. P., *Appl Microbiol Biotechnol* **2006,** *72*, 244.
437. Li, Y.; Qi, X. R.; Maitani, Y.; Nagai, T., *Nanotechnology* **2009,** *20*, 055106.
438. Jing, Y.; Quan, C.; Liu, B.; Jiang, Q.; Zhang, C., *Polymer Reviews* **2016,** *56*, 262.
439. Yu, Y. S.; Zhang, L. F.; Eisenberg, A., *Macromolecules* **1998,** *31*, 1144.
440. Kan, S. B. J.; Huang, X.; Gumulya, Y.; Chen, K.; Arnold, F. H., *Nature* **2017,** *552*, 132.
441. Arnold, F. H., *Angew Chem Int Ed Engl* **2018,** *57*, 4143.
442. Kan, S. B.; Lewis, R. D.; Chen, K.; Arnold, F. H., *Science* **2016,** *354*, 1048.